OCS Study
BOEM 2021-027

Characterizing Spatial Distributions of Deep-sea Corals and Chemosynthetic Communities in the US Gulf of Mexico through Data Synthesis and Predictive Modeling

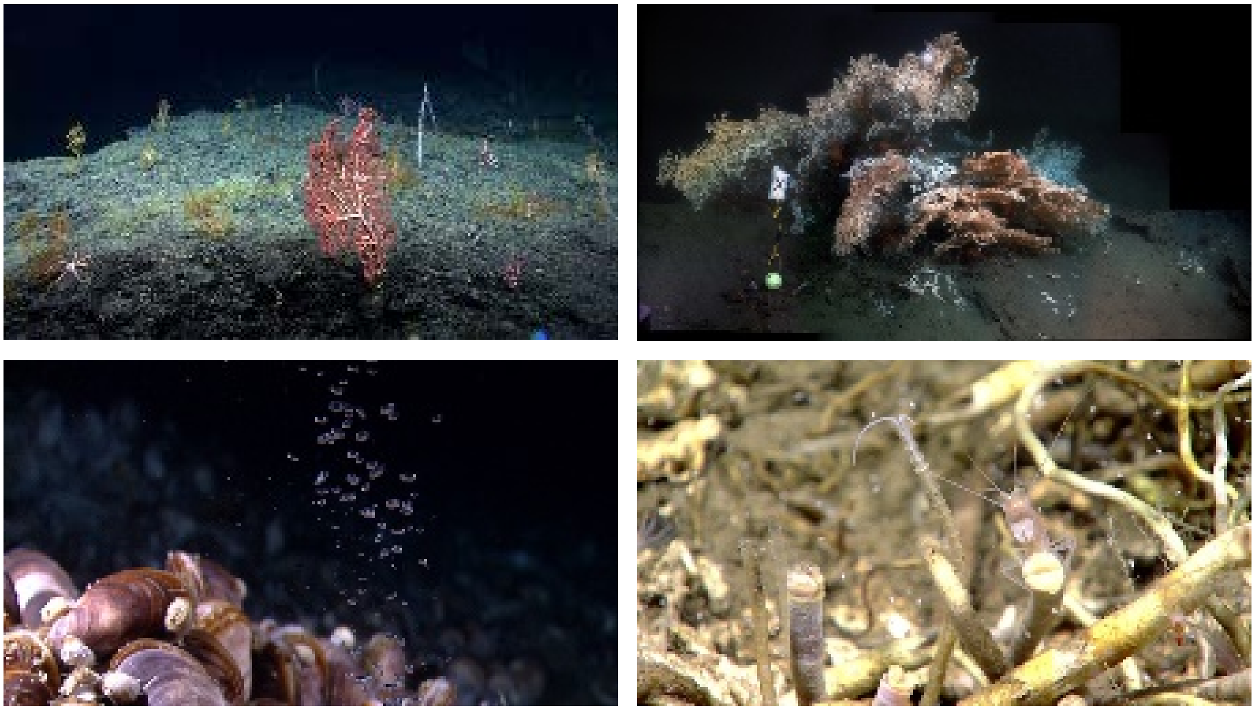

US Department of the Interior
Bureau of Ocean Energy Management
Gulf of Mexico Regional Office

BOEM
Bureau of Ocean Energy
Management

Characterizing Spatial Distributions of Deep-sea Corals and Chemosynthetic Communities in the US Gulf of Mexico through Data Synthesis and Predictive Modeling

February 2021

Authors:
Holly F. Goyert, Rachel Bassett, John Christensen, Heather Coleman, Michael Coyne, Peter J. Etnoyer, Janessy Frometa, Thomas F. Hourigan, Matthew Poti, Enrique J. Salgado, Bethany Williams, Arliss J. Winship

Prepared under NCCOS IAA MOA-2015-052-9159, and NCCOS BOEM IAA M15PG00020
by
National Oceanic and Atmospheric Administration
National Ocean Service
National Centers for Coastal Ocean Science
Marine Spatial Ecology Division
1305 East-West Hwy
SSMC-4, N/SCI-1
Silver Spring, MD 20910

US Department of the Interior
Bureau of Ocean Energy Management
Gulf of Mexico Regional Office

BOEM
Bureau of Ocean Energy Management

DISCLAIMER

This study was funded, in part, by the US Department of the Interior, Bureau of Ocean Energy Management (BOEM), Environmental Studies Program, Washington, DC, through Interagency Agreement Number M15PG00020 with the US Department of Commerce, National Oceanic and Atmospheric Administration, National Ocean Service, National Centers for Coastal Ocean Science, in Silver Spring, Maryland. This report has been technically reviewed by BOEM, and it has been approved for publication. The views and conclusions contained in this document are those of the authors and should not be interpreted as representing the opinions or policies of the US Government, nor does mention of trade names or commercial products constitute endorsement or recommendation for use.

REPORT AVAILABILITY

To download a PDF file of this report, go to the US Department of the Interior, Bureau of Ocean Energy Management Data and Information Systems webpage (http://www.boem.gov/Environmental-Studies-EnvData/), click on the link for the Environmental Studies Program Information System (ESPIS), and search on 2021-027. The report is also available at the National Technical Reports Library at https://ntrl.ntis.gov/NTRL/.

CITATION

Goyert HF, Bassett R, Christensen J, Coleman, H, Coyne M, Etnoyer PJ, Frometa J, Hourigan, TF, Poti M, Salgado EJ, Williams, B, Winship AJ. 2020. Characterizing spatial distributions of deep-sea corals and chemosynthetic communities in the US Gulf of Mexico through data synthesis and predictive modeling. New Orleans (LA): US Department of the Interior, Bureau of Ocean Energy Management. OCS Study BOEM 2021-027. 317 p.

ABOUT THE COVER

Cover photos: Top left: Diverse deep-sea coral community on the Florida Escarpment; credit: NOAA Office of Ocean Exploration and Research, Gulf of Mexico 2017. Top right: *Madrepora oculata* colony with several deep-sea red crab *Chaceon quinquedens*. The X marker was placed by deep-sea researchers in 2010 so they could return to this spot; credit: Lophelia II: Reefs, Rigs, and Wrecks 2009 Expedition, NOAA Office of Ocean Exploration and Research and BOEM. Bottom left: Bubbles of methane gas rise through a mussel bed at the Pascaguola Dome; credit: NOAA Office of Ocean Exploration and Research, Gulf of Mexico Expedition 2012. Bottom right: A dense cluster of *Escarpia* sp. chemosynthetic tubeworms at a cold seep, accompanied by an *Alvinocaris* sp. shrimp and a chaetopterid polychaete waving its pair of feeding palps from its slender bamboo-like tube; credit: NOAA Office of Ocean Exploration and Research, Gulf of Mexico 2017.

ACKNOWLEDGMENTS

We dedicate this report to the memory of Kody Kramer and Brian Kinlan, our colleagues who passed away before the completion of this study. Kody led the development of the Bureau of Ocean Energy Management (BOEM) Northern Gulf of Mexico Deepwater Bathymetry Grid that provided bathymetry data for much of our study area. Brian had a vision for using spatial predictive models to identify potential locations of deep-sea coral habitats in support of management. He was instrumental in the development of this study.

We thank the many scientists who contributed their data, time, and expertise over the course of this study. Mark Benfield (Louisiana State University), Robert Carney (Louisiana State University), Erik Cordes (Temple University), Charles Fisher (Pennsylvania State University), Peter Girguis (Harvard University), Emma Hickerson (Flower Garden Banks National Marine Sanctuary), Samantha Joye (University of Georgia), Elizabeth Lobecker (NOAA Office of Ocean Exploration and Research), Ian MacDonald (Florida State University), Charles Messing (Nova Southeastern University), Marissa Nuttall (Flower Garden Banks National Marine Sanctuary), John Reed (Harbor Branch Oceanographic Institute at Florida Atlantic University), George Schmahl (Flower Garden Banks National Marine Sanctuary), Stephanie Sharuga (BOEM, formerly Louisiana State University), Thomas Shirley (Harte Research Institute at Texas A&M, Corpus Christi), and Cindy Van Dover (Duke University) provided data and support in the development of the database of presence-absence records for deep-sea corals and chemosynthetic communities compiled as part of this study. Gregory Boland (BOEM), Sandra Brooke (Florida State University), Robert Carney (Louisiana State University), Charles Fisher (Pennsylvania State University), Paul Sammarco (Louisiana Universities Marine Consortium), and James Sinclair (Bureau of Safety and Environmental Enforcement) participated in a webinar review of the presence-absence database. Kody Kramer (BOEM) and William Shedd (BOEM) provided guidance on using the BOEM Northern Gulf of Mexico Deepwater Bathymetry Grid as part of the synthesis of bathymetry data used to derive several of the environmental predictor datasets. Yizhen Li (CSS Inc. and NOAA NCCOS) provided advice on the ocean circulation model data used to develop environmental predictor datasets depicting physical properties of bottom ocean water. Alicia Caporaso (BOEM), Erik Cordes (Temple University), Jeffery Leirness (CSS Inc. and NOAA NCCOS), Charles Menza (NOAA NCCOS), David Moran (BOEM), Mark Mueller (BOEM), Michelle Nannen (BOEM), Stephanie Sharuga (BOEM), and Mariana Steen (BOEM) reviewed this report and provided helpful comments and suggestions.

This study was funded by the BOEM through Interagency Agreement Number M15PG00020 with the US Department of Commerce, National Oceanic and Atmospheric Administration, National Ocean Service, National Centers for Coastal Ocean Science. Michael Coyne, Holly Goyert, Matthew Poti, Bethany Williams, and Arliss Winship were supported by NOAA Contracts No. GS-00F-217CA/EA133C-17-BA-0062 with CSS, Inc. Rachel Bassett, Janessy Frometa, and Enrique Salgado were supported by NOAA Contracts No. GS-00F-217CA/EA133C-17-BA-0049 with CSS, Inc.

Contents

List of Figures

List of Tables

List of Abbreviations and Acronyms

Short Form	Long Form
AUC	Area Under the Receiver Operating Characteristic Curve
AUV	Autonomous underwater vehicle
BOEM	Bureau of Ocean Energy Management
CCOM	Center for Coastal and Ocean Mapping
CV	coefficient of variation
DSC	deep-sea coral
DOI	US Department of the Interior
GEBCO	General Bathymetric Chart of the Oceans
HOV	human occupied vehicle
HYCOM	hybrid coordinate ocean model
km	kilometer
m	meter
MCMC	Markov Chain Monte Carlo
MODIS	Moderate Resolution Imaging Spectroradiometer
NASA	National Aeronautics and Space Administration
NCCOS	National Centers for Coastal Ocean Science
NEPA	National Environmental Policy Act
NMNH	National Museum of Natural History
NOAA	National Oceanic and Atmospheric Administration
NOS	National Ocean Service
NRDA	Natural Resource Damage Assessment
nm	nanometer
OER	Office of Ocean Exploration and Research
OCS	Outer Continental Shelf
ROV	remotely operated vehicle
SeaWiFS	Sea-viewing Wide Field-of-View Sensor
UNH	University of New Hampshire
USGS	US Geological Survey
VIF	variance inflation factor
VIIRS	Visible Infrared Imaging Radiometer Suite
WoRMS	World Register of Marine Species

1. Introduction

The Department of the Interior's Bureau of Ocean Energy Management (BOEM) is responsible for the environmentally and economically responsible stewardship of US Outer Continental Shelf (OCS) energy and mineral resources. This includes the approximately 160 million acres (650,000 km^2) of the Gulf of Mexico (Gulf) OCS. Offshore energy projects often include activities that may physically disturb the seafloor and could negatively affect benthic biota.

BOEM has identified deep-sea corals (DSCs), also known as cold-water corals or deepwater corals, and chemosynthetic communities as sensitive deep-water biota. Requirements were included in their Notices to Lessees (NTL No. 2009-G40) for oil and gas operators to avoid such habitats in the Gulf (MMS 2010). DSCs can create local hotspots of biodiversity by providing three-dimensional structure that increases the complexity of habitats available for use by other organisms such as fishes and echinoderms (Buhl-Mortensen et al. 2010). Recent reviews (Roberts et al. 2009; Cordes et al. 2016; Hourigan et al. 2017) have highlighted the importance of DSC communities and the habitats they create, and their vulnerability to impacts from human activities. Similar to DSCs, habitats created by chemosynthetic fauna at cold seeps (i.e., locations where fluids containing reduced chemicals like methane and sulfide emerge from beneath the seafloor) may increase habitat heterogeneity (Cordes et al. 2010).

Having the most comprehensive and up-to-date information on the spatial distribution of DSCs and chemosynthetic communities is essential for BOEM to assess potential impacts of offshore energy development on the marine environment in the Gulf. Although the intent of this study was to compile observations and model distributions of both DSCs and chemosynthetic communities, the primary focus was on DSCs because of challenges with the data available for characterizing distributions of chemosynthetic communities. First, chemosynthetic communities could only be recorded to category rather than taxon in the presence-absence database compiled as part of this study. Also, key environmental predictor variables needed to inform models of chemosynthetic community occurrence (e.g., presence of carbonates, backscatter, surface oil slicks) were not readily available for the entire study area and so were not included. As a result, although information on the spatial distributions of chemosynthetic communities is presented in this report and associated data products (both presence-absence records and model predictions), this information should be considered preliminary. This report provides information about what is needed to support improved models of chemosynthetic community distributions in the sections describing the observation data (Section 2.4) and environmental predictor variables (Section 2.5).

Many DSC taxa are found on exposed hard substrate at the seafloor. Consequently, the Gulf's complex geology and oceanography that controls exposed hard substrate also influences the spatial distribution of DSCs in the region. In the western and central Gulf (i.e., west of the Florida Escarpment), the continental shelf and slope are covered primarily by soft sediments (Darnell and Defenbaugh 1990; Rowe and Kennicutt 2009). However, the topography of the continental slope is extremely complex, with numerous banks and mounds (i.e., salt domes) having been formed by the movement of salt underneath the overlying sediments, a process known as salt diapirism (Boland et al. 2017). DSC communities can be found on exposed hard substrate that forms at these banks and mounds from the precipitation of authigenic carbonates associated with hydrocarbon seepage (Schroeder 1992; Brooks et al. 2016). In the eastern Gulf offshore of Florida, the continental shelf-slope complex lies on a broad carbonate platform (Darnell and Defenbaugh 1990; Hine et al. 2003). At the western edge of the platform is the extremely steep and high-relief Florida Escarpment, which contains areas of exposed rocky substrate that could support DSC communities (Newton et al. 1987; Hine et al. 2003). Newton et al. (1987) described an extensive area of DSC mounds at 500 m depth on the continental slope; however, the scleractinian corals sampled from the mounds, predominantly *Lophelia pertusa*, were all dead. Mapping of the seafloor on the west Florida slope by multibeam sonar has indicated a large number of mound, ridge, and scarp features with sufficient vertical relief to suggest the presence of exposed rock (Boland et al. 2017; Ross et al. 2017). Ross et al. (2017) reported on DSC communities observed on these habitats using underwater vehicles during six research cruises between 2008 and 2012.

Communities of chemosynthetic fauna associated with hydrocarbon seeps were first discovered in the Gulf during the 1980s at the Florida Escarpment (Paull et al. 1984) and in the Northern Gulf (Brooks et al. 1984; Kennicutt et al. 1985). Researchers have since identified and characterized numerous chemosynthetic communities in the Gulf (e.g., Brooks et al. 1987; Kennicutt et al. 1988; MacDonald et al. 1989; MacDonald et al. 2003; Cordes et al. 2007; Brooks et al. 2009). These chemosynthetic communities (i.e., that derive energy from chemical reactions) can include dense aggregations of mussels, clams, and tubeworms. In addition, the hard substrate associated with the hydrocarbon seeps may be inhabited by DSCs.

Brooke et al. (2007) and Boland et al. (2017) reviewed the state of knowledge of DSC communities in the Gulf and summarized the extensive exploration and research conducted to date to characterize these communities. Such research included, for example, large interdisciplinary projects involving federal and academic partners such as Lophelia I (Sulak et al. 2008), Lophelia II (Brooks et al. 2016; Demopoulos et al. 2017), and Chemo III (Brooks et al. 2009), along with standalone exploratory surveys by the R/V *Falkor* (Schmidt Ocean Institute), the E/V *Nautilus* (Ocean Exploration Trust), and the National Oceanic and Atmospheric Administration (NOAA) Ship *Okeanos Explorer*. In some cases, these expeditions investigated both DSC and chemosynthetic communities.

In spite of the considerable efforts to document and investigate DSCs and chemosynthetic communities, because of the expense and logistical challenges of deep-sea research, it is unlikely that more than a small fraction of all deep-water habitats in a region as large as the US Gulf will be explored through sampling or collection of imagery. Statistical models (i.e., species distribution models) have increasingly become an important and cost-effective tool for identifying locations of potential habitat for benthic biota such as DSCs. These models quantify relationships among species occurrence (e.g., presence, presence-absence, abundance) and environmental variables, and then use these relationships to predict and map locations of likely species occurrence.

Previous efforts to model the spatial distributions of DSCs at a regional scale across the entire US Gulf relied on presence data (Kinlan et al. 2013; Etnoyer et al. 2018). These models used environmental predictors derived from a regional bathymetry compilation that was too coarse to capture many of the fine-scale hard substrate features (e.g., mounds, ridges) where DSCs have been observed in the Gulf. Several of these models were generated for broader taxonomic groups (e.g., suborder, order) that combined taxa with different habitat requirements and may have overpredicted the extent of suitable habitat for these groups (Guinotte and Davies 2014; Kinlan et al. 2020). In addition, several studies have modeled distributions of DSCs for smaller (i.e., sub regional) extents at finer resolution using environmental predictors derived from high-resolution bathymetry data (Georgian et al. 2014; Silva and MacDonald 2017; Georgian et al. 2020; Sterne et al. 2020). Outputs from these previous modeling efforts have been integral to the Gulf of Mexico Fishery Management Council process for designating Habitat Areas of Particular Concern (NOAA Fisheries 2018; NOAA 2020a), the Flower Garden Banks National Marine Sanctuary Expansion Plan (NOAA 2020b), and the Open Ocean Restoration Plan for the Gulf of Mexico (NOAA 2019; Open Ocean Trustee Implementation Group 2019). The authors of this study are not aware of any studies that have modeled the spatial distributions of chemosynthetic communities in the Gulf.

Although models using presence data, but not absence data, (i.e., presence-only models or presence-background models) have been useful for informing management, presence-only models have important limitations. Most important, presence-only models may confound the distribution of sampling effort with the distribution of presence if they do not account for spatial sampling bias in the presence data (Phillips et al. 2009; Elith et al. 2011). Predictions from presence-only models are typically relative measures (e.g., habitat suitability) and, as such, should be interpreted with this caveat in mind (Royle et al. 2012). Models fit to presence-absence data provide a standardized measure of predicted occurrence (i.e., probability of occurrence) that allows predicted distributions to be directly compared, rather than being interpreted in relative terms (Winship et al. 2020).

Historically, many of the data describing DSC occurrence have tended to focus on documenting presences, and there have been concerns about whether it is possible to confirm the absence of a DSC (Vierod et al. 2014). Also, relatively few records of DSC occurrence have included measures of sampling effort (e.g., area surveyed). All else being equal, the greater the area surveyed the greater the probability that an organism will be observed and the greater the number of organisms that will be counted, so measures of sampling effort are critical for standardizing estimates of probability of occurrence and density. Although researchers have conducted numerous benthic surveys over the past few decades, imagery data from these surveys exist in a variety of formats and are in several repositories, many of which are not readily available for assessment. Many of these data have not been reviewed and digitized in a commonly formatted database. This information can be made more useful only by reviewing, analyzing, and organizing data for consistency and ease of access. Although the NOAA National Database for Deep-Sea Corals and Sponges (Hourigan et al. 2015) provides a framework within which to organize, standardize, and distribute deep-water benthic community data, NOAA funds alone do not allow for extensive effort to reanalyze previously collected field datasets to “rescue” the vast amount of data contained therein, including absence data and measures of sampling effort. In contrast to data for DSCs, no available database provides common information on chemosynthetic communities, though these communities are critical for and closely associated with DSCs in the Gulf.

In this study, BOEM funded the NOAA National Centers for Coastal Ocean Science (NCCOS) to provide information on the spatial distribution of DSCs and chemosynthetic communities to support environmental risk assessments, environmental impact statements, and other decision documents related to the review of proposed activities in the region. The study had two main objectives. The first was to compile a database of presence-absence observations for DSCs and chemosynthetic communities with associated measures of sampling effort (i.e., the survey area associated with each sample). Second, records in the database were used in spatial predictive models to characterize and map the potential spatial distributions of these organisms across the entire Gulf.

This report summarizes the approach used for this study. This chapter (Chapter 1) introduces the study, describes the management rationale for the analyses, provides background on the existing knowledge of DSC and chemosynthetic communities in the Gulf, and sets the stage for the subsequent sections. Chapter 2 describes the data and methods used to compile the database of presence-absence observations for DSCs and chemosynthetic communities, the set of gridded spatial datasets representing the environmental predictor variables, and the occupancy modeling approach used to predict the probability of occurrence for selected taxa. Chapter 3 presents and discusses the results of the occupancy models. This includes measures of model fit and performance, maps of the observed and predicted spatial distributions of DSCs and chemosynthetic communities, and an evaluation of the importance of the environmental predictor variables to model fitting. Chapter 4 provides conclusions about the advancements and limitations/caveats of the data, modeling approach, and maps and data products presented in this report as well as guidance about how this information can be used to inform marine resource management and future research and exploration.

2. Methods

2.1 Study area

The study area included waters within the US Gulf of Mexico (Gulf) from 50 m depth to the boundary of the Gulf Outer Continental Shelf (OCS) region (Figure 1). The 50 m depth contour ranged from approximately 5.6–150 km from shore. Though deep-sea coral (DSCs) are known to exist across a broad range of depths in the Gulf, the distribution of an individual taxon may be restricted to a specific depth range or zone. For this study, depth zones were defined as mesophotic (50–200 m), upper bathyal (200–1,000 m), and lower bathyal (1,000–3,000 m).

2.2 Data synthesis of observations of deep-sea corals and chemosynthetic communities

Available data from field surveys conducted during the 1980s–2010s were evaluated to create a comprehensive inventory of datasets to use in generating a database of georeferenced presence and absence information for DSCs and chemosynthetic communities in the study area. Datasets in the inventory contained still images and video collected by submersible (human occupied vehicle, or HOV), autonomous underwater vehicle (AUV), and remotely operated vehicle (ROV). Each dataset was assessed for accessibility, accuracy of navigation data, spatial coverage, temporal range, and data quality to prioritize datasets in the inventory. Twenty-two datasets were selected from the inventory and were analyzed to compile a database of presence-absence records for DSCs and chemosynthetic communities (Table 1, Figure 2). Additional information about these datasets can be found in Appendix A. The relational database is available as a Microsoft® Access® file as part of the data package available for the study.

Each record in the database corresponded to a sample (sometimes referred to as segment) of the imagery data. Each sample was assigned a spatial position (e.g., the point location of a still image or midpoint of a video transect), an estimate of the areal extent observed (i.e., sampling effort), and annotations of the DSCs and chemosynthetic communities present. A taxon was considered to be present in a sample if one or more occurrences of the taxon were recorded; otherwise the taxon could be inferred as absent for the sample.

Because of the differences in the methods used to collect the imagery data, the survey area represented by the samples varied across the source datasets. Samples included frame grabs (e.g., 1 m^2), photo mosaics (e.g., 10 m^2), submersible dives (e.g., 1,000 m^2), and ROV transects (e.g., 100–1,000 m^2). For reference, a five-minute ROV transect moving at 0.5 knots covers approximately 100 m with a field of view of 1–2 m, corresponding to an area surveyed of 100–200 m^2. The areal extent of each sample was calculated to the nearest order of magnitude based on vehicle specifications, such as camera frame width, and distance traveled.

Original still images or video were reanalyzed to obtain information on the absence of DSCs and chemosynthetic communities or the sampling effort for each sample when this information could not be inferred (e.g., if earlier analysis did not record presences for all taxa) or was missing or incomplete in the original data. For example, previous annotations for the Carney & Roberts Benthic Seeps datasets included only chemosynthetic biota. Annotations of DSCs were compiled for this dataset by reviewing the original video data. For some recently collected datasets, such as the ROV dives conducted by the National Oceanic and Atmospheric Administration (NOAA) Ship *Okeanos Explorer* in 2017 and 2018, imagery data were annotated for presence-absence of DSCs and chemosynthetic communities as part of this study.

2.3 Selection of DSC taxa for modeling

An initial list of potential DSC taxa for modeling was compiled by identifying the taxa that represented the top 95% of the occurrence records in the NOAA National Database for Deep-Sea Corals and Sponges (Hourigan et al. 2015) for each depth zone. This list was further refined using the records in the presence-absence database created in this study (Table 2).

For each DSC taxon, potential location or depth errors in the database records were identified using the reported depth for each sample and the depth extracted from the environmental predictor dataset depicting depth at the spatial position of the sample (see Section 2.4.2 for a description of the depth predictor dataset). In addition, a list of ‘expected’ depth ranges for each DSC taxon was compiled for further evaluation of potential errors in location, depth, or taxonomic identification. The expected depth range for each taxon was calculated from the 80–95% intervals of reported depths in the Smithsonian National Museum of Natural History (NMNH) database. This approach gave more reliable ranges (Table 2) that refined the minimum and maximum depth ranges published in the literature (Etnoyer and Cairns 2017). The ranges captured 85–100% of NMNH records while removing extreme and potentially erroneous values yet allowed some cushion for new discovery beyond previously observed depth ranges. Records in the presence-absence database that greatly exceeded these ranges were double-checked, and often corrected. The errors were attributed to clerical errors, typos, and misidentification of species in the images. For each taxon, occurrences that could not be corrected were treated as absences in the models but were still retained in the presence-absence database as occurrences.

The analysis focused on DSC taxa that are structure-forming (i.e., those that provide three-dimensional structure) that are of interest to the Bureau of Ocean Energy Management (BOEM) because these complex structures offer new microhabitats that are frequently used by other associated benthic species (e.g., crustaceans, brittle stars, fishes) and increase local biodiversity. The structure-forming DSCs selected for modeling included five genera and one family of branching stony corals in order Scleractinia; three species, 16 genera, and 11 families of gorgonian corals in order Alcyonacea; and two species, seven genera, and one family of black corals in order Antipatharia (Table 2). Only four taxa were identified to the species level in the presence-absence database: the stony coral *Lophelia pertusa*, the gorgonian octocoral *Swiftia exserta*, and two black corals *Antipathes furcata* and *Antipathes atlantica*. In addition, any records identified in the presence-absence database as *Paramuricea* (order Alcyonacea) that occurred deeper than 800 m were assumed to be *Paramuricea biscaya*. Records previously identified in the presence-absence database as *Hypnogorgia* were assumed to be *Muricea pendula*, because genetic studies have shown these taxa to be synonymous, although they appear very different. Taxonomic classifications were cross-referenced with the World Register of Marine Species (WoRMS Editorial Board 2020). Results are not presented in this report for *Plumarella* or *A. furcata* because the models for these taxa failed to converge numerically.

2.4 Selection of chemosynthetic communities for modeling

Although chemosynthetic communities were included in the presence-absence database, these observations were recorded only to general categories or habitats (Table 2) rather than at a finer taxonomic resolution (e.g., to species). Tubeworms consisted of any dead or living Siboglinid worms, associated with hydrocarbon or sulfide seeps in the seafloor. Bivalves included living or dead colonial bivalves (e.g., mussels, clams), associated with hydrocarbon or sulfide seeps in the seafloor. Bacterial mats represented observations of chemotrophic bacteria or archaea, often associated with seeps. A seep was identified as a hydrocarbon (oil, methane, or asphalt), sulfide, plume, mud, or volcanic ejection. Brine included brine pools or brine flows on the seafloor. Results are not presented in this report for tubeworms or seeps because the models for these taxa failed to converge numerically. It is important to note that the assignment of categories rather than taxonomic identifications for the chemosynthetic communities, along with the emphasis on DSCs in selecting environmental predictors (described in Section 2.5), limited the performance of these models. For example, the bivalve category included two very different groups of organisms — sessile mussels that live on the surface of the substrate, use methane and sulfide, and have no binding proteins for sulfides and mobile clams that live in the substrate, use sulfide only, and have binding proteins (E. Cordes, email message, August 27, 2020). Efforts to identify records within the tubeworm and bivalve categories at a finer taxonomic resolution would allow future studies to model distributions of the distinct groups of organisms within these categories.

2.5 Environmental predictor variables

An initial set of 27 environmental predictor variables (Table 3) that represented potential drivers (or proxies for drivers) of the occurrence of DSCs and chemosynthetic communities were identified. These variables included measures of depth, seafloor topography, seafloor substrate, oceanography, and geography. Additional environmental predictor variables, including other measures describing biological productivity, ocean chemistry, and seafloor substrate composition were considered. However, in situ and modeled measures of these variables generally had insufficient spatial coverage or were highly collinear (i.e., correlated) with other variables included in the models. In this section, the data sources and methods used to generate the environmental predictor datasets are described. In addition, maps are presented in Appendix B for each of the 27 environmental predictor variables.

It is important to note that the selection of environmental predictor variables reflected that the primary focus of the analysis was on structure-forming DSCs. Ideally, a more ecologically relevant set of environmental predictor variables would have been selected for the models of chemosynthetic communities. The emphasis on DSCs in the selection of environmental predictors limited the performance of the chemosynthetic community models. Key environmental predictor variables needed to inform models of chemosynthetic community occurrence include presence of carbonates, backscatter from seismic and/or multibeam surveys, oil-bearing cores, and surface oil slicks (E. Cordes, email message, August 27, 2020).

2.5.1 Map projection and spatial grid resolution

All environmental predictor datasets were projected onto an Orthographic coordinate system (origin = 28°N 90°W, datum = WGS84). This specific coordinate system was selected to minimize area distortion at the edges of the study area. The spatial resolution of the model grid was 100 x 100 m, chosen to reflect the approximate length of a five minute transect by an ROV traveling at 0.5 knots, a typical sample in the presence-absence database. A 100 m transect with a 1 m field of view sampled 100 m^2 representing 1% of a grid cell. The 100 x 100 m model grid contained 48,713,449 grid cells in the study area.

All source data for the environmental predictors were initially processed in their native coordinate systems and at their native spatial grid resolution prior to projection onto the model grid. Bilinear interpolation was used to resample the predictor values onto the model grid unless otherwise specified.

2.5.2 Depth and seafloor topography

Environmental predictors describing depth and seafloor topography were included to account for variability in the occurrence of DSCs resulting from the direct and indirect effects of the depth, shape, and spatial distribution of features on the seafloor. Seafloor depth can have an indirect effect as a proxy for other measures (e.g., temperature, salinity) that may directly relate to species distributions even if it does not directly influence the distributions of marine species (Wiltshire et al. 2018). In addition, variables depicting the shape and complexity of the seafloor can identify areas of exposed hard substrate, which provides habitat (e.g., available surface for attachment) for many DSCs. To capture hard features on the seafloor at finer scales, it is important to derive depth and seafloor topography variables from high-resolution bathymetry data (e.g., collected using multibeam acoustic sonar) when possible (Winship et al. 2020).

A comprehensive inventory of all available high-resolution bathymetry data for the study area was created (Appendix C). The inventory included a 12.5 x 12.5 m gridded dataset derived by BOEM using data collected from decades of industry-conducted seismic surveys (Kramer and Shedd 2017). This dataset provided depth data encompassing >90,000 square miles within the Northern Gulf. Additional high-resolution bathymetry data collected by multibeam sonar surveys were obtained from the NOAA National Centers for Environmental Information (NCEI 2004) and from the US Geological Survey (USGS) (Gardner et al. 2002a, 2002b, 2002c; Gardner et al. 2003; Cross et al. 2005). These data were evaluated for inconsistencies, artifacts, spatial coverage, and spatial resolution. Some data were excluded from the inventory following this review. For example, efforts were made to omit vessel transits from datasets when broader areas surrounding the transit lines had not been mapped by multibeam sonar. This was done to minimize boundary effects where the contrast in depth values between the multibeam-derived bathymetry and coarser surrounding bathymetry could result in identification of false seafloor features in the seafloor topography variables (e.g., areas incorrectly appearing to have high slope). In total, high-resolution bathymetry data was available for approximately 57% of the study area (Figure 3). Bathymetry data from the General Bathymetric Chart of the Oceans (GEBCO) (Weatherall et al. 2015) were used where no high-resolution bathymetry data existed.

Each bathymetry dataset was projected and resampled onto a 25 x 25 m grid (one that nested within the 100 x 100 m model grid). This spatial resolution represented a typical resolution of the available multibeam bathymetry data. Some datasets (e.g., the BOEM northern Gulf of Mexico deepwater bathymetry grid) had a native spatial resolution finer than 25 x 25 m. Resampling these datasets onto the coarser model grid resulted in the loss of some finer-scale information. In addition, some datasets, particularly from the deeper waters of the study area, had a native spatial resolution coarser than 25 x 25 m. Although these datasets were resampled onto the model grid, they did not include information at the resolution of the model grid. As a result, seafloor topography variables did not capture finer-scale features (e.g., those indicative of exposed hard substrate) in areas represented by these datasets.

The projected and resampled datasets were merged into a single gridded depth dataset (Figure B-1). In areas where datasets overlapped, depth values for the merged dataset were generally selected from the input dataset that had finer native spatial resolution or that was more recently collected. Depth values from the BOEM deepwater bathymetry grid were almost always selected where it overlapped with other bathymetry data.

In the areas where depth values from GEBCO were used in the merged bathymetry dataset, the depth and seafloor topography variables did not capture finer-scale seafloor features that could be associated with DSC habitat or chemosynthetic communities. Additional mapping of the seafloor in these areas would be useful for assessing model predictions and for supporting future research and exploration. GIS data layers depicting the extent of each high-resolution bathymetry dataset included in the bathymetry synthesis are provided as part of the digital data package associated with this study. These data layers can be used to identify targets for future mapping efforts.

Gridded spatial datasets were derived for 11 environmental predictor variables representing seafloor topography from the merged depth dataset. Focal statistics functions, where the value for each grid cell was calculated from the values of the eight surrounding grid cells in a 3 x 3 cell neighborhood, were used to generate each of these datasets with the “raster” package in R (Hijmans 2019). The seafloor slope (Figure B-2) and aspect (i.e., slope direction) were calculated using the ‘terrain’ function in this package. Aspect, a directional variable, was converted to datasets depicting the east-west and north-south gradients of aspect by calculating the sine and cosine, respectively (Figure B-3, Figure B-4). In addition, rugosity (Figure B-5) was derived following the arc-chord ratio method developed by Du Preez (2015). This approach calculates rugosity as the ratio of surface area to the area of a plane of best fit to avoid inflated rugosity values in areas of high slope. Finally, datasets were developed for several measures of seafloor curvature to characterize the shape of the seafloor (e.g., whether it is convex or concave). Slope of slope (Figure B-6) was calculated using the “terrain” function on the slope dataset rather than the merged depth dataset. The remaining measures — general curvature (Figure B-7), total curvature (Figure B-8), plan (i.e., planform) curvature (Figure B-9), cross-sectional curvature (Figure B-10), profile curvature (Figure B-11), and longitudinal curvature (Figure B-12) — were calculated following the descriptions in Jenness (2013). Additional measures of seafloor topography (e.g., bathymetric position index, terrain ruggedness) were considered, but previous experience indicated that these measures were generally highly correlated with other measures of seafloor topography and not as influential in fitting models to predict habitat suitability for DSCs.

2.5.3 Seafloor substrate

Gridded spatial datasets for environmental predictor variables depicting surficial sediment mean grain size (Figure B-13) and surficial sediment composition—percent gravel (Figure B-14), percent sand (Figure B-15), and percent mud (Figure B-16)—were first obtained in 2013 from Dr. Chris Jenkins (University of Colorado Boulder). These datasets were included to account for the effects of substrate characteristics (e.g., hard vs. soft substrate) on variability in the occurrence of DSCs. Jenkins derived these datasets from point data records representing seabed surveys (e.g., grab samples) using a custom interpolation algorithm (Williams et al. 2012; Kinlan et al. 2013). Each of these datasets (originally at approximately 370 x 370 m resolution) was projected and bilinearly resampled onto the model grid.

It is important to note that much of the substrate in the Gulf is unconsolidated sediment, and areas of hard substrate that are important for the attachment of DSCs are often in small patches. The interpolated substrate datasets used in this study may not resolve these small patches, particularly in deeper waters where data from sediment grabs were sparse. Bathymetry (and derived measures of seafloor topography) and backscatter data collected by multibeam sonar may be able to delineate these features; however, as noted in Section 2.5.2, data from multibeam sonar were not available for the entire study area. A dataset depicting seafloor features interpreted from seismic surveys was also considered for use in the models (i.e., the BOEM seismic anomalies dataset; BOEM 2019), but also was not available for the entire study area. The interpolated substrate datasets used in this study represented the best available data that existed for the entire study area.

2.5.4 Oceanography

Several gridded spatial datasets representing aspects of oceanography were derived to account for the direct and indirect effects of ocean productivity, ocean chemistry, and the physical state and dynamics of the ocean on variability in the occurrence of DSCs.

Datasets depicting long-term climatological patterns in sea surface chlorophyll-a concentration and sea surface reflectance (water-leaving radiance at 547 nm) were generated at approximately 4 x 4 km resolution from remotely sensed ocean color data to serve as proxies for measures of ocean productivity. Daily sea surface chlorophyll-a concentration data from multiple satellites were downloaded from the National Aeronautics and Space Administration (NASA) Ocean Biology Processing Group (NASA 2019). This included data from the Visible Infrared Imaging Radiometer Suite (VIIRS) collected from 2012 to 2019, data from the Moderate Resolution Imaging Spectroradiometer (MODIS) instruments collected from 2002 to 2019, and data from the Sea-Viewing Wide Field-of-View Sensor (SeaWiFS) collected from 1997 to 2001. Daily data from VIIRS and MODIS were blended together for best spatial coverage. Data from SeaWiFS were resampled from its native spatial resolution of approximately 9 x 9 km to match the resolution of the VIIRS and MODIS data. A long-term annual mean climatology of sea surface chlorophyll-a concentration (Figure B-17) was calculated from these daily data. Similarly, daily sea surface reflectance data from MODIS (NASA 2019) were downloaded, and a long-term annual mean climatology (Figure B-18) was calculated. The gridded datasets depicting these climatologies were projected and bilinearly resampled onto the model grid.

A gridded dataset depicting annual mean bottom dissolved oxygen was initially created from in situ point records (e.g., from bottom trawls, CTD casts, ocean stations) of dissolved oxygen in 2013 for models of DSC habitat suitability (Kinlan et al. 2013). The point data were filtered to extract only records near the seafloor. Ordinary kriging was used to interpolate the gridded dataset from the extracted records. Kriging is a stochastic interpolation method that assumes that values are more similar for neighboring data than for data farther apart (i.e., that data are spatially autocorrelated) and uses this assumption to fit a statistical model to the data in order to estimate values at locations that do not have data (Tobler 1970; Cressie 1993). The gridded dataset for annual mean bottom dissolved oxygen was initially created at 370 x 370 m resolution. This dataset was projected and bilinearly resampled onto the 100 x 100 m model grid (Figure B-19). In addition to providing a gridded prediction from the point data, kriging also provided a measure of prediction uncertainty (i.e., standard error) at each grid cell that can be used to assess confidence in the predictions. However, these measures of uncertainty were not incorporated directly into the models of DSC and chemosynthetic community occurrence as this would require different models than were used in this study. Nonetheless, they can be used to evaluate the quality of the bottom dissolved oxygen dataset and to identify areas where this environmental predictor dataset could be improved through additional collection of water samples.

Data describing long-term trends in the physical properties of ocean bottom water were obtained from a data assimilating ocean circulation model, HYbrid Coordinate Ocean Model (HYCOM) (HYCOM Consortium 2019). Daily data at 0.04° grid resolution (approximately 4 x 4 km) spanning 25 years (1993–2019) were downloaded from the regional Gulf HYCOM. Annual mean climatologies were calculated from the daily data for bottom temperature (Figure B-20), bottom salinity (Figure B-21), bottom current speed (i.e., the magnitude of bottom current velocity; Figure B-22), bottom current east-west velocity (Figure B-23), bottom current north-south velocity (Figure B-24), and mixed layer depth (Figure B-25). These climatologies were projected and resampled onto the model grid.

2.5.5 Geography

To account for variation in the distribution of DSCs and chemosynthetic communities arising from spatial location, gridded spatial datasets depicting the longitude (Figure B-26) and latitude (Figure B-27) were generated on the model grid. These were included because some DSC taxa were known to be restricted to portions of the study area.

2.6 Environmental predictor variable selection

The initial set of 27 environmental predictor variables was reduced to avoid the inclusion of highly correlated predictors, to avoid extreme model extrapolations, and to ensure numerical convergence for successful model fitting.

First, pairs of environmental predictor variables that were highly collinear (i.e., correlated) were identified by calculating the variance inflation factor (VIF) (Zuur et al. 2010) for all 27 predictors using the subset of grid cells sampled (surveyed) within the study area. Starting with the most highly collinear predictors (i.e., highest VIFs), one of each pair of collinear predictors was removed to reduce the remaining VIFs to values <3 (i.e., roughly equivalent to eliminating collinearity with correlation coefficients >0.6). Thus, the information content in the removed predictors was largely captured in the remaining predictors. The subset of 12 predictors that remained following this step of the variable reduction process was depth, slope, east-west aspect, north-south aspect, general curvature, surficial sediment mean grain size, surficial sediment percent sand, annual mean bottom dissolved oxygen, annual mean east-west bottom current velocity, annual mean north-south bottom current velocity, annual mean surface chlorophyll-a concentration, and longitude.

Next, on the basis of preliminary model tests, the predictor subset was further revised to avoid extreme model extrapolations (Conn et al. 2015). Some predictors exhibited extreme values in unsampled areas that did not occur in sampled areas. Thus, predictions from models fit only to the sample data were extreme extrapolations in unsampled areas. In very deep waters there were extreme values for east-west and north-south bottom current velocity as well as for mixed layer depth. Therefore, the directional bottom current velocity predictors were replaced with annual mean bottom current speed, which did not exhibit such extremes. Annual mean surface chlorophyll concentration was extremely high in nearshore waters close to Louisiana, so alternatives were tested including log-transformed chlorophyll and latitude (which was highly correlated with annual mean surface chlorophyll concentration). However, both of these tests resulted in poorer model convergence. Therefore, annual mean surface chlorophyll concentration was retained in the subset of environmental predictors. The preliminary model tests also identified environmental predictor variables that resulted in poorer model convergence, and this information was used to further revise the predictor subset. In particular, surficial sediment mean grain size was removed, which improved convergence.

The final predictor set consisted of 10 predictors: depth, slope, east-west aspect, north-south aspect, general curvature, surficial sediment percent sand, annual mean bottom dissolved oxygen, annual mean bottom current speed, annual mean surface chlorophyll-a concentration, and longitude (Table 3). The selected predictor set consisted of 10 predictor variables represented by 20 predictor terms including both linear and quadratic (i.e., squared) terms to accommodate nonlinearity.

Models for all taxa incorporated all 10 environmental predictor variables. However, the magnitude of the effect of each predictor on the probability of occurrence was allowed to vary between taxa. Predictors with negligible estimated effects for a given taxon would be inferred to be minimally influential on the probability of occurrence of that taxon.

2.7 Model framework

2.7.1 Occupancy analysis

An occupancy approach for species distribution modeling was used in this study (MacKenzie et al. 2002; Kéry and Royle 2016). Models were fit to the occurrence data compiled in the presence-absence database and the selected environmental predictors. The estimated relationships between occurrence and the predictors from the fitted models were then used to predict the probability of occurrence at each grid cell across the entire study area, including unsampled areas. The occupancy framework separates the probability of occurrence at a site (occupancy probability) from the probability of detecting an organism present at a site and provides estimates of both quantities. The ability to distinguish occupancy probability from detection probability relies on replicate samples within sites. By accounting for detection probability, the occupancy framework provides an estimate of the absolute probability of occurrence at a given site, in contrast to some presence-only methods (e.g., MaxEnt) that only provide an estimate of the relative suitability of a given site. Estimates of absolute probabilities of occurrence are directly comparable across models and taxa, which allowed the implementation of a hierarchical multi-taxon approach. Furthermore, estimates of absolute probabilities of occurrence are more interpretable than relative habitat suitability and can be more useful for management (Winship et al. 2020).

The model grid cell (100 x 100 m) was selected as the smallest unit of interest since the environmental predictor datasets did not vary at finer resolutions. Therefore, each grid cell was treated as a site. This offered the opportunity to treat the samples at each site as spatial replicates (Figure 4). DSCs are particularly well suited to this assumption because they are very long-lived. The survey data compiled in the presence-absence database spanned 31 years, which was a short time frame relative to the life span of these organisms. Therefore, local colonization or extinction was unlikely to occur across spatial replicates at any given site, enabling the implementation of static models, as opposed to dynamic models (see Section 2.7.3).

2.7.2 Space-for-time substitution

In an occupancy framework, temporal replicates are most commonly used to procure repeated samples, where the same site is visited multiple times. However, the nature of the data compiled for this study served as a candidate for the analogous ‘space-for-time substitution’ (Kéry and Royle 2016). Within-site variation was used advantageously—spatially replicated samples allowed the estimation of detection probability (Kéry and Royle 2016). Space-for-time substitutions have been used in occupancy modeling with other taxa, including birds (Sadoti et al. 2013; Jiménez-Franco et al. 2019) and mammals (Charbonnel et al. 2014; Srivathsa et al. 2018; Petracca et al. 2020). They have also been used to approximate historical baselines of exploited marine fauna (Lotze and Worm 2009).

By using the space-for-time substitution, estimates of ‘detection’ probability are a combination of true detection probability and availability probability. Both of these probabilities account for the fact that, although an organism might have occupied a site, it could have been undetected by the observer for a couple of reasons. For example, consider a hypothetical situation where two grid cells are both occupied by corals (Figure 5). The true occupancy state of these grid cells $(z) = 1$. Samples are collected during a dive by taking images along a submersible’s path that covers only part of the grid cell. In the first grid cell, the coral is undetected because it is obscured by a rock in the image. In the second grid cell, the coral is undetected because the submersible did not visit the part of the site where the coral was present. These two cases represent separate detection and availability processes, respectively. However, in both cases observed occurrence $(y) = 0$ because no corals were detected. The analysis conducted for this study could not distinguish these different types of recorded absences, thus the estimated detection probability represented a combination of the detection and availability processes, even though these processes are technically different.

The issue of availability arises when using spatial replicates instead of temporal replicates in an occupancy framework (Guillera-Arroita 2011). Traditionally, with temporal replicates, one would observe the entire site, or grid cell, on each visit. In this study, each spatial replicate was a subunit of the site (e.g., Figure 5). Therefore, three processes occur: detection, availability, and occupancy. These correspond to three levels of analysis: small- mid-, and large-scale, respectively (Kéry and Royle 2016). Conventionally, in a space-for-time substitution, availability is treated as part of either the observation-level (detection) or site-level (occupancy) process. Therefore, by combining availability with detection probability, the three levels can be collapsed to two: occupancy and detection. Kéry and Royle (2016) tested this approach through simulation and found that a two-level model performed equivalently to a three-level model in a space-for-time substitution framework, supporting the treatment of availability and detection probability as a single process. However, they did suggest the need for more investigation of this topic, and several subsequent studies have provided additional support for space-for-time substitutions (Srivathsa et al. 2018; Jiménez-Franco et al. 2019; Petracca et al. 2020). Hereafter, any mention of detection probability implies availability as well.

2.7.3 Model assumptions

By distinguishing probabilities of detection and occurrence, occupancy models offer appropriate interpretation of sampled absences by distinguishing true absences (“true negatives”) from false absences (“false negatives”). One does not have to assume that every sampled absence is a true absence. However, the occupancy framework has several important assumptions (MacKenzie et al. 2002; Kéry and Royle 2016) that were made here:

1. Imperfect detection: sampled absences are not treated as true absences. False negatives are explicitly accounted for through the estimation of detection probability.

2. No false positives: no corals are misidentified. This assumption was addressed by identifying taxa only to the finest taxonomic level for which the organism could be identified with confidence (usually genus).

3. Closure: the sampling time window is short relative to the system dynamics. DSCs are sessile and long-lived and thus make exemplary study organisms under the assumption that their distributions remain static over the course of the study period. Therefore, static occupancy models were implemented, in contrast to dynamic occupancy models, which relax this assumption and explicitly estimate colonization and extinction.

4. Independence of occurrence and detection probabilities. Because corals are sessile, they should show no behavioral response to the observer that could influence detection probability between visits.

5. Homogeneity of detection probability: detectability is consistent throughout the study area. This assumption was unlikely to be met in this study given the numerous surveys in the presence-absence database. To account for heterogeneity in detection probability, the area sampled per occasion was included as an effort offset. Taxon- and site-level effects on detection probability were also included (see Section 2.8.4 for more details).

A further consideration in species distribution modeling is sampling design. Unbalanced and non-random spatial sampling designs can bias estimates of occurrence and density, even with model-based inference (Kéry and Royle 2016; Conn et al. 2017). The combination of multiple surveys in the presence-absence database resulted in a non-random sampling design. Preferential sampling at sites with higher densities typically results in overestimates of the probability of occurrence; however, an occupancy modeling framework applied to such samples may result in overestimates of the probability of detection and underestimates of the probability of occupancy (Kéry and Royle 2016). Thus, in the presence of positive sampling bias, occupancy analysis is a conservative approach in terms of estimated probabilities of occurrence.

2.7.4 Multi-taxon occupancy analysis

Occupancy analysis provides estimates of absolute probabilities of occurrence that are directly comparable across models and taxa. For example, if the estimated probability of occupancy is 0.2 for one taxon, and 0.4 for another, one can reasonably estimate that the second occurs twice as often. These estimates are an improvement over presence-only models, which predict relative occurrence (Kéry and Royle 2016). An occupancy modeling approach inherently provides the opportunity to model multiple taxa jointly in a hierarchical modeling framework, and to estimate multi-taxon richness (i.e., combine the predicted distributions for multiple species, genera, or families into a single map). Multi-taxon occupancy models have become increasingly popular for describing the distributions of several taxa, including birds (Zipkin et al. 2009; Kéry and Royle 2008; Flanders et al. 2015; Jiménez-Franco et al. 2019) and mammals (Zipkin et al. 2010; Petracca et al. 2020). In this study, multi-taxon occupancy models were developed based on the approach of Dorazio and Royle (2005), limiting inference only to those taxa observed during surveys (Kéry and Royle 2016).

2.8 Model structure

2.8.1 Taxonomic composition of model runs

As previously stated, the modeling presented in this report focused on structure-forming DSCs. Models included a combination of single-taxon and multi-taxon occupancy models (Table 4). Multi-taxon models were hierarchical, facilitating the modeling of less common taxa by drawing information from data on more common taxa. The member taxa in a given multi-taxon model all had the same taxonomic rank and were members of the same next higher-ranked taxon; e.g., all genera in the same family. However, member taxa in a multi-taxon model did not necessarily have the same spatial distributions or co-occur. The multi-taxon models allowed for different environmental relationships and spatial distributions among member taxa. Groups of taxa were modeled together for the statistical advantage of improved estimation for less common taxa, not because they were ecologically similar or part of the same ecological community.

A multi-genus model was run for branching stony corals in order Scleractinia because *Lophelia pertusa* was the only Scleractinian identified to species level (Table 4). Hereafter, any reference to genus *Lophelia* refers to observations of *Lophelia pertusa*. In addition, a single-family model was run for family Oculinidae since these records were not identified to genus level (Table 4). However, records identified as *Madrepora* were not included in the Oculinidae model. The assumption was that the model for Oculinidae would essentially represent genus *Oculina*; however, because it was not certain that this subset of records consisted exclusively of records of the genus *Oculina*, these records and the genus *Oculina* were not included in the multi-genus model of branching stony corals.

Because most records within order Alcyonacea were identified only to family level, a multi-family model was run that included all the families of gorgonian corals represented in the presence-absence database (Table 4). For family Plexauridae, records identified to the genus level were included in a multi-genus model (Table 4). Similarly, records identified to the genus level within family Isididae were also included in a multi-genus model (Table 4). Additionally, single-taxon models were run for three genera and three species of gorgonian corals in order Alcyonacea (Table 4). All records within families Plexauridae and

Isididae identified to genus or species level were also included in the multi-family model, while only those identified to genus level were included in the respective multi-genus models.

A multi-genus model was run for black corals in order Antipatharia (Table 4). A single-taxon model for family Aphanipathidae was also run (Table 4). The records included in this model were only identified to family level and were not included in the multi-genus model for order Antipatharia. Two single-taxon models were also run for the black corals *Antipathes atlantica* and *Antipathes furcata* (Table 4). Records identified to the species level within genus *Antipathes* were also included in the multi-genus model.

Finally, single-taxon models were run for each category of chemosynthetic communities (Table 4).

2.8.2 Overall structure

Occupancy models were fit in a Bayesian statistical framework. The models had two main components: a state process (occupancy) and an observation process (detection). The response data (i.e., dependent variable) were binary, observed presence-absence data y_{ijk} (= 0 or 1), where i = site (grid cell), j = occasion (spatial replicate), and k = taxon. The expected probability of a presence at a given site on a given occasion was the product of detection and occupancy. As such, the presence-absence data were assumed to be Bernoulli distributed with probability equal to the product of the estimated occupancy state and the probability of detection:

$$y_{ijk} \sim Bernoulli\left(z_{ik}p_{ijk}\right)$$

where z_{ik} (= 0 or 1) is the true but unobserved state of occupancy at each sampled site and p_{ijk} is the probability of detection.

2.8.3 State process (occupancy)

In the state process, the estimated occupancy state, z_{ik}, for site *i* and taxon *k* was assumed to be a Bernoulli distributed variable with estimated occupancy probability, Ψ_{ik}, which was a function of the site-level environmental predictors:

$$z_{ik} \sim Bernoulli\ (\Psi_{ik})$$
$$cloglog(\Psi_{ik}) = \beta_{0k} + \beta_{vk} \times predictor_{vi}$$

where β_{0k} is the occupancy intercept for taxon *k*, β_{vk} is the coefficient for the effect of predictor *v* on occupancy for taxon *k*, and $predictor_{vi}$ is the value of predictor *v* (or its square) for site *i*. Effects of predictor terms were assumed to be linear on the complementary log-log scale, but the inclusion of quadratic terms for each predictor allowed for nonlinear responses in the probability of occupancy. The global model for all taxa included the aforementioned set of 10 environmental predictors (Table 3) and their 10 quadratic terms. Orthogonal transformations were applied to center and scale each predictor term prior to modeling to remove collinearity between polynomial terms.

The taxon- and predictor-specific occupancy intercepts (β_{0k}) and effects (β_{vk}) were assumed to come from common normal distributions with associated mean (μ) and precision (τ) hyper-parameters:

$$\beta_{0k} \sim Normal\left(u_{\beta 0}, \tau_{\beta 0}\right)$$
$$\beta_{vk} \sim Normal(u_{\beta}, \tau_{\beta})$$

Vague normal prior probability distributions (mean = 0, precision = 1 x 10^{-6}) were assumed for mean hyper-parameters, and vague gamma prior probability distributions (shape = 0.001, rate = 0.001) were assumed for precision hyper-parameters.

Multi-taxon models were structured hierarchically whereby effects across taxa were assumed to come from the same common distributions described above with their estimated hyper-parameters (i.e., a random effect; Zipkin et al. 2009). Though taxa within a given multi-taxon model were not constrained to have the same responses to environmental predictors, the hierarchical structure still allowed for the sharing of information among taxa within the model, which enabled the inclusion of rare taxa that would otherwise be difficult to model due to small numbers of observed presences (Zipkin et al. 2009).

Multiple alternative hierarchical model structures were tested. For example, hyper-parameters were specified that varied by either predictor (Kéry and Royle 2016) or depth (observed at either <1,000 m or ≥1,000 m). However, the selected configuration (common intercept and effect distributions across all taxa and predictors) resulted in the best performance with respect to model convergence.

2.8.4 Observation process (detection)

The probability of detection, p_{ijk}, was assumed to be a function of sampling effort, as well as site- and taxon-specific effects:

$$cloglog(p_{ijk}) = \alpha_0 + \alpha_{1,i} + \alpha_{2,k} + \log(effort_{ij})$$

where α_0 is the intercept for detection, $\alpha_{1,i}$ is the effect of site i on detection, $\alpha_{2,k}$ is the effect of taxon k on detection, and $effort_{ij}$ is the sampling effort associated with sample j from site i. Sampling effort was estimated as the area viewed for each sample (m^2), and the log of sampling effort was treated as an effort offset. Sampling effort was divided by 100 m^2 prior to the log transformation, so the presented estimates of detection probability correspond to a sample of 100 m^2. Additive site- and taxon-specific effects on the complementary log-log scale were assumed to follow normal distributions across sites and taxa, respectively (random effects):

$$\alpha_{1,i} \sim Normal(0, \tau_{clp1})$$
$$\alpha_{2,k} \sim Normal(0, \tau_{clp2})$$

with means equal to 0 and estimated precision hyper-parameters, τ_{clp1} and τ_{clp2} (Pinheiro and Bates 2004). A vague normal prior probability distribution (mean = 0, precision = 1×10^{-6}) was assumed for the detection intercept, α_0, and vague gamma prior probability distributions (shape = 0.001, rate = 0.001) were assumed for the precision hyper-parameters, τ_{clp1} and τ_{clp2}.

Many factors could have influenced the probability of detection. It is likely that different taxa have different probabilities of detection, so it seemed reasonable to include an explicit effect of taxon. Other factors are more difficult to quantify from the data (e.g., survey technology, observer expertise, visual background), and those factors likely varied across survey datasets and sites. The site effect was included to capture additional variation in detection probability arising from these various factors. Essentially, it was expected that these factors would result in overdispersion of the presence-absence data relative to a simpler model, and thus a site effect was included in an attempt to reduce that overdispersion and to adjust statistical inferences about other parameters accordingly.

An interaction between the effects of site and taxon, where the detection effect varied by combination of site and taxon, was also tested. However, this structure resulted in most of the variation being attributed to site such that mean detection probabilities were estimated to vary little between taxa. Thus, independent, additive effects of site and taxon were retained because that structure aligned more closely with a priori ecological expectations that detection probability should vary by taxa.

A survey effect on detection was considered as an alternative to the site effect, but models with a site effect were similar to or slightly better than models with a survey effect in terms of convergence and fit. It is acknowledged that other factors, aside from survey and site, may have affected detectability (e.g., such as observer), but those conditions were not modeled explicitly, and it was assumed that their influence was captured in the additive random effects of site and taxon on detection.

2.9 Model fitting and assessment

All models were implemented using JAGS (v4.3.0), via package "rjags" (Plummer 2018) in R (R Core Team 2018), which implements Markov chain Monte Carlo (MCMC) sampling. Model runs included 100,000 iterations of five independent chains, following a burn-in of 100,000 updates after an adaptation phase of 100,000 iterations. Thinning by 100 resulted in 5,000 samples from the joint posterior. Convergence was evaluated by visually inspecting MCMC trace plots and scatterplots of posterior samples for pairs of parameters and by calculating $\hat{R}$, a measure of between- and within-chain variation (Gelman and Rubin 1992). Satisfactory model convergence was assumed when $\hat{R}$ <1.1.

Three different fit statistics (chi-squared, Pearson's and Freeman-Tukey) were calculated on two different levels of the data (site and taxon). For example, the site-level fit statistics were calculated using the raw residuals aggregated by site; i.e., where the observed (y_{ijk}) and expected detections ($z_{ik}p_{ijk}$) were summed across occasion and taxon. The raw residuals were calculated as the difference between the observed and expected values. Additionally, a spatial correlogram was generated of the raw site-level residuals to assess spatial autocorrelation.

From the fit statistics, the Bayesian p-values (Conn et al. 2018) were computed. These calculate the proportion of times (out of the total number of model iterations) that the fit statistics computed using observed data (y_{ijk}), were greater than those from simulated data ($ysim_{ijk} \sim Bernoulli\left(z_{ik}p_{ijk}\right)$). Thus, a Bayesian p-value of 0.5 is good, but if closer to 0 or 1, it is poor.

As additional assessments of model fit, the point-biserial correlation coefficient and the area under the receiver operating characteristic curve (AUC) were calculated for the observed presence-absence data and the corresponding predicted probabilities ($z_{ik}p_{ijk}$). However, predicted values that are calculated from the estimated occupancy states (z_{ik}) and estimated detection probabilities (p_{ijk}) that incorporate estimated site effects ($\alpha_{1,i}$) do not reflect the expected performance of the model at new sites where the occupancy states and site effects on detection are unknown. To better characterize fit in terms of new sites, these performance metrics were also calculated substituting the probability of occupancy (Ψ_{ik}) for z_{ik} in the calculation of predicted values ($\Psi_{ik}p_{ijk}$), and setting the site-level effect on detection ($\alpha_{1,i}$) to zero. This alternative way of calculating performance metrics corresponds better to the maps of predicted occupancy probabilities (Section 2.11) and is more comparable to the assessment of model predictive performance (see Section 2.10). A model that fits well to the data yields a higher point-biserial correlation between the observed data and the expected occupancy probabilities. AUC compares an observed binary outcome (e.g., observed presence-absence) to a continuous predicted value (e.g., expected probability of occurrence) and measures the ratio of true positives to the inverse of false positives across a range of thresholds for the predicted value (estimated presences at observed absences; Zipkin et al. 2012). AUC ≤0.5 is no better than random, while AUC closer to 1 is desirable, being indicative of few false positives relative to true positives.

2.10 Model predictive performance

To assess the ability of the models to predict occurrence in novel areas, the data were divided into training and test subsets representing different geographic areas within the study area. Models were fit to the training data, and performance of model predictions was assessed with respect to the test data. The R package "blockCV" (version 1.0) was used to divide the data into the training (~70%) and test (~30%) subsets (Valavi et al. 2019). First the study area was divided into spatial blocks, the size of which (117,616 m x 117,616 m) was determined from the spatial autocorrelation in the 10 predictors (Figure 6). The data were then divided into 10 different subsets or "folds" each assigned to unique sets of spatial blocks while attempting to achieve a relatively even number of presences and absences in each fold. Seven of the folds were then randomly chosen as the training subset with the remaining three folds making up the test subset. For models with multiple taxa it was not possible to achieve a 70/30 split for presences and absences across all taxa given the same set of folds and spatial blocks. In those cases, 7 and 3 folds were manually assigned to the training and test subsets, respectively, to achieve as close to a 70/30 split for presence and absence data for as many taxa as possible while maintaining a substantial number of presences in both the training and test subsets for all taxa. Model performance was compared with respect to the training and test data subsets using the point bi-serial correlation coefficient and AUC. Because predicted values for the test data corresponded to new sites, there were no corresponding estimated occupancy states (z_{ik}) or site effects on detection ($\alpha_{1,i}$), thus predicted values were calculated with the posterior predicted occupancy probabilities (Ψ_{ik}) and with the site effect on detection ($\alpha_{1,i}$) set to zero. It is important to note that this assessment of predictive performance did not strictly apply to the final global models since those models were fit to all of the data, but it does give some indication of how well those models may predict occurrence in novel areas.

2.11 Maps of observed and predicted spatial distributions

The Bayesian framework used in this study generated posterior probability distributions for estimated model parameters and quantities, from which the predicted posterior mean occupancy probability (Ψ_{ik}) was calculated for each grid cell in the study area along with the posterior coefficient of variation (CV) as a measure of prediction variability, or uncertainty, at each grid cell. The CV was calculated as the posterior standard deviation divided by the mean, such that a higher value indicates a less precise estimate (more uncertainty), while a lower value indicates a more precise estimate (less uncertainty). A set of maps was created for each DSC taxon and chemosynthetic community to depict its observed distribution from the presence-absence database compiled for this study and its predicted spatial distribution using the posterior mean occupancy probability and posterior coefficient of variation of the occupancy probability. Note that fine-scale features may be difficult to discern in the map pages given the resolution of the model predictions and the extent of the map display. However, these features can be examined using the GIS data products associated with the report.

The first map displays the locations of presences and absences from the presence-absence database. For each DSC taxon, it also includes the presence records in the NOAA National Database for the taxon. These additional records are not visible in the maps when they coincide with records also included in the presence-absence database, but in some cases the additional records identify areas where the taxon had been observed outside the spatial extent of the survey datasets included in the presence-absence database. The records from the NOAA National Database were not used in the models, however, because they included only information on the locations of DSC presence and could not be used to infer absence or quantify sampling effort.

The second map depicts the predicted mean probability of occurrence (i.e., the predicted posterior mean occupancy probability) for the taxon from the occupancy models. These maps indicate the expected occupancy probability based on the environmental predictor values at each grid cell, not the actual occupancy states (z). For example, if a taxon was observed in a grid cell, then the actual occupancy state would be 1. Because estimates of occurrence probabilities were standardized across taxa (i.e., by accounting for absences), they are directly comparable among taxa and are estimates of absolute probability of occurrence, not relative. In addition to examining spatial patterns in the areas where DSCs or chemosynthetic communities are predicted to occur, these maps can be used to identify potential targets for future exploration (e.g., an area predicted to have high probability of occurrence that has not been previously surveyed).

The third map depicts the predicted CV of the probability of occurrence (i.e., the predicted posterior CV of the occupancy probability). Maps of the CV can be used to identify areas with greater variability or uncertainty (i.e., less precision) in the model predictions. It is important to note that in addition to areas of greater variability, higher values of the CV can also result from extremely low values of the predicted mean probability of occurrence. Therefore, maps of the CV should be interpreted in conjunction with the maps of the presence-absence records and the mean probability of occurrence to distinguish areas where variability was high and the taxon was predicted to occur from areas where the CV was high because the mean was extremely low.

In addition to the maps depicting the observed and predicted spatial distributions for each individual DSC taxon and chemosynthetic community, for each multi-taxon model there are maps depicting the predicted taxon richness (i.e., the number of taxa expected at each grid cell) and corresponding maps of the variability in predicted taxon richness. Taxon richness was calculated as the sum of the predicted posterior mean occupancy probabilities for each taxon. Conceptually, this procedure stacked the maps of the predicted occurrence of each taxon within a multi-taxon model to produce a single map of taxon richness (Calabrese et al. 2014).

Although the occupancy models generated predictions of the probability of occurrence for each grid cell in the study area, predictions at unsampled grid cells where the environmental predictor values were outside the range of predictor values found at the sample locations should be interpreted with caution. Conn et al. (2015) demonstrated that extrapolation of statistical relationships from fitted models outside the range of observed data may result in biased predictions. In this study, some unsampled parts of the study area had unexpectedly high values for the predicted probability of occurrence. An environmental predictor mask comprised of grid cells where one or more environmental predictors had values outside the range of values at sample locations was created for this study to identify areas that may be affected by extrapolation. This mask was overlaid on the maps depicting predicted spatial distributions to obscure these areas.

2.12 Analysis of predicted genus richness by depth zone

For the 28 genera of structure-forming DSCs modeled in this study, the genus richness was derived across each planning area (Western, Central, and Eastern) and depth zone (mesophotic, upper bathyal, and lower bathyal) within the Gulf OCS region. The 28 genera were modeled in either the single- or multi-genus occupancy models of orders Scleractinia, Alcyonacea, and Antipatharia (Table 4). The posterior mean genus occupancy was extracted from each of the nine regional depth zones. The genus richness was calculated as the sum of the estimated posterior mean genus occupancies from the multi-taxon models, and the estimated posterior mean occupancy from the single-taxon models. The mean occupancy and richness were then calculated across each of the nine regional depth zones, excluding sites covered by the environmental predictor mask. This effectively standardized occupancy and richness by the number of sites in each zone, to allow for direct comparisons between zones. Taxon richness provides some indication of taxon diversity, and the results of these analyses can be used to determine where more or fewer taxa would be expected to occur. Note that many factors influence patterns of taxon richness across planning areas and depth zones, for example the amount of suitable hard substrate for DSCs.

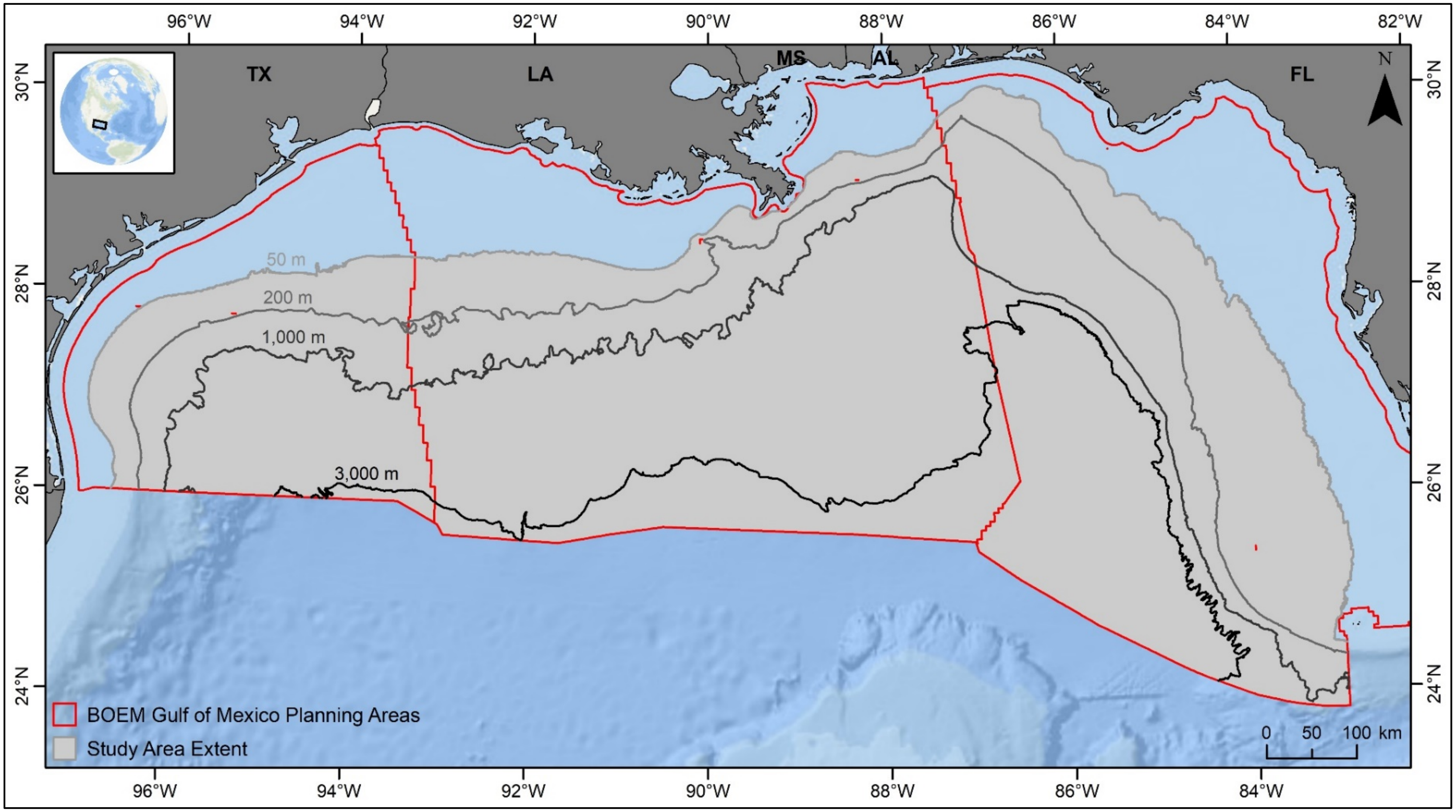

Figure 1. Study area.

The study area covers federal waters >50 m deep to the boundary of the BOEM Gulf of Mexico OCS region. Depth contours define the three zones within which DSCs exist in the Gulf: mesophotic (50–200 m), upper bathyal (200–1,000 m), and lower bathyal (1,000–3,000 m).

Table 1. Survey datasets included in the synthesis of DSC and chemosynthetic community observations

Survey Dataset	Principal Investigators	Years	Number of Dives	Sites	Samples	Total Area (m^2)
Carney & Roberts Benthic Seeps 1988	R. Carney, H. Roberts	1988	10	8	74	1,249
Carney & Roberts Benthic Seeps 1989–1997	R. Carney, H. Roberts	1989–1997	121	80	1,502	39,237
Carney & Roberts Benthic Seeps 1990	R. Carney, H. Roberts	1990	10	10	299	9,860
MS-AL Pinnacle Trend Ecosystem Monitoring	I. MacDonald, M. Silva	1997–1999	15	34	1,176	353
Deep Slope Chemosynthetic	C. Fisher	2007	16	423	7,821	58,658
Lophelia II 2008	E. Cordes, R. Church	2008	7	47	74	4,927
Lophelia II 2009	E. Cordes, C. Fisher	2009	14	69	161	1,569
Lophelia II 2010	E. Cordes, C. Fisher	2010	15	78	128	2,131
Florida Shelf Edge Expedition	J. Reed	2010	13	10	15	77
Deepwater Horizon Soft Sediment Megafauna	M. Benfield	2011–2012	6	52	128	54,630
Potentially Sensitive Benthic Features	M. Nuttall, E. Hickerson, G. Schmahl	2011–2013	132	682	6,026	5,572
Ecosystem Impacts of Oil and Gas Inputs	C. Fisher, E. Cordes	2011–2017	35	69	135	14,407
Okeanos Explorer 2012	E. Lobecker	2012	15	122	2,126	5,614
Deep Sea Coral Shakedown Cruises	P. Etnoyer, E. Cordes	2012	7	41	155	10,595
Mapping South Texas Banks	T. Shirley, D. Hicks	2012	8	33	445	4,434
AT-26	P. Girguis, E. Cordes, S. Joye, C. Van Dover	2014	58	154	201	17,392
Mesophotic Pinnacles	P. Etnoyer	2014	10	24	30	9,767
Okeanos Explorer 2014	E. Lobecker	2014	14	169	2,239	6,619
Deep Fish Habitat 28	E. Hickerson	2015	24	67	137	6,194
Okeanos Explorer 2017	D. Amon, C. Messing	2017	17	171	659	48,862
SEDCI NF1708	P. Etnoyer	2017	13	95	111	43,792
Okeanos Explorer 2018	D. Wagner, A. Skarke	2018	13	75	77	11,453

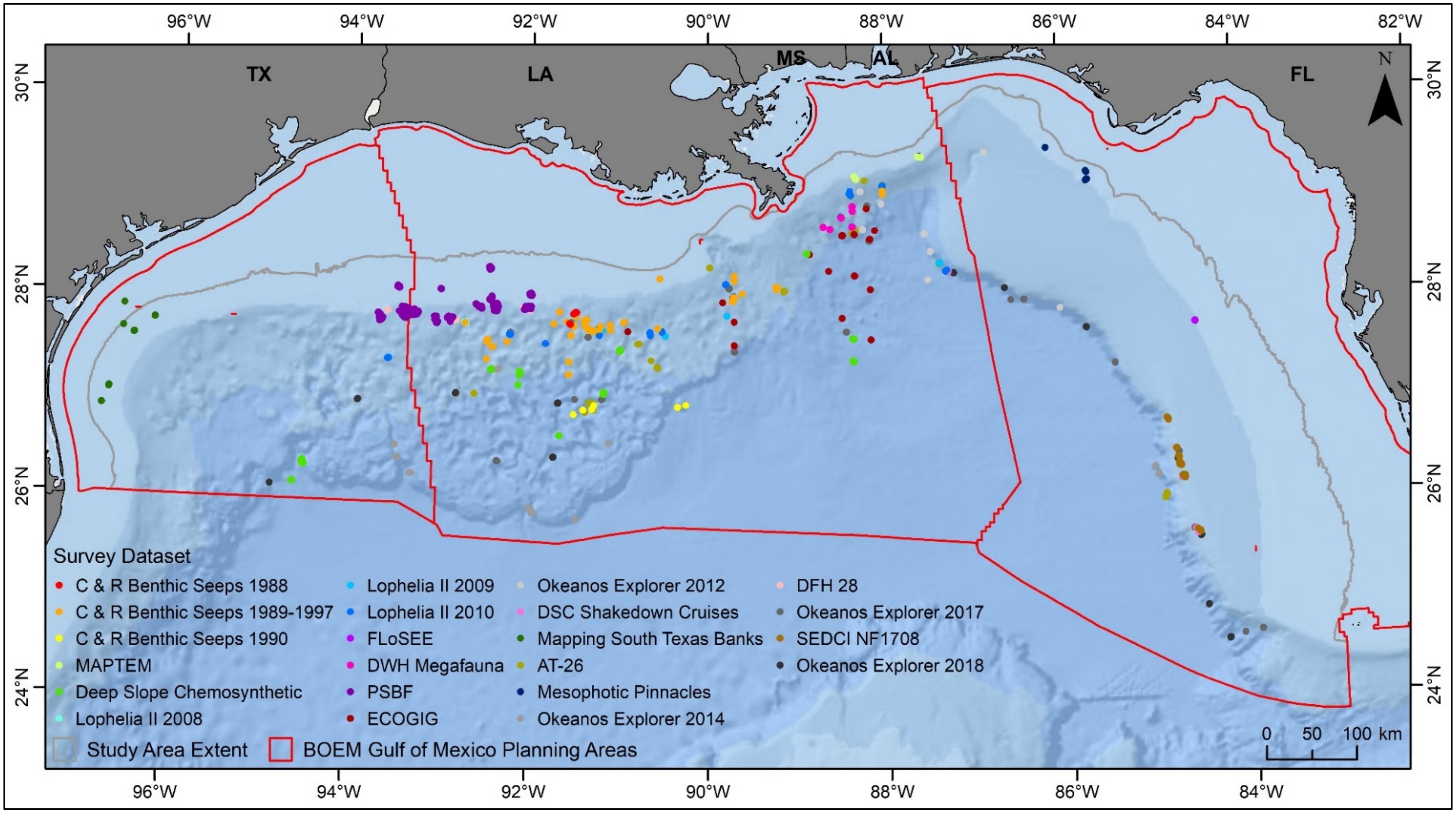

Figure 2. Survey dataset locations.

This map depicts the locations of surveys (e.g., dives) from the 22 datasets used to create the presence-absence database of DSCs and chemosynthetic communities. C & R = Carney & Roberts, MAPTEM = MS-AL Pinnacle Trend Ecosystem Monitoring, FLoSEE = Florida Shelf Edge Expedition, DWH = Deepwater Horizon, PSBF = Potentially Sensitive Benthic Features, ECOGIG = Ecosystem Impacts of Oil and Gas Inputs, DFH = Deep Fish Habitat. For additional details about each dataset, see Table 1 and Appendix A.

Table 2. DSC taxa and chemosynthetic communities selected for modeling

Taxon	Order	Family	Depth Zones	Expected Depth Range (m)	Datasets	Sites	Samples
Madracis	Scleractinia	Pocilloporidae	M	20–200	3	189	426
Lophelia pertusa	Scleractinia	Caryophylliidae	UB	300–900	12	153	327
Madrepora	Scleractinia	Oculinidae	M, UB, LB	50–1,500	11	45	97
Solenosmilia	Scleractinia	Caryophylliidae	UB, LB	300–2,000	5	14	26
Enallopsammia	Scleractinia	Dendrophylliidae	UB, LB	300–1,800	5	14	18
Oculinidae	Scleractinia	Oculinidae	M	20–200	4	241	722
Plexauridae	Alcyonacea	Plexauridae	M, UB, LB	50–2,500	21	894	4,473
Bebryce	Alcyonacea	Plexauridae	M, UB	50–300	5	213	1,051
Swiftia	Alcyonacea	Plexauridae	M, UB, LB	20–1,500	10	91	613
Paramuricea	Alcyonacea	Plexauridae	M, UB, LB	50–2,500	15	210	569
Caliacis	Alcyonacea	Plexauridae	M	30–150	2	188	478
Muricea (*Hypnogorgia*)	Alcyonacea	Plexauridae	M	20–125	5	147	436
Scleracis	Alcyonacea	Plexauridae	M	50–200	2	146	368
Thesea	Alcyonacea	Plexauridae	M	50–300	4	113	224
Placogorgia	Alcyonacea	Plexauridae	M	50–200	5	50	199
Villogorgia	Alcyonacea	Plexauridae	M	50–200	1	19	22
Swiftia exserta	Alcyonacea	Plexauridae	M	20–200	4	74	587
Muricea pendula	Alcyonacea	Plexauridae	M	20–125	5	147	436
Paramuricea biscaya	Alcyonacea	Plexauridae	UB, LB	800–2,500	13	109	347
Ellisellidae	Alcyonacea	Ellisellidae	M, UB	20–300	8	531	3,243
Nicella	Alcyonacea	Ellisellidae	M, UB	40–300	4	453	2,621
Primnoidae	Alcyonacea	Primnoidae	M, UB, LB	100–1,500	17	315	831
Callogorgia	Alcyonacea	Primnoidae	M, UB	30–1,000	13	292	793
Plumarella	Alcyonacea	Primnoidae	M, UB, LB	150–1,200	6	47	73
Isididae	Alcyonacea	Isididae	UB, LB	300–3,000	13	210	565

Taxon	Order	Family	Depth Zones	Expected Depth Range (m)	Datasets	Sites	Samples
Lepidisis	Alcyonacea	Isididae	UB, LB	300–3,000	6	31	35
Keratoisis	Alcyonacea	Isididae	UB, LB	300–2,500	6	20	26
Chelidonisis	Alcyonacea	Isididae	UB	300–800	5	8	9
Acanella	Alcyonacea	Isididae	UB, LB	300–3,000	2	6	8
Chrysogorgiidae	Alcyonacea	Chrysogorgiidae	UB, LB	200–2,500	10	88	185
Acanthogorgiidae	Alcyonacea	Acanthogorgiidae	UB, LB	200–1,200	11	59	129
Paragorgiidae	Alcyonacea	Paragorgiidae	UB, LB	400–2,500	12	36	65
Gorgoniidae	Alcyonacea	Gorgoniidae	M	20–200	3	35	48
Keroeididae	Alcyonacea	Keroeididae	M, UB	30–300	3	40	48
Spongiodermidae	Alcyonacea	Spongiodermidae	M	20–200	1	34	39
Coralliidae	Alcyonacea	Coralliidae	UB, LB	500–2,500	7	18	38
Tanacetipathes	Antipatharia	Myriopathidae	M	50–150	5	448	1,709
Stichopathes	Antipatharia	Antipathidae	M	20–200	7	326	1,288
Antipathes	Antipatharia	Antipathidae	M	20–200	6	349	1,231
Antipathes furcata	Antipatharia	Antipathidae	M	20–200	3	293	834
Antipathes atlantica	Antipatharia	Antipathidae	M	20–200	6	89	531
Leiopathes	Antipatharia	Leiopathidae	M, UB	150–800	12	135	244
Bathypathes	Antipatharia	Schizopathidae	UB, LB	300–2,200	10	69	114
Stauropathes	Antipatharia	Schizopathidae	LB	1,000–3,500	3	10	13
Plumapathes	Antipatharia	Myriopathidae	M	20–80	2	6	9
Aphanipathidae	Antipatharia	Aphanipathidae	M, UB	50–500	4	410	2,319
Tubeworms	N/A	N/A	N/A	N/A	10	201	1,531
Bivalves	N/A	N/A	N/A	N/A	9	242	775
Bacterial Mats	N/A	N/A	N/A	N/A	2	69	174
Seeps	N/A	N/A	N/A	N/A	13	122	440
Brine	N/A	N/A	N/A	N/A	6	37	167

M = Mesophotic, UB = Upper Bathyal, LB = Lower Bathyal

Table 3. Environmental predictors considered for models of DSC and chemosynthetic communities

X denotes the subset selected for use in models.

Environmental Predictor Variable	Category	Subset
Depth	Depth and Seafloor Topography	X
Slope	Depth and Seafloor Topography	X
Slope of Slope	Depth and Seafloor Topography	
East-West Aspect	Depth and Seafloor Topography	X
North-South Aspect	Depth and Seafloor Topography	X
Rugosity	Depth and Seafloor Topography	
General Curvature	Depth and Seafloor Topography	X
Total Curvature	Depth and Seafloor Topography	
Planform Curvature	Depth and Seafloor Topography	
Cross-Sectional Curvature	Depth and Seafloor Topography	
Profile Curvature	Depth and Seafloor Topography	
Longitudinal Curvature	Depth and Seafloor Topography	
Surficial Sediment Mean Grain Size	Seafloor Substrate	
Surficial Sediment Percent Gravel	Seafloor Substrate	
Surficial Sediment Percent Sand	Seafloor Substrate	X
Surficial Sediment Percent Mud	Seafloor Substrate	
Annual Mean Bottom Dissolved Oxygen	Oceanography	X
Annual Mean Bottom Salinity	Oceanography	
Annual Mean Bottom Temperature	Oceanography	
Annual Mean Bottom Current Speed	Oceanography	X
Annual Mean East-West Bottom Current Velocity	Oceanography	
Annual Mean North-South Bottom Current Velocity	Oceanography	
Annual Mean Surface Chlorophyll-a Concentration	Oceanography	X
Annual Mean Surface Reflectance	Oceanography	
Annual Mean Mixed Layer Depth	Oceanography	
Longitude	Geography	X
Latitude	Geography	

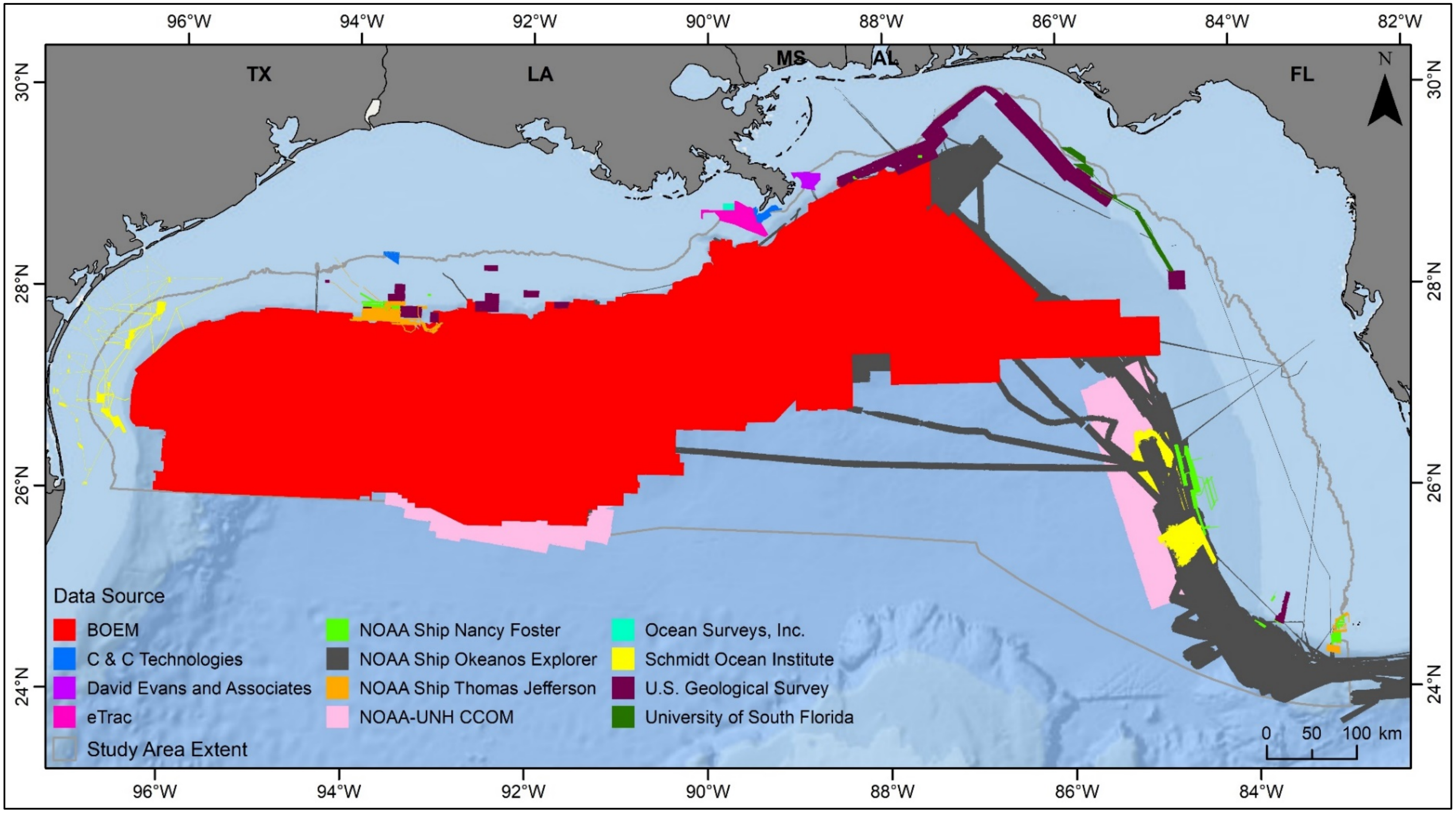

Figure 3. Coverage of available high-resolution bathymetry datasets.

This map depicts footprints of the high-resolution bathymetry datasets, symbolized by data source, used in the bathymetry synthesis. For additional details of each individual dataset, see Appendix C. UNH = University of New Hampshire, CCOM = Center for Coastal and Ocean Mapping.

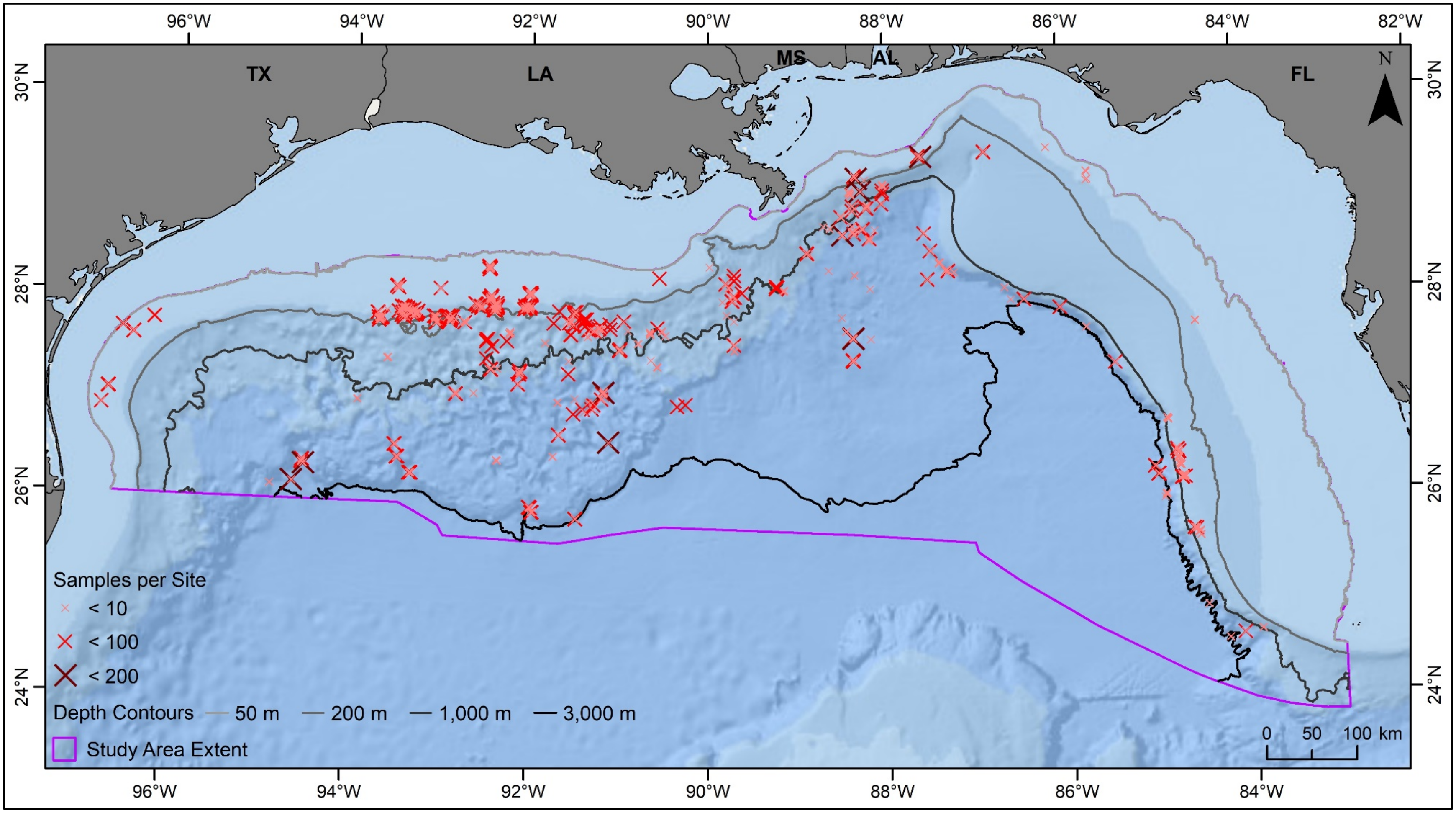

Figure 4. Spatial distribution of sampling effort.

This map depicts the number of samples (segments) within each site (100 x 100 m grid cell). Samples within each site were treated as spatial replicates.

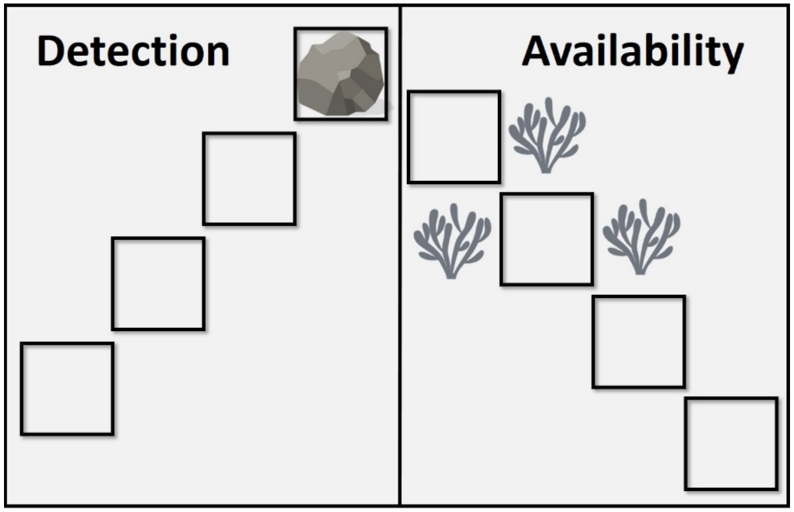

Figure 5. Illustration of detection and availability processes.

The two grid cells shown are a hypothetical subsample of the model grid, with both cells (sites) occupied by corals. Squares indicate spatial replicate samples (e.g., images) along a dive transect through these grid cells. Corals could go undetected because they are obscured by a rock in an image (left; detection process), or because they are not present at the sampled locations (right; availability process). The data would indicate absence in both grid cells, but technically these are different processes leading to recorded absence.

Table 4. List of models and the taxa included in each model

Model	Taxa Included
Multi-genus model of branching stony corals in order Scleractinia	*Madracis*, *Lophelia pertusa*, *Madrepora*, *Solenosmilia*, *Enallopsammia*
Single-taxon model of family Oculinidae	Oculinidae (without *Madrepora*)
Multi-family model of gorgonian corals in order Alcyonacea	Plexauridae, Ellisellidae, Primnoidae, Isididae, Chrysogorgiidae, Acanthogorgiidae, Paragorgiidae, Gorgoniidae, Keroeididae, Spongiodermidae, Coralliidae
Multi-genus model of family Plexauridae	*Bebryce*, *Swiftia*, *Paramuricea*, *Caliacis*, *Muricea* (*Hypnogorgia*), *Scleracis*, *Thesea*, *Placogorgia*, *Villogorgia*
Single-taxon model of *Swiftia exserta*	*Swiftia exserta*
Single-taxon model of *Muricea pendula*	*Muricea* (*Hypnogorgia*)
Single-taxon model of *Paramuricea biscaya*	*Paramuricea* (800–2,500 m)
Single-taxon model of genus *Nicella*	*Nicella*
Single-taxon model of genus *Callogorgia*	*Callogorgia*
Single-taxon model of genus *Plumarella*	*Plumarella*
Multi-genus model of family Isididae	*Lepidisis*, *Keratoisis*, *Chelidonisis*, *Acanella*
Multi-genus model of black corals in order Antipatharia	*Tanacetipathes*, *Stichopathes*, *Antipathes*, *Leiopathes*, *Bathypathes*, *Stauropathes*, *Plumapathes*
Single-taxon model of *Antipathes atlantica*	*Antipathes atlantica*
Single-taxon model of *Antipathes furcata*	*Antipathes furcata*
Single-taxon model of family Aphanipathidae	Aphanipathidae
Single-taxon model of tubeworms	Tubeworms
Single-taxon model of bivalves	Bivalves
Single-taxon model of bacterial mats	Bacterial Mat
Single-taxon model of seeps	Seep
Single-taxon model of brine	Brine

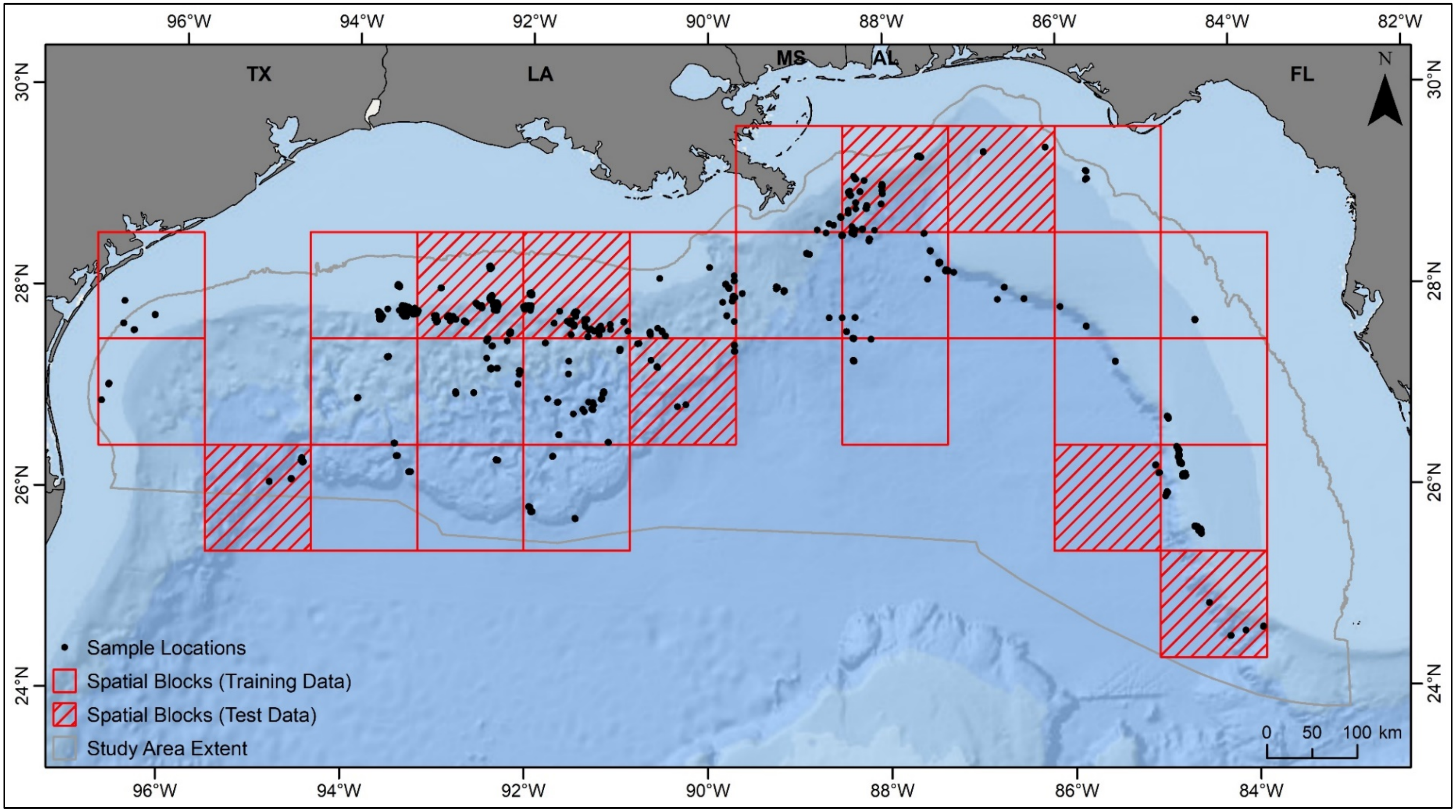

Figure 6. Example spatial blocks used in model validation.

This map depicts the spatial blocks used to partition the training and test sample data for the multi-genus model of branching stony corals in order Scleractinia.

3. Results and Discussion

3.1 Model fit

Model fit was assessed by calculating the Bayesian p-values (Conn et al. 2018) for the chi-squared, Pearson's, and Freeman-Tukey fit statistics (Table 5). Models that fit well to the data will have Bayesian p-values close to 0.5 (rather than 0 or 1) for the fit statistics. Models that fit well to the data based on one of more of these goodness-of-fit tests included the multi-genus model of branching stony corals (Bayesian p-value = 0.584 for the site-level Freeman-Tukey statistic; Table 5) and the multi-genus model of family Isididae (Bayesian p-values of 0.516, 0.450, and 0.527 for the taxon-level chi-squared, Pearson, and Freeman-Tukey fit statistics; Table 5). Some models performed poorly (i.e., had Bayesian p-values close to 0 or 1) by one or more of these measures of goodness-of-fit. The point-biserial correlation coefficients and area under the receiver operating characteristic curve (AUC) values indicated reasonably good model fit across taxa when calculated using the estimated occupancy states (z_{ik}). Over 80% of correlation coefficients were >0.4, while AUC values were all ≥0.93 (Table 6). Performance was generally degraded when predicted values were calculated using mean probabilities of occupancy (Ψ_{ik}) and ignoring site effects on detection. Only 19% of correlation coefficients were ≥0.4, while 40% of AUC values were <0.9 (Table 6). All models presented in this report were considered to have sufficient model fit to be useful for informing management.

3.2 Model predictive performance

Predictive performance of the models (i.e., with respect to test data from novel areas) was usually lower than the performance indicated by the fit of the global models or the fit of the models to training subsets of the data (Table 7). Sixty-five percent of correlation coefficients were <0.2, while 45% of AUC values were <0.8. Five models had very poor predictive performance with correlation coefficients near zero and AUC ≤0.6, while five models had decent predictive performance with correlation coefficients >0.4 and AUC ≥0.87. Thus, while the global models provided a reasonably good fit to the entire sample data, the ability of the models to predict to unsampled geographic areas that were not represented in the presence-absence database may be limited.

3.3 Probability of detection

In general, more frequently observed taxa were estimated to have higher detectability, but also higher occupancy probability than less frequently observed taxa (e.g., Figures 7–9). These patterns were not surprising because abundant taxa are more likely to be widespread and easily detectable compared to rare taxa (Dorazio et al. 2006; Kéry and Royle 2016). This can lead to positive correlations between occpancy and detection. Detection probability was usually estimated as higher than occupancy probability, but this was not always the case (Figures 7–9). Models may have had some difficulty distinguishing occupancy from detection probability, in part because of the space-for-time substitution. This is because availability (i.e., "small-scale occupancy") can be confounded with either detection or occupancy (Guillera-Arroita 2011; Kéry and Royle 2016). The space-for-time substitution meant that three levels of analysis (small-, mid-, and large-scale, corresponding to detection, availability, and occupancy) were collapsed into two (detection and occupancy), treating detection and availability as a single process. The space-for-time substitution is well-supported (Sadoti et al. 2013; Charbonnel et al. 2014; Srivathsa et al. 2018; Jiménez-Franco et al. 2019; Petracca et al. 2020) because it provides the flexibility to estimate detection probability. Implementing the space-for-time substition allowed for the implementation of an occupancy modeling framework rather than a more conventional approach that does not account for detectability.

3.4 Maps of observed and predicted spatial distributions

This section describes the set of maps produced for each deep-sea coral (DSC) taxon and chemosynthetic community selected for modeling. The first map displays the locations of presences and absences from the presence-absence database compiled for this study. For each DSC taxon, it also includes the presence records in the National Oceanic and Atmospheric Administration (NOAA) National Database for the taxon. These additional records are not visible in the maps when they coincide with records also included in the presence-absence database, but in some cases the additional records identify areas where the taxon had been observed outside the spatial extent of the survey datasets included in the presence-absence database. The records from the NOAA National Database were not used in the models, however, because they only included information on the locations of DSC presence and could not be used to infer absence or quantify sampling effort.

The second map depicts the predicted mean probability of occurrence (i.e., the predicted posterior mean occupancy probability) for the taxon from the occupancy models. Because estimates of occurrence probabilities were standardized across taxa (i.e., by accounting for absences), they are directly comparable among taxa and are estimates of absolute probability of occurrence, not relative. Values of the predicted mean probability of occurrence have been classified as very high (0.8–1), high (0.6–0.8), medium (0.4–0.6), low (0.2–0.4), and very low (0–0.2) for the purpose of facilitating descriptions of the spatial patterns observed. In addition to examining spatial patterns in the areas where DSCs or chemosynthetic communities are predicted to occur, these maps can be used to identify potential targets for future surveys (e.g., an area predicted to have high probability of occurrence that has not been previously surveyed).

The third map depicts the predicted coefficient of variation (CV) of the probability of occurrence (i.e., the predicted posterior CV of the occupancy probability). Maps of the CV can be used to identify areas with greater variability or uncertainty (i.e., less precision) in the model predictions. It is important to note that in addition to areas of greater variability, higher values of the CV can also result from extremely low values of the predicted mean probability of occurrence. Therefore, maps of the CV should be interpreted in conjunction with the maps of the presence-absence records and the mean probability of occurrence to distinguish areas where variability was high and the taxon was predicted to occur from areas where the CV was high because the mean was extremely low. There was generally greater variability in data poor areas with fewer or no sample data, particularly in regions at the extreme ends of the predictor values. In addition to providing information about the level of confidence in model predictions, the CV maps can be used to suggest potential targets for future surveys (e.g., areas with higher variability and limited sample data).

In addition to the maps depicting the observed and predicted spatial distributions for each individual DSC taxon and chemosynthetic community, for each multi-taxon model there are maps depicting the predicted taxon richness (i.e., the number of taxa expected at each grid cell) with corresponding maps of the variability (CV) in predicted taxon richness. These maps provide information about the number of taxa expected to occur at each grid cell and can be used to identify areas where more or fewer of the taxa in each multi-taxon model may co-occur.

3.4.1 Branching stony corals (order Scleractinia)

The most commonly observed branching stony corals in the presence-absence database were *Madracis*, *Lophelia pertusa*, and Oculinidae (Table 2). Records of *Madracis* presence in the database (n = 426 samples) and patchy areas with very high predicted probability of occurrence were primarily on the Texas-Louisiana continental shelf in the northwestern Gulf of Mexico (Gulf) (Figure 10, Figure 11). Although there were fewer observations of *Madracis* on the continental shelf in the western and eastern Gulf (Figure 10), there were some areas with low–medium predicted probability of occurrence in these areas (Figure 11), and additional records of *Madracis* presence in the NOAA National Database were located on the continental shelf throughout the study area (Figure 10). Predictions of low probability of occurrence near edges of the environmental predictor mask in deep (>3,000 m) parts of the study area should be considered unreliable, as these areas are unsampled and far deeper than the maximum expected depth for *Madracis* (Figure 11). Variability in the model predictions (i.e., the CV) was relatively low in the areas predicted to have higher probability of occurrence for *Madracis* and throughout most of its expected depth range (Figure 12). Higher variability was found deeper than the maximum expected depth for *Madracis* in areas with very low predicted probability of occurrence (Figure 12). Incorporating sample data where there were additional *Madracris* presences (e.g., by reviewing the original data to infer absence or by applying an integrated model framework that could use both presence-absence and presence-only records) may improve model predictions on the continental shelf in the western and eastern Gulf (e.g., on the west Florida shelf).

There were observations of *L. pertusa* in the presence-absence database (n = 327 samples) and additional records of *L. pertusa* presence in the NOAA National Database on the continental slope in the central Gulf and on the west Florida slope within its expected depth range (Figure 13). Most of the areas with very high predicted probability of occurrence for *L. pertusa* were on the west Florida slope, including large areas extending southeast from De Soto Canyon where there were no samples in the presence-absence database and some areas slightly shallower than its expected depth range (Figure 14). There were also some small areas with medium–very high predicted probability of occurrence for *L. pertusa* on the edge of the continental shelf and on the continental slope off south Texas, where there were no sample data in the presence-absence database (Figure 14). There was relatively low variability in the model predictions in the areas with highest predicted probability of occurrence for *L. pertusa* and throughout its expected depth range (Figure 15). Predictions had higher variability in some areas outside the expected depth range for *L. pertusa* where the predicted probability of occurrence was very low (Figure 15). Although few surveys have been conducted on the continental slope in the northeastern Gulf where there was very high predicted probability of occurrence for *L. pertusa*, these surveys have found only *Lophelia* rubble (i.e., dead corals) and no living corals (E. Cordes, email message, July 21, 2020). In contrast to the occupancy model for *L. pertusa* developed for this study, the presence-only model from Kinlan et al. (2013) predicted low relative habitat suitability in this area. However, the presence-only model provided only a prediction of relative habitat suitability (as opposed to an absolute probability of occurrence) and may be somewhat overfit to (i.e., constrained by) the presence records available to the model. The presence-only model did not incorporate absence data and instead contrasted locations of *L. pertusa* presence with randomly selected background locations from across the Gulf. As a result, while both the occupancy model and the presence-only model predicted that *L. pertusa* was likely to occur in the southern part of the west Florida slope, predictions were considerably different for the central Gulf. The presence-only model predicted high relative habitat suitability for a wide stretch of the central Gulf where there are records of *L. pertusa* presence. However, because the occupancy model also used the numerous records of *L. pertusa* absence in this area, the occupancy model predicted only a few small patches with very high probability of occurrence in the central Gulf , and most of this area was predicted to have low–medium probability of occurrence. This comparison of the occupancy model and earlier presence-only model is intended to demonstrate some of the advancements in the data and modeling approach used in this study. Even with these advancements, some caution should be taken when using predictions from the occupancy model for *L. pertusa* in the areas where there were no samples in the presence-absence database (e.g., on the west Florida slope in the northeastern Gulf), particularly given that there were surveys not included in the database that found no living *L. pertusa*. Additional surveys in these areas should be a high priority for ground truthing the occupancy model predictions for *L. pertusa*.

There were fewer records of *Madrepora* presence in the presence-absence database (n = 97 samples), and these were found in the central Gulf and on the west Florida slope. Additional records of *Madrepora* presence in the NOAA National Database were located across the study area within its expected depth range (Figure 16). The predicted probability of occurrence for *Madrepora* was generally very low across most of the study area, with some areas on the continental slope in the central and eastern Gulf having low predicted probability of occurrence and a few small patches (difficult to discern in the map page) within these areas that had medium predicted probability of occurrence (Figure 17). Areas with highest variability in model predictions for *Madrepora* were mostly in unsampled areas deeper than its expected depth range where the predicted probability of occurrence was very low (Figure 18). Variability was relatively low in the areas with higher predicted probability of occurrence, but there were areas with slightly higher variability within the expected depth range for *Madrepora* in the western and eastern Gulf , again where the predicted probability of occurrence was very low (Figure 18).

There were very few records of *Solenosmilia* presence in the presence-absence database (n = 26 samples) on the continental slope in the central and eastern Gulf and few additional records in the NOAA National Database (Figure 19). The predicted probability of occurrence for *Solenosmilia* was generally very low throughout the study area, and the few areas with predicted probability of occurrence >0.2 were far too small to be seen in the mag page (Figure 20). The low predicted probability of occurrence for *Solenosmilia* was not surprising given how infrequently it was recorded in the presence-absence database. There was relatively higher variability in the model predictions for *Solenosmilia*, although the highest variability was generally outside the expected depth range and in unsampled areas (Figure 21).

Like *Solenosmilia*, there were very few records of *Enallopsammia* presence in the presence-absence database (n = 18 samples) on the continental slope in the central and eastern Gulf and few additional records in the NOAA National Database (Figure 22). Near the observations of *Enallopsammia* presence there were some small areas of low–medium predicted probability of occurrence for *Enallopsammia* in the central Gulf and even smaller patches of low predicted probability of occurrence on the west Florida slope (Figure 23). Elsewhere in the study area the predicted probability of occurrence was generally very low (Figure 23). Variability in the model predictions for *Enallopsammia* was relatively low in the areas with higher predicted probability of occurrence, but was considerably higher in some parts of the expected depth range (e.g., in the eastern and western Gulf) as well as large areas outside the expected depth range where the predicted probability of occurrence was very low (Figure 24).

Observations of the family Oculinidae (excluding records identified as *Madrepora*) in the presence-absence database were more numerous (n = 722 samples) and concentrated on the Texas-Louisiana continental shelf (Figure 25). Areas with very high predicted probability of occurrence were also found on the Texas-Louisiana continental shelf among additional areas with low–high predicted probability of occurrence (Figure 26). Although there were some additional records of Oculinidae presence in the NOAA National Database on the Mississippi-Alabama continental shelf and west Florida shelf (Figure 25), the predicted probability of occurrence was very low in the eastern Gulf (Figure 26). Model predictions for Oculinidae had relatively low variability where the predicted probability of occurrence was higher and across much of the continental shelf and slope in the western and central Gulf (Figure 27). Areas with relatively higher variability in model predictions for Oculinidae were widespread in the eastern Gulf where the predicted probability of occurrence was very low, including on the continental shelf where there were records of Oculinidae in the NOAA National Database but no samples in the presence-absence database (Figure 27). As with *Madracis*, incorporating sample data where there were additional Oculinidae presences on the continental shelf (e.g., by reviewing the original data to infer absence or by applying an integrated model framework that could use both presence-absence and presence-only records) may improve model predictions for Oculinidae in these areas.

The five genera of branching stony corals in order Scleractinia selected for modeling included two that occur at mesophotic depths (50–200 m), four found in the upper bathyal zone (200–1,000 m), and three found deeper (1,000–3,000 m) in the lower bathyal zone (Table 2). Areas with the highest predicted genus richness (1–2) for branching stony corals were primarily on the west Florida slope, where there were also broader areas of low (0–0.25) to medium (0.5–1) predicted genus richness (Figure 28). Smaller patches of low–medium predicted genus richness were found on the continental shelf and slope in the western and central Gulf (Figure 28). Variability in the predicted genus richness was relatively low in the areas with higher predicted genus richness, but was higher within the expected depth range for the selected stony coral genera in areas with very low predicted genus richness on the shallow edge of the study area, particularly around the environmental predictor mask, and where there were only recorded absences of stony corals or no sample data (Figure 29).

3.4.2 Gorgonian corals (order Alcyonacea)

3.4.2.1 Plexauridae

The family Plexauridae is very diverse, with taxa in the presence-absence database found in mesophotic (50–200 m), upper bathyal (200–1,000 m), and lower bathyal (1,000–2,000 m) depths (Table 2). Not surprisingly, records of Plexauridae (or taxa within family Plexauridae) presence in the presence-absence database (n = 4,473 samples) and in the NOAA National Database were widespread across the continental shelf and slope (Figure 30). Areas predicted to have very high probability of occurrence were also widespread on the continental shelf and upper continental slope (Figure 31). Model predictions had relatively low variability across the entire study area (Figure 32).

Observations of the genus *Bebryce* in the presence-absence database (n = 1,051 samples) were found on the continental shelf across much of the study area, with additional records of *Bebryce* presence in the NOAA National Database in some areas with no samples in the presence-absence database (Figure 33). Predicted probability of occurrence for *Bebryce* was very high on the continental shelf in the western and central Gulf , and there were additional smaller areas on the west Florida shelf with medium–high predicted probability of occurrence (Figure 34). Variability in model predictions for *Bebryce* was relatively low where there was higher predicted probability of occurrence as well as other areas within its expected depth range where there was very low predicted probability of occurrence (Figure 35). Areas of slightly higher variability within the expected depth range for *Bebryce* were found around the edges of the environmental predictor mask on the upper continental slope in the northeastern Gulf , but other areas with higher variability were deeper than its maximum expected depth and where the predicted probability of occurrence was very low (Figure 35).

Records of *Swiftia* presence in the presence-absence database (n = 613 samples) were found most often on the Texas-Louisiana continental shelf and Mississippi-Alabama continental shelf but were also found on the continental slope in both the central and eastern Gulf of Mexico (Figure 36). Additional records of *Swiftia* presence in the NOAA National Database were located on the continental shelf and slope across the study area (Figure 36). There were areas of very high predicted probability of occurrence for *Swiftia* on the continental shelf off eastern Louisiana and Mississippi on either side of the environmental predictor mask (Figure 37). Smaller patches of low–high predicted probability of occurrence were found on the continental shelf off Louisiana, Alabama, and northern Florida (Figure 37). Variability in model predictions for *Swiftia* was relatively low in the areas with higher predicted probability of occurrence and some parts of the continental shelf and slope within its expected depth range where the predicted probability of occurrence was very low (Figure 38). Within the expected depth range for *Swiftia*, variability was slightly higher around the edges of the environmental predictor mask in the western and eastern Gulf (Figure 38). Areas with higher variability were generally in unsampled locations deeper than the expected depth range of *Swiftia* (Figure 38). Records identified as *Swiftia exserta* comprised most of the *Swiftia* records in the presence-absence data (n = 587 samples) and were constrained to the Texas-Louisiana continental shelf and Mississippi-Alabama continental shelf in the central Gulf. There were additional records of *S. exserta* presence in the NOAA National Database on the Mississippi-Alabama continental shelf as well as on the west Florida shelf (Figure 39). Similar to the model for the genus *Swiftia*, there was a large area of very high predicted probability of occurrence for *S. exserta* along the continental shelf off Louisiana, Mississippi, and Alabama, with additional smaller patches with low–high predicted probability of occurrence on the Texas-Louisiana continental shelf and on the continental shelf off northern Florida (Figure 40). There was also a large area at the deepest edge of the study area in the central Gulf with low–high predicted probability of occurrence (Figure 40). The model predictions for this area should be considered unreliable as there were no sample data in this area and it is far deeper than the expected depth range for *S. exserta*. Model predictions for *S. exserta* had relatively low variability were there was higher predicted probability of occurrence, but there were areas with higher variability within its expected depth range where there was very low predicted probability of occurrence in the western and eastern Gulf (Figure 41). Areas with considerably higher variability around the environmental predictor mask in the western and eastern Gulf and on the west Florida slope were deeper than the maximum expected depth for *S. exserta* (Figure 41).

Taxa in the genus *Paramuricea* had a wide expected depth range in the study area, but most of the observations of *Paramuricea* in the presence-absence database (n = 569 samples) were found on the continental slope in the central and eastern Gulf (Figure 42). Additional records of *Paramurciea* presence in the NOAA National Database were located on the continental shelf and slope across the study area (Figure 42). Areas of medium probability of occurrence for *Paramuricea* were predicted on parts of the west Florida slope, and there were large areas with low predicted probability of occurrence on the continental slope in the central Gulf and along the extent of the west Florida slope (Figure 43). Variability in model predictions for *Paramuricea* was relatively low across much of the study area, including the areas with higher predicted probability of occurrence as well as areas with very low predicted probability of occurrence (Figure 44). Slightly higher variability was found within the expected depth range for *Paramuricea* in some places on the continental shelf in the western and eastern Gulf where there was very low predicted probability of occurrence (Figure 44). Within the genus *Paramuricea*, the species *Paramuricea biscaya* occurs in the deeper waters of the upper and lower bathyal zones. Observation identified as *P. biscaya* (including records of *Paramuricea* at depths >800 m) in the presence-absence database (n = 347 samples) were located on the continental slope in the central Gulf and along the west Florida slope near its maximum expected depth (Figure 45). There was a narrow band of high and very high predicted probability of occurrence for *P. biscaya* along the northern part of the west Florida slope and near its maximum expected depth that is too narrow to discern in the map page (Figure 46). In addition, there were extensive areas of low–medium predicted probability of occurrence on the continental slope in the central Gulf of Mexico and along the west Florida slope (Figure 46). Model predictions for *P. biscaya* had relatively low variability where there was higher predicted probability of occurrence within its expected depth range, but areas with higher variability were found in some parts of the continental shelf and in deeper waters near the environmental predictor mask where there was very low predicted probability of occurrence (Figure 47).

Caliacis presences in the presence-absence database (n = 478 samples) were concentrated near the edge of the Texas-Louisiana continental shelf in the northwestern Gulf, while there were some additional presence records for *Caliacis* in the NOAA National Database (including some deeper than its expected depth range) across the study area (Figure 48). Areas with very high and high predicted probability of occurrence for *Caliacis* were found along the Texas-Louisiana continental shelf and were surrounded by broader areas with low–medium predicted probability of occurrence (Figure 49). *Caliacis* had only very low predicted probability of occurrence in the eastern Gulf of Mexico where there were some records in the NOAA National Database but no sample data in the presence-absence database (Figure 49). Variability in model predictions for *Caliacis* was relatively low in the northwestern Gulf where there was higher predicted probability of occurrence, but was considerably higher in the eastern Gulf where there was very low predicted probability of occurrence, including some areas within the expected depth range on the west Florida shelf (Figure 50). Additional surveys in these areas or models that incorporate the additional *Caliacis* presences found here in the NOAA National Database (e.g., by reviewing the original data to infer absence or by applying an integrated model framework that could use both presence-absence and presence-only records) may improve the model predictions for *Caliacis* on the west Florida shelf.

Records in the presence-absence database identified as *Hypnogorgia* (n = 436 samples) were assumed to be *Muricea pendula* as described in Section 2.3 and included in the multi-genus model for family Plexauridae. These records were found on the continental shelf off Texas, the Texas-Louisiana continental shelf (including some records that were deeper than the expected depth range for *Muricea*), the Mississippi-Alabama continental shelf, and off northern Florida (Figure 51). There were additional records in the NOAA National Database on the continental shelf in the central Gulf and on the west Florida shelf where there were no samples in the presence-absence database (Figure 51). A wide band of very high predicted probability of occurrence for *Muricea* extended along the continental shelf across the western and central Gulf, and additional areas of very high and high predicted probability of occurrence were found along the Mississippi-Alabama continental shelf and west Florida shelf (Figure 52). Model predictions for *Muricea* had relatively low variability where there was high predicted probability of occurrence on the continental shelf or elsewhere within its expected depth range, but there were two areas of considerably higher variability around the environmental predictor mask in the western and northeastern Gulf (Figure 53). The single-taxon model for *Muricea pendula* used the same records from the presence-absence database (Figure 54) that were used in the multi-genus model, and the patterns in the predicted probability of occurrence for *M. pendula* (Figure 55, Figure 56) were nearly identical to the predictions from the multi-genus model.

Observations of *Scleracis* presence in the presence-absence database (n = 368 samples) were restricted to the Texas-Louisiana continental shelf in the northwestern Gulf, although there were some additional records of *Scleracis* presence in the NOAA National Database on the west Florida shelf (Figure 57). A few small patches with medium–very high predicted probability of occurrence for *Scleracis* were found near the edge of the Texas-Louisiana continental shelf where the presence records were concentrated, but the predicted probability of occurrence was very low across most of the continental shelf, including on the west Florida shelf where there were *Scleracis* presences in the NOAA National Database (Figure 58). Model predictions for *Scleracis* had relatively low variability on the continental shelf in the northwestern Gulf where there was higher predicted probability of occurrence, but there was considerably higher variability in the eastern Gulf, including in some areas within its expected depth range, where there was very low predicted probability of occurrence (Figure 59). Similar to *Caliacis*, additional surveys on the west Florida shelf or models that incorporate the additional *Scleracis* presences found in the NOAA National Database (e.g., by reviewing the original data to infer absence or by applying an integrated model framework that could use both presence-absence and presence-only records) may improve the model predictions for *Scleracis* on the west Florida shelf.

Records of *Thesea* presence in the presence-absence database (n = 224 samples) were located on the Texas-Louisiana continental shelf, the Mississippi-Alabama continental shelf, and on the continental shelf off northern Florida, with many additional *Thesea* records in the NOAA National Database on the continental shelf across the study area (Figure 60). There was a wide band of very high predicted probability of occurrence for *Thesea* on the continental shelf extending from the Texas-Louisiana continental shelf to the northern part of the west Florida shelf (Figure 61). Although there were *Thesea* presences in the NOAA National Database on the continental shelf off Texas and the southern part of the west Florida shelf, the predicted probability of occurrence was very low in these areas because there were no presence records in the presence-absence database (Figure 61). Similar to *Swiftia*, there were also large areas in locations far deeper than the expected depth range for *Thesea* with low–high predicted probability of occurrence but no sample data (Figure 61). Model predictions for *Thesea* in these areas should be considered unreliable. Variability in model predictions for *Thesea* were relatively low where the predicted probability of occurrence was higher on the continental shelf but was slightly higher on parts of the continental shelf where there was very low predicted probability of occurrence (Figure 62). Areas with highest variability were outside the expected depth range on the continental slope in the western and eastern Gulf where there was very low predicted probability of occurrence (Figure 62). As with *Caliacis* and *Scleracis*, additional surveys on the west Florida shelf or models that incorporate the additional *Thesea* presences found in the NOAA National Database (e.g., by reviewing the original data to infer absence or by applying an integrated model framework that could use both presence-absence and presence-only records) may improve the model predictions for *Scleracis*.

Placogorgia presences in the presence-absence database (n = 199 samples) were also found on the continental shelf across much of the study area, and additional records of *Placogorgia* presence in the NOAA National Database were located on the continental shelf in areas where there were no samples in the presence-absence database (e.g., the southern part of the west Florida shelf; Figure 63). Fairly large areas with very high predicted probability of occurrence for *Placogorgia* were located on the continental shelf off Texas and eastern Louisiana, with smaller patches of very high predicted probability of occurrence along the Mississippi-Alabama continental shelf and the west Florida shelf (Figure 64). These areas of very high predicted probability of occurrence were typically surrounded by areas of low–high predicted probability of occurrence (Figure 64). There were again some areas deeper than the expected depth range for *Placogorgia* in the central and eastern Gulf where there was low–medium predicted probability of occurrence but no sample data (Figure 64). Model predictions for *Placogorgia* should be considered unreliable in these areas. Although model predictions for *Placogorgia* had relatively low variability where there was higher predicted probability of occurrence, there was higher variability on other parts of the continental shelf as well as in deeper waters on the continental slope around the environmental predictor mask where there was very low predicted probability of occurrence (Figure 65). Unlike some of the previously described genera in Plexauridae, there were some areas on the southern part of the west Florida shelf with high–very high predicted probability of occurrence for *Placogorgia* farther south than any of the sample data locations in the presence-absence database. Nonetheless, additional surveys on the west Florida shelf or models that incorporate the additional *Placogorgia* presences found in the NOAA National Database (e.g., by reviewing the original data to infer absence or by applying an integrated model framework that could use both presence-absence and presence-only records) may still improve the model predictions for *Placogorgia* in this area.

Villogorgia was the least frequently observed genus in family Plexauridae in the presence-absence database (n = 22 samples). Like *Placogorgia*, records of *Villogorgia* presence in the presence-absence database were found on the continental shelf across the study area, and there were also additional records of *Villogorgia* presence in the NOAA National Database across the continental shelf (Figure 66). Small patches with very high predicted probability of occurrence for *Villogorgia* were primarily on the shallow edge of the study area on the Mississippi-Alabama continental shelf and the west Florida shelf (Figure 67). These patches were generally surrounded by additional areas with low–high predicted probability of occurrence (Figure 67). Although there were *Villogorgia* presences in the presence-absence database and the NOAA National Database in the western and central Gulf of Mexico, these areas generally had very low predicted probability of occurrence for *Villogorgia* (Figure 67). Variability in model predictions for *Villogorgia* was relatively low in the limited areas on the continental shelf with higher predicted probability of occurrence, but there were areas with higher variability on the continental shelf (typically highest in unsampled areas) as well as in deeper waters at the edge of the study area and around the environmental predictor mask where there was very low predicted probability of occurrence (Figure 68).

Although the taxa in the gorgonian coral family Plexauridae are very diverse and span all the depth zones included in the study area, all nine of the genera included in the multi-genus model of family Plexauridae are found at mesophotic depths (50–200 m), while only five are found in the upper bathyal zone (200–1,000 m), and only two are found deeper (1,000–3,000 m) in the lower bathyal zone (Table 2). There were large areas on the continental shelf with high (2–3) and very high (>3) predicted genus richness (Figure 69). This was expected since most of the genera selected for modeling from family Plexauridae are found at mesophotic depths. There were unexpected areas with low–medium predicted genus richness in deeper (>2,500 m), unsampled parts of the central and eastern Gulf (Figure 69) that coincide with areas deemed to have unreliable predictions for some taxa (e.g., *Muricea*, *Placogorgia*, *Thesea*). Variability in the predicted genus richness for Plexauridae was relatively low in the areas with higher predicted genus richness (Figure 70). There were some areas of slightly higher variability within the expected depth range for Plexauridae on the edge of the environmental predictor mask and in deeper waters outside the expected depth range (e.g., near the base of the west Florida slope) where the predicted genus richness was very low (Figure 70).

3.4.2.2 Ellisellidae

Records within the presence-absence database in family Ellisellidae (n = 3,243 samples) were located on the continental shelf across the study area, with some records just deeper than the expected depth range on the upper continental slope off Louisiana (Figure 71). There were additional records of Ellisellidae presence in the NOAA National Database along the continental shelf, including the southern part of the west Florida shelf where there were no sample locations in the presence-absence database (Figure 71). There were large areas with very high predicted probability of occurrence for Ellisellidae on the Texas-Louisiana continental shelf, the Mississippi-Alabama continental shelf, and the west Florida shelf (Figure 72). Smaller areas of very high and high predicted probability of occurrence were found on the continental shelf off south Texas (Figure 72). Model predictions for Ellisellidae should be considered unreliable in the areas with low–medium predicted probability of occurrence in the central and eastern Gulf of Mexico deeper than the expected depth range and where there were no sample data (Figure 72). Model predictions for Ellisellidae had relatively low variability across most of the study area, including where there was higher predicted probability of occurrence and areas with very low predicted probability of occurrence (Figure 73). Areas with slightly higher variability were found around the environmental predictor mask in the western Gulf and along the base of the west Florida slope where there was also very low predicted probability of occurrence (Figure 73).

Nicella presences in the presence-absence database (n = 2,621 samples) were primarily on the Texas-Louisiana continental shelf in the northwestern Gulf but were also found on the Mississippi-Alabama continental shelf and west Florida shelf (Figure 74). Additional records of *Nicella* presence in the NOAA National Database were found on the continental shelf across the study area, including the southern part of the west Florida shelf where there were no sample locations in the presence-absence database (Figure 74). Areas with very high and high predicted probability of occurrence for *Nicella* were found on the Texas-Louisiana continental shelf and west Florida shelf with additional areas of low–medium predicted probability of occurrence (Figure 75). There were also small areas of high predicted probability of occurrence surrounded by areas with low–medium probability of occurrence on the continental shelf off south Texas (Figure 75). Although there were observations of *Nicella* in the presence-absence database in the northeastern Gulf, there were only a few small patches with low predicted probability of occurrence in this area (Figure 75). Variability in model predictions for *Nicella* was relatively low in the areas with higher predicted probability of occurrence as well as other areas within its expected depth range where the predicted probability of occurrence was very low (Figure 76). Variability was only slightly higher in some areas deeper than the maximum expected depth for *Nicella* with very low predicted probability of occurrence (Figure 76).

3.4.2.3 Primnoidae

Records identified as family Primnoidae in the presence-absence database (n = 831 samples) were found on the continental shelf and slope in the central Gulf of Mexico and on the west Florida slope (Figure 77). There were small areas of very high, high, and medium predicted probability of occurrence for Primnoidae surrounded by broader areas of low predicted probability of occurrence on the continental shelf and slope off east Texas and Louisiana (Figure 78). A band of medium–high probability of occurrence surrounded by broader areas of low probability of occurrence was predicted along the southern part of the west Florida slope (Figure 78). Similar to *L. pertusa*, there were also large areas with very high and high predicted probability of occurrence on the west Florida slope in the northeastern Gulf of Mexico where there were no sample locations in the presence-absence database (Figure 78). There were also extensive areas on the continental shelf shallower than the minimum expected depth for Primnoidae that had low–medium predicted probability of occurrence (Figure 78). Model predictions for Primnoidae had relatively low variability throughout its expected depth range, both in the areas where there were observations of Primnoidae presence and higher predicted probability of occurrence and in the areas unexpectedly predicted to have higher probability of occurrence where there were no sample data (Figure 79). Additional surveys in these unsampled areas should be a high priority for ground truthing the occupancy model predictions.

Observations of *Callogorgia* in the presence-absence database (n = 793 samples) were also on the continental shelf and slope off Louisiana and Mississippi and on the west Florida slope (Figure 80). There was a large area with very high predicted probability of occurrence for *Callogorgia* on the Texas-Louisiana continental shelf and upper continental slope in the northwestern to central Gulf that extended shallower than the majority of the *Callogorgia* observations in the presence-absence database and NOAA National Database (Figure 81). In addition, there were also areas of very high predicted probability of occurrence on the continental shelf and upper continental slope in the northeastern Gulf of Mexico (Figure 81). This was somewhat unexpected since there were no observations of *Callogorgia* in the presence-absence database or NOAA National Database in the vicinity, but there were observations of *Callogorgia* at similar depths in the central Gulf. Although there were records of *Callogorgia* presence in the presence-absence database and NOAA National Database on the southern part of the west Florida slope, the predicted probability of occurrence was very low (Figure 81). Variability in model predictions for *Callogorgia* was relatively low in the areas with higher predicted probability occurrence, although there were some areas within its expected depth range in the eastern Gulf with slightly higher variability where there was very low predicted probability of occurrence (Figure 82). There were also areas with somewhat higher variability deeper than the maximum expected depth for *Callogorgia* in the eastern Gulf where the predicted probability of occurrence was also very low (Figure 82).

3.4.2.4 Isididae

Bamboo corals (family Isididae) in the study area occur on the continental slope in the upper bathyal (200–1,000 m) and lower bathyal (1,000–3,000 m) depth zones (Table 2). Observations of bamboo corals in the presence-absence database were generally identified to the family level, although some records were identified to the genus level (Table 2). Records within family Isididae in the presence-absence database (n = 565 samples) and in the NOAA National Database were widespread on the continental slope across the study area (Figure 83). Similar to *P. biscaya*, there was a narrow band of very high and high predicted probability of occurrence for Isididae along the northern part of the west Florida slope near its maximum expected depth that is difficult to discern in the map page (Figure 84). Farther to the south on the west Florida slope, there were broader areas of medium–very high predicted probability of occurrence for Isididae (Figure 84). In addition, there were large areas of low predicted probability of occurrence along the shallower part of the west Florida slope and across parts of the continental slope in the central Gulf, although some areas in the central Gulf with Isididae presences (as well as absences) in the presence-absence database had very low predicted probability of occurrence (Figure 84). Model predictions for Isididae had relatively low variability across its expected depth range, both where there was higher predicted probability of occurrence and where the predicted probability of occurrence was very low (Figure 85). Some large areas with slightly higher variability were located shallower than the minimum expected depth for Isididae on the west Florida shelf (Figure 85).

Lepidisis presences in the presence-absence database were infrequent (n = 35 samples) and generally found in deeper waters on the continental slope in the central Gulf and on the west Florida slope (Figure 86). Areas of very high predicted probability of occurrence for *Lepidisis* included a narrow band along the west Florida slope near its maximum expected depth and narrow patches on the continental slope in the central Gulf that were consistent with the locations where there were observations of *Lepidisis* (Figure 87). However, there were also large areas of medium–very high predicted probability of occurrence near and sometimes deeper than the maximum expected depth for *Lepidisis* (e.g., at the edge of the study area in the central Gulf) that do not appear reliable because they are in unsampled areas and because of apparent artifacts that may be related to tracklines not sufficiently removed from the bathymetry synthesis (Figure 87). Variability in model predictions for *Lepidisis* was relatively low in the areas predicted to have higher probability of occurrence (Figure 88) and did not help distinguish the areas with unreliable predictions (i.e., outside of the expected depth range with no sample data) from the predictions that may be reliable. Variability was considerably higher in some shallower parts of the expected depth range where there was very low predicted probability of occurrence, including areas near the environmental predictor mask (Figure 88). Predictions for *Lepidisis* should be used with caution outside the sampled areas and in the areas with bathymetry artifacts.

Like *Lepidisis*, observations of *Keratoisis* in the presence-absence database were infrequent (n = 26 samples) on the continental slope in the central Gulf and on the west Florida slope (Figure 89). There were areas with very high, high, and medium predicted probability of occurrence for *Keratoisis* along southern parts of the west Florida slope near observations of *Keratoisis* presence, but only patchy areas of low–medium predicted probability of occurrence in the central Gulf (Figure 90). Model predictions for *Keratoisis* had relatively low variability in the areas with higher predicted probability of occurrence, but variability was higher across other parts of its expected depth range, including near the environmental predictor mask, and outside the expected depth range where there was very low predicted probability of occurrence (Figure 91).

Records of *Chelidonisis* presence in the presence-absence database were extremely rare (n = 9 samples) and found on the upper continental slope in the central and eastern Gulf (Figure 92). In spite of this, there were bands of very high and high predicted probability of occurrence for *Chelidonisis* along the southern part of the west Florida slope and areas of medium–very high predicted probability of occurrence farther north on the west Florida slope where there were no sample locations in the presence-absence database (Figure 93). Though variability in model predictions for *Chelidonisis* was relatively low in these areas (Figure 94), some caution should be taken in using these model predictions since the areas with higher predicted probability of occurrence were in unsampled areas. Variability was higher within the expected depth range for *Chelidonisis* where there was very low predicted probability of occurrence in the western and central Gulf as well as outside the expected depth range (Figure 94).

Similar to *Chelidonisis*, observations of *Acanella* presence in the presence-absence database were extremely rare (n = 8 samples) and mostly on the west Florida slope (Figure 95). However, records of *Acanella* presence in the NOAA National Database were much more widespread across its expected depth range (Figure 95). Not surprisingly, because it was only rarely recorded in the presence-absence database, there was very low predicted probability of occurrence for *Acanella* across most of the study area and only a few small areas with low predicted probability of occurrence, primarily on the southern part of the west Florida slope (Figure 96). Model predictions for *Acanella* had relatively low variability in the limited places it was predicted to have higher probability of occurrence, but variability was higher throughout much of its expected depth range as well as outside its expected depth range where there was very low predicted probability of occurrence (Figure 97). The model predictions for *Acanella* presented here clearly appear to underpredict the extent of *Acanella* in the study area given the distribution of records from the NOAA National Database. Increasing the availability of presence-absence data for *Acanella* (e.g., by trying to recover information on absence and sampling effort where *Acanella* has been recorded in the NOAA National Database) or using models that integrate presence records with presence-absence data would improve future model predictions.

As stated earlier, the four genera representing family Isididae in the presence-absence database are found at upper bathyal (200–1,000 m) and lower bathyal (1,000–3,000 m) depths (Table 2). Areas with higher (>2) predicted genus richness for family Isididae were along the west Florida slope, in a narrow band near the maximum expected depth to the north and in slightly large patches to the south (Figure 98). There were additional very small patches (difficult to discern in the map page) with high (2–3) predicted genus richness surrounded by larger areas with low (0.5–1) and medium (1–2) predicted genus richness on the continental slope in the central Gulf (Figure 98). In addition, there were unexpected areas with low–medium predicted genus richness near and sometimes deeper than the maximum expected depth for Isididae in unsampled parts of the central and eastern Gulf of Mexico that coincided with areas deemed to have unreliable predictions for *Lepidisis* (Figure 98). Variability in the predicted genus richness for Isididae was relatively low in the areas with higher predicted genus richness, but was higher in other areas within the expected depth range for Isididae as well as on the continental shelf outside the expected depth range where predicted genus richness was very low (Figure 99).

3.4.2.5 Other families of gorgonian corals

Similar to family Isididae, gorgonian corals in family Chrysogorgiidae tend to be found on the continental slope. Records of Chrysogorgiidae presence in the presence-absence database (n = 185 samples) were located on the continental slope in the central Gulf of Mexico and along the west Florida slope near its maximum expected depth (Figure 100). In addition to these locations, Chrysogorgiidae presences in the NOAA National Database were also found in the western and northeastern Gulf of Mexico where there were no sample data in the presence-absence database (Figure 100). There were areas with very high predicted probability of occurrence for Chrysogorgiidae along the west Florida slope near its maximum expected depth, and these areas were generally surrounded by slightly shallower areas with low–high predicted probability of occurrence (Figure 101). In the central Gulf, there were some areas with medium and low predicted probability of occurrence on the continental slope (Figure 101). Model predictions for Chrysogorgiidae had relatively low variability within its expected depth range across the study area, including areas with higher predicted probability of occurrence and areas with very low predicted probability of occurrence (Figure 102). There were some areas with higher variability but very low predicted probability of occurrence outside the expected depth range for Chrysogorgiidae on the continental shelf and areas deeper than 2,500 m (Figure 102).

Acanthogorgiidae presences in the presence-absence database (n = 129 samples) were also found on the continental slope in the central and eastern Gulf but were shallower than observations of Chrysogorgiidae (Figure 103). Very high probability of occurrence for Acanthogorgiidae was predicted at an area on the southern part of the west Florida slope at its maximum expected depth (Figure 104). Other areas with very high predicted probability of occurrence for Acanthogorgiidae were adjacent to the environmental predictor mask and deeper than its expected depth range on the continental slope in the western Gulf (Figure 104). Although model predictions in these areas with very high predicted probability of occurrence had relatively low variability (Figure 105), caution should be taken in using the model predictions where there was higher predicted probability of occurrence in unsampled areas outside the expected depth range.

Records of Paragorgiidae presence in the presence-absence database were less common (n = 65 samples) but were again located on the continental shelf in the central and eastern Gulf (Figure 106). There were was a narrow band (too small to discern in the map page) with medium predicted probability of occurrence for Paragorgiidae near its maximum expected depth along the west Florida slope and slightly larger areas with low–medium predicted probability of occurrence farther south on the west Florida slope (Figure 107). There were also areas of low–medium predicted probability of occurrence on the edges of the environmental predictor mask on the continental slope in the western and northeastern Gulf (Figure 107). There were only very small (difficult to discern) patches of low predicted probability of occurrence on the continental slope in the central Gulf (Figure 107). Variability in model predictions for Paragorgiidae was relatively low within its expected depth range both where there was higher predicted probability of occurrence and where the predicted probability of occurrence was very low (Figure 108). Variability was slightly higher in some areas with very low predicted probability of occurrence for Paragorgiidae outside its expected depth range on the continental shelf and in areas deeper than 2,500 m (Figure 108). Although variability was relatively low in the areas predicted to have low–medium probability of occurrence on the edges of the environmental predictor mask (Figure 107), predictions in these unsampled areas should be used with some caution. Additional surveys in these areas would be beneficial for ground truthing the occupancy model predictions.

Observations of Gorgoniidae in the presence-absence database were also less common (n = 48 samples) but were found on the Texas-Louisiana continental shelf and the Mississippi-Alabama continental shelf rather than on the continental slope (Figure 109). Additional records of Gorgoniidae presence in the NOAA National Database spanned broader (and shallower) areas along the continental shelf, including on the west Florida shelf (Figure 109). Only a few very small patches of very high probability of occurrence were predicted for Gorgoniidae on the Texas-Louisiana continental shelf, while there were broader areas of low–medium predicted probability of occurrence on the Texas-Louisiana continental shelf and Mississippi-Alabama continental shelf (Figure 110). There was also a large area on the deepest edge of the study area in the central Gulf with low–high predicted probability of occurrence (Figure 110). The model predictions for this area should be considered unreliable as there were no sample data in this area, and it is far deeper than the maximum expected depth for Gorgoniidae. Model predictions for Gorgoniidae had relatively low variability where there was higher predicted probability of occurrence, but there were areas with higher variability within its expected depth range where there was very low predicted probability of occurrence on the shallower edge of the study area and on the west Florida slope (Figure 111).

Like Gorgoniidae, records of Keroeididae presence in the presence-absence database were less common (n = 48 samples) and were found at mesophotic depths at the edge of the Texas-Louisiana continental shelf and on the continental shelf off south Texas (Figure 112). Patchy areas with medium–high predicted probability of occurrence for Keroeididae surrounded by areas of low predicted probability of occurrence were found along the continental shelf off Texas and Louisiana (Figure 113). There was again an area on the deepest edge of the study area in the central Gulf where model predictions should be considered unreliable. The predicted probability of occurrence for this area was low–medium, but there were no sample data in this area, and it is far deeper than the maximum expected depth for Keroeididae (Figure 113). Variability in model predictions for Keroeididae was relatively low on the parts of the continental shelf in the western and central Gulf where there was higher predicted probability of occurrence, but there were areas with higher variability on the continental shelf in the eastern Gulf and near areas of the environmental predictor mask on the continental slope where the model predicted very low probability of occurrence (Figure 114).

Records of Spongiodermidae presence in the presence-absence database were uncommon (n = 39 samples) and concentrated on the edge of the Texas-Louisiana continental shelf, although there were some additional records in the NOAA National Database on the west Florida shelf (Figure 115). Spatial patterns in the predicted probability of occurrence for Spongiodermidae were similar to the patterns predicted for Keroeididae, with patchy areas of medium–high predicted probability of occurrence for Spongiodermidae surrounded by areas of low predicted probability of occurrence along the continental shelf off Texas and Louisiana (Figure 116). There was again an area on the deepest edge of the study area in the central Gulf where model predictions should be considered unreliable. The predicted probability of occurrence for this area ranged from low–medium, but there were no sample data in this area, and it is far deeper than the maximum expected depth for Spongiodermidae (Figure 116). Model predictions for Spongiodermidae had relatively low variability where it had higher predicted probability of occurrence on the continental shelf in the western and central Gulf, but similar to Keroeididae there were areas with higher variability on the continental shelf in the eastern Gulf where there was very low predicted probability of occurrence (Figure 117).

Observations of Coralliidae in the presence-absence database were also uncommon (n = 38 samples) but were found on the continental slope in the central Gulf and near its maximum expected depth on the west Florida slope (Figure 118). The predicted probability of occurrence for Coralliidae was very low across most of the study area, with only very small areas of medium and low predicted probability of occurrence on the southern part of the west Florida slope (Figure 119). Variability in model predictions for Coralliidae was relatively low in the areas where it was occasionally observed, even when predicted probability of occurrence was very low, and was highest within its expected depth range in the western and northeastern Gulf surrounding areas of the environmental predictor mask (Figure 120).

3.4.2.6 Multi-family model

Of the 12 families of gorgonian corals in order Alcyonacea that were selected for modeling, six are found at mesophotic depths (50–200 m), nine are found in the upper bathyal zone (200–1,000 m), and seven are found in the deeper waters (1,000–3,000 m) of the lower bathyal zone (Table 2). There were areas with the highest (>3) predicted family richness for gorgonian corals both at mesophotic depths across the Texas-Louisiana continental shelf and in deeper waters in a narrow band along the west Florida slope (Figure 121). Broad areas with relatively high (2–3) and medium (1–2) predicted family richness were found along much of the continental shelf and on the west Florida slope (Figure 121). There were fewer areas with medium predicted family richness on the continental slope in the western and central Gulf of

Mexico, but there were large patches of low (0.5–1) predicted family richness (Figure 121). Predictions of low–medium predicted family richness near or deeper than the maximum expected depth for the selected gorgonian coral families in the central and eastern Gulf (Figure 121) should be considered unreliable and in some cases may have been caused by artifacts in the seafloor topography predictor variables (e.g., from tracklines not sufficiently removed from the bathymetry synthesis) or by model extrapolation in unsampled areas. Variability in the predicted family richness for gorgonian corals was relatively low for most of their expected depth range, including where there was higher predicted family richness as well as areas with very low predicted family richness, but variability was slightly higher in areas around the environmental predictor mask and in deeper unsampled areas (Figure 122).

3.4.3 Black corals (order Antipatharia)

Observations of *Tanacetipathes* in the presence-absence database (n = 1,709 samples) were predominantly near the edge of the continental shelf (and close to or past its maximum expected depth) on the Texas-Louisiana continental shelf, but it was also found on the continental shelf off Texas, the Mississippi-Alabama continental shelf, and the west Florida shelf (Figure 123). There were large areas of very high predicted probability of occurrence for *Tanacetipathes* on the continental shelf off Texas, but there were only very small patches of medium–very high predicted probability of occurrence near the South Texas Banks where *Tanacetipathes* was observed in samples (Figure 124). There was also a continuous stretch of very high predicted probability of occurrence along much of the west Florida shelf (Figure 124), where there were limited samples in the presence-absence database but some records of *Tanacetipathes* presence in the NOAA National Database (Figure 123). This broad stretch of very high predicted probability of occurrence extended onto the west Florida slope well past the expected depth range for *Tanacetipathes* (Figure 124). In addition to near the South Texas Banks, smaller patches of medium–very high predicted probability of occurrence were found on the continental shelf off Louisiana and off northern Florida near the samples from the Mesophotic Pinnacles dataset where *Tanacetipathes* was observed (Figure 124). The areas with highest predicted probability of occurrence for *Tanacetipathes* had relatively low variability in model predictions, and variability was also relatively low throughout its expected depth range including areas with very low predicted probability of occurrence (Figure 125). Highest variability was in areas with very low predicted probability of occurrence deeper than the maximum expected depth for *Tanacetipathes*, including parts of the continental slope in the central Gulf of Mexico and a narrow band on the west Florida slope (Figure 125).

Like *Tanacetipathes*, records of *Stichopathes* occurrence in the presence-absence database (n = 1,288 samples) were located on the continental shelf across much of the study area (Figure 126). Although there were few sample data in the presence-absence database on the west Florida shelf, there were a number of *Stichopathes* presences in the NOAA National Database in this area as well as records (likely a different species) deeper than the expected range for *Stichopathes* on the west Florida slope (Figure 126). A wide band of very high predicted probability of occurrence for *Stichopathes* extended along the continental shelf from off south Texas to off Alabama (Figure 127). Areas of high–very high predicted probability of occurrence were patchier on the continental shelf off north Florida and transitioned to areas of low–medium predicted probability of occurrence farther south on the west Florida shelf (Figure 127). Variability in model predictions for *Stichopathes* was relatively low along the continental shelf and throughout its expected depth range both in areas with higher predicted probability of occurrence and very low predicted probability of occurrence (Figure 128). Variability was higher in areas with very low predicted probability of occurrence deeper than the maximum expected depth for *Stichopathes* and was highest along the edge of the west Florida slope (Figure 128). Interestingly, this narrow band of higher variability on the west Florida slope coincided with records of *Stichopathes* presence in the NOAA National Database (Figure 126).

Records identified as genus *Antipathes* or as *A. atlantica* or *A. furcata* in the presence-absence database (n = 1,231 samples) were also found on the continental shelf across much of the study area (Figure 129). Additional records of *Antipathes* presence in the NOAA National Database were in areas where no samples existed in the presence-absence database, including on the west Florida shelf (Figure 129). Similar to *Stichopathes*, there large bands of very high predicted probability of occurrence for *Antipathes* along the continental shelf (Figure 130). Predicted probability of occurrence appeared to decrease (i.e., transitioning from very high to high, high to medium, medium to low) with increasing depth on the continental shelf (Figure 130). Model predictions for *Antipathes* had relative low variability within its expected depth range on the continental shelf where there was highest predicted probability of occurrence (Figure 131). Highest variability was in areas with very low predicted probability of occurrence deeper than the maximum expected depth for *Antipathes*, including parts of the continental slope in the central Gulf and a narrow band on the west Florida slope (Figure 131). Records of *A. atlantica* presence in the presence-absence database (n = 531 samples) were also found along much of the continental shelf but were less numerous in the central Gulf because these samples either had records of *A. furcata* or records identified only to the genus level (Figure 132). While there were again areas of very high predicted probability of occurrence for *A. atlantica* along the continental shelf, these areas were less extensive compared to the genus level model for *Antipathes*, especially on the Texas-Louisiana continental shelf (Figure 133). Variability in the model predictions for *A. atlantica* was relatively low in the areas with very high predicted probability of occurrence, but there were some areas of higher variability on the continental shelf within the expected depth range for *A. atlantica* where the predicted probability of occurrence was very low (Figure 134). There was also considerably higher variability in areas with very low predicted probability of occurrence almost everywhere deeper than the maximum expected depth for *A. atlantica* (Figure 134).

Leiopathes presences in the presence-absence database (n = 244 samples) were located on the continental slope in the central and eastern Gulf (Figure 135). Large areas with very high predicted probability of occurrence for *Leiopathes* were found on the continental slope off Mississippi and Alabama and on the west Florida slope (Figure 136). There were also patches of very high predicted probability of occurrence on the edge of the continental shelf and upper continental slope off eastern Louisiana and areas with low–medium predicted probability of occurrence on the edge of the continental shelf and upper continental slope off Texas (Figure 136). Model predictions for *Leiopathes* had relatively low variability on the continental slope where there was higher predicted probability of occurrence and where there was very low predicted probability of occurrence, but variability was considerably higher in a few spots on the continental slope in the central Gulf and deeper than the maximum expected depth for *Leiopathes* where the predicted probability of occurrence was very low (Figure 137).

Records of *Bathypathes* occurrence in the presence-absence database (n = 114 samples) were generally found in deeper waters than *Leiopathes* on the continental slope in the central and eastern Gulf (Figure 138). A wide band of very high predicted probability of occurrence for *Bathypathes* extended along the west Florida slope (Figure 139). Narrower bands of low–high predicted probability of occurrence were found higher up the slope in this area, particularly the northern part of the west Florida slope (Figure 139). In the central Gulf, there were patchy areas of low–high predicted probability of occurrence on the continental slope off Louisiana and over to De Soto Canyon (Figure 139). Variability in model predictions for *Bathypathes* was relatively low where it was observed and predicted to have higher probability of occurrence within its expected depth range in the central and eastern Gulf (Figure 140). There was considerably higher variability in model predictions for *Bathypathes* within its expected depth range in the western Gulf and just deeper than the environmental predictor mask offshore of Louisiana, where there was very low predicted probability of occurrence (Figure 140). Variability was also considerably higher outside the expected depth range for *Bathypathes* where the predicted probability of occurrence was also very low (Figure 140).

Observations of *Stauropathes* in the presence-absence database were rare (n = 13 samples) and located on the west Florida slope (Figure 141). Very high probability of occurrence for *Stauropathes* was predicted along a band of varying width between 1,000–3,000 m depth on the west Florida slope (Figure 142). Predictions of low–high probability of occurrence in unsampled areas on the Florida Plain at >3,000 m depth should be used with some caution, as should predictions of low–medium probability of occurrence on the west Florida shelf and west Florida slope shallower than the minimum expected depth for *Stauropathes* (Figure 142). Model predictions for *Stauropathes* had relatively low variability on the west Florida slope where there was very high predicted probability of occurrence and much higher variability across much of the study area where the predicted probability of occurrence was very low (Figure 143).

Plumapathes presences in the presence-absence database were also rare (n = 9 samples) and were found at relatively shallow depths on the Texas-Louisiana continental shelf (Figure 144). There were some small patches of high–very high predicted probability of occurrence for Plumapathes on the Texas-Louisiana continental shelf, as well some small patches at similar depths on the Mississippi-Alabama continental shelf and west Florida shelf with low–medium predicted probability of occurrence (Figure 145). Predictions of low–medium probability of occurrence on the deepest edge of the study area in the central Gulf (Figure 145) should be considered unreliable as this area is unsampled and far outside the expected depth range for *Plumapathes*. Variability in model predictions for *Plumapathes* was relatively low in the small areas where predicted probability of occurrence was higher but was considerably higher across much of the study area where there was very low predicted probability of occurrence (Figure 146). The areas with higher variability included parts of the continental shelf within the expected depth range for *Plumapathes* (Figure 146).

Records in the presence-absence database for black corals in family Aphanipathidae were only identified to the family level. Observations of Aphanipathidae were numerous (n = 2,319 samples) but generally concentrated on the Texas-Louisiana continental shelf, with records in a few locations on the west Florida shelf and upper west Florida slope (Figure 147). Additional Aphanipathidae presences in the NOAA National Database were located in these areas as well (Figure 147). Very high probability of occurrence was predicted for areas on the continental shelf off south Texas where Aphanipathidae was not recorded in the presence-absence database, on the Texas-Louisiana continental shelf, and on the west Florida shelf where there were no samples in the presence-absence database but there were Aphanipathidae presences in the NOAA National Database (Figure 148). Model predictions for Aphanipathidae had low variability on the continental shelf where there was very high predicted probability of occurrence, but variability was considerably higher where there was very low predicted probability of occurrence on the continental shelf off eastern Louisiana, Mississippi, and Alabama and outside the expected depth range for Aphanipathidae (Figure 149).

The seven genera of black corals in order Antipatharia selected for modeling included five that are found at mesophotic depths (50–200 m), four that occur in the upper bathyal zone (200–1,000 m), and only two found deeper (1,000–3,000 m) in the lower bathyal zone (Table 2). Because most of the genera of black corals included in the multi-genus model were known to occur at mesophotic depths, it was not surprising that areas with higher (>2) predicted genus richness for black corals were primarily on the continental shelf, although there were also some areas with higher predicted genus richness on the west Florida slope (Figure 150). There were also wide swaths with low (0.25–1) to medium (1–2) predicted genus richness along the continental shelf and the west Florida slope (Figure 150). Predictions of low genus richness on the Florida Plain at >3,000 m depth were likely caused by the inclusion of *Stauropathes* and should be used with caution in this unsampled and poorly known area (Figure 150). Variability in the predicted genus richness for black corals was relatively low on the continental shelf where there was generally higher predicted genus richness, but there were areas with considerably higher variability on the continental slope in the central and western Gulf where there was very low predicted genus richness (Figure 151).

3.4.4 Chemosynthetic communities

As stated previously, the intent of this study was to compile observations and model distributions of both DSCs and chemosynthetic communities. However, challenges with the data available for characterizing distributions of chemosynthetic communities limited the performance of the chemosynthetic community models. First, chemosynthetic communities could only be recorded to category rather than taxon in the presence-absence database compiled as part of this study. In addition, key environmental predictor variables needed to inform models of chemosynthetic community occurrence (e.g., presence of carbonates, backscatter, surface oil slicks) were not readily available for the entire study area and thus were not included. As a result, the primary focus was on DSCs in the selection of environmental predictor variables. Although information on the spatial distributions of chemosynthetic communities is presented in this report and associated data products, the presence-absence records and model predictions for chemosynthetic communities should be considered preliminary.

Records of bivalve presence (n = 775 samples) were widespread throughout the central Gulf and less common in the western and eastern Gulf of Mexico (Figure 152). There were large areas of very high predicted probability of occurrence for bivalves on the continental slope as well as areas on the abyssal plain far deeper than the sample locations (Figure 153). Variability in the predicted probability of occurrence for bivalves was highest on the continental shelf where the predicted probability of occurrence was very low, but variability was relatively low in the areas with highest predicted probability of occurrence (Figure 154).

Bacterial mats were only observed (n = 174 samples) on the continental slope in the central Gulf (Figure 155). Areas with very high predicted probability of occurrence were found near the observations of bacterial mats in the central Gulf and on the edge of the study area in the northeastern Gulf (Figure 156). Model predictions for bacterial mats had relatively low variability in the central Gulf where there were areas of high predicted probability of occurrence, but there was higher variability on the continental shelf and on the abyssal plain in the deepest part of the study area where the predicted probability of occurrence was very low (Figure 157).

Records identified as brine (n = 167 samples) were also primarily in the central Gulf (Figure 158). Areas with high and very high predicted probability of occurrence were found in the western Gulf in an area where there were few samples, although there were also patchy areas with medium–high predicted probability of occurrence in the central Gulf closer to the sample locations where brine was observed surrounded by broader areas with low predicted probability of occurrence (Figure 159). The areas with the highest variability in model predictions for brine were in the eastern Gulf on the shallow edge of the study area where there was very low predicted probability of occurrence, and there was relatively low variability where there was higher predicted probability of occurrence (Figure 160).

3.5 Predicted genus richness by depth zone

The 28 genera of structure-forming DSCs selected for multi-taxon and single-taxon occupancy models included 22 that occur at mesophotic depths (50–200 m), 19 found in the upper bathyal zone (200–1,000 m), and seven found deeper in the lower bathyal zone (1,000–3,000 m). As would be expected with most of the genera occurring at mesophotic depths, areas with the highest (>9) cumulative predicted genus richness in the study area were found exclusively at mesophotic depths in the Western Planning Area and Central Planning Area (Figure 161). There were also extensive areas in the mesophotic zone predicted to have medium (3–5) or high (5–9) genus richness across all three planning areas, although the proportion of high predicted genus richness was lower in the Eastern Planning Area where there were fewer samples (Figure 161). The mean predicted genus richness for grid cells in the mesophotic zone was highest in the Central Planning Area, where *Thesea*, *Callogorgia*, and *Stichopathes* had the highest mean predicted probability of occurrence (Table 8). *Bebryce*, *Stichopathes*, and *Muricea* had the highest mean predicted probability of occurrence in the mesophotic zone in the Western Planning Area (Table 8). In the Eastern Planning Area, which had the lowest mean predicted genus richness for grid cells in the mesophotic zone, *Antipathes* and *Tanacetipathes* had the highest mean predicted probability of occurrence at mesophotic depths (Table 8).

Predicted genus richness was generally very low (0–1) to low (1–3) across the upper bathyal depth zone in the Western Planning Area and Central Planning Area, but in the Eastern Planning Area the upper bathyal zone had some areas with medium predicted genus richness and was predominantly predicted to have low genus richness (Figure 161). The mean predicted genus richness for grid cells in the upper bathyal zone was highest in the Eastern Planning Area, where *Lophelia*, *Chelidonisis*, and *Leiopathes* had the highest mean predicted probability of occurrence (Table 8). *Callogorgia*, *Leiopathes*, and *Paramuricea* had the highest mean predicted probability of occurrence in the upper bathyal zone in the Central Planning Area (Table 8). The Western Planning Area had the lowest mean predicted genus richness for grid cells in the upper bathyal zone, and *Lophelia*, *Callogorgia*, and *Leiopathes* had the highest mean predicted probability of occurrence at upper bathyal depths in this planning area, although at considerably lower probabilities than in the Eastern Planning Area (Table 8).

Similar to the upper bathyal zone, predicted genus richness in the lower bathyal zone was low–medium in the Eastern Planning Area but was generally very low with smaller areas of low predicted genus richness in the Western Planning Area and Central Planning Area (Figure 161). The mean predicted genus richness for grid cells in the lower bathyal zone was highest in the Eastern Planning Area, where *Bathypathes*, *Stauropathes*, *Paramuricea*, and *Lepidisis* had the highest mean predicted probability of occurrence (Table 8). *Lepidisis*, *Stauropathes*, and *Paramuricea* had the highest mean predicted probability of occurrence in the lower bathyal zone in the Central Planning Area (Table 8). The Western Planning Area had the lowest mean predicted genus richness for grid cells in the lower bathyal zone, with *Lepidisis*, *Lophelia*, and *Chelidonisis* having the highest mean predicted probability of occurrence at lower bathyal depths in this planning area, although at low probabilities (Table 8).

3.6 Predictor effects

As stated previously, the global occupancy models included 10 environmental predictor variables (Table 3) represented by 20 predictor terms comprising both linear and quadratic terms to allow for nonlinear relationships. Predictor effects are summarized for the multi-taxon models for orders Scleractinia (Figure 162), Alcyonacea (Figure 163), and Antipatharia (Figure 164) to identify the environmental predictor variables with significant effects in each model. The multi-taxon models maintained heterogeneity in taxon-specific predictor effects, despite their being drawn from a common distribution. For example, the effect of the quadratic depth term was positive for the most frequently observed genus of stony coral, *Madracis*, and negative for the least frequently observed, *Enallopsammia* (Figure 162). This demonstrated the ability to include genera that partition habitats (e.g., by depth) and do not co-occur in multi-taxon models.

The environmental predictor variables with predictor terms that most frequently had significant effects (i.e., the credible interval did not contain zero) across the models were identified as the most important environmental predictor variables. Not surprisingly, depth was the most important environmental predictor across the DSC taxa selected for modeling (Figures 162–164). Many of the taxa are generally confined to specific depth ranges (Tables 2; Etnoyer and Cairns 2017), and depth can act as a proxy for other measures (e.g., temperature, salinity) that may directly influence the distributions of DSCs (Wiltshire et al. 2018). Longitude was the second most important environmental predictor variable (Figures 162–164), suggesting that the DSC taxa modeled may have geographically restricted distributions while only more cosmopolitan taxa spanned the entire study area. This pattern with respect to longitude could, however, also reflect sampling bias in the presence-absence database (e.g., that there were far fewer samples at mesophotic depths in the eastern Gulf). Annual mean surface chlorophyll concentration was the third most important predictor variable (Figures 162–164), representing ocean surface productivity that inevitably impacts the seafloor through subsequent processes such as marine snow. Seafloor slope and general curvature ranked next in importance, along with annual mean bottom dissolved oxygen, which was less important for taxa in order Scleractinia than it was for taxa in orders Alcyonacea and Antipatharia (Figures 162–164). Annual mean speed of bottom ocean currents, a predictor variable not included in the previous regional models of DSC occurrence (Kinlan et al. 2013), had a significant negative effect for family Isididae (Figure 163). Surficial sediment percent sand and mean grain size were not particularly important predictors in the models. As described in Section 2.5.3, the surficial sediment variables were interpolated from grab sample data and may not be able to resolve the small, patchy hard features that are important for the attachment of DSCs. East-west aspect and north-south aspect were the least important predictor variables, but still accounted for enough variability to warrant inclusion in the models. Although the environmental predictor variables with significant effects in the models of chemosynthetic communities were similar to those in the models for DSCs, it is important to note that this finding may be different if a more ecologically relevant set of environmental predictor variables were used for the models of chemosynthetic communities.

In addition to the predictor effect size plots, marginal effects plots are presented for the two most frequently observed genera of branching stony corals in order Scleractinia (Figure 165, Figure 166). Although care must be taken when making inferences about the ecological drivers of DSC and chemosynthetic community occurrence from the models presented in this report, marginal effects plots are sometimes used to examine the relationships between predicted occurrence and each individual environmental predictor variable. These plots depict how the predicted probability of occurrence varies across the range of environmental predictor values while holding each of the other environmental predictors at its mean value at the sample locations. For example, *Lophelia pertusa* was most likely to occur in the upper bathyal depth zone within the study area and within its expected depth range of 300–900 m (Figure 166).

Table 5. Model goodness-of-fit based on Bayesian p-values for three fit statistics

Model	Fit Statistic					
	Chi-squared (site level)	**Chi-squared (taxon level)**	**Pearson's (site level)**	**Pearson's (taxon level)**	**Freeman-Tukey (site level)**	**Freeman-Tukey (taxon level)**
Multi-genus model of branching stony corals in order Scleractinia	0.195	0.193	0.041	0.095	0.584	0.211
Single-taxon model of family Oculinidae	0.147	N/A	0.025	N/A	0.682	N/A
Multi-family model of gorgonian corals in order Alcyonacea	0.079	0.012	0.001	0.002	0.359	0.014
Multi-genus model of family Plexauridae	0.016	0.001	0.001	0.000	0.016	0.001
Single-taxon model of *Swiftia exserta*	0.366	N/A	0.328	N/A	0.788	N/A
Single-taxon model of *Muricea pendula*	0.127	N/A	0.066	N/A	0.055	N/A
Single-taxon model of *Paramuricea biscaya*	0.172	N/A	0.138	N/A	0.292	N/A
Single-taxon model of genus *Nicella*	0.117	N/A	0.108	N/A	0.349	N/A
Single-taxon model of genus *Callogorgia*	0.279	N/A	0.105	N/A	0.541	N/A
Multi-genus model of family Isididae	0.250	0.516	0.211	0.450	0.344	0.527
Multi-genus model of black corals in order Antipatharia	0.030	0.018	0.001	0.014	0.055	0.023
Single-taxon model of *Antipathes atlantica*	0.278	N/A	0.170	N/A	0.679	N/A
Single-taxon model of family Aphanipathidae	0.255	N/A	0.167	N/A	0.207	N/A
Single-taxon model of bivalves	0.580	N/A	0.470	N/A	0.380	N/A
Single-taxon model of bacterial mats	0.778	N/A	0.636	N/A	0.561	N/A
Single-taxon model of brine	0.653	N/A	0.674	N/A	0.479	N/A

Table 6. Model fit for each taxon based on the point-biserial correlation (r_{pb}) and AUC

Taxon	r_{pb}		AUC	
	z_{ik}	Ψ_k	z_{ik}	Ψ_k
Madracis	0.44	0.09	0.97	0.89
Lophelia pertusa	0.76	0.42	1.00	0.97
Madrepora	0.60	0.24	1.00	0.92
Solenosmilia	0.41	0.06	0.99	0.92
Enallopsammia	0.27	0.14	0.99	0.96
Oculinidae	0.58	0.23	0.97	0.91
Plexauridae	0.67	0.16	0.93	0.59
Bebryce	0.64	0.27	0.97	0.87
Swiftia	0.61	0.12	0.98	0.83
Swiftia exserta	0.69	0.27	0.99	0.96
Paramuricea	0.62	0.29	0.97	0.81
Paramuricea biscaya	0.54	0.23	0.98	0.84
Caliacis	0.43	0.09	0.97	0.89
Muricea	0.36	0.15	0.95	0.85
Muricea pendula	0.42	0.16	0.96	0.86
Scleracis	0.42	0.08	0.97	0.91
Thesea	0.36	0.23	0.95	0.86
Placogorgia	0.30	0.01	0.98	0.91
Villogorgia	0.93	0.87	1.00	1.00
Ellisellidae	0.71	0.29	0.96	0.89
Nicella	0.79	0.60	0.98	0.94
Primnoidae	0.58	0.22	0.97	0.80
Callogorgia	0.61	0.23	0.97	0.86
Isididae	0.62	0.40	0.98	0.88
Lepidisis	0.52	0.20	0.99	0.95
Keratoisis	0.48	0.29	0.99	0.95
Chelidonisis	0.46	0.20	1.00	0.95
Acanella	0.52	0.26	1.00	0.99
Chrysogorgiidae	0.56	0.39	0.99	0.94
Acanthogorgiidae	0.74	0.50	1.00	0.96
Paragorgiidae	0.33	0.08	0.99	0.82
Gorgoniidae	0.52	0.31	0.99	0.91
Keroeididae	0.18	0.05	0.96	0.86
Spongiodermidae	0.15	0.01	0.98	0.87
Coralliidae	0.44	0.26	0.99	0.93
Tanacetipathes	0.55	0.37	0.95	0.91
Stichopathes	0.66	0.58	0.97	0.93

Taxon	**r_{pb}**		**AUC**	
Antipathes	0.58	0.44	0.96	0.89
Antipathes atlantica	0.70	0.51	0.99	0.98
Leiopathes	0.69	0.38	0.99	0.97
Bathypathes	0.48	0.30	0.99	0.96
Stauropathes	0.23	0.10	0.99	0.97
Plumapathes	0.55	0.19	1.00	0.99
Aphanipathidae	0.82	0.56	0.99	0.94
Bivalves	0.62	0.20	0.96	0.85
Bacterial Mats	0.87	0.57	1.00	0.98
Brine	0.49	0.11	0.99	0.91

Table 7. Model predictive performance for training and test data based on the point-biserial correlation (r_{pb}) and AUC

Taxon	Samples				r_{pb}			AUC		
	Training		Test		Training		Test	Training		Test
	Presence	Absence	Presence	Absence	z_{ik}	Ψ_k	Ψ_k	z_{ik}	Ψ_k	Ψ_k
Madracis	280	12,630	146	10,663	0.50	0.15	0.03	0.97	0.92	0.75
Lophelia pertusa	246	12,664	81	10,728	0.75	0.42	0.06	0.99	0.96	0.76
Madrepora	69	12,841	28	10,781	0.52	0.17	0.01	0.99	0.92	0.82
Solenosmilia	18	12,892	8	10,801	0.46	0.06	0.02	0.99	0.91	0.75
Enallopsammia	12	12,898	6	10,803	0.24	0.12	0.01	0.99	0.94	0.92
Oculinidae	442	16,525	280	6,472	0.59	0.28	0.18	0.98	0.95	0.83
Plexauridae	2,889	13,843	1,584	5,403	0.70	0.12	0.20	0.94	0.50	0.70
Bebryce	846	16,249	205	6,419	0.66	0.27	0.21	0.98	0.91	0.75
Swiftia	565	16,530	48	6,576	0.63	0.16	0.01	0.98	0.90	0.53
Swiftia exserta	535	14,968	52	8,164	---	---	---	---	---	---
Paramuricea	468	16,627	101	6,523	0.62	0.33	0.16	0.97	0.82	0.83
Paramuricea biscaya	253	14,614	94	8,758	---	---	---	---	---	---
Caliacis	253	16,842	225	6,399	0.48	0.16	0.01	0.98	0.96	0.61
Muricea	277	16,818	159	6,465	0.35	0.12	0.07	0.96	0.91	0.65
Muricea pendula	309	15,604	127	7,679	---	---	---	---	---	---
Scleracis	237	16,858	131	6,493	0.43	0.12	0.00	0.98	0.96	0.68
Thesea	112	16.983	112	6,512	0.36	0.34	0.11	0.96	0.93	0.56
Placogorgia	184	16,911	15	6,609	0.32	0.02	0.00	0.97	0.94	0.56
Villogorgia	12	17,083	10	6,614	0.88	0.80	0.58	1.00	1.00	0.97
Ellisellidae	1,884	14,848	1,359	5,628	0.67	0.26	0.22	0.95	0.88	0.84
Nicella	1,459	14,409	1,162	6,689	---	---	---	---	---	---
Primnoidae	386	16,346	445	6,542	0.55	0.32	0.13	0.97	0.86	0.73
Callogorgia	544	17,859	249	5,067	0.64	0.23	0.25	0.98	0.90	0.76
Isididae	322	16,410	243	6,744	0.61	0.36	0.35	0.98	0.83	0.85

Taxon	**Samples**				**r_{pb}**			**AUC**		
	Training		**Test**		**Training**		**Test**	**Training**		**Test**
	Presence	**Absence**	**Presence**	**Absence**	z_{ik}	Ψ_k	Ψ_k	z_{ik}	Ψ_k	Ψ_k
Lepidisis	15	17,543	20	6,141	0.34	0.06	0.14	0.99	0.95	0.84
Keratoisis	20	17,538	6	6,155	0.47	0.33	0.13	0.99	0.92	0.97
Chelidonisis	7	17,551	2	6,159	0.54	0.28	0.00	1.00	0.94	0.81
Acanella	6	17,552	2	6,159	0.51	0.20	0.26	1.00	0.99	0.93
Chrysogorgiidae	107	16,625	78	6,909	0.56	0.33	0.35	0.98	0.90	0.94
Acanthogorgiidae	41	16,691	88	6,899	0.62	0.15	0.41	1.00	0.87	0.95
Paragorgiidae	26	16,706	39	6,948	0.42	0.14	0.01	0.99	0.88	0.60
Gorgoniidae	36	16,696	12	6,975	0.60	0.29	0.11	0.99	0.91	0.76
Keroeididae	22	16,710	26	6,961	0.26	0.10	0.00	0.98	0.90	0.59
Spongiodermidae	31	16,701	8	6,979	0.16	0.01	0.00	0.98	0.87	0.72
Coralliidae	22	16,710	16	6,971	0.54	0.28	0.09	1.00	0.95	0.86
Tanacetipathes	1,468	15,421	241	6,589	0.55	0.37	0.44	0.94	0.90	0.94
Stichopathes	1,034	15,855	254	6,576	0.63	0.60	0.45	0.96	0.91	0.96
Antipathes	1,035	15,854	196	6,634	0.58	0.45	0.38	0.95	0.88	0.92
Antipathes atlantica	411	16,743	120	6,445	---	---	---	---	---	---
Leiopathes	180	16,709	64	6,766	0.72	0.43	0.13	1.00	0.97	0.93
Bathypathes	90	16,799	24	6,806	0.51	0.33	0.14	0.99	0.96	0.94
Stauropathes	9	16,880	4	6,826	0.08	0.03	0.10	0.99	0.98	0.83
Plumapathes	7	16,882	2	6,828	0.41	0.33	0.00	1.00	1.00	0.65
Aphanipathidae	1,200	15,088	1,119	6,312	0.83	0.68	0.44	0.99	0.97	0.87
Bivalves	532	14,467	243	8,477	---	---	---	---	---	---
Bacterial Mats	126	15,787	48	7,758	0.87	0.49	0.23	1.00	0.98	0.98
Brine	114	16,367	53	7,185	---	---	---	---	---	---

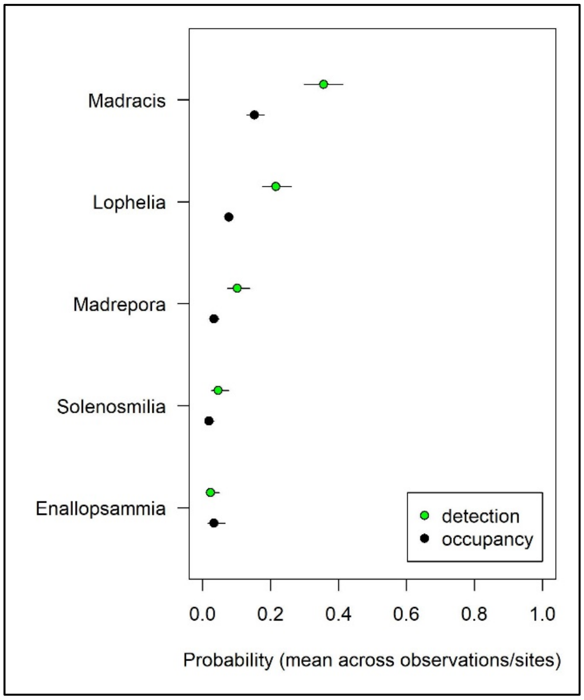

Figure 7. Mean probability of detection and occupancy for genera of branching stony corals.

Genera of stony corals (order Scleractinia) are shown in decreasing order of frequency (i.e., number of samples where observed) on the y-axis. The x-axis is on the probability scale (0–1). In green are the posterior mean (point) and 95% credible interval (lines) for genus-specific detection probability averaged across sites and occasions (p_k). In black are the posterior mean (points) and 95% credible interval (lines) for occupancy probability averaged across sites (ψ_k).

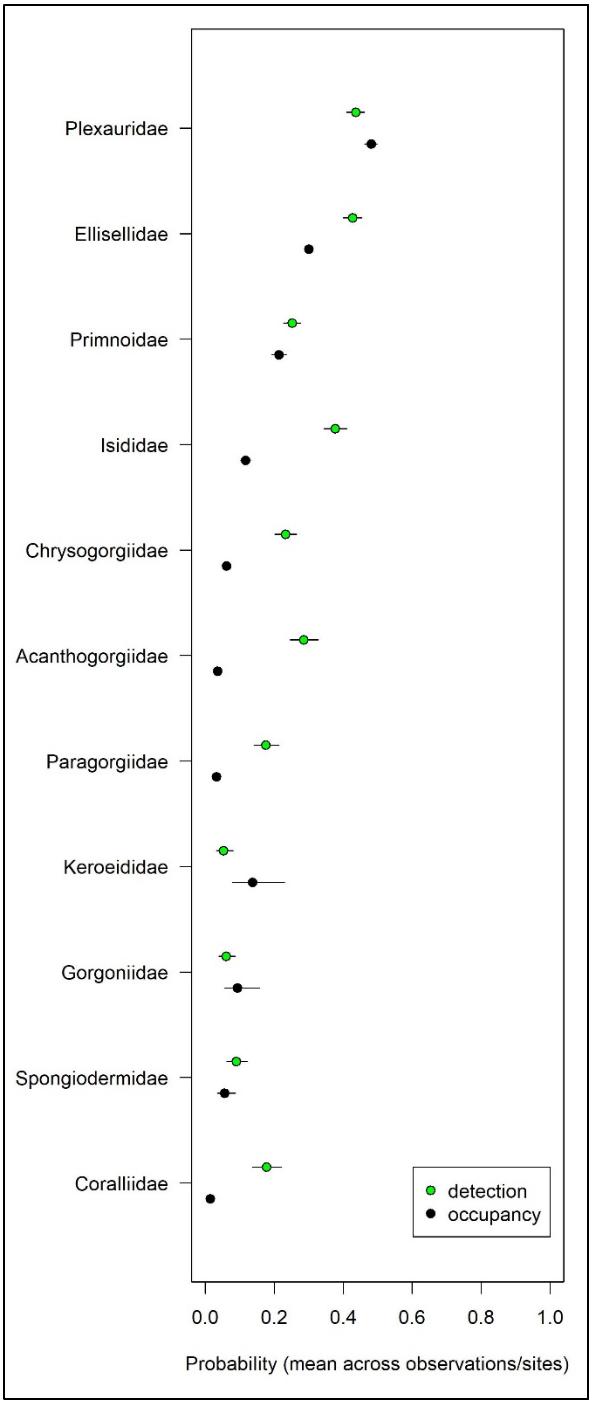

Figure 8. Mean probability of detection and occupancy for families of gorgonian corals.

Families of gorgonian corals (order Alcyonacea) are shown in decreasing order of frequency (i.e., number of samples where observed) on the y-axis. The x-axis is on the probability scale (0–1). In green are the posterior mean (point) and 95% credible interval (lines) for family-specific detection probability averaged across sites and occasions (p_k). In black are the posterior mean (points) and 95% credible interval (lines) for occupancy probability averaged across sites (ψ_k).

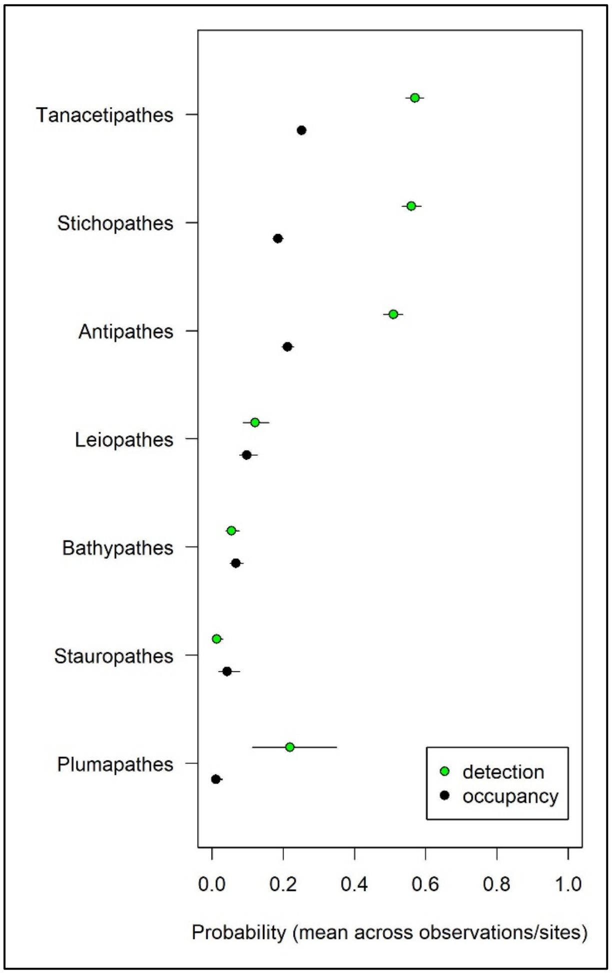

Figure 9. Mean probability of detection and occupancy for genera of black corals.

Genera of black corals (order Antipatharia) are shown in decreasing order of frequency (i.e., number of samples where observed) on the y-axis. The x-axis is on the probability scale (0–1). In green are the posterior mean (point) and 95% credible interval (lines) for genus-specific detection probability averaged across sites and occasions (p_k). In black are the posterior mean (points) and 95% credible interval (lines) for occupancy probability averaged across sites (ψ_k).

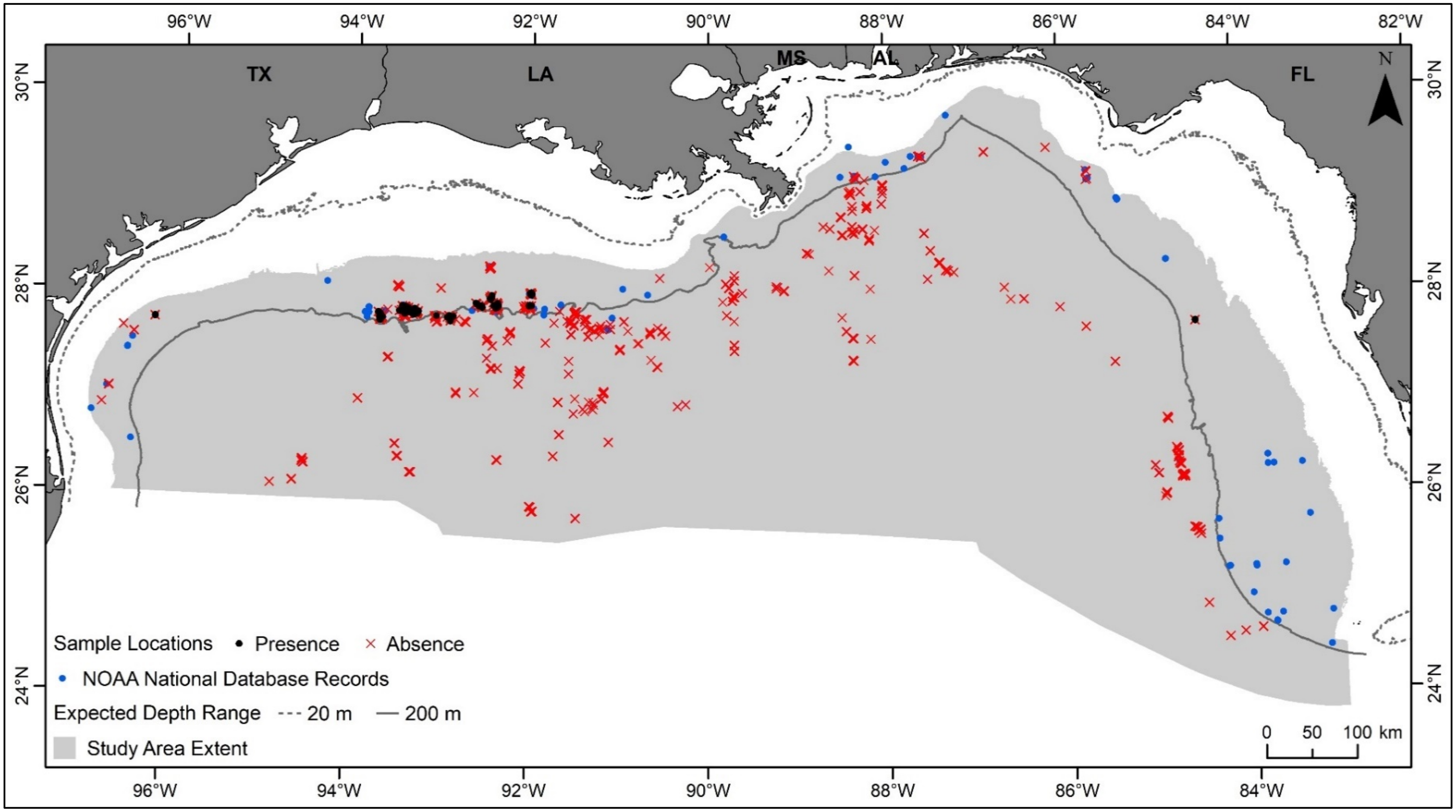

Figure 10. Occurrence records for the branching stony coral *Madracis* (order Scleractinia).

This map shows the observed occurrence (presence-absence) of *Madracis* at sample locations in the presence-absence database compiled for this study. Additional records of occurrence in the NOAA National Database are also displayed. Gray lines denote the expected depth range for *Madracis*.

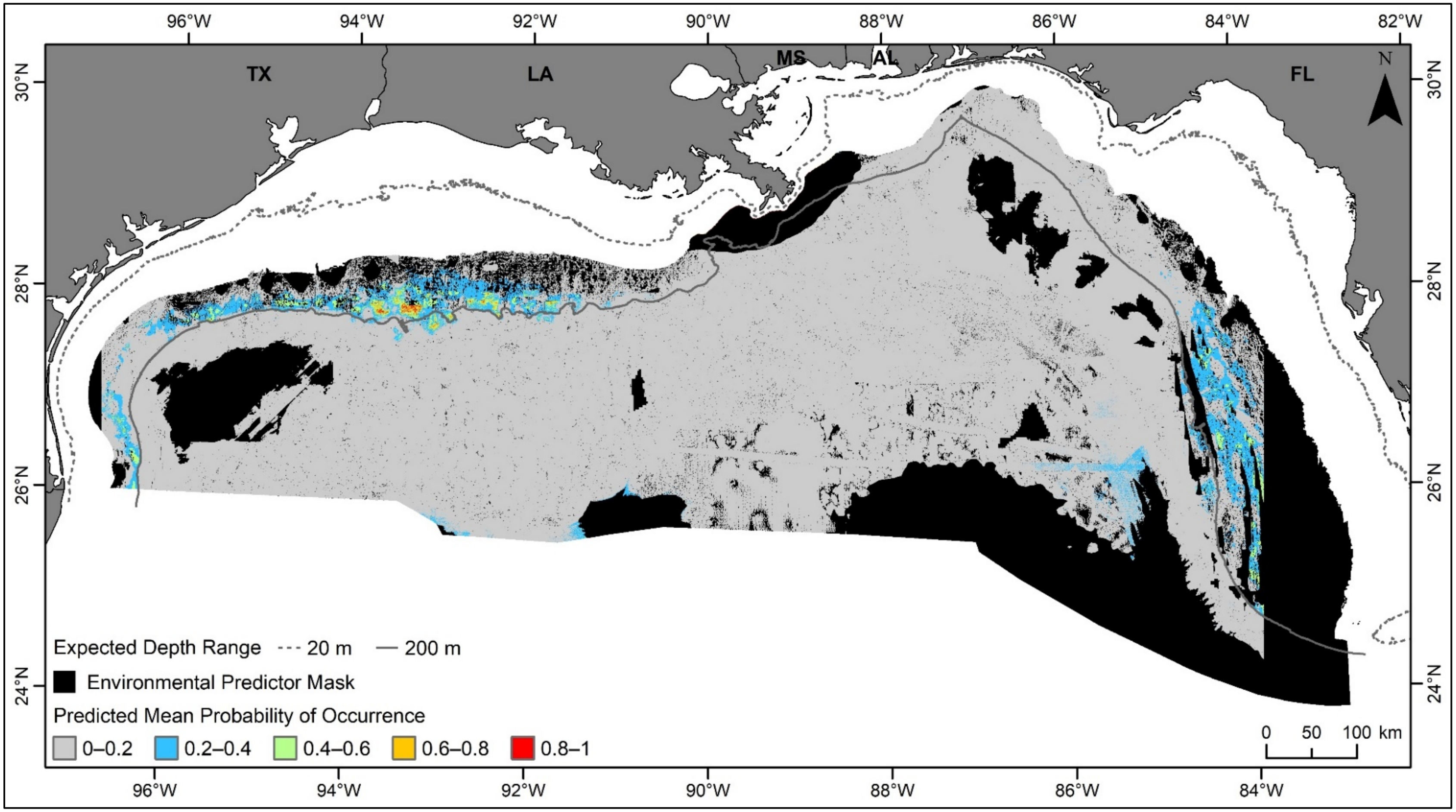

Figure 11. Predicted occurrence of the branching stony coral *Madracis* (order Scleractinia).

This map shows the predicted mean probability of occurrence (i.e., the predicted posterior mean occupancy probability) for *Madracis* from the multi-genus occupancy model of order Scleractinia. The environmental predictor mask overlays areas where predictor values were outside the range of values at the sample locations and model predictions may be affected by extrapolation. Gray lines denote the expected depth range for *Madracis*.

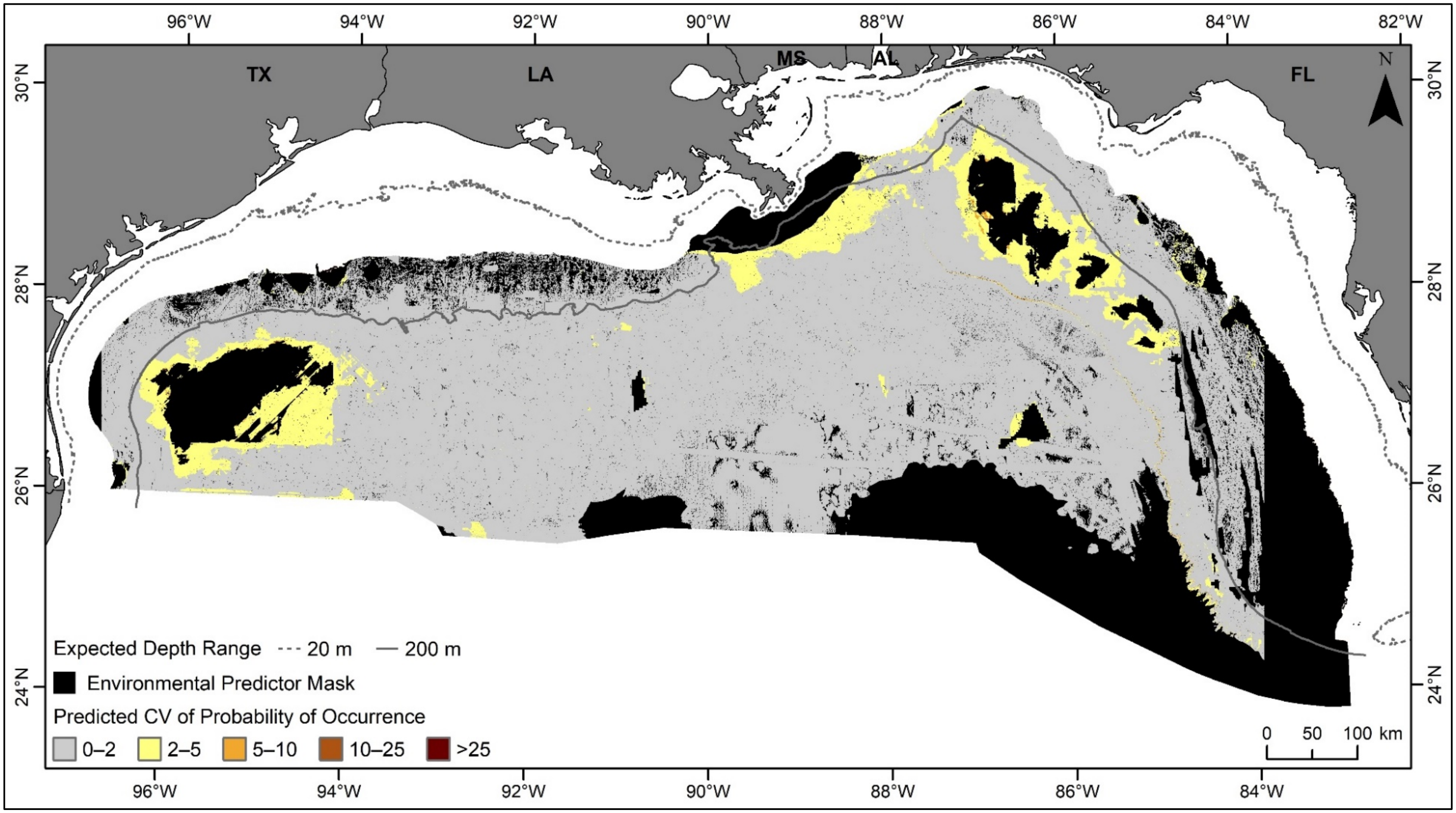

Figure 12. Variability in the predicted occurrence of the branching stony coral *Madracis* (order Scleractinia).

This map shows the predicted coefficient of variation (CV) of the probability of occurrence (i.e., the predicted posterior CV of occupancy probability) for *Madracis* from the multi-genus occupancy model of order Scleractinia. The environmental predictor mask overlays areas where predictor values were outside the range of values at the sample locations and model predictions may be affected by extrapolation. Gray lines denote the expected depth range for *Madracis*.

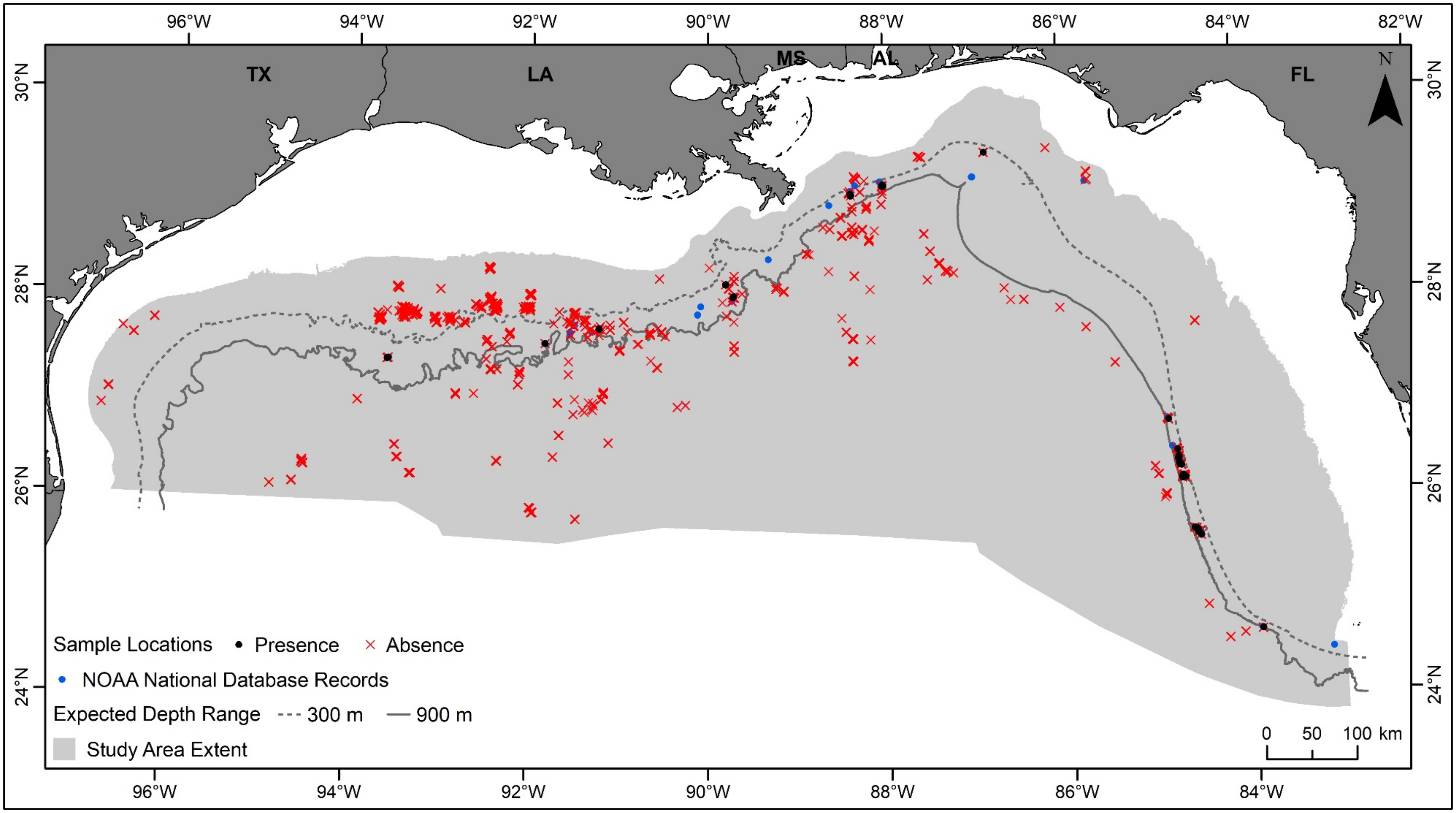

Figure 13. Occurrence records for the branching stony coral *Lophelia pertusa* (order Scleractinia).

This map shows the observed occurrence (presence-absence) of *L. pertusa* at sample locations in the presence-absence database compiled for this study. Additional records of occurrence in the NOAA National Database are also displayed. Gray lines denote the expected depth range for *L. pertusa*.

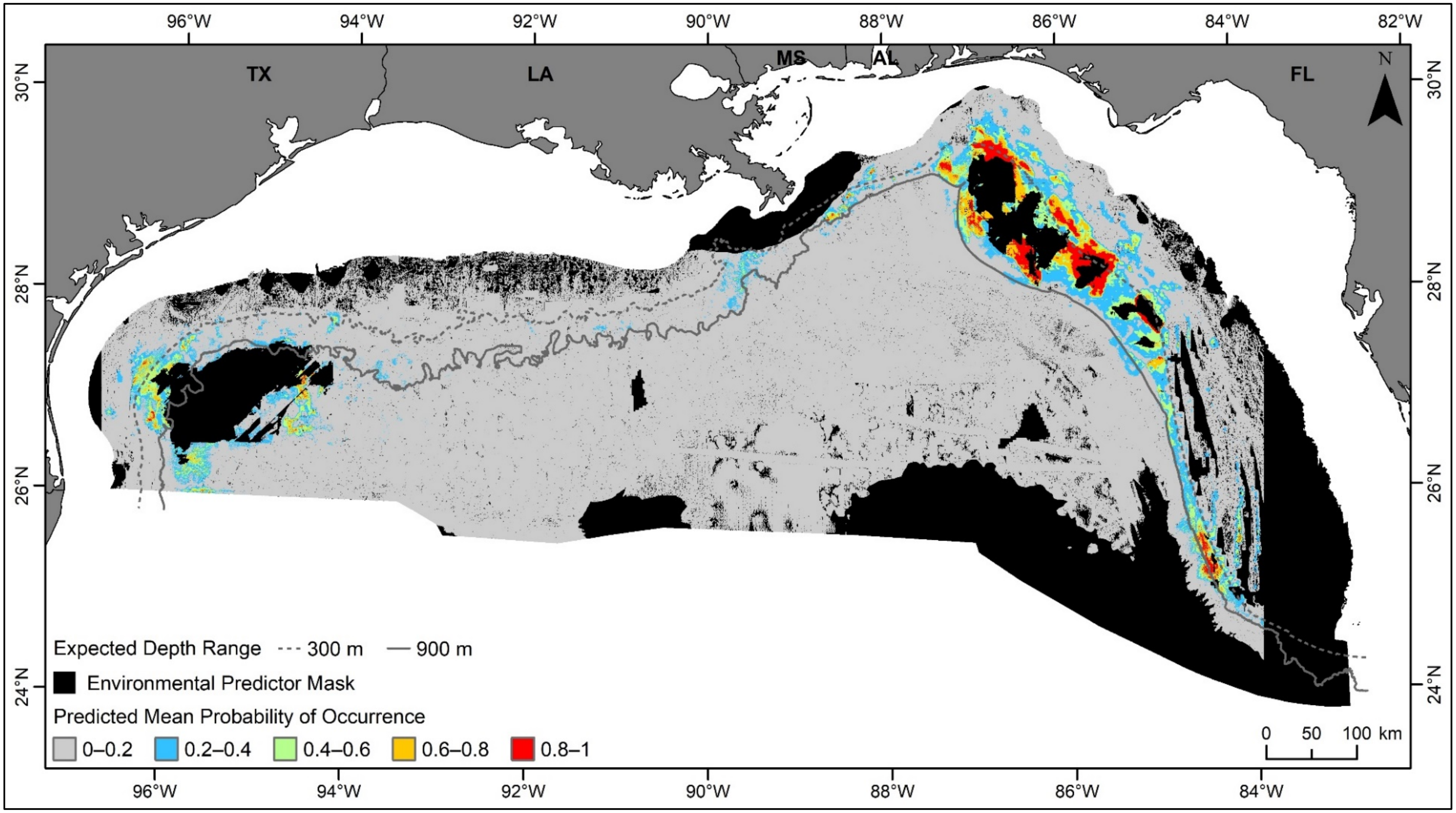

Figure 14. Predicted occurrence of the branching stony coral *Lophelia pertusa* (order Scleractinia).

This map shows the predicted mean probability of occurrence (i.e., the predicted posterior mean occupancy probability) for *L. pertusa* from the multi-genus occupancy model of order Scleractinia. The environmental predictor mask overlays areas where predictor values were outside the range of values at the sample locations and model predictions may be affected by extrapolation. Gray lines denote the expected depth range for *L. pertusa*.

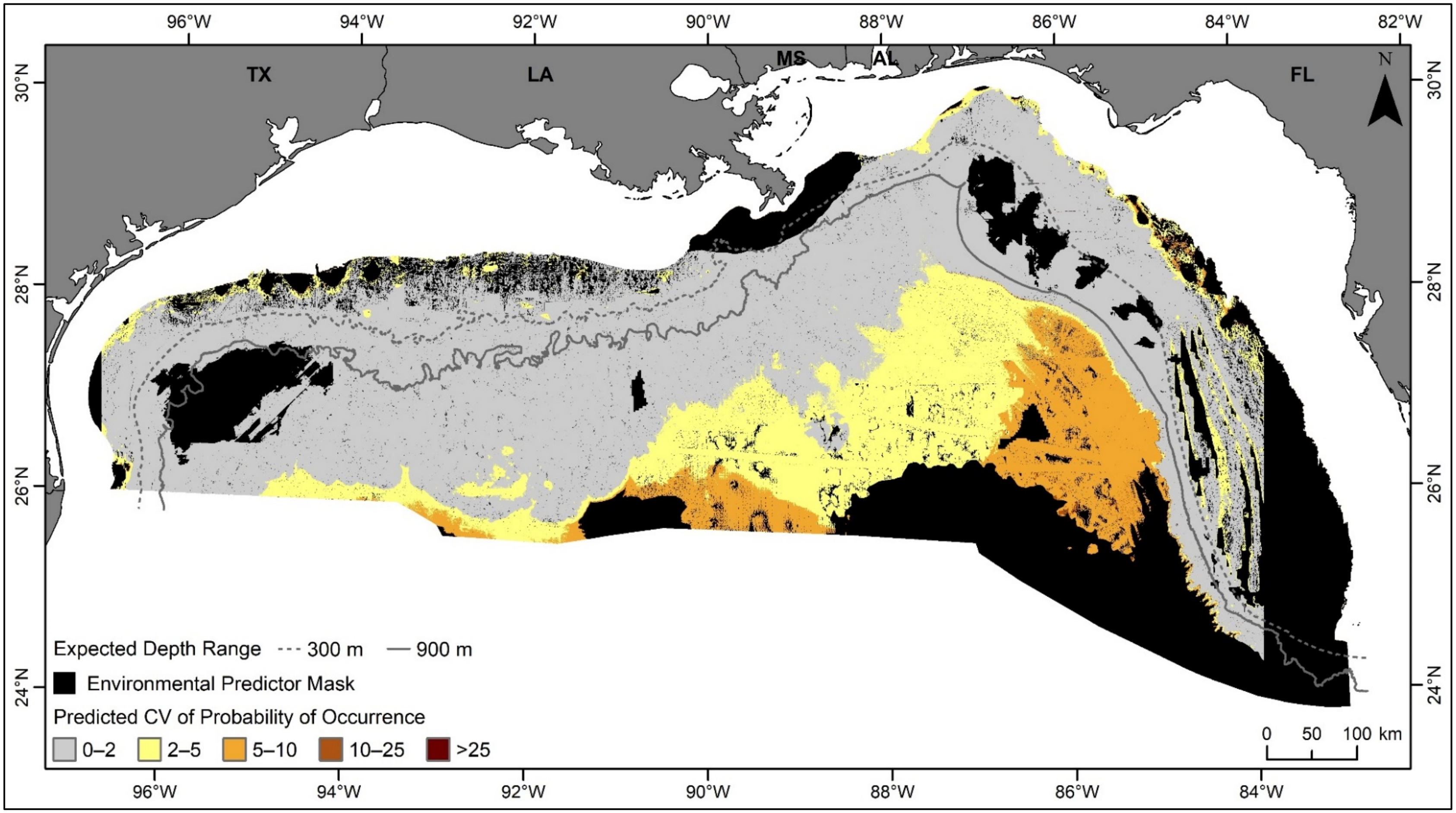

Figure 15. Variability in the predicted occurrence of the branching stony coral *Lophelia pertusa* (order Scleractinia).

This map shows the predicted coefficient of variation (CV) of the probability of occurrence (i.e., the predicted posterior CV of occupancy probability) for *L. pertusa* from the multi-genus occupancy model of order Scleractinia. The environmental predictor mask overlays areas where predictor values were outside the range of values at the sample locations and model predictions may be affected by extrapolation. Gray lines denote the expected depth range for *L. pertusa*.

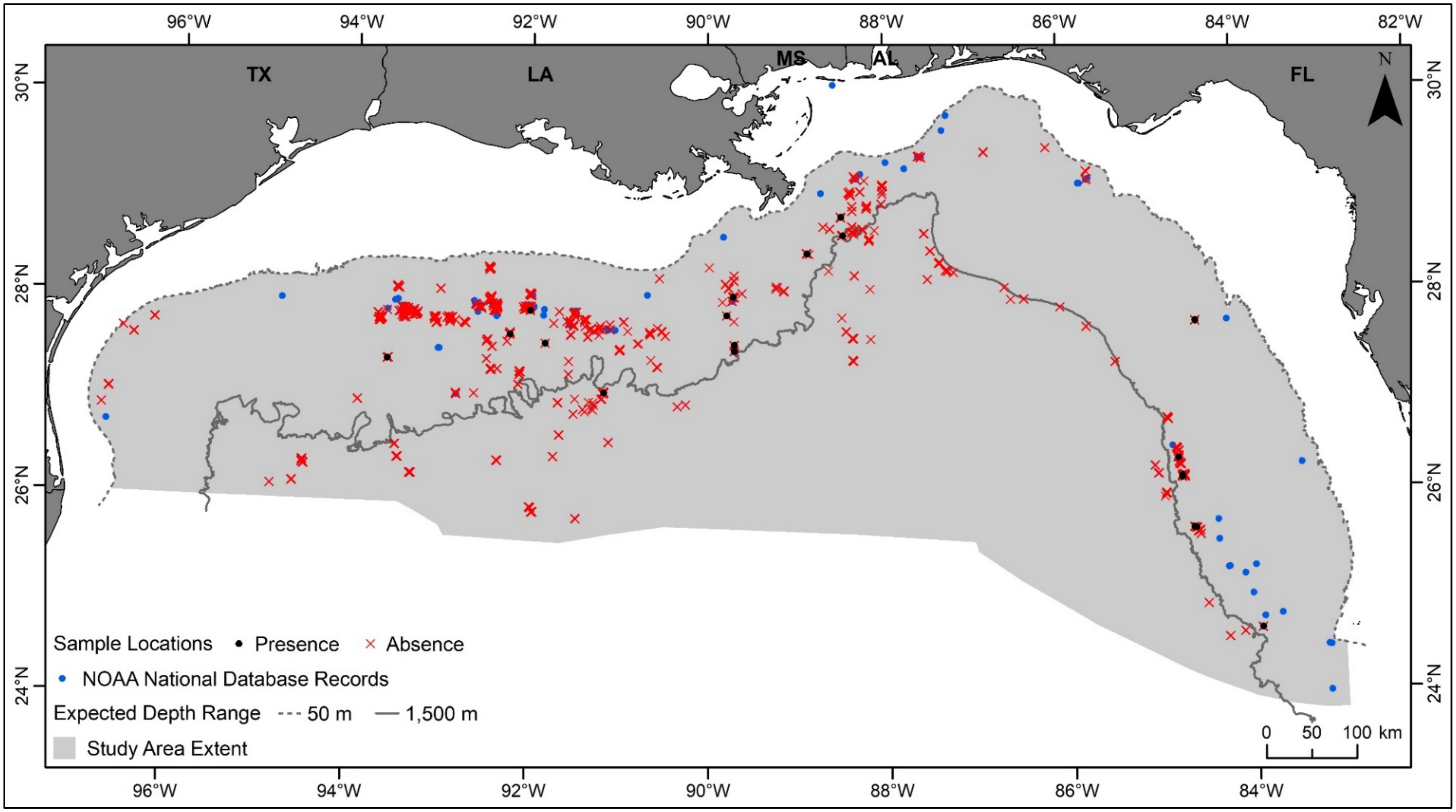

Figure 16. Occurrence records for the branching stony coral *Madrepora* (order Scleractinia).

This map shows the observed occurrence (presence-absence) of *Madrepora* at sample locations in the presence-absence database compiled for this study. Additional records of occurrence in the NOAA National Database are also displayed. Gray lines denote the expected depth range for *Madrepora*.

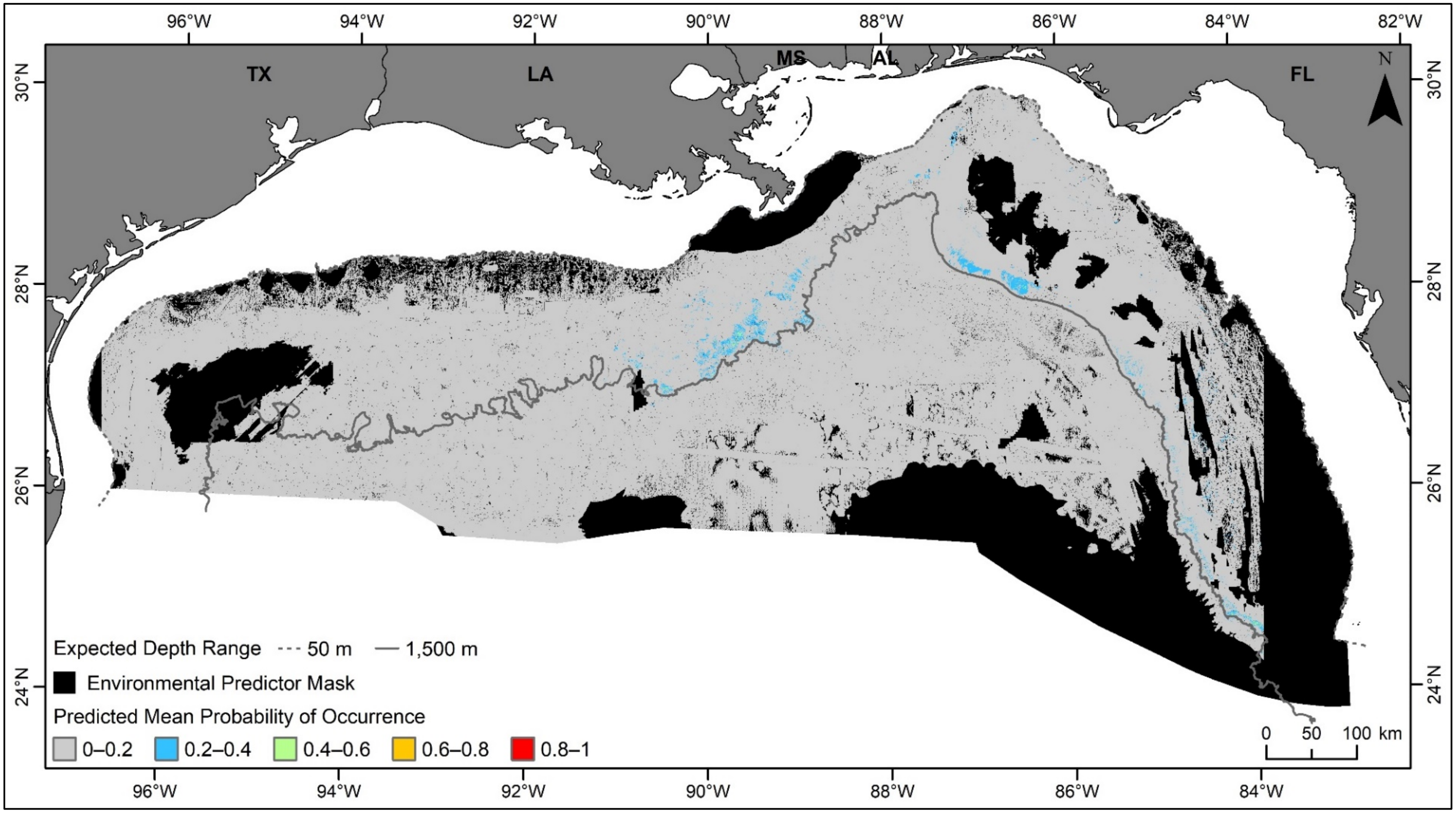

Figure 17. Predicted occurrence of the branching stony coral *Madrepora* (order Scleractinia).

This map shows the predicted mean probability of occurrence (i.e., the predicted posterior mean occupancy probability) for *Madrepora* from the multi-genus occupancy model of order Scleractinia. The environmental predictor mask overlays areas where predictor values were outside the range of values at the sample locations and model predictions may be affected by extrapolation. Gray lines denote the expected depth range for *Madrepora*.

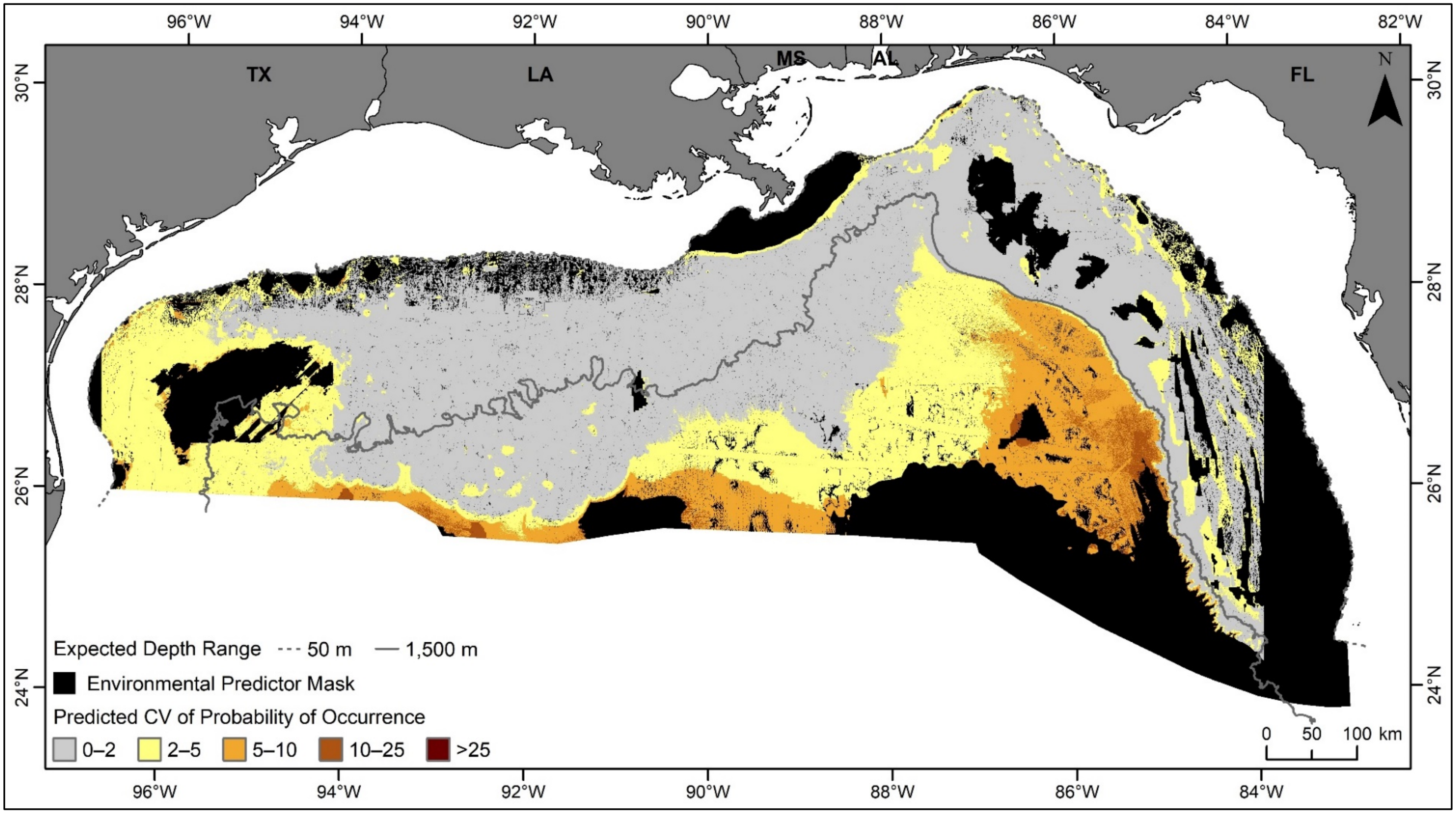

Figure 18. Variability in the predicted occurrence of the branching stony coral *Madrepora* (order Scleractinia).

This map shows the predicted coefficient of variation (CV) of the probability of occurrence (i.e., the predicted posterior CV of occupancy probability) for *Madrepora* from the multi-genus occupancy model of order Scleractinia. The environmental predictor mask overlays areas where predictor values were outside the range of values at the sample locations and model predictions may be affected by extrapolation. Gray lines denote the expected depth range for *Madrepora*.

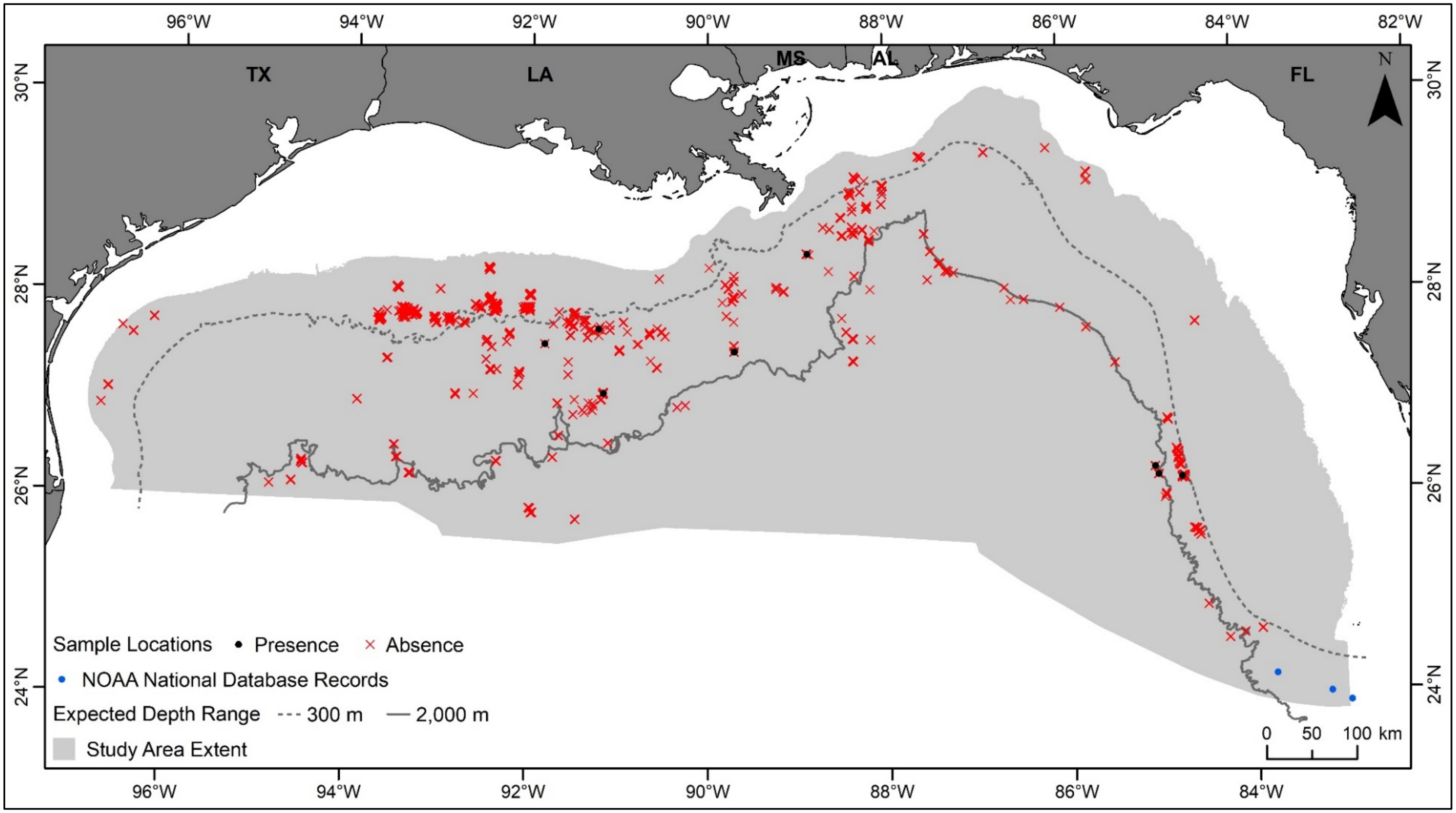

Figure 19. Occurrence records for the branching stony coral *Solenosmilia* (order Scleractinia).

This map shows the observed occurrence (presence-absence) of *Solenosmilia* at sample locations in the presence-absence database compiled for this study. Additional records of occurrence in the NOAA National Database are also displayed. Gray lines denote the expected depth range for *Solenosmilia*.

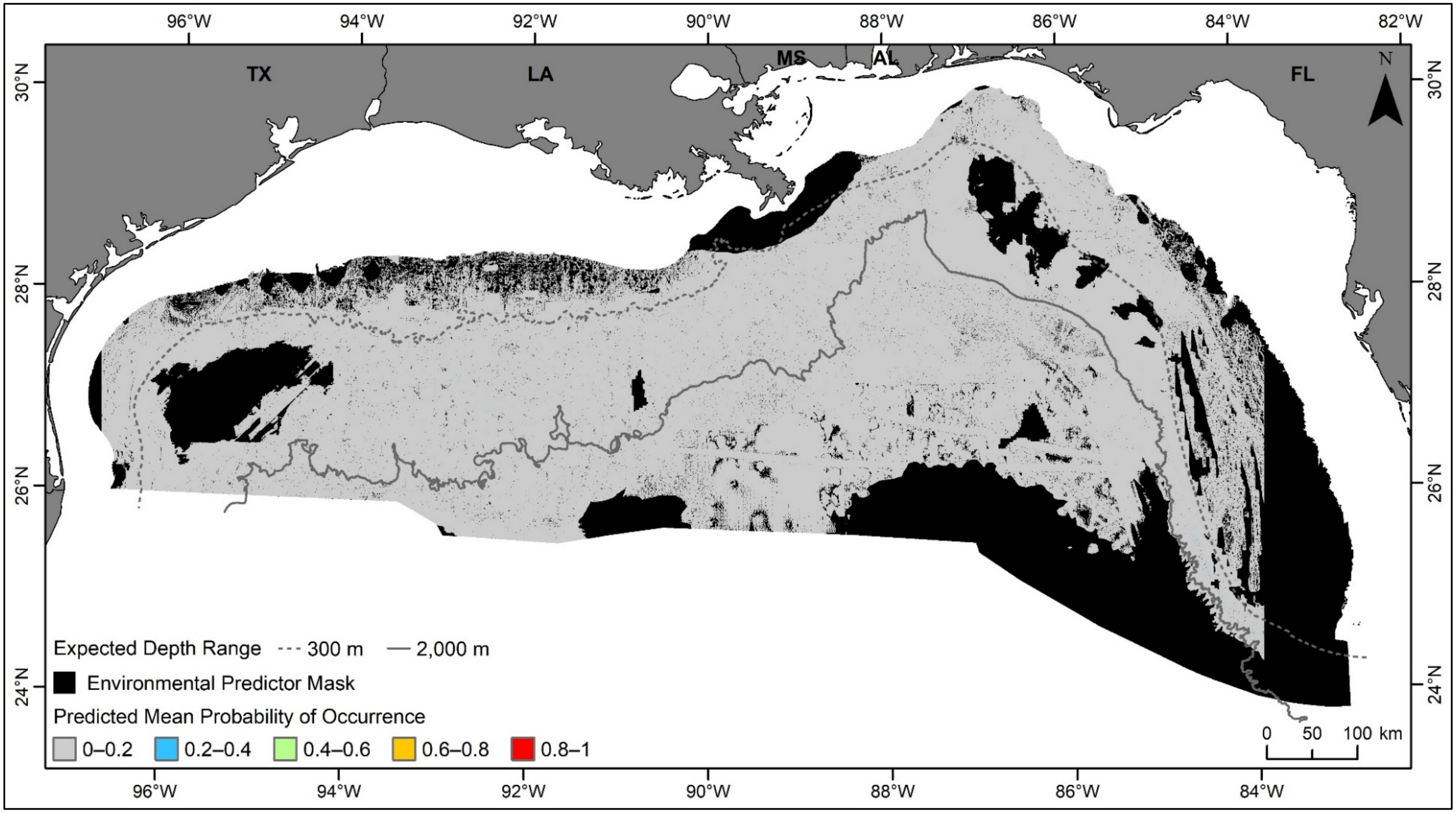

Figure 20. Predicted occurrence of the branching stony coral *Solenosmilia* (order Scleractinia).

This map shows the predicted mean probability of occurrence (i.e., the predicted posterior mean occupancy probability) for *Solenosmilia* from the multi-genus occupancy model of order Scleractinia. The environmental predictor mask overlays areas where predictor values were outside the range of values at the sample locations and model predictions may be affected by extrapolation. Gray lines denote the expected depth range for *Solenosmilia*.

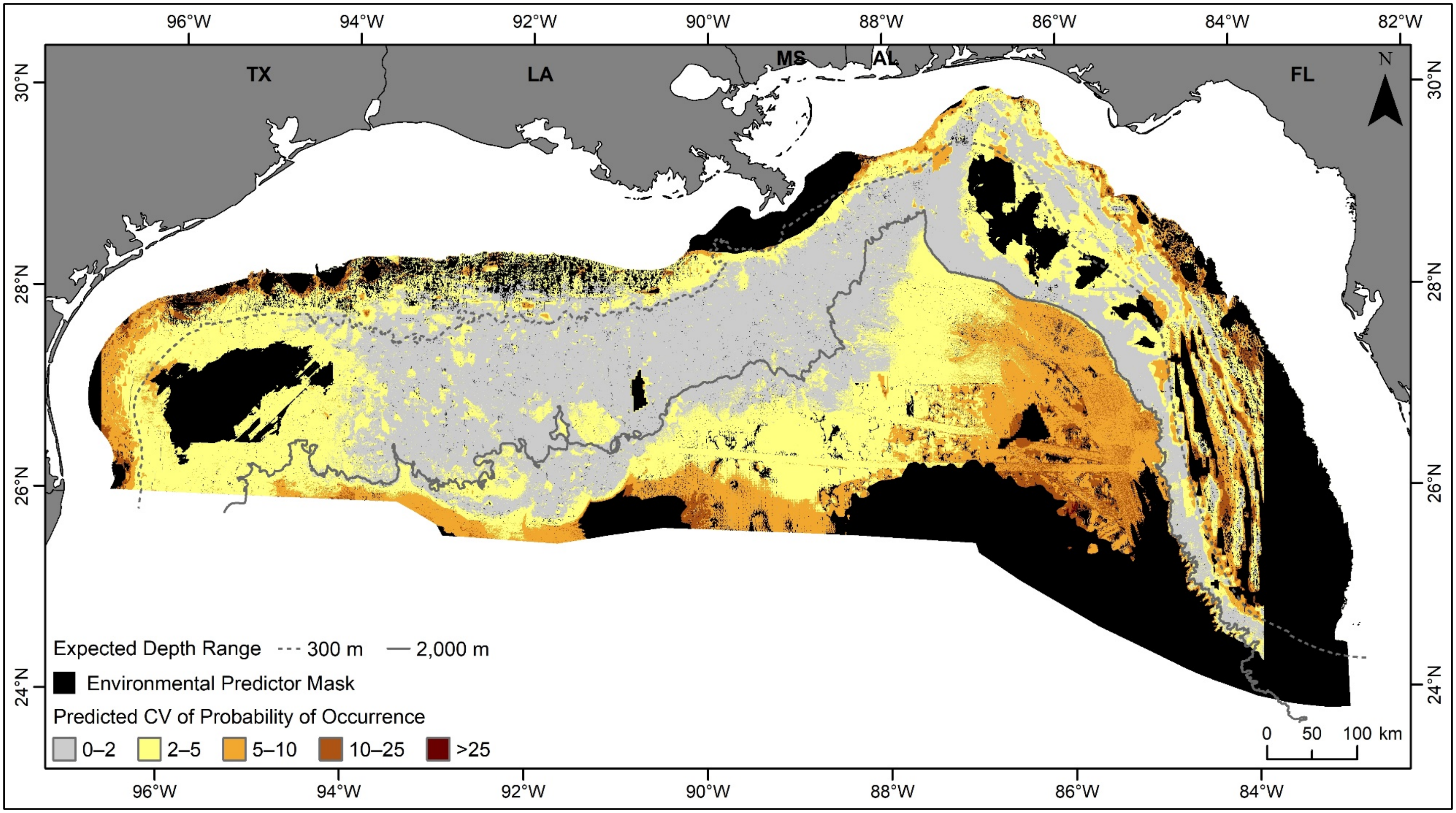

Figure 21. Variability in the predicted occurrence of the branching stony coral *Solenosmilia* (order Scleractinia).

This map shows the predicted coefficient of variation (CV) of the probability of occurrence (i.e., the predicted posterior CV of occupancy probability) for *Solenosmilia* from the multi-genus occupancy model of order Scleractinia. The environmental predictor mask overlays areas where predictor values were outside the range of values at the sample locations and model predictions may be affected by extrapolation. Gray lines denote the expected depth range for *Solenosmilia*.

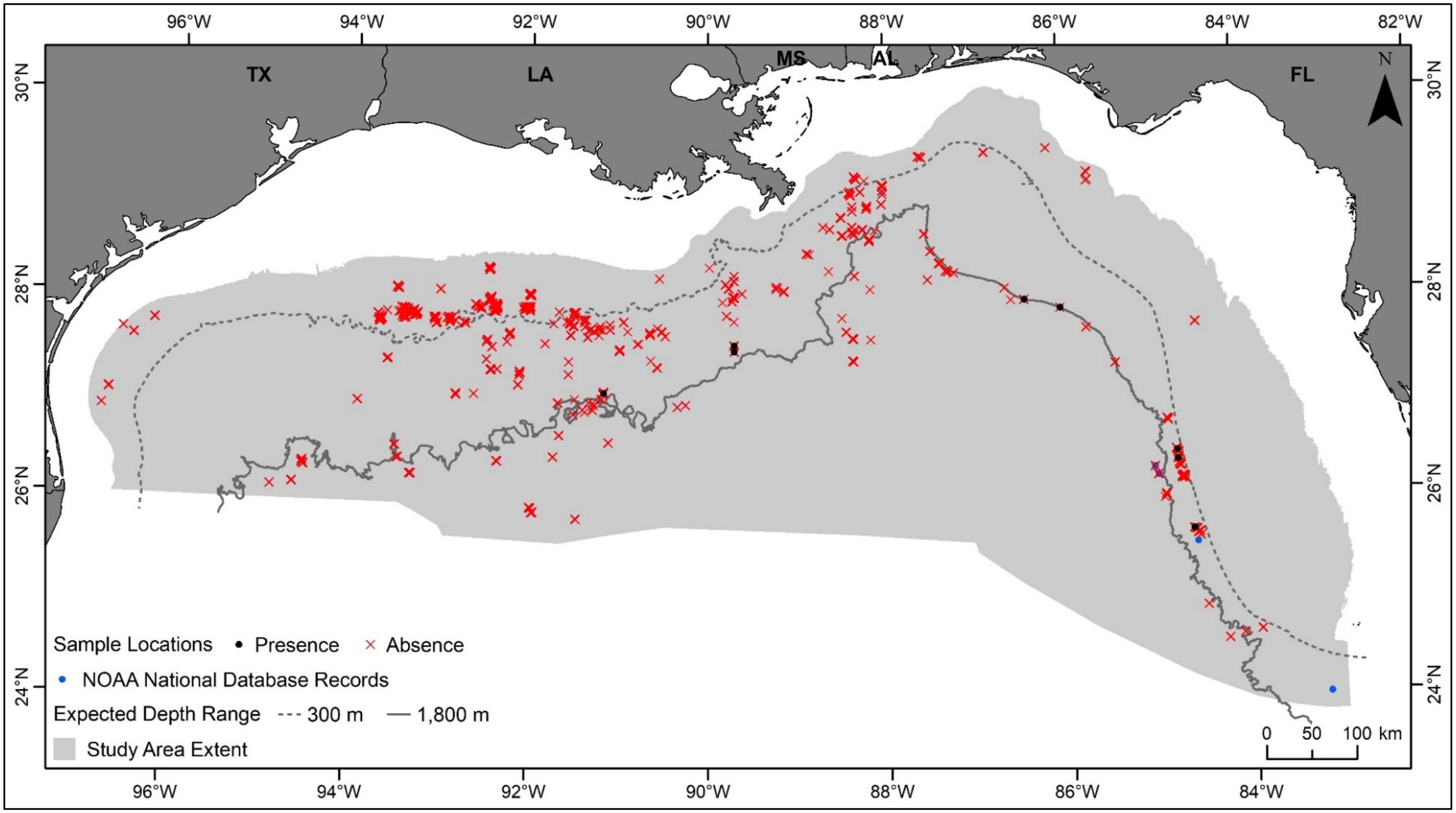

Figure 22. Occurrence records for the branching stony coral *Enallopsammia* (order Scleractinia).

This map shows the observed occurrence (presence-absence) of *Enallopsammia* at sample locations in the presence-absence database compiled for this study. Additional records of occurrence in the NOAA National Database are also displayed. Gray lines denote the expected depth range for *Enallopsammia*.

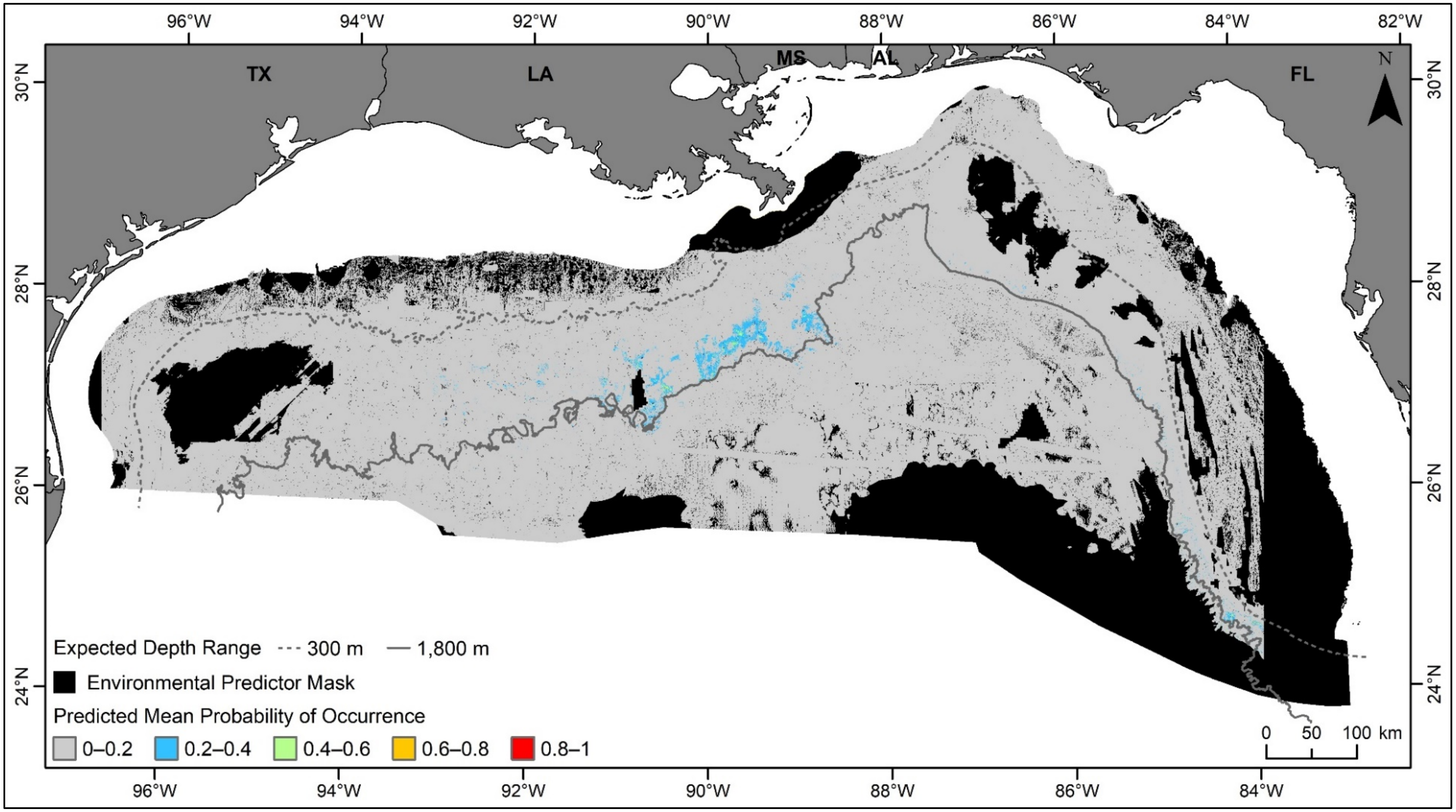

Figure 23. Predicted occurrence of the branching stony coral *Enallopsammia* (order Scleractinia).

This map shows the predicted mean probability of occurrence (i.e., the predicted posterior mean occupancy probability) for *Enallopsammia* from the multi-genus occupancy model of order Scleractinia. The environmental predictor mask overlays areas where predictor values were outside the range of values at the sample locations and model predictions may be affected by extrapolation. Gray lines denote the expected depth range for *Enallopsammia*.

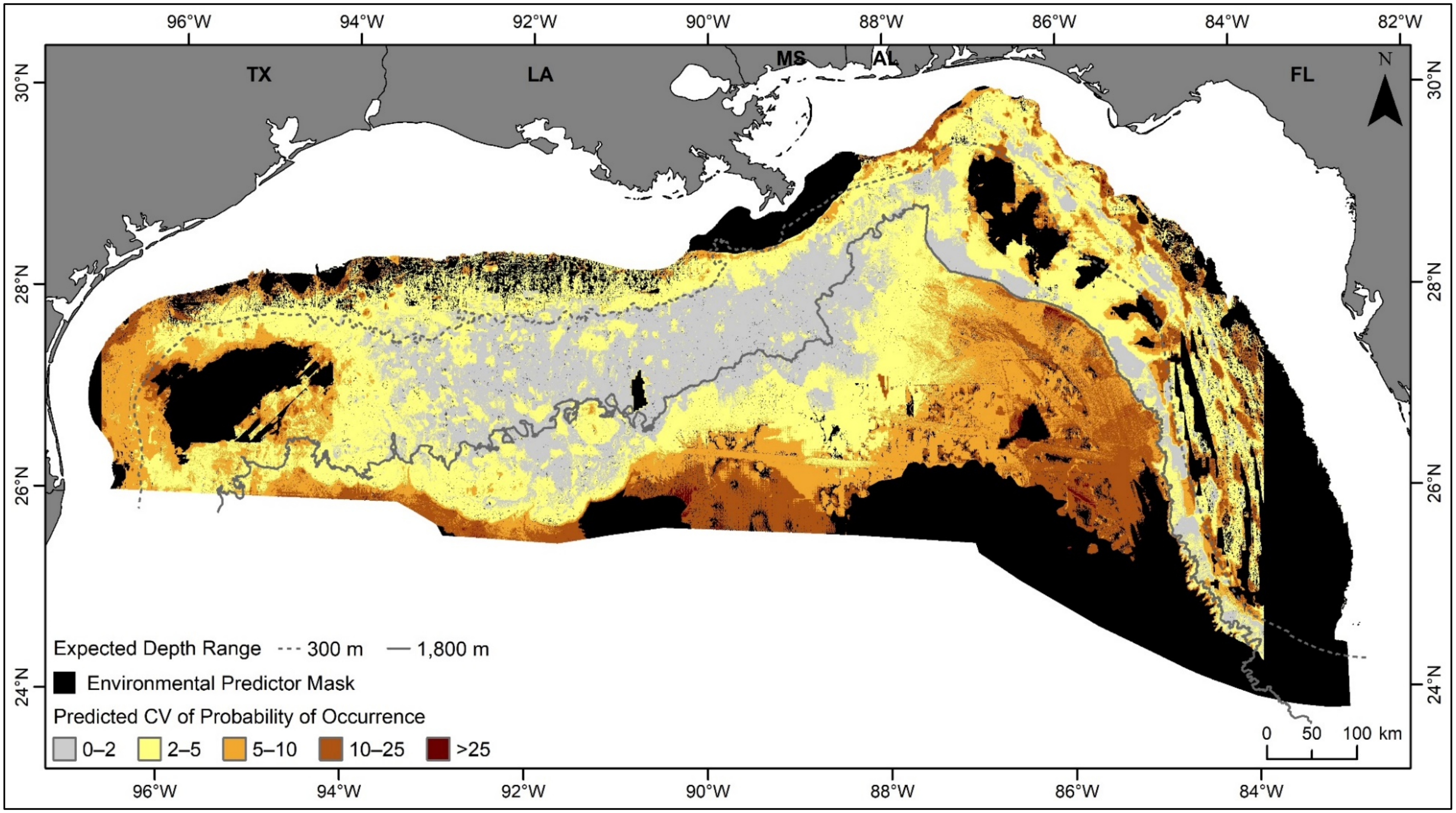

Figure 24. Variability in the predicted occurrence of the branching stony coral *Enallopsammia* (order Scleractinia).

This map shows the predicted coefficient of variation (CV) of the probability of occurrence (i.e., the predicted posterior CV of occupancy probability) for *Enallopsammia* from the multi-genus occupancy model of order Scleractinia. The environmental predictor mask overlays areas where predictor values were outside the range of values at the sample locations and model predictions may be affected by extrapolation. Gray lines denote the expected depth range for *Enallopsammia*.

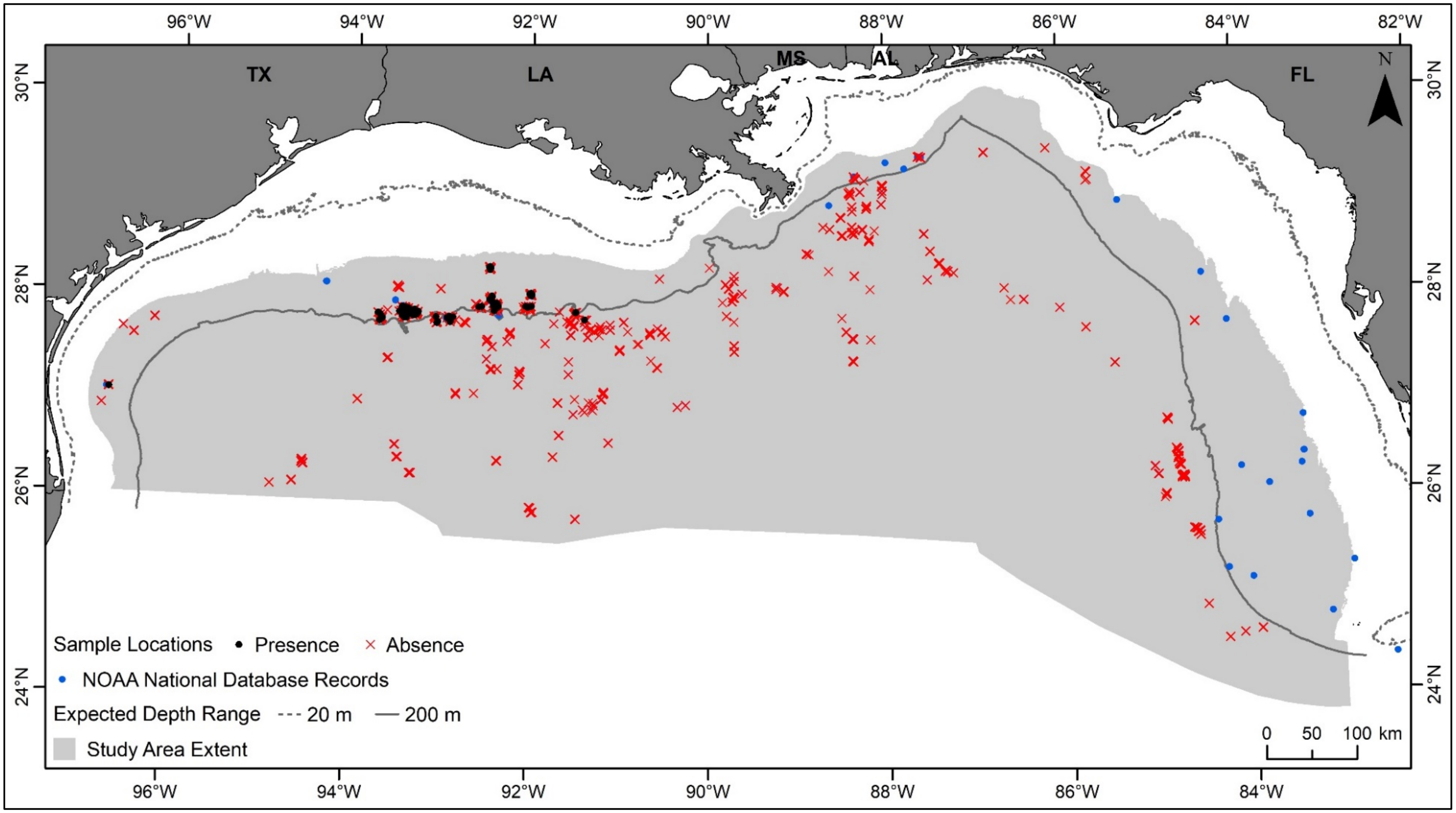

Figure 25. Occurrence records for the branching stony corals family Oculinidae (order Scleractinia).

This map shows the observed occurrence (presence-absence) of Oculinidae (excluding records identified as *Madrepora*) at sample locations in the presence-absence database compiled for this study. Additional records of occurrence in the NOAA National Database are also displayed. Gray lines denote the expected depth range for Oculinidae.

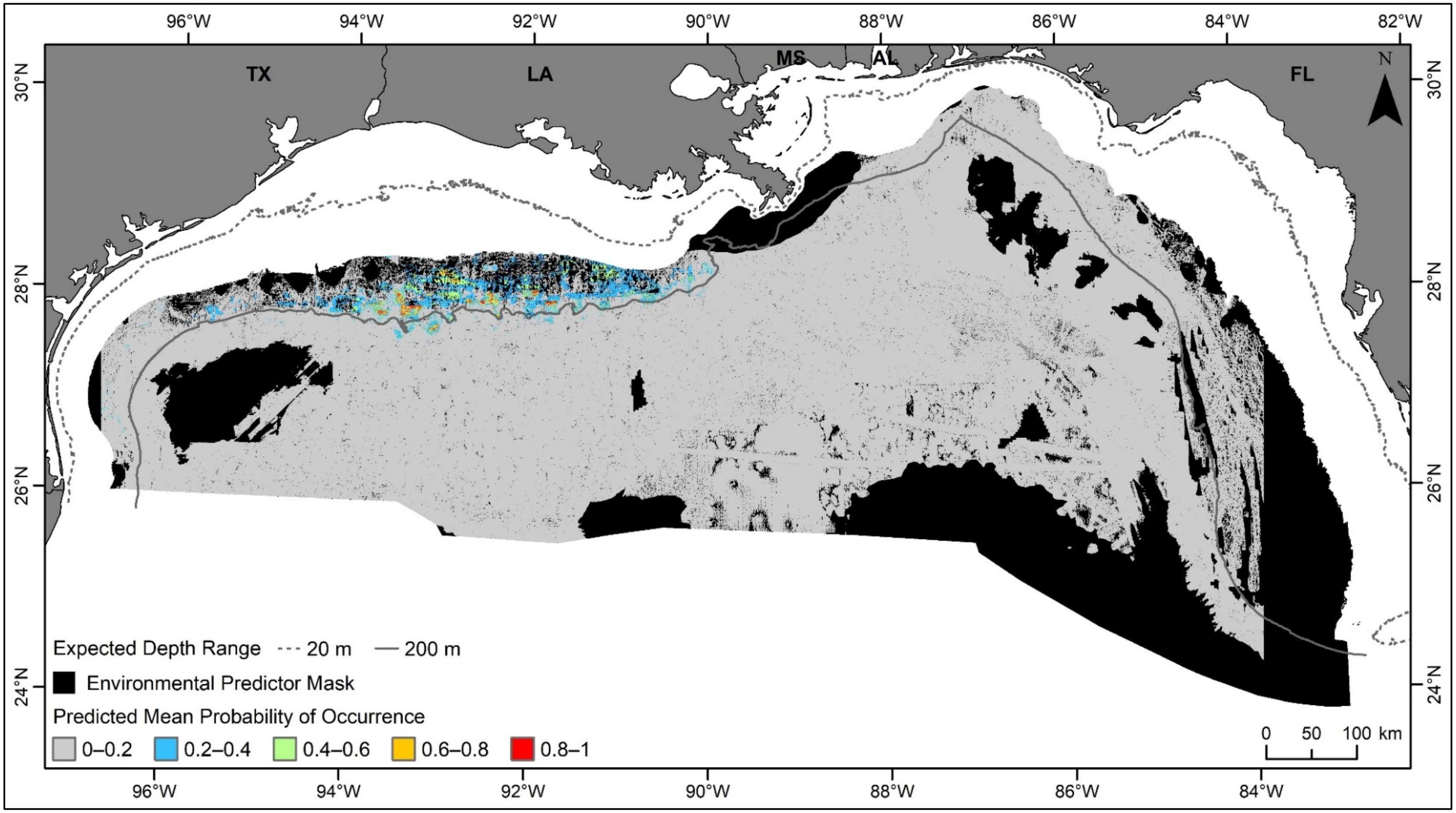

Figure 26. Predicted occurrence of the branching stony coral family Oculinidae (order Scleractinia).

This map shows the predicted mean probability of occurrence (i.e., the predicted posterior mean occupancy probability) for Oculinidae from the single-taxon occupancy model. The environmental predictor mask overlays areas where predictor values were outside the range of values at the sample locations and model predictions may be affected by extrapolation. Gray lines denote the expected depth range for Oculinidae.

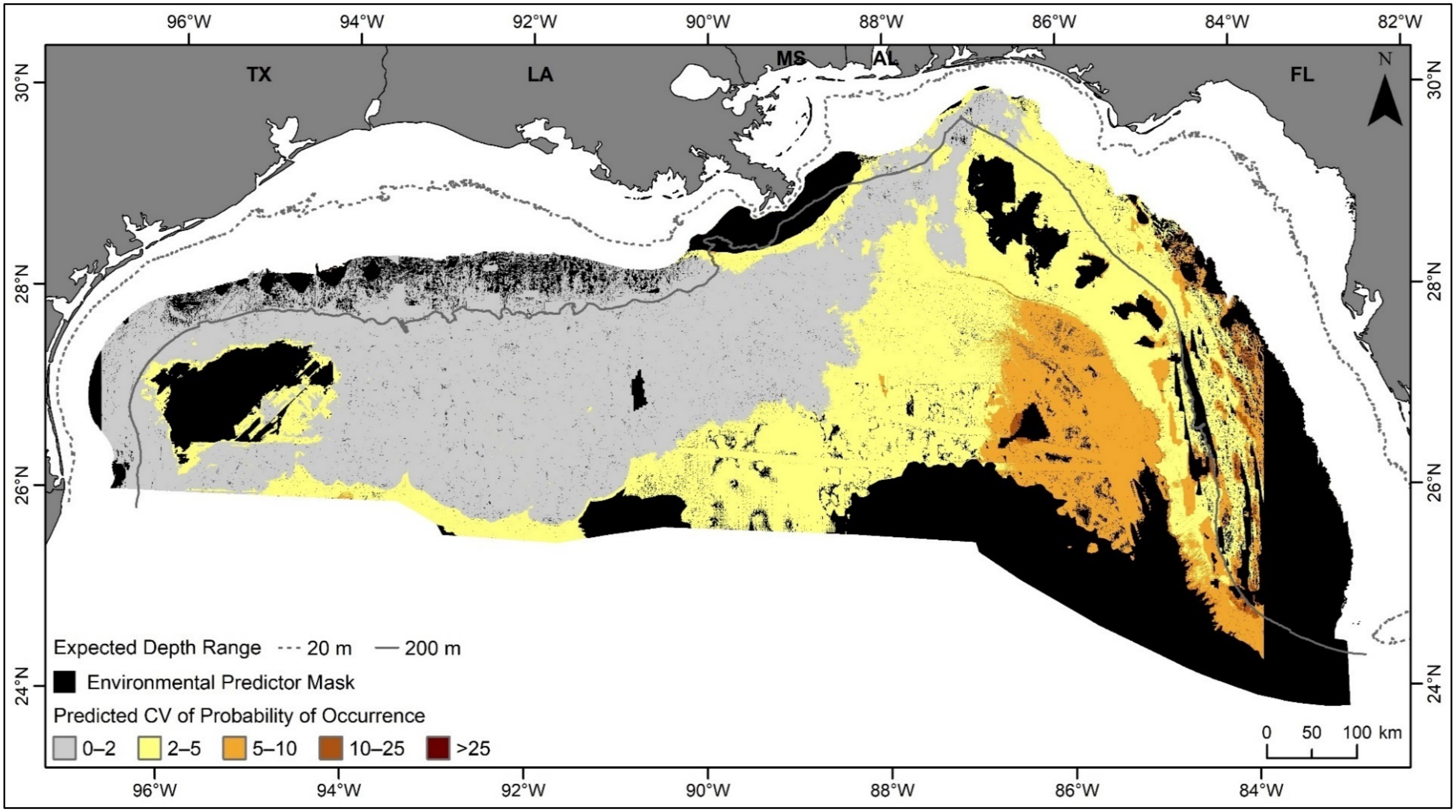

Figure 27. Variability in the predicted occurrence of the branching stony coral family Oculinidae (order Scleractinia).

This map shows the predicted coefficient of variation (CV) of the probability of occurrence (i.e., the predicted posterior CV of occupancy probability) for Oculinidae from the single-taxon occupancy model. The environmental predictor mask overlays areas where predictor values were outside the range of values at the sample locations and model predictions may be affected by extrapolation. Gray lines denote the expected depth range for Oculinidae.

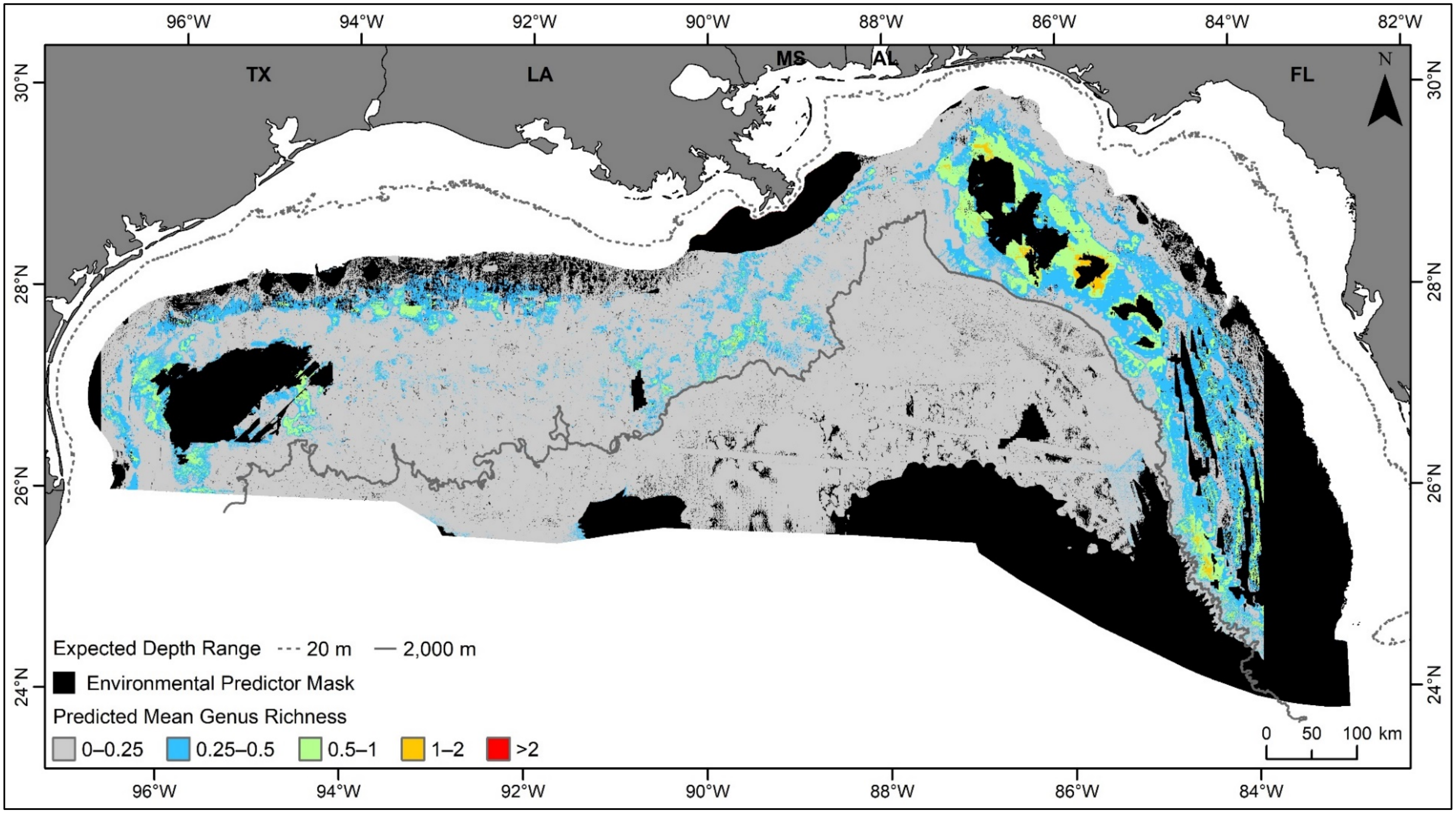

Figure 28. Predicted genus richness of branching stony corals (order Scleractinia).

This map shows the predicted mean genus richness (i.e., the posterior mean genus richness) from the multi-genus occupancy model of order Scleractinia. The environmental predictor mask overlays areas where predictor values were outside the range of values at the sample locations and model predictions may be affected by extrapolation. Gray lines denote the combined expected depth range for the genera included in the model.

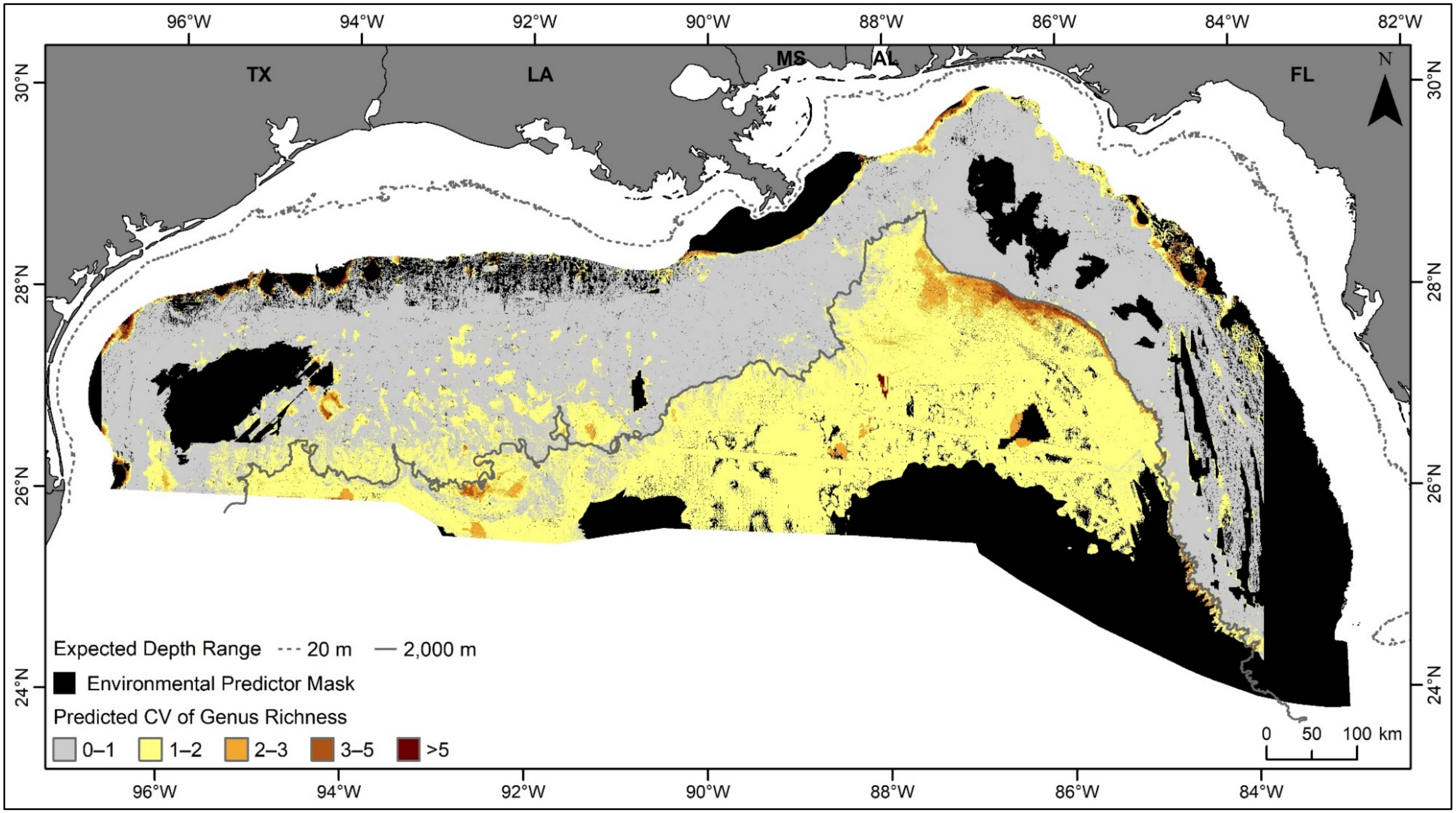

Figure 29. Variability in the predicted genus richness of branching stony corals (order Scleractinia).

This map shows the predicted coefficient of variation of genus richness (i.e., the posterior CV of genus richness) from the multi-genus occupancy model of order Scleractinia. The environmental predictor mask overlays areas where predictor values were outside the range of values at the sample locations and model predictions may be affected by extrapolation. Gray lines denote the combined expected depth range for the genera included in the model.

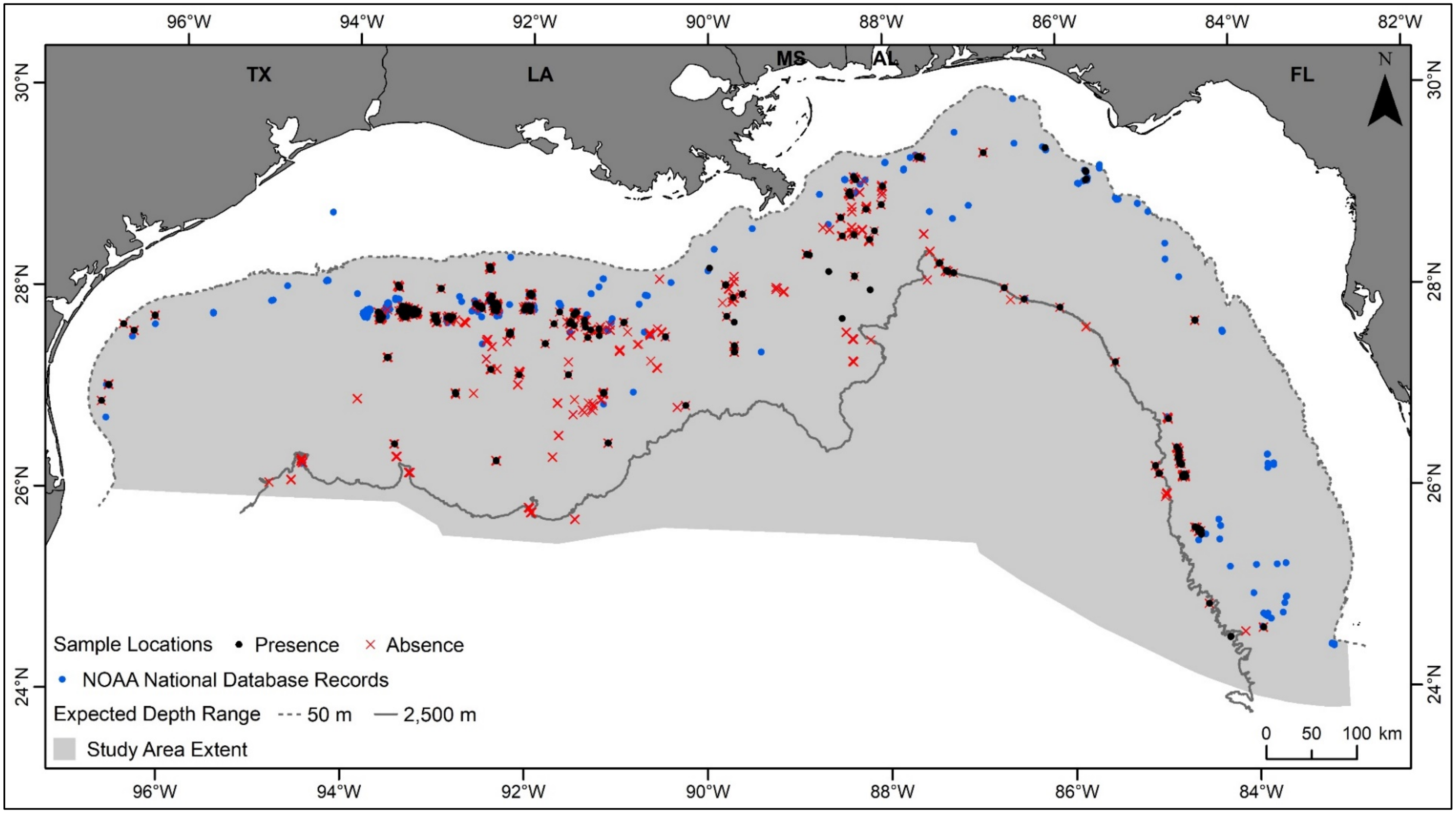

Figure 30. Occurrence records for the gorgonian coral family Plexauridae (order Alcyonacea).

This map shows the observed occurrence (presence-absence) of Plexauridae at sample locations in the presence-absence database compiled for this study. Additional records of occurrence in the NOAA National Database are also displayed. Gray lines denote the expected depth range for Plexauridae.

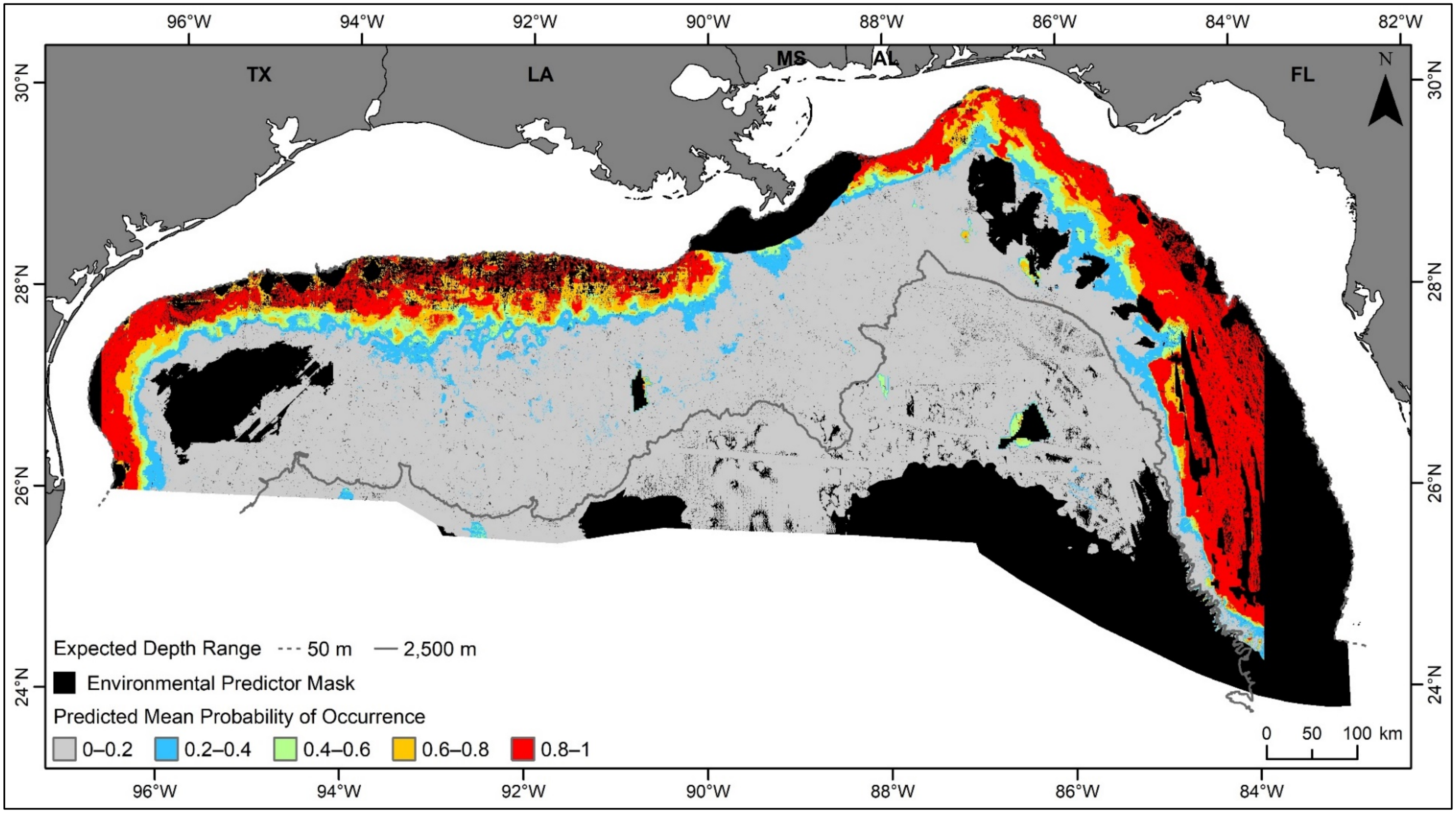

Figure 31. Predicted occurrence of the gorgonian coral family Plexauridae (order Alcyonacea).

This map shows the predicted mean probability of occurrence (i.e., the predicted posterior mean occupancy probability) for Plexauridae from the multi-family occupancy model of order Alcyonacea. The environmental predictor mask overlays areas where predictor values were outside the range of values at the sample locations and model predictions may be affected by extrapolation. Gray lines denote the expected depth range for Plexauridae.

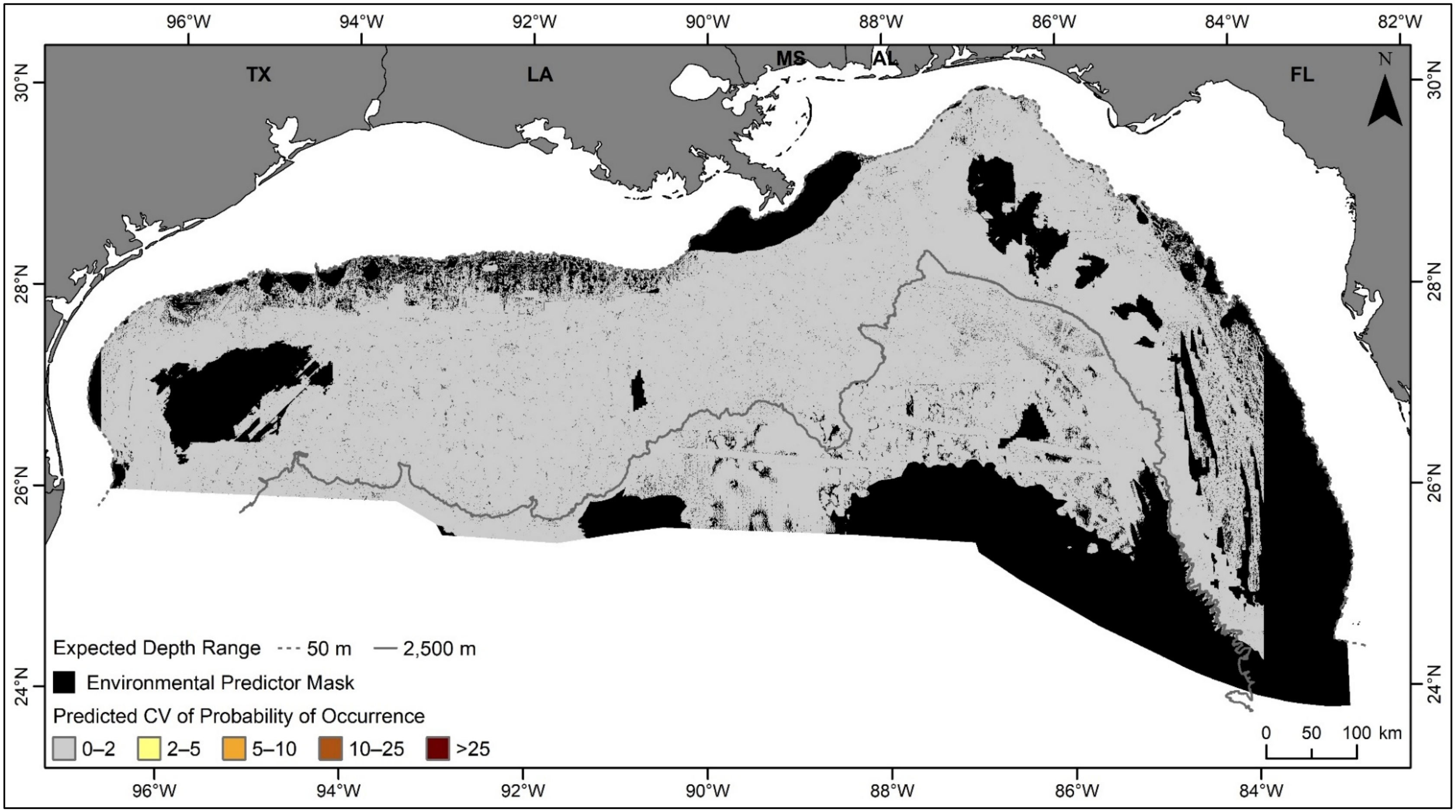

Figure 32. Variability in the predicted occurrence of the gorgonian coral family Plexauridae (order Alcyonacea).

This map shows the predicted coefficient of variation (CV) of the probability of occurrence (i.e., the predicted posterior CV of occupancy probability) for Plexauridae from the multi-family occupancy model of order Alcyonacea. The environmental predictor mask overlays areas where predictor values were outside the range of values at the sample locations and model predictions may be affected by extrapolation. Gray lines denote the expected depth range for Plexauridae.

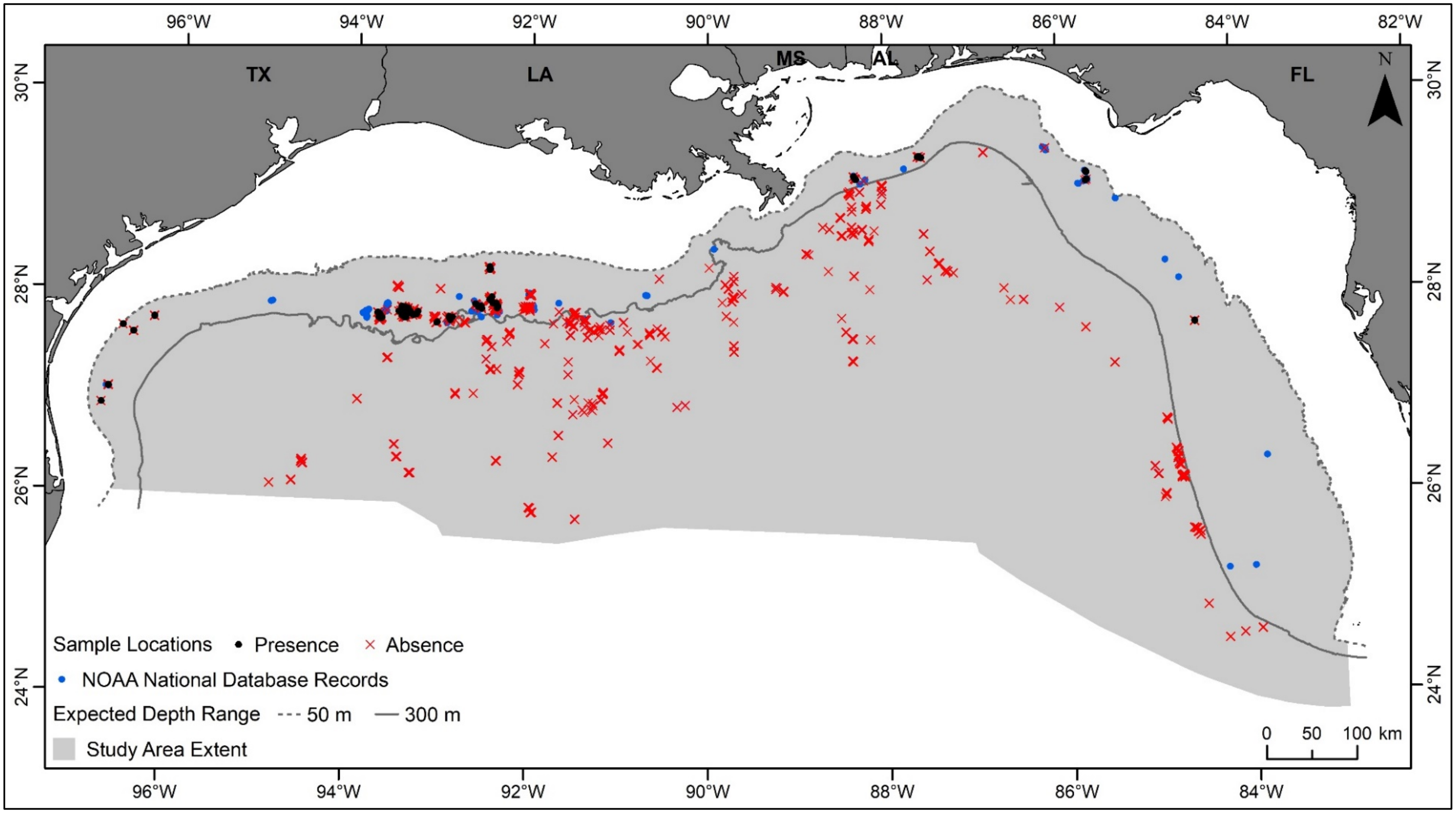

Figure 33. Occurrence records for the gorgonian coral *Bebryce* (order Alcyonacea, family Plexauridae).

This map shows the observed occurrence (presence-absence) of *Bebryce* at sample locations in the presence-absence database compiled for this study. Additional records of occurrence in the NOAA National Database are also displayed. Gray lines denote the expected depth range for *Bebryce*.

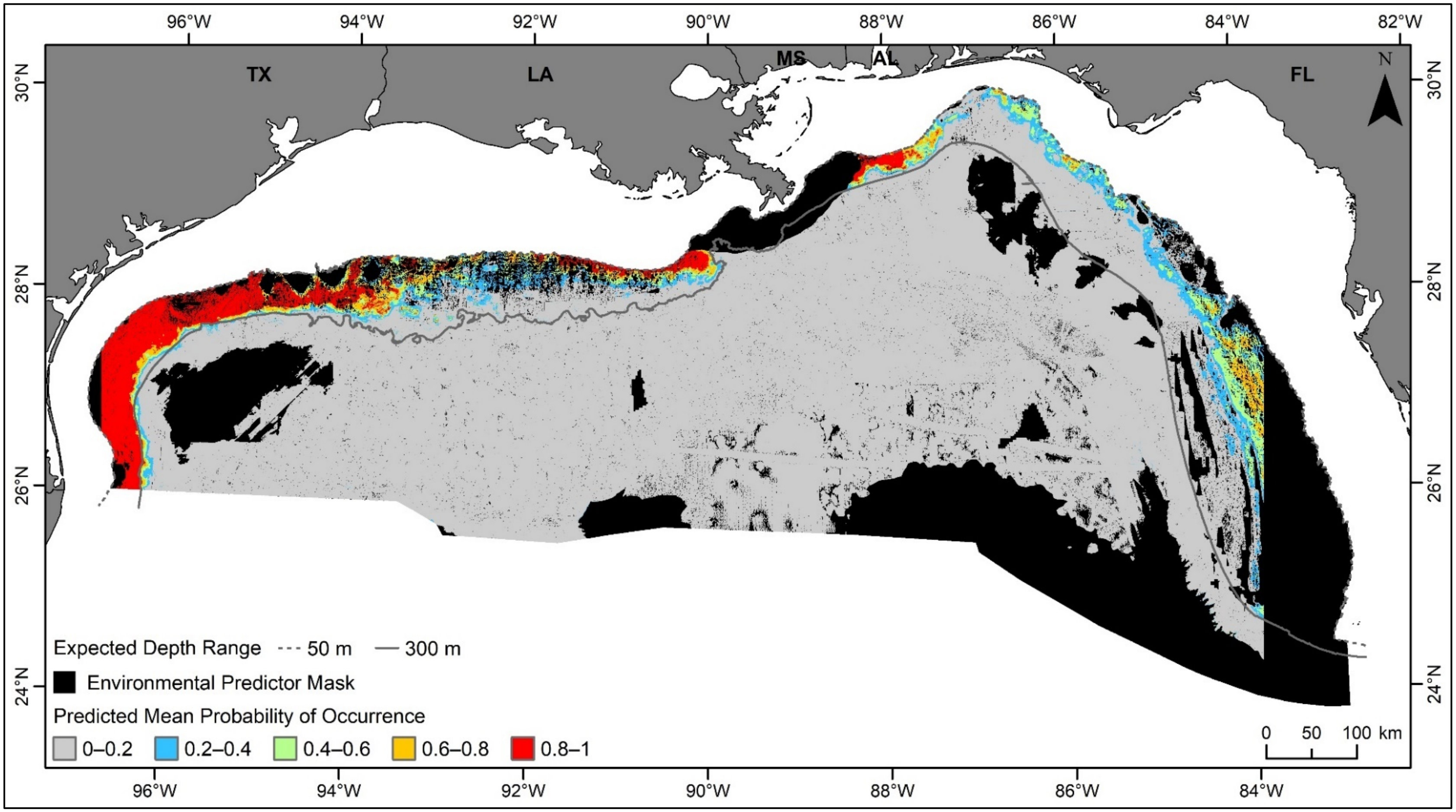

Figure 34. Predicted occurrence of the gorgonian coral *Bebryce* (order Alcyonacea, family Plexauridae).

This map shows the predicted mean probability of occurrence (i.e., the predicted posterior mean occupancy probability) for *Bebryce* from the multi-genus occupancy model of family Plexauridae. The environmental predictor mask overlays areas where predictor values were outside the range of values at the sample locations and model predictions may be affected by extrapolation. Gray lines denote the expected depth range for *Bebryce*.

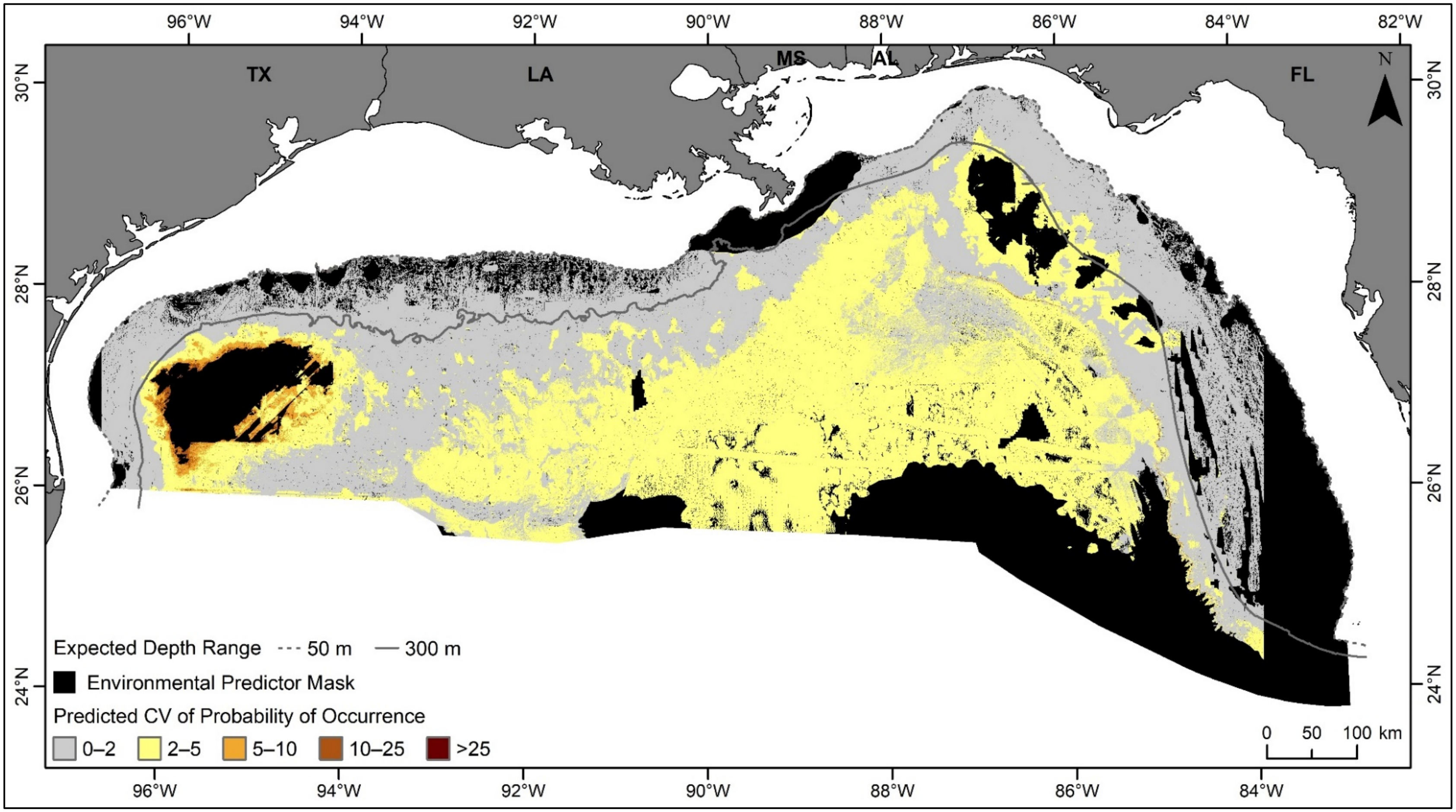

Figure 35. Variability in the predicted occurrence of the gorgonian coral *Bebryce* (order Alcyonacea, family Plexauridae).

This map shows the predicted coefficient of variation (CV) of the probability of occurrence (i.e., the predicted posterior CV of occupancy probability) for *Bebryce* from the multi-genus occupancy model of family Plexauridae. The environmental predictor mask overlays areas where predictor values were outside the range of values at the sample locations and model predictions may be affected by extrapolation. Gray lines denote the expected depth range for *Bebryce*.

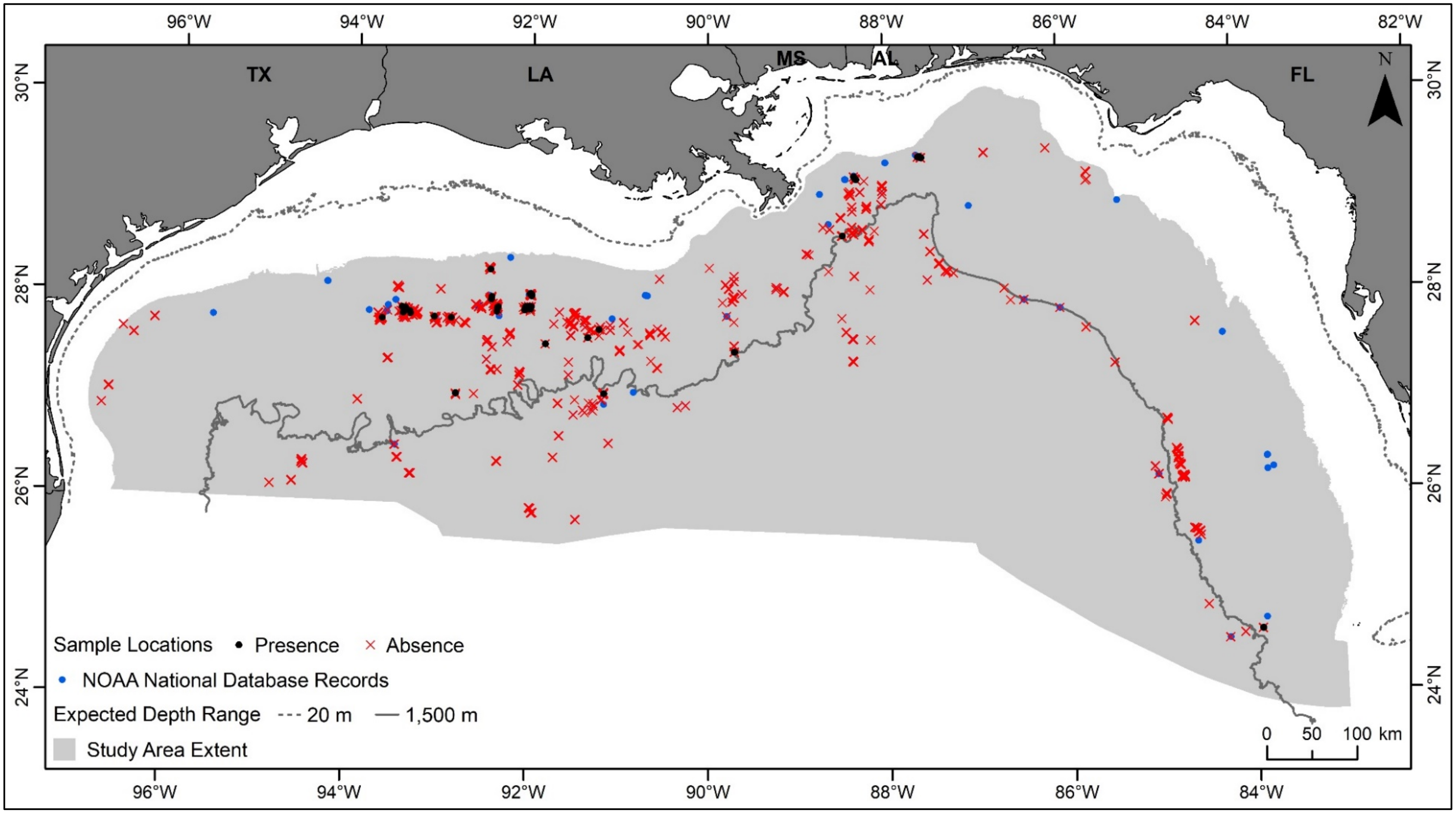

Figure 36. Occurrence records for the gorgonian coral *Swiftia* (order Alcyonacea, family Plexauridae).

This map shows the observed occurrence (presence-absence) of *Swiftia* at sample locations in the presence-absence database compiled for this study. Additional records of occurrence in the NOAA National Database are also displayed. Gray lines denote the expected depth range for *Swiftia*.

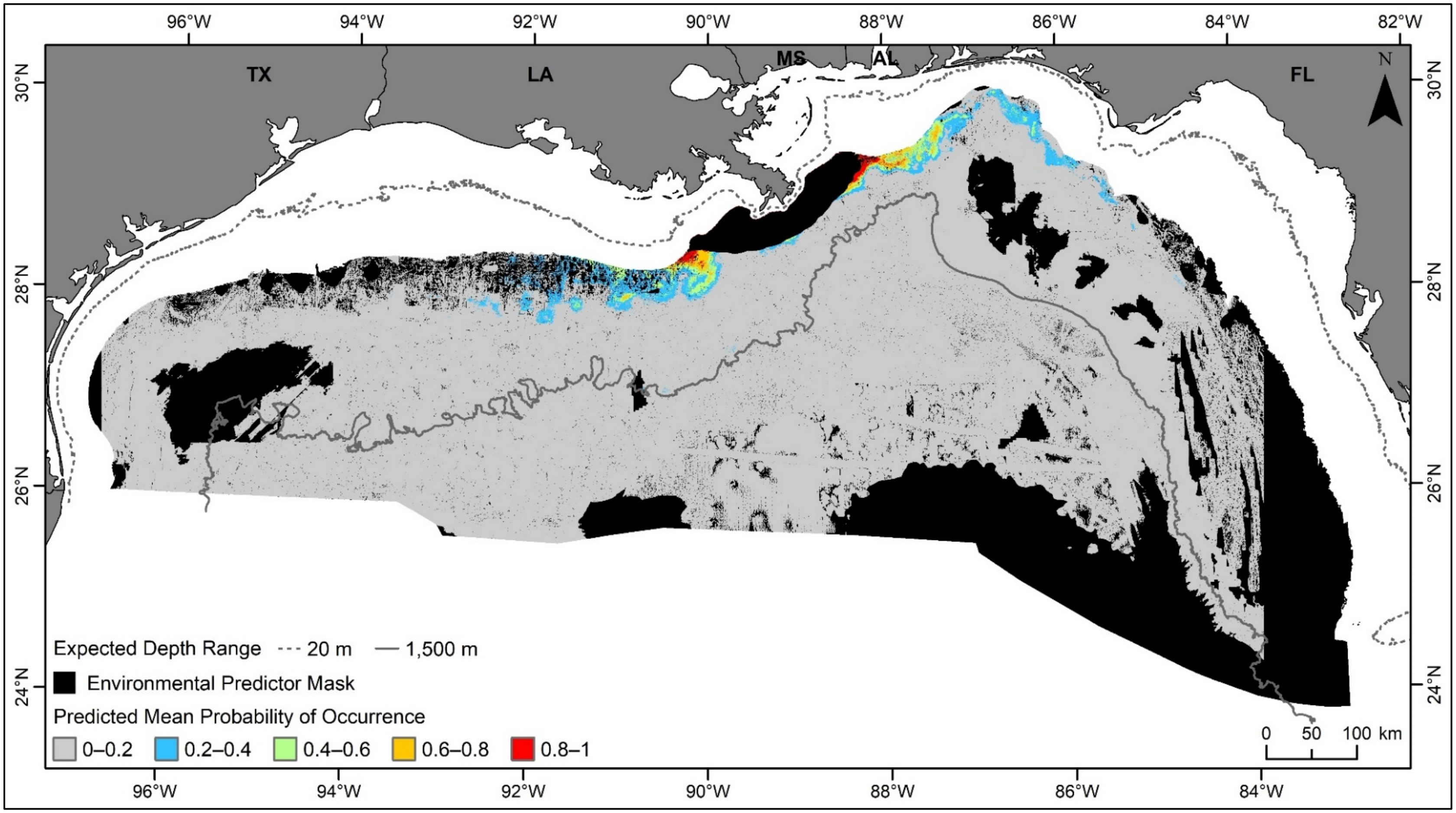

Figure 37. Predicted occurrence of the gorgonian coral *Swiftia* (order Alcyonacea, family Plexauridae).

This map shows the predicted mean probability of occurrence (i.e., the predicted posterior mean occupancy probability) for *Swiftia* from the multi-genus occupancy model of family Plexauridae. The environmental predictor mask overlays areas where predictor values were outside the range of values at the sample locations and model predictions may be affected by extrapolation. Gray lines denote the expected depth range for *Swiftia*.

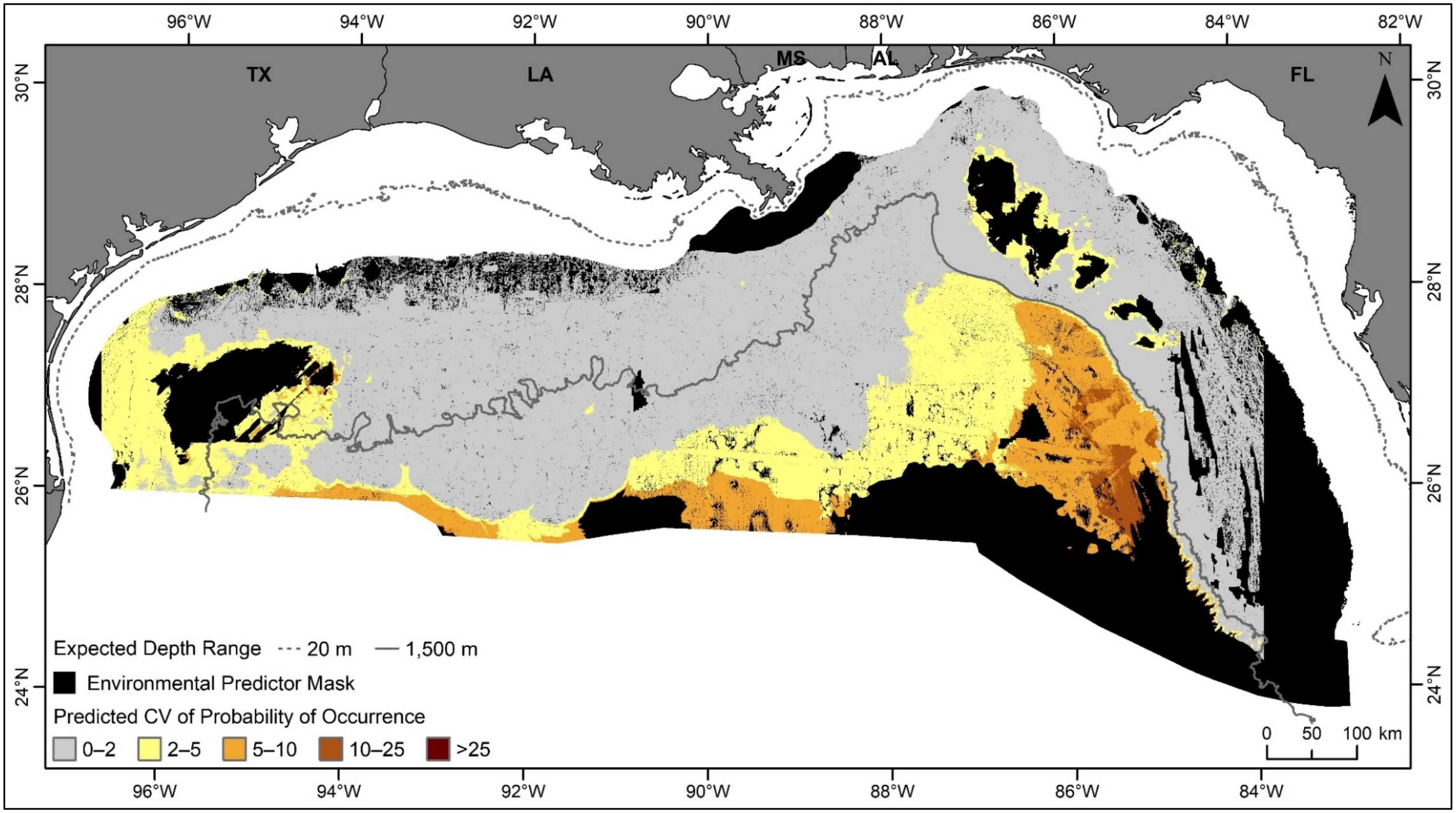

Figure 38. Variability in the predicted occurrence of the gorgonian coral *Swiftia* (order Alcyonacea, family Plexauridae).

This map shows the predicted coefficient of variation (CV) of the probability of occurrence (i.e., the predicted posterior CV of occupancy probability) for *Swiftia* from the multi-genus occupancy model of family Plexauridae. The environmental predictor mask overlays areas where predictor values were outside the range of values at the sample locations and model predictions may be affected by extrapolation. Gray lines denote the expected depth range for *Swiftia*.

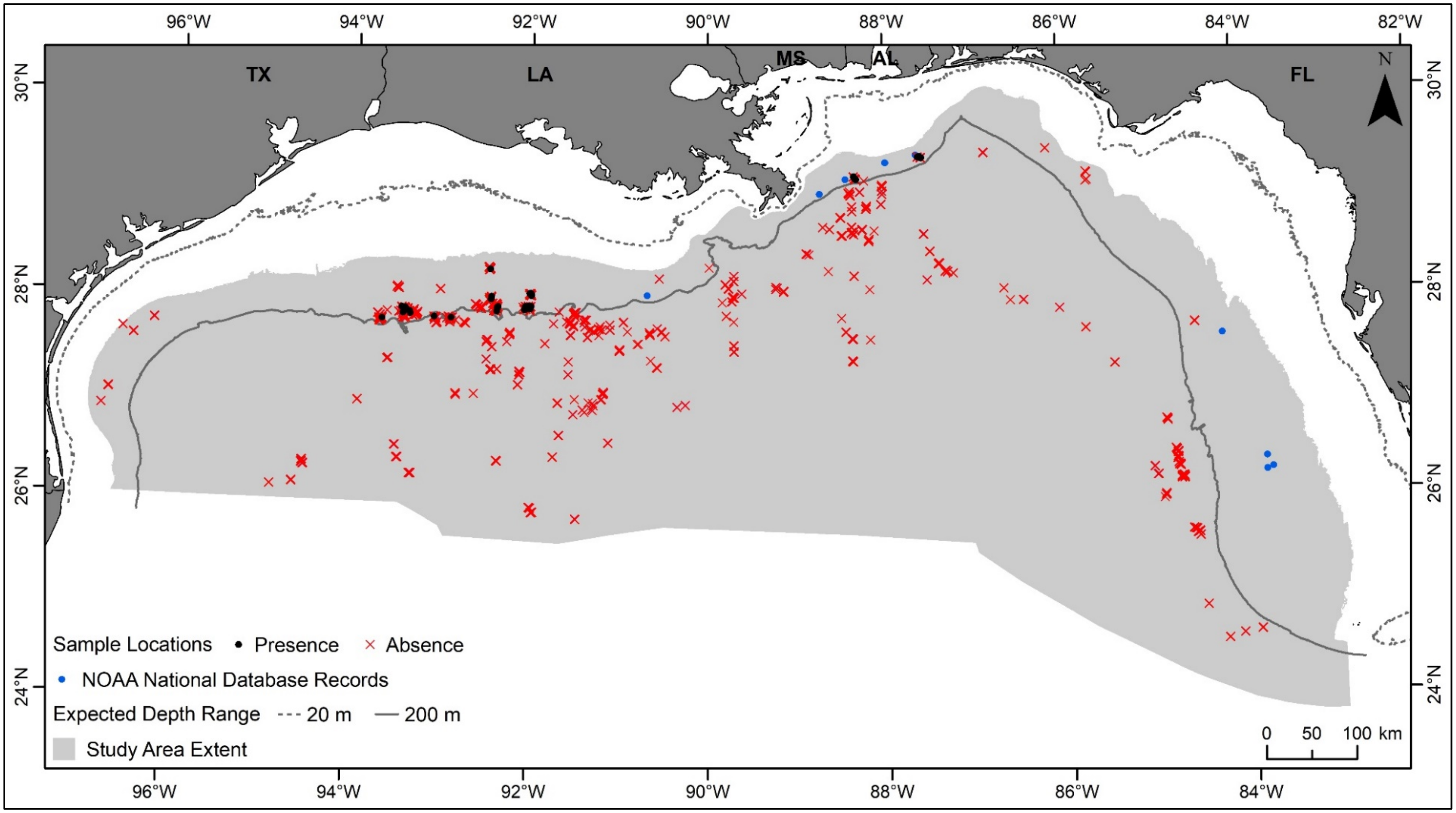

Figure 39. Occurrence records for the gorgonian coral *Swiftia exserta* (order Alcyonacea, family Plexauridae).

This map shows the observed occurrence (presence-absence) of *S. exserta* at sample locations in the presence-absence database compiled for this study. Additional records of occurrence in the NOAA National Database are also displayed. Gray lines denote the expected depth range for *S. exserta*.

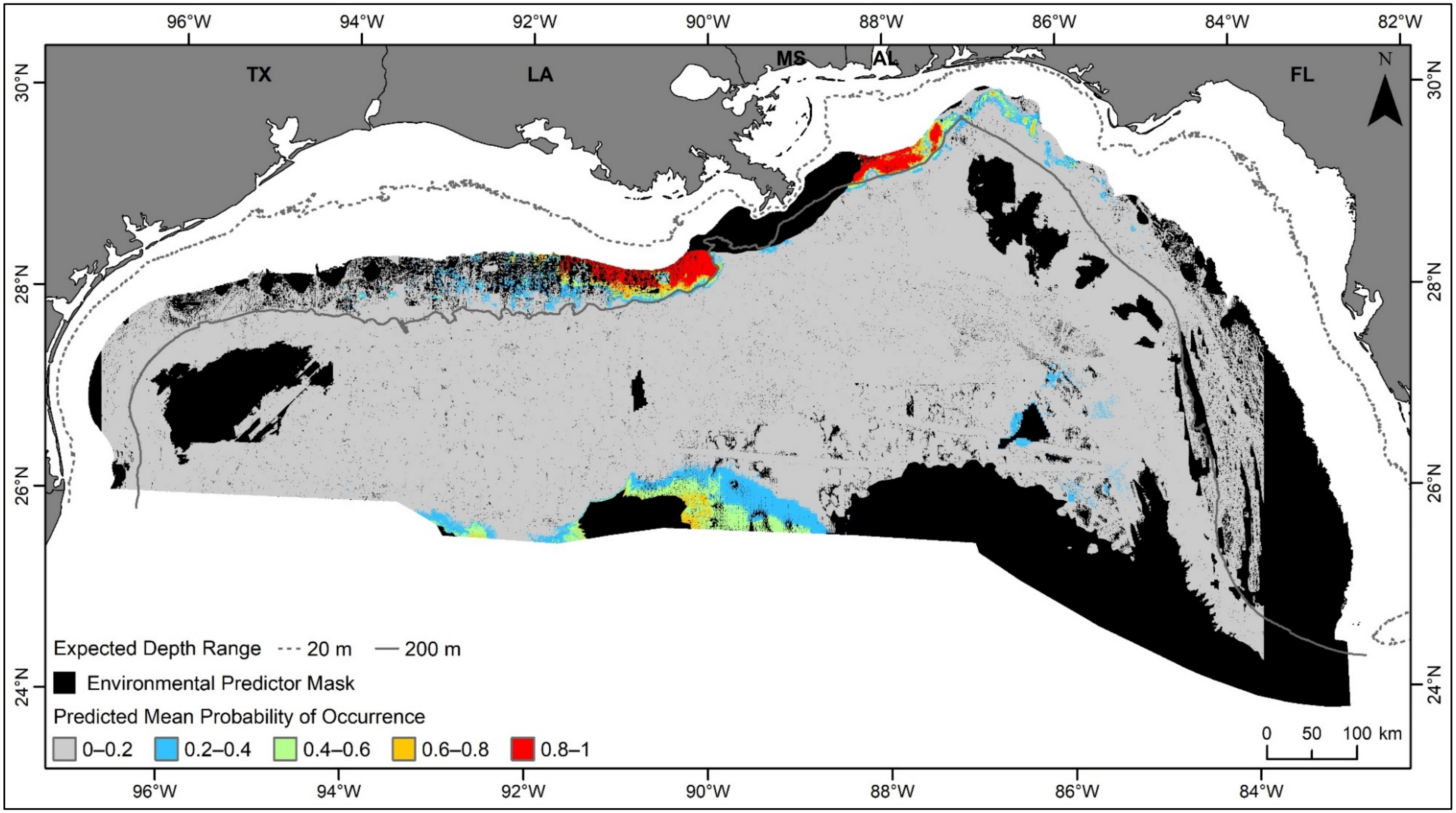

Figure 40. Predicted occurrence of the gorgonian coral *Swiftia exserta* (order Alcyonacea, family Plexauridae).

This map shows the predicted mean probability of occurrence (i.e., the predicted posterior mean occupancy probability) for *S. exserta* from the single-taxon occupancy model. The environmental predictor mask overlays areas where predictor values were outside the range of values at the sample locations and model predictions may be affected by extrapolation. Gray lines denote the expected depth range for *S. exserta*.

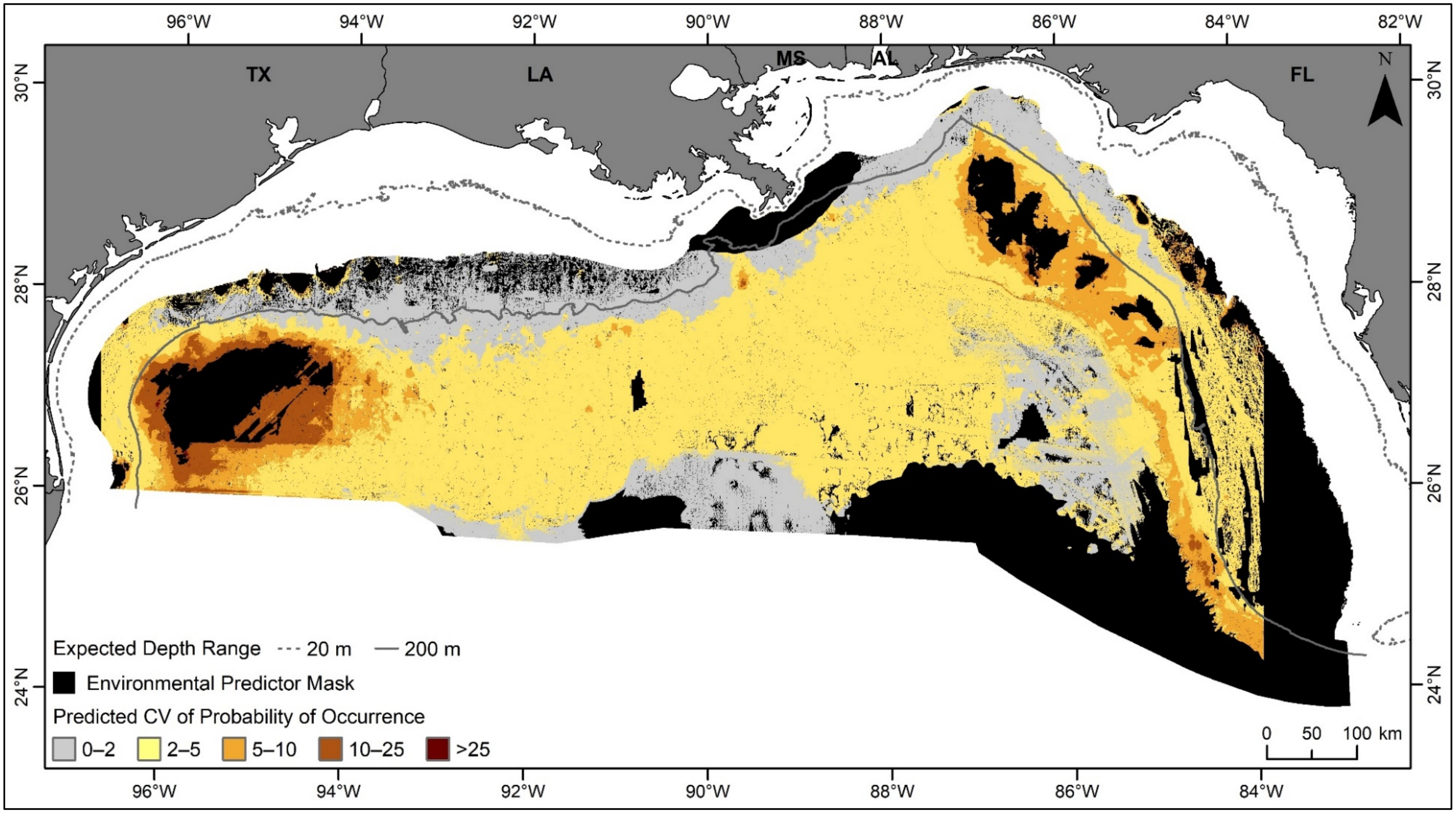

Figure 41. Variability in the predicted occurrence of the gorgonian coral *Swiftia exserta* (order Alcyonacea, family Plexauridae).

This map shows the predicted coefficient of variation (CV) of the probability of occurrence (i.e., the predicted posterior CV of occupancy probability) for *S. exserta* from the single-taxon occupancy model. The environmental predictor mask overlays areas where predictor values were outside the range of values at the sample locations and model predictions may be affected by extrapolation. Gray lines denote the expected depth range for *S. exserta*.

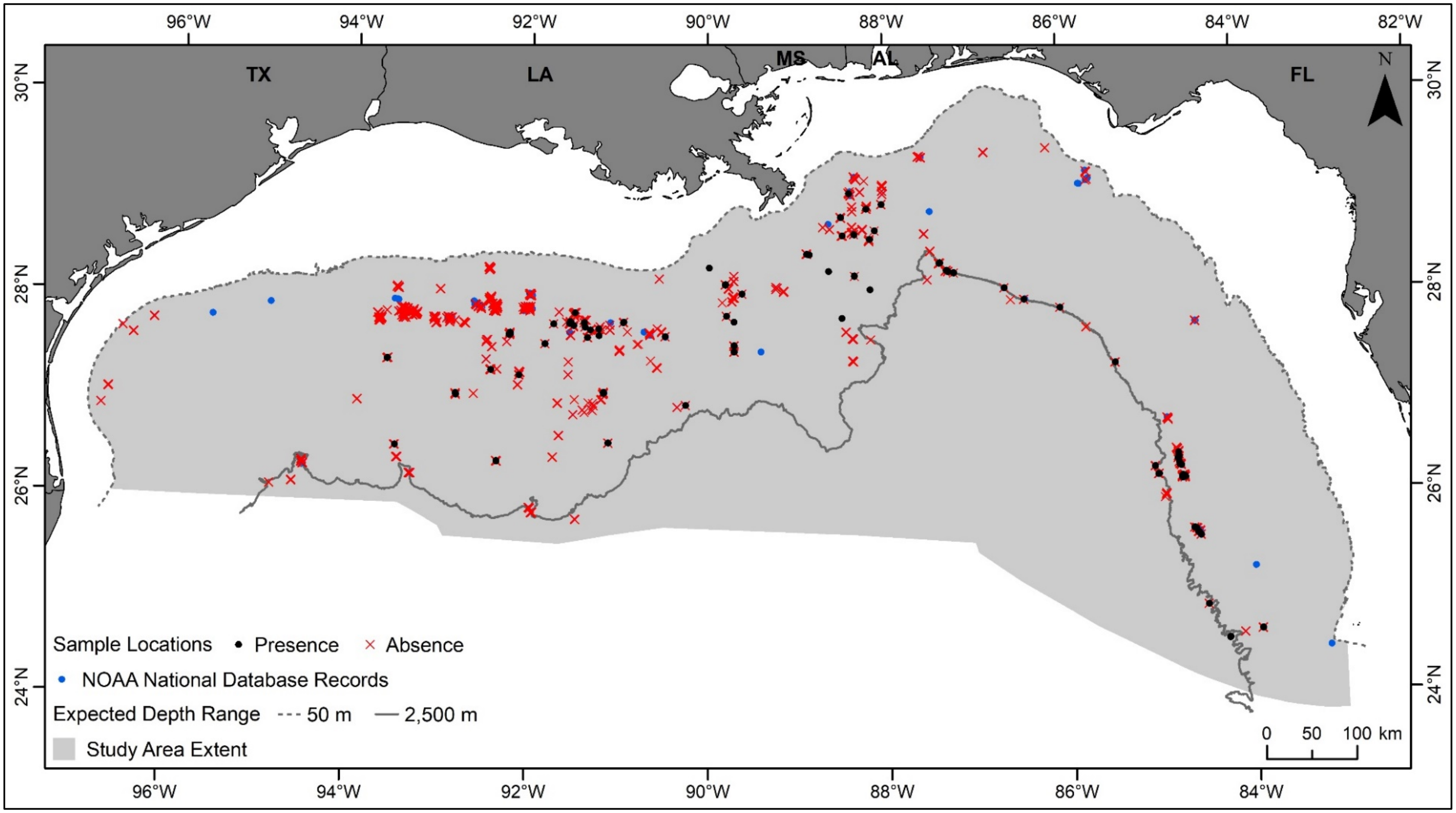

Figure 42. Occurrence records for the gorgonian coral *Paramuricea* (order Alcyonacea, family Plexauridae).

This map shows the observed occurrence (presence-absence) of *Paramuricea* at sample locations in the presence-absence database compiled for this study. Additional records of occurrence in the NOAA National Database are also displayed. Gray lines denote the expected depth range for *Paramuricea*.

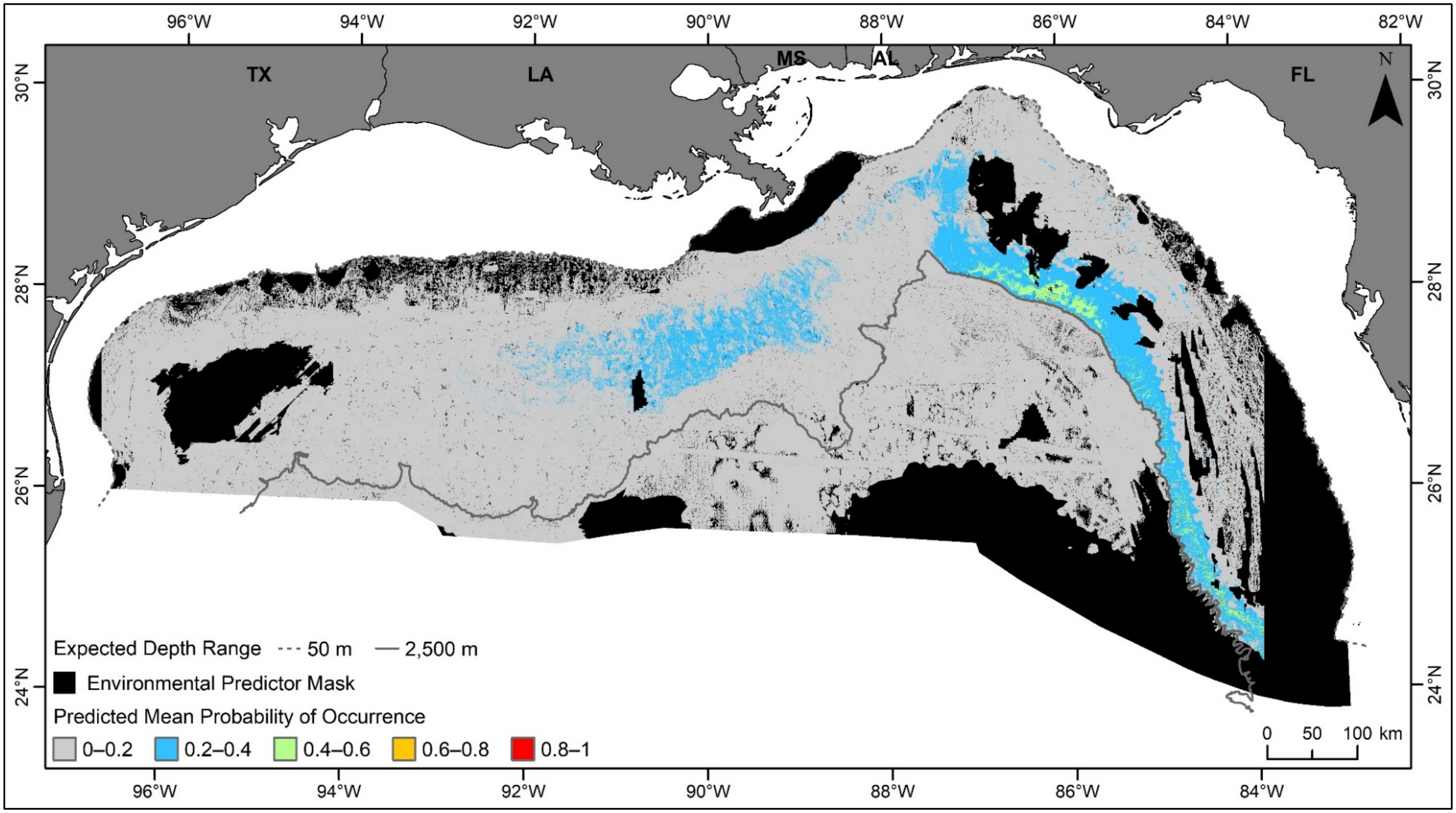

Figure 43. Predicted occurrence of the gorgonian coral *Paramuricea* (order Alcyonacea, family Plexauridae).

This map shows the predicted mean probability of occurrence (i.e., the predicted posterior mean occupancy probability) for *Paramuricea* from the multi-genus occupancy model of family Plexauridae. The environmental predictor mask overlays areas where predictor values were outside the range of values at the sample locations and model predictions may be affected by extrapolation. Gray lines denote the expected depth range for *Paramuricea*.

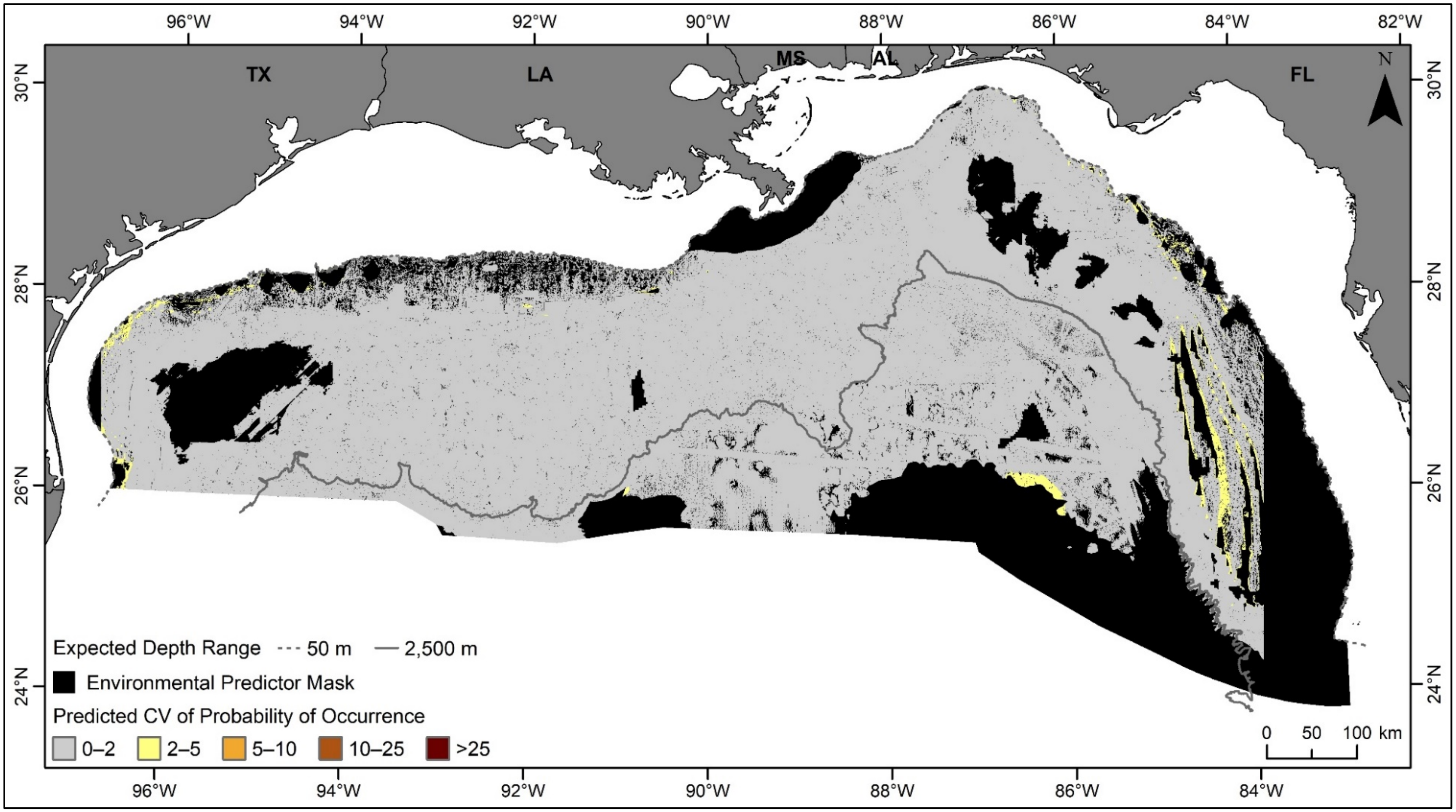

Figure 44. Variability in the predicted occurrence of the gorgonian coral *Paramuricea* (order Alcyonacea, family Plexauridae).

This map shows the predicted coefficient of variation (CV) of the probability of occurrence (i.e., the predicted posterior CV of occupancy probability) for *Paramuricea* from the multi-genus occupancy model of family Plexauridae. The environmental predictor mask overlays areas where predictor values were outside the range of values at the sample locations and model predictions may be affected by extrapolation. Gray lines denote the expected depth range for *Paramuricea*.

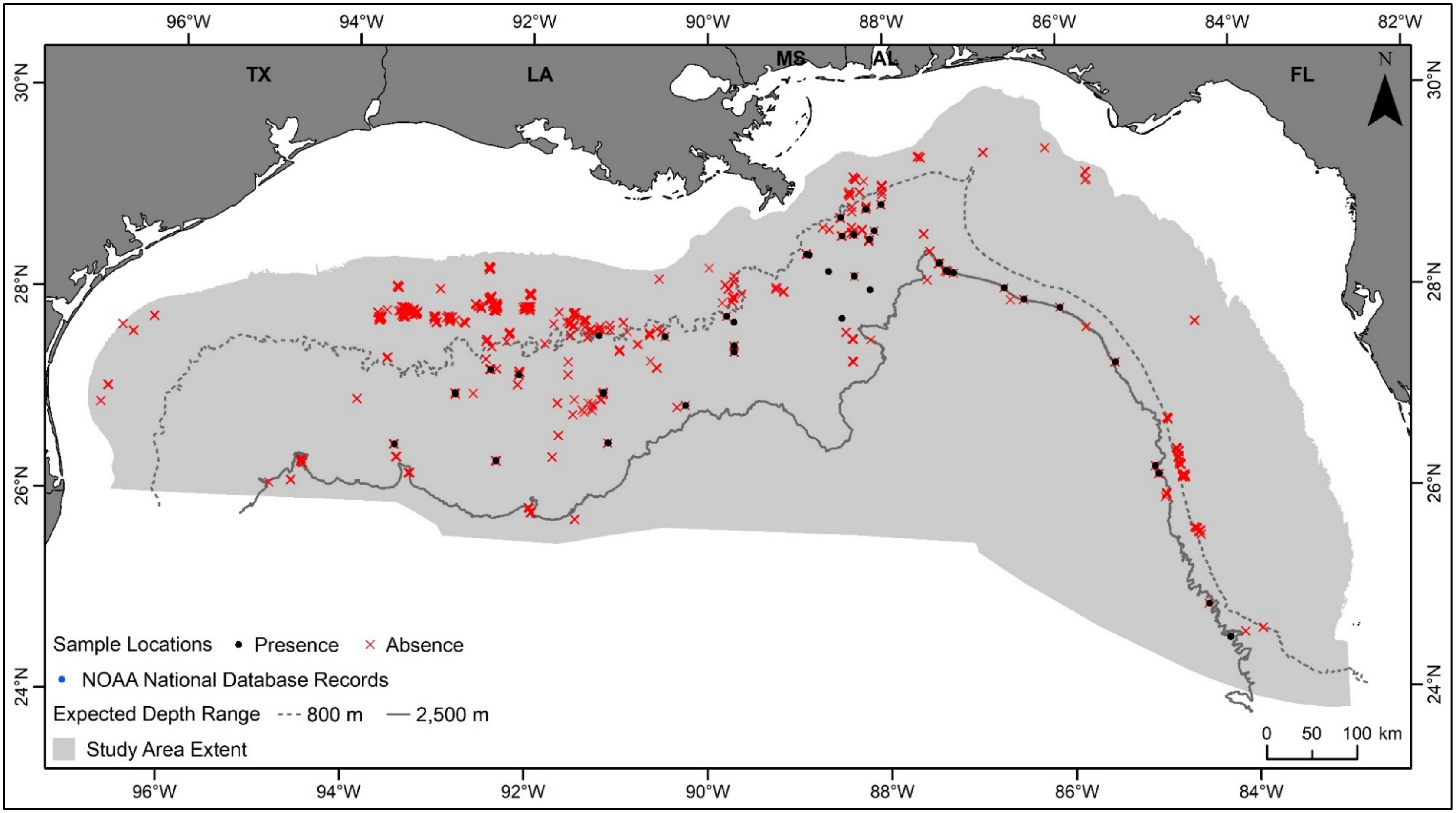

Figure 45. Occurrence records for the gorgonian coral *Paramuricea biscaya* (order Alcyonacea, family Plexauridae).

This map shows the observed occurrence (presence-absence) of *P. biscaya* at sample locations in the presence-absence database compiled for this study. Additional records of occurrence in the NOAA National Database are also displayed. Gray lines denote the expected depth range for *P. biscaya*.

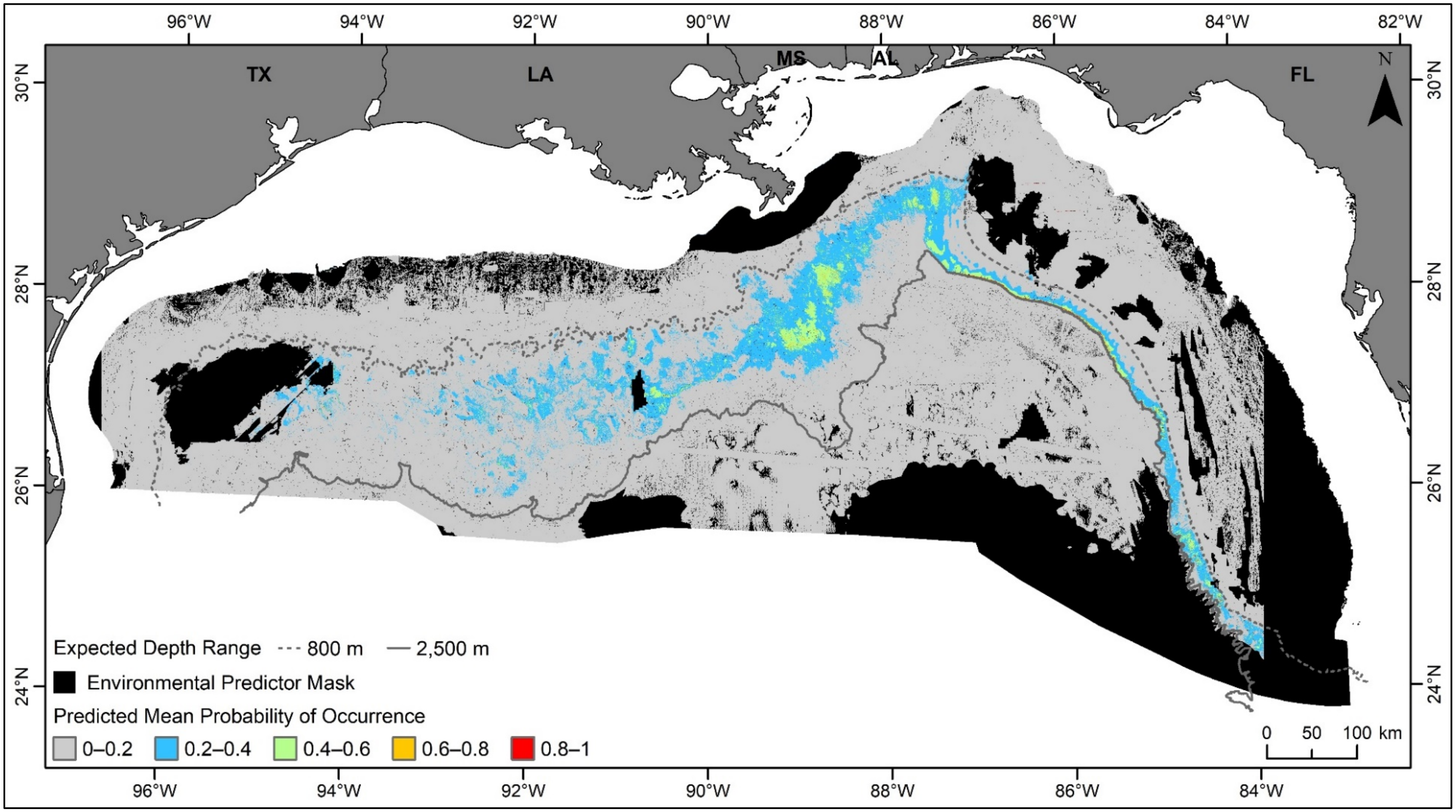

Figure 46. Predicted occurrence of the gorgonian coral *Paramuricea biscaya* (order Alcyonacea, family Plexauridae).

This map shows the predicted mean probability of occurrence (i.e., the predicted posterior mean occupancy probability) for *P. biscaya* from the single-taxon occupancy model. The environmental predictor mask overlays areas where predictor values were outside the range of values at the sample locations and model predictions may be affected by extrapolation. Gray lines denote the expected depth range for *P. biscaya*.

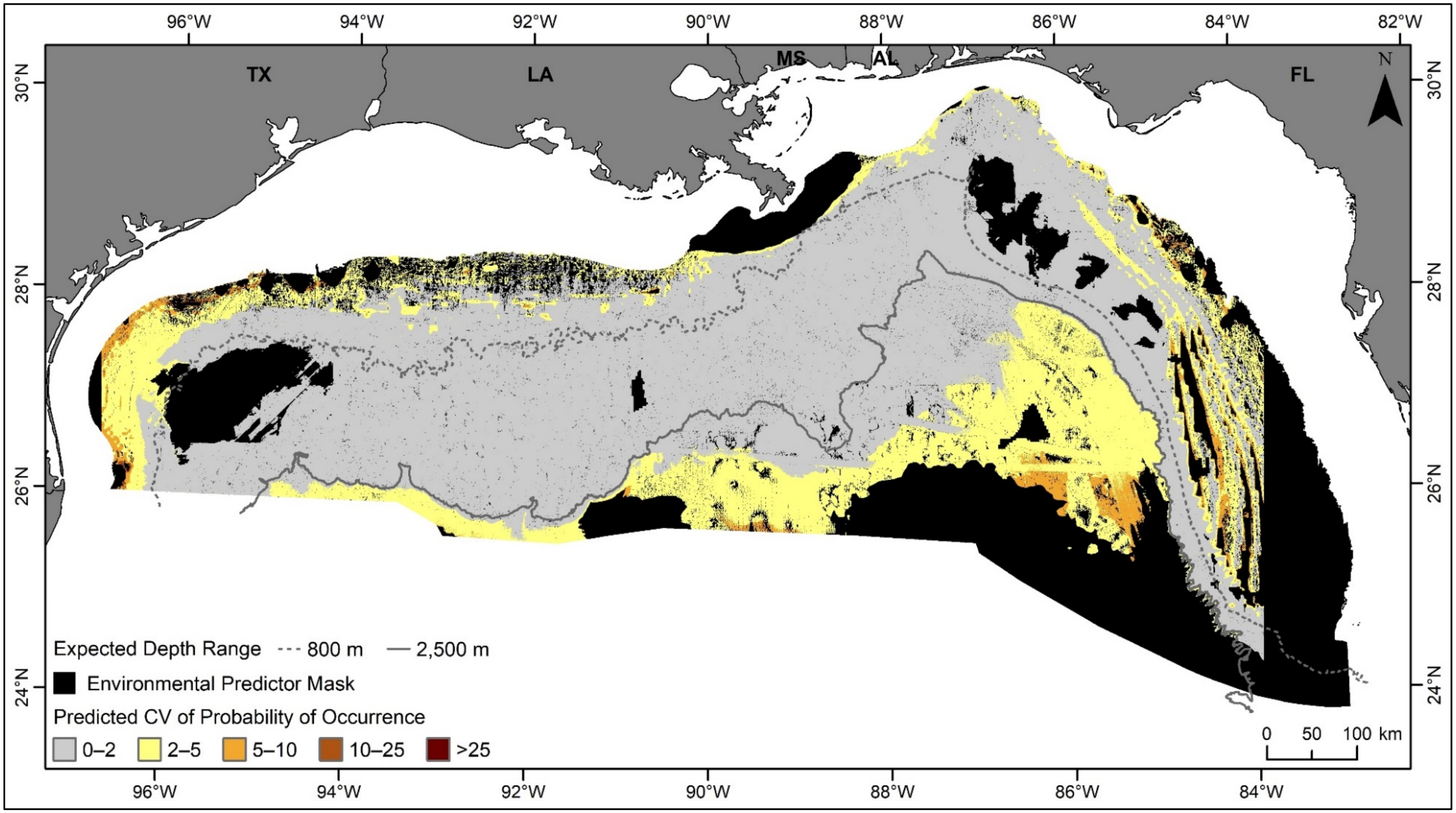

Figure 47. Variability in the predicted occurrence of the gorgonian coral *Paramuricea biscaya* (order Alcyonacea, family Plexauridae).

This map shows the predicted coefficient of variation (CV) of the probability of occurrence (i.e., the predicted posterior CV of occupancy probability) for *P. biscaya* from the single-taxon occupancy model. The environmental predictor mask overlays areas where predictor values were outside the range of values at the sample locations and model predictions may be affected by extrapolation. Gray lines denote the expected depth range for *P. biscaya*.

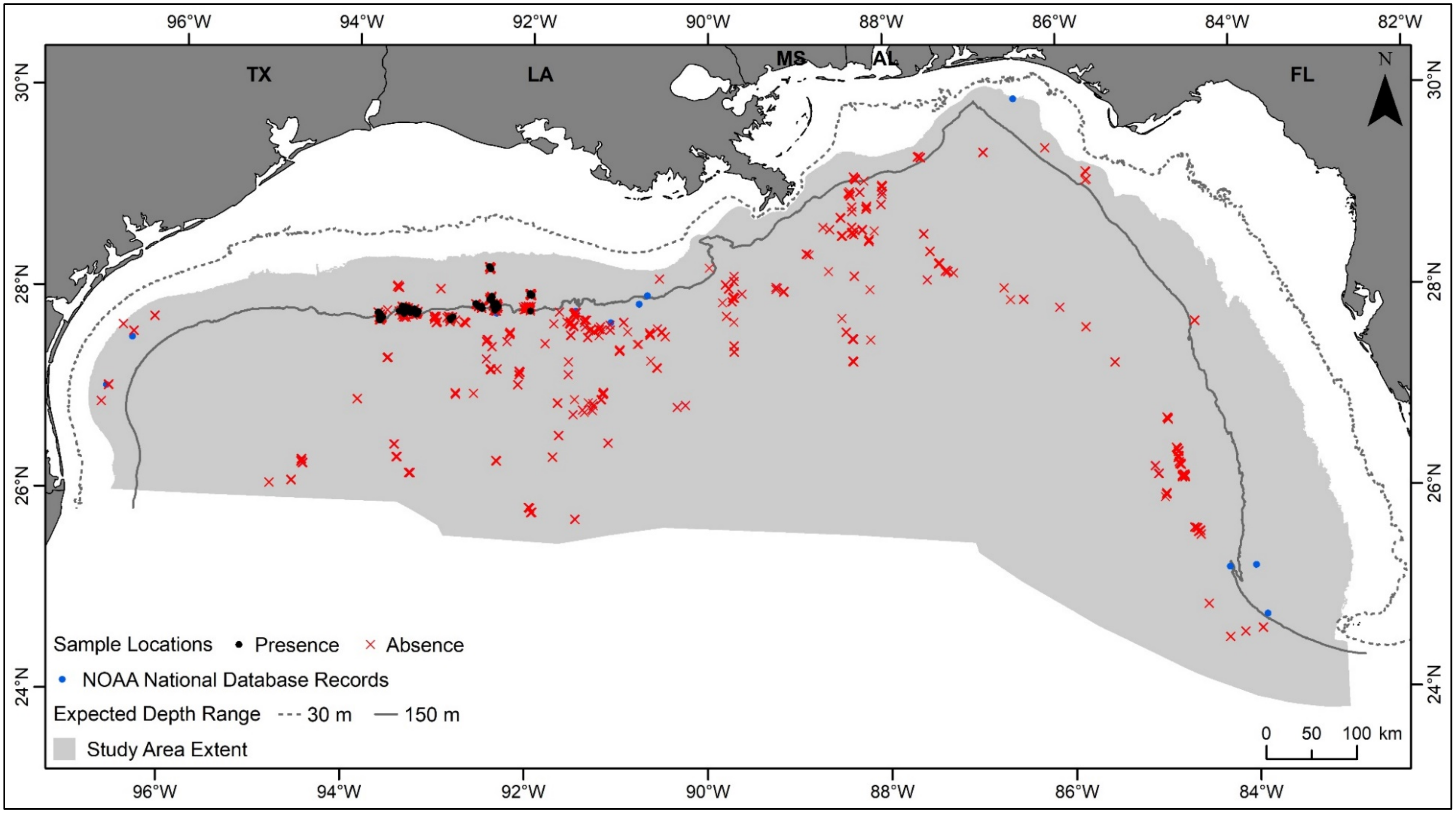

Figure 48. Occurrence records for the gorgonian coral *Caliacis* (order Alcyonacea, family Plexauridae).

This map shows the observed occurrence (presence-absence) of *Caliacis* at sample locations in the presence-absence database compiled for this study. Additional records of occurrence in the NOAA National Database are also displayed. Gray lines denote the expected depth range for *Caliacis*.

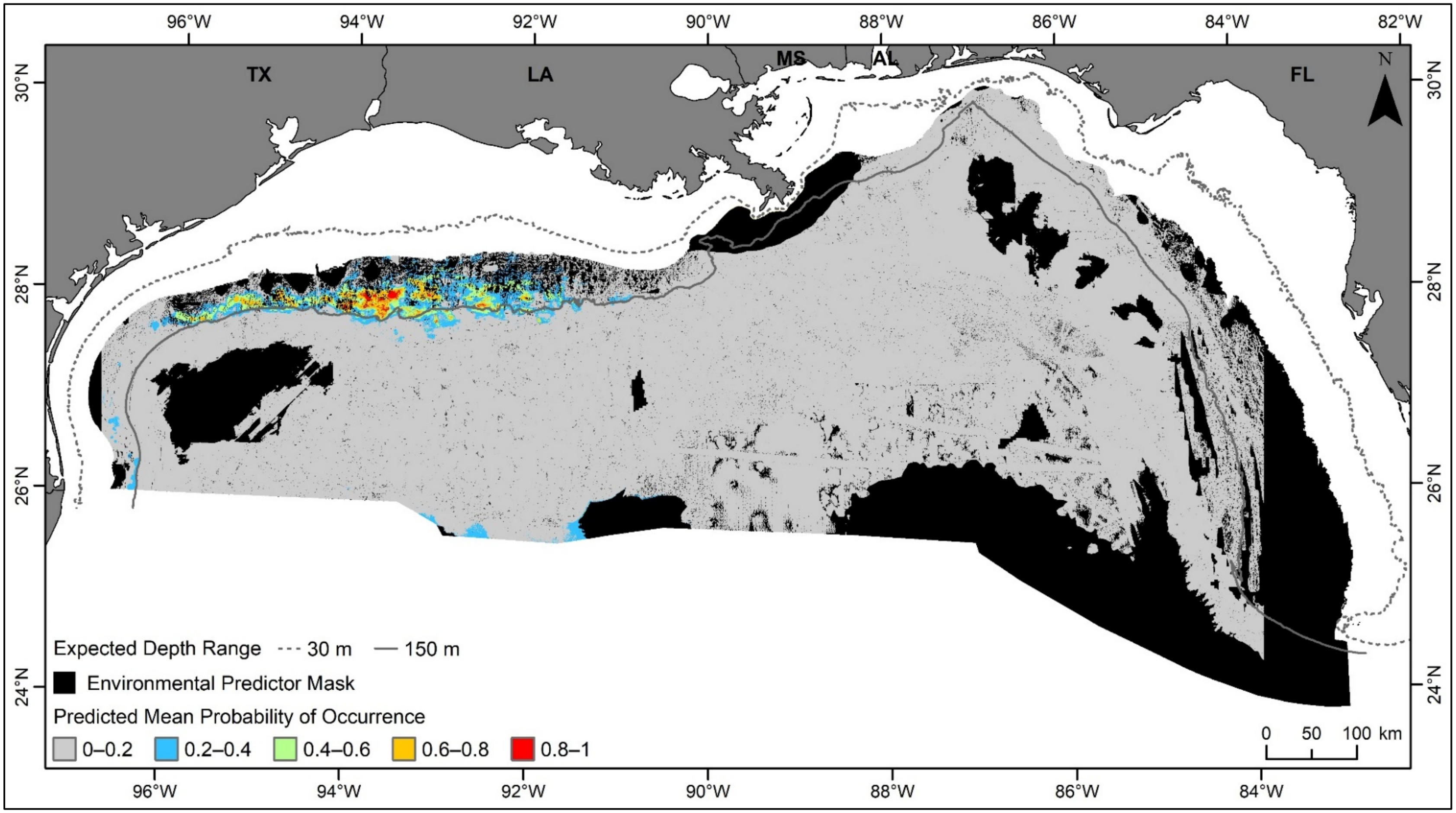

Figure 49. Predicted occurrence of the gorgonian coral *Caliacis* (order Alcyonacea, family Plexauridae).

This map shows the predicted mean probability of occurrence (i.e., the predicted posterior mean occupancy probability) for *Caliacis* from the multi-genus occupancy model of family Plexauridae. The environmental predictor mask overlays areas where predictor values were outside the range of values at the sample locations and model predictions may be affected by extrapolation. Gray lines denote the expected depth range for *Caliacis*.

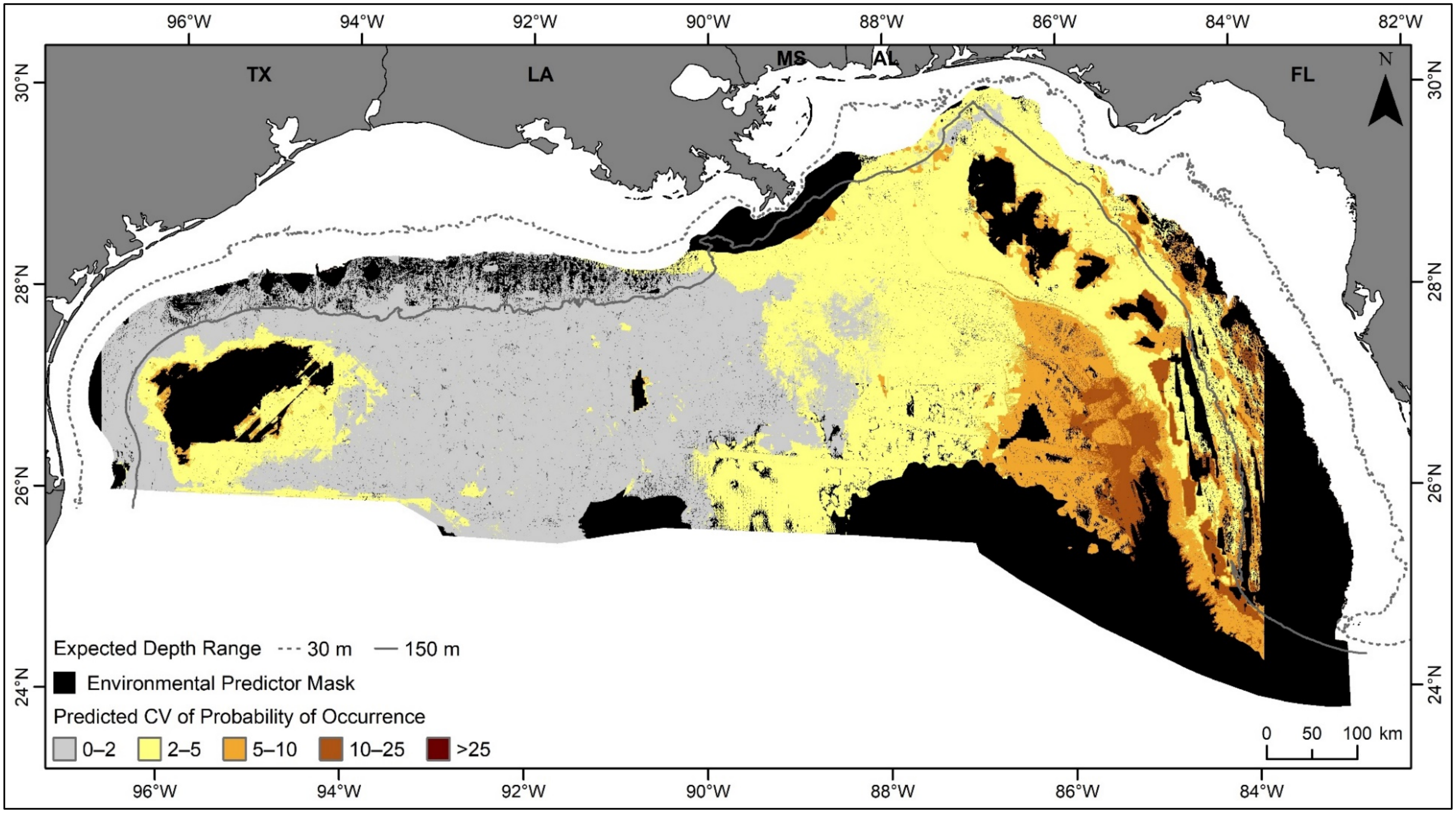

Figure 50. Variability in the predicted occurrence of the gorgonian coral *Caliacis* (order Alcyonacea, family Plexauridae).

This map shows the predicted coefficient of variation (CV) of the probability of occurrence (i.e., the predicted posterior CV of occupancy probability) for *Caliacis* from the multi-genus occupancy model of family Plexauridae. The environmental predictor mask overlays areas where predictor values were outside the range of values at the sample locations and model predictions may be affected by extrapolation. Gray lines denote the expected depth range for *Caliacis*.

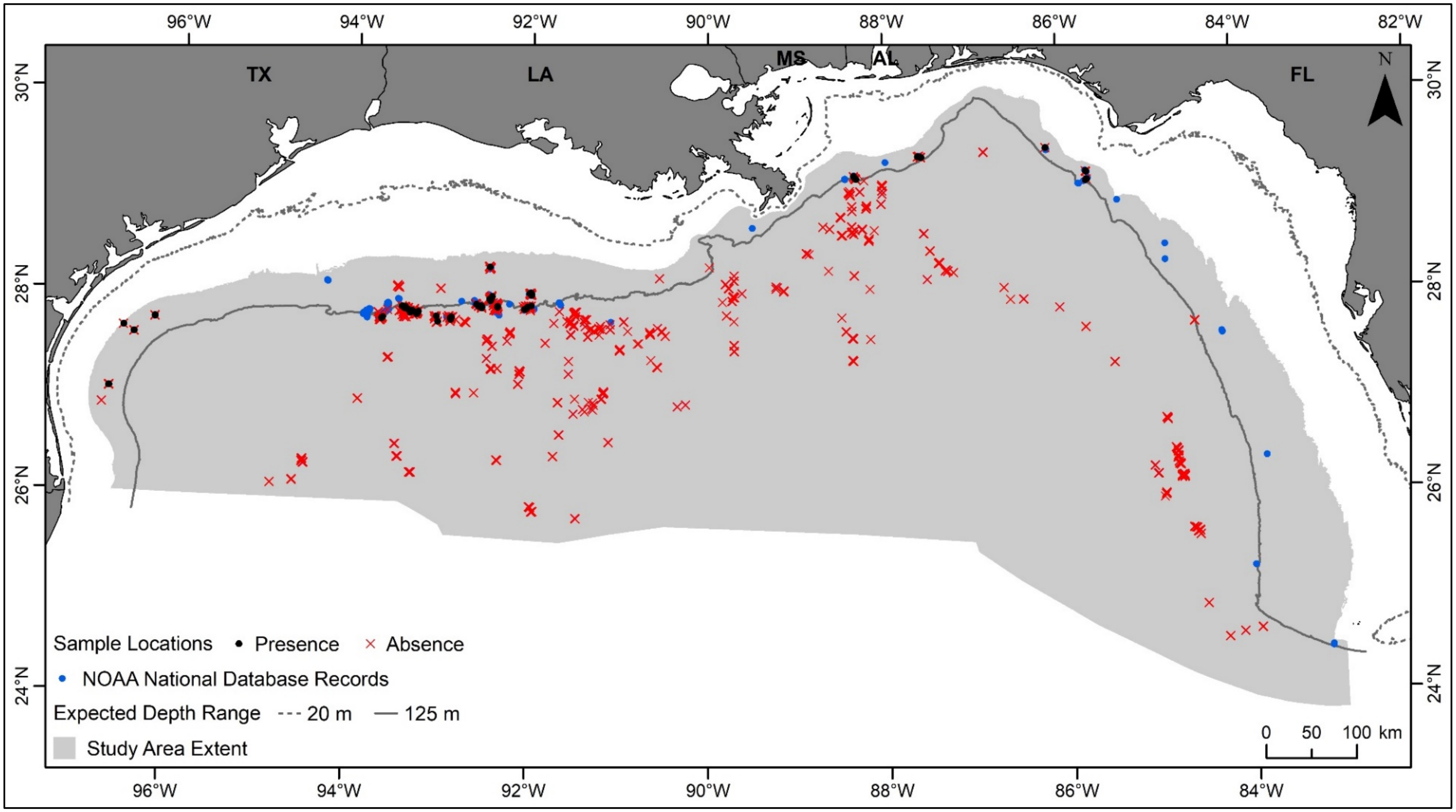

Figure 51. Occurrence records for the gorgonian coral *Muricea* (order Alcyonacea, family Plexauridae).

This map shows the observed occurrence (presence-absence) of *Muricea* at sample locations in the presence-absence database compiled for this study. Additional records of occurrence in the NOAA National Database are also displayed. Gray lines denote the expected depth range for *Muricea*.

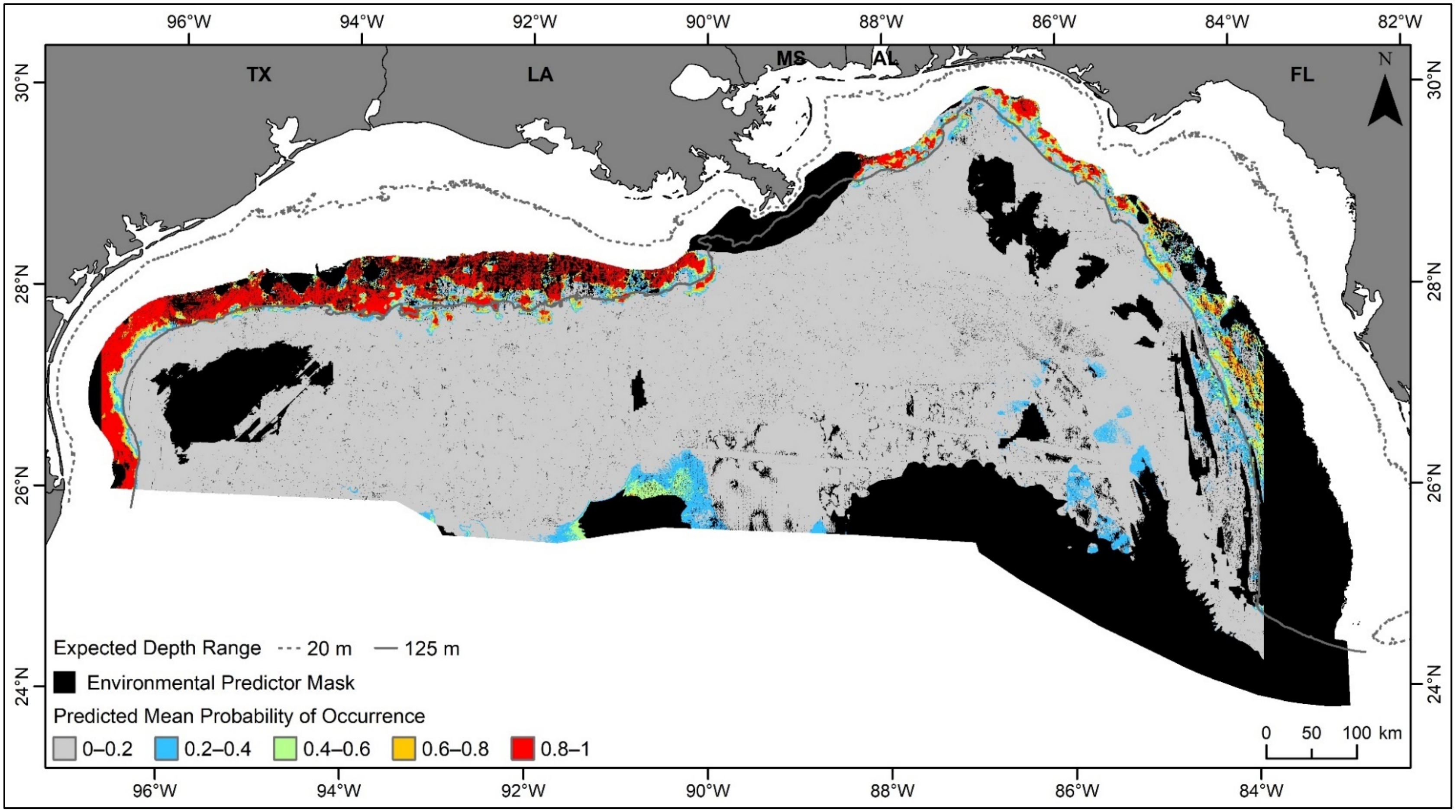

Figure 52. Predicted occurrence of the gorgonian coral *Muricea* (order Alcyonacea, family Plexauridae).

This map shows the predicted mean probability of occurrence (i.e., the predicted posterior mean occupancy probability) for *Muricea* from the multi-genus occupancy model of family Plexauridae. The environmental predictor mask overlays areas where predictor values were outside the range of values at the sample locations and model predictions may be affected by extrapolation. Gray lines denote the expected depth range for *Muricea*.

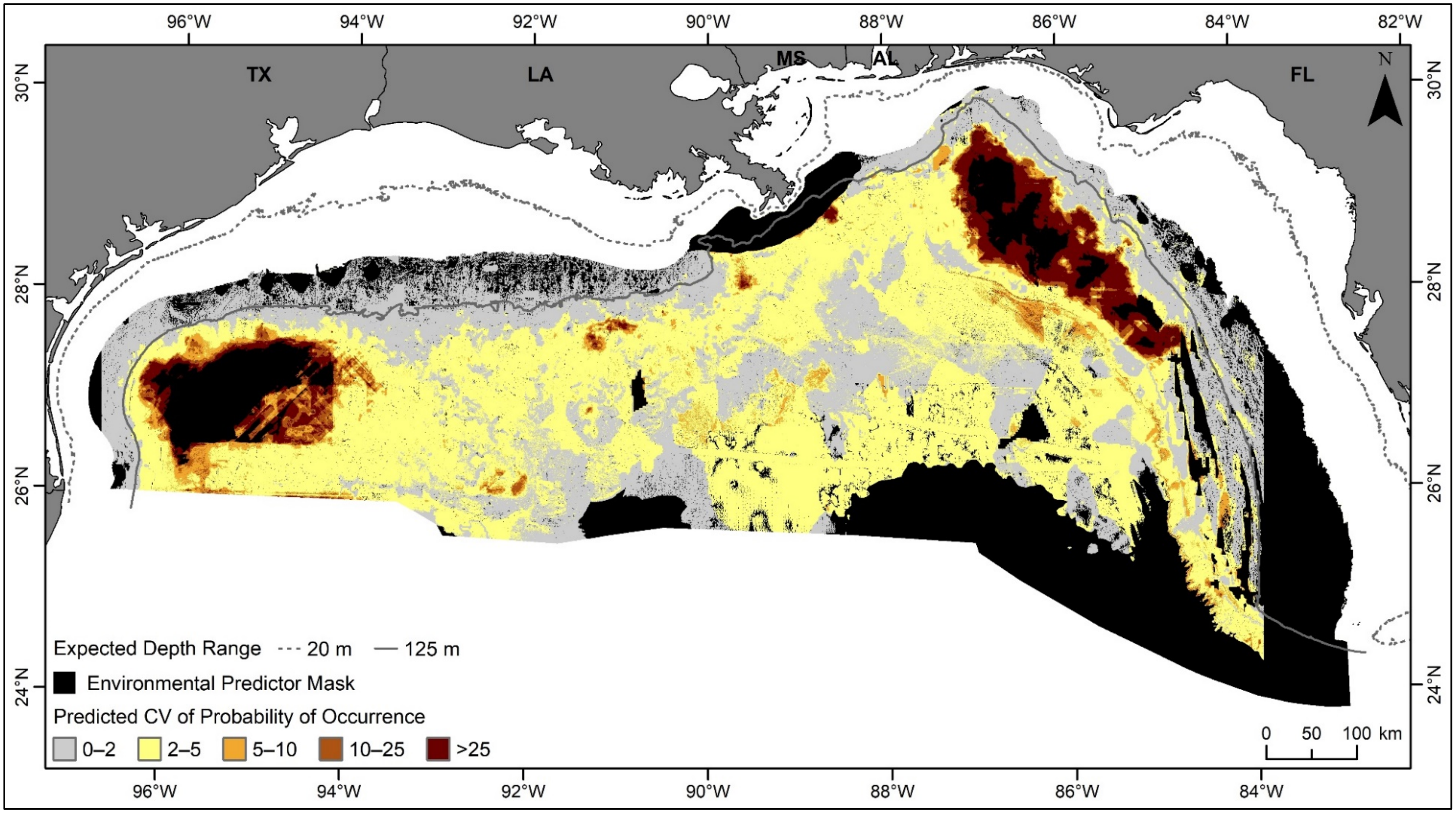

Figure 53. Variability in the predicted occurrence of the gorgonian coral *Muricea* (order Alcyonacea, family Plexauridae).

This map shows the predicted coefficient of variation (CV) of the probability of occurrence (i.e., the predicted posterior CV of occupancy probability) for *Muricea* from the multi-genus occupancy model of family Plexauridae. The environmental predictor mask overlays areas where predictor values were outside the range of values at the sample locations and model predictions may be affected by extrapolation. Gray lines denote the expected depth range for *Muricea*.

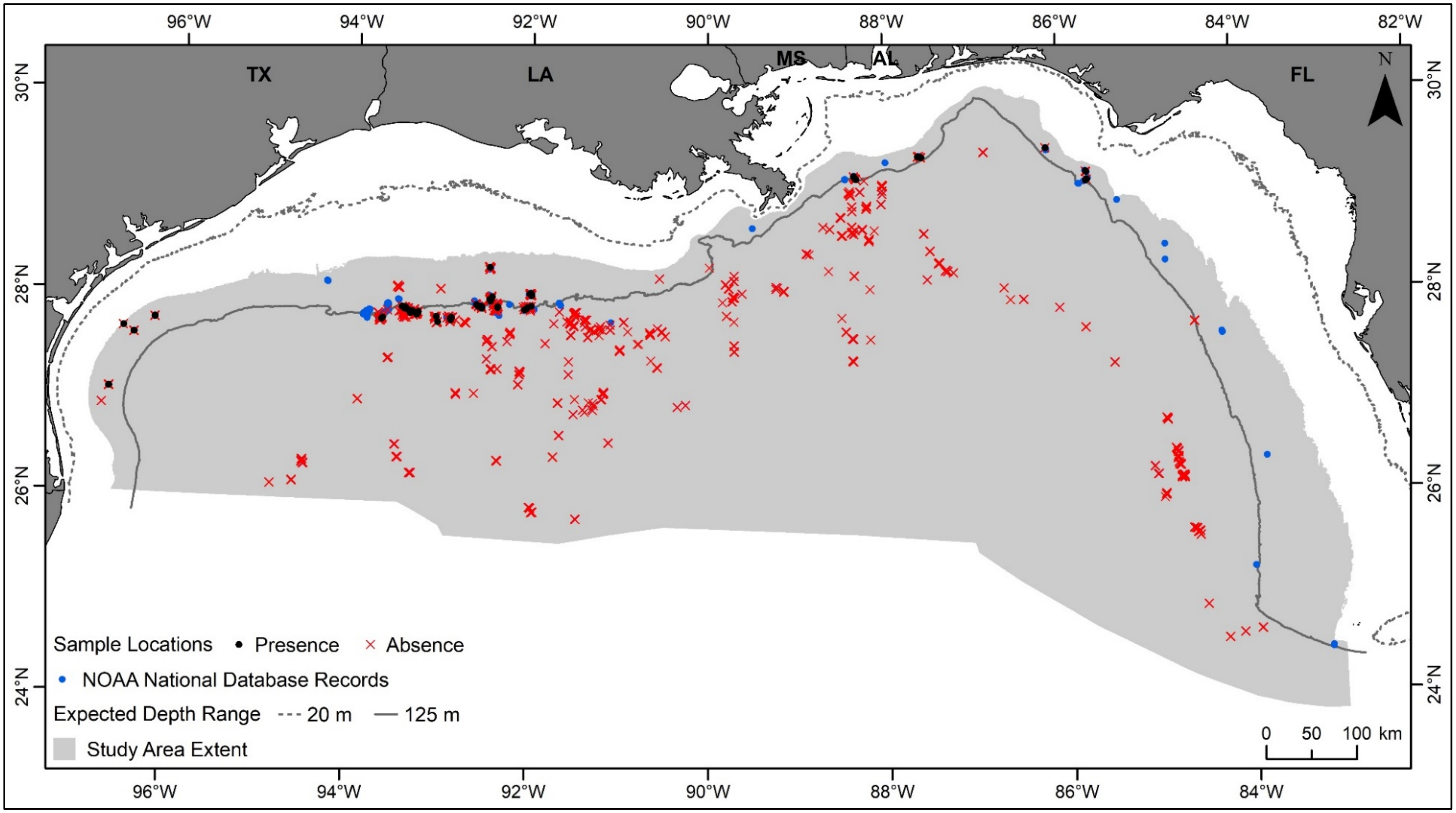

Figure 54. Occurrence records for the gorgonian coral *Muricea pendula* (order Alcyonacea, family Plexauridae).

This map shows the observed occurrence (presence-absence) of *M. pendula* at sample locations in the presence-absence database compiled for this study. Additional records of occurrence in the NOAA National Database are also displayed. Gray lines denote the expected depth range for *M. pendula*.

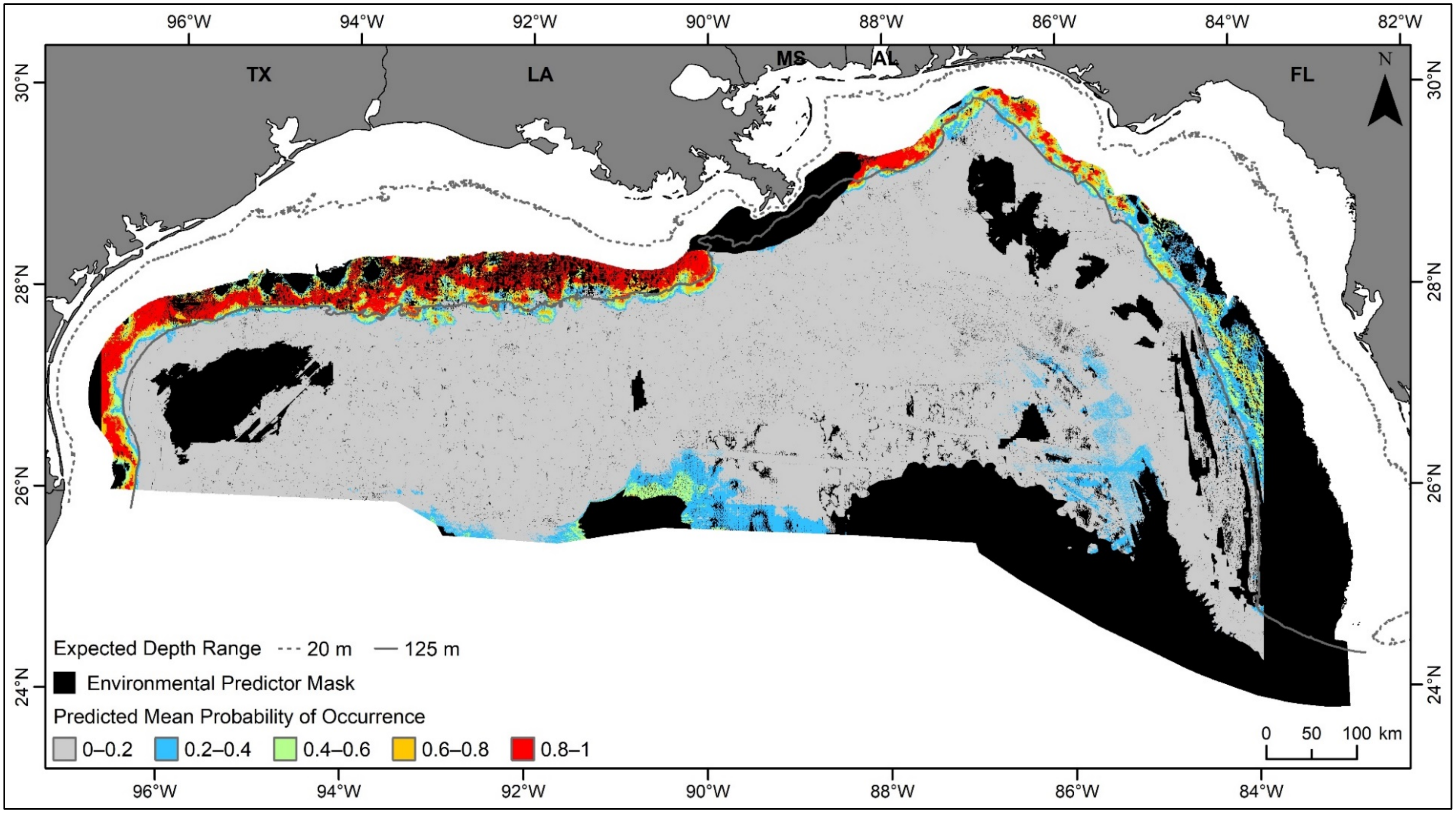

Figure 55. Predicted occurrence of the gorgonian coral *Muricea pendula* (order Alcyonacea, family Plexauridae).

This map shows the predicted mean probability of occurrence (i.e., the predicted posterior mean occupancy probability) for *M. pendula* from the single-taxon occupancy model. The environmental predictor mask overlays areas where predictor values were outside the range of values at the sample locations and model predictions may be affected by extrapolation. Gray lines denote the expected depth range for *M. pendula*.

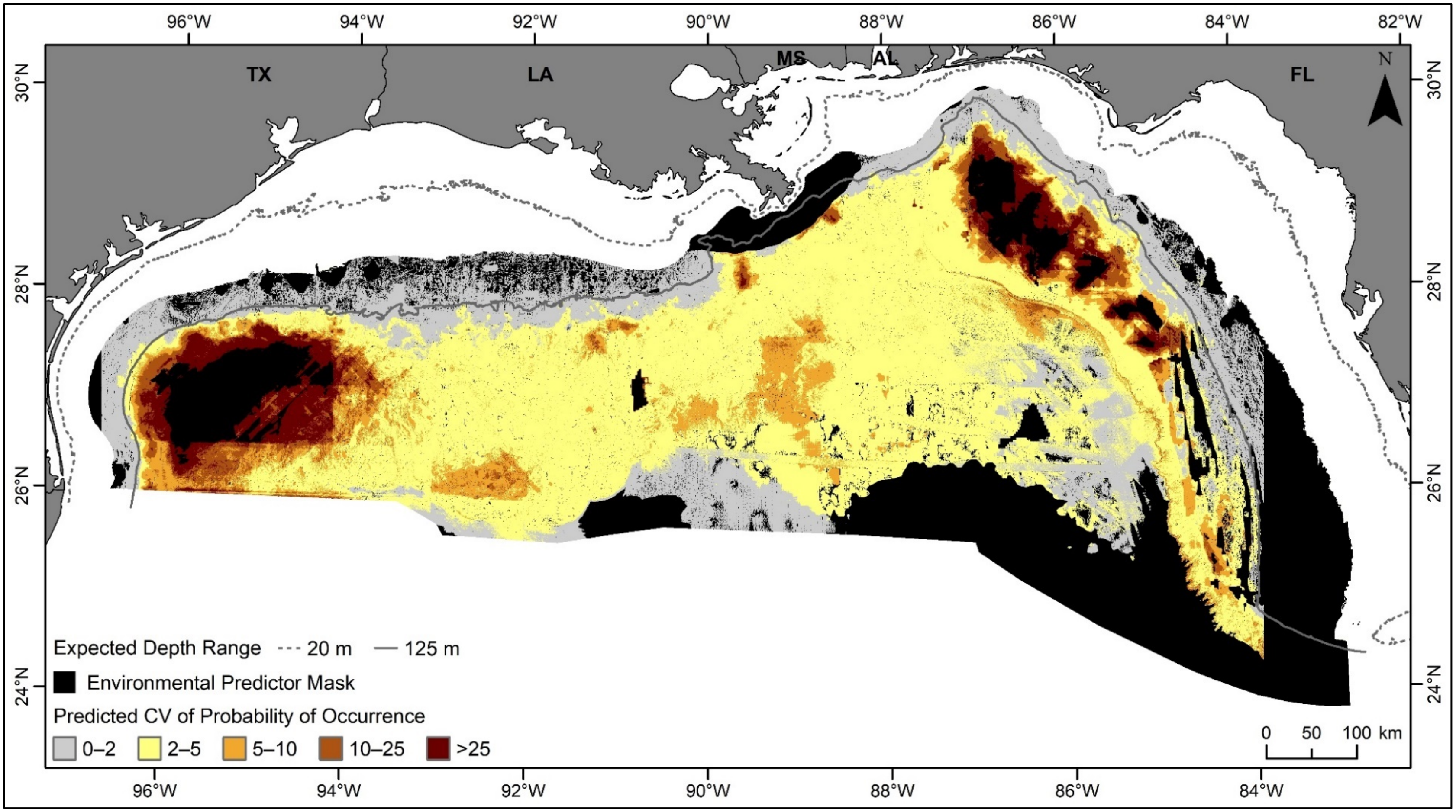

Figure 56. Variability in the predicted occurrence of the gorgonian coral *Muricea pendula* (order Alcyonacea, family Plexauridae).

This map shows the predicted coefficient of variation (CV) of the probability of occurrence (i.e., the predicted posterior CV of occupancy probability) for *M. pendula* from the single-taxon occupancy model. The environmental predictor mask overlays areas where predictor values were outside the range of values at the sample locations and model predictions may be affected by extrapolation. Gray lines denote the expected depth range for *M. pendula*.

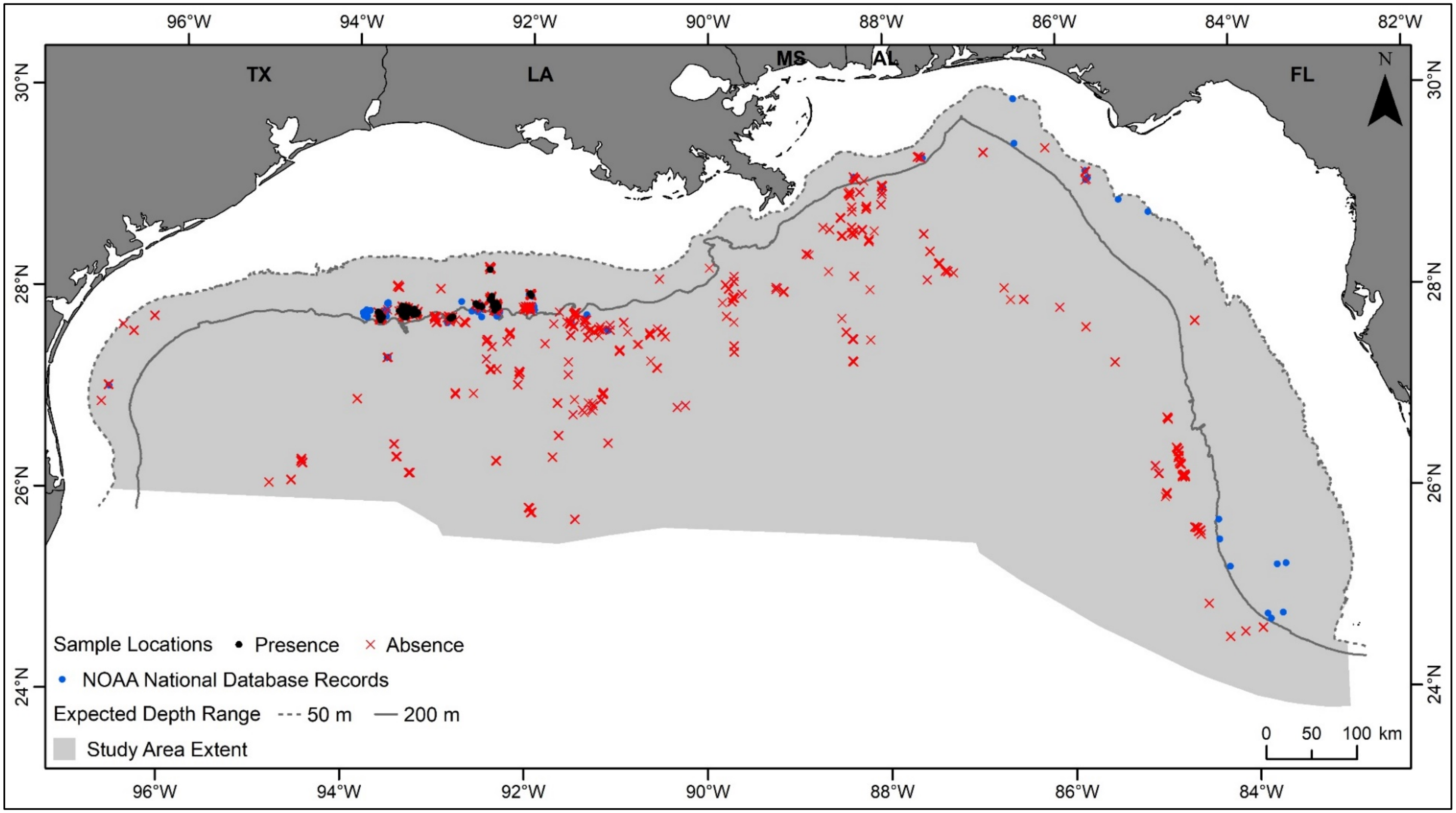

Figure 57. Occurrence records for the gorgonian coral *Scleracis* (order Alcyonacea, family Plexauridae).

This map shows the observed occurrence (presence-absence) of *Scleracis* at sample locations in the presence-absence database compiled for this study. Additional records of occurrence in the NOAA National Database are also displayed. Gray lines denote the expected depth range for *Scleracis*.

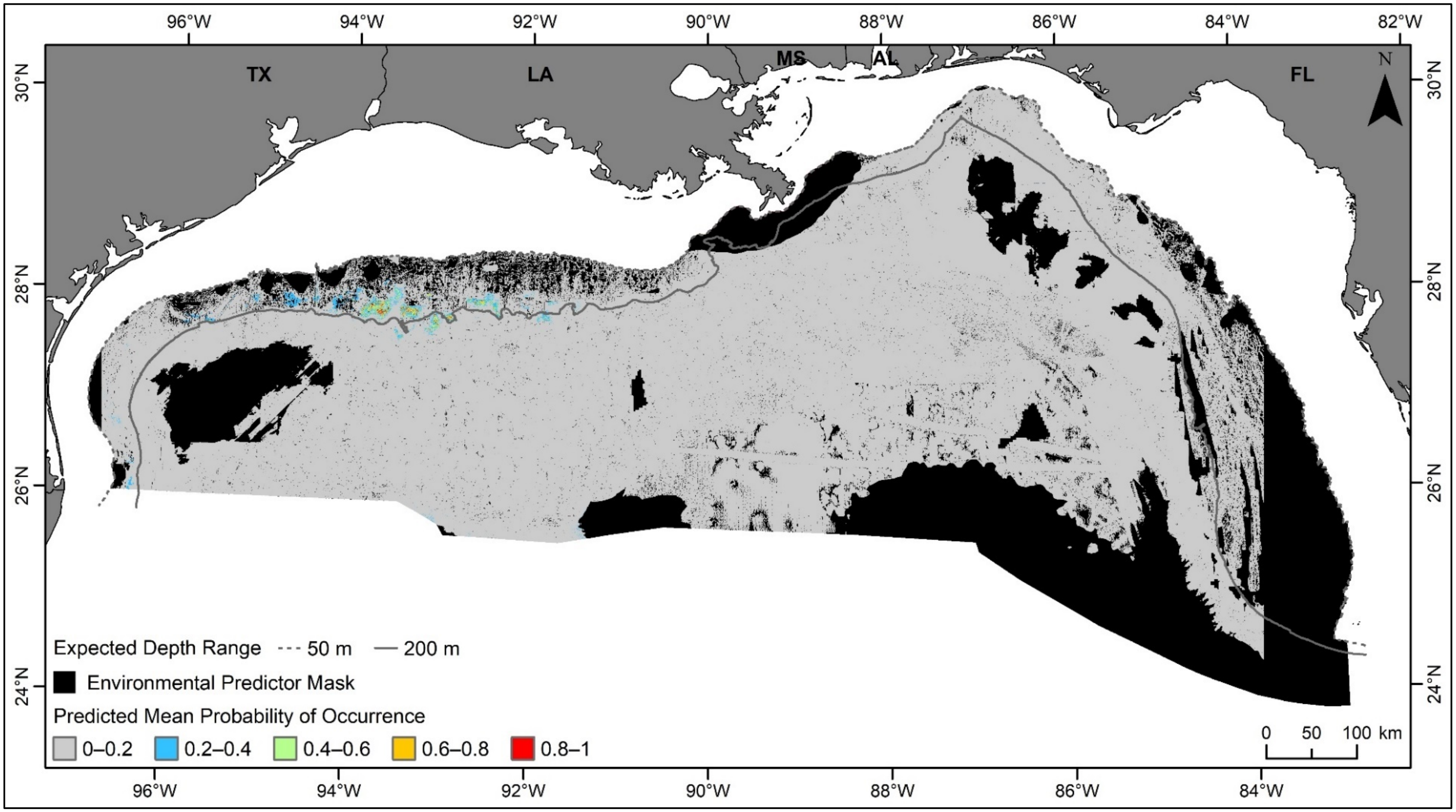

Figure 58. Predicted occurrence of the gorgonian coral *Scleracis* (order Alcyonacea, family Plexauridae).

This map shows the predicted mean probability of occurrence (i.e., the predicted posterior mean occupancy probability) for *Scleracis* from the multi-genus occupancy model of family Plexauridae. The environmental predictor mask overlays areas where predictor values were outside the range of values at the sample locations and model predictions may be affected by extrapolation. Gray lines denote the expected depth range for *Scleracis*.

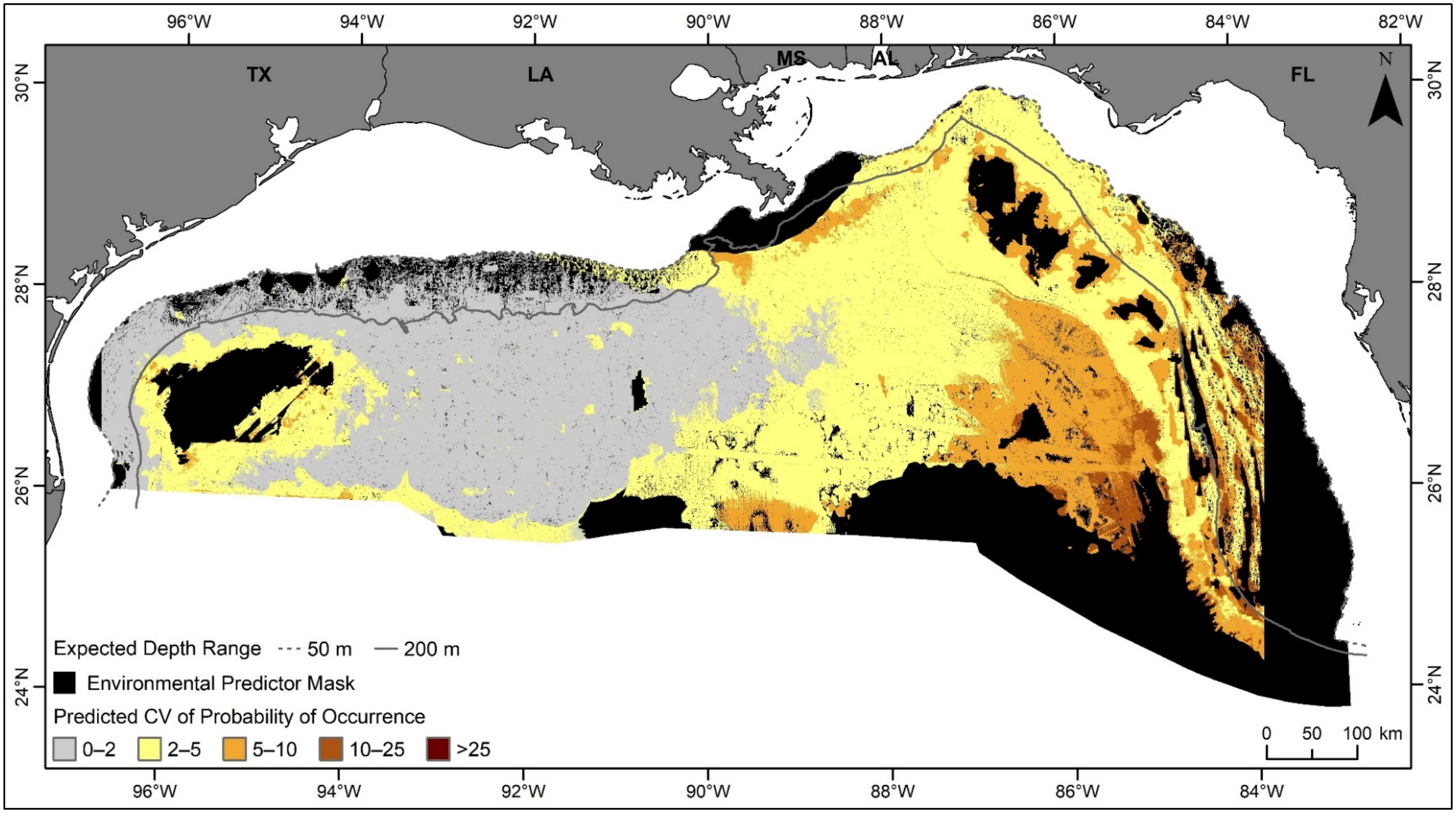

Figure 59. Variability in the predicted occurrence of the gorgonian coral *Scleracis* (order Alcyonacea, family Plexauridae).

This map shows the predicted coefficient of variation (CV) of the probability of occurrence (i.e., the predicted posterior CV of occupancy probability) for *Scleracis* from the multi-genus occupancy model of family Plexauridae. The environmental predictor mask overlays areas where predictor values were outside the range of values at the sample locations and model predictions may be affected by extrapolation. Gray lines denote the expected depth range for *Scleracis*.

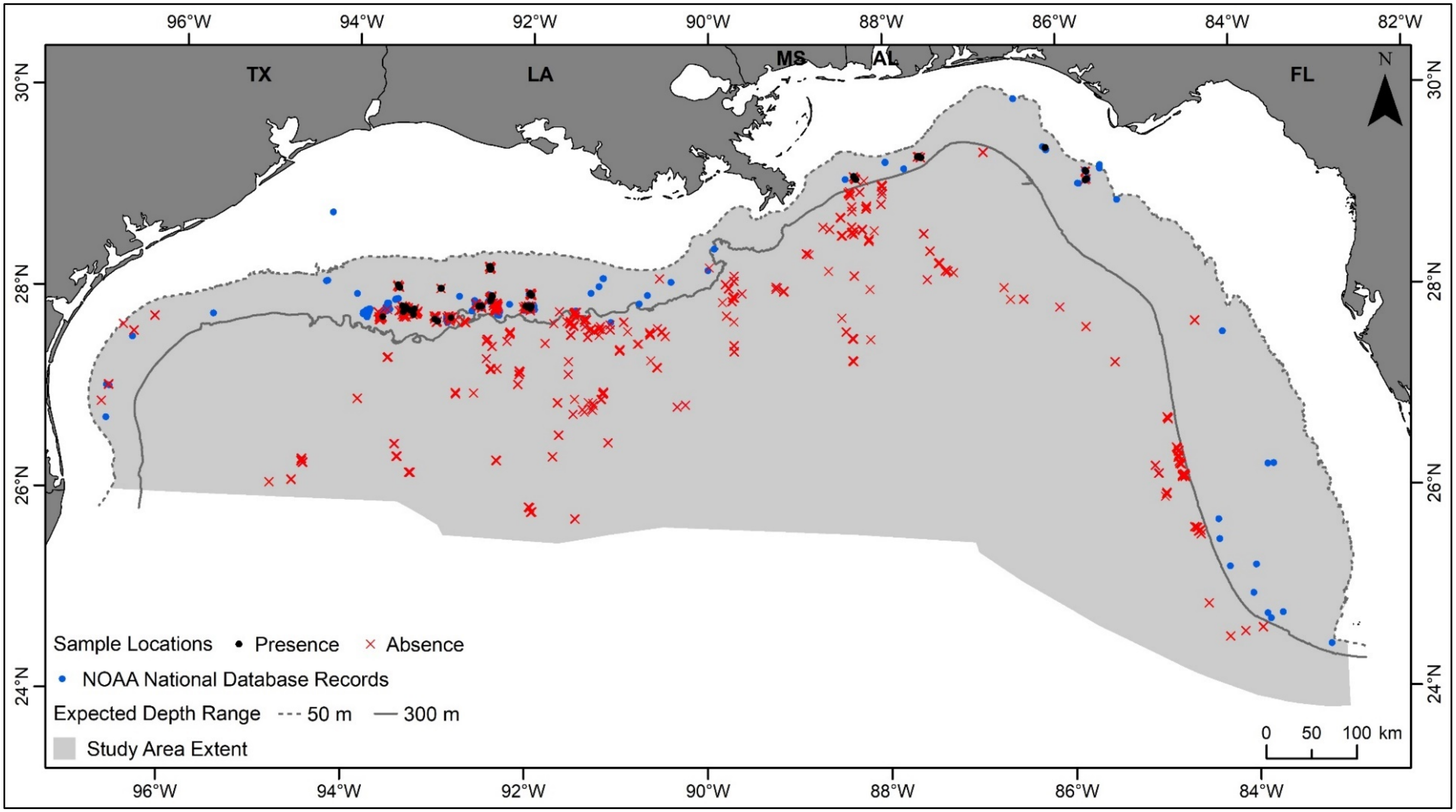

Figure 60. Occurrence records for the gorgonian coral *Thesea* (order Alcyonacea, family Plexauridae).

This map shows the observed occurrence (presence-absence) of *Thesea* at sample locations in the presence-absence database compiled for this study. Additional records of occurrence in the NOAA National Database are also displayed. Gray lines denote the expected depth range for *Thesea*.

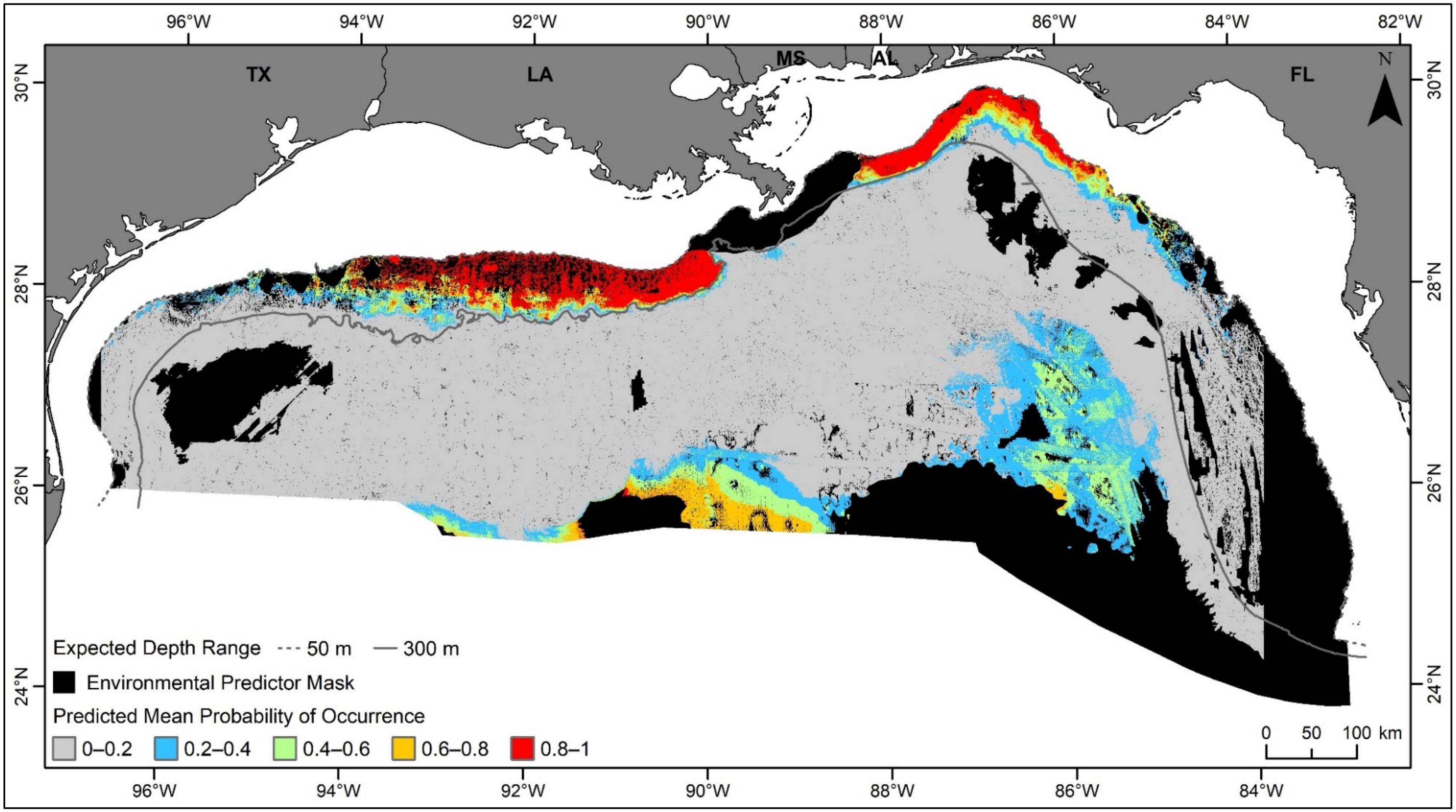

Figure 61. Predicted occurrence of the gorgonian coral *Thesea* (order Alcyonacea, family Plexauridae).

This map shows the predicted mean probability of occurrence (i.e., the predicted posterior mean occupancy probability) for *Thesea* from the multi-genus occupancy model of family Plexauridae. The environmental predictor mask overlays areas where predictor values were outside the range of values at the sample locations and model predictions may be affected by extrapolation. Gray lines denote the expected depth range for *Thesea*.

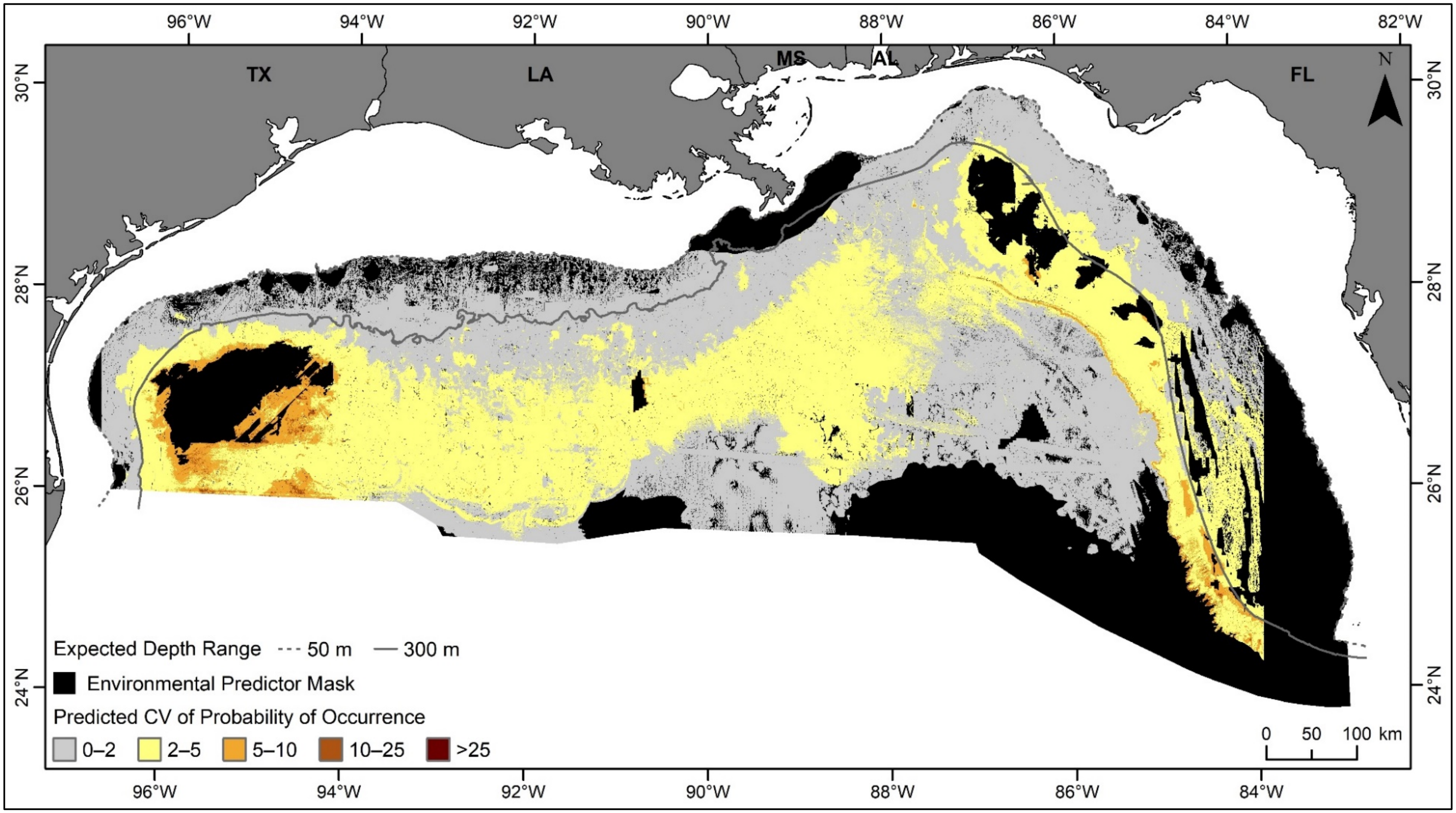

Figure 62. Variability in the predicted occurrence of the gorgonian coral *Thesea* (order Alcyonacea, family Plexauridae).

This map shows the predicted coefficient of variation (CV) of the probability of occurrence (i.e., the predicted posterior CV of occupancy probability) for *Thesea* from the multi-genus occupancy model of family Plexauridae. The environmental predictor mask overlays areas where predictor values were outside the range of values at the sample locations and model predictions may be affected by extrapolation. Gray lines denote the expected depth range for *Thesea*.

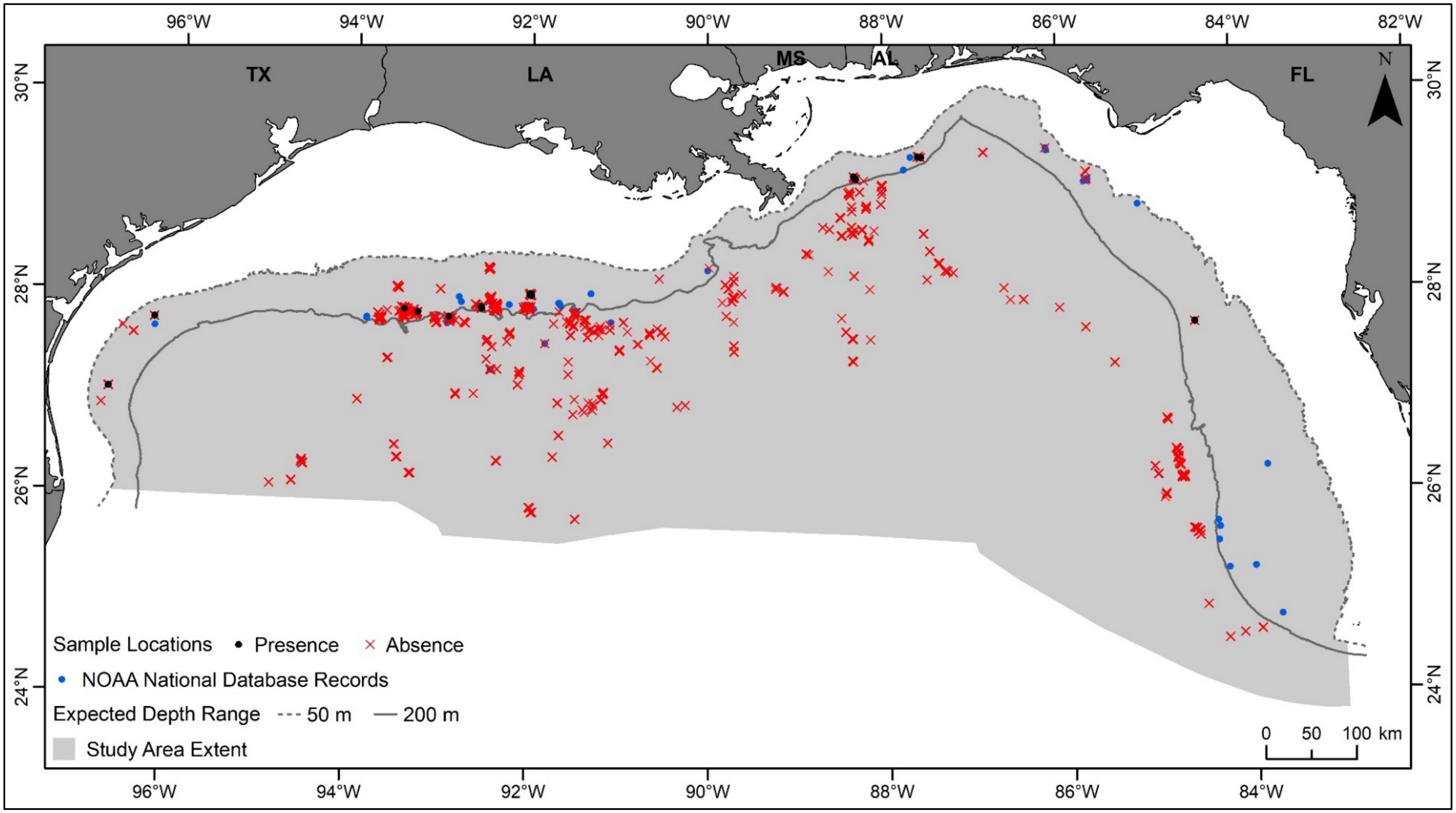

Figure 63. Occurrence records for the gorgonian coral *Placogorgia* (order Alcyonacea, family Plexauridae).

This map shows the observed occurrence (presence-absence) of *Placogorgia* at sample locations in the presence-absence database compiled for this study. Additional records of occurrence in the NOAA National Database are also displayed. Gray lines denote the expected depth range for *Placogorgia*.

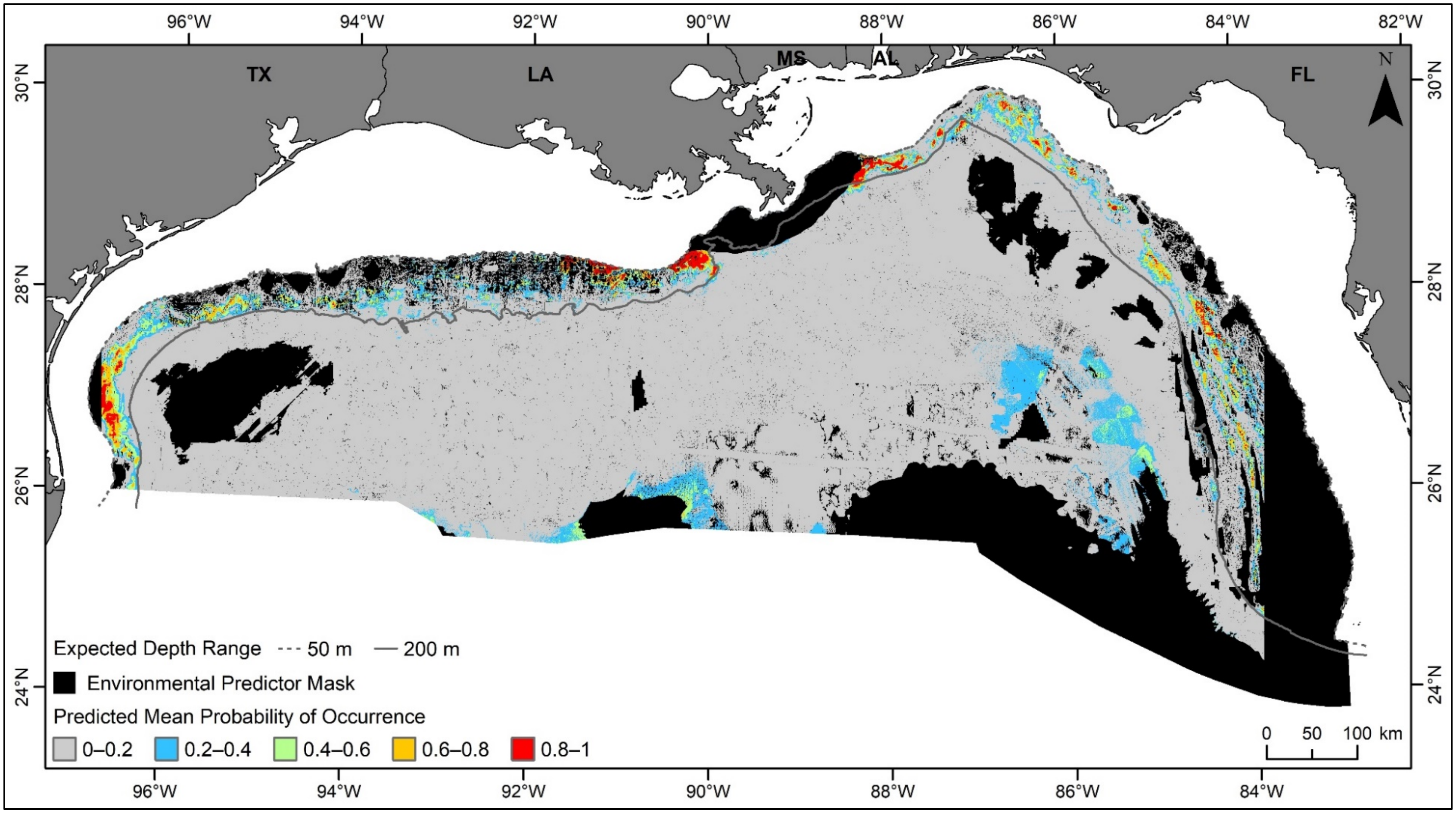

Figure 64. Predicted occurrence of the gorgonian coral *Placogorgia* (order Alcyonacea, family Plexauridae).

This map shows the predicted mean probability of occurrence (i.e., the predicted posterior mean occupancy probability) for *Placogorgia* from the multi-genus occupancy model of family Plexauridae. The environmental predictor mask overlays areas where predictor values were outside the range of values at the sample locations and model predictions may be affected by extrapolation. Gray lines denote the expected depth range for *Placogorgia*.

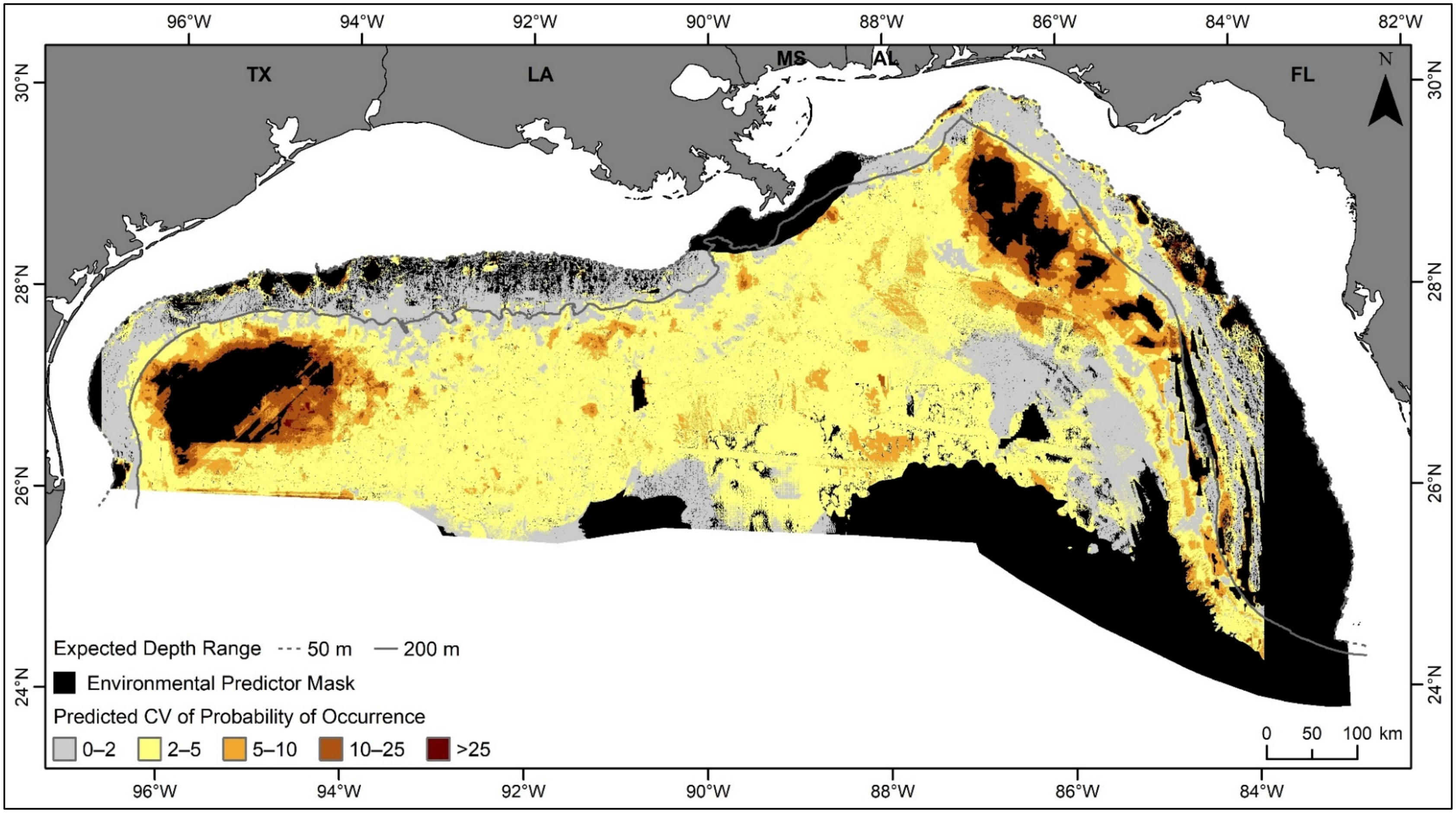

Figure 65. Variability in the predicted occurrence of the gorgonian coral *Placogorgia* (order Alcyonacea, family Plexauridae).

This map shows the predicted coefficient of variation (CV) of the probability of occurrence (i.e., the predicted posterior CV of occupancy probability) for *Placogorgia* from the multi-genus occupancy model of family Plexauridae. The environmental predictor mask overlays areas where predictor values were outside the range of values at the sample locations and model predictions may be affected by extrapolation. Gray lines denote the expected depth range for *Placogorgia*.

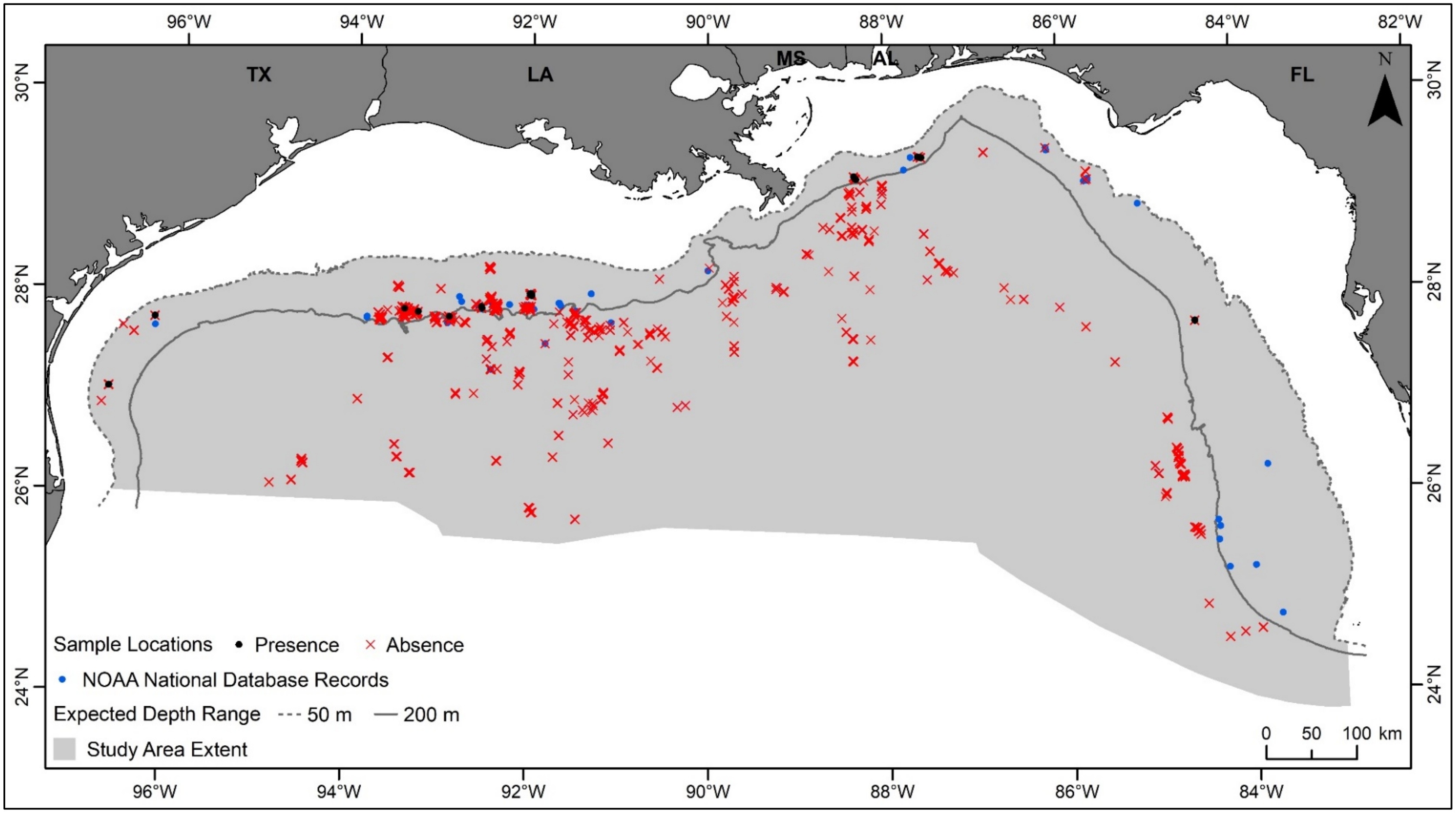

Figure 66. Occurrence records for the gorgonian coral *Villogorgia* (order Alcyonacea, family Plexauridae).

This map shows the observed occurrence (presence-absence) of *Villogorgia* at sample locations in the presence-absence database compiled for this study. Additional records of occurrence in the NOAA National Database are also displayed. Gray lines denote the expected depth range for *Villogorgia*.

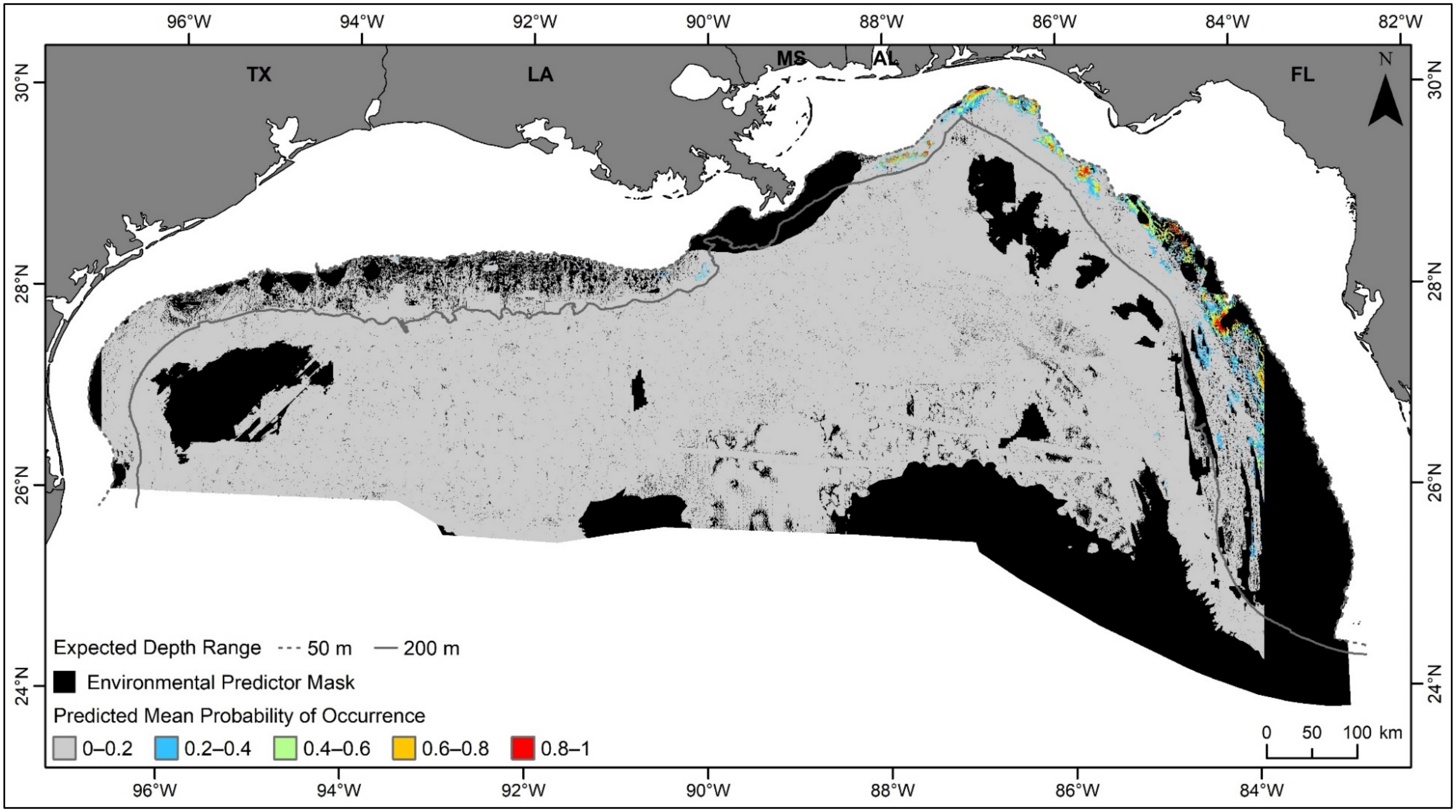

Figure 67. Predicted occurrence of the gorgonian coral *Villogorgia* (order Alcyonacea, family Plexauridae).

This map shows the predicted mean probability of occurrence (i.e., the predicted posterior mean occupancy probability) for *Villogorgia* from the multi-genus occupancy model of family Plexauridae. The environmental predictor mask overlays areas where predictor values were outside the range of values at the sample locations and model predictions may be affected by extrapolation. Gray lines denote the expected depth range for *Villogorgia*.

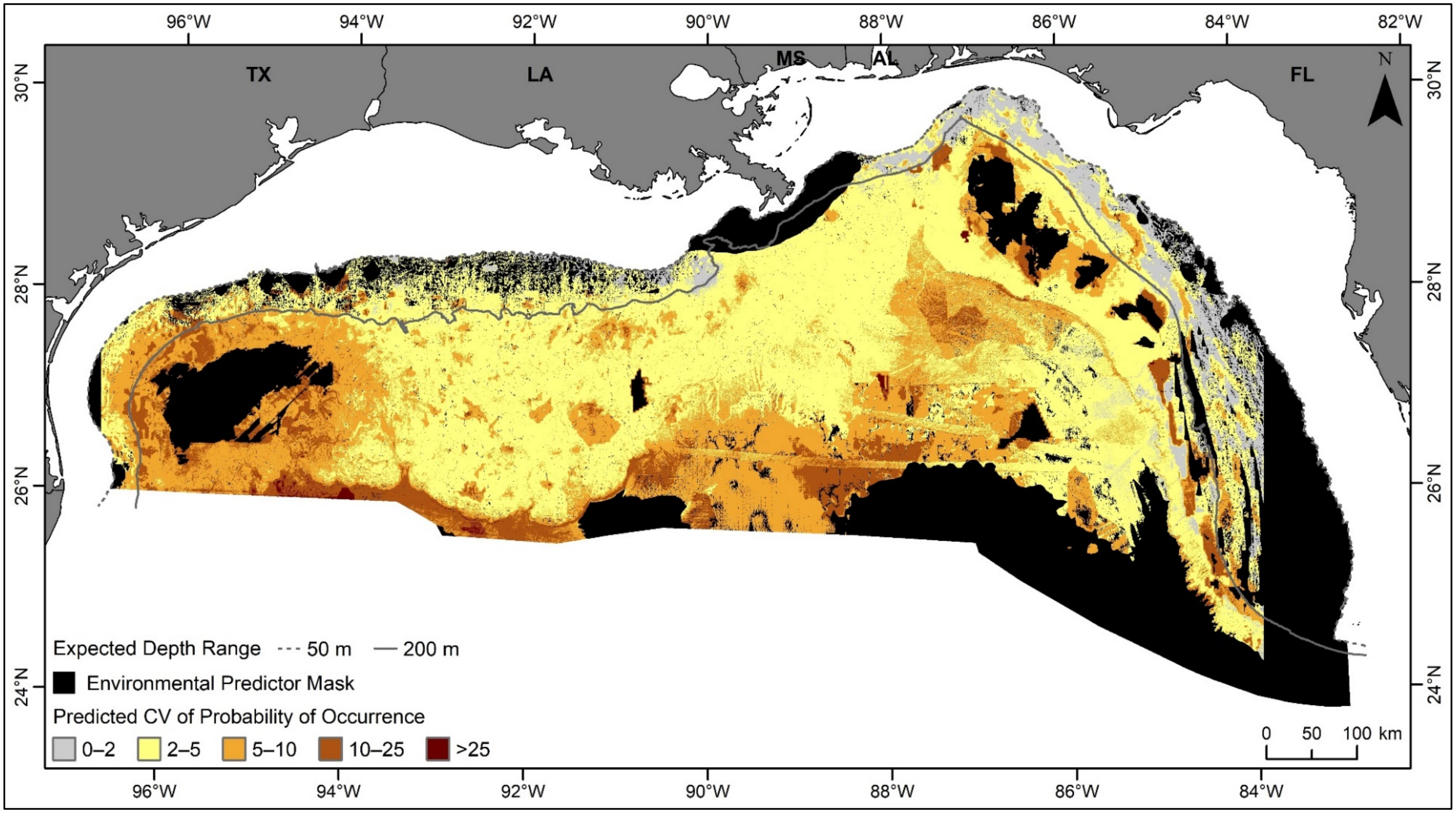

Figure 68. Variability in the predicted occurrence of the gorgonian coral *Villogorgia* (order Alcyonacea, family Plexauridae).

This map shows the predicted coefficient of variation (CV) of the probability of occurrence (i.e., the predicted posterior CV of occupancy probability) for *Villogorgia* from the multi-genus occupancy model of family Plexauridae. The environmental predictor mask overlays areas where predictor values were outside the range of values at the sample locations and model predictions may be affected by extrapolation. Gray lines denote the expected depth range for *Villogorgia*.

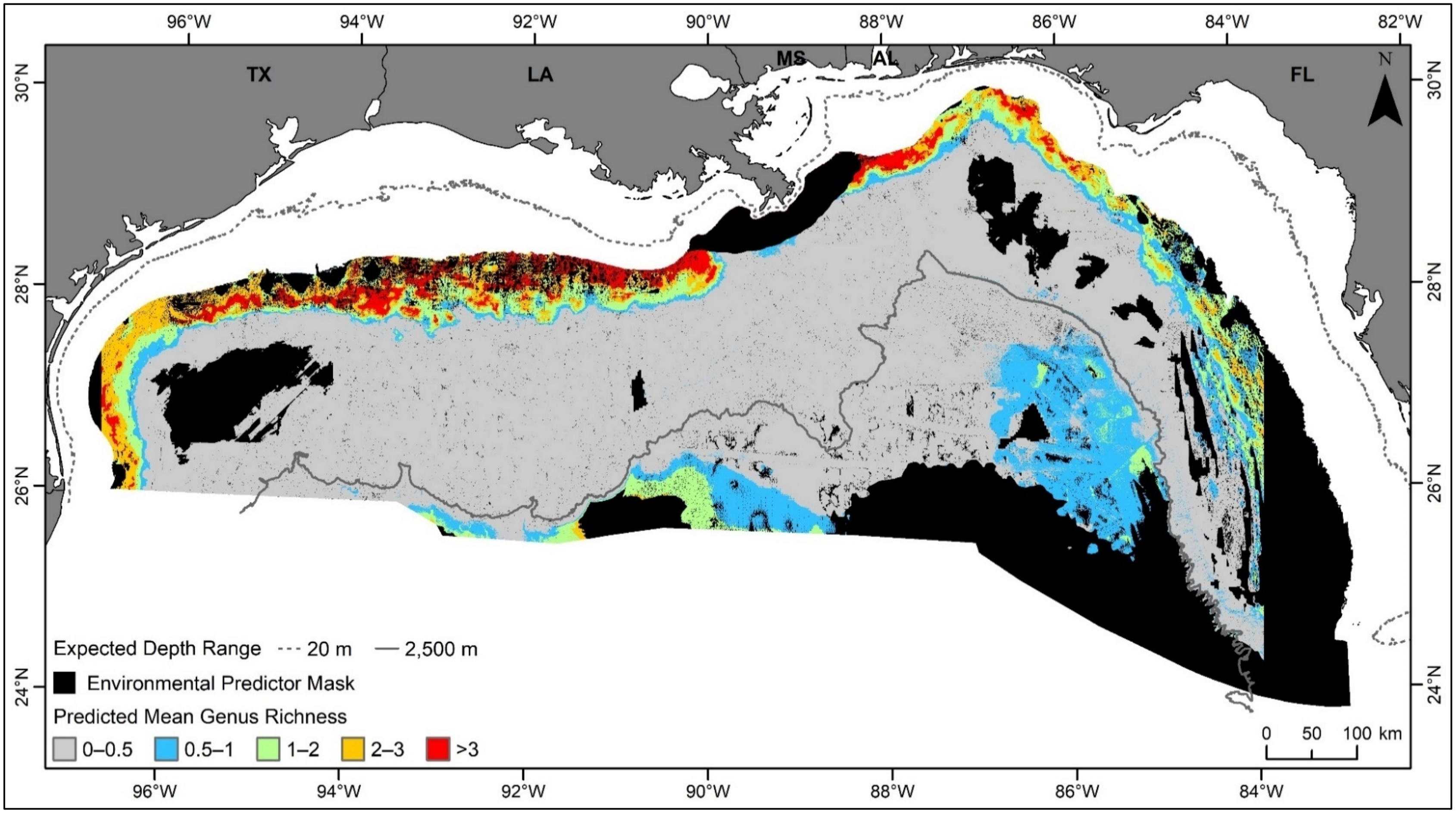

Figure 69. Predicted genus richness of gorgonian corals in family Plexauridae (order Alcyonacea).

This map shows the predicted mean genus richness (i.e., the posterior mean genus richness) from the multi-genus occupancy model of family Plexauridae. The environmental predictor mask overlays areas where predictor values were outside the range of values at the sample locations and model predictions may be affected by extrapolation. Gray lines denote the combined expected depth range for the genera included in the model.

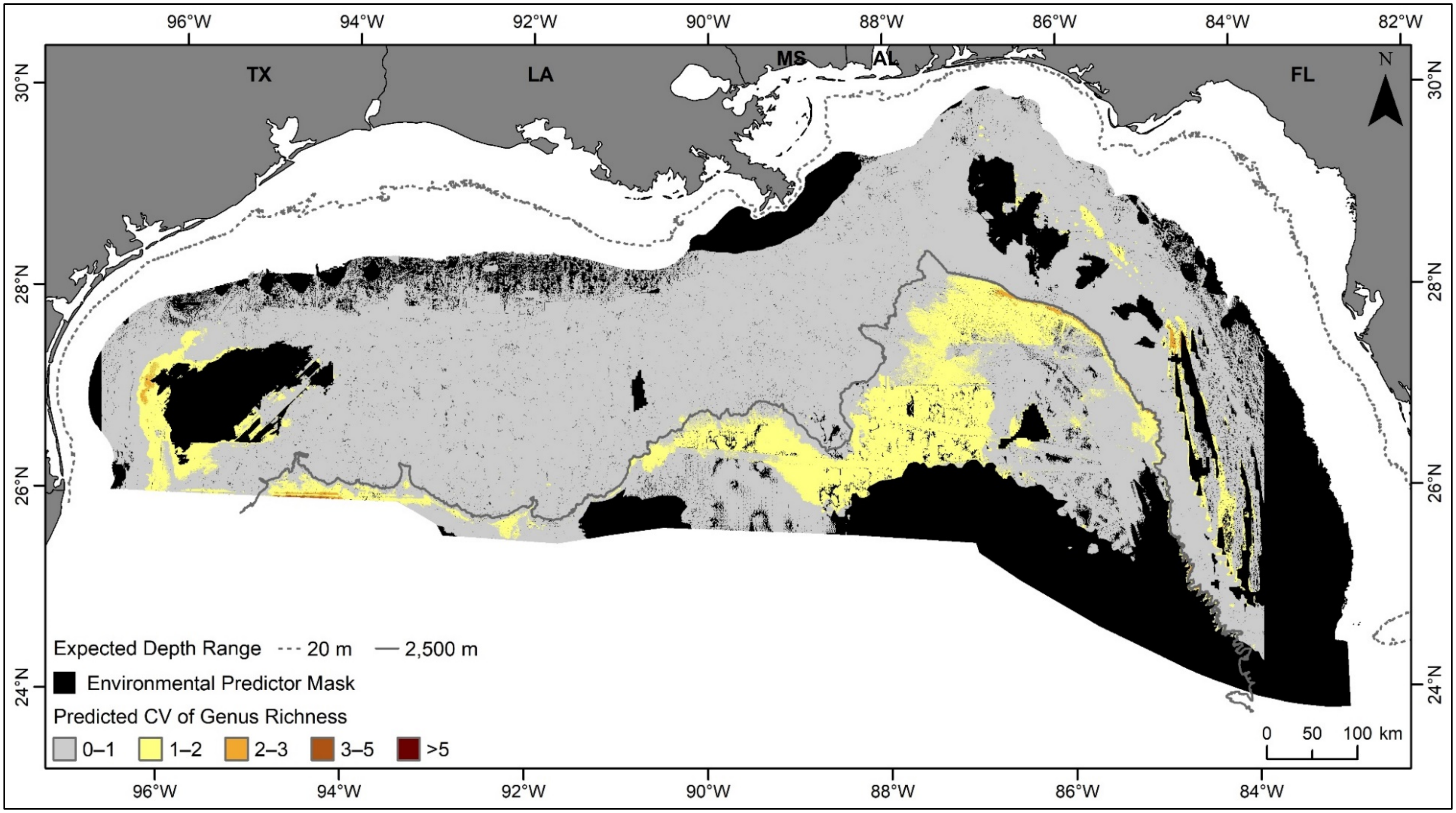

Figure 70. Variability in the predicted genus richness of gorgonian corals in family Plexauridae (order Alcyonacea).

This map shows the predicted coefficient of variation of genus richness (i.e., the posterior CV of genus richness) from the multi-genus occupancy model of family Plexauridae. The environmental predictor mask overlays areas where predictor values were outside the range of values at the sample locations and model predictions may be affected by extrapolation. Gray lines denote the combined expected depth range for the genera included in the model.

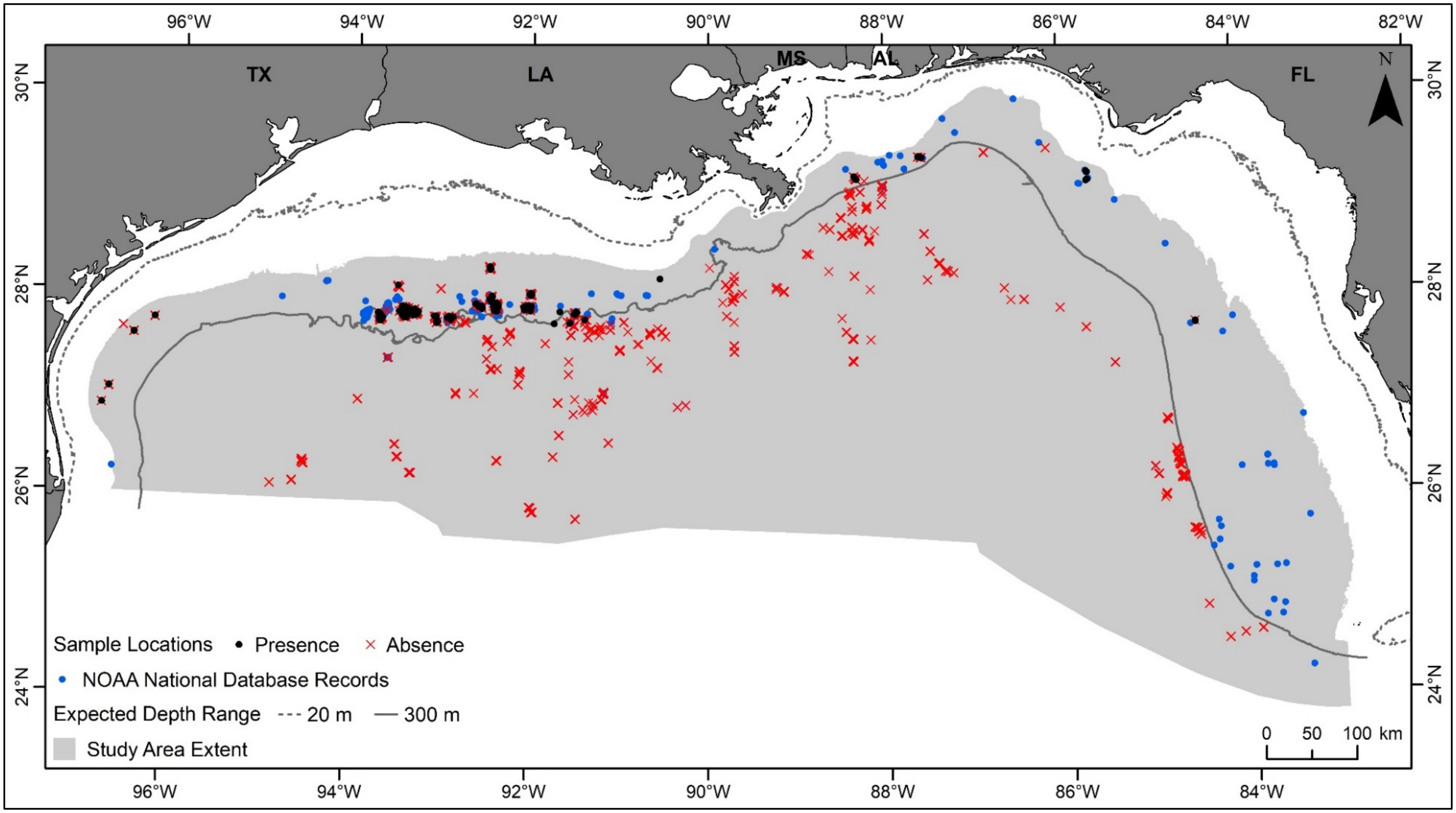

Figure 71. Occurrence records for the gorgonian coral family Ellisellidae (order Alcyonacea).

This map shows the observed occurrence (presence-absence) of Ellisellidae at sample locations in the presence-absence database compiled for this study. Additional records of occurrence in the NOAA National Database are also displayed. Gray lines denote the expected depth range for Ellisellidae.

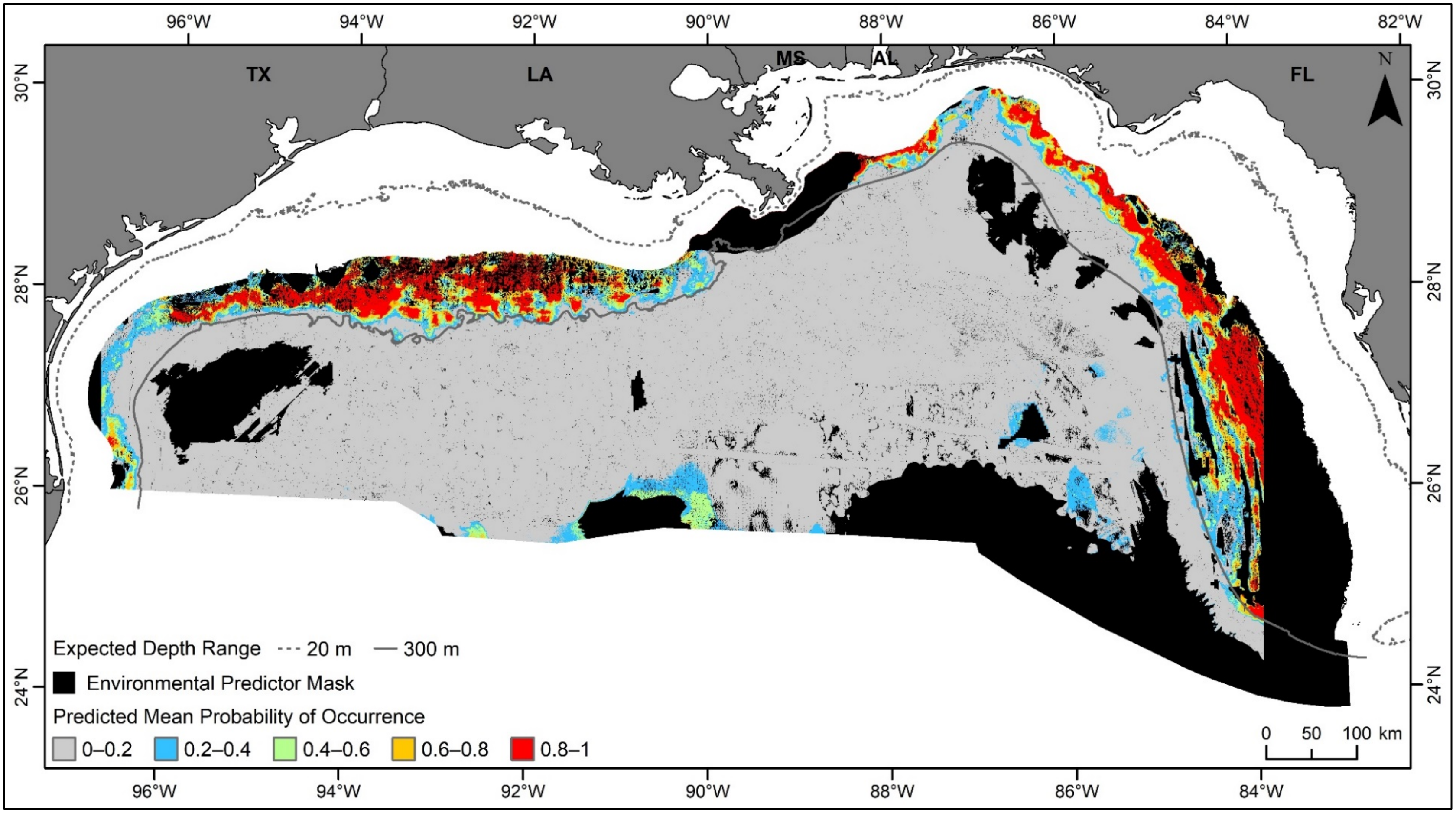

Figure 72. Predicted occurrence of the gorgonian coral family Ellisellidae (order Alcyonacea).

This map shows the predicted mean probability of occurrence (i.e., the predicted posterior mean occupancy probability) for Ellisellidae from the multi-family occupancy model of order Alcyonacea. The environmental predictor mask overlays areas where predictor values were outside the range of values at the sample locations and model predictions may be affected by extrapolation. Gray lines denote the expected depth range for Ellisellidae.

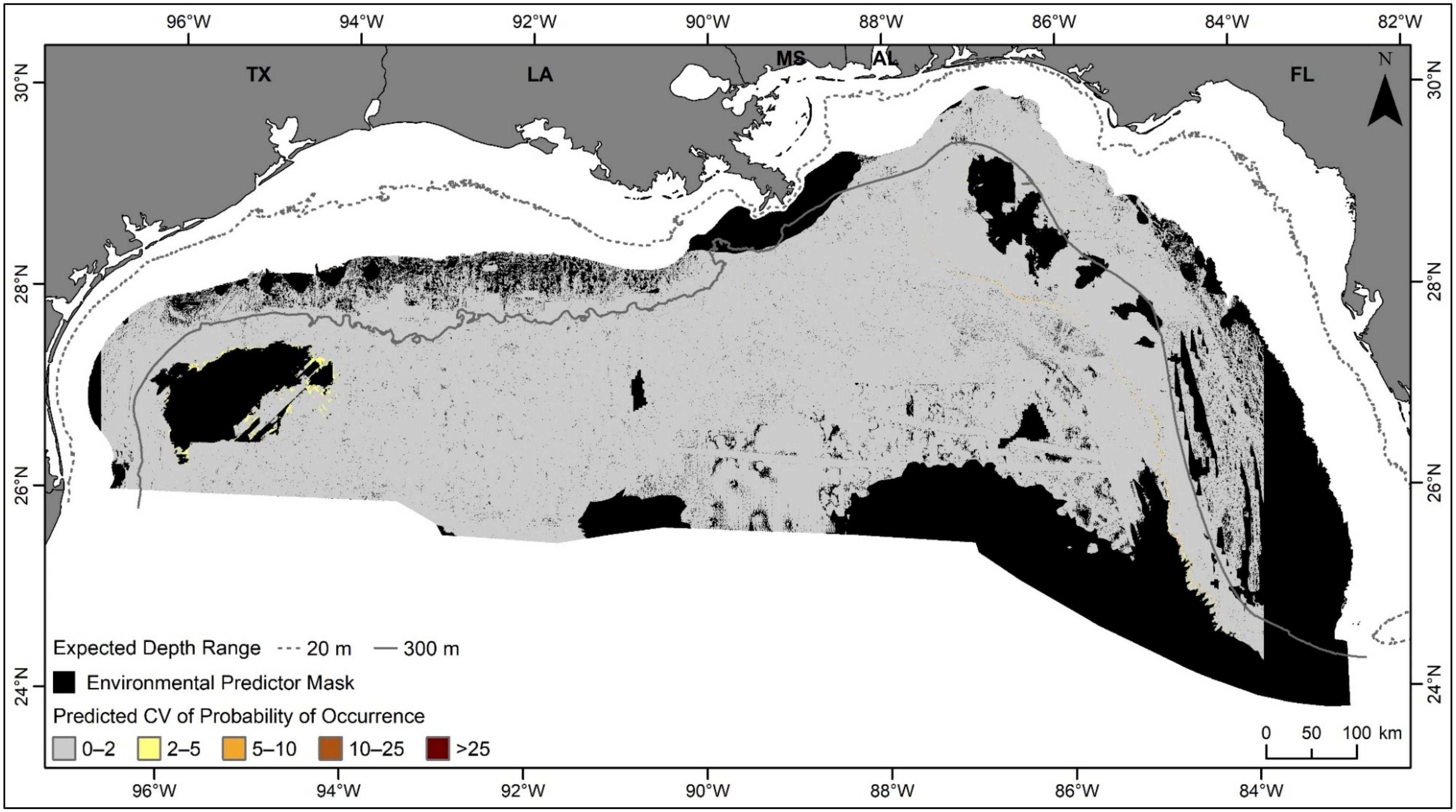

Figure 73. Variability in the predicted occurrence of the gorgonian coral family Ellisellidae (order Alcyonacea).

This map shows the predicted coefficient of variation (CV) of the probability of occurrence (i.e., the predicted posterior CV of occupancy probability) for Ellisellidae from the multi-family occupancy model of order Alcyonacea. The environmental predictor mask overlays areas where predictor values were outside the range of values at the sample locations and model predictions may be affected by extrapolation. Gray lines denote the expected depth range for Ellisellidae.

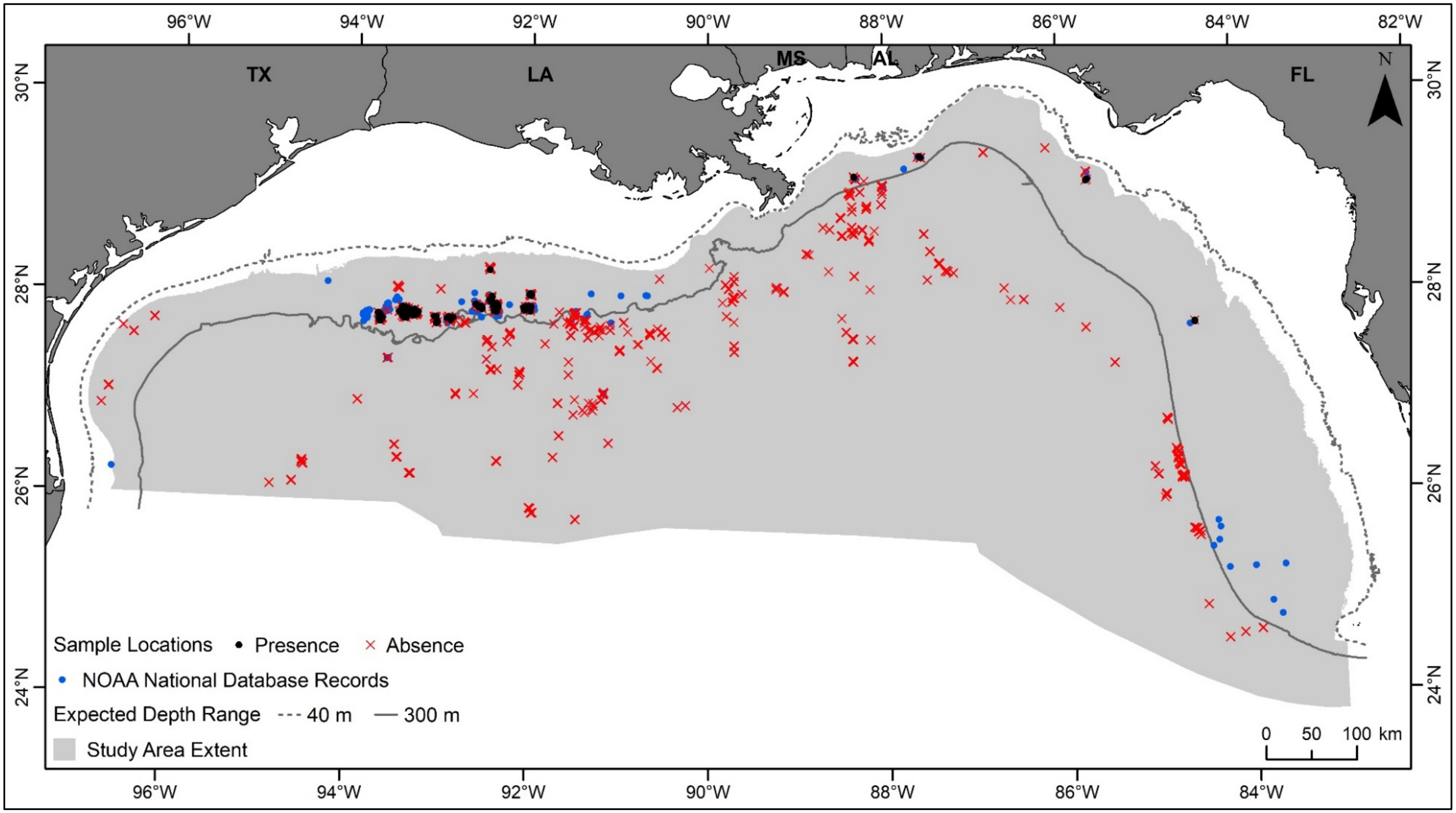

Figure 74. Occurrence records for the gorgonian coral *Nicella* (order Alcyonacea, family Ellisellidae).

This map shows the observed occurrence (presence-absence) of *Nicella* at sample locations in the presence-absence database compiled for this study. Additional records of occurrence in the NOAA National Database are also displayed. Gray lines denote the expected depth range for *Nicella*.

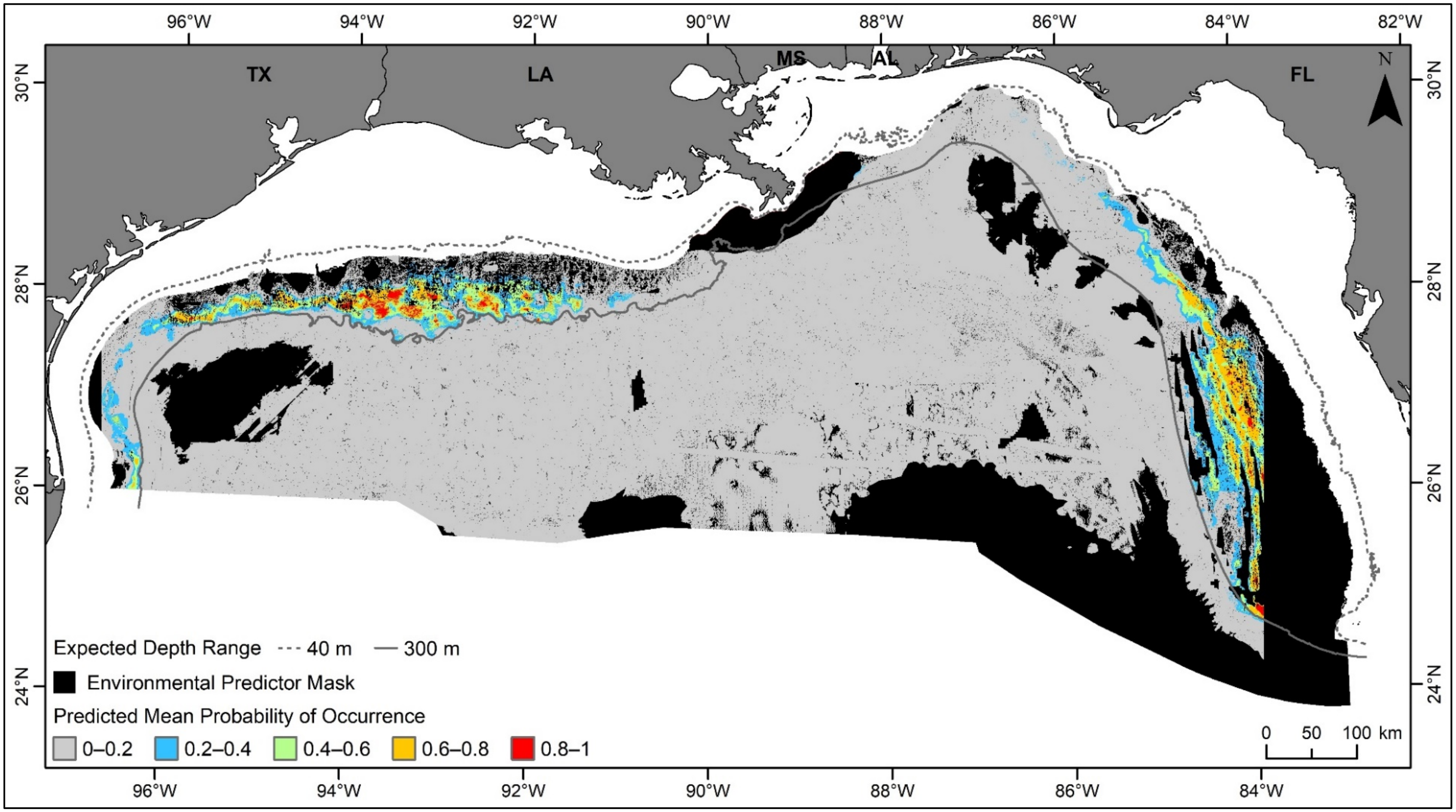

Figure 75. Predicted occurrence of the gorgonian coral *Nicella* (order Alcyonacea, family Ellisellidae).

This map shows the predicted mean probability of occurrence (i.e., the predicted posterior mean occupancy probability) for *Nicella* from the single-taxon occupancy model. The environmental predictor mask overlays areas where predictor values were outside the range of values at the sample locations and model predictions may be affected by extrapolation. Gray lines denote the expected depth range for *Nicella*.

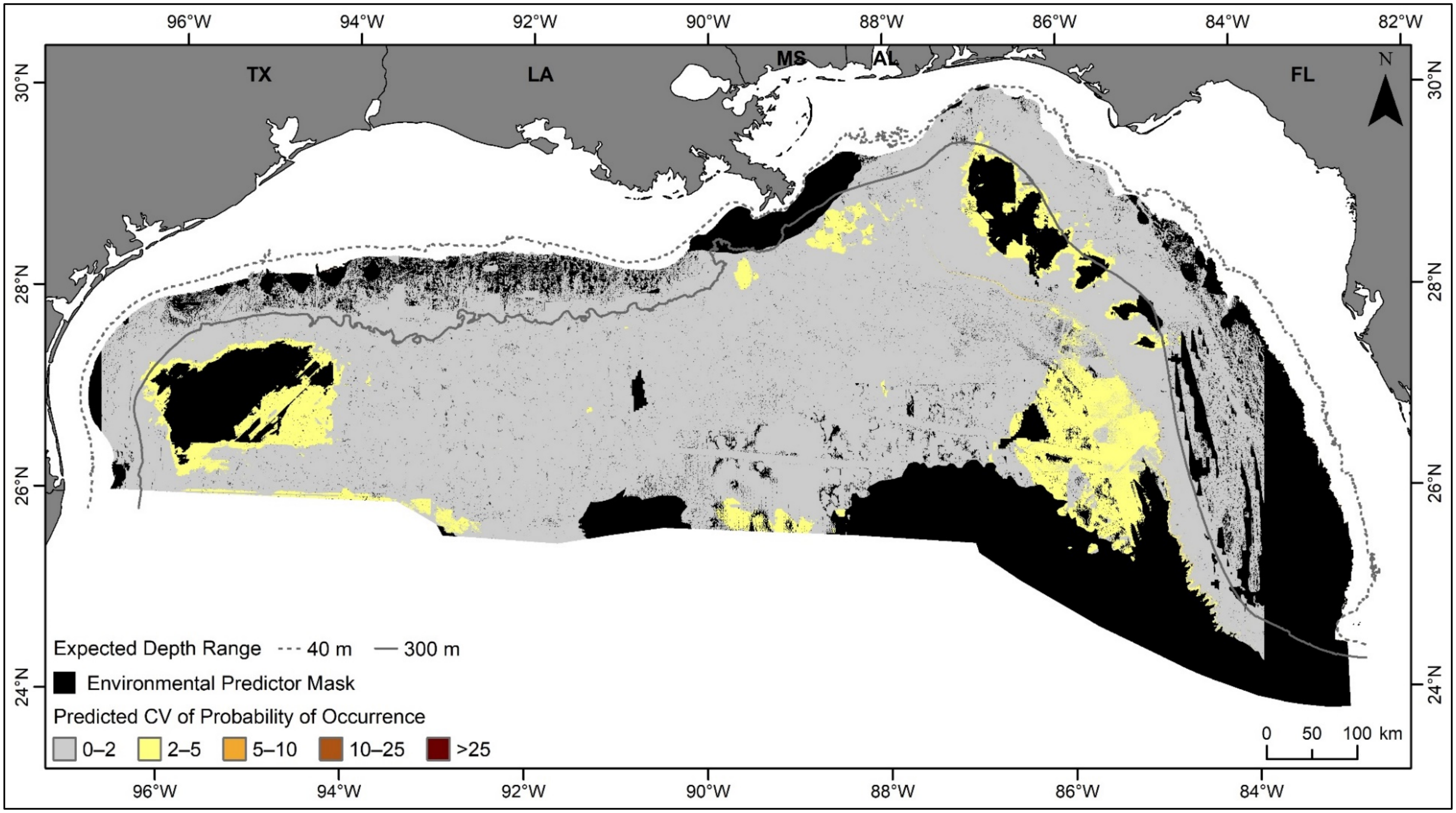

Figure 76. Variability in the predicted occurrence of the gorgonian coral *Nicella* (order Alcyonacea, family Ellisellidae).

This map shows the predicted coefficient of variation (CV) of the probability of occurrence (i.e., the predicted posterior CV of occupancy probability) for *Nicella* from the single-taxon occupancy model. The environmental predictor mask overlays areas where predictor values were outside the range of values at the sample locations and model predictions may be affected by extrapolation. Gray lines denote the expected depth range for *Nicella*.

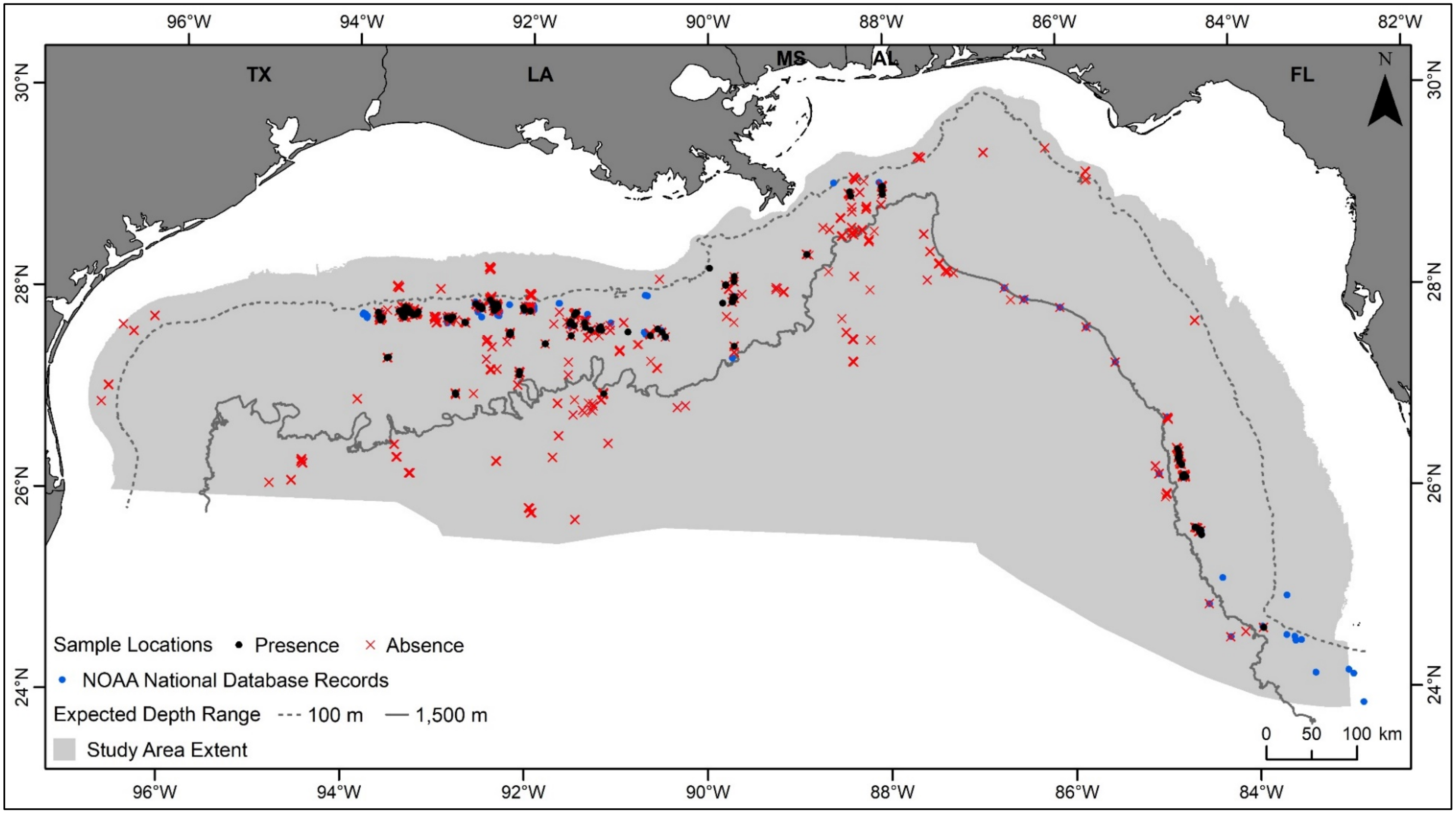

Figure 77. Occurrence records for the gorgonian coral family Primnoidae (order Alcyonacea).

This map shows the observed occurrence (presence-absence) of Primnoidae at sample locations in the presence-absence database compiled for this study. Additional records of occurrence in the NOAA National Database are also displayed. Gray lines denote the expected depth range for Primnoidae.

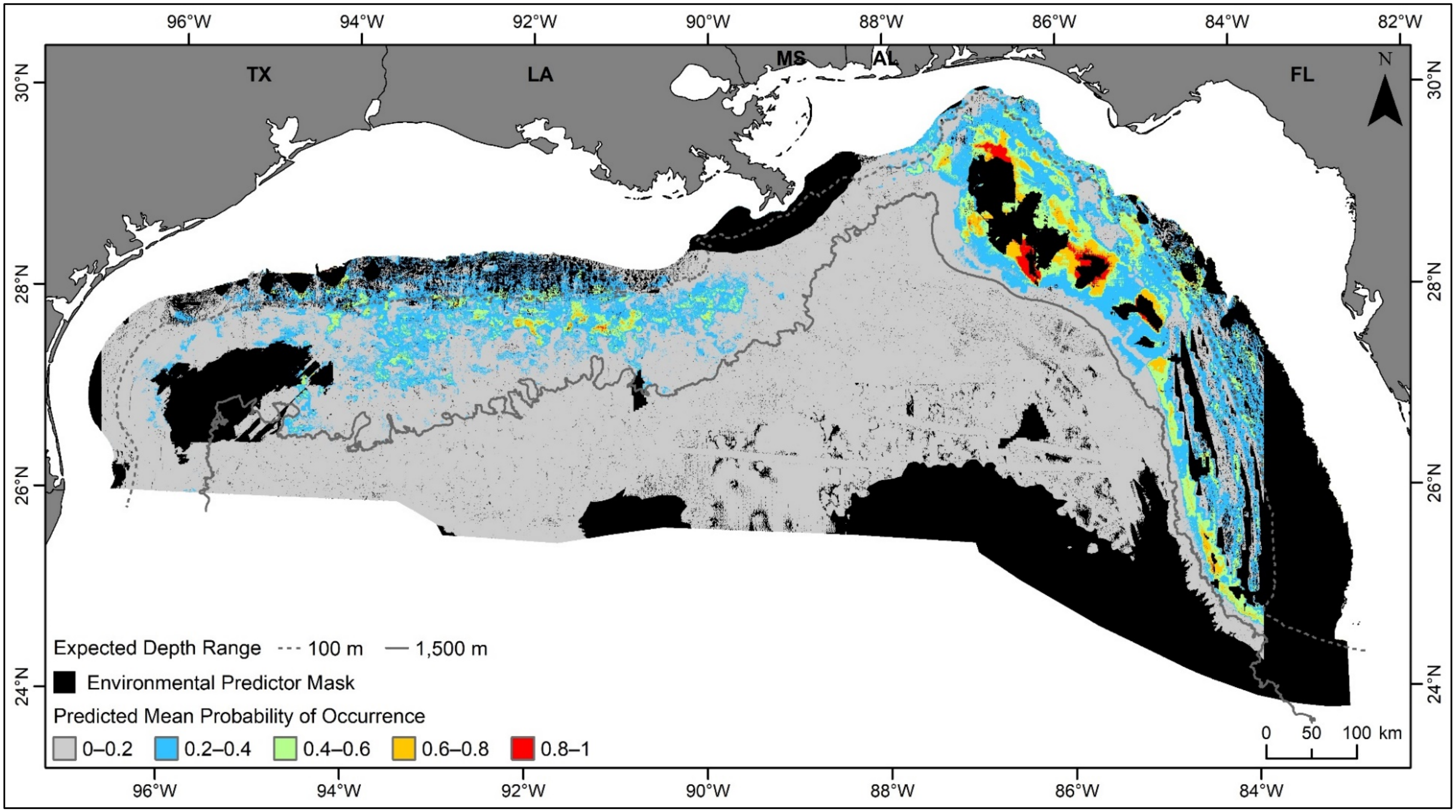

Figure 78. Predicted occurrence of the gorgonian coral family Primnoidae (order Alcyonacea).

This map shows the predicted mean probability of occurrence (i.e., the predicted posterior mean occupancy probability) for Primnoidae from the multi-family occupancy model of order Alcyonacea. The environmental predictor mask overlays areas where predictor values were outside the range of values at the sample locations and model predictions may be affected by extrapolation. Gray lines denote the expected depth range for Primnoidae.

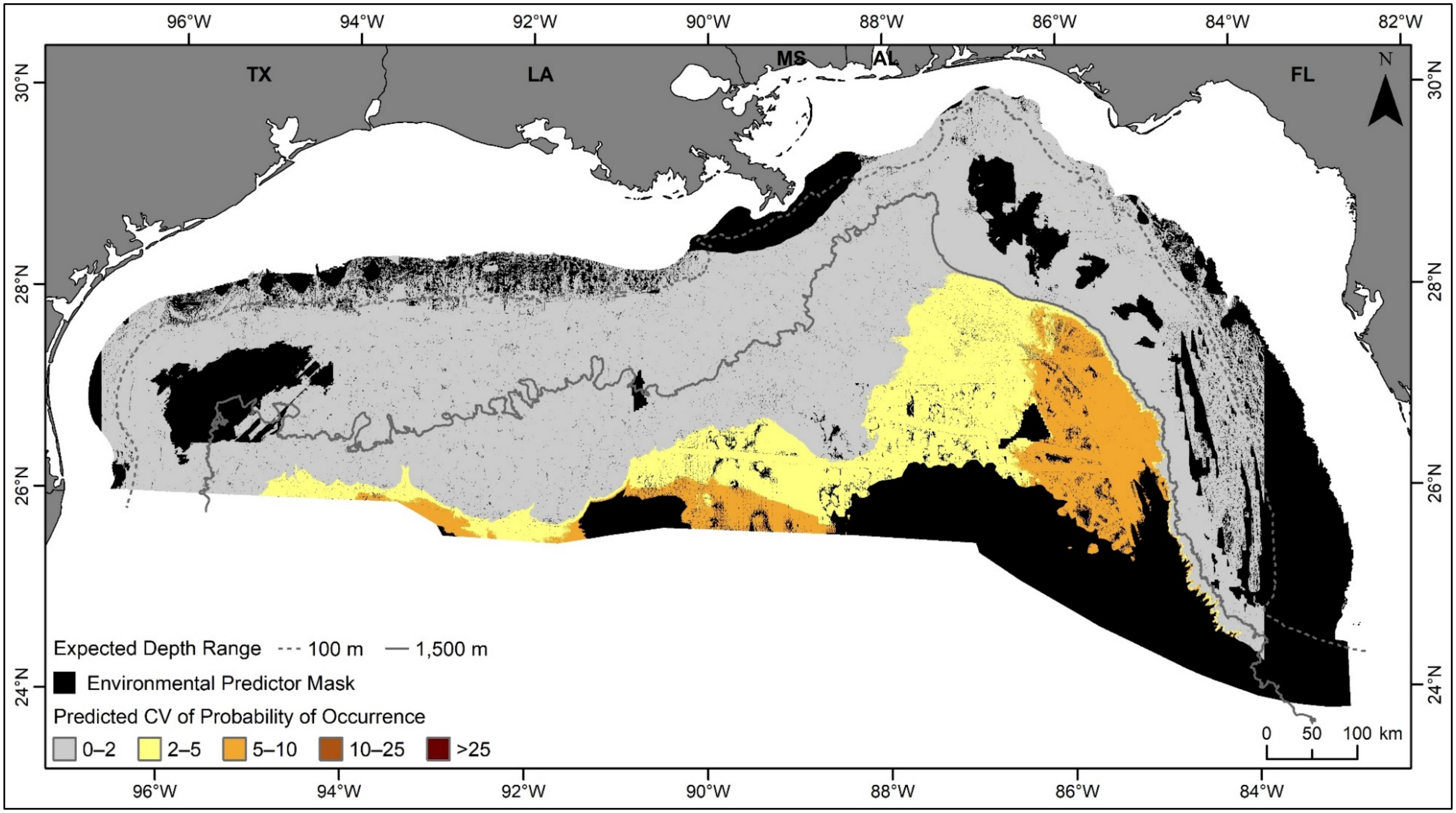

Figure 79. Variability in the predicted occurrence of the gorgonian coral family Primnoidae (order Alcyonacea).

This map shows the predicted coefficient of variation (CV) of the probability of occurrence (i.e., the predicted posterior CV of occupancy probability) for Primnoidae from the multi-family occupancy model of order Alcyonacea. The environmental predictor mask overlays areas where predictor values were outside the range of values at the sample locations and model predictions may be affected by extrapolation. Gray lines denote the expected depth range for Primnoidae.

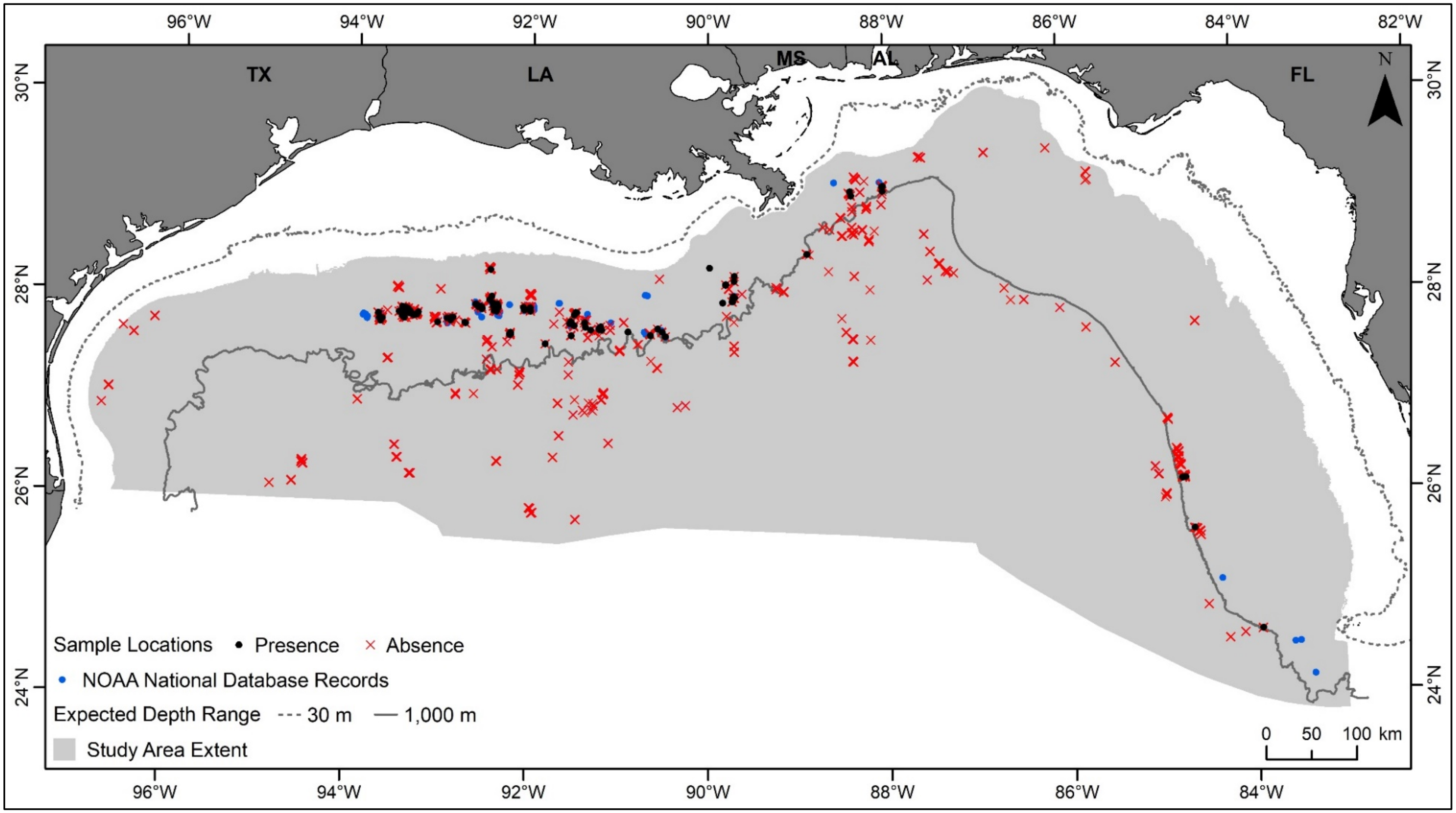

Figure 80. Occurrence records for the gorgonian coral *Callogorgia* (order Alcyonacea, family Primnoidae).

This map shows the observed occurrence (presence-absence) of *Callogorgia* at sample locations in the presence-absence database compiled for this study. Additional records of occurrence in the NOAA National Database are also displayed. Gray lines denote the expected depth range for *Callogorgia*.

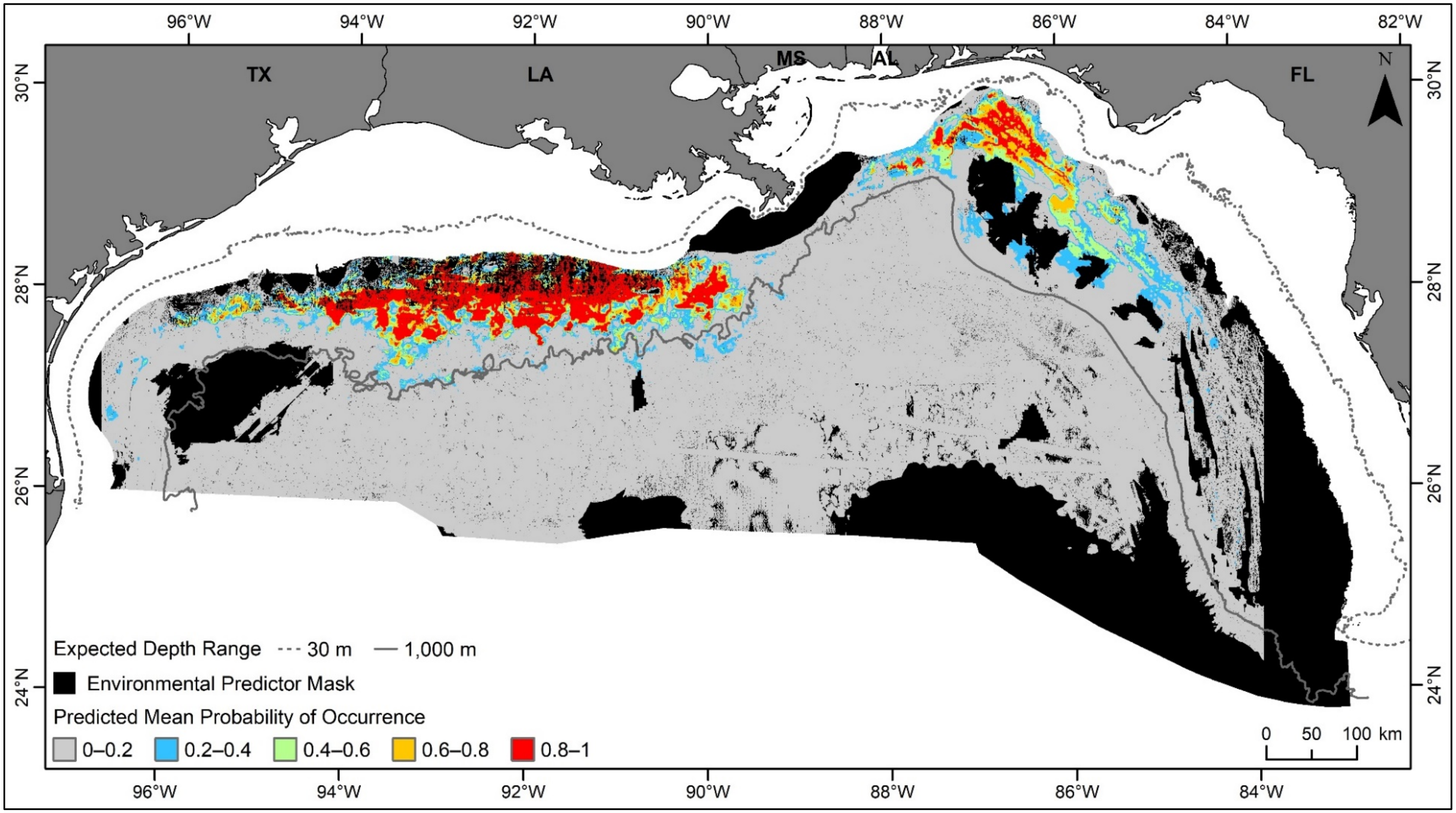

Figure 81. Predicted occurrence of the gorgonian coral *Callogorgia* (order Alcyonacea, family Primnoidae).

This map shows the predicted mean probability of occurrence (i.e., the predicted posterior mean occupancy probability) for *Callogorgia* from the single-taxon occupancy model. The environmental predictor mask overlays areas where predictor values were outside the range of values at the sample locations and model predictions may be affected by extrapolation. Gray lines denote the expected depth range for *Callogorgia*.

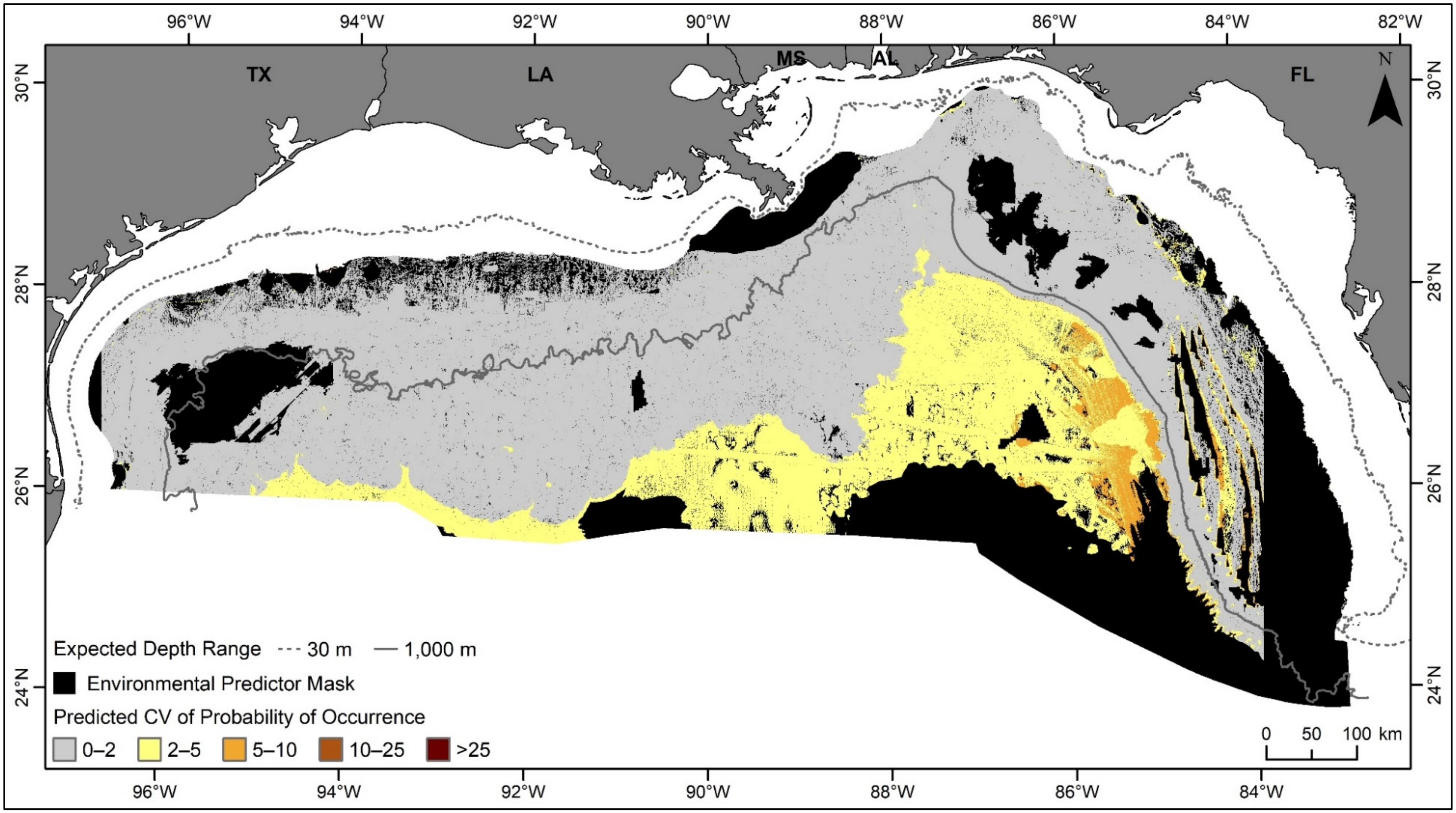

Figure 82. Variability in the predicted occurrence of the gorgonian coral *Callogorgia* (order Alcyonacea, family Primnoidae).

This map shows the predicted coefficient of variation (CV) of the probability of occurrence (i.e., the predicted posterior CV of occupancy probability) for *Callogorgia* from the single-taxon occupancy model. The environmental predictor mask overlays areas where predictor values were outside the range of values at the sample locations and model predictions may be affected by extrapolation. Gray lines denote the expected depth range for *Callogorgia*.

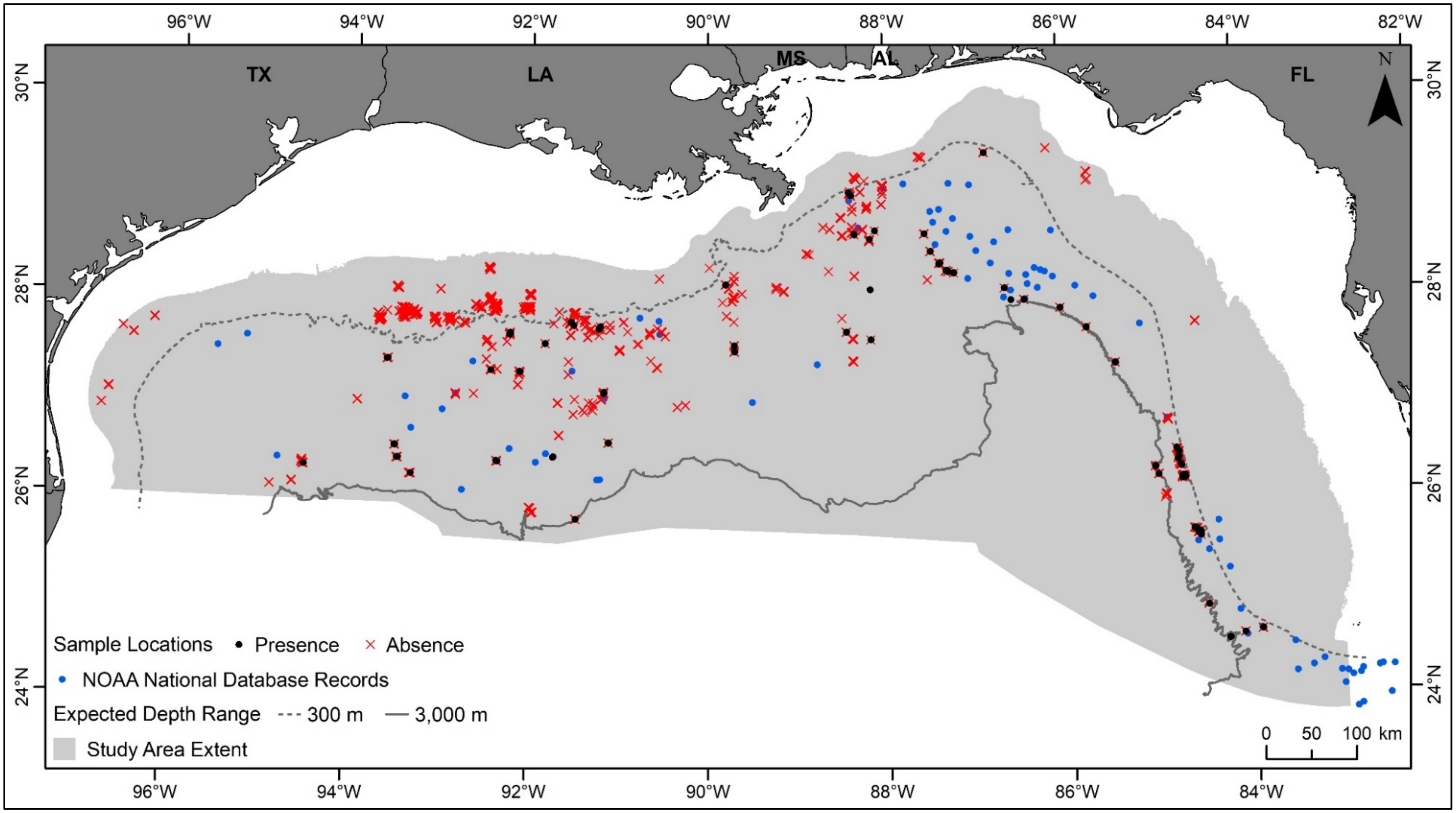

Figure 83. Occurrence records for the gorgonian coral family Isididae (order Alcyonacea).

This map shows the observed occurrence (presence-absence) of Isididae at sample locations in the presence-absence database compiled for this study. Additional records of occurrence in the NOAA National Database are also displayed. Gray lines denote the expected depth range for Isididae.

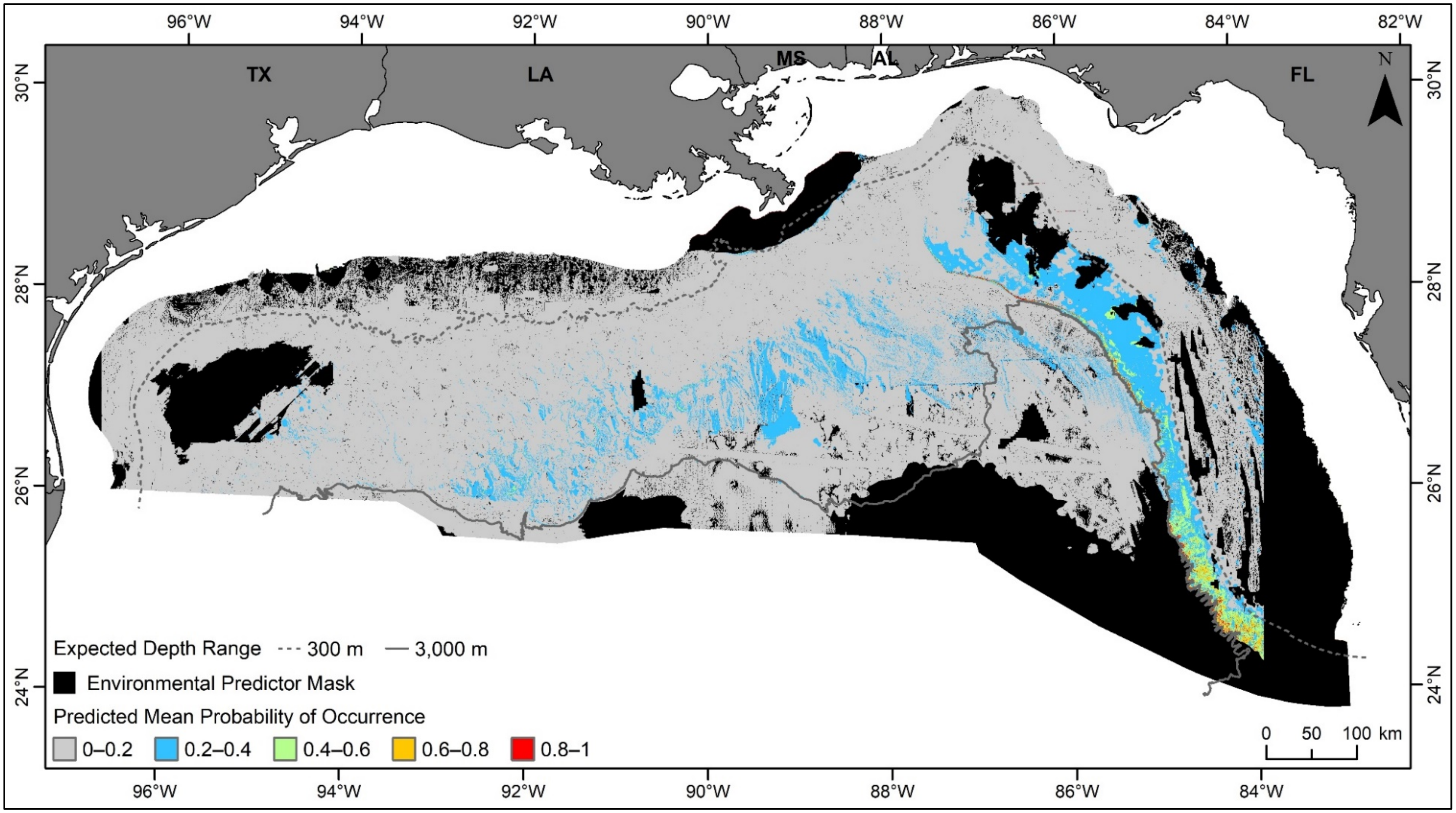

Figure 84. Predicted occurrence of the gorgonian coral family Isididae (order Alcyonacea).

This map shows the predicted mean probability of occurrence (i.e., the predicted posterior mean occupancy probability) for Isididae from the multi-family occupancy model of order Alcyonacea. The environmental predictor mask overlays areas where predictor values were outside the range of values at the sample locations and model predictions may be affected by extrapolation. Gray lines denote the expected depth range for Isididae.

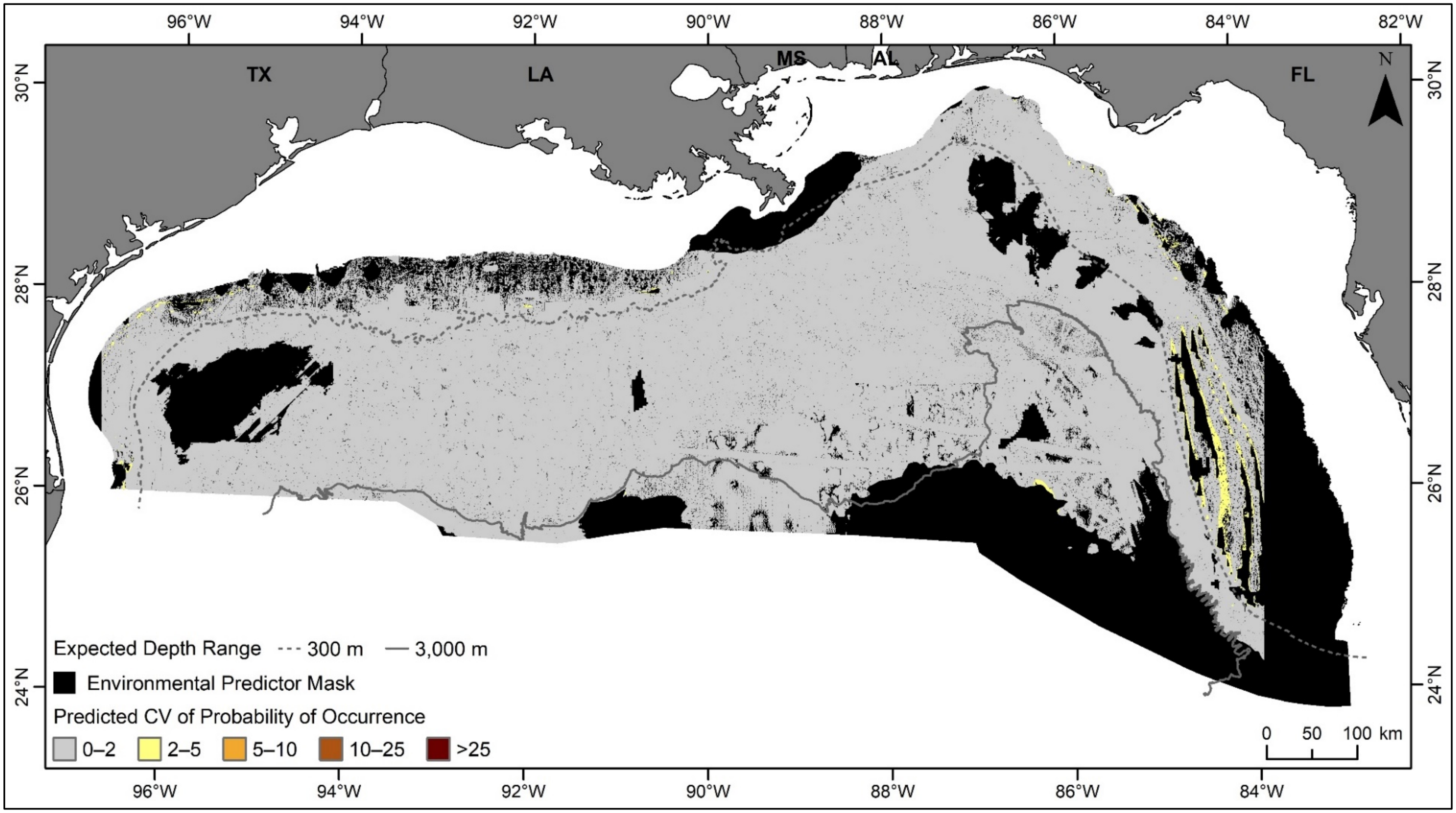

Figure 85. Variability in the predicted occurrence of the gorgonian coral family Isididae (order Alcyonacea).

This map shows the predicted coefficient of variation (CV) of the probability of occurrence (i.e., the predicted posterior CV of occupancy probability) for Isididae from the multi-family occupancy model of order Alcyonacea. The environmental predictor mask overlays areas where predictor values were outside the range of values at the sample locations and model predictions may be affected by extrapolation. Gray lines denote the expected depth range for Isididae.

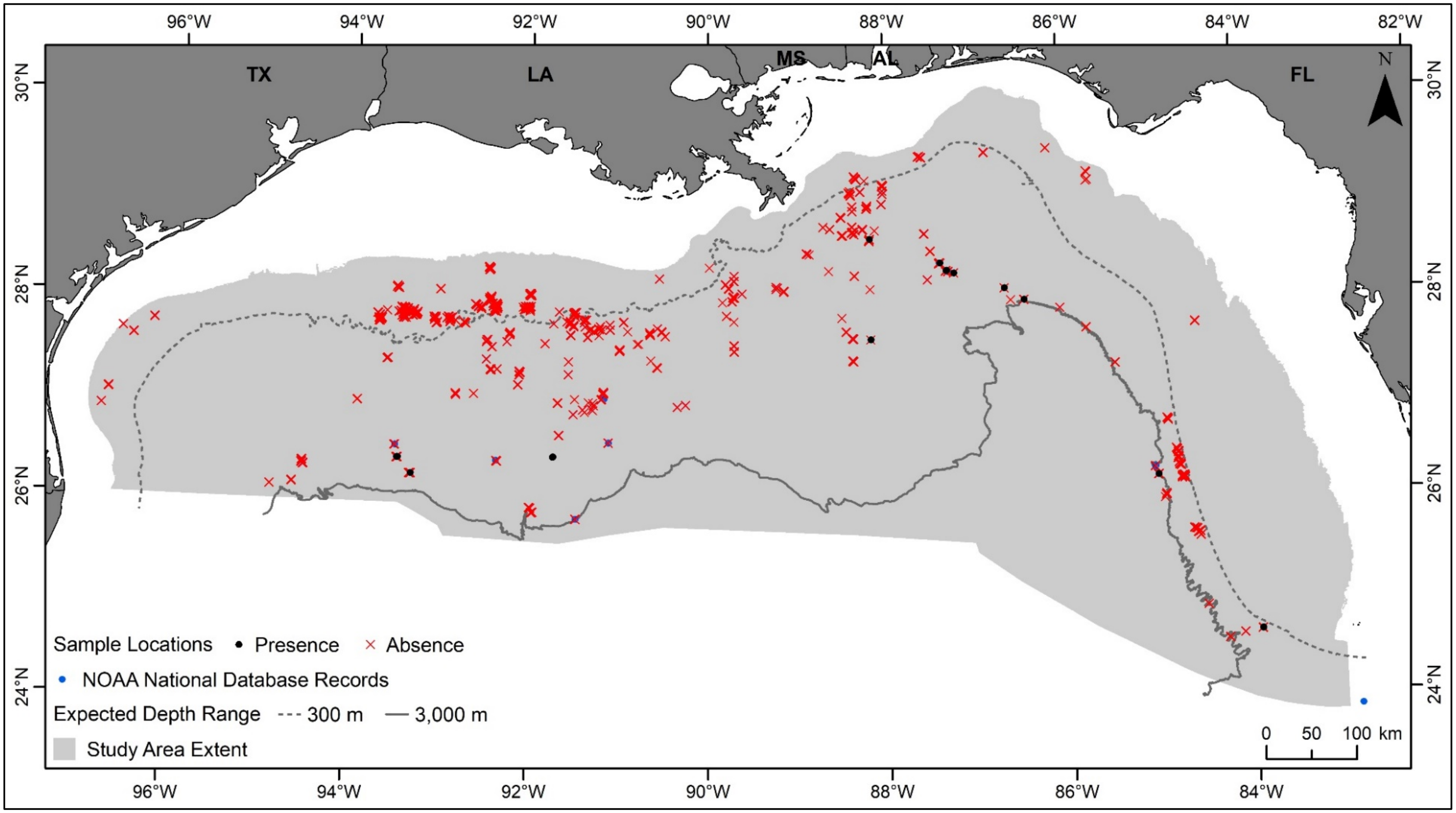

Figure 86. Occurrence records for the gorgonian coral *Lepidisis* (order Alcyonacea, family Isididae).

This map shows the observed occurrence (presence-absence) of *Lepidisis* at sample locations in the presence-absence database compiled for this study. Additional records of occurrence in the NOAA National Database are also displayed. Gray lines denote the expected depth range for *Lepidisis*.

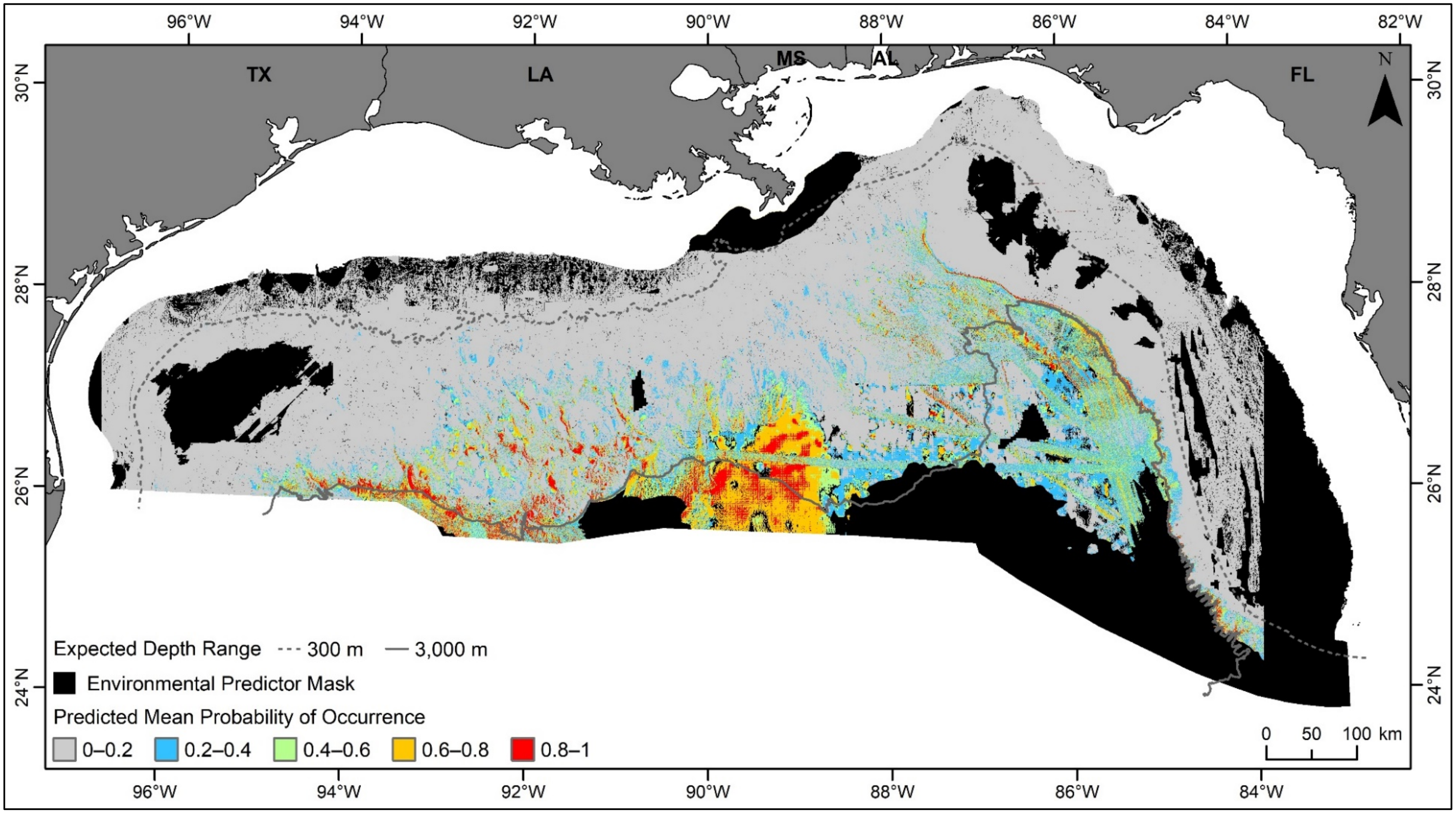

Figure 87. Predicted occurrence of the gorgonian coral *Lepidisis* (order Alcyonacea, family Isididae).

This map shows the predicted mean probability of occurrence (i.e., the predicted posterior mean occupancy probability) for *Lepidisis* from the multi-genus occupancy model of family Isididae. The environmental predictor mask overlays areas where predictor values were outside the range of values at the sample locations and model predictions may be affected by extrapolation. Gray lines denote the expected depth range for *Lepidisis*.

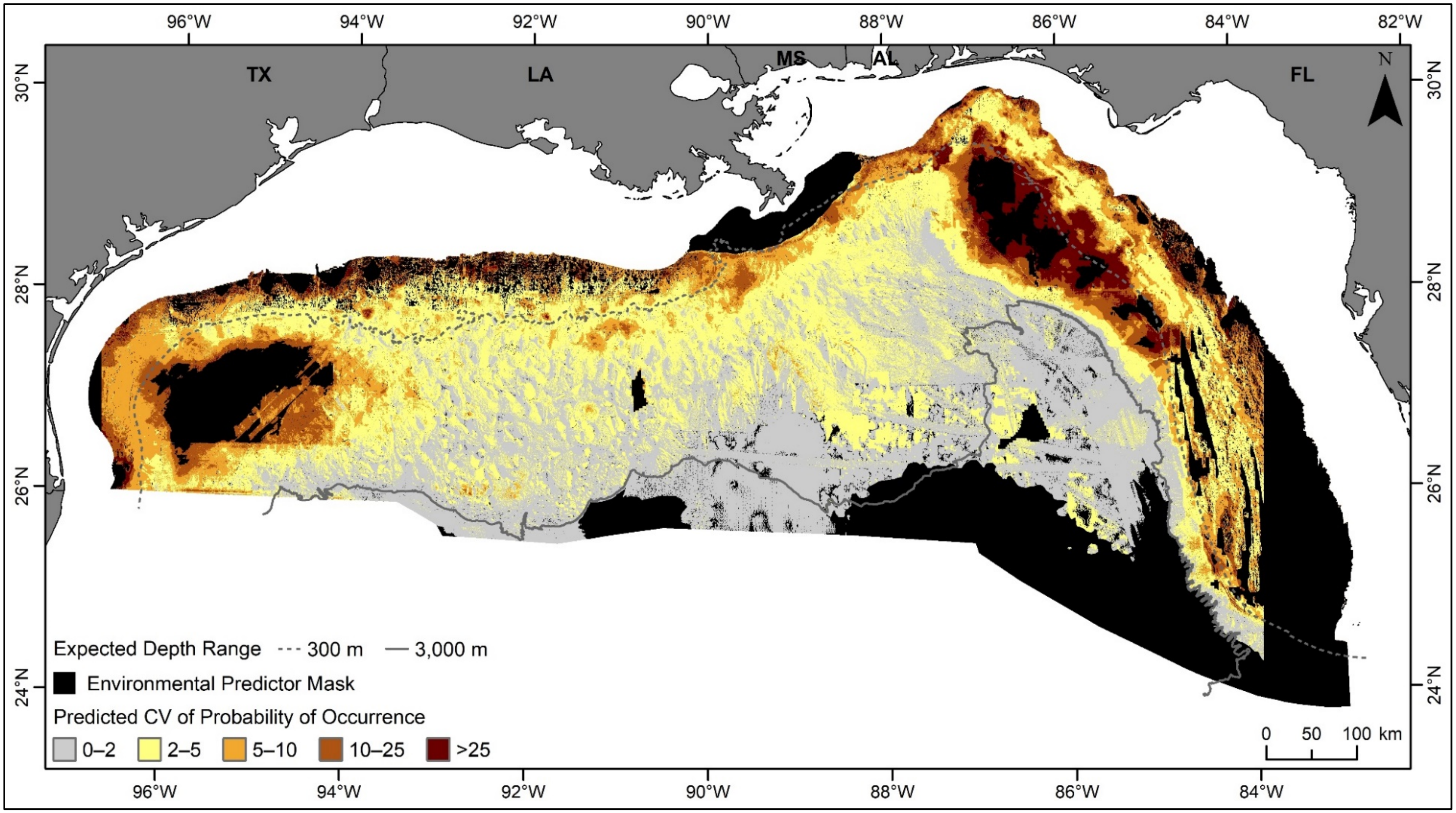

Figure 88. Variability in the predicted occurrence of the gorgonian coral *Lepidisis* (order Alcyonacea, family Isididae).

This map shows the predicted coefficient of variation (CV) of the probability of occurrence (i.e., the predicted posterior CV of occupancy probability) for *Lepidisis* from the multi-genus occupancy model of family Isididae. The environmental predictor mask overlays areas where predictor values were outside the range of values at the sample locations and model predictions may be affected by extrapolation. Gray lines denote the expected depth range for *Lepidisis*.

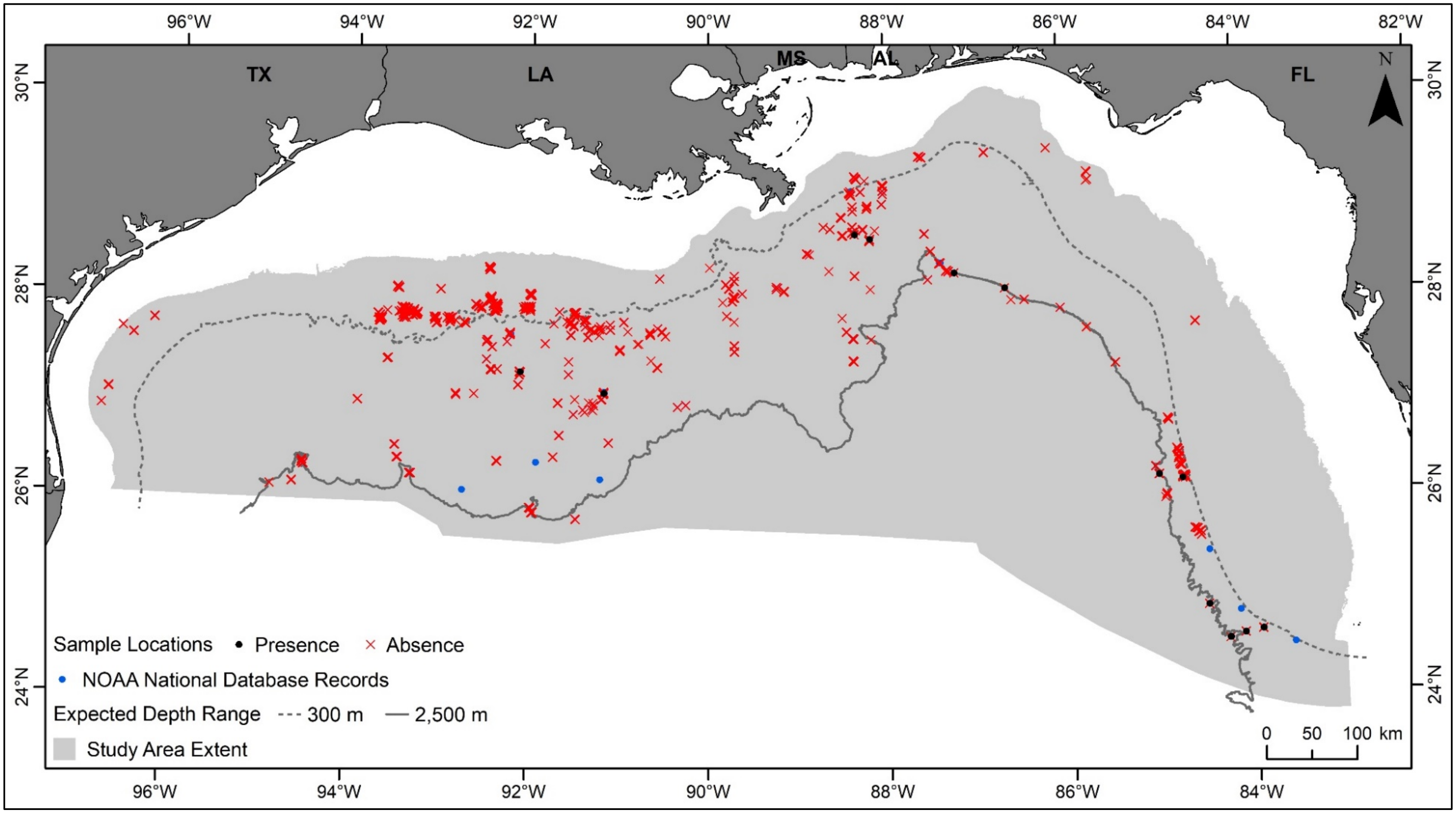

Figure 89. Occurrence records for the gorgonian coral *Keratoisis* (order Alcyonacea, family Isididae).

This map shows the observed occurrence (presence-absence) of *Keratoisis* at sample locations in the presence-absence database compiled for this study. Additional records of occurrence in the NOAA National Database are also displayed. Gray lines denote the expected depth range for *Keratoisis*.

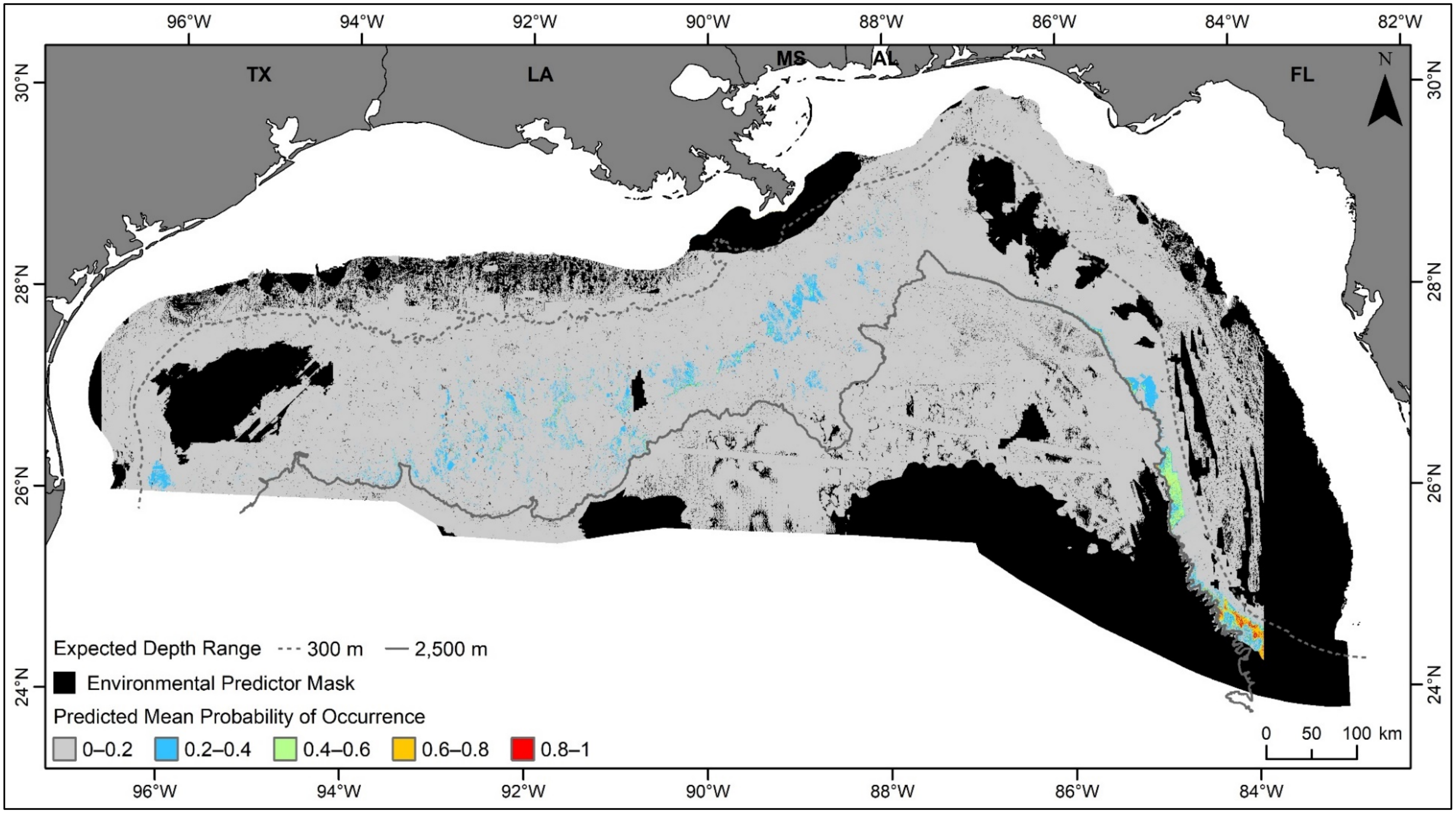

Figure 90. Predicted occurrence of the gorgonian coral *Keratoisis* (order Alcyonacea, family Isididae).

This map shows the predicted mean probability of occurrence (i.e., the predicted posterior mean occupancy probability) for *Keratoisis* from the multi-genus occupancy model of family Isididae. The environmental predictor mask overlays areas where predictor values were outside the range of values at the sample locations and model predictions may be affected by extrapolation. Gray lines denote the expected depth range for *Keratoisis*.

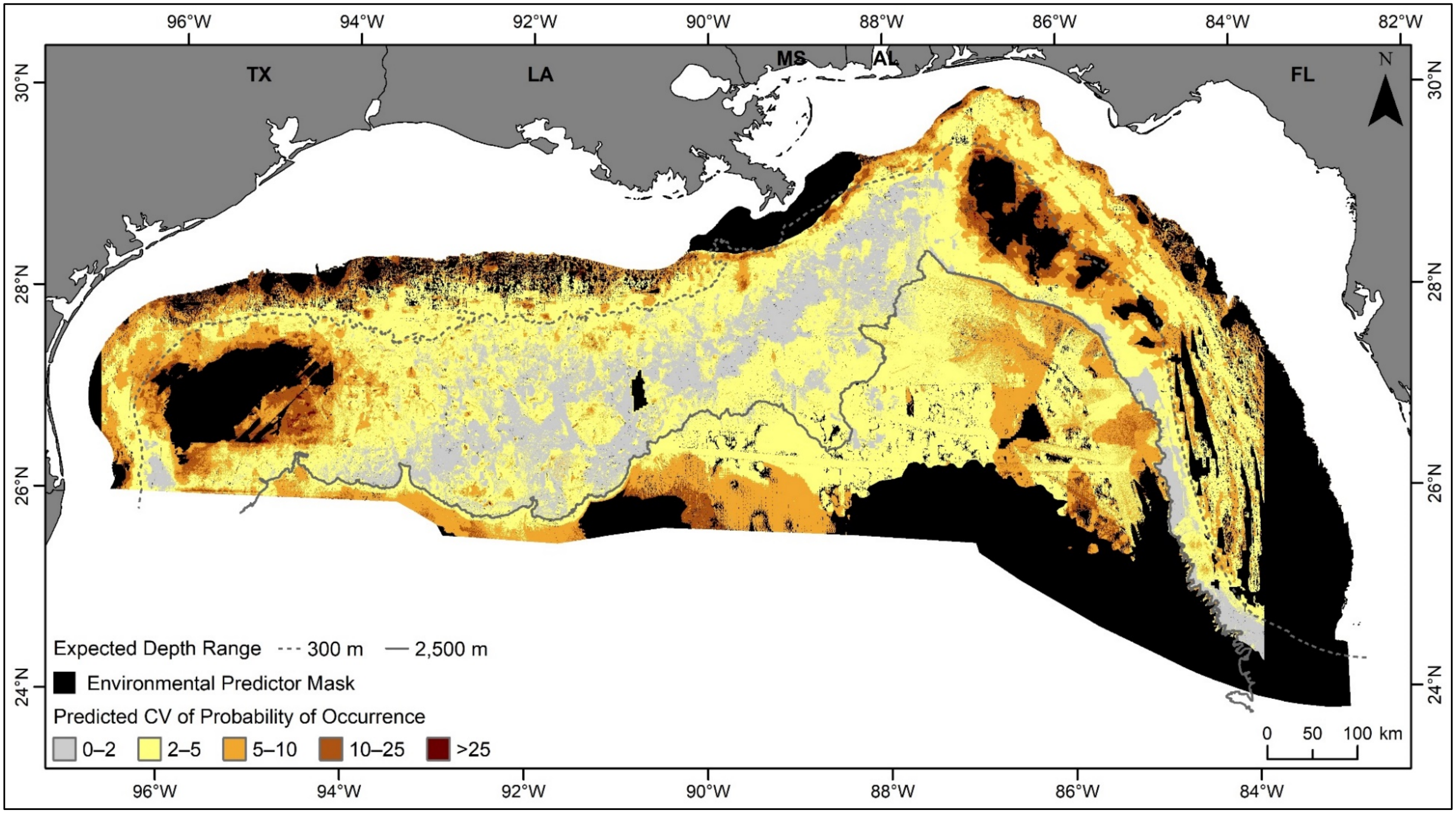

Figure 91. Variability in the predicted occurrence of the gorgonian coral *Keratoisis* (order Alcyonacea, family Isididae).

This map shows the predicted coefficient of variation (CV) of the probability of occurrence (i.e., the predicted posterior CV of occupancy probability) for *Keratoisis* from the multi-genus occupancy model of family Isididae. The environmental predictor mask overlays areas where predictor values were outside the range of values at the sample locations and model predictions may be affected by extrapolation. Gray lines denote the expected depth range for *Keratoisis*.

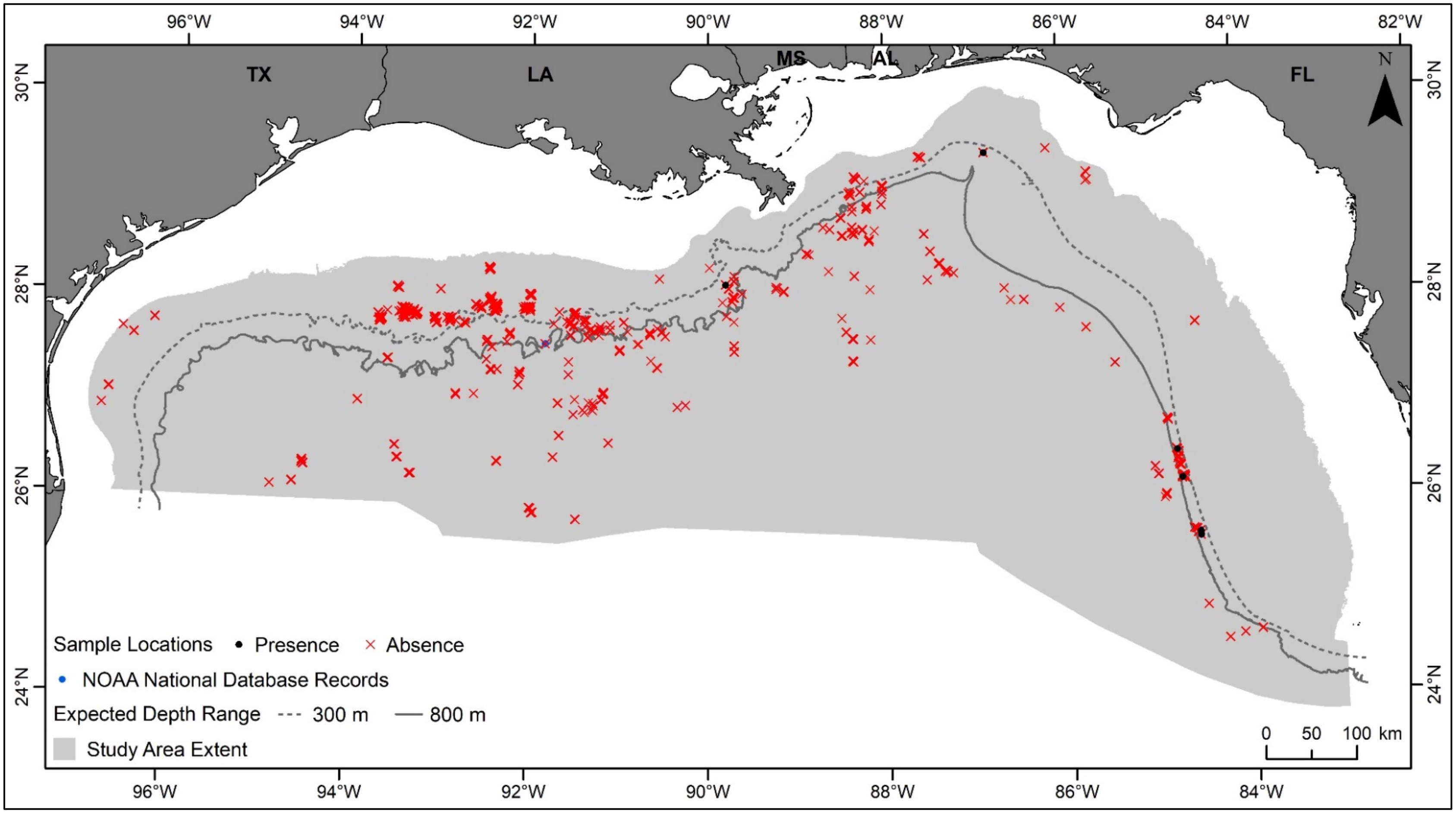

Figure 92. Occurrence records for the gorgonian coral *Chelidonisis* (order Alcyonacea, family Isididae).

This map shows the observed occurrence (presence-absence) of *Chelidonisis* at sample locations in the presence-absence database compiled for this study. Additional records of occurrence in the NOAA National Database are also displayed. Gray lines denote the expected depth range for *Chelidonisis*.

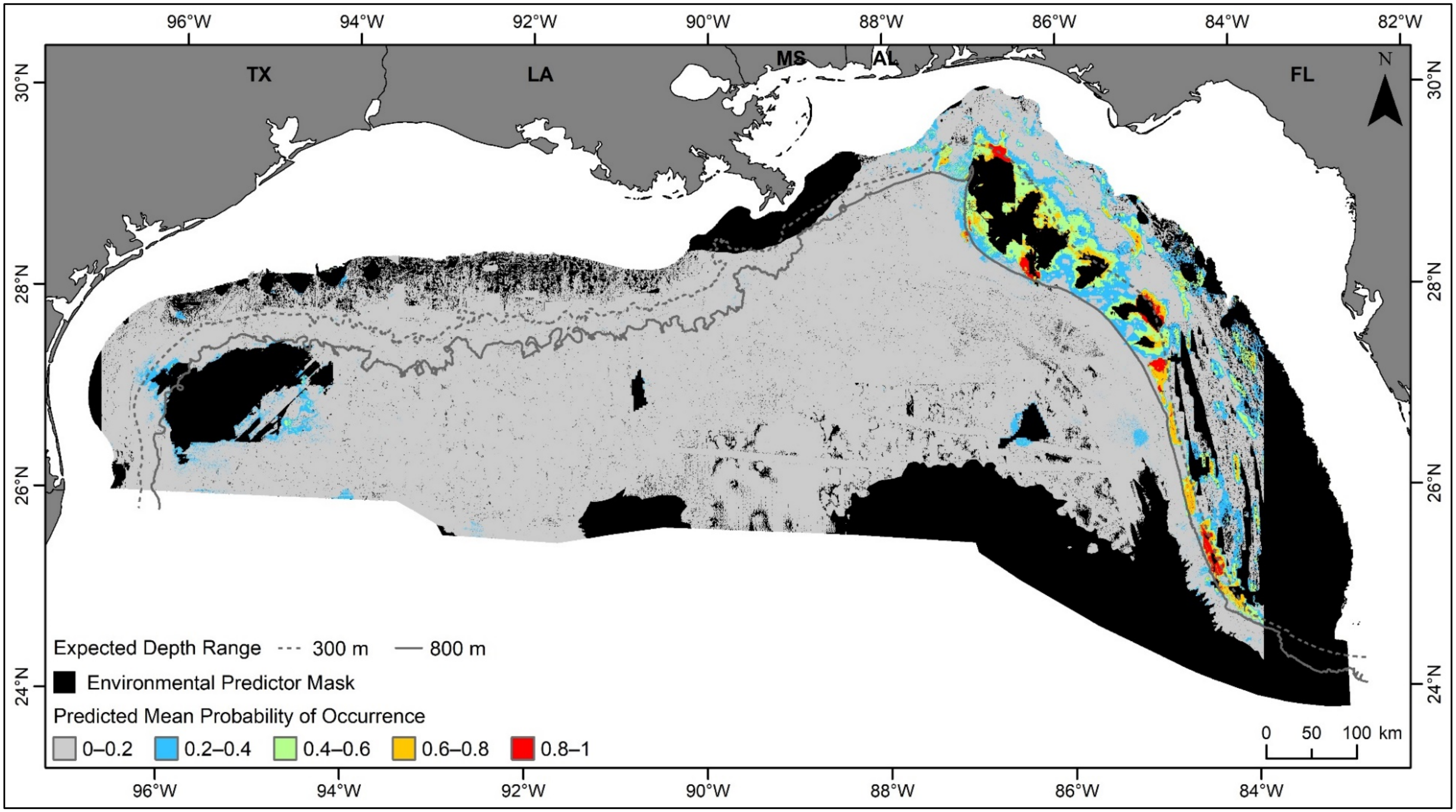

Figure 93. Predicted occurrence of the gorgonian coral *Chelidonisis* (order Alcyonacea, family Isididae).

This map shows the predicted mean probability of occurrence (i.e., the predicted posterior mean occupancy probability) for *Chelidonisis* from the multi-genus occupancy model of family Isididae. The environmental predictor mask overlays areas where predictor values were outside the range of values at the sample locations and model predictions may be affected by extrapolation. Gray lines denote the expected depth range for *Chelidonisis*.

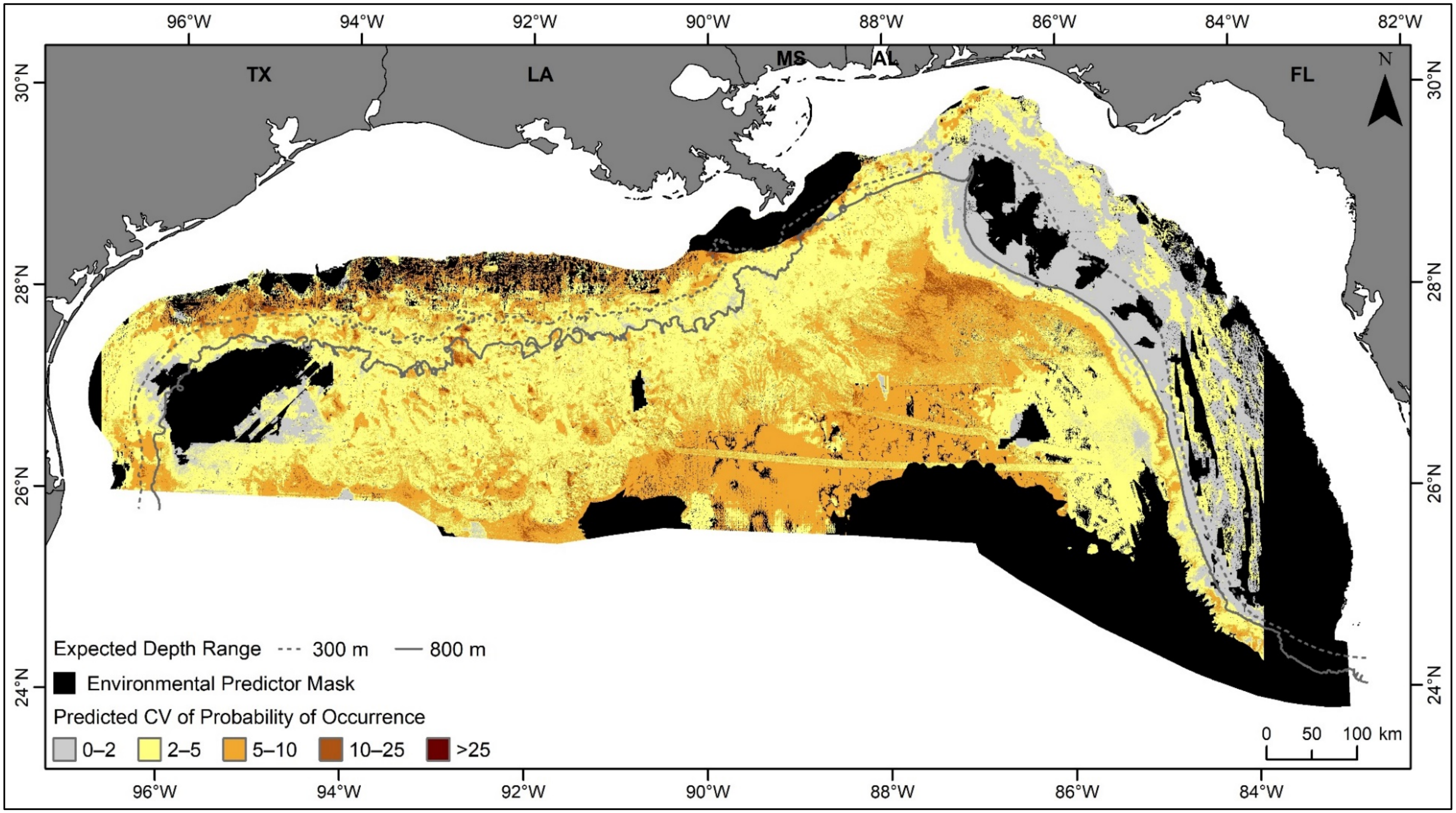

Figure 94. Variability in the predicted occurrence of the gorgonian coral *Chelidonisis* (order Alcyonacea, family Isididae).

This map shows the predicted coefficient of variation (CV) of the probability of occurrence (i.e., the predicted posterior CV of occupancy probability) for *Chelidonisis* from the multi-genus occupancy model of family Isididae. The environmental predictor mask overlays areas where predictor values were outside the range of values at the sample locations and model predictions may be affected by extrapolation. Gray lines denote the expected depth range for *Chelidonisis*.

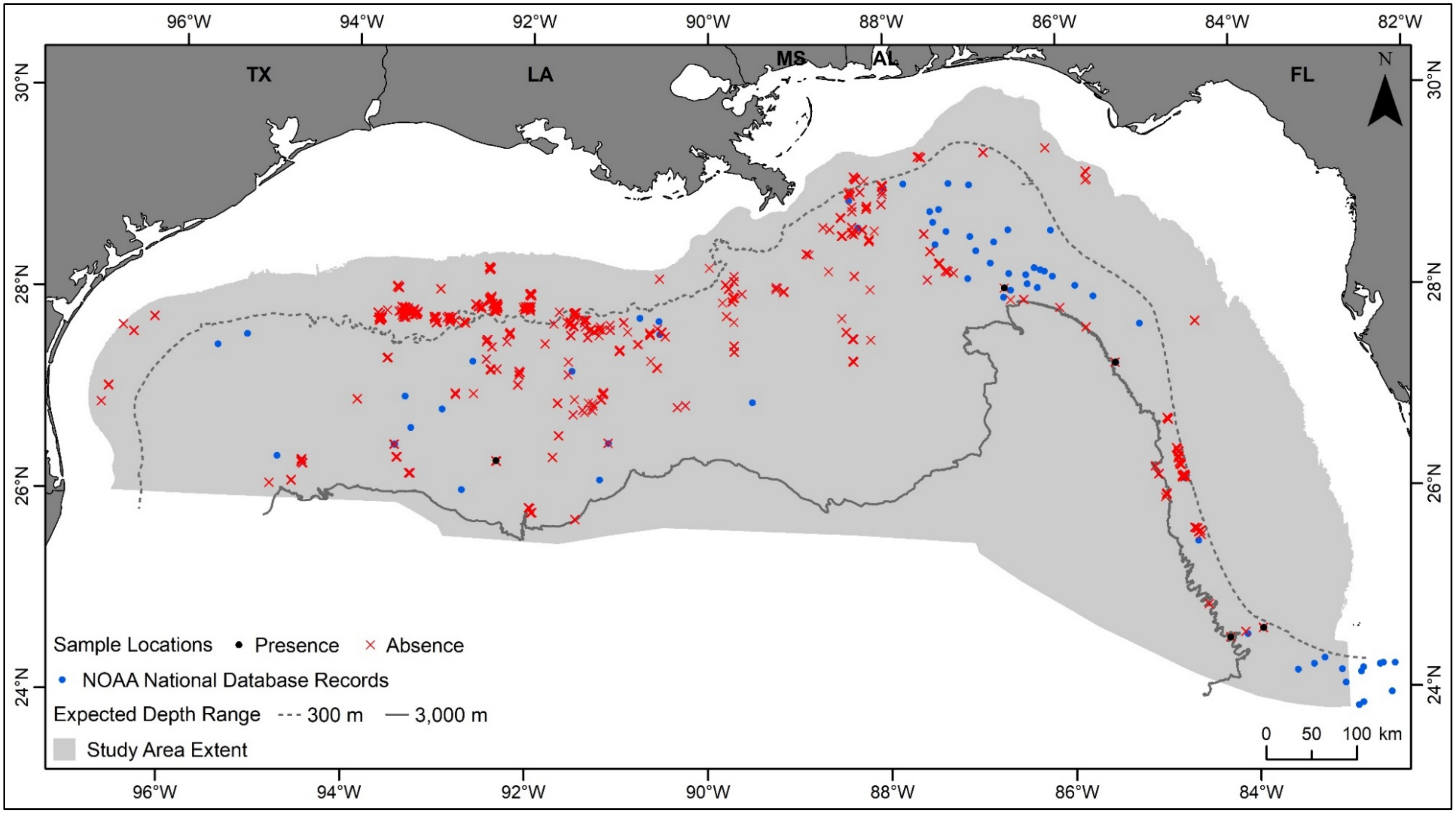

Figure 95. Occurrence records for the gorgonian coral *Acanella* (order Alcyonacea, family Isididae).

This map shows the observed occurrence (presence-absence) of *Acanella* at sample locations in the presence-absence database compiled for this study. Additional records of occurrence in the NOAA National Database are also displayed. Gray lines denote the expected depth range for *Acanella*.

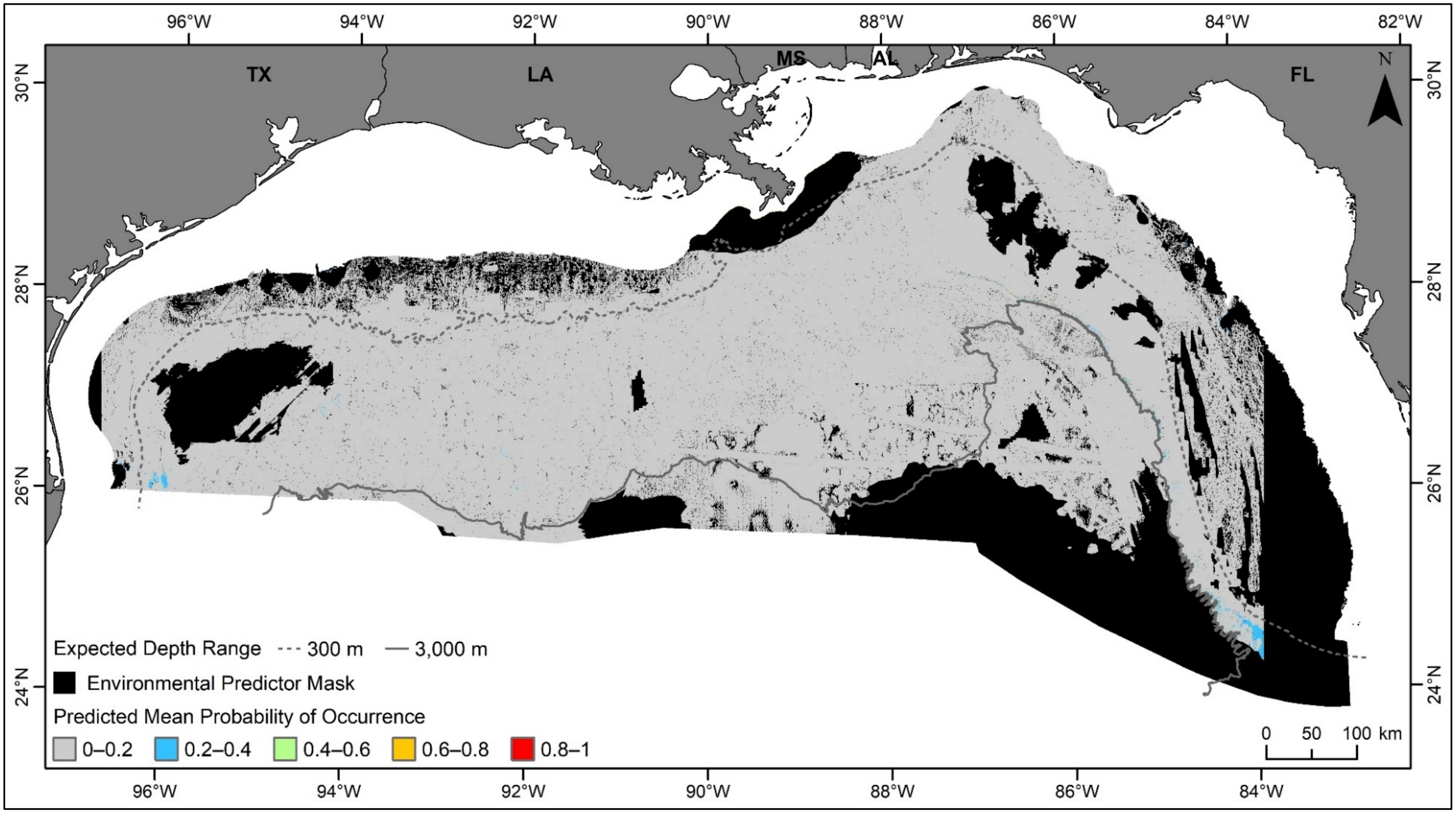

Figure 96. Predicted occurrence of the gorgonian coral *Acanella* (order Alcyonacea, family Isididae).

This map shows the predicted mean probability of occurrence (i.e., the predicted posterior mean occupancy probability) for *Acanella* from the multi-genus occupancy model of family Isididae. The environmental predictor mask overlays areas where predictor values were outside the range of values at the sample locations and model predictions may be affected by extrapolation. Gray lines denote the expected depth range for *Acanella*.

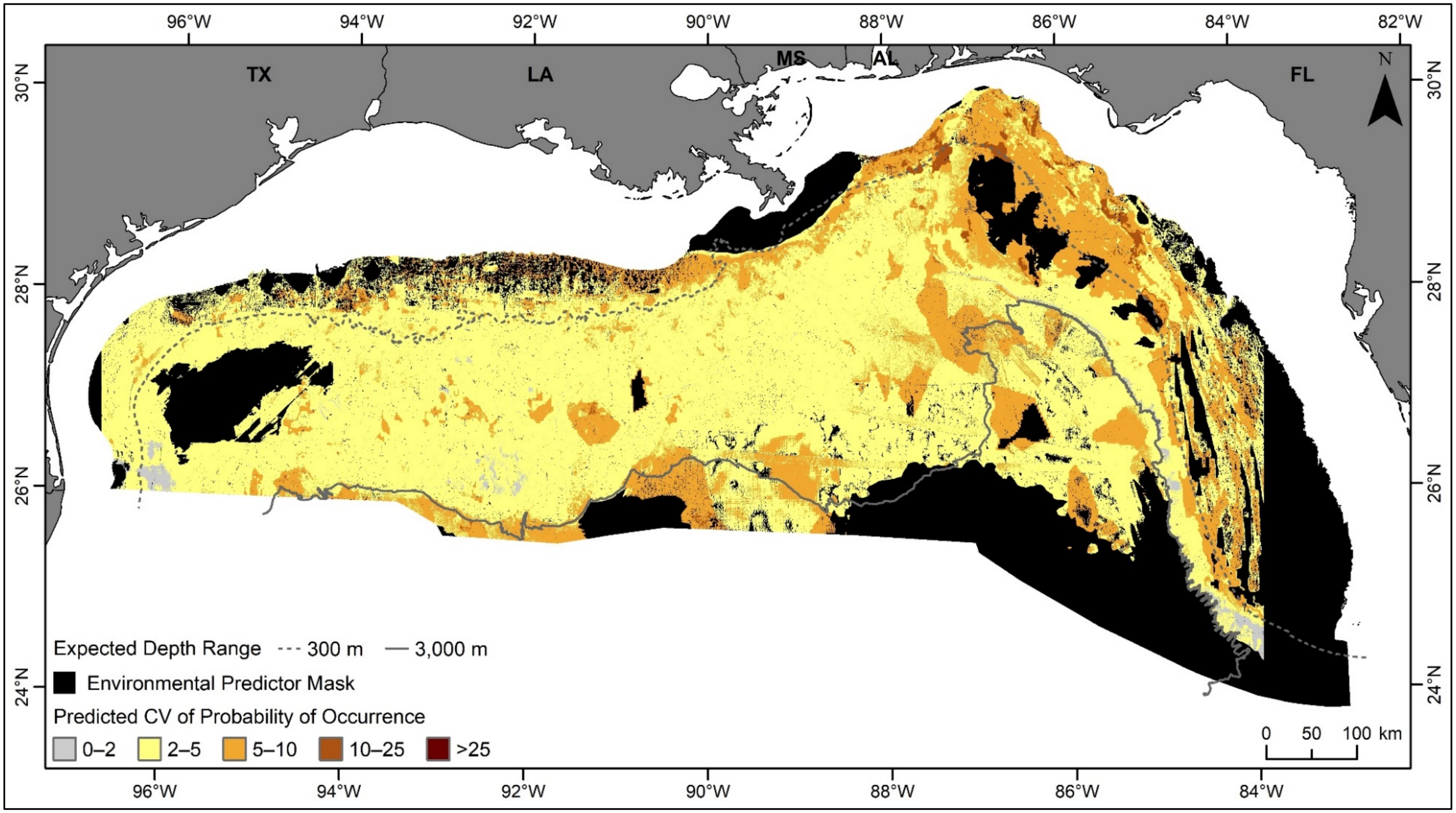

Figure 97. Variability in the predicted occurrence of the gorgonian coral *Acanella* (order Alcyonacea, family Isididae).

This map shows the predicted coefficient of variation (CV) of the probability of occurrence (i.e., the predicted posterior CV of occupancy probability) for *Acanella* from the multi-genus occupancy model of family Isididae. The environmental predictor mask overlays areas where predictor values were outside the range of values at the sample locations and model predictions may be affected by extrapolation. Gray lines denote the expected depth range for *Acanella*.

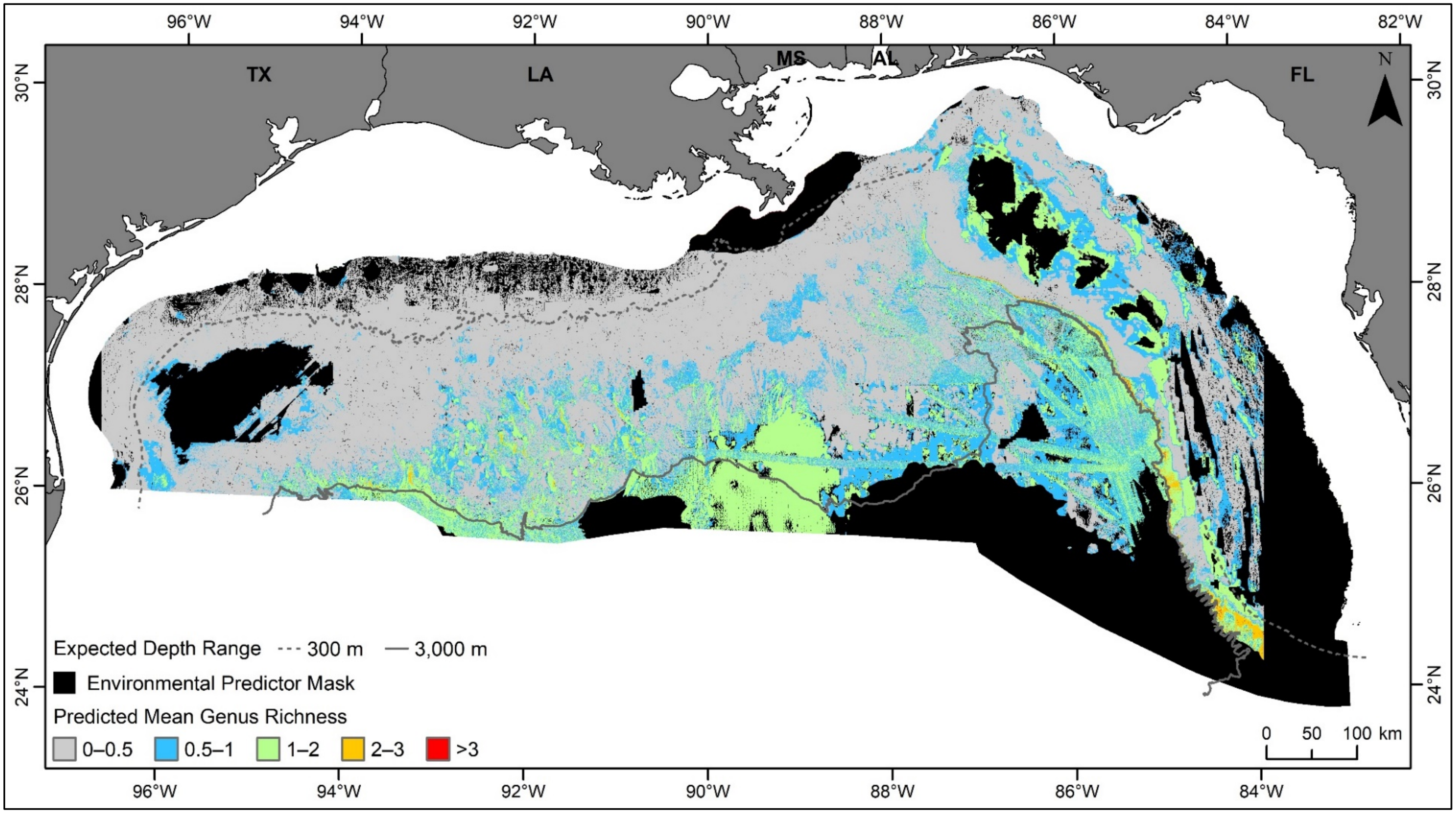

Figure 98. Predicted genus richness of gorgonian corals in family Isididae (order Alcyonacea).

This map shows the predicted mean genus richness (i.e., the posterior mean genus richness) from the multi-genus occupancy model of family Isididae. The environmental predictor mask overlays areas where predictor values were outside the range of values at the sample locations and model predictions may be affected by extrapolation. Gray lines denote the combined expected depth range for the genera included in the model.

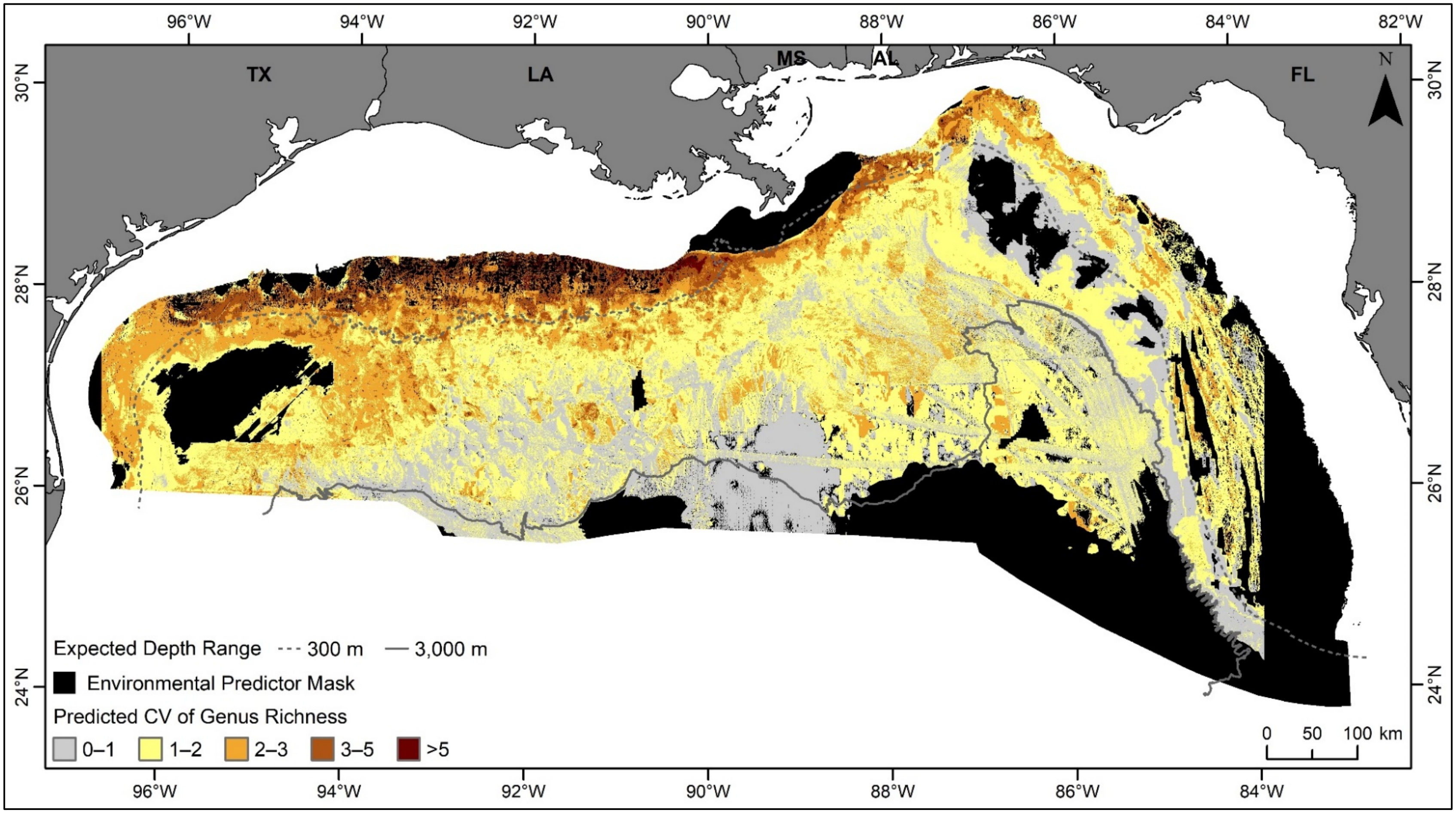

Figure 99. Variability in the predicted genus richness of gorgonian corals in family Isididae (order Alcyonacea).

This map shows the predicted coefficient of variation of genus richness (i.e., the posterior CV of genus richness) from the multi-genus occupancy model of family Isididae. The environmental predictor mask overlays areas where predictor values were outside the range of values at the sample locations and model predictions may be affected by extrapolation. Gray lines denote the combined expected depth range for the genera included in the model.

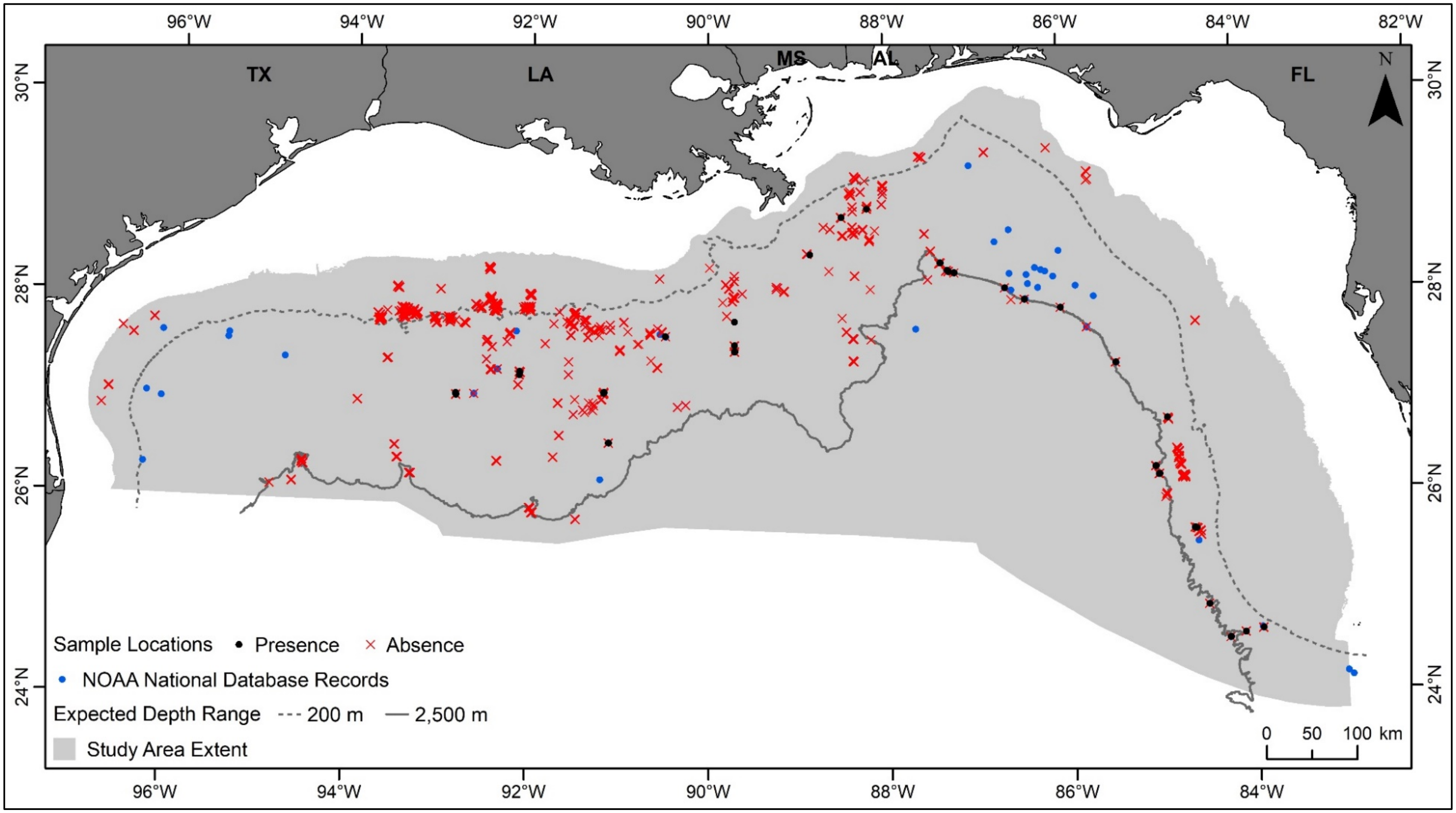

Figure 100. Occurrence records for the gorgonian coral family Chrysogorgiidae (order Alcyonacea).

This map shows the observed occurrence (presence-absence) of Chrysogorgiidae at sample locations in the presence-absence database compiled for this study. Additional records of occurrence in the NOAA National Database are also displayed. Gray lines denote the expected depth range for Chrysogorgiidae.

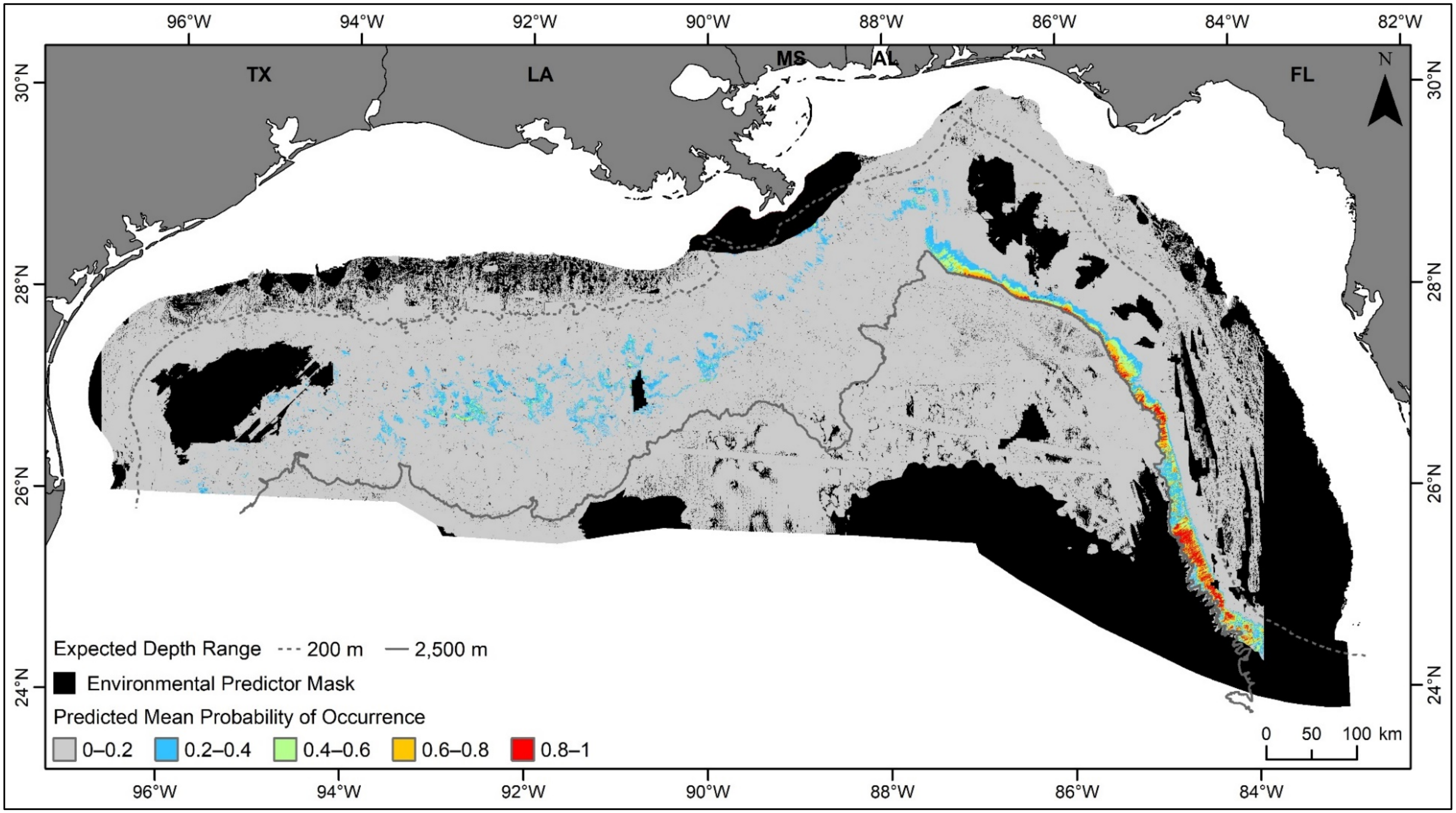

Figure 101. Predicted occurrence of the gorgonian coral family Chrysogorgiidae (order Alcyonacea).

This map shows the predicted mean probability of occurrence (i.e., the predicted posterior mean occupancy probability) for Chrysogorgiidae from the multi-family occupancy model of order Alcyonacea. The environmental predictor mask overlays areas where predictor values were outside the range of values at the sample locations and model predictions may be affected by extrapolation. Gray lines denote the expected depth range for Chrysogorgiidae.

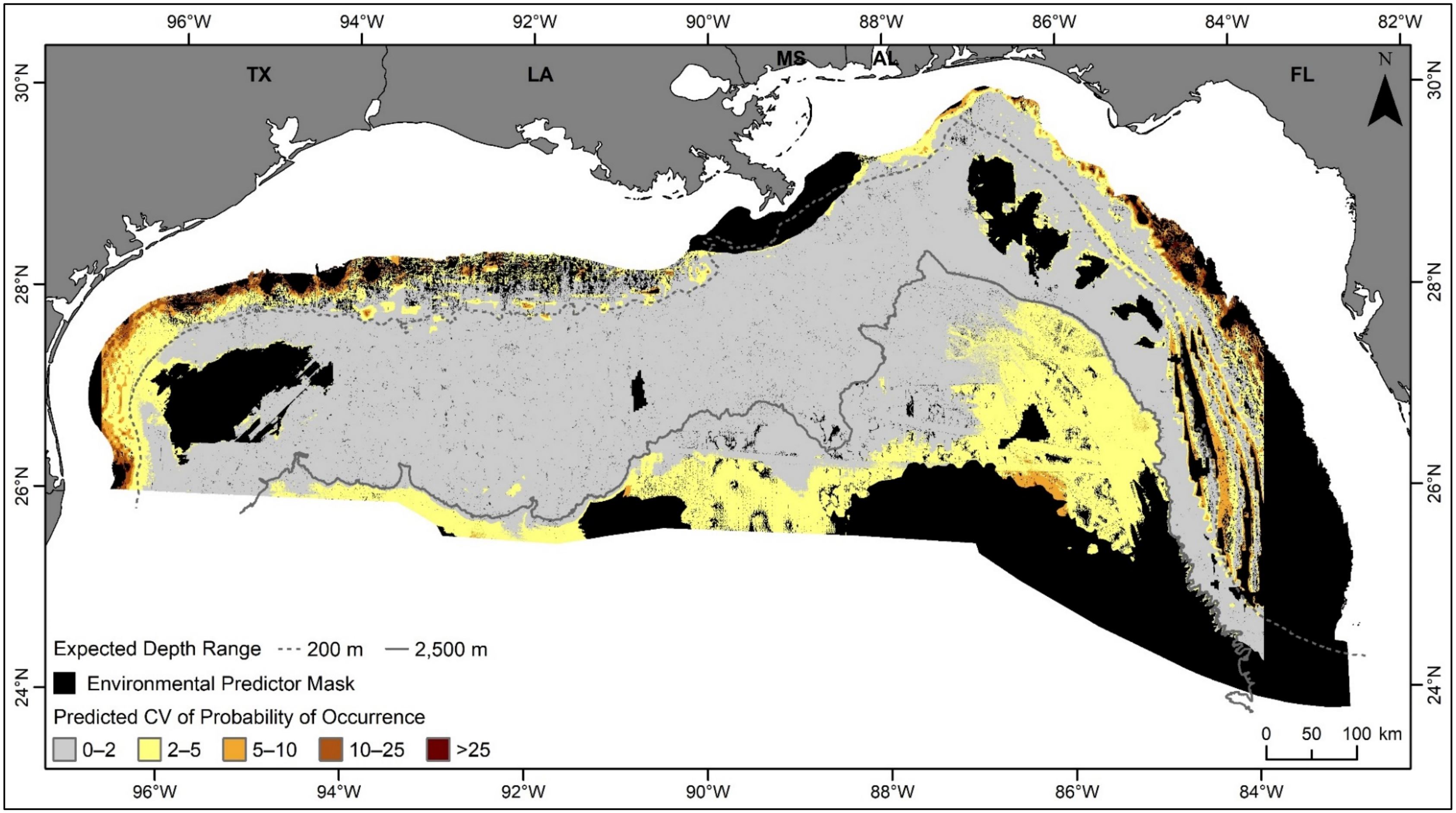

Figure 102. Variability in the predicted occurrence of the gorgonian coral family Chrysogorgiidae (order Alcyonacea).

This map shows the predicted coefficient of variation (CV) of the probability of occurrence (i.e., the predicted posterior CV of occupancy probability) for Chrysogorgiidae from the multi-family occupancy model of order Alcyonacea. The environmental predictor mask overlays areas where predictor values were outside the range of values at the sample locations and model predictions may be affected by extrapolation. Gray lines denote the expected depth range for Chrysogorgiidae.

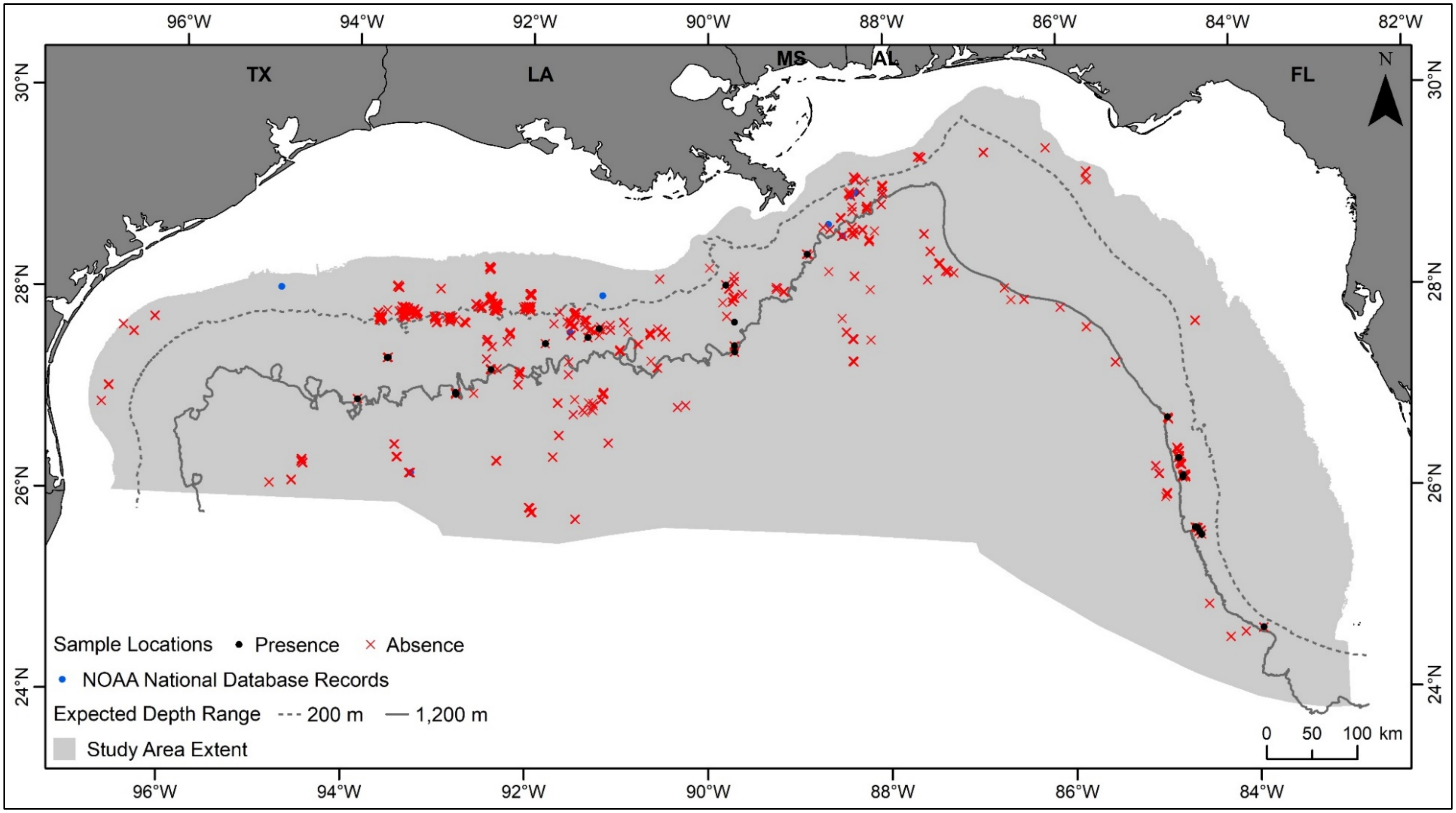

Figure 103. Occurrence records for the gorgonian coral family Acanthogorgiidae (order Alcyonacea).

This map shows the observed occurrence (presence-absence) of Acanthogorgiidae at sample locations in the presence-absence database compiled for this study. Additional records of occurrence in the NOAA National Database are also displayed. Gray lines denote the expected depth range for Acanthogorgiidae.

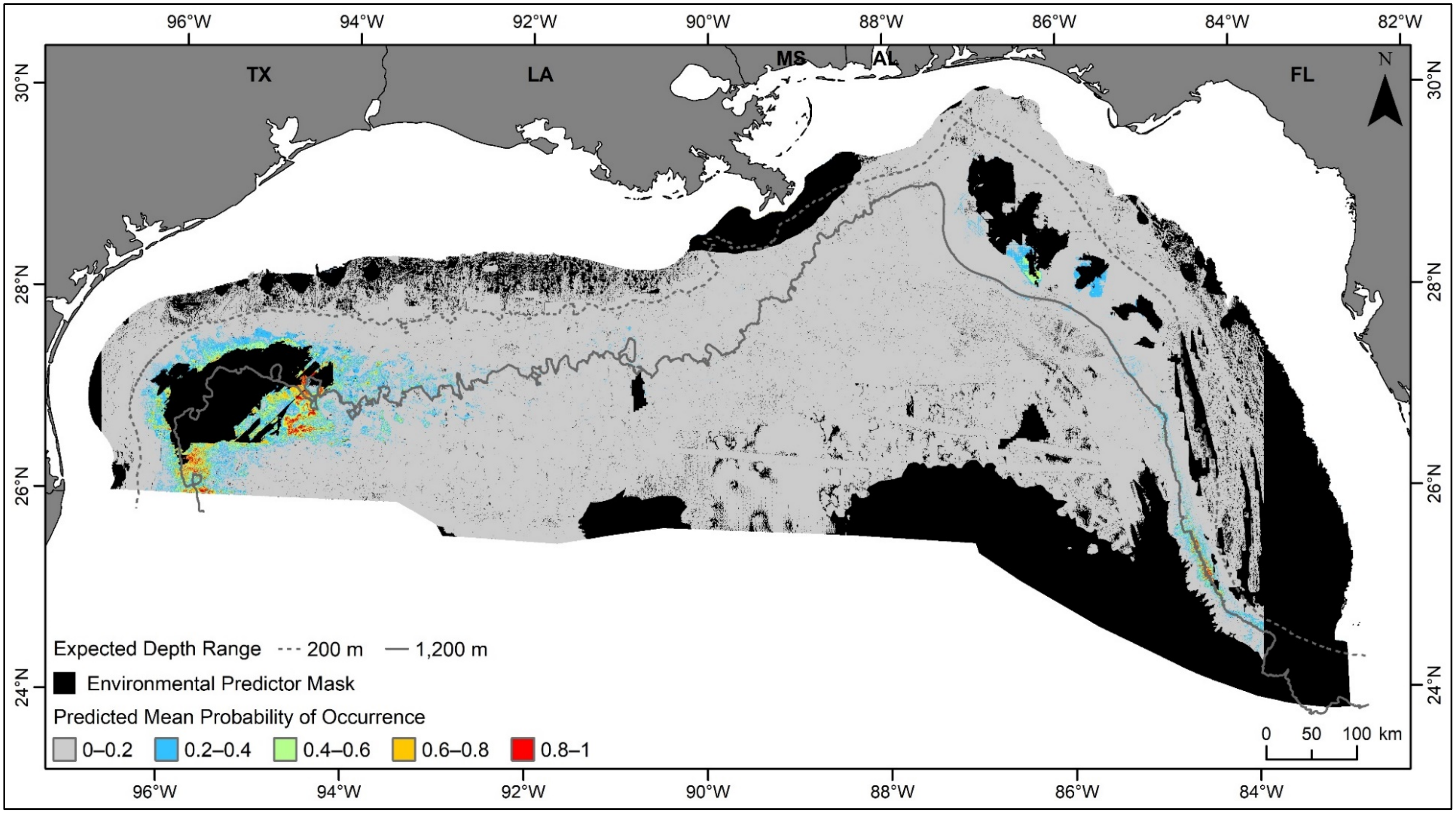

Figure 104. Predicted occurrence of the gorgonian coral family Acanthogorgiidae (order Alcyonacea).

This map shows the predicted mean probability of occurrence (i.e., the predicted posterior mean occupancy probability) for Acanthogorgiidae from the multi-family occupancy model of order Alcyonacea. The environmental predictor mask overlays areas where predictor values were outside the range of values at the sample locations and model predictions may be affected by extrapolation. Gray lines denote the expected depth range for Acanthogorgiidae.

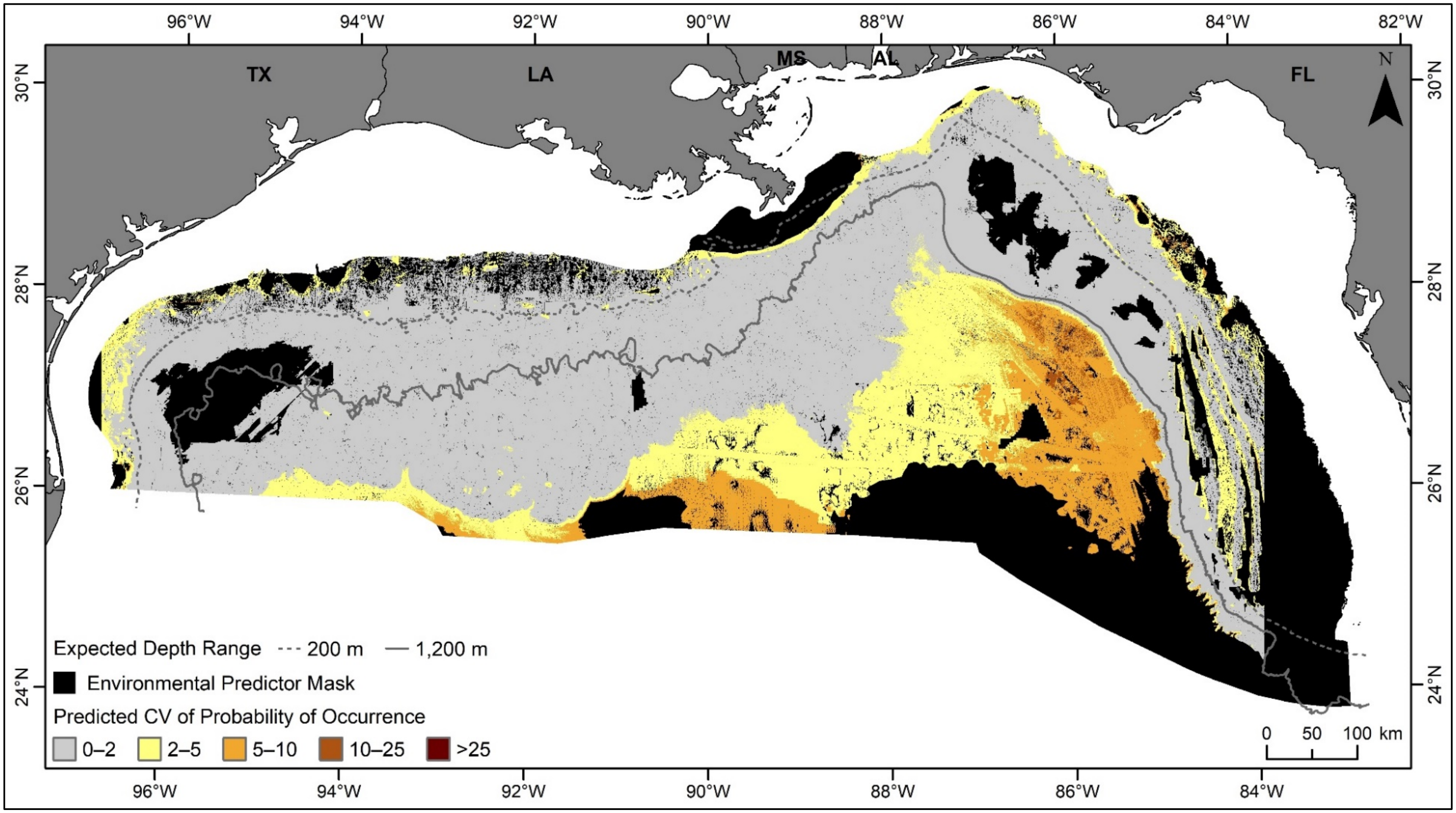

Figure 105. Variability in the predicted occurrence of the gorgonian coral family Acanthogorgiidae (order Alcyonacea).

This map shows the predicted coefficient of variation (CV) of the probability of occurrence (i.e., the predicted posterior CV of occupancy probability) for Acanthogorgiidae from the multi-family occupancy model of order Alcyonacea. The environmental predictor mask overlays areas where predictor values were outside the range of values at the sample locations and model predictions may be affected by extrapolation. Gray lines denote the expected depth range for Acanthogorgiidae.

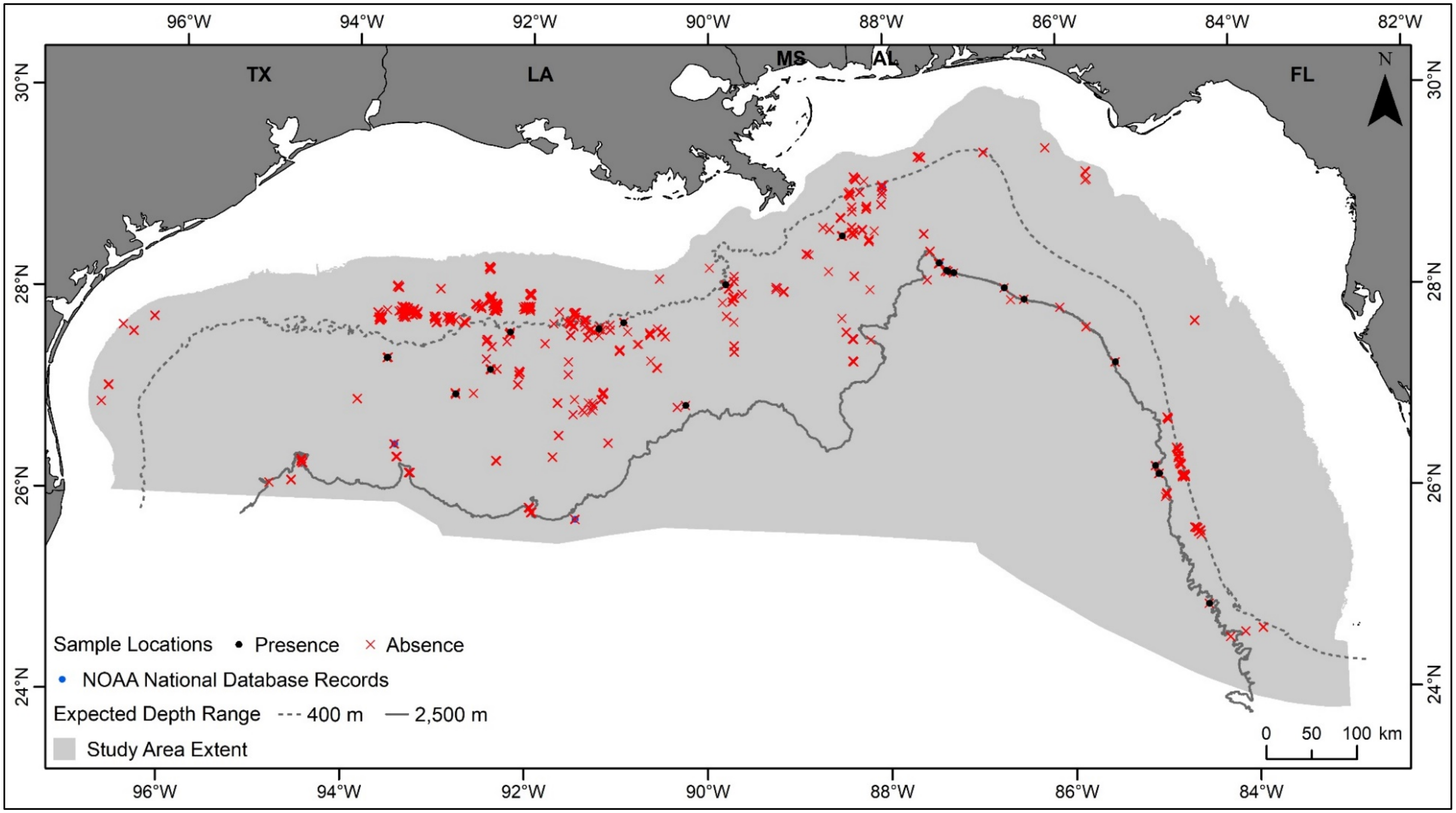

Figure 106. Occurrence records for the gorgonian coral family Paragorgiidae (order Alcyonacea).

This map shows the observed occurrence (presence-absence) of Paragorgiidae at sample locations in the presence-absence database compiled for this study. Additional records of occurrence in the NOAA National Database are also displayed. Gray lines denote the expected depth range for Paragorgiidae.

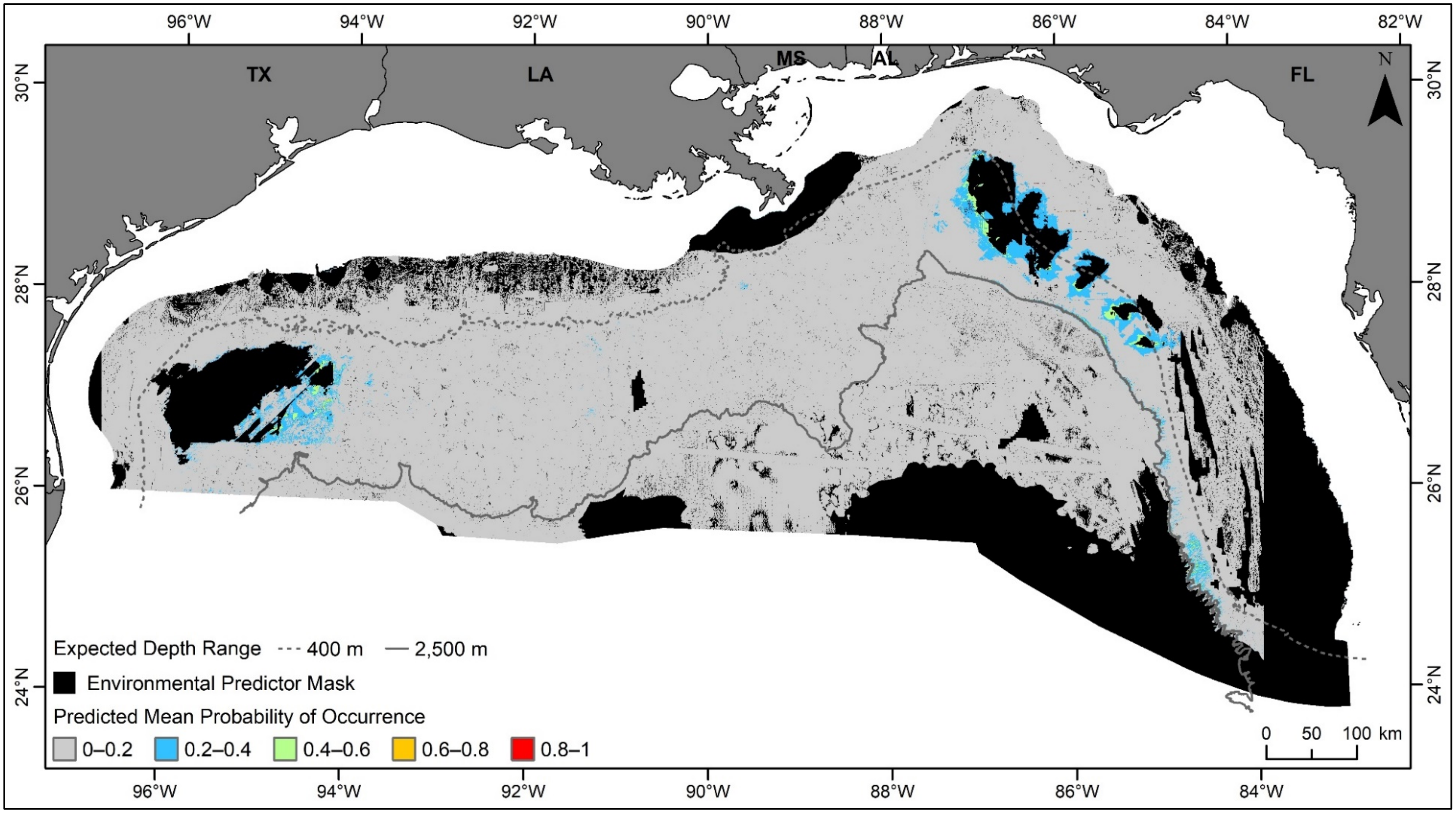

Figure 107. Predicted occurrence of the gorgonian coral family Paragorgiidae (order Alcyonacea).

This map shows the predicted mean probability of occurrence (i.e., the predicted posterior mean occupancy probability) for Paragorgiidae from the multi-family occupancy model of order Alcyonacea. The environmental predictor mask overlays areas where predictor values were outside the range of values at the sample locations and model predictions may be affected by extrapolation. Gray lines denote the expected depth range for Paragorgiidae.

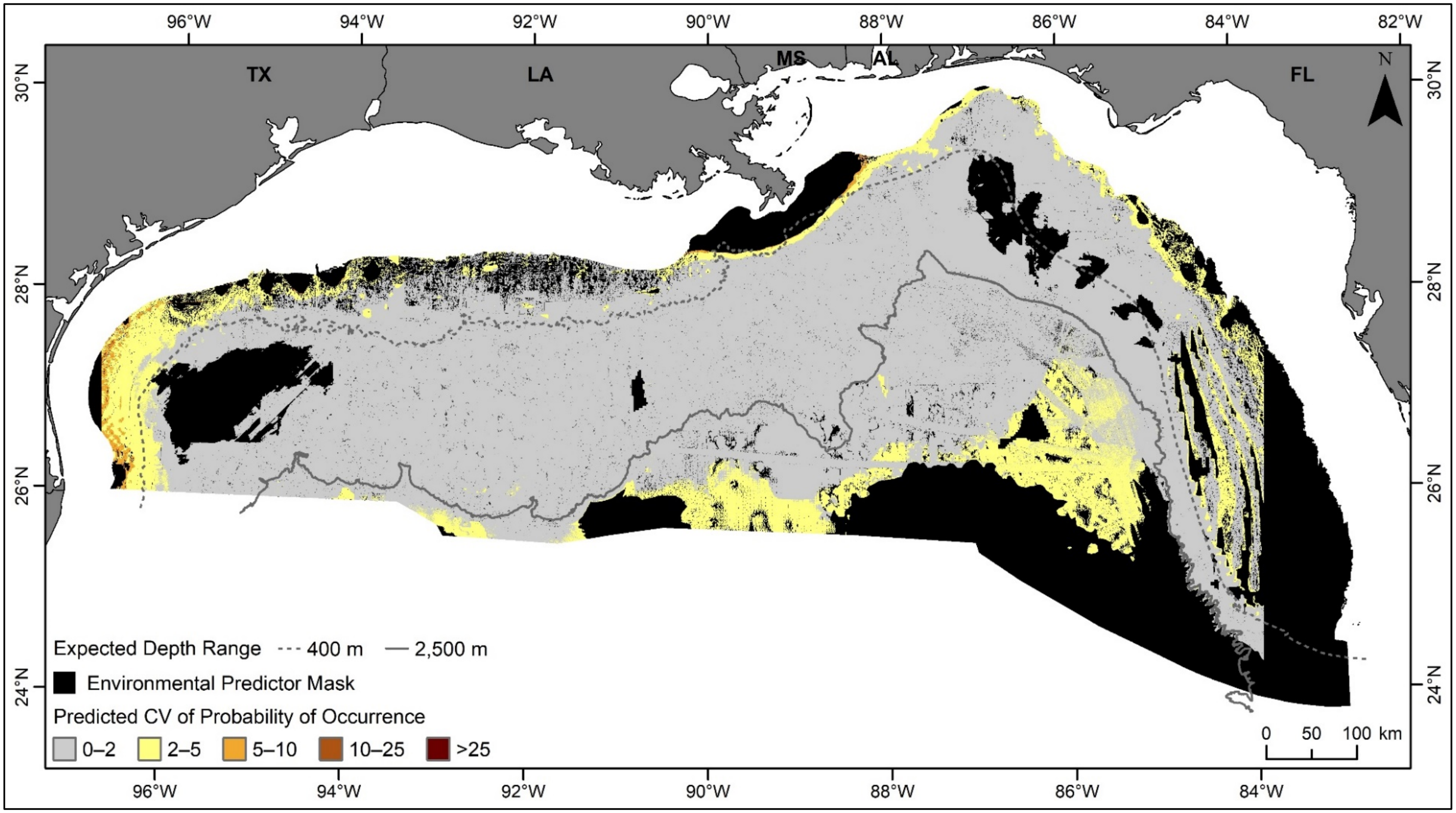

Figure 108. Variability in the predicted occurrence of the gorgonian coral family Paragorgiidae (order Alcyonacea).

This map shows the predicted coefficient of variation (CV) of the probability of occurrence (i.e., the predicted posterior CV of occupancy probability) for Paragorgiidae from the multi-family occupancy model of order Alcyonacea. The environmental predictor mask overlays areas where predictor values were outside the range of values at the sample locations and model predictions may be affected by extrapolation. Gray lines denote the expected depth range for Paragorgiidae.

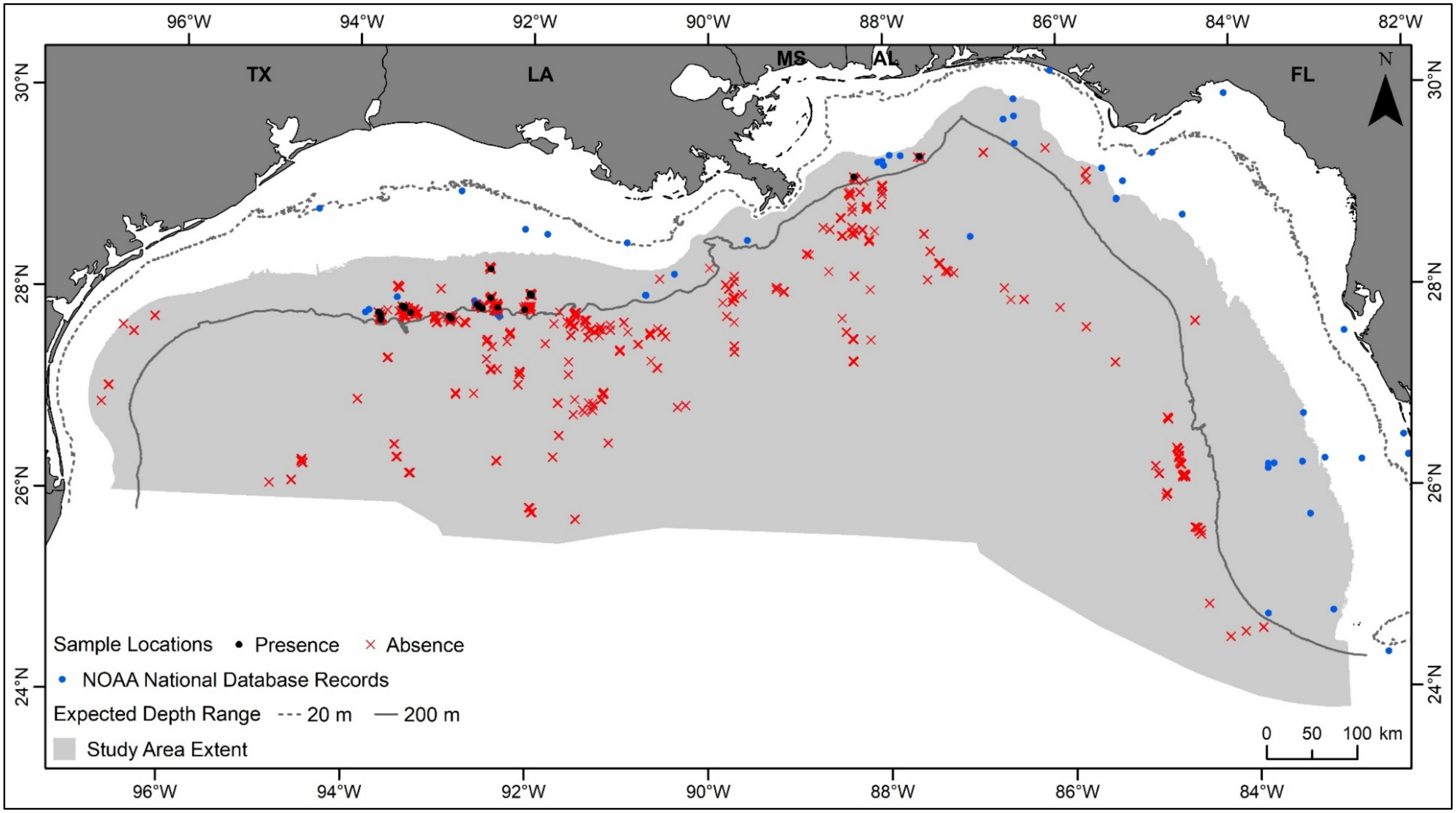

Figure 109. Occurrence records for the gorgonian coral family Gorgoniidae (order Alcyonacea).

This map shows the observed occurrence (presence-absence) of Gorgoniidae at sample locations in the presence-absence database compiled for this study. Additional records of occurrence in the NOAA National Database are also displayed. Gray lines denote the expected depth range for Gorgoniidae.

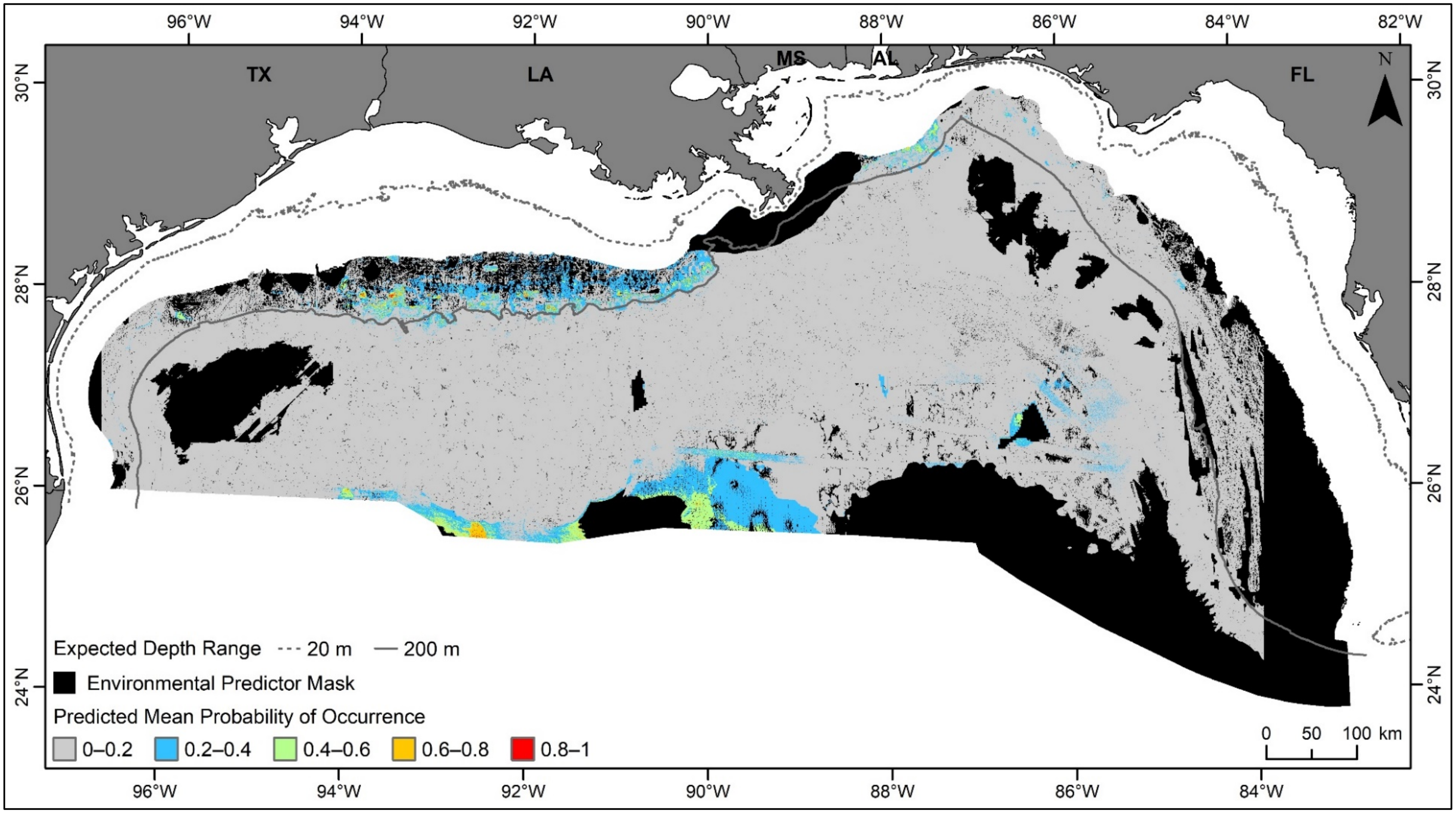

Figure 110. Predicted occurrence of the gorgonian coral family Gorgoniidae (order Alcyonacea).

This map shows the predicted mean probability of occurrence (i.e., the predicted posterior mean occupancy probability) for Gorgoniidae from the multi-family occupancy model of order Alcyonacea. The environmental predictor mask overlays areas where predictor values were outside the range of values at the sample locations and model predictions may be affected by extrapolation. Gray lines denote the expected depth range for Gorgoniidae.

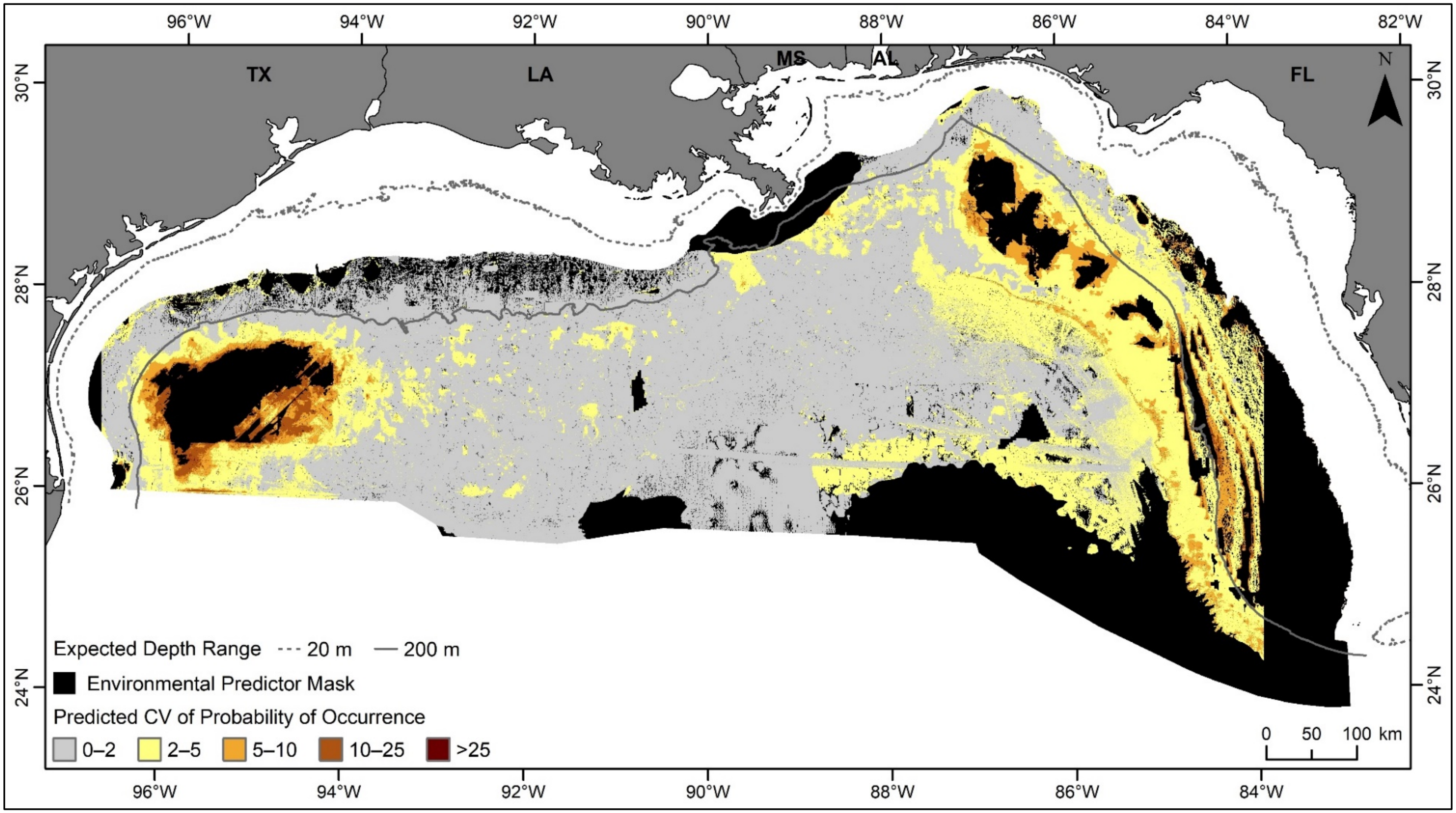

Figure 111. Variability in the predicted occurrence of the gorgonian coral family Gorgoniidae (order Alcyonacea).

This map shows the predicted coefficient of variation (CV) of the probability of occurrence (i.e., the predicted posterior CV of occupancy probability) for Gorgoniidae from the multi-family occupancy model of order Alcyonacea. The environmental predictor mask overlays areas where predictor values were outside the range of values at the sample locations and model predictions may be affected by extrapolation. Gray lines denote the expected depth range for Gorgoniidae.

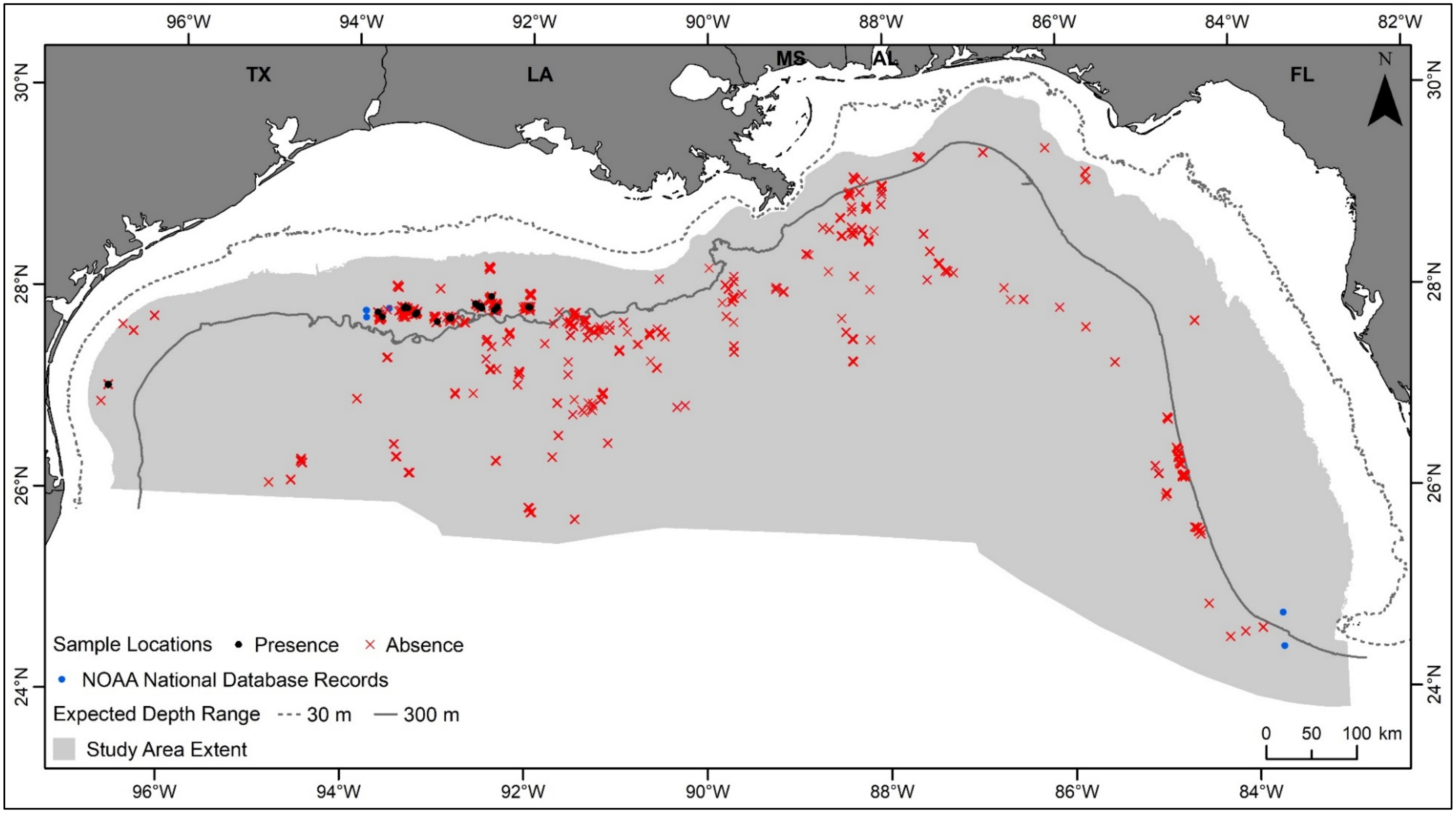

Figure 112. Occurrence records for the gorgonian coral family Keroeididae (order Alcyonacea).

This map shows the observed occurrence (presence-absence) of Keroeididae at sample locations in the presence-absence database compiled for this study. Additional records of occurrence in the NOAA National Database are also displayed. Gray lines denote the expected depth range for Keroeididae.

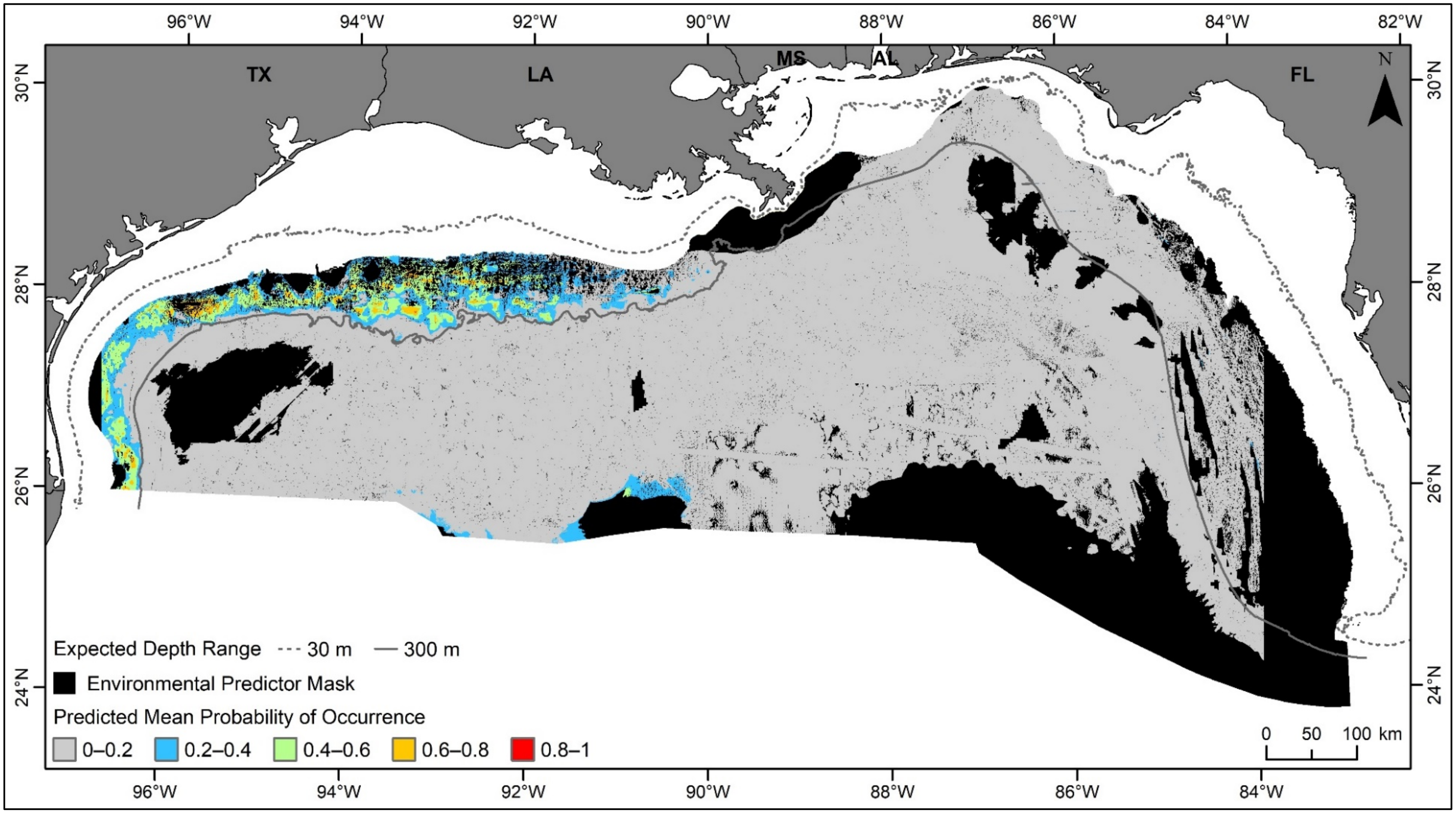

Figure 113. Predicted occurrence of the gorgonian coral family Keroeididae (order Alcyonacea).

This map shows the predicted mean probability of occurrence (i.e., the predicted posterior mean occupancy probability) for Keroeididae from the multi-family occupancy model of order Alcyonacea. The environmental predictor mask overlays areas where predictor values were outside the range of values at the sample locations and model predictions may be affected by extrapolation. Gray lines denote the expected depth range for Keroeididae.

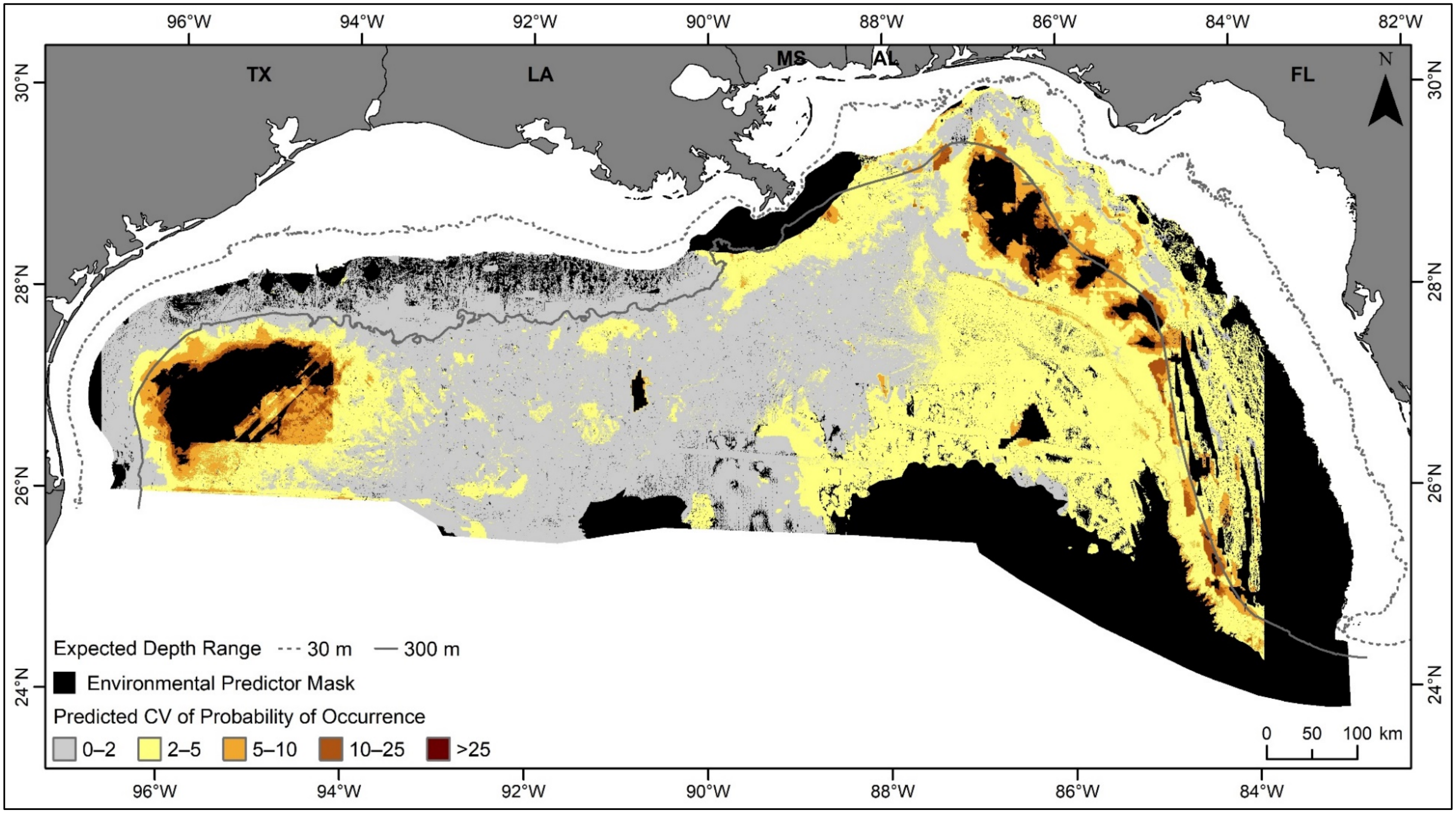

Figure 114. Variability in the predicted occurrence of the gorgonian coral family Keroeididae (order Alcyonacea).

This map shows the predicted coefficient of variation (CV) of the probability of occurrence (i.e., the predicted posterior CV of occupancy probability) for Keroeididae from the multi-family occupancy model of order Alcyonacea. The environmental predictor mask overlays areas where predictor values were outside the range of values at the sample locations and model predictions may be affected by extrapolation. Gray lines denote the expected depth range for Keroeididae.

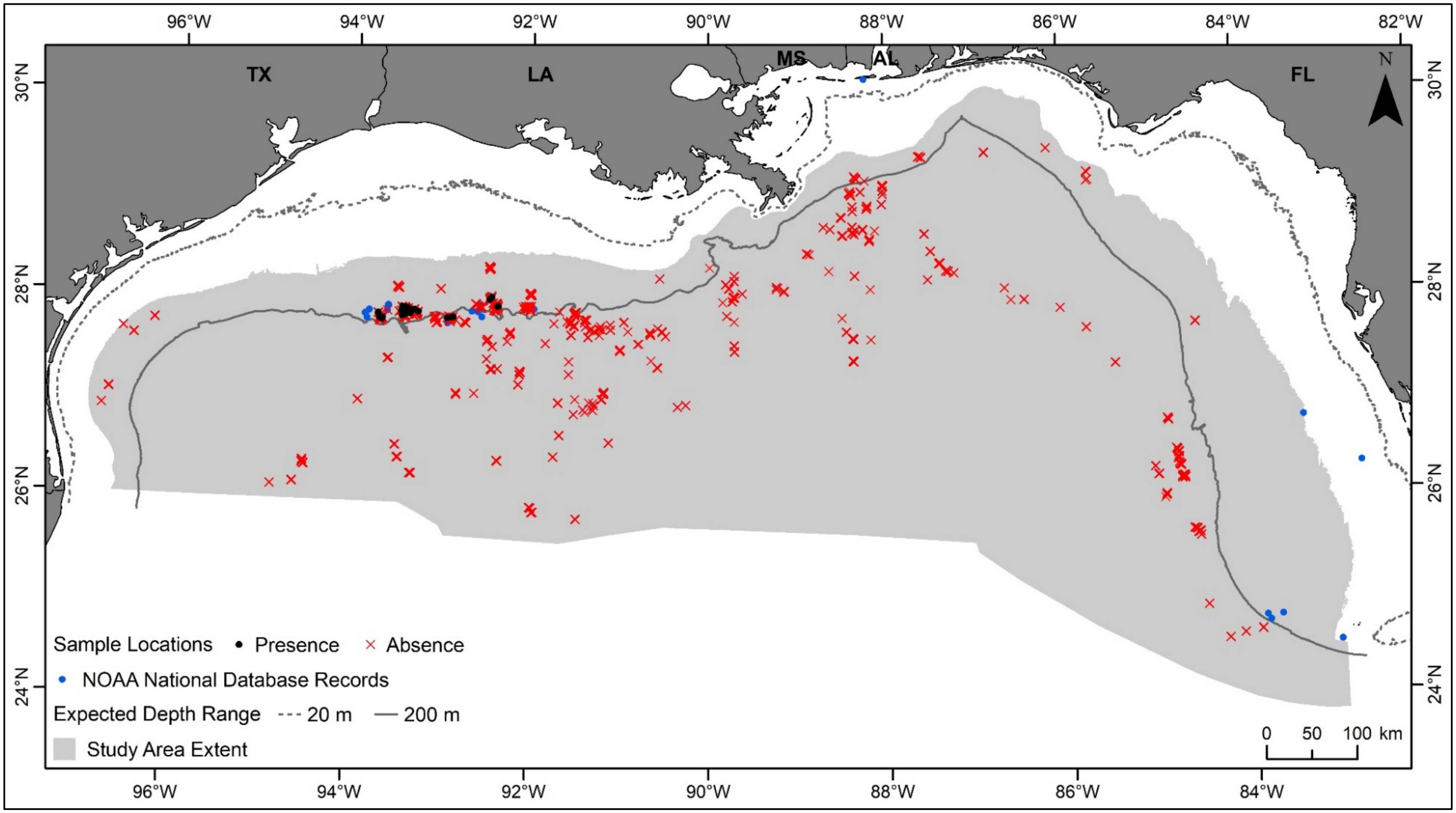

Figure 115. Occurrence records for the gorgonian coral family Spongiodermidae (order Alcyonacea).

This map shows the observed occurrence (presence-absence) of Spongiodermidae at sample locations in the presence-absence database compiled for this study. Additional records of occurrence in the NOAA National Database are also displayed. Gray lines denote the expected depth range for Spongiodermidae.

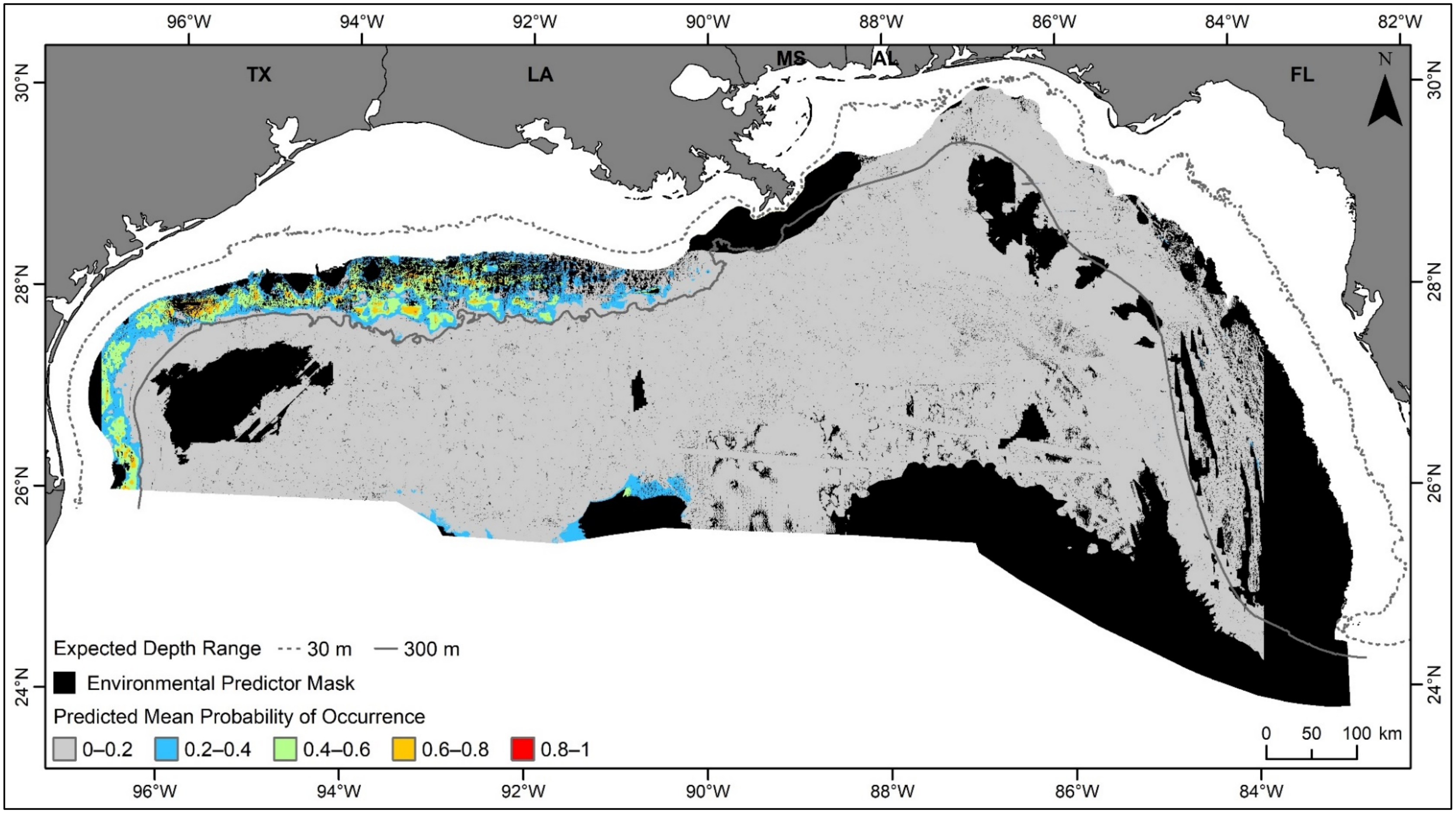

Figure 116. Predicted occurrence of the gorgonian coral family Spongiodermidae (order Alcyonacea).

This map shows the predicted mean probability of occurrence (i.e., the predicted posterior mean occupancy probability) for Spongiodermidae from the multi-family occupancy model of order Alcyonacea. The environmental predictor mask overlays areas where predictor values were outside the range of values at the sample locations and model predictions may be affected by extrapolation. Gray lines denote the expected depth range for Spongiodermidae.

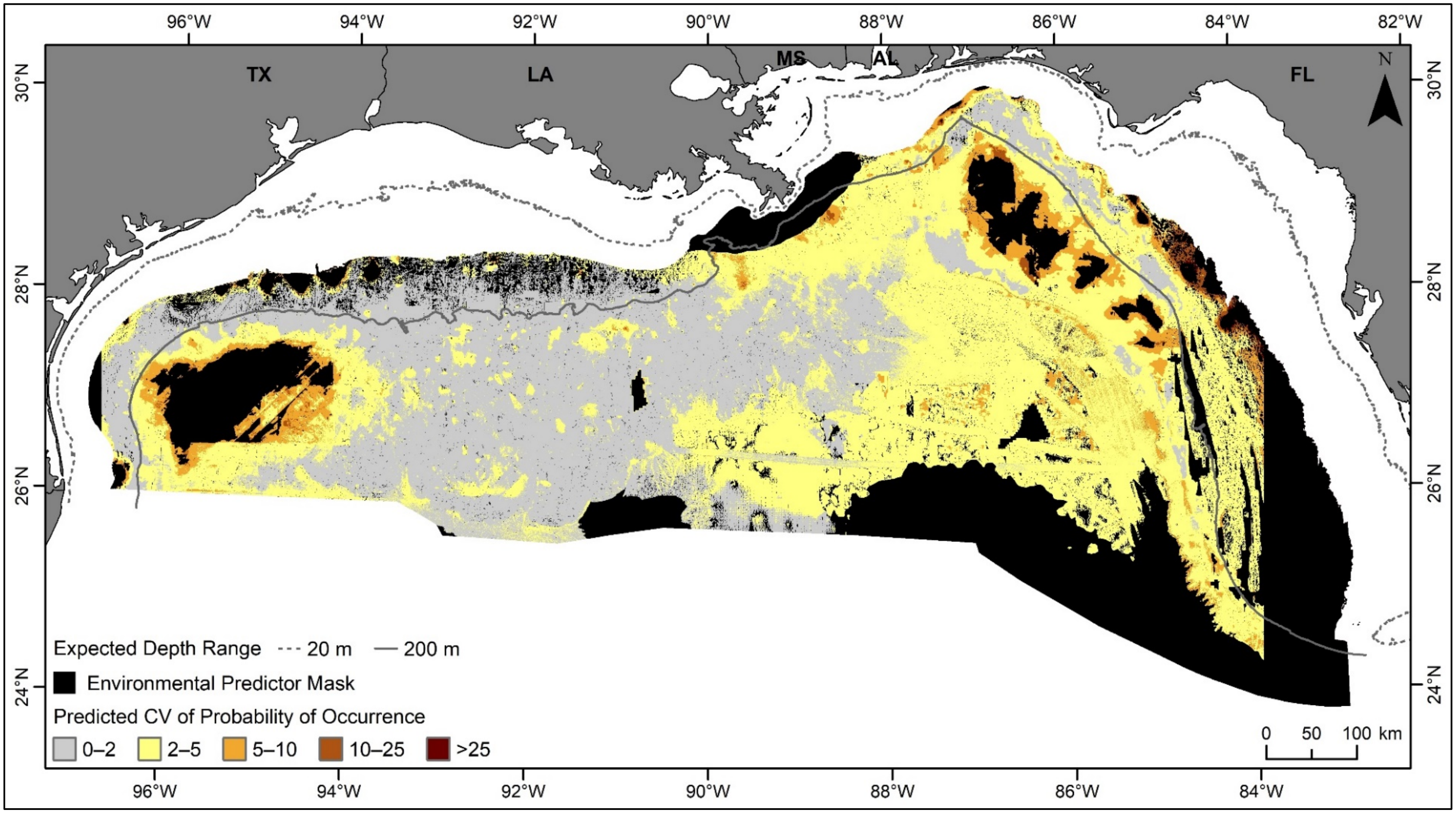

Figure 117. Variability in the predicted occurrence of the gorgonian coral family Spongiodermidae (order Alcyonacea).

This map shows the predicted coefficient of variation (CV) of the probability of occurrence (i.e., the predicted posterior CV of occupancy probability) for Spongiodermidae from the multi-family occupancy model of order Alcyonacea. The environmental predictor mask overlays areas where predictor values were outside the range of values at the sample locations and model predictions may be affected by extrapolation. Gray lines denote the expected depth range for Spongiodermidae.

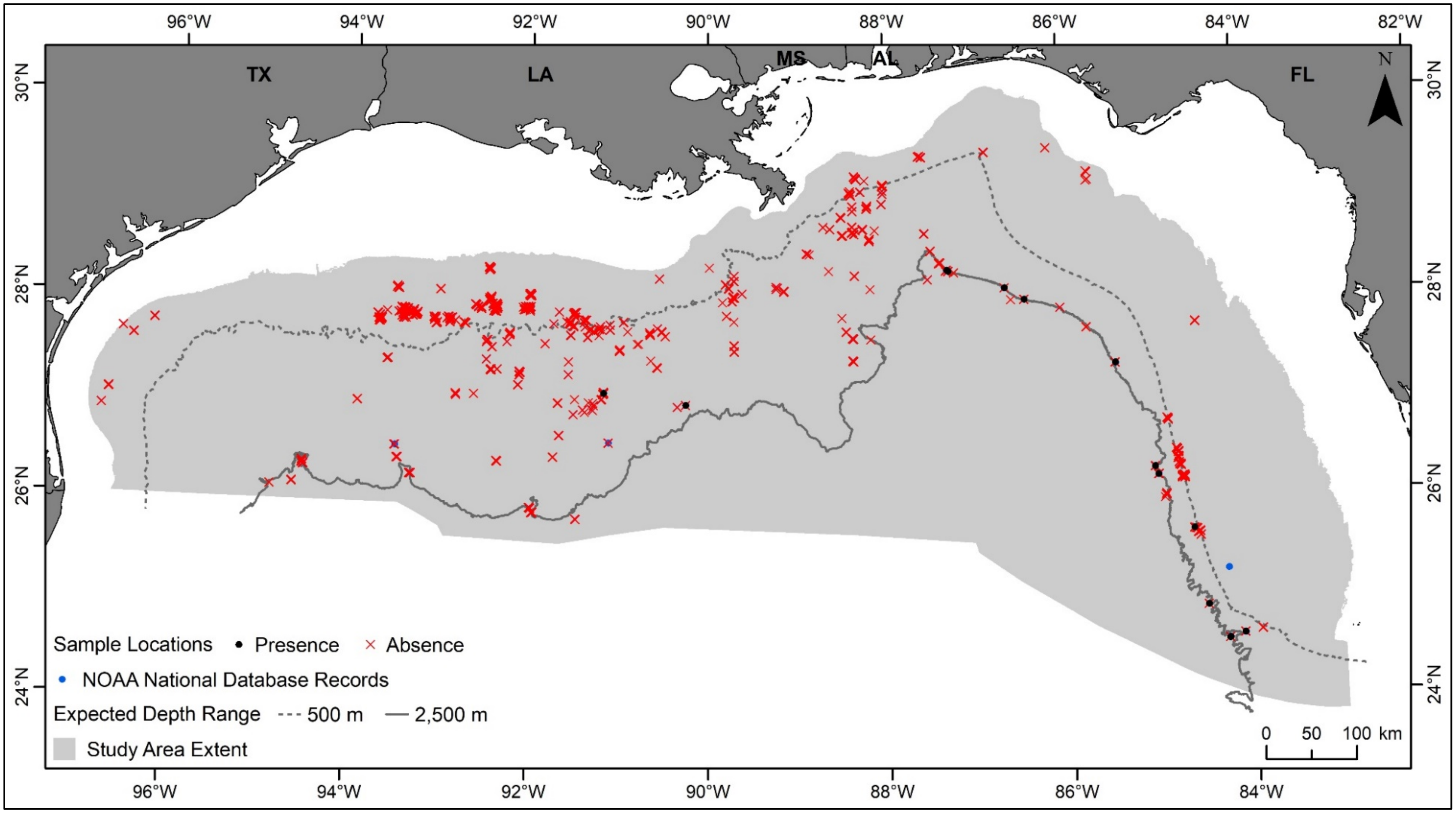

Figure 118. Occurrence records for the gorgonian coral family Coralliidae (order Alcyonacea).

This map shows the observed occurrence (presence-absence) of Coralliidae at sample locations in the presence-absence database compiled for this study. Additional records of occurrence in the NOAA National Database are also displayed. Gray lines denote the expected depth range for Coralliidae.

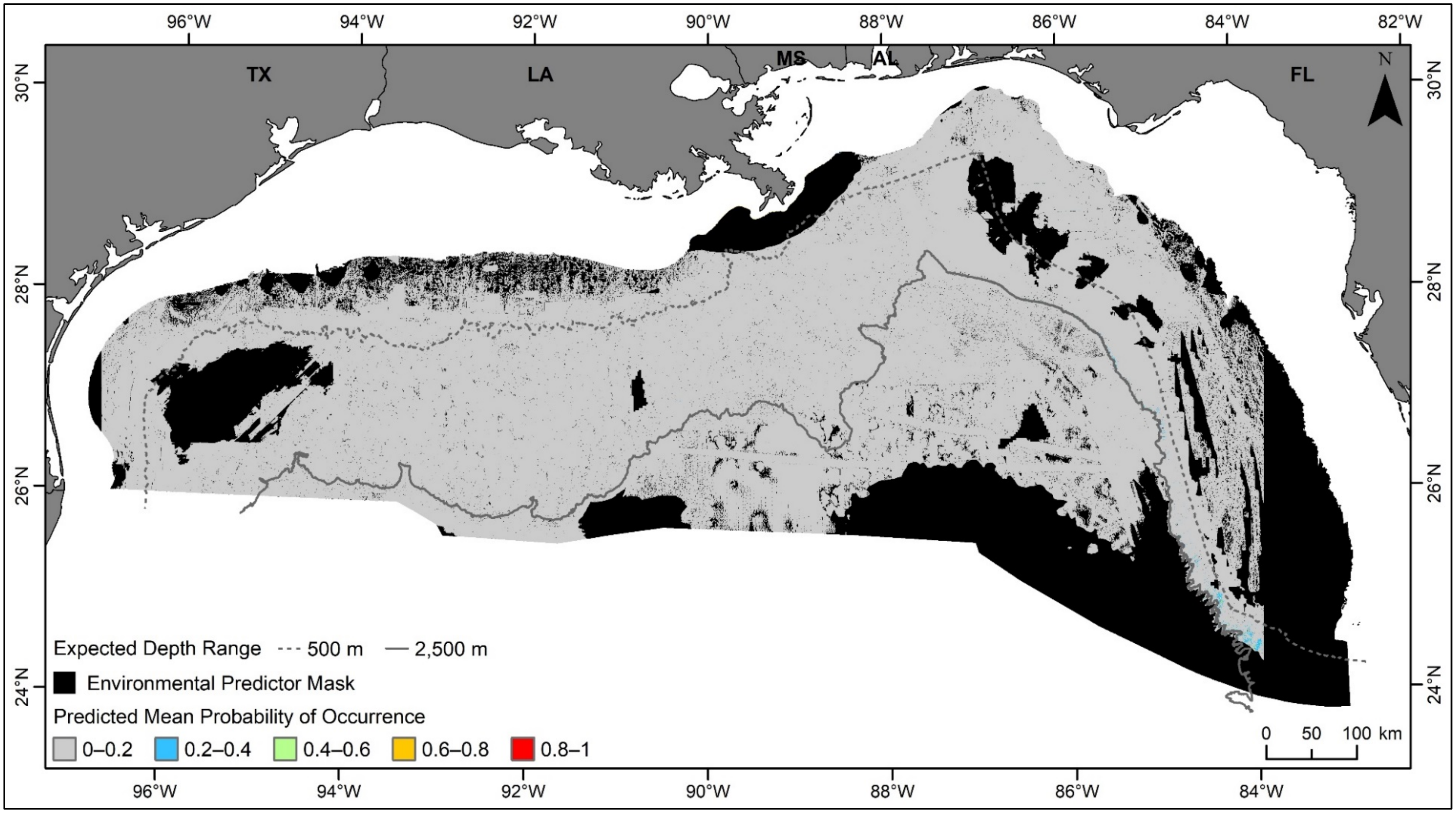

Figure 119. Predicted occurrence of the gorgonian coral family Coralliidae (order Alcyonacea).

This map shows the predicted mean probability of occurrence (i.e., the predicted posterior mean occupancy probability) for Coralliidae from the multi-family occupancy model of order Alcyonacea. The environmental predictor mask overlays areas where predictor values were outside the range of values at the sample locations and model predictions may be affected by extrapolation. Gray lines denote the expected depth range for Coralliidae.

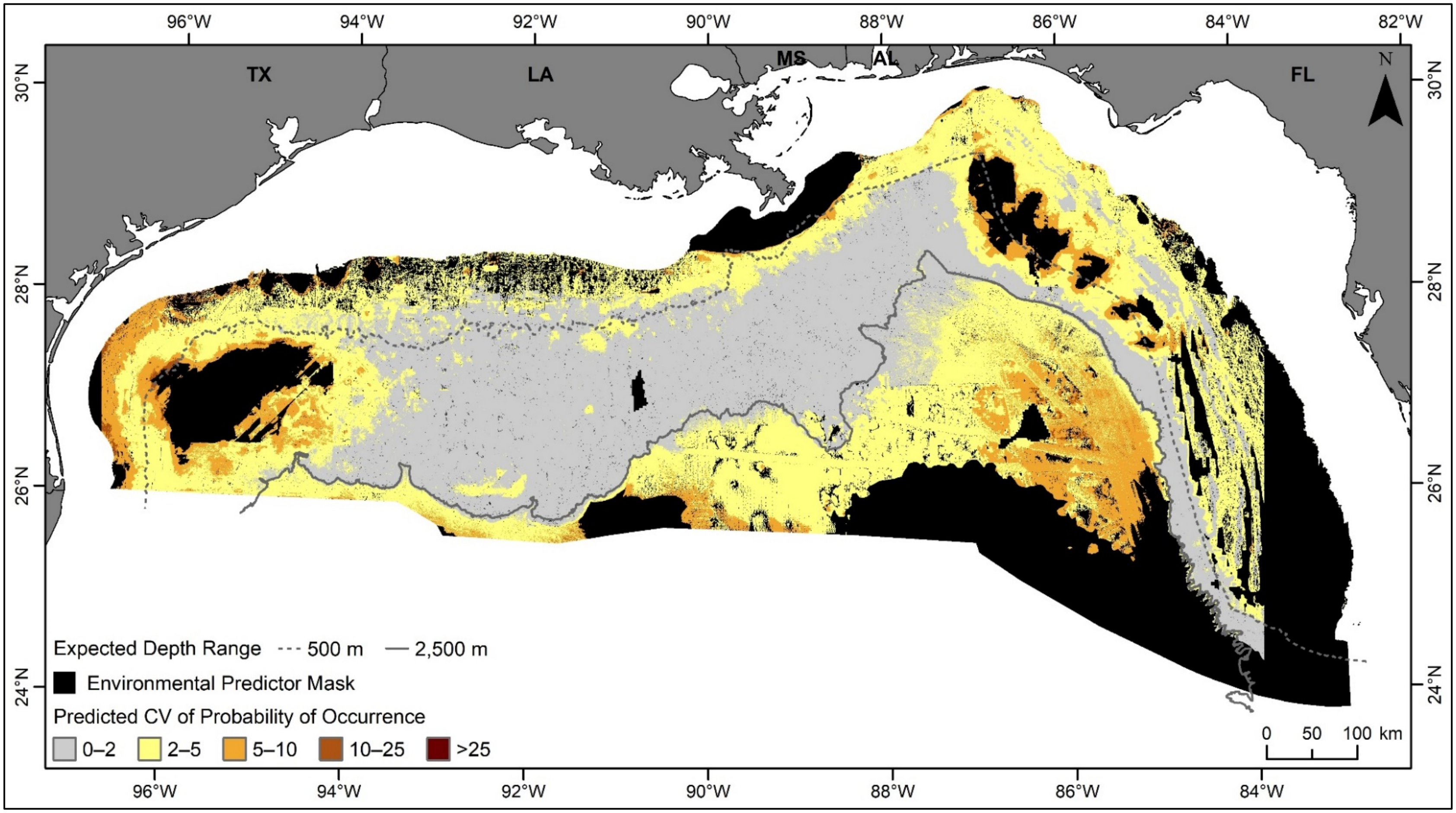

Figure 120. Variability in the predicted occurrence of the gorgonian coral family Coralliidae (order Alcyonacea).

This map shows the predicted coefficient of variation (CV) of the probability of occurrence (i.e., the predicted posterior CV of occupancy probability) for Coralliidae from the multi-family occupancy model of order Alcyonacea. The environmental predictor mask overlays areas where predictor values were outside the range of values at the sample locations and model predictions may be affected by extrapolation. Gray lines denote the expected depth range for Coralliidae.

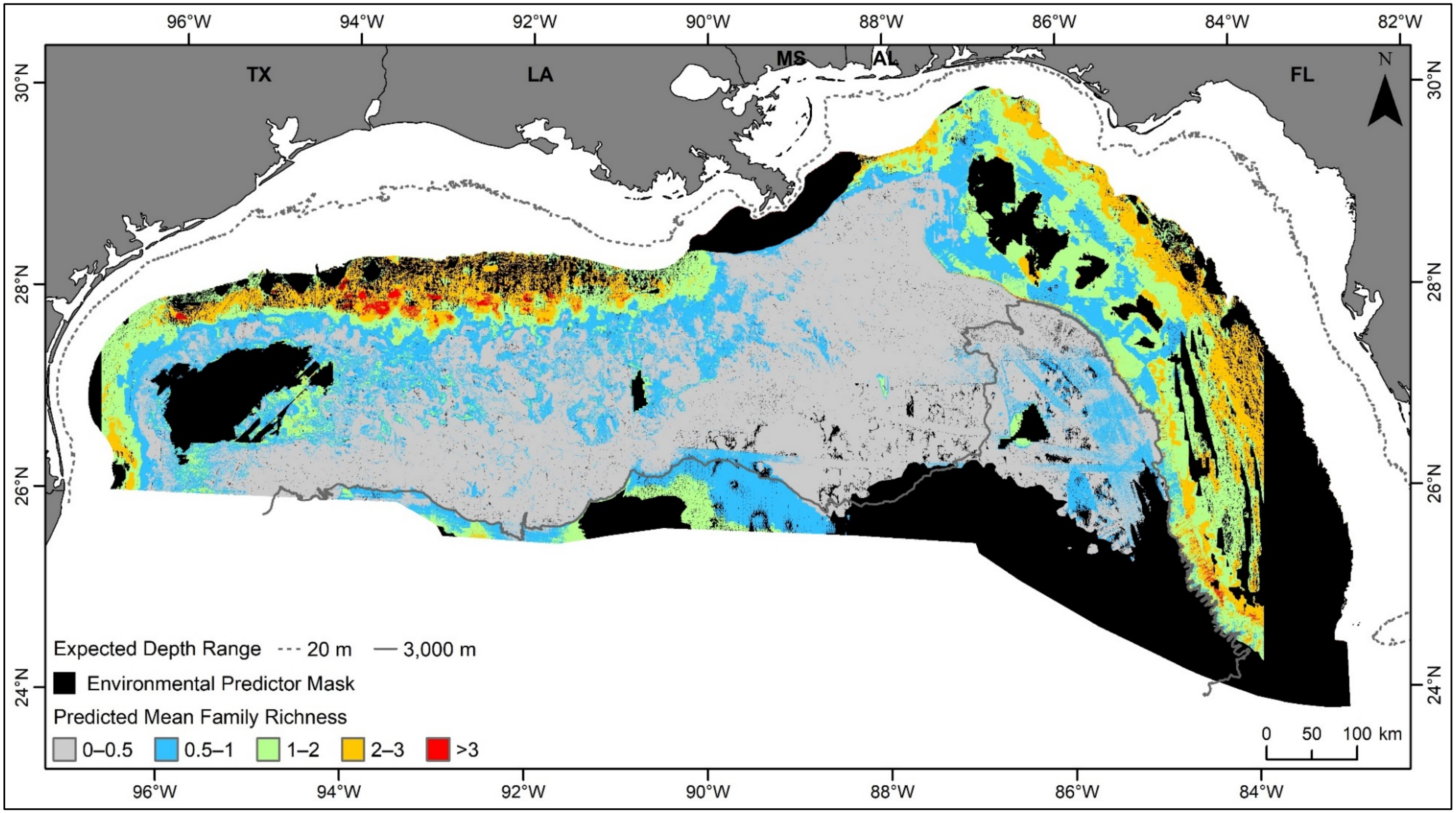

Figure 121. Predicted family richness of gorgonian corals (order Alcyonacea).

This map shows the predicted mean family richness (i.e., the posterior mean genus richness) from the multi-family occupancy model of order Alcyonacea. The environmental predictor mask overlays areas where predictor values were outside the range of values at the sample locations and model predictions may be affected by extrapolation. Gray lines denote the combined expected depth range for the families included in the model.

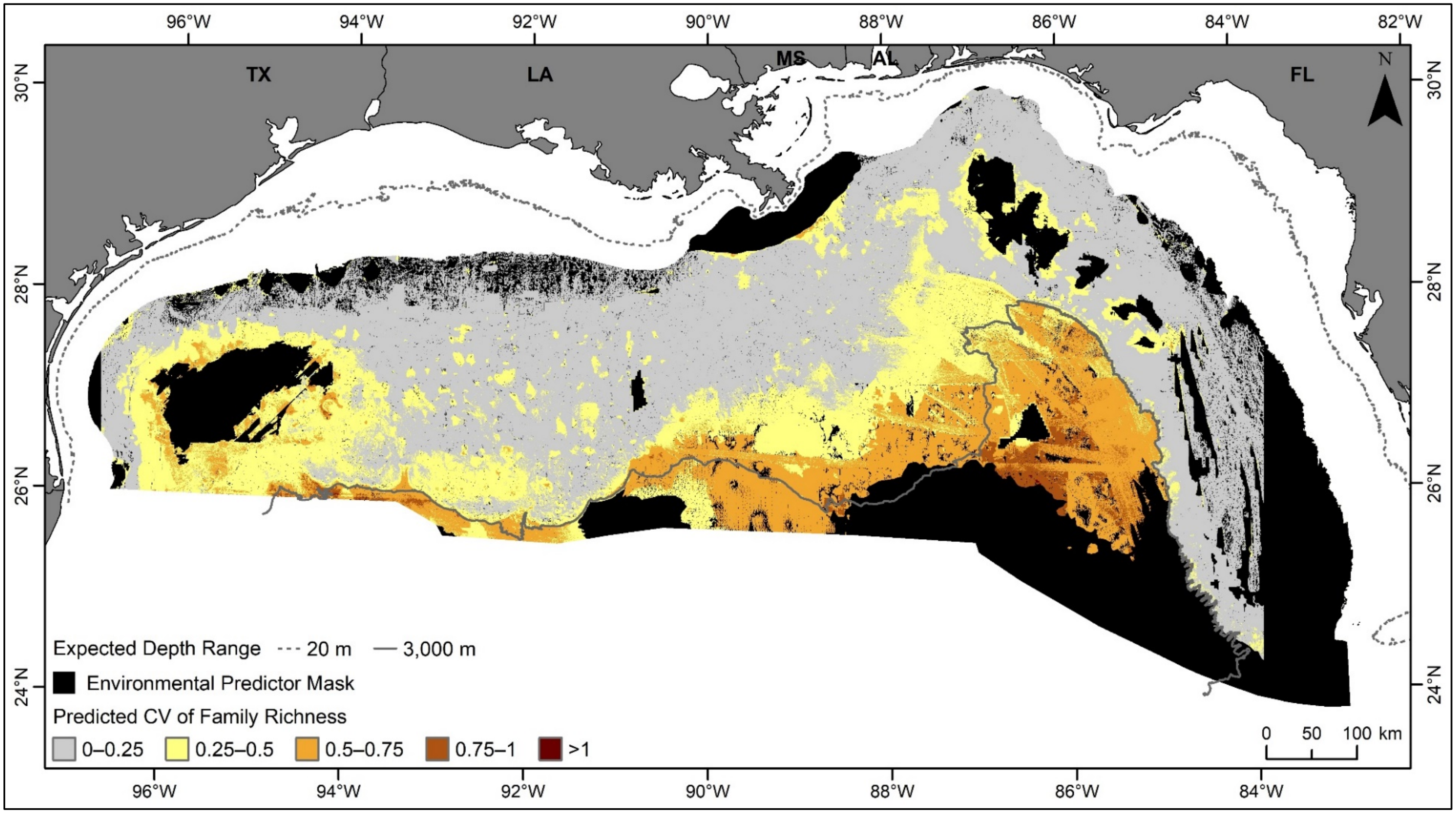

Figure 122. Variability in the predicted family richness of gorgonian corals (order Alcyonacea).

This map shows the predicted coefficient of variation of family richness (i.e., the posterior CV of genus richness) from the multi-family occupancy model of order Alcyonacea. The environmental predictor mask overlays areas where predictor values were outside the range of values at the sample locations and model predictions may be affected by extrapolation. Gray lines denote the combined expected depth range for the families included in the model.

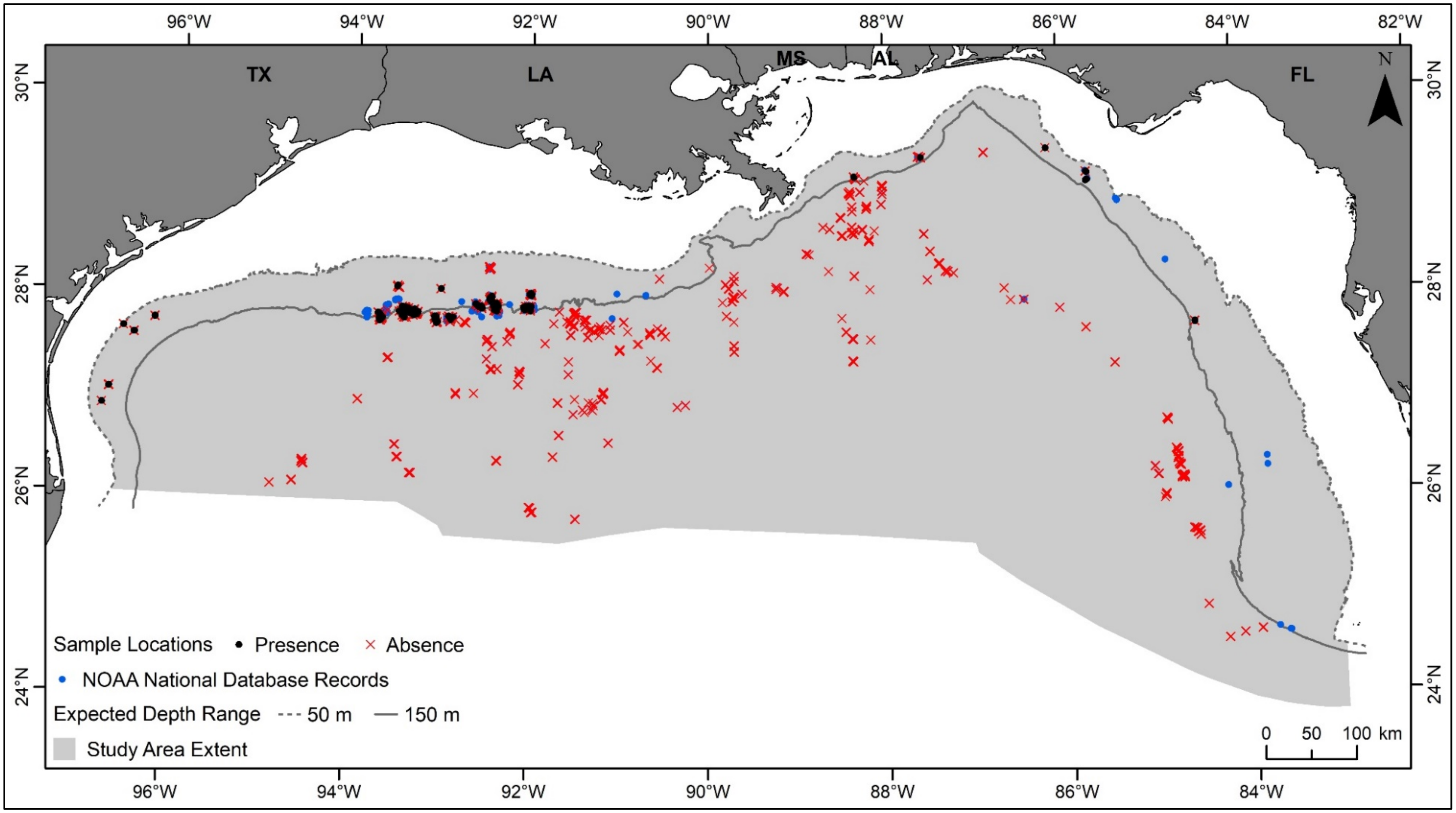

Figure 123. Occurrence records for the black coral *Tanacetipathes* (order Antipatharia).

This map shows the observed occurrence (presence-absence) of *Tanacetipathes* at sample locations in the presence-absence database compiled for this study. Additional records of occurrence in the NOAA National Database are also displayed. Gray lines denote the expected depth range for *Tanacetipathes*.

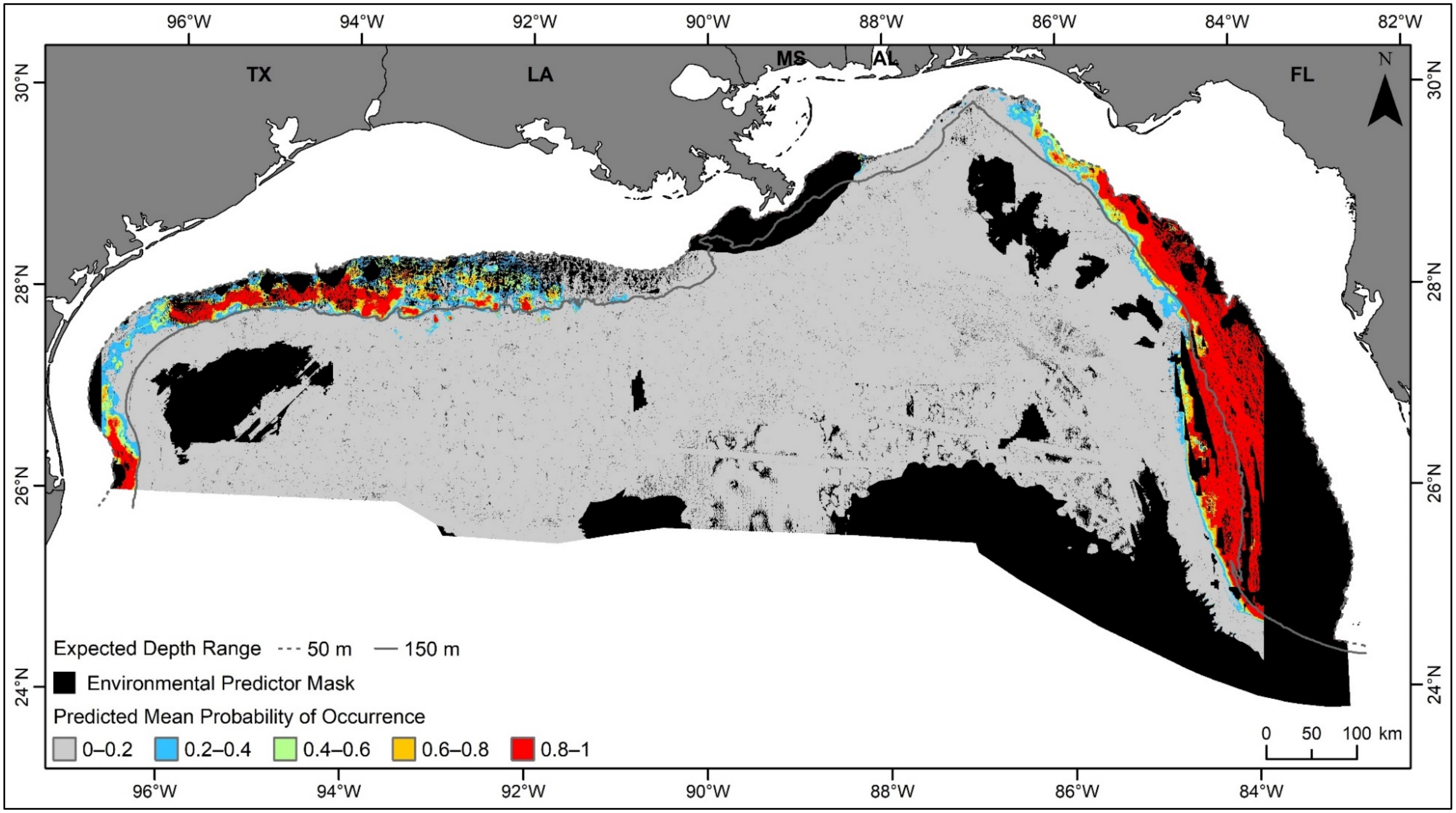

Figure 124. Predicted occurrence of the black coral *Tanacetipathes* (order Antipatharia).

This map shows the predicted mean probability of occurrence (i.e., the predicted posterior mean occupancy probability) for *Tanacetipathes* from the multi-genus occupancy model of order Antipatharia. The environmental predictor mask overlays areas where predictor values were outside the range of values at the sample locations and model predictions may be affected by extrapolation. Gray lines denote the expected depth range for *Tanacetipathes*.

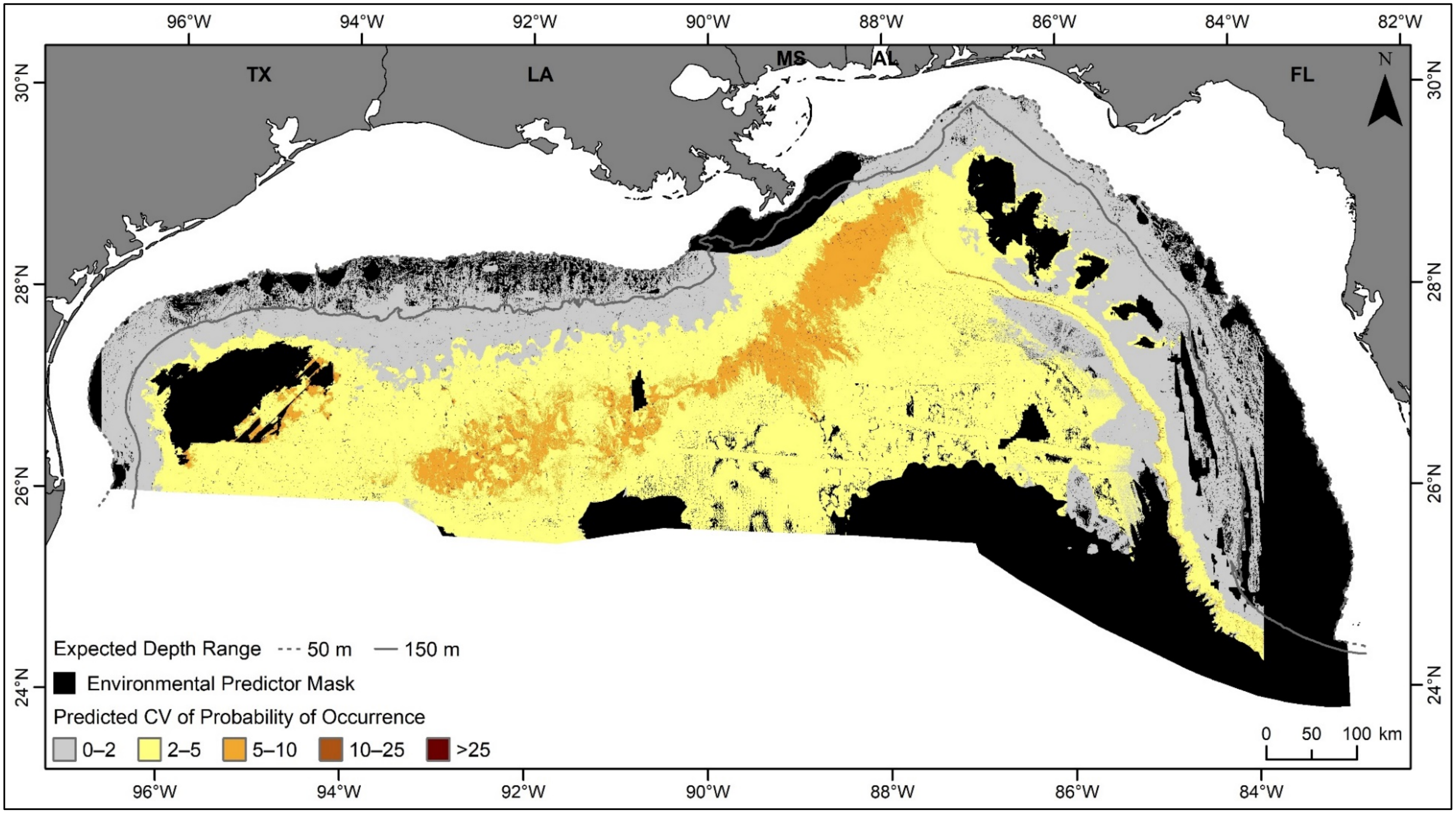

Figure 125. Variability in the predicted occurrence of the black coral *Tanacetipathes* (order Antipatharia).

This map shows the predicted coefficient of variation (CV) of the probability of occurrence (i.e., the predicted posterior CV of occupancy probability) for *Tanacetipathes* from the multi-genus occupancy model of order Antipatharia. The environmental predictor mask overlays areas where predictor values were outside the range of values at the sample locations and model predictions may be affected by extrapolation. Gray lines denote the expected depth range for *Tanacetipathes*.

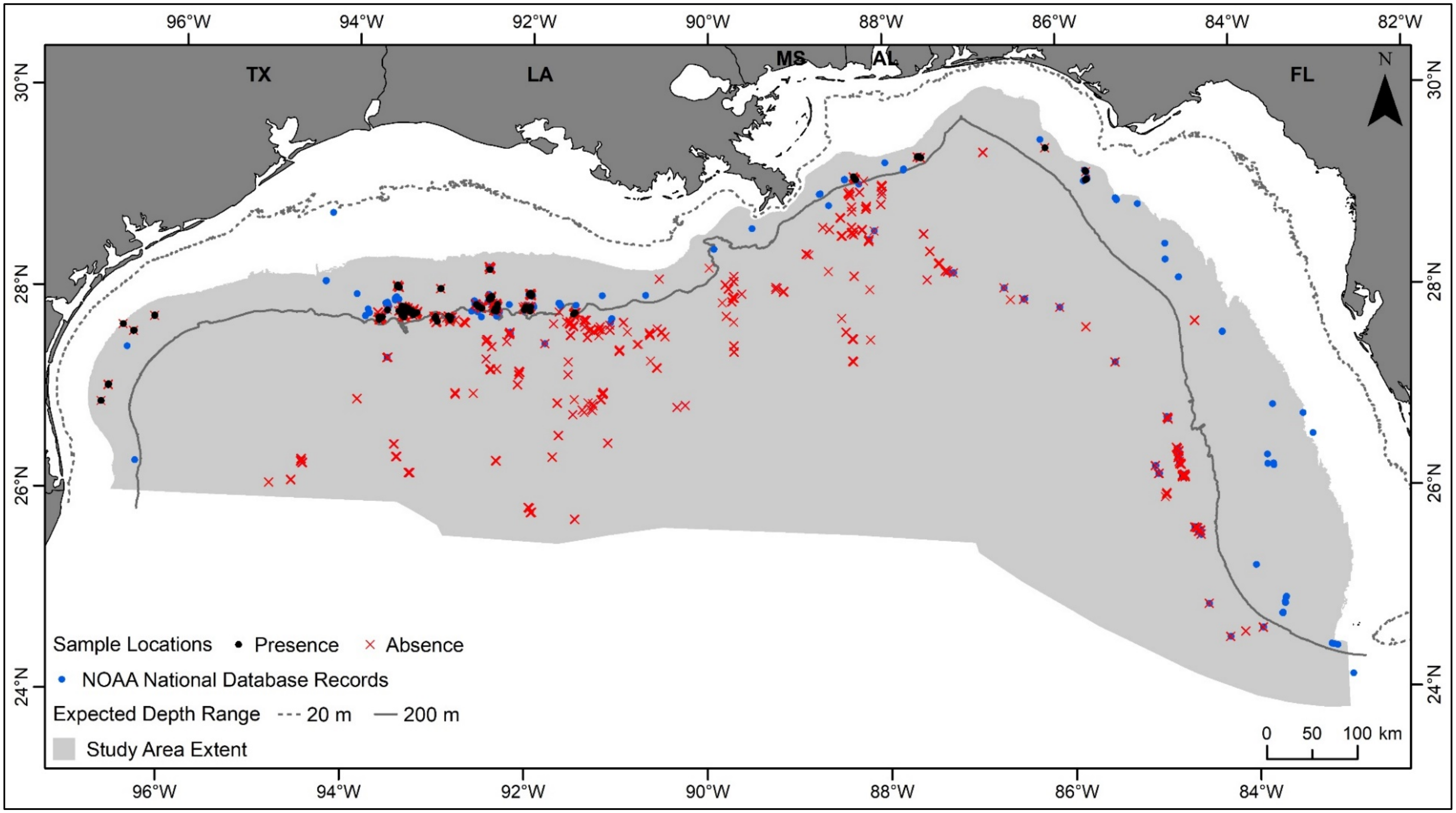

Figure 126. Occurrence records for the black coral *Stichopathes* (order Antipatharia).

This map shows the observed occurrence (presence-absence) of *Stichopathes* at sample locations in the presence-absence database compiled for this study. Additional records of occurrence in the NOAA National Database are also displayed. Gray lines denote the expected depth range for *Stichopathes*.

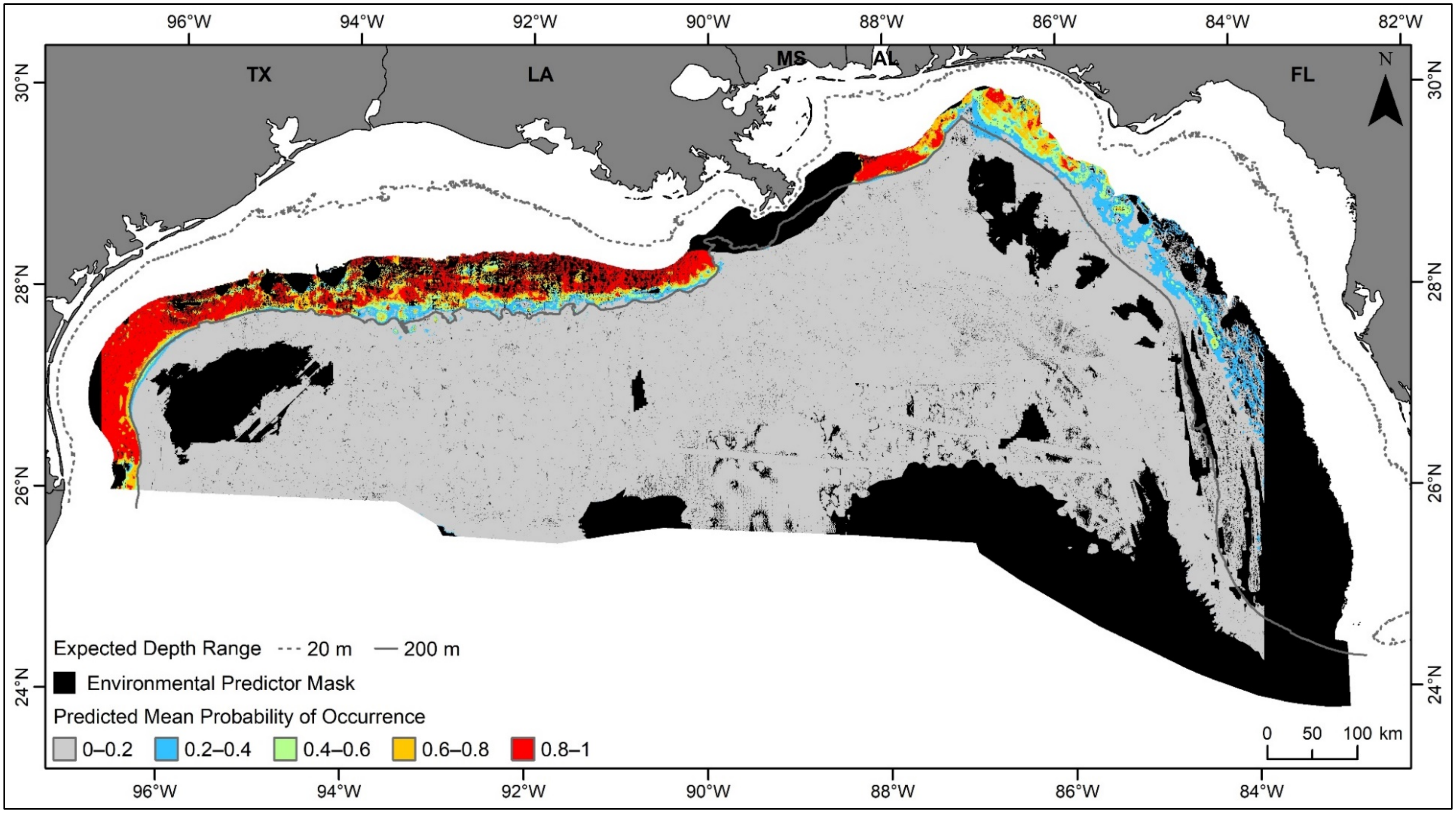

Figure 127. Predicted occurrence of the black coral *Stichopathes* (order Antipatharia).

This map shows the predicted mean probability of occurrence (i.e., the predicted posterior mean occupancy probability) for *Stichopathes* from the multi-genus occupancy model of order Antipatharia. The environmental predictor mask overlays areas where predictor values were outside the range of values at the sample locations and model predictions may be affected by extrapolation. Gray lines denote the expected depth range for *Stichopathes*.

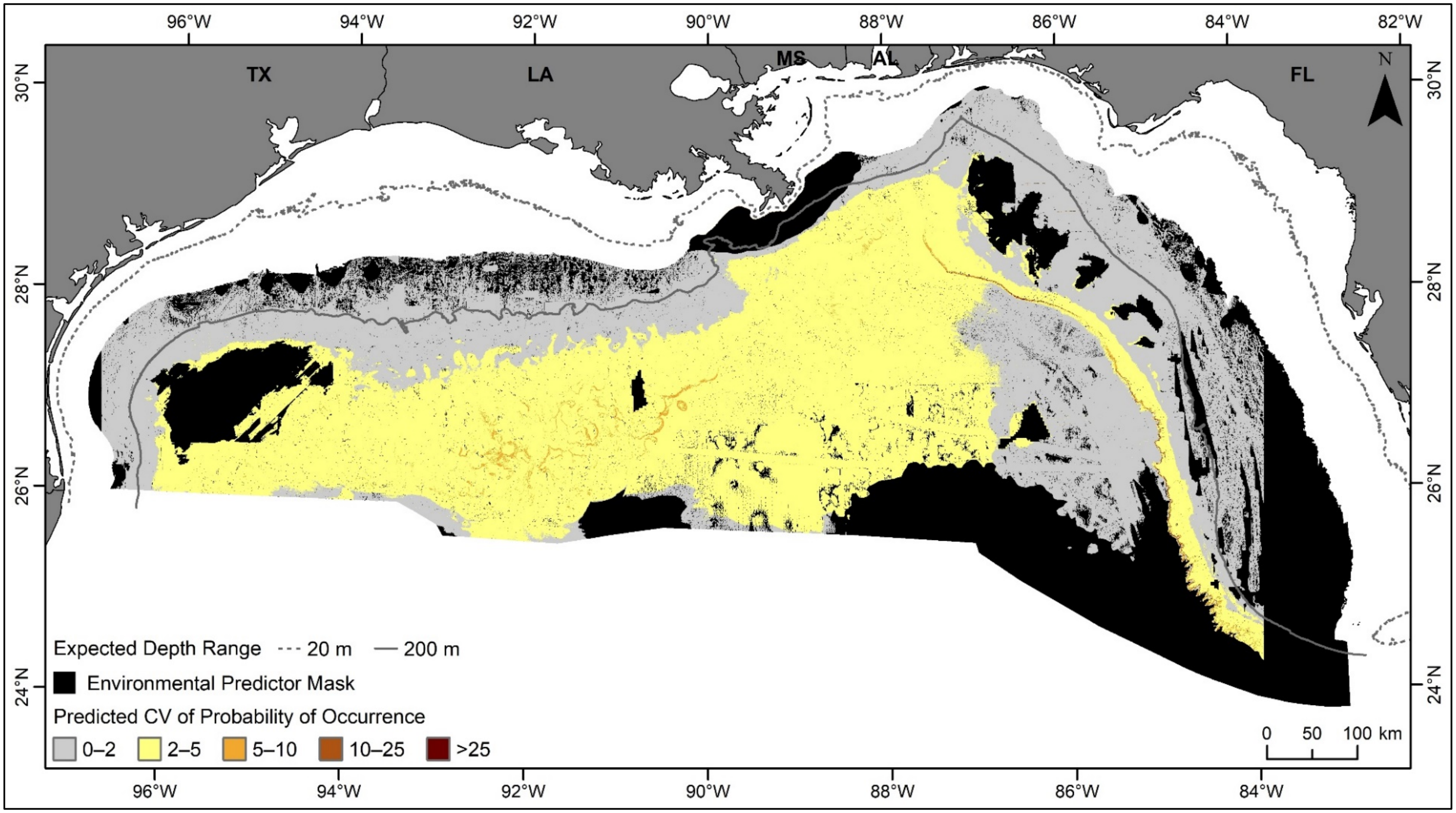

Figure 128. Variability in the predicted occurrence of the black coral *Stichopathes* (order Antipatharia).

This map shows the predicted coefficient of variation (CV) of the probability of occurrence (i.e., the predicted posterior CV of occupancy probability) for *Stichopathes* from the multi-genus occupancy model of order Antipatharia. The environmental predictor mask overlays areas where predictor values were outside the range of values at the sample locations and model predictions may be affected by extrapolation. Gray lines denote the expected depth range for *Stichopathes*.

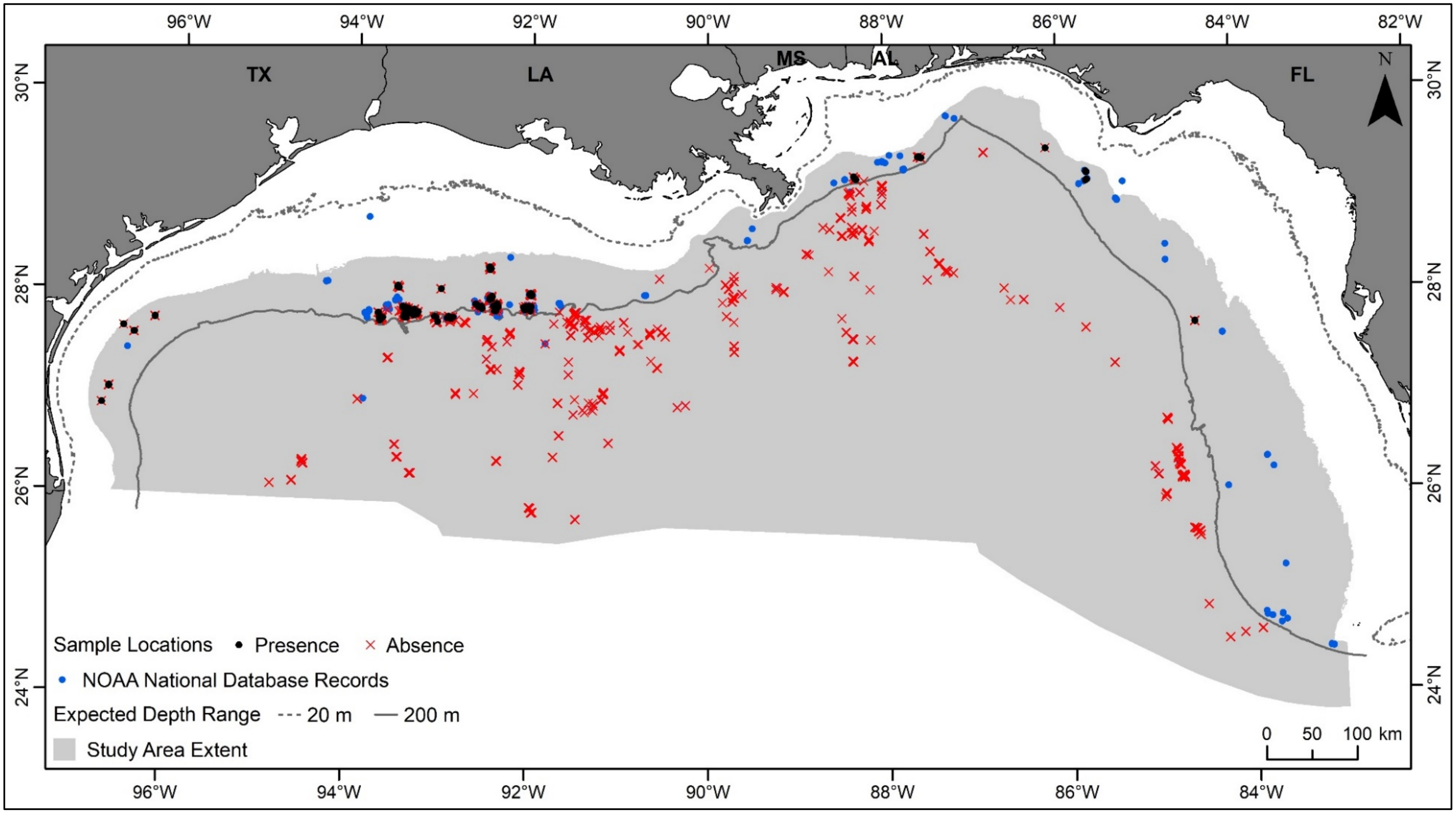

Figure 129. Occurrence records for the black coral *Antipathes* (order Antipatharia).

This map shows the observed occurrence (presence-absence) of *Antipathes* at sample locations in the presence-absence database compiled for this study. Additional records of occurrence in the NOAA National Database are also displayed. Gray lines denote the expected depth range for *Antipathes*.

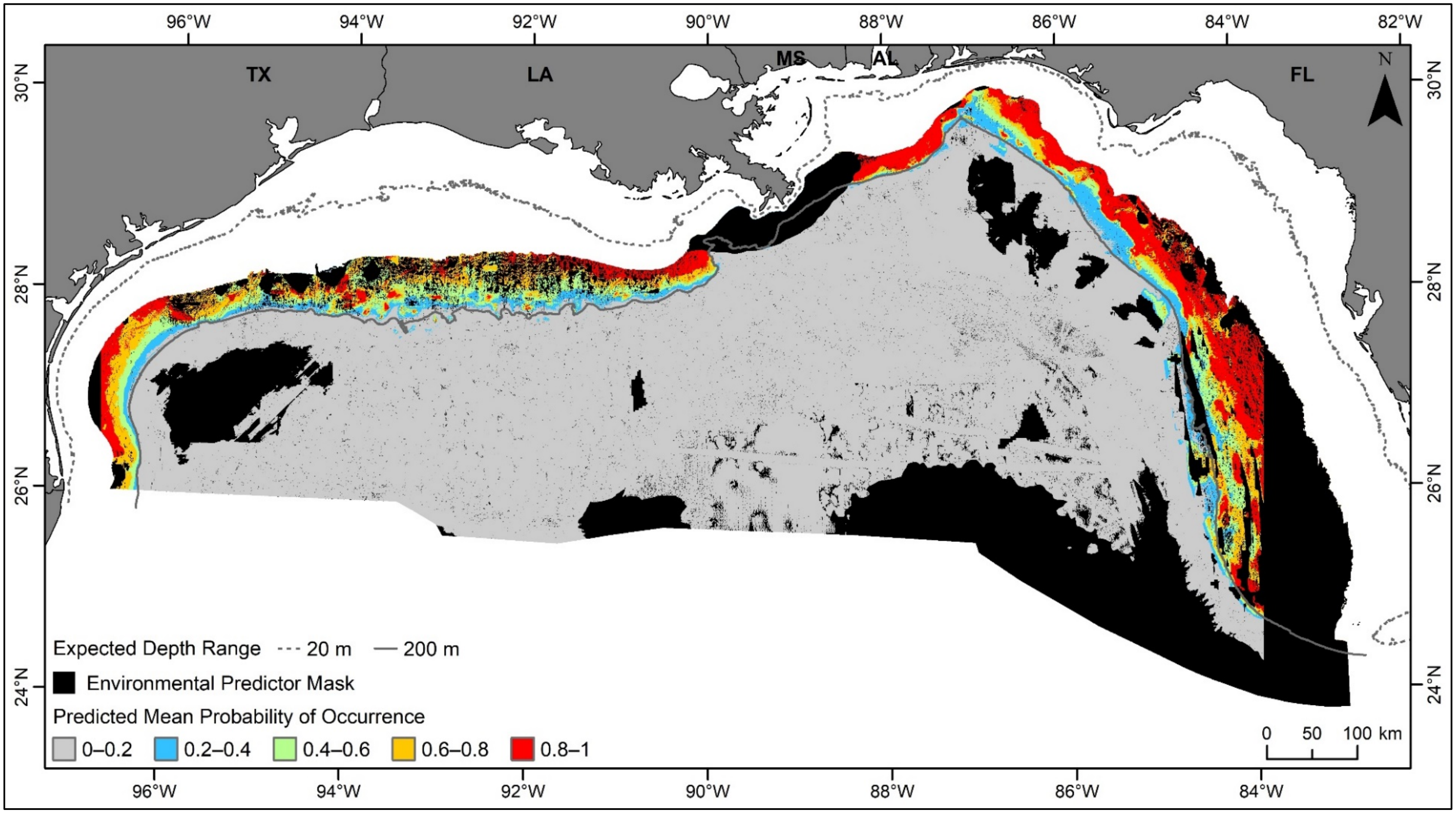

Figure 130. Predicted occurrence of the black coral *Antipathes* (order Antipatharia).

This map shows the predicted mean probability of occurrence (i.e., the predicted posterior mean occupancy probability) for *Antipathes* from the multi-genus occupancy model of order Antipatharia. The environmental predictor mask overlays areas where predictor values were outside the range of values at the sample locations and model predictions may be affected by extrapolation. Gray lines denote the expected depth range for *Antipathes*.

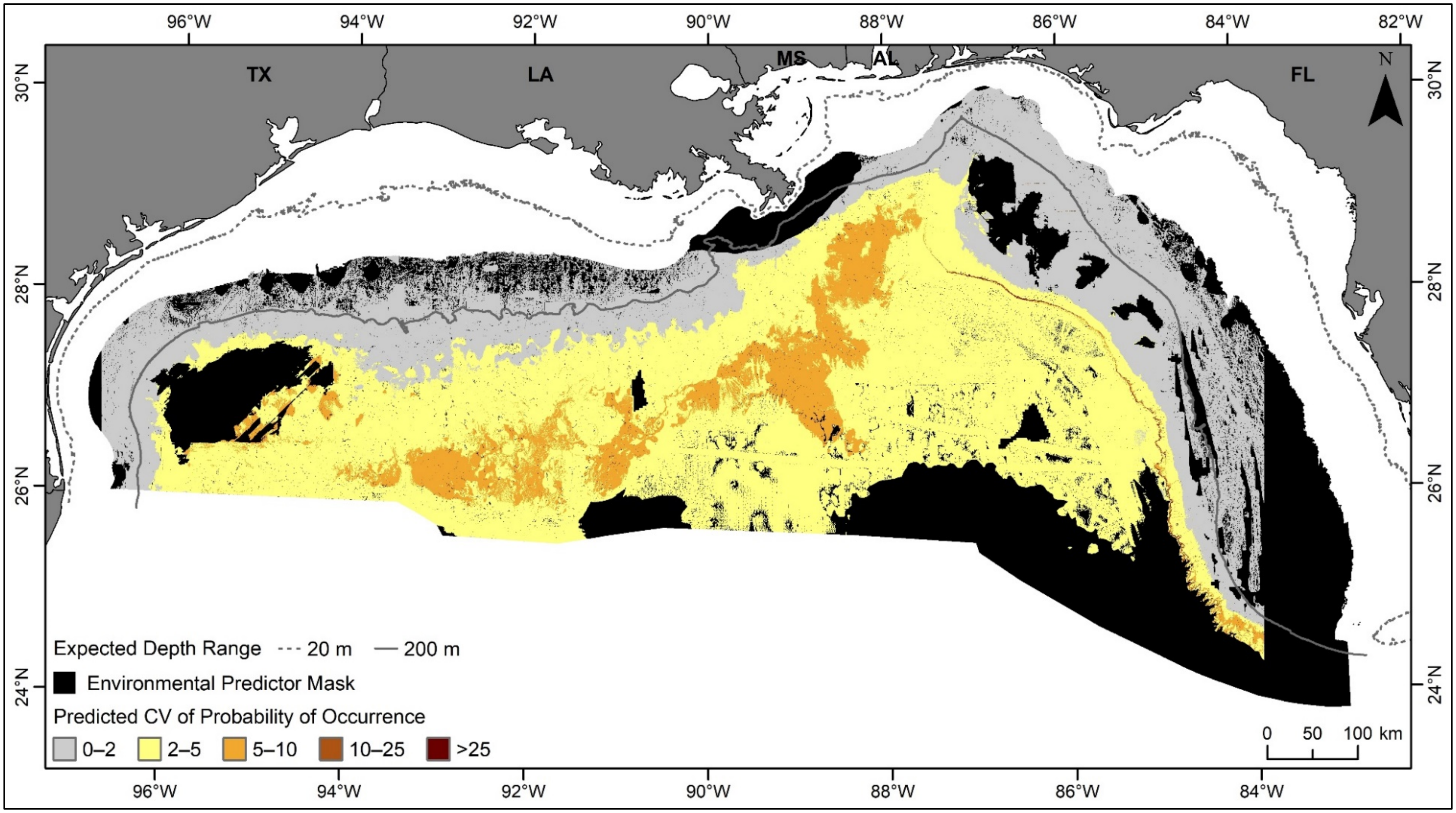

Figure 131. Variability in the predicted occurrence of the black coral *Antipathes* (order Antipatharia).

This map shows the predicted coefficient of variation (CV) of the probability of occurrence (i.e., the predicted posterior CV of occupancy probability) for *Antipathes* from the multi-genus occupancy model of order Antipatharia. The environmental predictor mask overlays areas where predictor values were outside the range of values at the sample locations and model predictions may be affected by extrapolation. Gray lines denote the expected depth range for *Antipathes*.

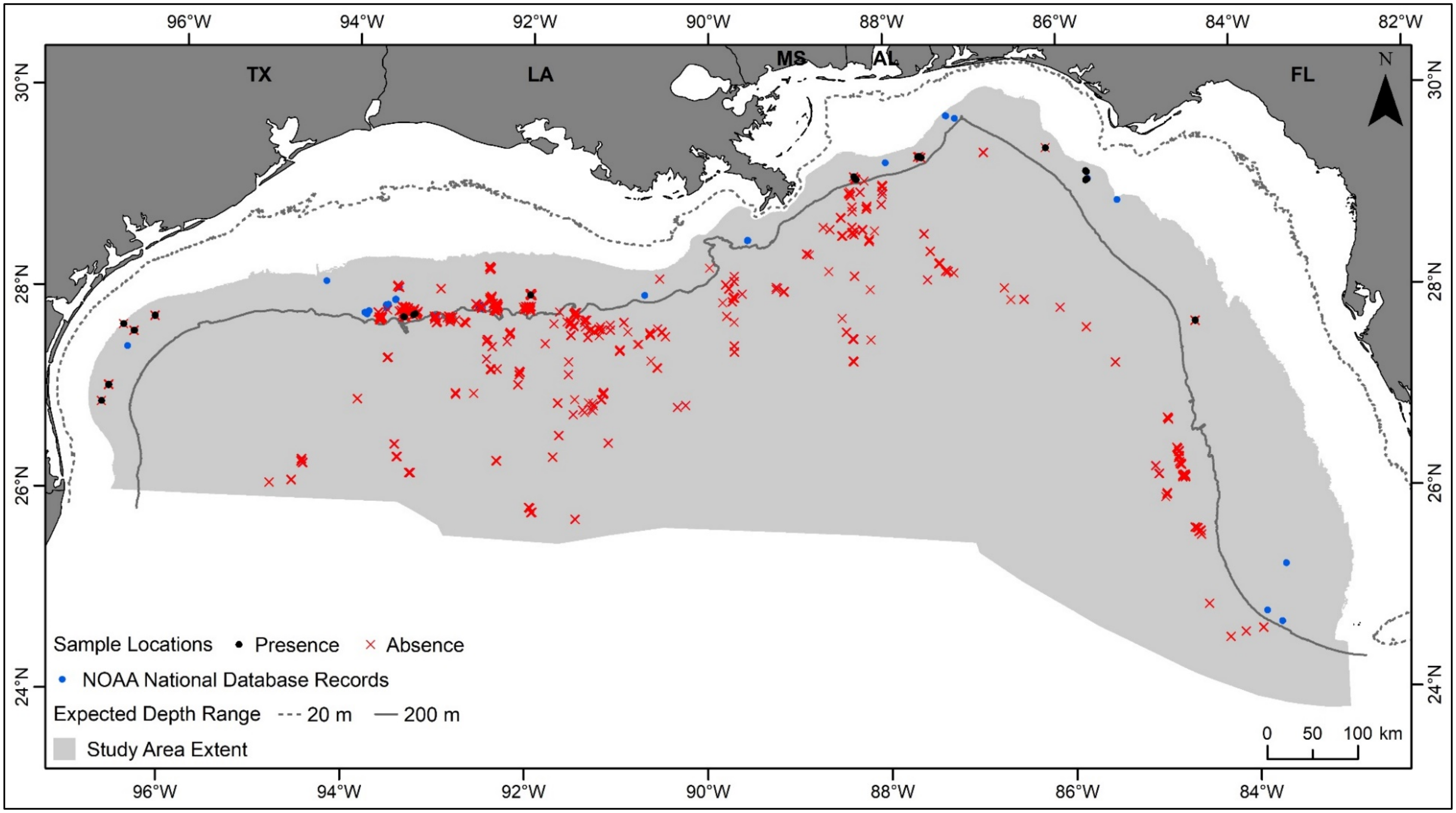

Figure 132. Occurrence records for the black coral *Antipathes atlantica* (order Antipatharia).

This map shows the observed occurrence (presence-absence) of *A. atlantica* at sample locations in the presence-absence database compiled for this study. Additional records of occurrence in the NOAA National Database are also displayed. Gray lines denote the expected depth range for *A. atlantica*.

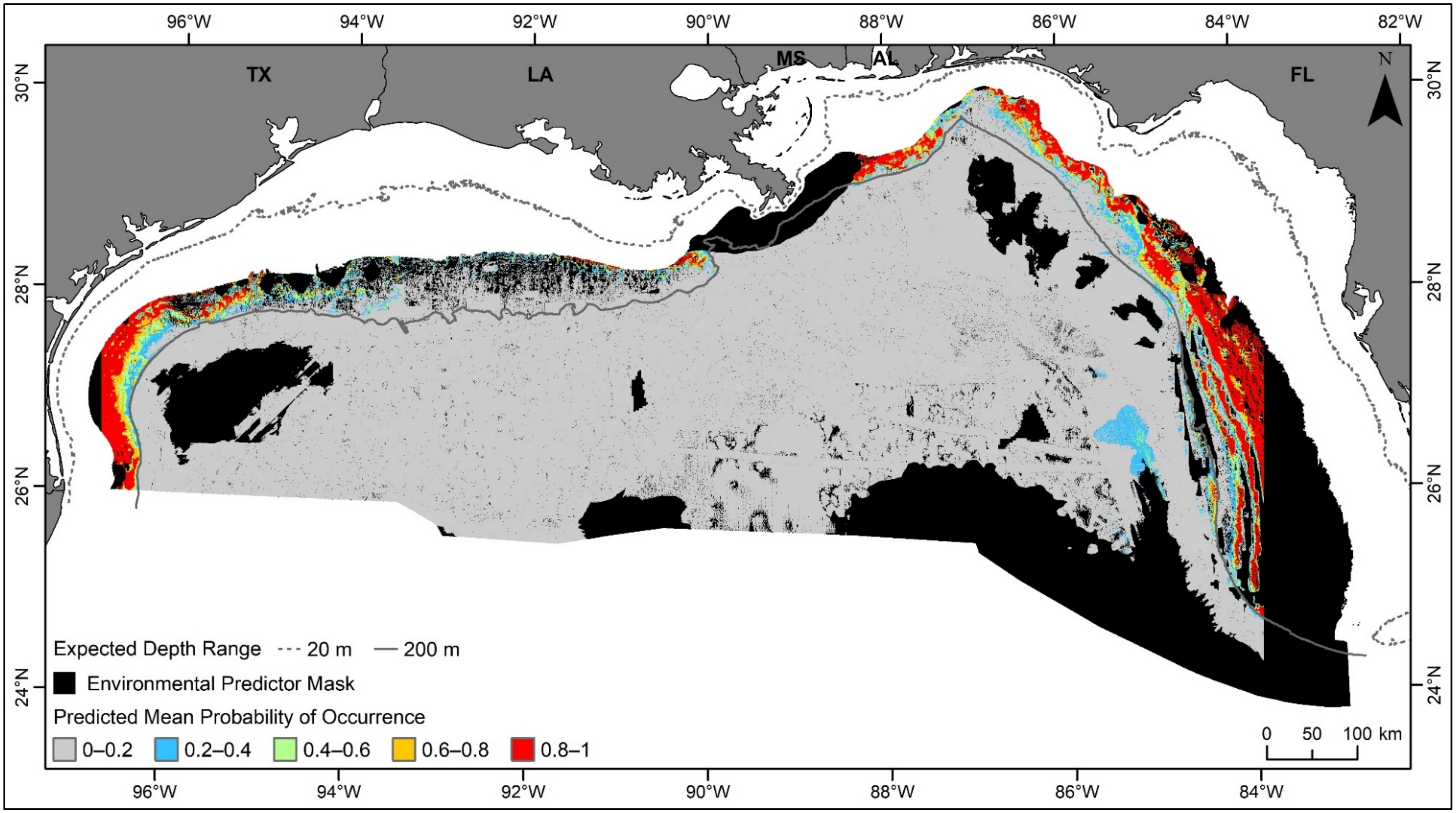

Figure 133. Predicted occurrence of the black coral *Antipathes atlantica* (order Antipatharia).

This map shows the predicted mean probability of occurrence (i.e., the predicted posterior mean occupancy probability) for *A. atlantica* from the single-taxon occupancy model. The environmental predictor mask overlays areas where predictor values were outside the range of values at the sample locations and model predictions may be affected by extrapolation. Gray lines denote the expected depth range for *A. atlantica*.

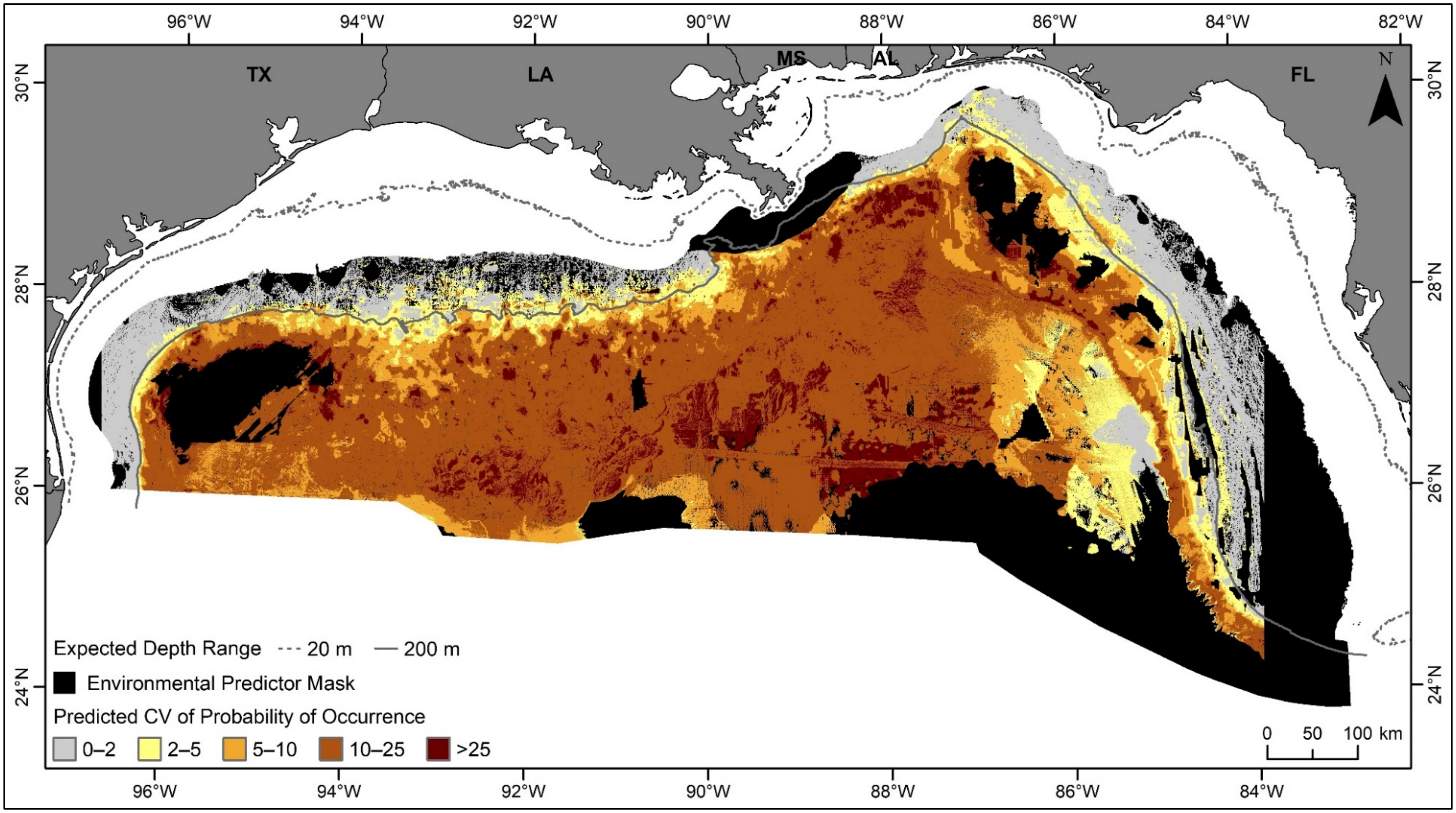

Figure 134. Variability in the predicted occurrence of the black coral *Antipathes atlantica* (order Antipatharia).

This map shows the predicted coefficient of variation (CV) of the probability of occurrence (i.e., the predicted posterior CV of occupancy probability) for *A. atlantica* from the single-taxon occupancy model. The environmental predictor mask overlays areas where predictor values were outside the range of values at the sample locations and model predictions may be affected by extrapolation. Gray lines denote the expected depth range for *A. atlantica*.

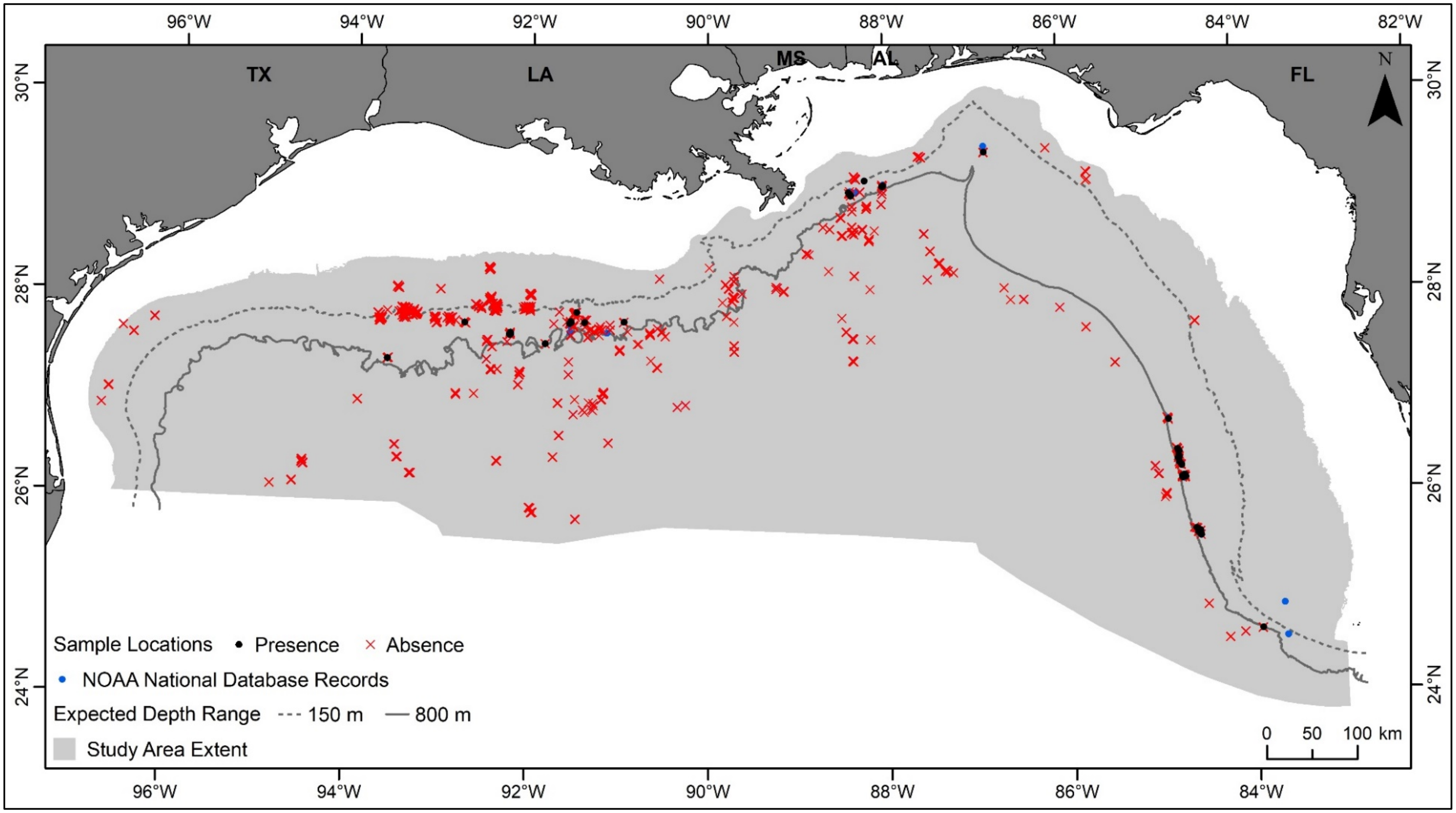

Figure 135. Occurrence records for the black coral *Leiopathes* (order Antipatharia).

This map shows the observed occurrence (presence-absence) of *Leiopathes* at sample locations in the presence-absence database compiled for this study. Additional records of occurrence in the NOAA National Database are also displayed. Gray lines denote the expected depth range for *Leiopathes*.

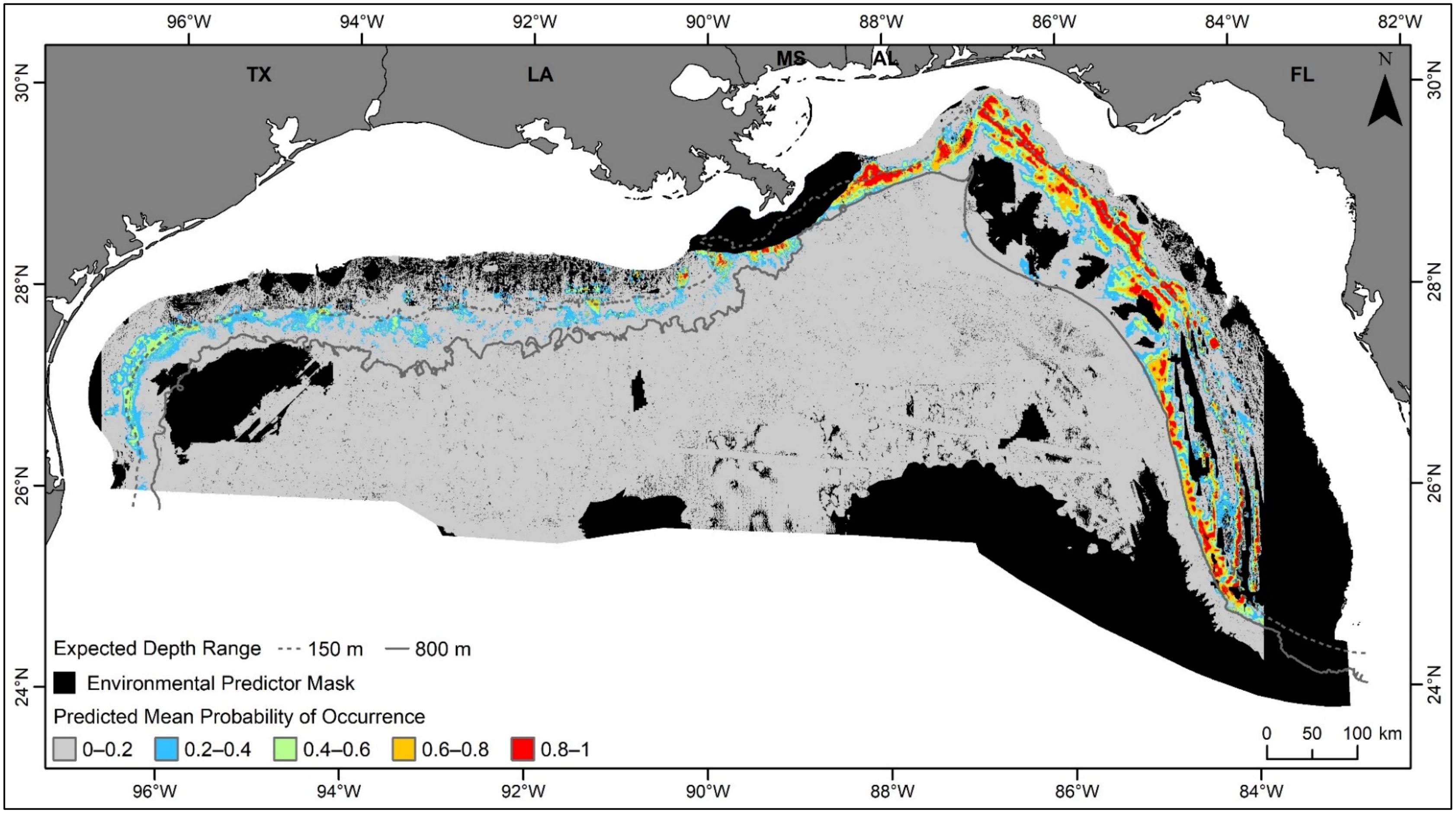

Figure 136. Predicted occurrence of the black coral *Leiopathes* (order Antipatharia).

This map shows the predicted mean probability of occurrence (i.e., the predicted posterior mean occupancy probability) for *Leiopathes* from the multi-genus occupancy model of order Antipatharia. The environmental predictor mask overlays areas where predictor values were outside the range of values at the sample locations and model predictions may be affected by extrapolation. Gray lines denote the expected depth range for *Leiopathes*.

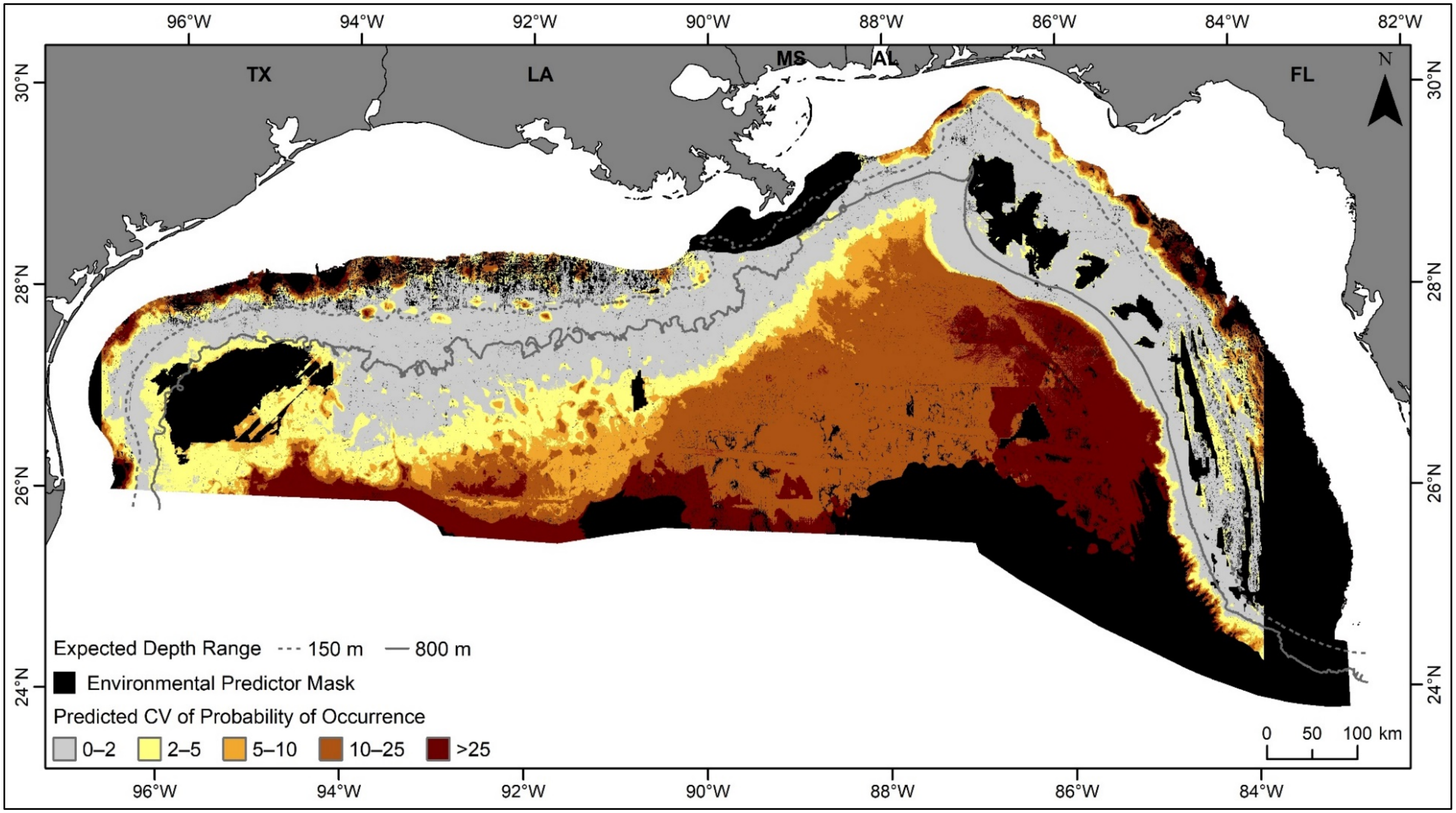

Figure 137. Variability in the predicted occurrence of the black coral *Leiopathes* (order Antipatharia).

This map shows the predicted coefficient of variation (CV) of the probability of occurrence (i.e., the predicted posterior CV of occupancy probability) for *Leiopathes* from the multi-genus occupancy model of order Antipatharia. The environmental predictor mask overlays areas where predictor values were outside the range of values at the sample locations and model predictions may be affected by extrapolation. Gray lines denote the expected depth range for *Leiopathes*.

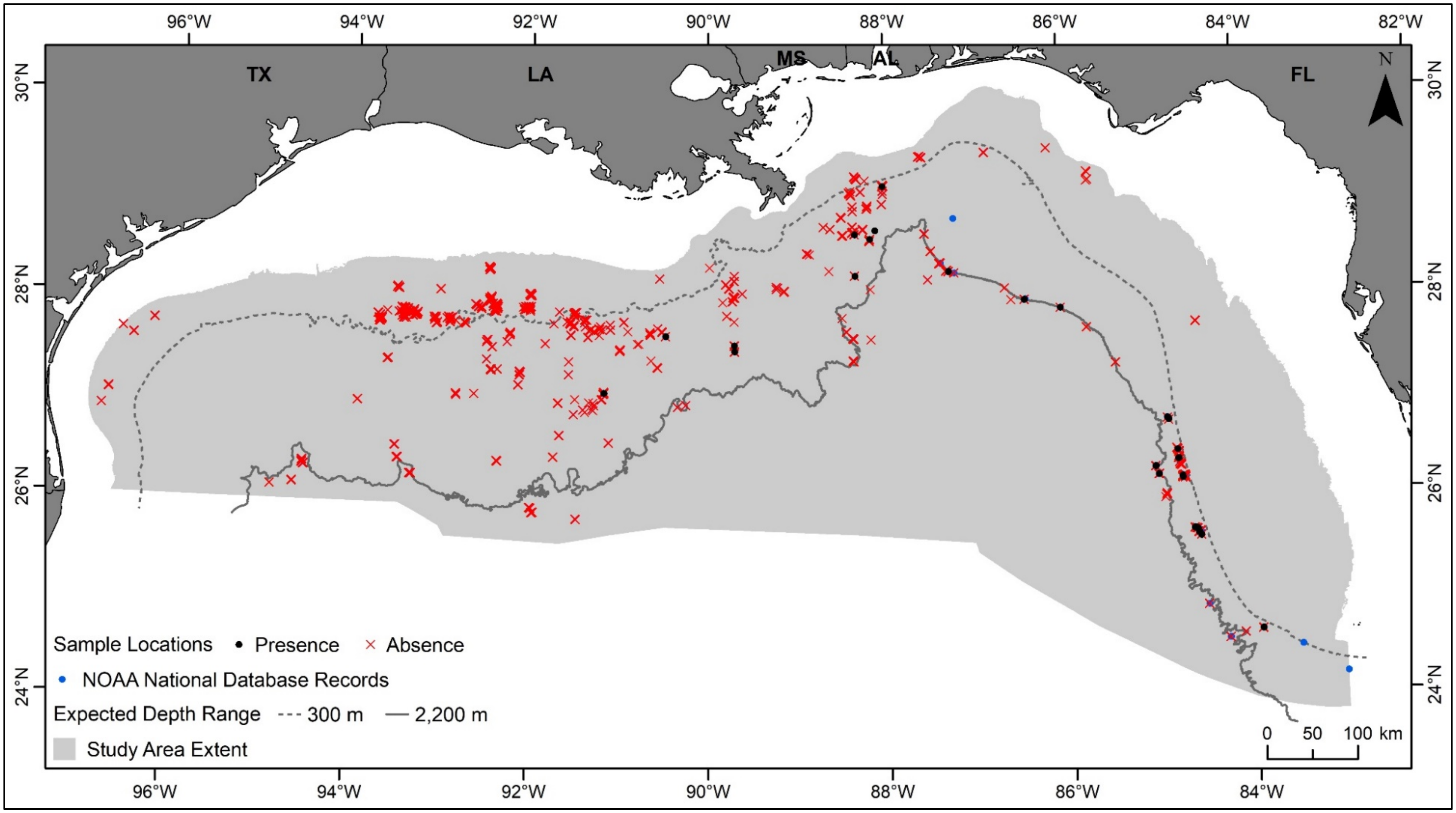

Figure 138. Occurrence records for the black coral *Bathypathes* (order Antipatharia).

This map shows the observed occurrence (presence-absence) of *Bathypathes* at sample locations in the presence-absence database compiled for this study. Additional records of occurrence in the NOAA National Database are also displayed. Gray lines denote the expected depth range for *Bathypathes*.

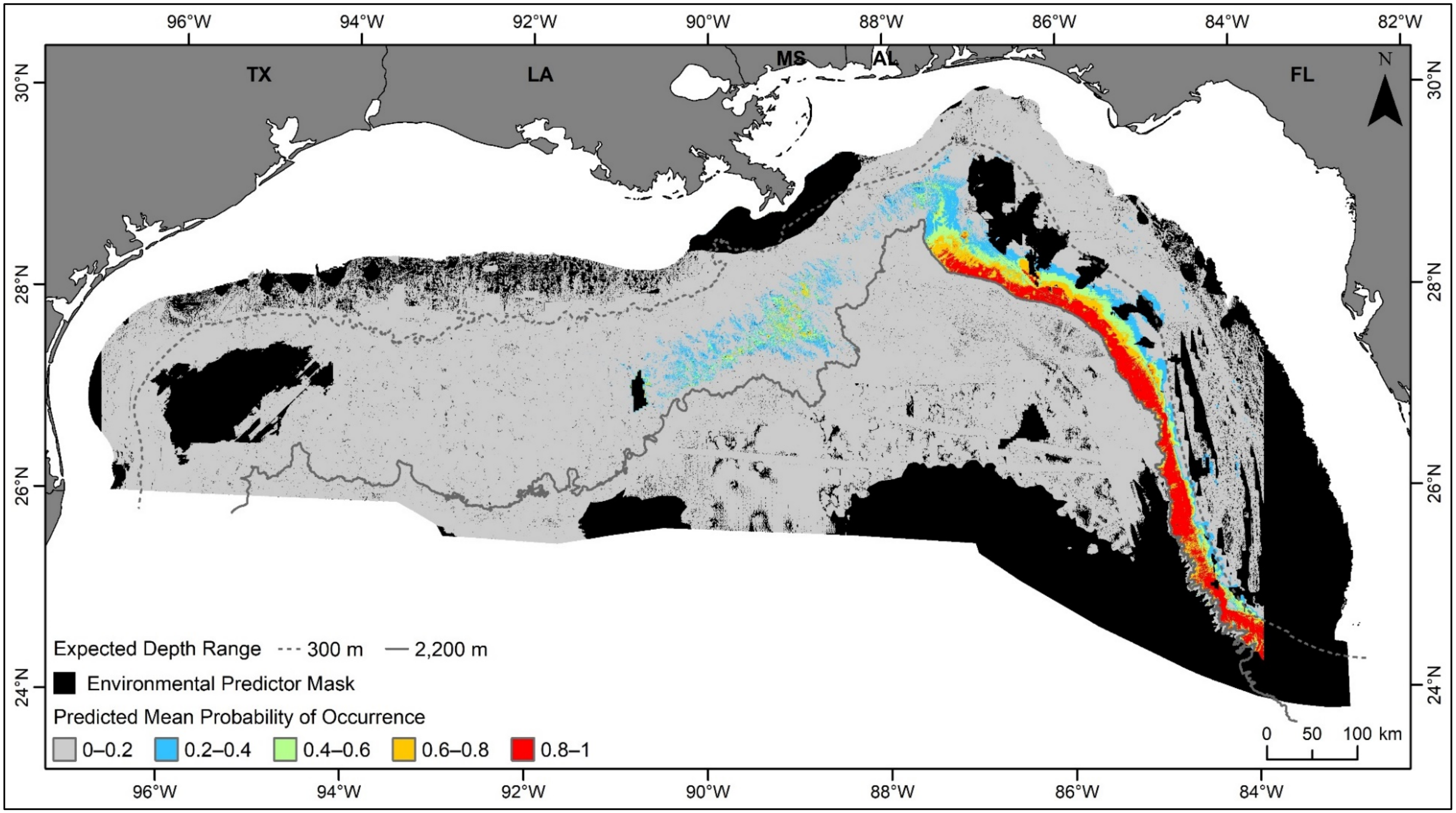

Figure 139. Predicted occurrence of the black coral *Bathypathes* (order Antipatharia).

This map shows the predicted mean probability of occurrence (i.e., the predicted posterior mean occupancy probability) for *Bathypathes* from the multi-genus occupancy model of order Antipatharia. The environmental predictor mask overlays areas where predictor values were outside the range of values at the sample locations and model predictions may be affected by extrapolation. Gray lines denote the expected depth range for *Bathypathes*.

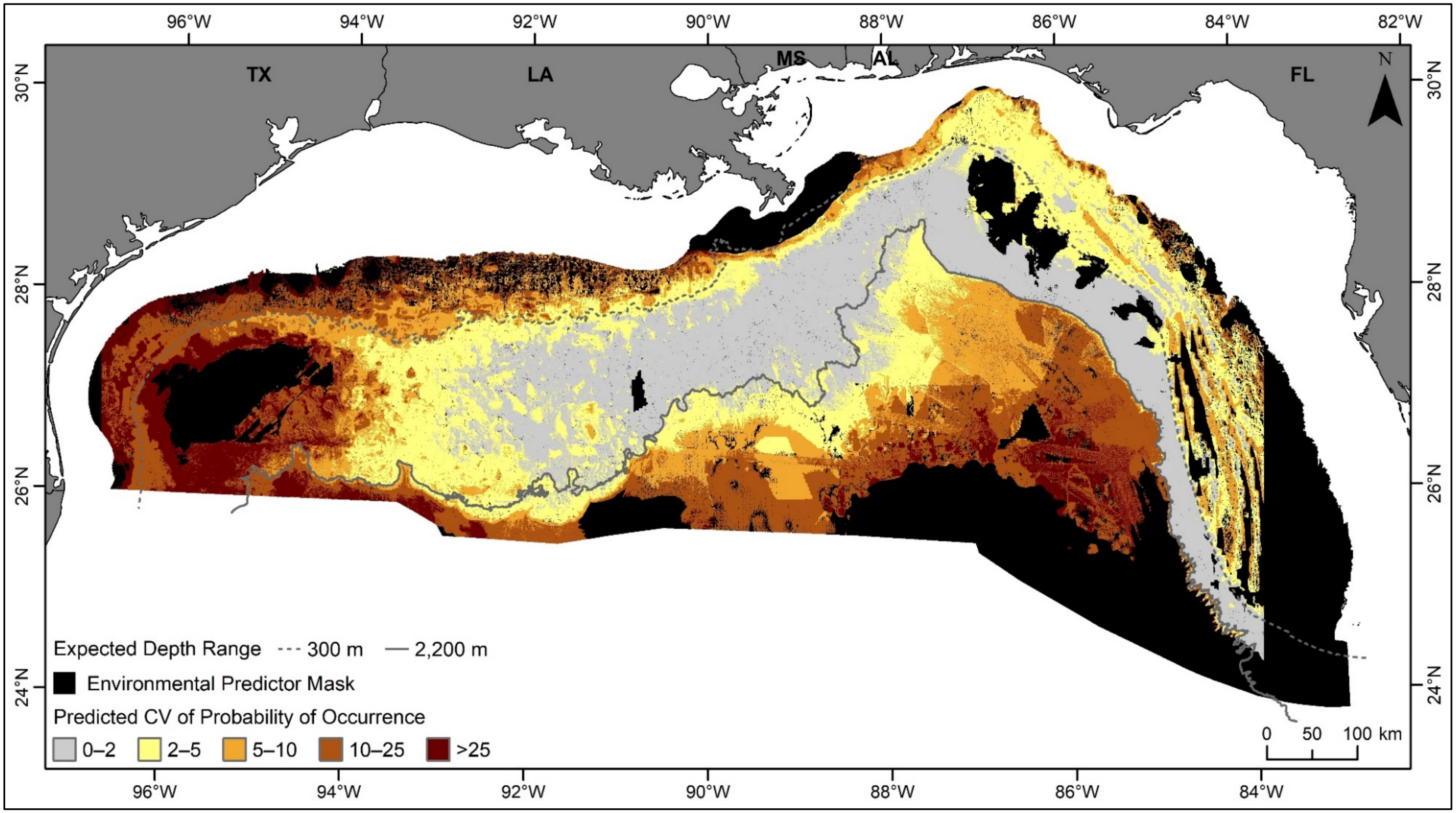

Figure 140. Variability in the predicted occurrence of the black coral *Bathypathes* (order Antipatharia).

This map shows the predicted coefficient of variation (CV) of the probability of occurrence (i.e., the predicted posterior CV of occupancy probability) for *Bathypathes* from the multi-genus occupancy model of order Antipatharia. The environmental predictor mask overlays areas where predictor values were outside the range of values at the sample locations and model predictions may be affected by extrapolation. Gray lines denote the expected depth range for *Bathypathes*.

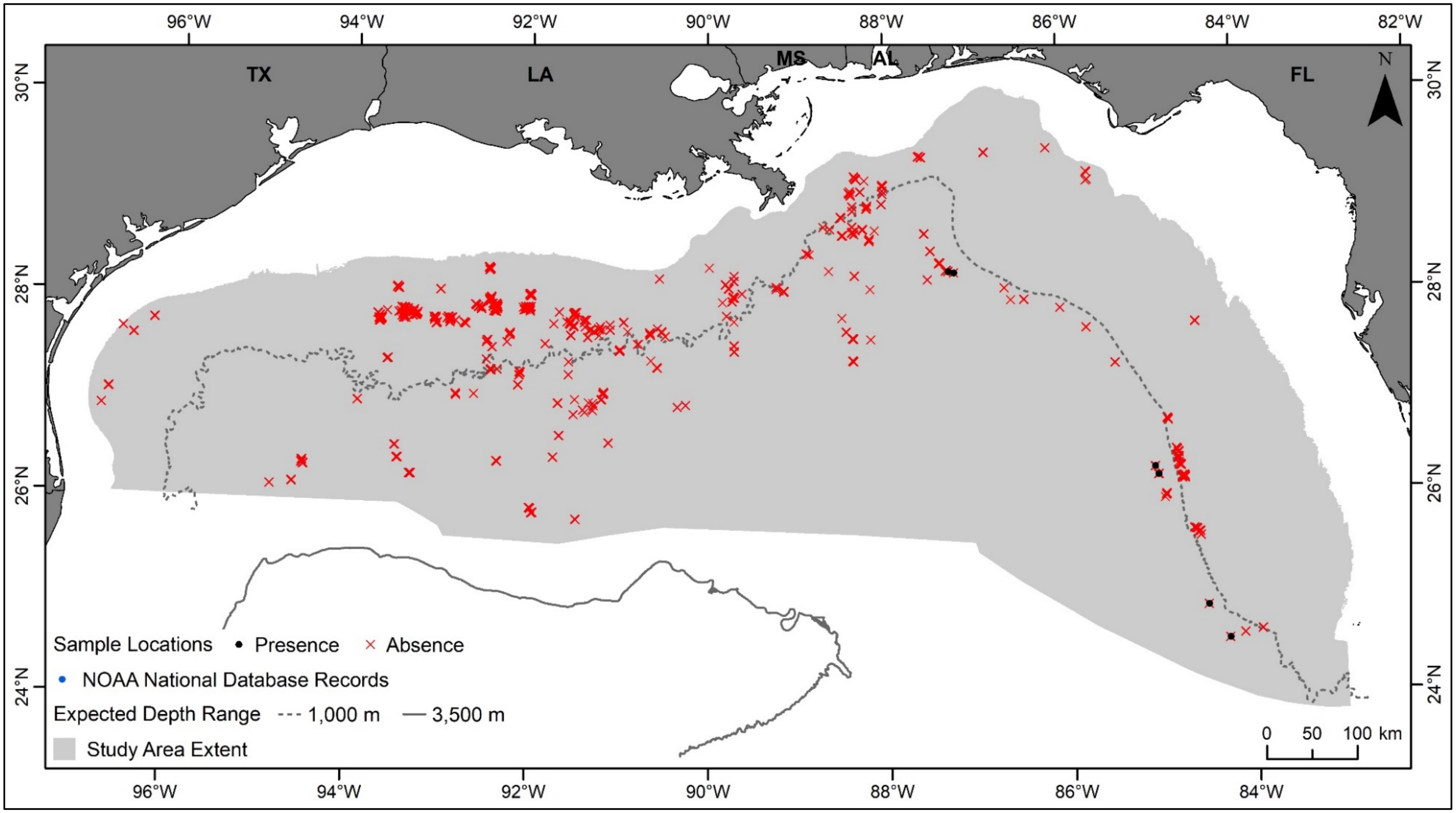

Figure 141. Occurrence records for the black coral *Stauropathes* (order Antipatharia).

This map shows the observed occurrence (presence-absence) of *Stauropathes* at sample locations in the presence-absence database compiled for this study. Additional records of occurrence in the NOAA National Database are also displayed. Gray lines denote the expected depth range for *Stauropathes*.

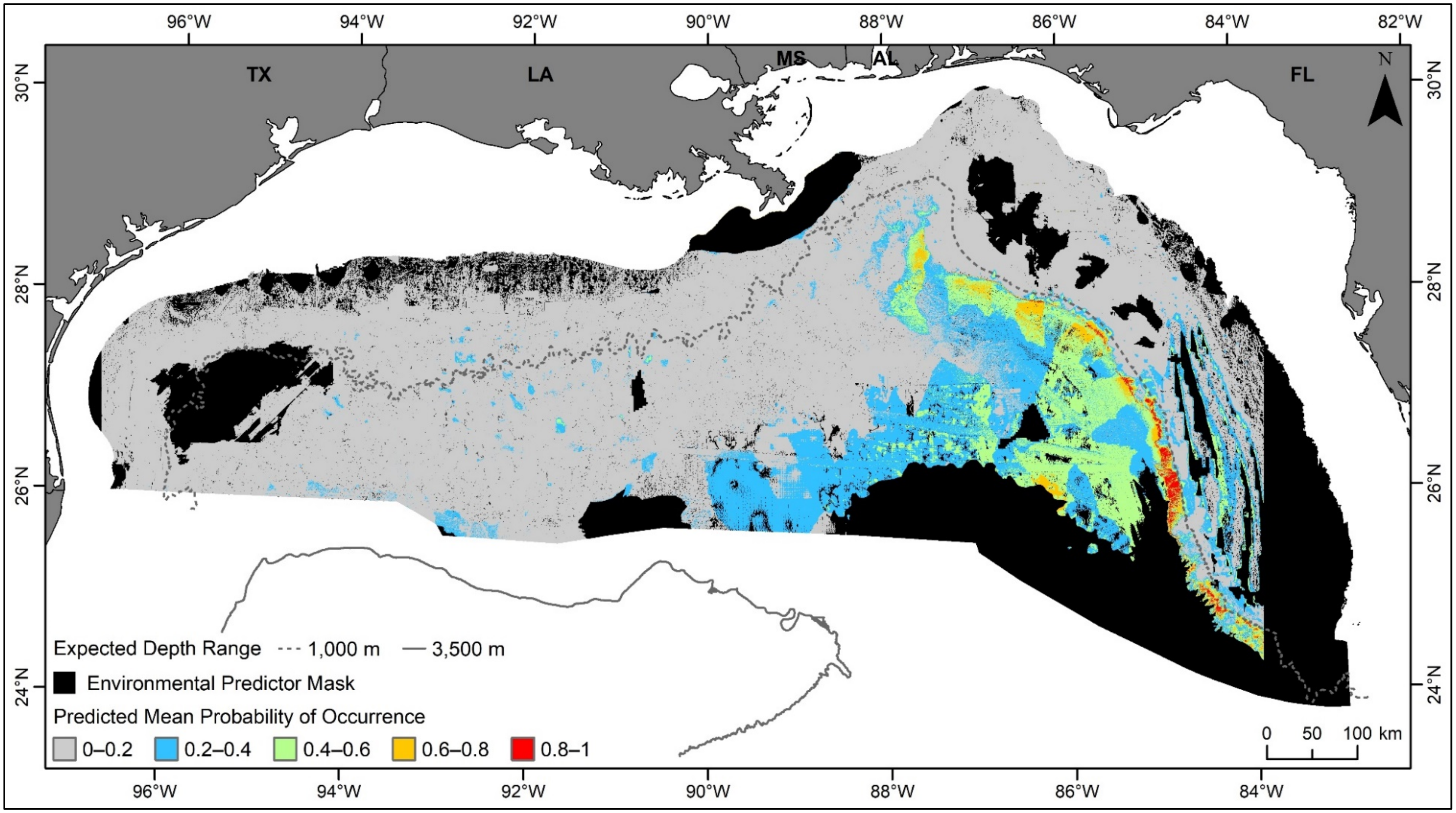

Figure 142. Predicted occurrence of the black coral *Stauropathes* (order Antipatharia).

This map shows the predicted mean probability of occurrence (i.e., the predicted posterior mean occupancy probability) for *Stauropathes* from the multi-genus occupancy model of order Antipatharia. The environmental predictor mask overlays areas where predictor values were outside the range of values at the sample locations and model predictions may be affected by extrapolation. Gray lines denote the expected depth range for *Stauropathes*.

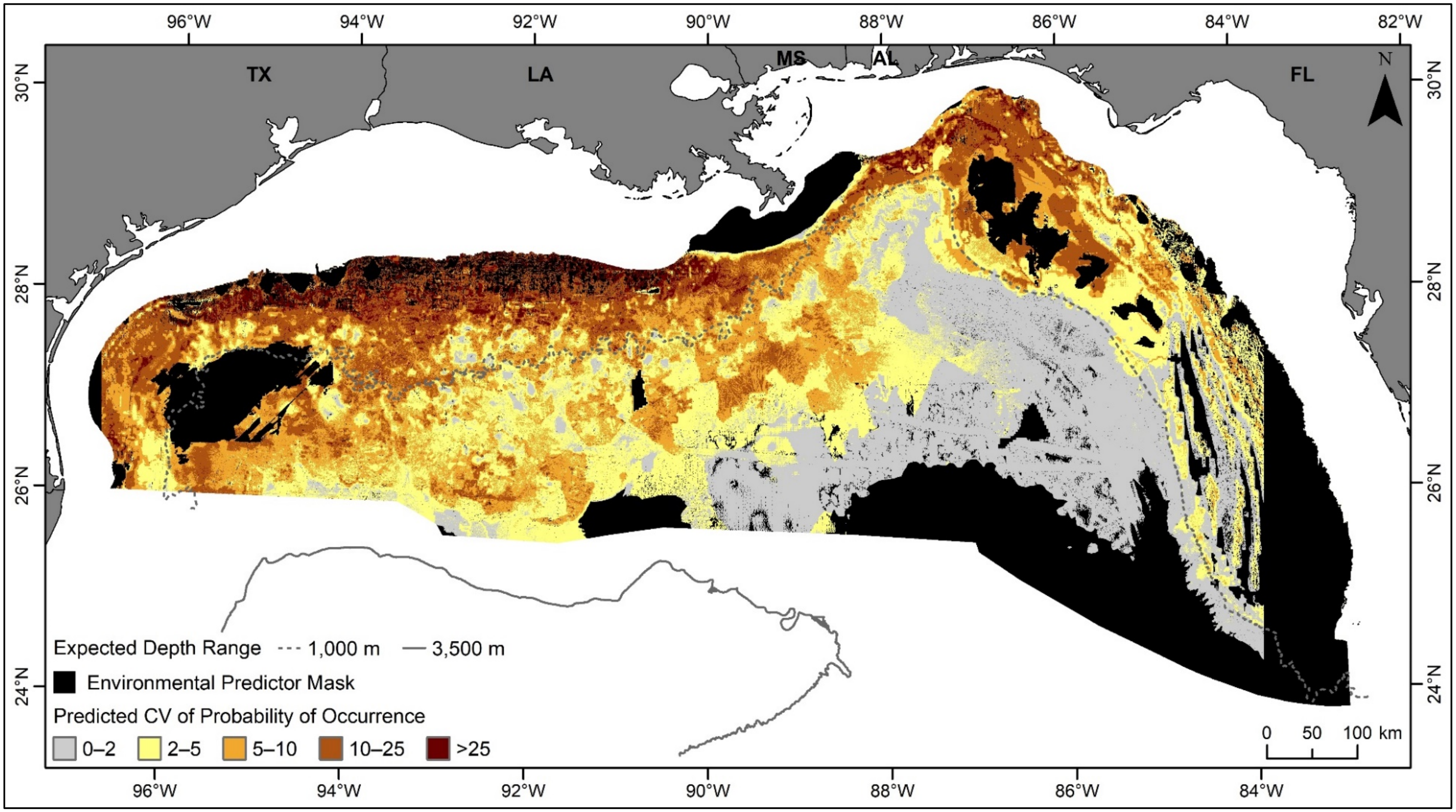

Figure 143. Variability in the predicted occurrence of the black coral *Stauropathes* (order Antipatharia).

This map shows the predicted coefficient of variation (CV) of the probability of occurrence (i.e., the predicted posterior CV of occupancy probability) for *Stauropathes* from the multi-genus occupancy model of order Antipatharia. The environmental predictor mask overlays areas where predictor values were outside the range of values at the sample locations and model predictions may be affected by extrapolation. Gray lines denote the expected depth range for *Stauropathes*.

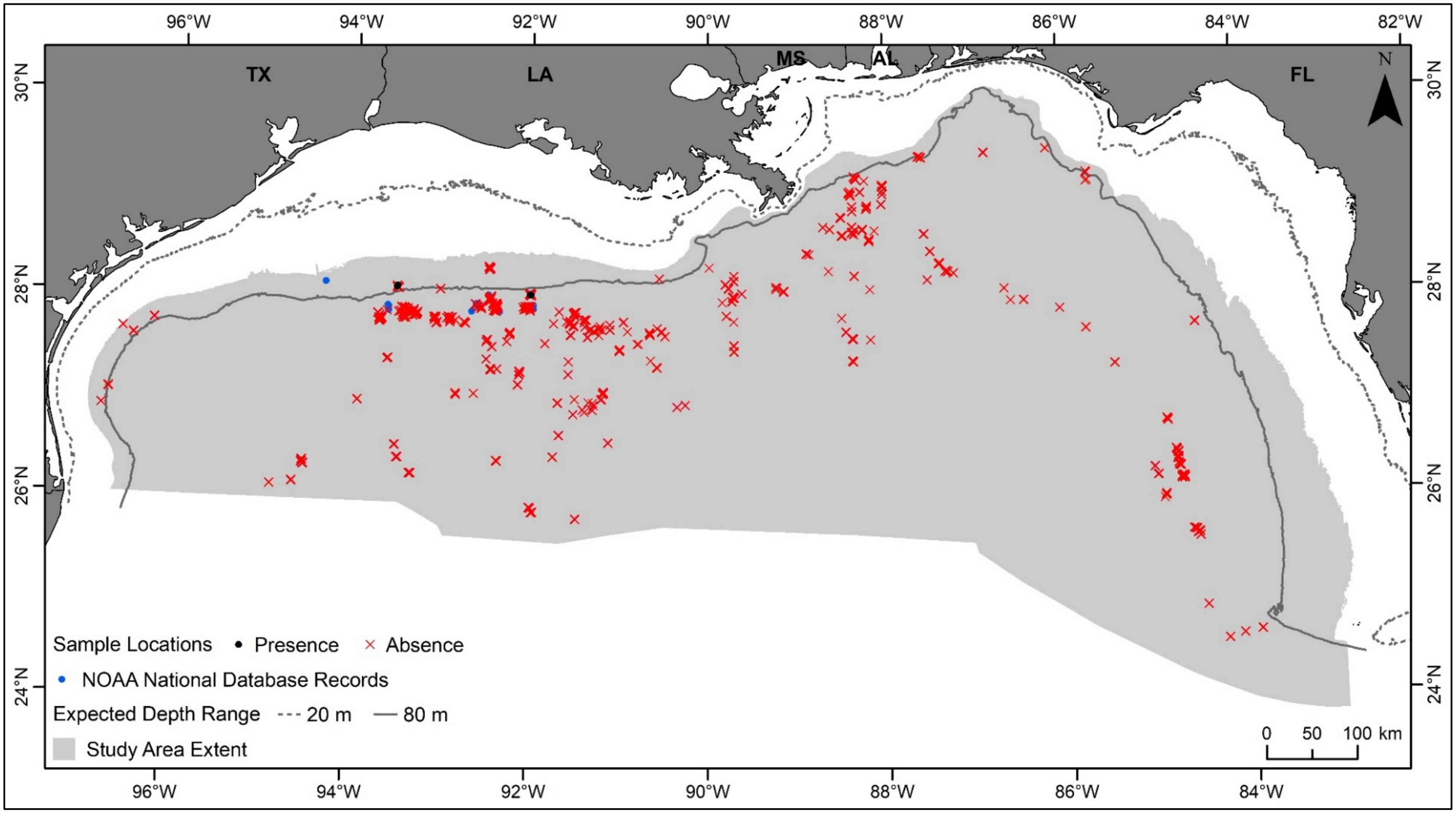

Figure 144. Occurrence records for the black coral *Plumapathes* (order Antipatharia).

This map shows the observed occurrence (presence-absence) of *Plumapathes* at sample locations in the presence-absence database compiled for this study. Additional records of occurrence in the NOAA National Database are also displayed. Gray lines denote the expected depth range for *Plumapathes*.

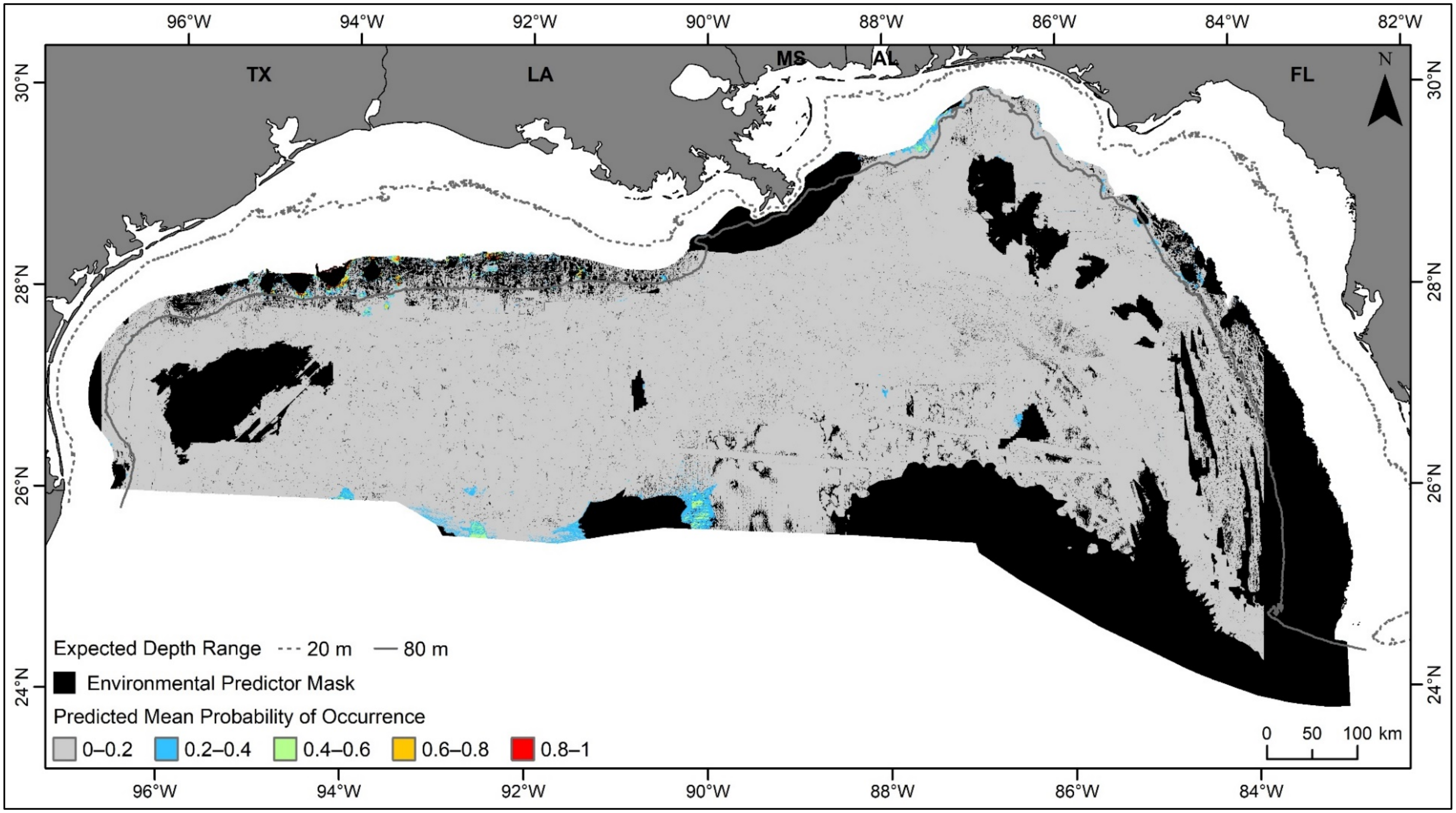

Figure 145. Predicted occurrence of the black coral *Plumapathes* (order Antipatharia).

This map shows the predicted mean probability of occurrence (i.e., the predicted posterior mean occupancy probability) for *Plumapathes* from the multi-genus occupancy model of order Antipatharia. The environmental predictor mask overlays areas where predictor values were outside the range of values at the sample locations and model predictions may be affected by extrapolation. Gray lines denote the expected depth range for *Plumapathes*.

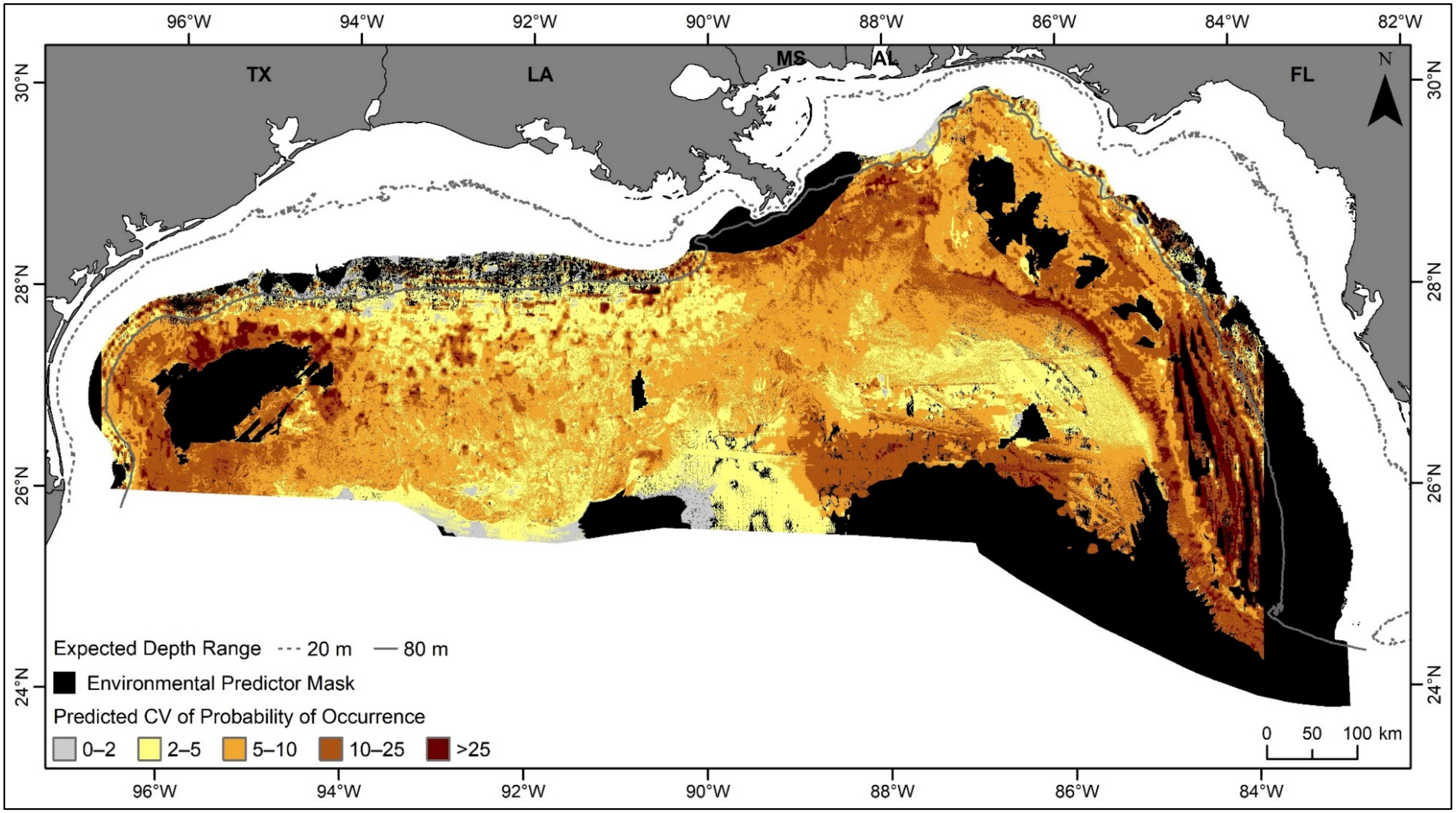

Figure 146. Variability in the predicted occurrence of the black coral *Plumapathes* (order Antipatharia).

This map shows the predicted coefficient of variation (CV) of the probability of occurrence (i.e., the predicted posterior CV of occupancy probability) for *Plumapathes* from the multi-genus occupancy model of order Antipatharia. The environmental predictor mask overlays areas where predictor values were outside the range of values at the sample locations and model predictions may be affected by extrapolation. Gray lines denote the expected depth range for *Plumapathes*.

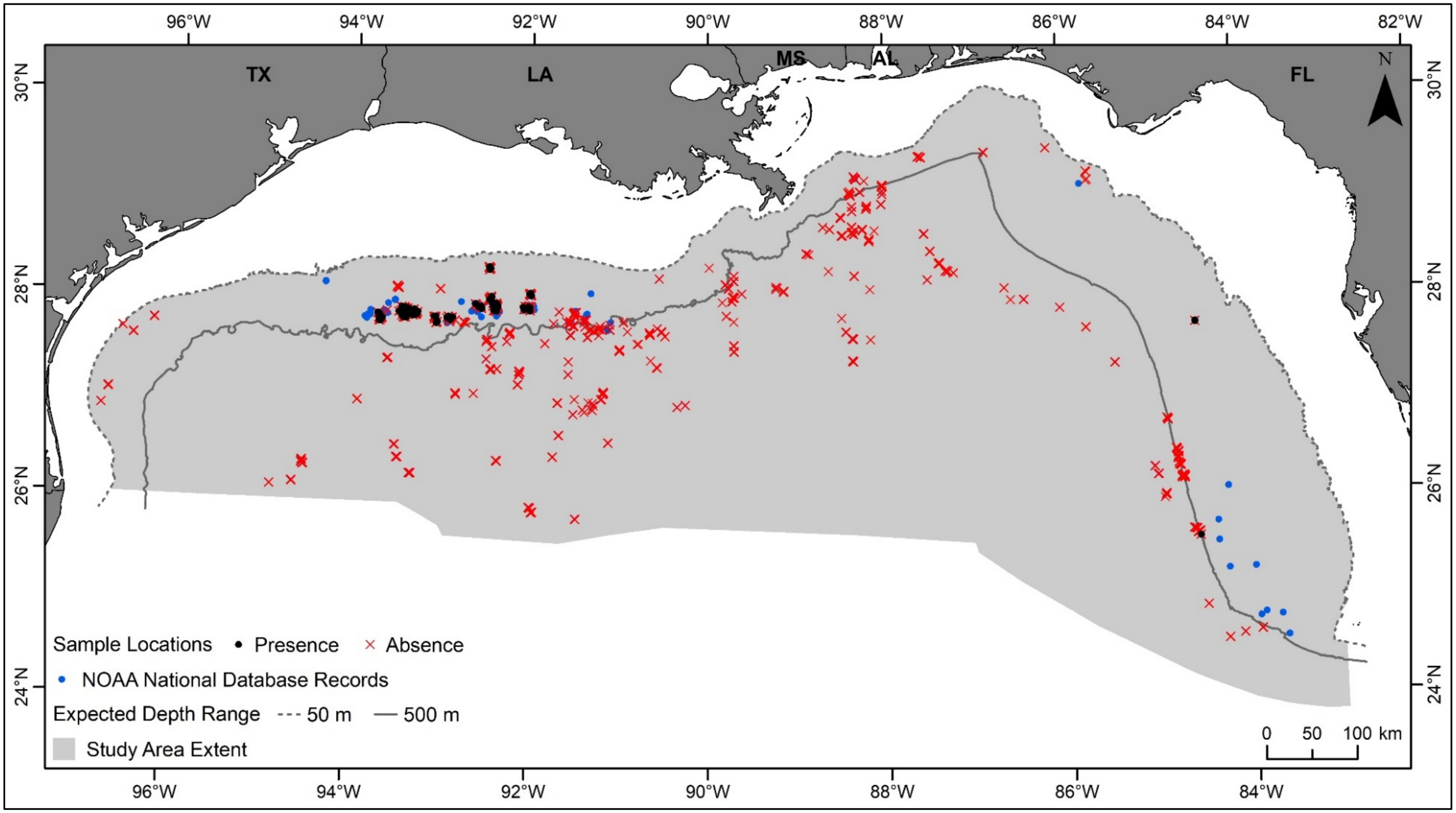

Figure 147. Occurrence records for the black coral family Aphanipathidae (order Antipatharia).

This map shows the observed occurrence (presence-absence) of Aphanipathidae at sample locations in the presence-absence database compiled for this study. Additional records of occurrence in the NOAA National Database are also displayed. Gray lines denote the expected depth range for Aphanipathidae.

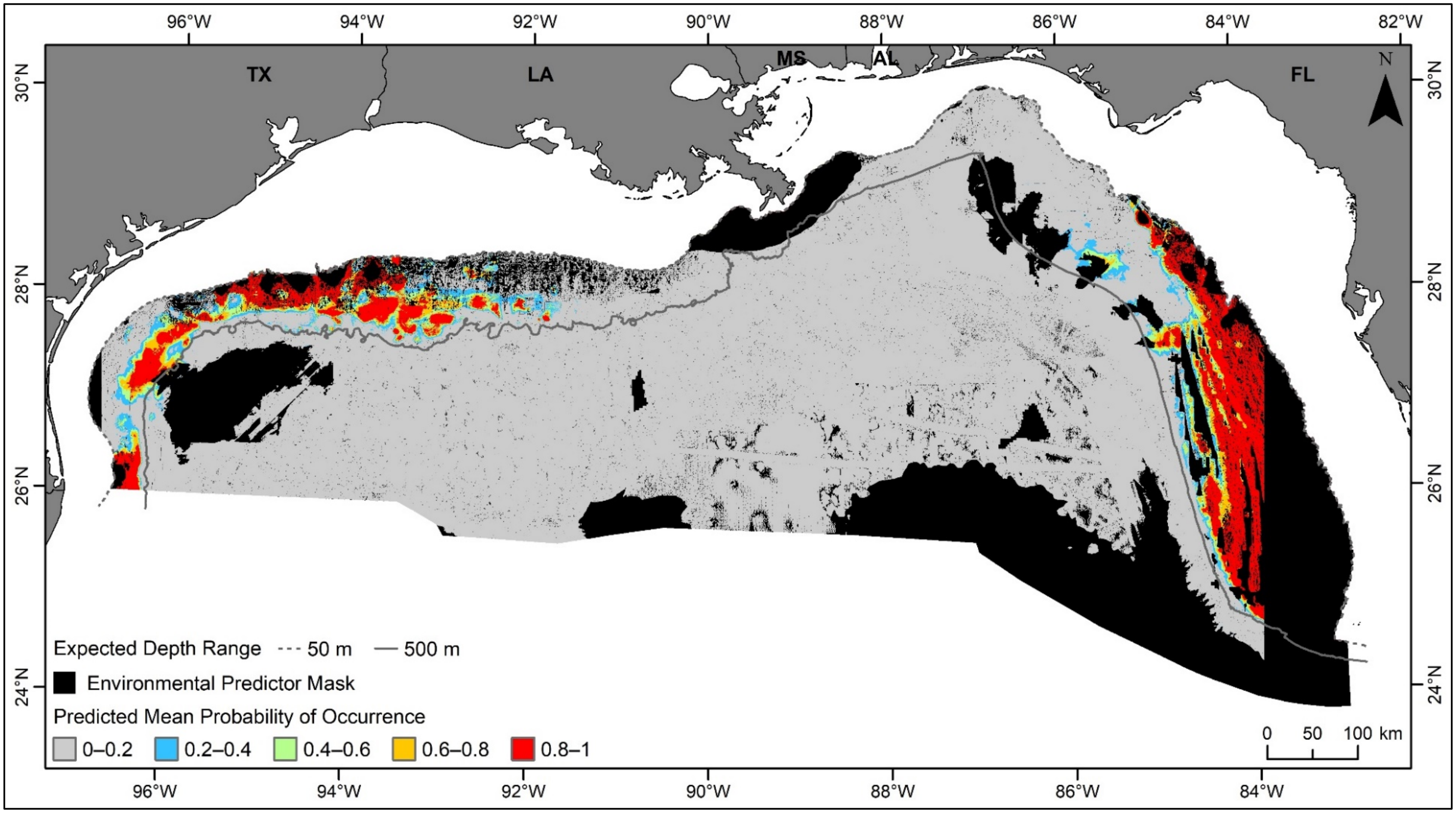

Figure 148. Predicted occurrence of the black coral family Aphanipathidae (order Antipatharia).

This map shows the predicted mean probability of occurrence (i.e., the predicted posterior mean occupancy probability) for Aphanipathidae from the single-taxon occupancy model. The environmental predictor mask overlays areas where predictor values were outside the range of values at the sample locations and model predictions may be affected by extrapolation. Gray lines denote the expected depth range for Aphanipathidae.

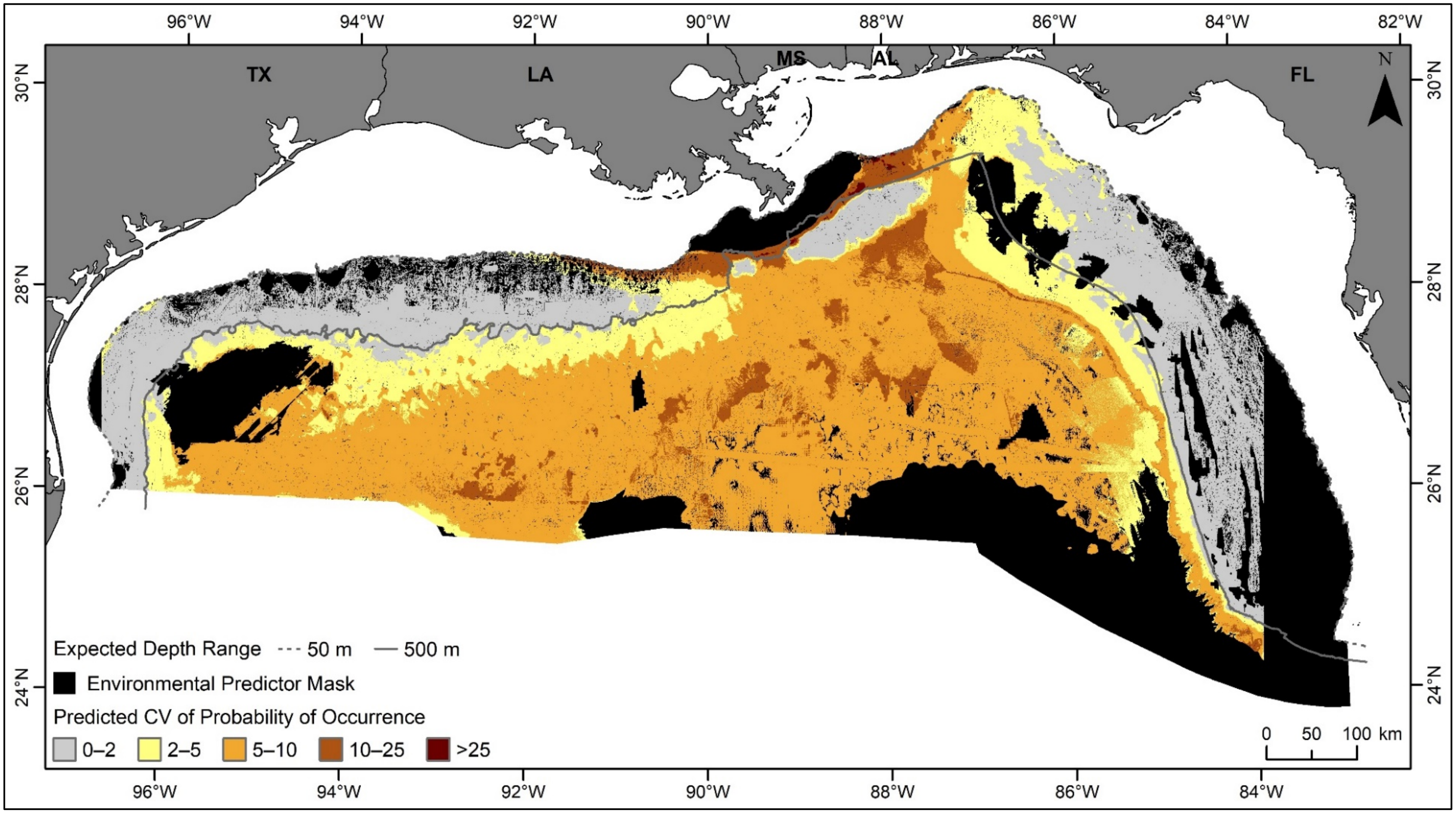

Figure 149. Variability in the predicted occurrence of the black coral family Aphanipathidae (order Antipatharia).

This map shows the predicted coefficient of variation (CV) of the probability of occurrence (i.e., the predicted posterior CV of occupancy probability) for Aphanipathidae from the single-taxon occupancy model. The environmental predictor mask overlays areas where predictor values were outside the range of values at the sample locations and model predictions may be affected by extrapolation. Gray lines denote the expected depth range for Aphanipathidae.

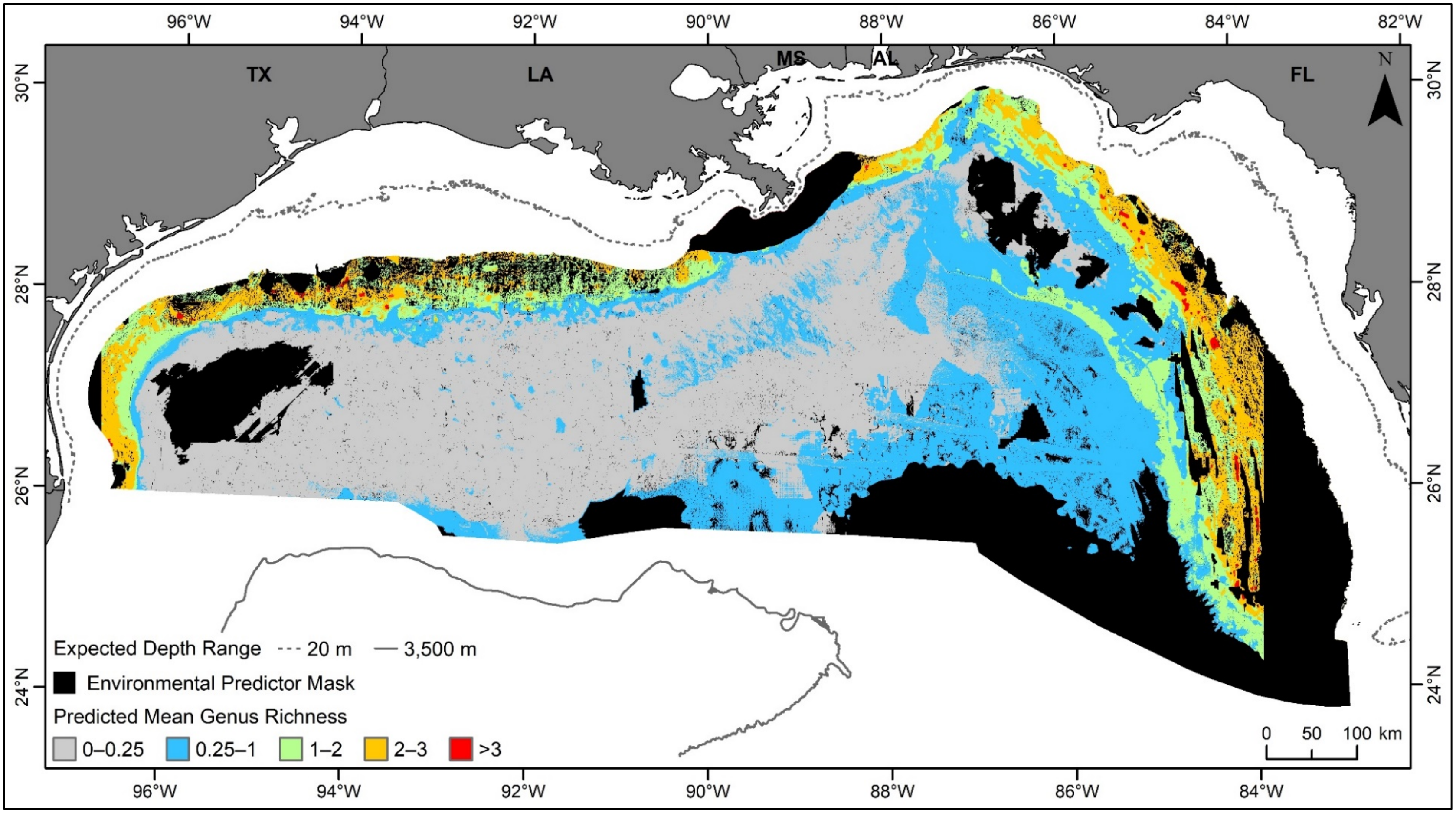

Figure 150. Predicted genus richness of black corals (order Antipatharia).

This map shows the predicted mean genus richness (i.e., the posterior mean genus richness) from the multi-genus occupancy model of order Antipatharia. The environmental predictor mask overlays areas where predictor values were outside the range of values at the sample locations and model predictions may be affected by extrapolation. Gray lines denote the combined expected depth range for the genera included in the model.

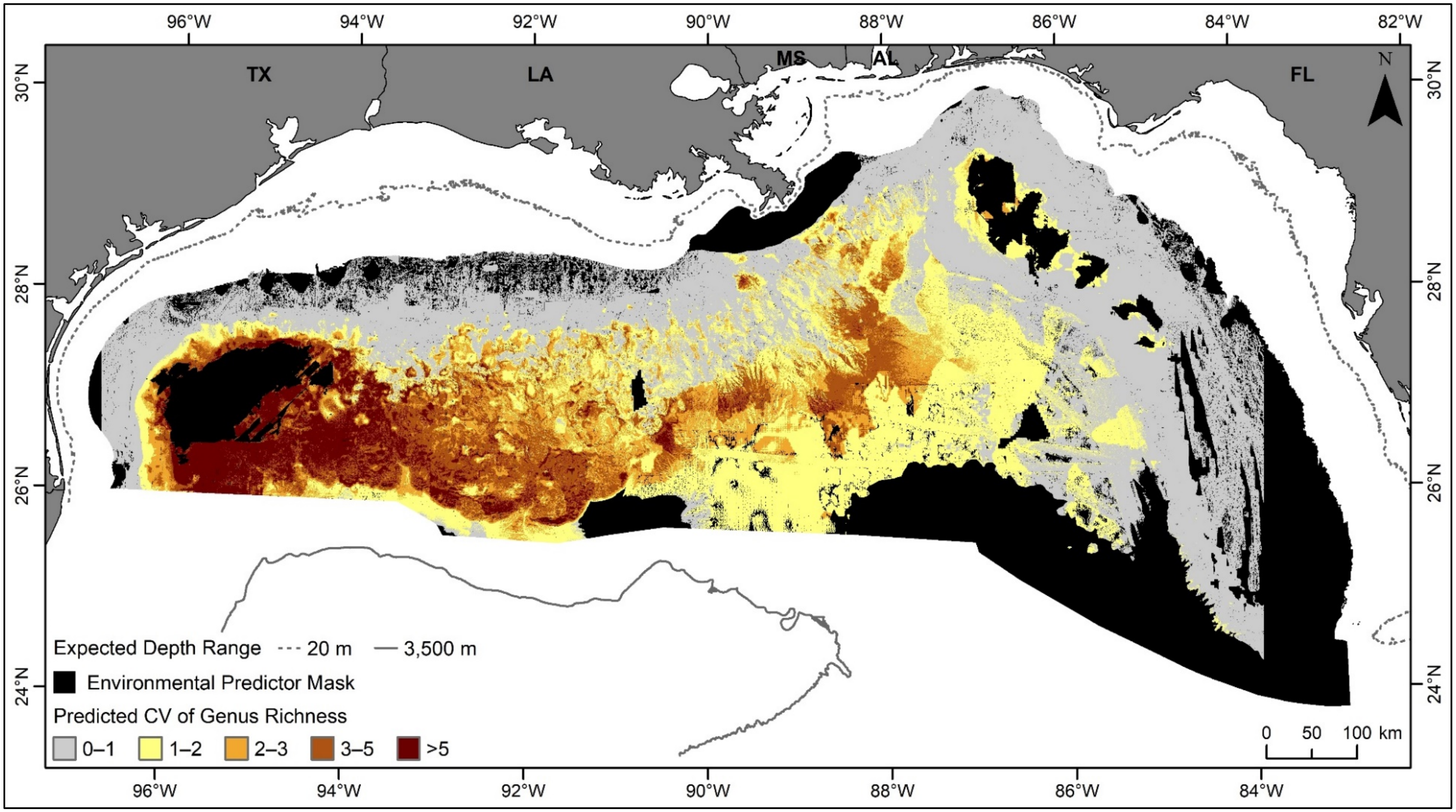

Figure 151. Variability in the predicted genus richness of black corals (order Antipatharia).

This map shows the predicted coefficient of variation of genus richness (i.e., the posterior CV of genus richness) from the multi-genus occupancy model of order Antipatharia. The environmental predictor mask overlays areas where predictor values were outside the range of values at the sample locations and model predictions may be affected by extrapolation. Gray lines denote the combined expected depth range for the genera included in the model.

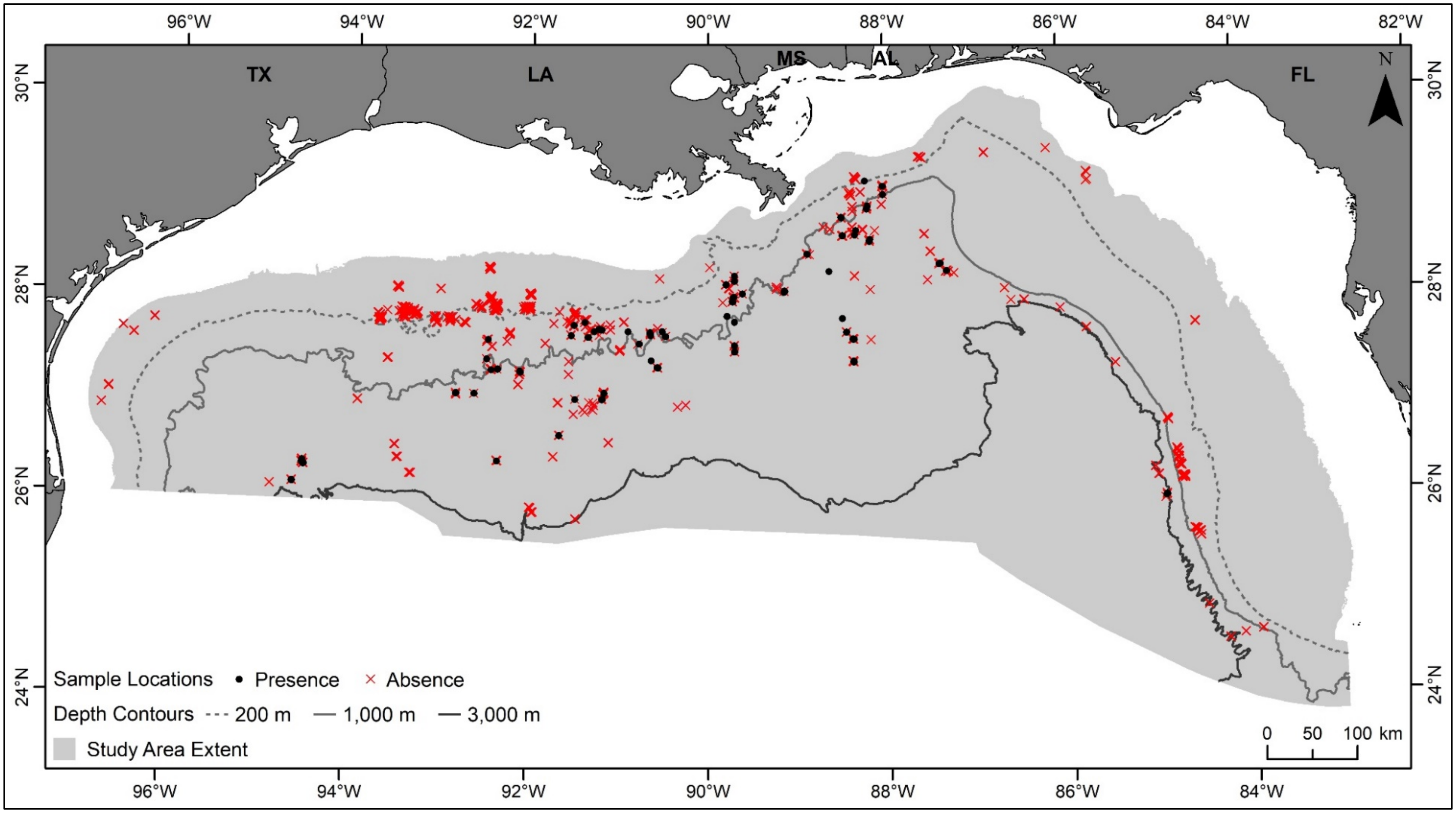

Figure 152. Occurrence records for bivalves.

This map shows the observed occurrence (presence-absence) of bivalves at sample locations in the presence-absence database compiled for this study. Depth contours define the mesophotic, upper bathyal, and lower bathyal depth zones.

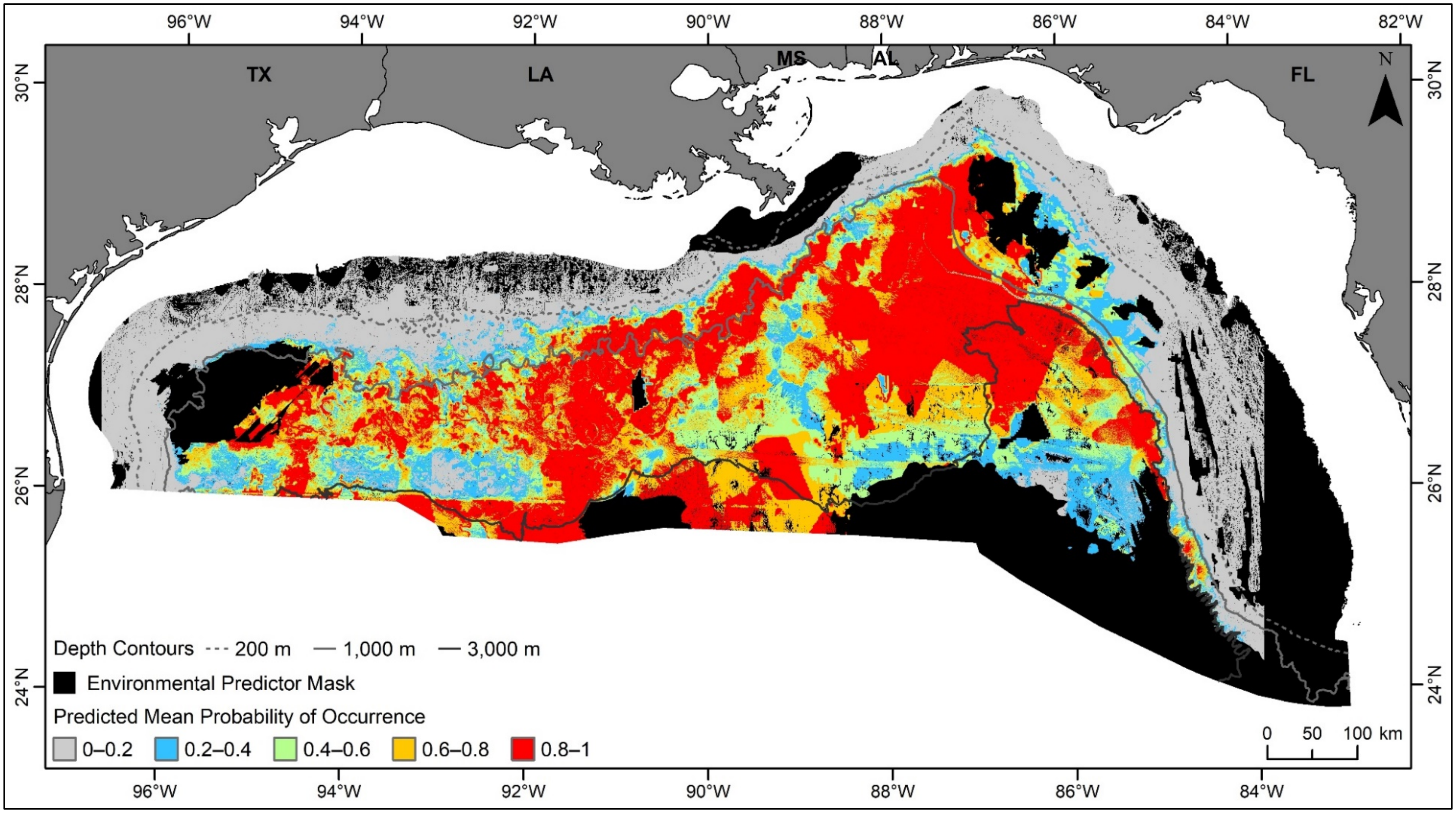

Figure 153. Predicted occurrence of bivalves.

This map shows the predicted mean probability of occurrence (i.e., the predicted posterior mean occupancy probability) for bivalves from the single-taxon occupancy model. The environmental predictor mask overlays areas where predictor values were outside the range of values at the sample locations and model predictions may be affected by extrapolation. Depth contours define the mesophotic, upper bathyal, and lower bathyal depth zones.

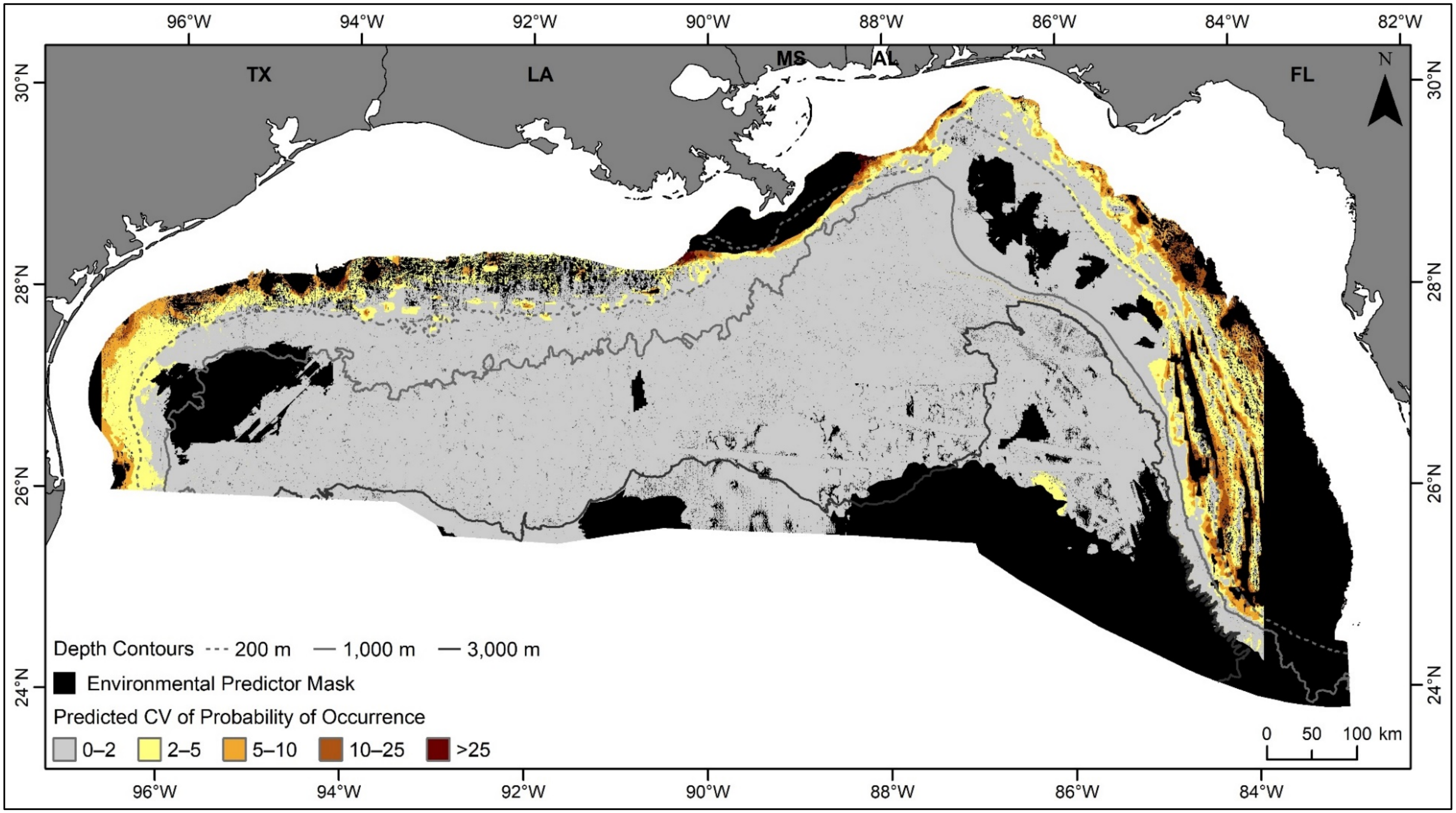

Figure 154. Variability in the predicted occurrence of bivalves.

This map shows the predicted coefficient of variation (CV) of the probability of occurrence (i.e., the predicted posterior CV of occupancy probability) for bivalves from the single-taxon occupancy model. The environmental predictor mask overlays areas where predictor values were outside the range of values at the sample locations and model predictions may be affected by extrapolation. Depth contours define the mesophotic, upper bathyal, and lower bathyal depth zones.

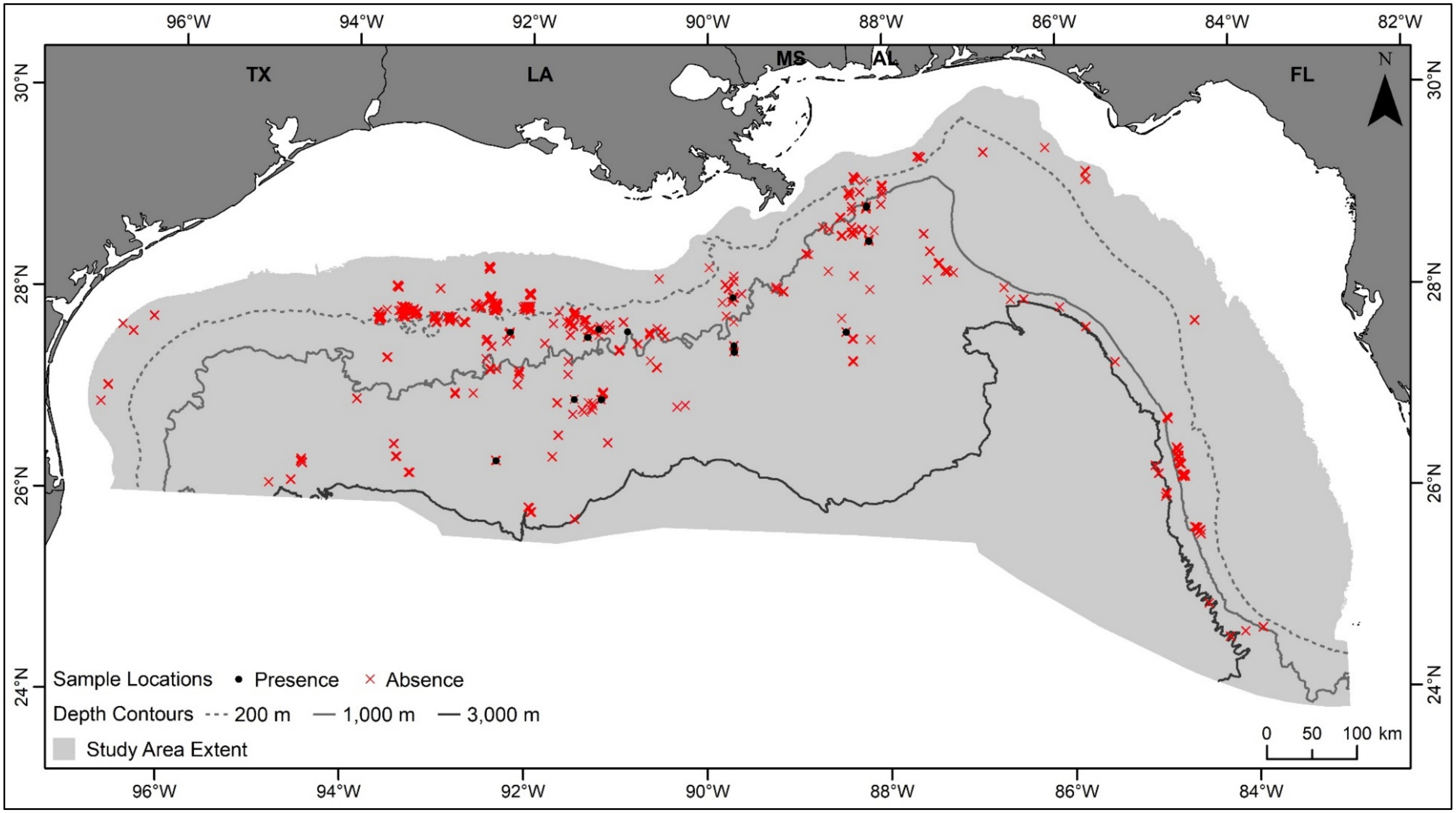

Figure 155. Occurrence records for bacterial mats.

This map shows the observed occurrence (presence-absence) of bacterial mats at sample locations in the presence-absence database compiled for this study. Depth contours define the mesophotic, upper bathyal, and lower bathyal depth zones.

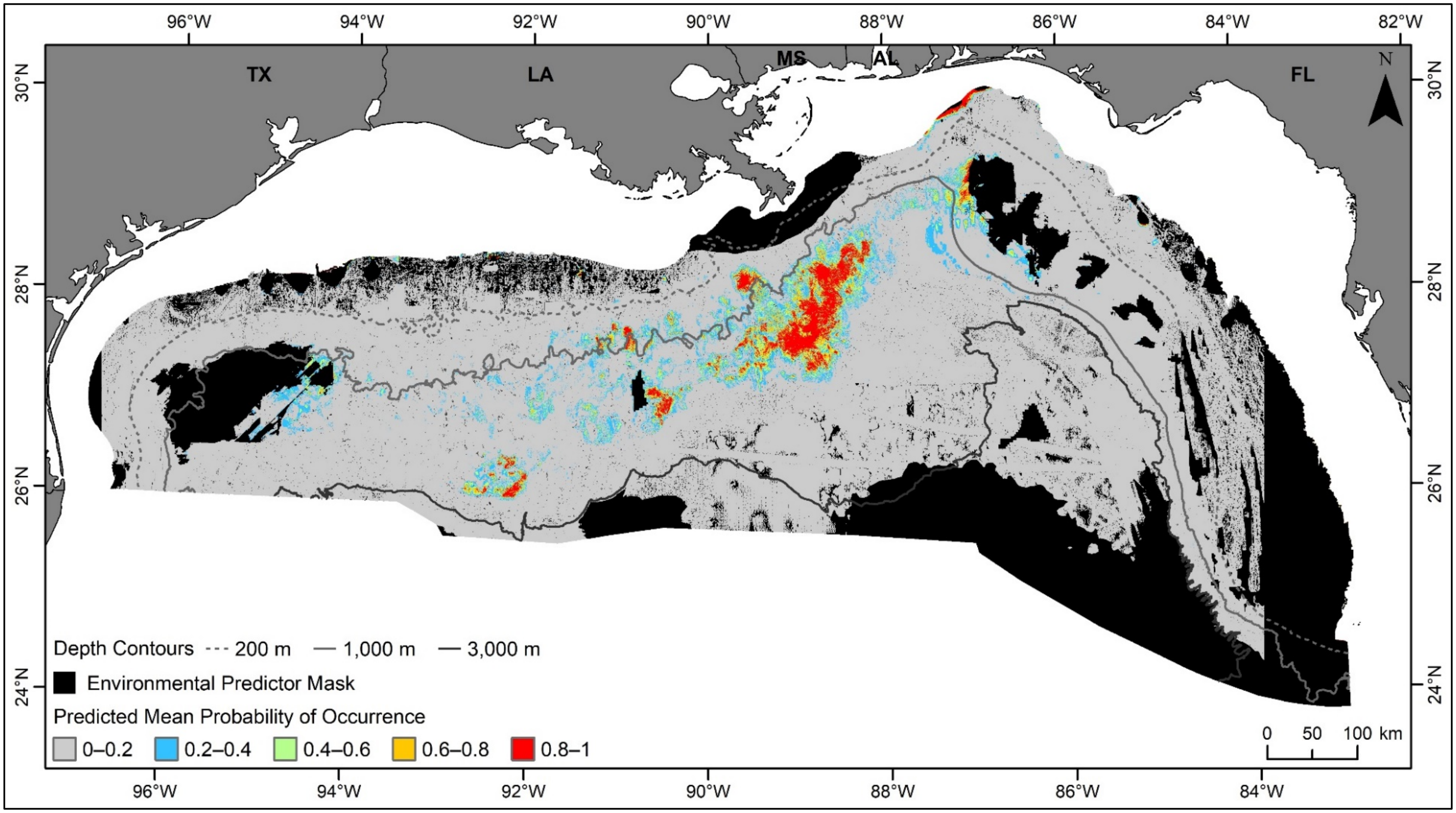

Figure 156. Predicted occurrence of bacterial mats.

This map shows the predicted mean probability of occurrence (i.e., the predicted posterior mean occupancy probability) for bacterial mats from the single-taxon occupancy model. The environmental predictor mask overlays areas where predictor values were outside the range of values at the sample locations and model predictions may be affected by extrapolation. Depth contours define the mesophotic, upper bathyal, and lower bathyal depth zones.

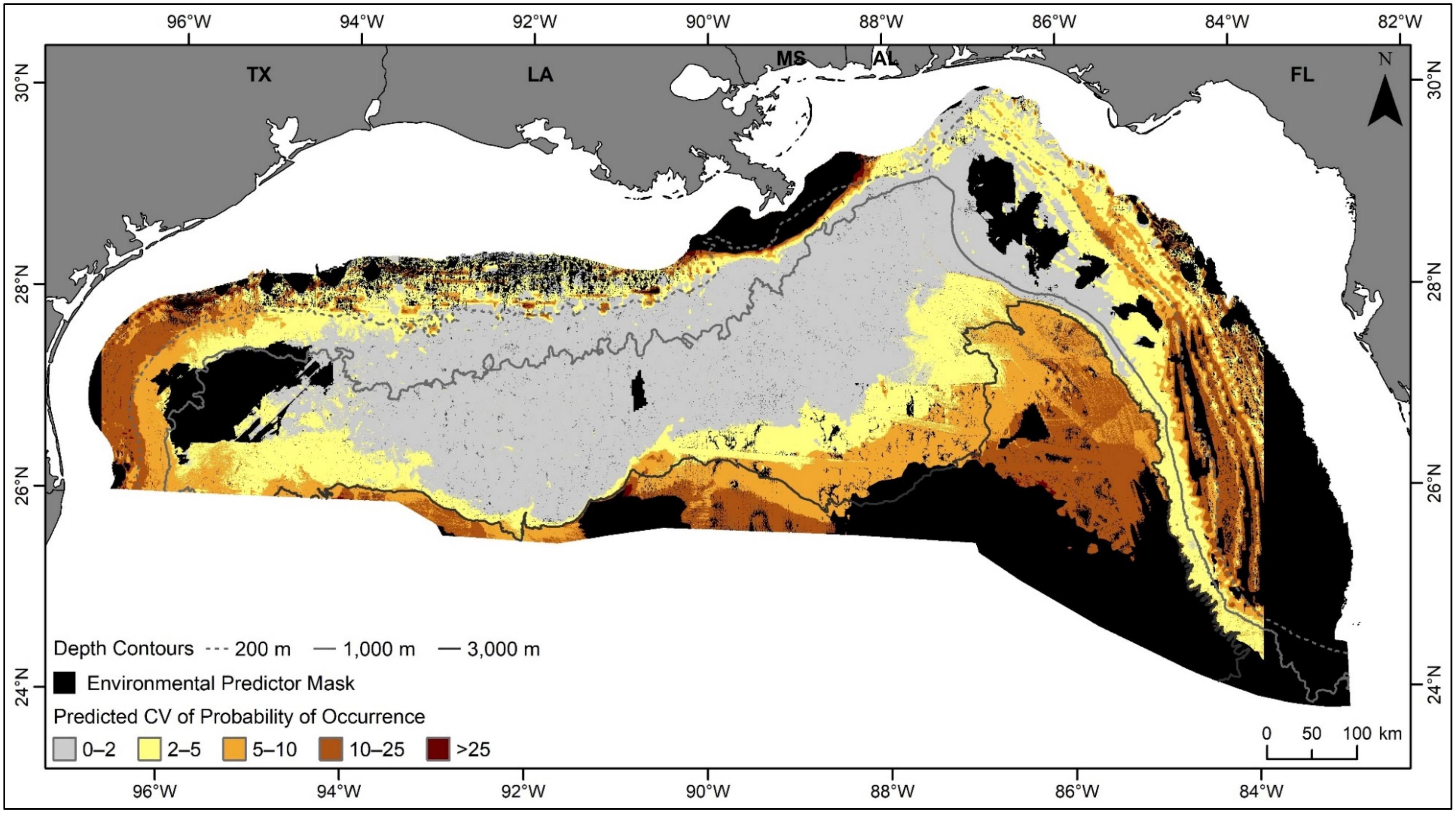

Figure 157. Variability in the predicted occurrence of bacterial mats.

This map shows the predicted coefficient of variation (CV) of the probability of occurrence (i.e., the predicted posterior CV of occupancy probability) for bacterial mats from the single-taxon occupancy model. The environmental predictor mask overlays areas where predictor values were outside the range of values at the sample locations and model predictions may be affected by extrapolation. Depth contours define the mesophotic, upper bathyal, and lower bathyal depth zones.

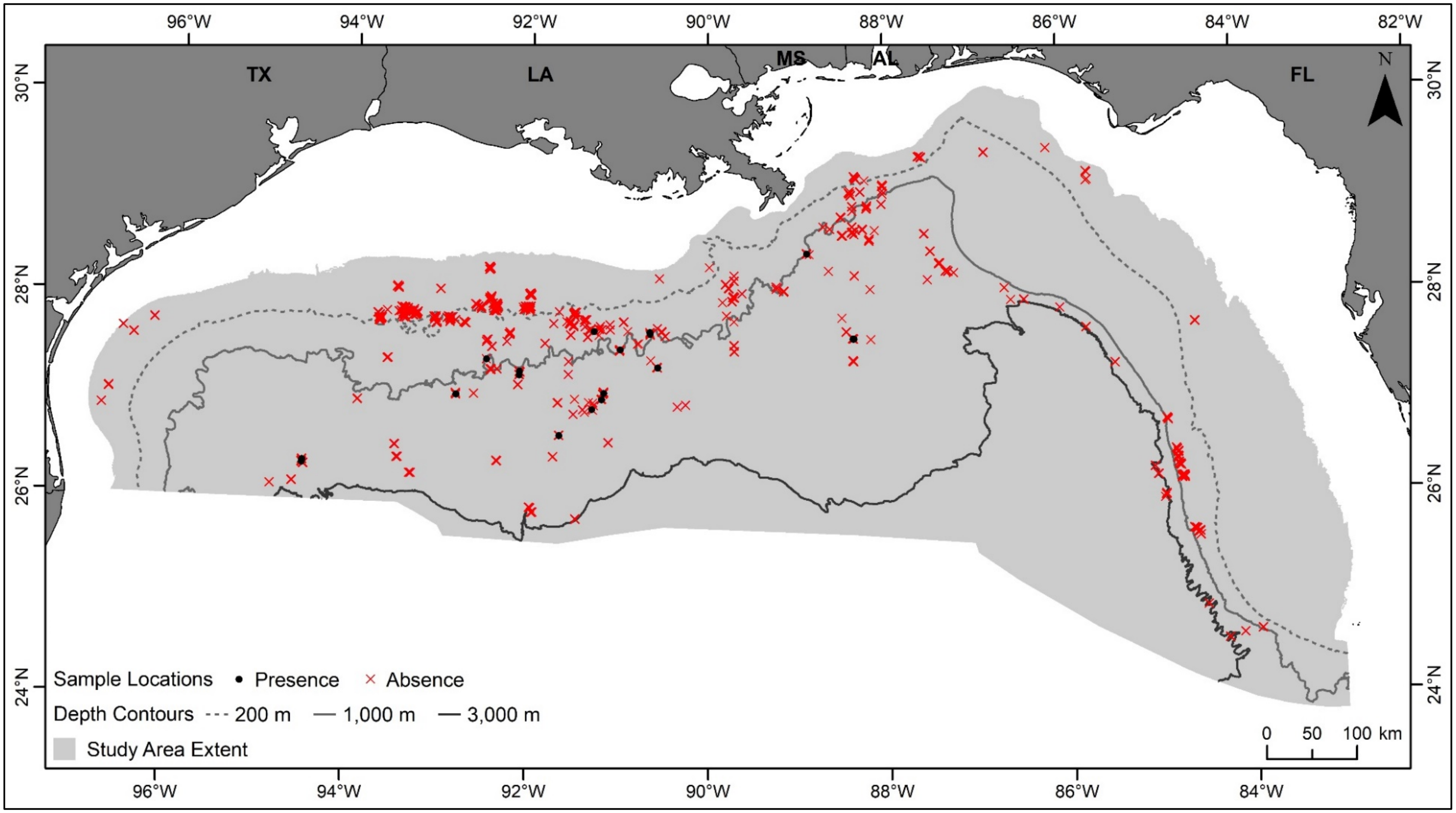

Figure 158. Occurrence records for brine.

This map shows the observed occurrence (presence-absence) of brine at sample locations in the presence-absence database compiled for this study. Depth contours define the mesophotic, upper bathyal, and lower bathyal depth zones.

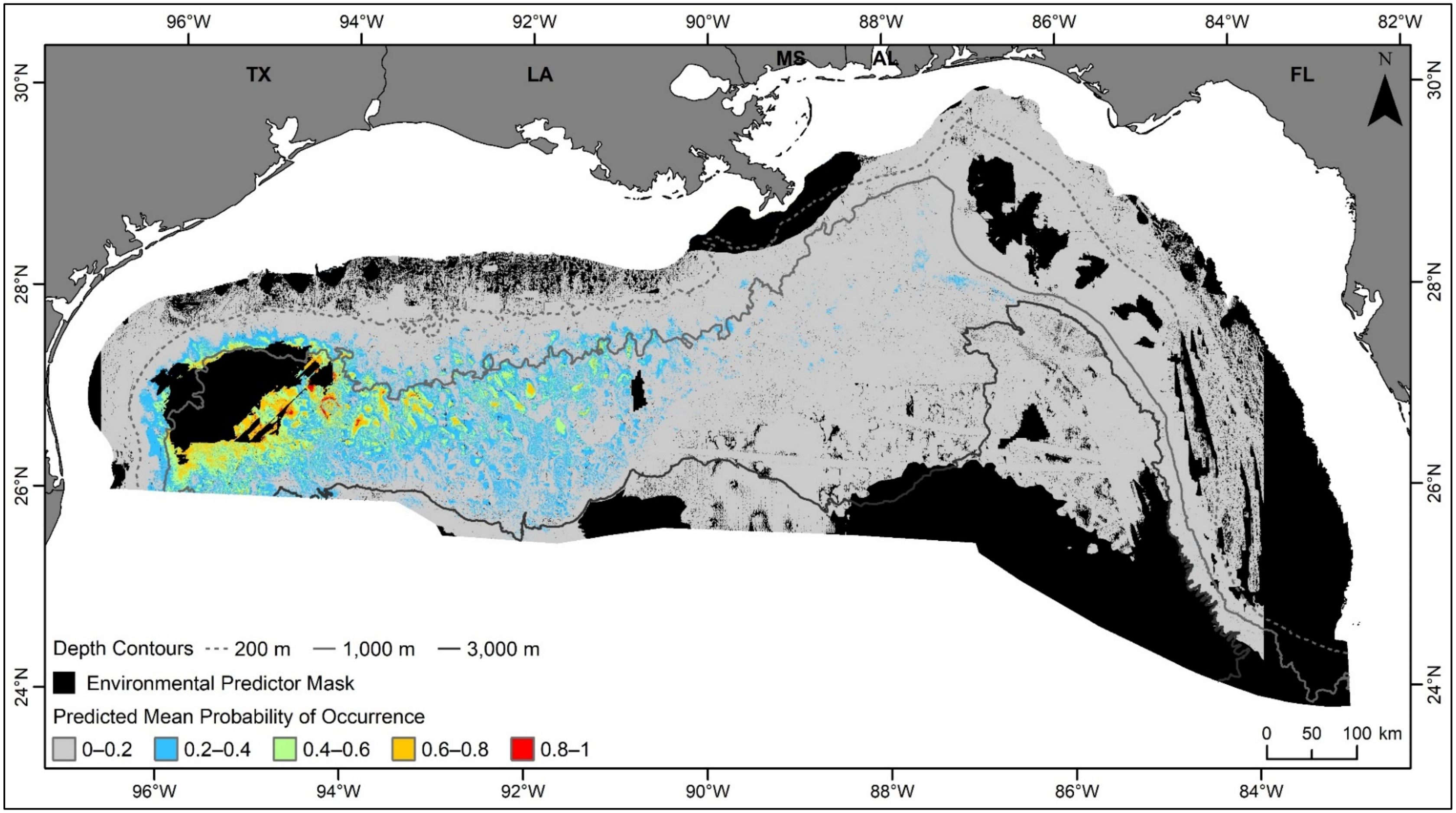

Figure 159. Predicted occurrence of brine.

This map shows the predicted mean probability of occurrence (i.e., the predicted posterior mean occupancy probability) for brine from the single-taxon occupancy model. The environmental predictor mask overlays areas where predictor values were outside the range of values at the sample locations and model predictions may be affected by extrapolation. Depth contours define the mesophotic, upper bathyal, and lower bathyal depth zones.

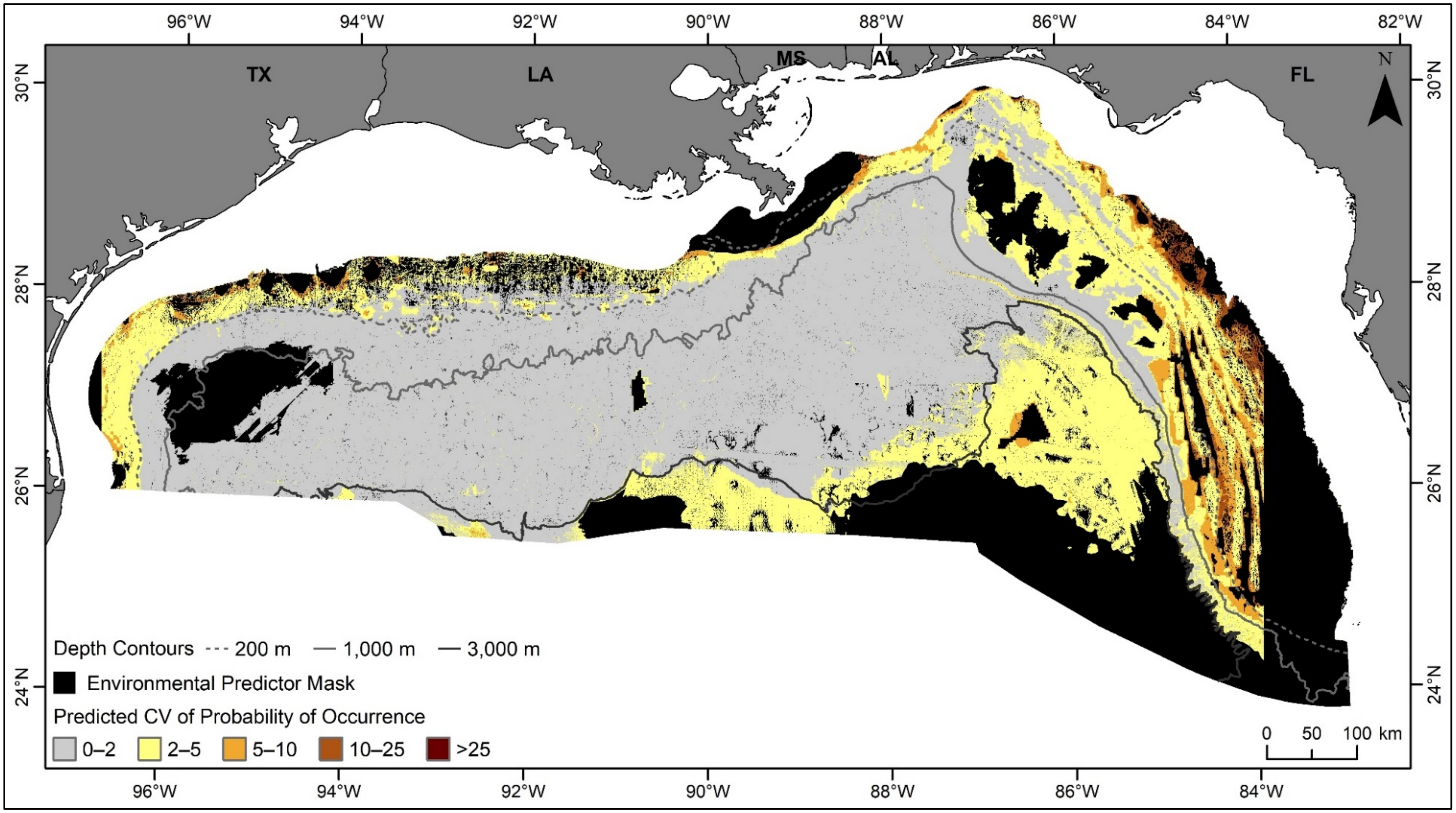

Figure 160. Variability in the predicted occurrence of brine.

This map shows the predicted coefficient of variation (CV) of the probability of occurrence (i.e., the predicted posterior CV of occupancy probability) for brine from the single-taxon occupancy model. The environmental predictor mask overlays areas where predictor values were outside the range of values at the sample locations and model predictions may be affected by extrapolation. Depth contours define the mesophotic, upper bathyal, and lower bathyal depth zones.

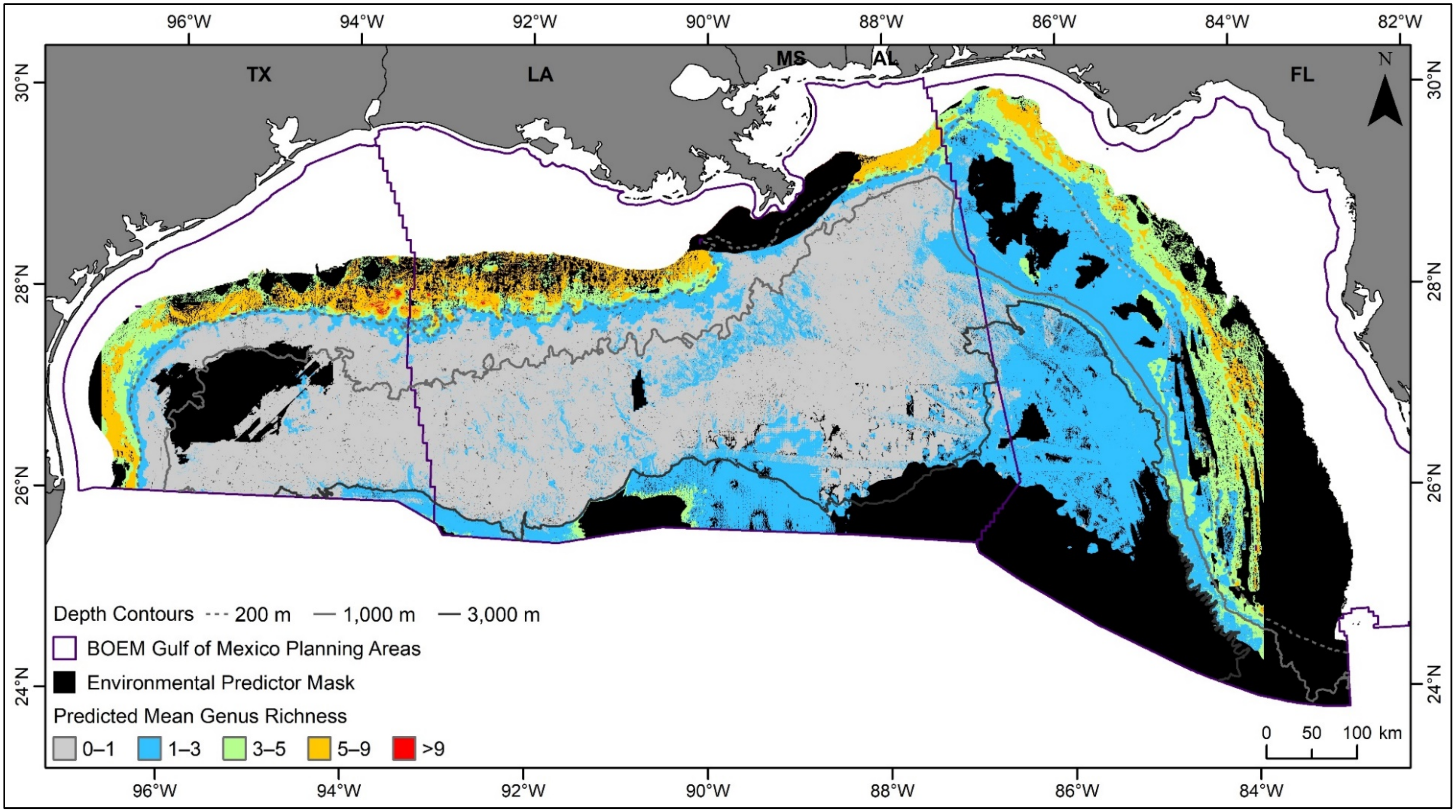

Figure 161. Cumulative predicted genus richness of structure-forming deep-sea corals.

This map shows the predicted mean genus richness (i.e., the posterior mean genus richness) for all 28 genera modeled from orders Scleractinia, Alcyonacea, and Antipatharia. The environmental predictor mask overlays areas where predictor values were outside the range of values at the sample locations and model predictions may be affected by extrapolation. Depth contours define the mesophotic, upper bathyal, and lower bathyal depth zones.

Table 8. Predicted mean probability of occurrence (occupancy) for all 28 genera modeled from orders Scleractinia, Alcyonacea, and Antipatharia and predicted mean genus richness by BOEM Gulf of Mexico planning area and depth zone

Taxon			BOEM Gulf of Mexico Planning Areas								
			Western			Central			Eastern		
Order	**Family**	**Genus**	**M**	**UB**	**LB**	**M**	**UB**	**LB**	**M**	**UB**	**LB**
Scleractinia	Caryophylliidae	*Lophelia*	0.04	0.13	0.08	0.01	0.07	0.00	0.08	0.38	0.06
		Solenosmilia	0.00	0.01	0.01	0.00	0.01	0.01	0.00	0.01	0.04
	Dendrophylliidae	*Enallopsammia*	0.00	0.01	0.01	0.01	0.02	0.03	0.01	0.01	0.05
	Oculinidae	*Madrepora*	0.00	0.00	0.00	0.02	0.04	0.02	0.05	0.06	0.05
		Oculina	0.09	0.01	0.00	0.19	0.02	0.00	0.00	0.00	0.00
	Pocilloporidae	*Madracis*	0.17	0.02	0.00	0.13	0.02	0.00	0.11	0.02	0.00
Alcyonacea	Ellisellidae	*Nicella*	0.25	0.02	0.00	0.21	0.02	0.00	0.24	0.03	0.00
	Isididae	*Acanella*	0.04	0.04	0.04	0.01	0.01	0.02	0.02	0.01	0.08
		Chelidonisis	0.03	0.04	0.05	0.02	0.02	0.00	0.16	0.34	0.03
		Keratoisis	0.01	0.02	0.02	0.00	0.01	0.04	0.01	0.02	0.19
		Lepidisis	0.00	0.01	0.08	0.00	0.01	0.20	0.01	0.01	0.27
	Plexauridae	*Bebryce*	0.85	0.08	0.00	0.36	0.01	0.00	0.21	0.01	0.00
		Caliacis	0.21	0.02	0.00	0.17	0.02	0.00	0.00	0.00	0.00
		Muricea	0.68	0.01	0.00	0.57	0.02	0.01	0.24	0.01	0.00
		Paramuricea	0.01	0.03	0.03	0.03	0.13	0.08	0.06	0.18	0.27
		Placogorgia	0.24	0.00	0.00	0.25	0.01	0.01	0.17	0.02	0.00
		Scleracis	0.07	0.01	0.00	0.04	0.01	0.00	0.00	0.00	0.00
		Swiftia	0.01	0.00	0.00	0.26	0.04	0.01	0.06	0.01	0.00
		Thesea	0.18	0.00	0.00	0.84	0.07	0.03	0.23	0.02	0.01
		Villogorgia	0.00	0.00	0.00	0.03	0.00	0.00	0.12	0.01	0.01
	Primnoidae	*Callogorgia*	0.27	0.10	0.01	0.69	0.29	0.01	0.18	0.15	0.00
Antipatharia	Antipathidae	*Antipathes*	0.59	0.01	0.00	0.59	0.01	0.00	0.70	0.08	0.00
		Stichopathes	0.80	0.03	0.00	0.68	0.01	0.00	0.23	0.02	0.00
	Leiopathidae	*Leiopathes*	0.10	0.10	0.00	0.11	0.13	0.00	0.27	0.30	0.01
	Myriopathidae	*Plumapathes*	0.04	0.00	0.00	0.04	0.00	0.01	0.01	0.00	0.00
		Tanacetipathes	0.47	0.00	0.00	0.20	0.01	0.00	0.68	0.09	0.00
	Schizopathidae	*Bathypathes*	0.00	0.00	0.00	0.00	0.02	0.04	0.02	0.25	0.62
		Stauropathes	0.01	0.02	0.02	0.00	0.02	0.11	0.10	0.08	0.44
Genus Richness			5.2	0.7	0.4	5.5	1.1	0.6	4.0	2.1	2.1

M = Mesophotic, UB = Upper Bathyal, LB = Lower Bathyal

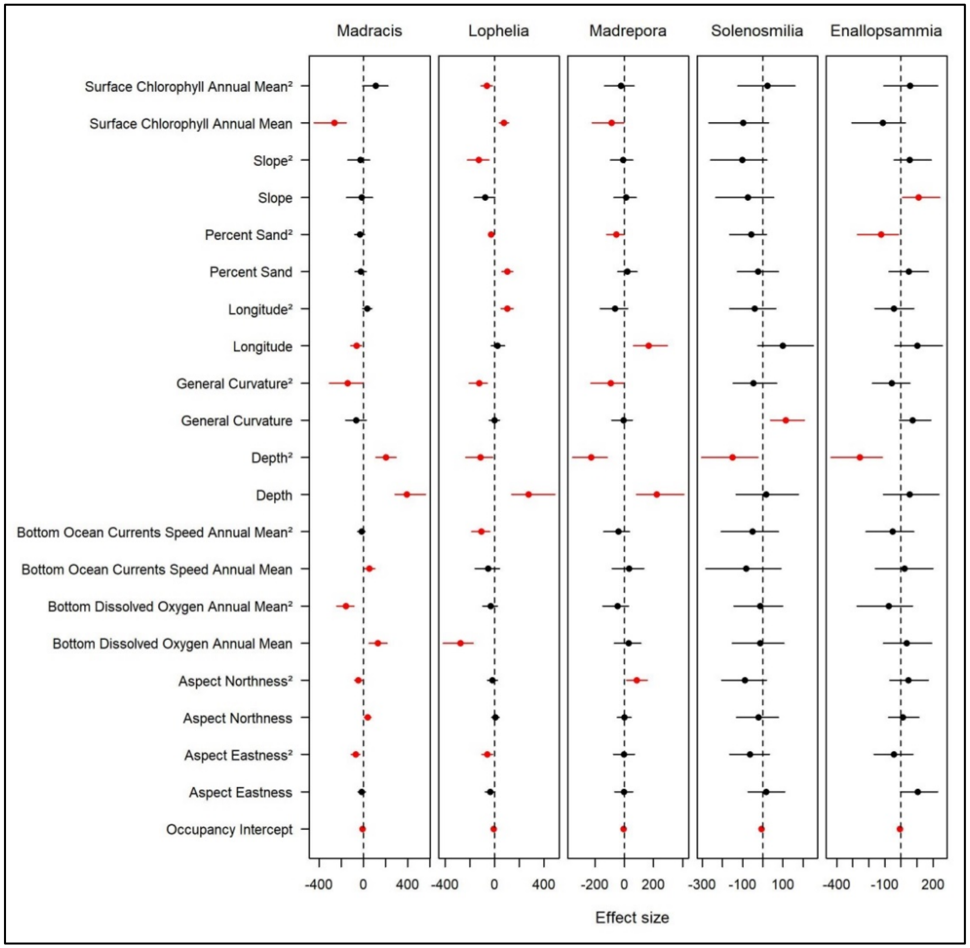

Figure 162. Effect size of environmental predictors for stony corals (order Scleractinia).

Genera within order Scleractinia are listed from left to right in decreasing order of frequency observed. The 21 terms of the occupancy model (state process) are shown on the y-axis, including the occupancy intercept and both the main effects of the 10 predictors and their quadratic (i.e., squared) terms. The x-axis shows the effect size for that predictor, indicating whether effects were more positive (right of zero) or negative (left of zero) for each genus. Effect sizes appear large because their values correspond to orthogonal scales used to standardize the predictors. Dots indicate posterior mean effect estimates and lines indicate the 95% posterior credible interval. Genus-specific effects that were significantly different from zero (i.e., credible interval did not contain zero) are shown in red.

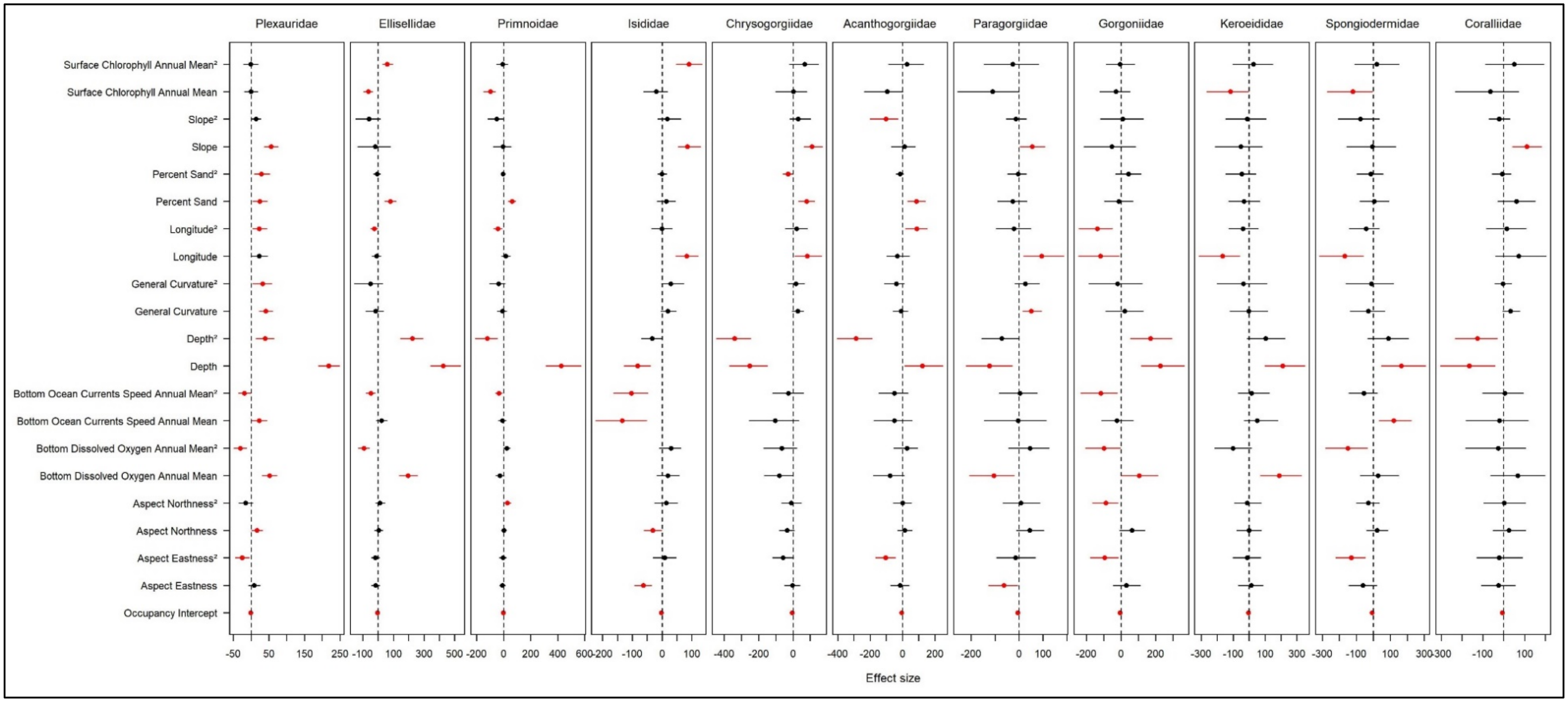

Figure 163. Effect size of environmental predictors for gorgonian corals (order Alcyonacea).

Families within order Alcyonacea are listed from left to right in decreasing order of frequency observed. The 21 terms of the occupancy model (state process) are shown on the y-axis, including the occupancy intercept and both the main effects of the 10 predictors and their quadratic (i.e., squared) terms. The x-axis shows the effect size for that predictor, indicating whether effects were more positive (right of zero) or negative (left of zero) for each family. Effect sizes appear large because their values correspond to orthogonal scales used to standardize the predictors. Dots indicate posterior mean effect estimates and lines indicate the 95% posterior credible interval. Family-specific effects that were significantly different from zero (i.e., credible interval did not contain zero) are shown in red.

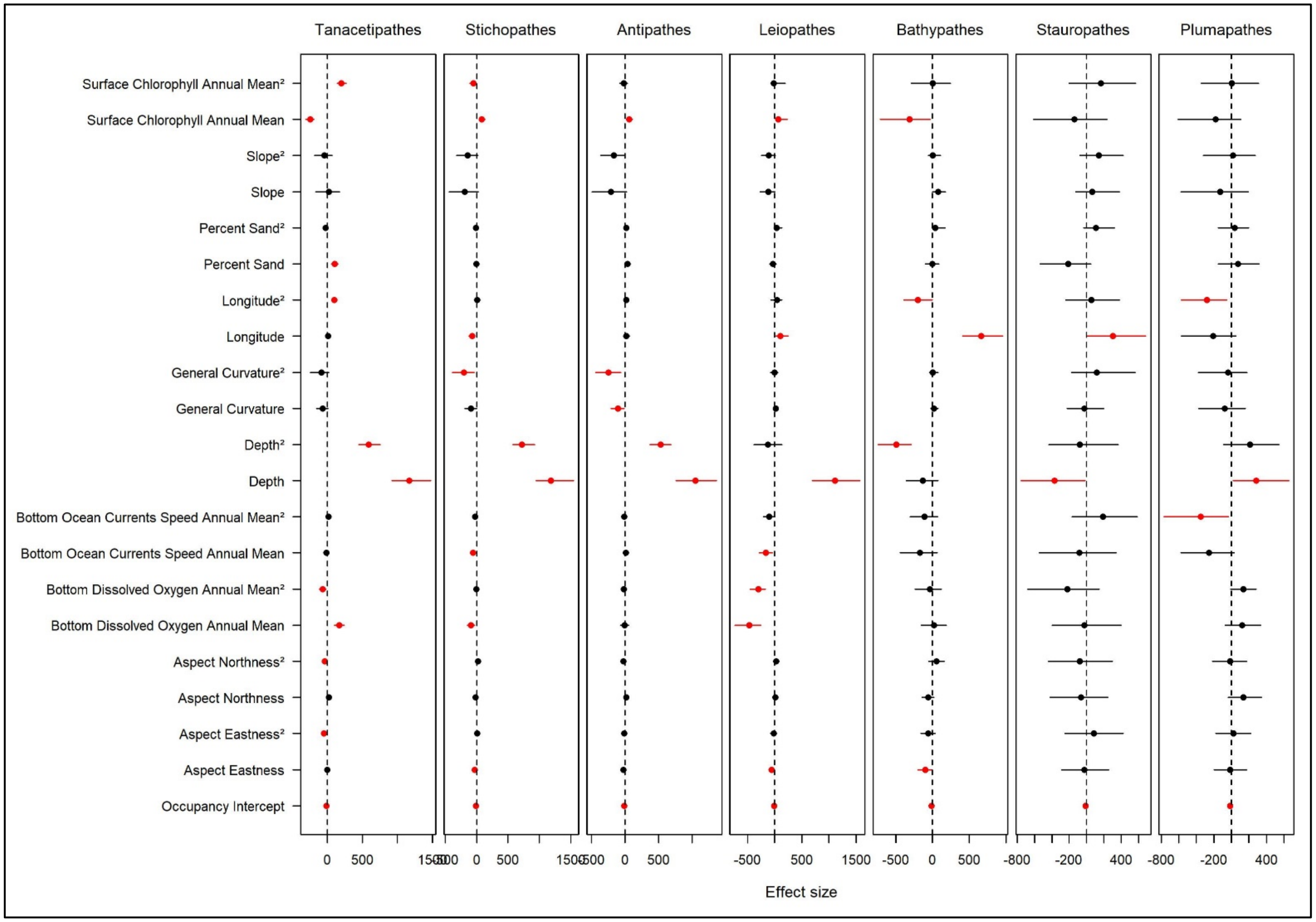

Figure 164. Effect size of predictors for black corals (order Antipatharia).

Genera within order Antipatharia are listed from left to right in decreasing order of frequency observed. The 21 terms of the occupancy model (state process) are shown on the y-axis, including the occupancy intercept and both the main effects of the 10 predictors and their quadratic (i.e., squared) terms. The x-axis shows the effect size for that predictor, indicating whether effects were more positive (right of zero) or negative (left of zero) for each genus. Effect sizes appear large because their values correspond to orthogonal scales used to standardize the predictors. Dots indicate posterior mean effect estimates and lines indicate the 95% posterior credible interval. Genus-specific effects that were significantly different from zero (i.e., credible interval did not contain zero) are shown in red.

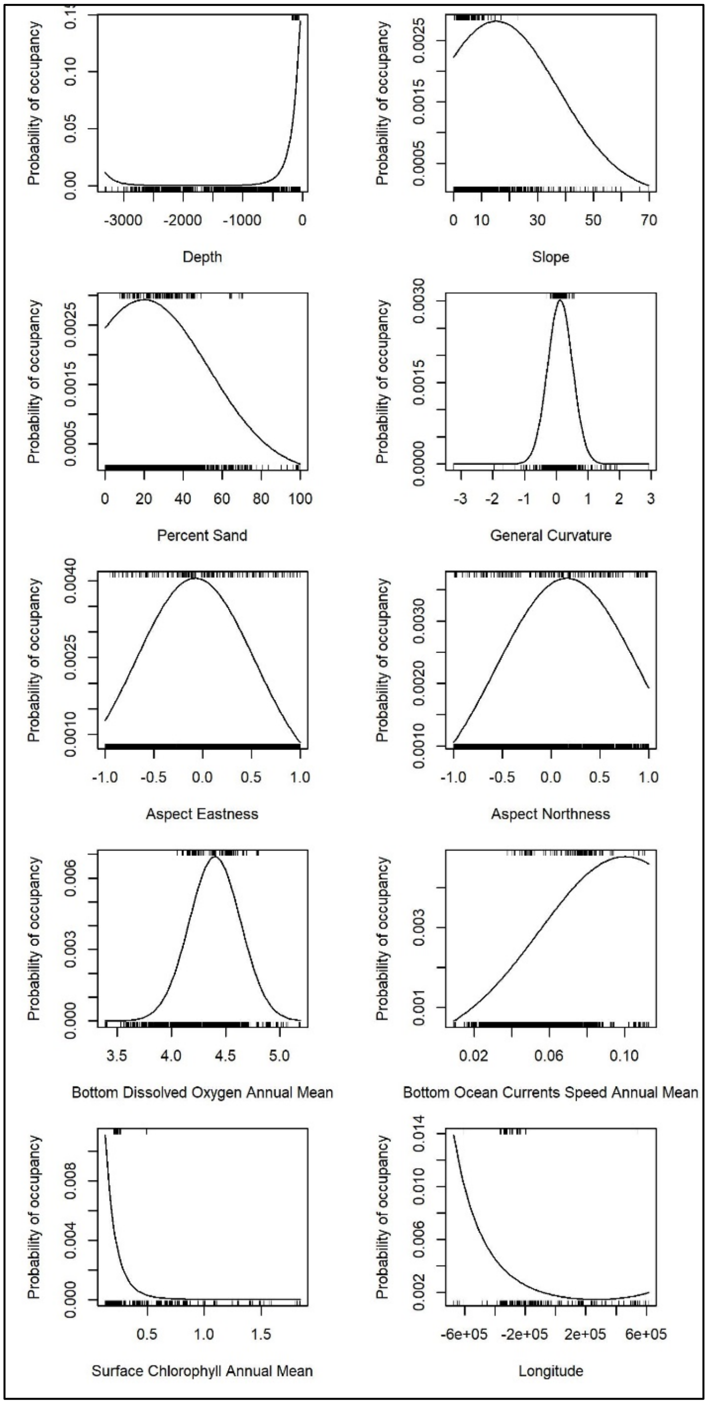

Figure 165. Marginal effects of predictors on the predicted probability of occurrence for the stony coral *Madracis* (order Scleractinia).

The y-axes show the predicted mean probability of occurrence (i.e., the predicted posterior mean occupancy probability) for *Madracis*, and the x-axes indicate the values of each predictor. This marginal effects plot should be interpreted with caution because it illustrates the estimated effect of each predictor while all others are set at their mean value; i.e., each plot ignores the realized range of effects from all predictors. Hash marks (i.e., rug plots) indicate the sampled predictor values at which *Madracis* was observed present (top) or absent (bottom).

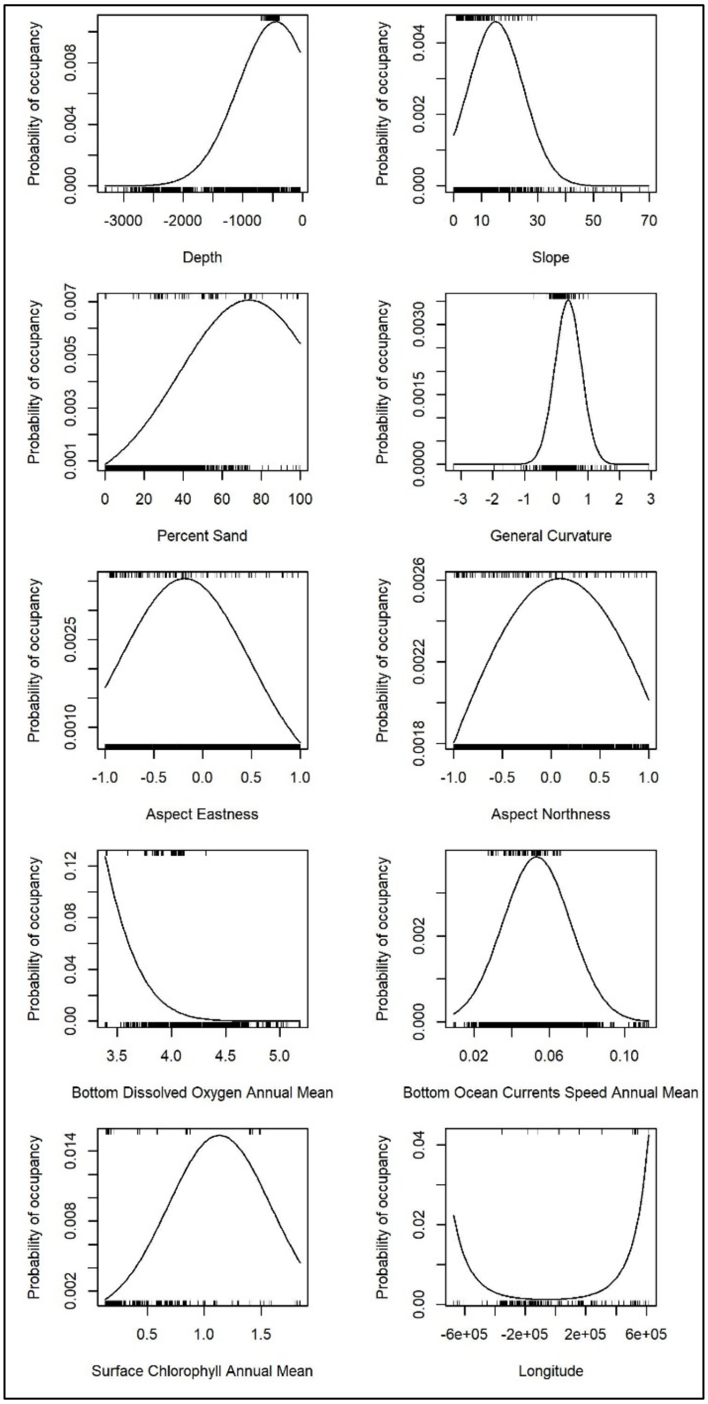

Figure 166. Marginal effects of predictors on the predicted probability of occurrence for the stony coral *Lophelia pertusa* (order Scleractinia).

The y-axes show the predicted mean probability of occurrence (i.e., the predicted posterior mean occupancy probability) for *L. pertusa*, and the x-axes indicate the values of each predictor. This marginal effects plot should be interpreted with caution because it illustrates the estimated effect of each predictor while all others are set at their mean value; i.e., each plot ignores the realized range of effects from all predictors. Hash marks (i.e., rug plots) indicate the sampled predictor values at which *L. pertusa* was observed present (top) or absent (bottom).

4. Conclusion

In this study, predictive modeling was used to synthesize information from deep-sea surveys spanning 31 years into a new database of deep-sea coral (DSC) and chemosynthetic community occurrences (presences and absences) in the US Gulf of Mexico (Gulf) and to predict the spatial distributions of selected taxa across the region on the basis of estimated environmental relationships. The modeling approach used (i.e., occupancy modeling) had several advancements over the previous regional modeling effort for deep-sea taxa and communities in the Gulf (Kinlan et al. 2013). First, the spatial resolution of the model predictions (100 x 100 m) was finer than that of previous regional models (~370 x 370 m), providing more detailed information for management. Second, the modeling employed here incorporated absence data which allowed the estimation of absolute probabilities of occurrence rather than relative measures of habitat suitability that previous presence-only models provided (Winship et al. 2020). The occupancy modeling technique in particular attempted to distinguish true from false absences thereby accounting for imperfect detection and providing estimates of the true probability of occurrence (Kéry and Royle 2016). Third, some of the models were hierarchical and modeled the distributions of multiple taxa simultaneously, which statistically allowed for the modeling of rare taxa (Zipkin et al. 2009). Fourth, the precision (i.e., variability) of the model predictions was estimated which provides measures of confidence or uncertainty associated with the predicted probabilities of occurrence in any given area.

The modeling advancements were more demanding in terms of data requirements. For example, ideally the occupancy modeling framework used here would be applied to well-balanced data with each survey covering every site and similar numbers of data replicates per site. However, the cost and logistics of deep-sea surveys are such that systematic region-wide surveys are not feasible, so databases like that compiled here entail substantial sampling heterogeneity and some data imbalances. As a result, it was sometimes challenging to estimate detection and occupancy probabilities, so model estimates of these quantities should be interpreted with proper attention to their associated estimates of uncertainty (e.g., predicted coefficient of variation [CV] of probability of occurrence). To the extent possible, future modeling would benefit from data collected using more systematic survey designs. Temporally replicated survey transects operated from different perspectives (e.g., in opposing directions) would provide additional information to help estimate detection probabilities. The authors of this study were not aware of any previous models of DSC or chemosynthetic community occurrence that used occupancy modeling. Addition research on this approach for modeling deep-sea taxa would be beneficial, e.g. to determine if there is some minimum number of replicate samples per grid cell below which the data are insufficient to provide good estimates of occupancy, especially if there is a high rate of false absences because only a small fraction of each site has been sampled. Although the models used here require presence-absence data, the large number of historical presence-only records collected throughout the Gulf (e.g., in the NOAA National Database) could potentially boost the effective sample size if they could be used in an integrated modeling framework along with the presence-absence data (Fithian et al. 2015; Gelfand and Shirota 2019). It would be beneficial to compare the predictions from the occupancy models to predictions from other presence-absence approaches (e.g., generalized additive models, boosted regression trees) that have been used to model DSC occurrence in other places (e.g., Rooper et al. 2017; Georgian et al. 2019).

The models presented in this study took advantage of the presence-absence records compiled for the study and the increased availability of high-resolution bathymetry and ocean model data; however, there are still data limitations that need to be considered. First, though efforts were made to incorporate sample data that was as evenly distributed across the planning areas and depth zones as possible, there have been fewer surveys collected in the western and eastern Gulf compared to the central Gulf and far more surveys have been collected at mesophotic depths than in the upper bathyal and lower bathyal zones. In addition, while the models incorporated environmental data that was not available for previous regional models, there are still improvements that can be made to the environmental predictors. Selecting the best spatial scale at which to analyze deep-sea biota is an ongoing area of research and involves several considerations and tradeoffs (Scales et al. 2017; Frishkoff et al. 2019). For example, analyzing data at a resolution that is too coarse could dilute any fine-scale habitat relationships, such as at bioherms (i.e., mounds of DSC and/or chemosynthetic communities). On the other hand, analyzing data at a resolution that is too fine would result in fewer spatial replicates and reduce the power of estimating detectability. Ideally, high-resolution bathymetry data (e.g., collected using multibeam acoustic sonar) should be used to capture the fine-scale features on the seafloor that may provide habitat for deep-sea biota (Winship et al. 2020). This study included extensive coverage of high-resolution bathymetry data (Appendix C), but this only accounted for approximately 57% of the study area. As a result, depth and seafloor topography variables could not delineate finer-scale features (e.g., those indicative of exposed hard substrate) in areas where there were not high-resolution bathymetry data. Collection of additional data using multibeam sonar surveys and expansion of the Bureau of Ocean Energy Management (BOEM) deepwater bathymetry grid would improve these predictors for future models of deep-sea biota. Maps of the existing coverage of high-resolution bathymetry (Figure 3) can be used to identify targets for future mapping surveys. Environmental predictor variables representing seafloor substrate were limited to measures of surficial sediment characteristics interpolated from fairly sparse (particular in deeper waters) sediment grab samples. Additional sampling could improve the characterization of surficial sediments. Modeling efforts at sub regional extents (e.g., Silva and MacDonald 2017 in the Gulf) have used acoustic backscatter data and benthic habitat maps derived from backscatter data to represent locations with hard substrate in models. However, the interpretation of acoustic backscatter data is not perfect (e.g., in addition to exposed hard rock, deposits of sand and gravel might also provide high backscatter reflectance values; Silva and MacDonald 2017) and creating a composite of acoustic backscatter collected by different multibeam surveys (e.g., the many multibeam datasets used in the bathymetry synthesis) would be far more challenging and costly than the creation of the bathymetry synthesis for this study. Georgian et al. (2020) used the BOEM seismic anomalies dataset to create an environmental predictor representing locations with hard substrate, but currently the BOEM seismic anomalies dataset does not include all of the eastern Gulf of Mexico within the study area and could not be used in this modeling effort. Expansion of the geographic footprint of the seismic anomalies dataset would be beneficial for future models of both DSCs and chemosynthetic communities. Environmental predictor variables depicting measures of oceanography were primarily derived from remotely sensed data or ocean models because in situ measures of ocean water properties at or near the seafloor are limited. Datasets derived from remote sensing and ocean models may have insufficient resolution to depict fine-scale patterns that may be important for estimating relationships between these oceanographic measures and the occurrence of deep-sea biota.

The maps presented in this report provide information about the observed and predicted distributions of individual DSC taxa and chemosynthetic communities across the study area in the Gulf. For each taxon or community, the maps depict the presence or absence at sample locations in the database compiled for this study and model predictions (mean and CV) of the probability of occurrence across the study area at a spatial grid resolution of 100 x 100 m. For multi-taxon models, maps are also presented that depict the predicted taxon richness (i.e., the number of taxa expected to occur at each grid cell) for the taxa included in the model. Such information could be used for example to plan activities in areas where the predicted probability of occurrence for some taxon or taxa of interest or the predicted taxon richness was below a specific threshold.

The maps presented here can themselves be used to inform future data collection for the purposes of validating the model predictions and developing future models. For model validation and ground truthing, areas where taxon richness was estimated to be high but sampling effort was low (e.g., the northern and southern sections of the west Florida slope, the ‘sticky grounds’ off Florida, west of the Sigsbee Escarpment) should be given high priority. The maps of prediction variability and the environmental predictor mask revealed areas that would benefit from more survey effort because environmental conditions in those areas were outside the range of sampled data, resulting in model extrapolation. Locations where there were particularly large areas in the environmental predictor mask, including the region with high surface chlorophyll-a concentration within a radius of approximately 50 km of the Mississippi River Delta, the northern part of the west Florida slope to the southeast of De Soto Canyon, and the continental slope off Texas, should be given high priority. Such efforts would help reduce areas of extrapolation for future models. Moreover, while it is seemingly less intuitive to sample areas with expected absences of coral, absence data are just as important as presence data when predicting to unsampled areas. Therefore, the use of a stratified survey design for even sampling of environmental gradients is strongly recommended (Hirzel and Guisan 2002; Williams and Brown 2019).

The maps presented in this report and associated digital data products can be used to support environmental risk assessments, environmental impact statements, and other decision documents related to the review of proposed activities in the US Gulf of Mexico. In addition, it is hoped that these maps and products will also be used to inform other aspects of marine resource management for the region, including fisheries management and future research and exploration. The analyses and products presented in this report were not designed to replace, but rather to help inform, additional analyses required by law under the National Environmental Policy Act (NEPA) and other environmental statutes. For more information about how these products may be used, please see the BOEM Gulf of Mexico OCS Region (https://boem.gov/regions/gulf-mexico-ocs-region), the BOEM Environmental Studies Program (https://www.boem.gov/environmental-studies), or the BOEM Office of Public Affairs (https://www.boem.gov/newsroom).

References

BOEM. 2019. Seismic water bottom anomalies map gallery [dataset]. New Orleans (LA): US Department of the Interior, Bureau of Ocean Energy Management, Gulf of Mexico OCS Region; [accessed 25 Oct 2020]. https://www.boem.gov/oil-gas-energy/mapping-and-data/map-gallery/seismic-water-bottom-anomalies-map-gallery.

Boland GS, Etnoyer PJ, Fisher CR, Hickerson EL. 2017. Chapter 11: state of deep-sea coral and sponge ecosystems of the Gulf of Mexico region. In: Hourigan T, Etnoyer P, Cairns S, editors. The state of deep-sea coral and sponge ecosystems of the United States: 2017. Silver Spring (MD): National Ocean and Atmospheric Administration, National Marine Fisheries Service. 467 p. Report No.: NOAA Technical Memorandum NMFS-OHC-4. p. 319–378.

Brooke S, Schroeder WW. 2007. Chapter 7: state of deep coral ecosystems in the Northern Gulf of Mexico region: Florida Straits to Texas. In: Lumsden SE, Hourigan TF, Bruckner AW, Dorr G, editors. The state of deep coral ecosystems of the United States: 2007. Silver Spring (MD): National Ocean and Atmospheric Administration, Coral Reef Conservation Program. 365 p. Report No.: NOAA Technical Memorandum CRCP 3. p. 271–306.

Brooks JM, Kennicutt MC, Fay RR, McDonald TJ, Sassen R. 1984. Thermogenic gas hydrates in the Gulf of Mexico. Science. 225:409–411.

Brooks JM, Kennicutt MC, Fisher CR, Macko SA, Cole K, et al. 1987. Deep-sea hydrocarbon seep communities: evidence for energy and nutritional carbon sources. Science. 238:1138–1142.

Brooks JM, Fisher C, Roberts H, Bernard B, MacDonald I, et al. (TDI-Brooks Internal, Inc, College Station, TX). 2009. Investigations of chemosynthetic communities on the lower continental slope of the Gulf of Mexico: interim report 2. New Orleans (LA): US Department of the Interior, Minerals Management Service. 360 p. Contract No.: 1435-01-05-CT-39187 (M05PC00018). Report No.: OCS Study MMS 2009-046. [accessed 4 Jan 2020]; https://marinecadastre.gov/espis/#/search/study/239

Brooks JM, Fisher C, Cordes E, Baums I, Bernard B, et al. (TID-Brooks International, Inc., College Station, TX) 2016. Exploration and research of northern Gulf of Mexico deepwater natural and artificial hard-bottom habitats with emphasis on coral communities: reefs, rigs, and wrecks — "*Lophelia* II" final report, volume I: technical report. New Orleans (LA): US Department of the Interior, Bureau of Ocean Energy Management. 628 p. Contract No.: M08PC20028. Report No.: OCS Study BOEM 2016-021. [accessed 4 Jan 2020]; https://marinecadastre.gov/espis/#/search/study/27140

Buhl-Mortensen L, Vanreusel A, Gooday AJ, Levin LA, Priede IG, et al. 2010. Biological structures as a source of habitat heterogeneity and biodiversity on the deep ocean margins. Mar Ecol. 31(1):21–50.

Calabrese JM, Certain G, Kraan C, Dormann CF. 2014. Stacking species distribution models and adjusting bias by linking them to macroecological models. Glob Ecol Biogeogr. 23(1):99–112.

Charbonnel A, D'Amico F, Besnard A, Blanc F, Buisson L, et al. 2014. Spatial replicates as an alternative to temporal replicates for occupancy modelling when surveys are based on linear features of the landscape. J Appl Ecol. 51(5):1425–1433.

Conn PB, Johnson DS, Boveng PL. 2015. On extrapolating past the range of observed data when making statistical predictions in ecology. PLoS One. 10(10): e0141416.

Conn PB, Thorson JT, Johnson DS. 2017. Confronting preferential sampling when analysing population distributions: diagnosis and model-based triage. Methods Ecol Evol. 8(11):1535–1546.

Conn PB, Johnson DS, Williams PJ, Melin SR, Hooten MB. 2018. A guide to Bayesian model checking for ecologists. Ecol Monogr. 88(4):526–542.

Cordes EE, Carney SL, Hourdez S, Carney RS, Brooks JM, et al. 2007. Cold seeps of the deep Gulf of Mexico: community structure and biogeographic comparisons to Atlantic equatorial belt seep communities. Deep Sea Res Part I. 54:637–653.

Cordes EE, Cunha MR, Galéron J, Mora C, Olu-Le Roy K, et al. 2010. The influence of geological, geochemical, and biogenic habitat heterogeneity on seep biodiversity. Mar Ecol. 31:51–65.

Cordes EE, Arnaud-Haond S, Bergstad O-A, da Costa Falcão AP, Freiwald A, et al. 2016. Chapter 42–Cold-water corals. In: United Nations, editor. The first global integrated marine assessment: world ocean assessment I. Cambridge (GB): Cambridge University Press. p. 803–816.

Cressie NAC. 1993. Statistics for spatial data. revised ed. New York (NY): John Wiley & Sons. 900 p.

Cross VA, Twichell DC, Halley RB, Ciembronowicz KT, Jarrett BD, et al. 2005. GIS compilation of data collected from the Pulley Ridge deep coral reef region. Reston (VA): US Department of the Interior, US Geological Survey. Report No.: US Geological Survey Open-File Report 2005-1089.

Darnell RM, Defenbaugh RE. 1990. Gulf of Mexico: environmental overview and history of environmental research. Am Zool. 30:3–6.

Demopoulos AWJ, Ross SW, Kellogg CA, Morrison CL, Nizinski M, et al. 2017. Deepwater program: Lophelia II, continuing ecological research on deep-sea corals and deep-reef habitats in the Gulf of Mexico. Reston (VA): US Department of the Interior, US Geological Survey. 269 p. Report No.: US Geological Survey Open-File Report 2017-1139.

Dorazio RM, Royle JA. 2005. Estimating size and composition of biological communities by modeling the occurrence of species. J Am Stat Assoc. 100(470):389–398.

Dorazio RM, Royle JA, Söderström B, Glimskär A. 2006. Estimating species richness and accumulation by modeling species occurrence and detectability. Ecology. 87(4):842–854.

Du Preez C. 2015. A new arch-chord ratio (ACR) rugosity index for quantifying three-dimensional landscape structural complexity. Landsc Ecol. 30:181–192.

Elith J, Phillips SJ, Hastie T, Dudik M, Chee YE, Yates CJ. 2011. A statistical explanation of MaxEnt for ecologists. Divers Distrib. 17(1):43–57.

Etnoyer P, Cairns S. 2017. Deep-sea coral taxa in the US Gulf of Mexico: depth and geographical distribution. In: Hourigan T, Etnoyer P, Cairns S, editors. The state of deep-sea coral and sponge ecosystems of the United States: 2017. Silver Spring (MD): National Ocean and Atmospheric

Administration, National Marine Fisheries Service. 467 p. Report No.: NOAA Technical Memorandum NMFS-OHC-4.

Etnoyer PJ, Wagner D, Fowle HA, Poti M, Kinlan B, et al. 2018. Models of habitat suitability, size, and age-class structure for the deep-sea black coral *Leiopathes glaberrima* in the Gulf of Mexico. Deep Sea Res 2 Top Stud Oceanogr. 150:218–228.

Fithian W, Elith J, Hastie T, Keith DA. 2015. Bias correction in species distribution models: pooling survey and collection data for multiple species. Methods Ecol Evol. 6:424–438.

Flanders NP, Gardner B, Winiarski KJ, Paton PWC, Allison T, O'Connell AF. 2015. Key seabird areas in southern New England identified using a community occupancy model. Mar Ecol Prog Ser. 533:277–290.

Frishkoff LO, Mahler DL, Fortin M-J. 2019. Integrating over uncertainty in spatial scale of response within multispecies occupancy models yields more accurate assessments of community composition. Ecography. 42(12):2132–2143.

Gardner JV, Dartnell P, Sulak KJ. 2002a. Multibeam mapping of the West Florida Shelf, Gulf of Mexico. Reston (VA): US Department of the Interior, US Geological Survey. Report No.: US Geological Survey Open-File Report 02-005.

Gardner JV, Dartnell P, Sulak KJ. 2002b. Multibeam mapping of the Pinnacles region, Gulf of Mexico. Reston (VA): US Department of the Interior, US Geological Survey. Report No.: US Geological Survey Open-File Report 02-006.

Gardner JV, Beaudoin JD, Hughes Clarke JE, Dartnell P. 2002c. Multibeam mapping of selected areas of the outer continental shelf, northwestern Gulf of Mexico—data, images, and GIS. Reston (VA): US Department of the Interior, US Geological Survey. Report No.: US Geological Survey Open-File Report 02-411.

Gardner JV, Hughes Clarke JE, Mayer LA, Dartnell P. 2003. Bathymetry and acoustic backscatter of the mid and outer continental shelf, head of De Soto Canyon, northeastern Gulf of Mexico—data, images, and GIS. Reston (VA): US Department of the Interior, US Geological Survey. Report No.: US Geological Survey Open-File Report 03-007.

Gelfand AE, Shirota S. 2019. Preferential sampling for presence/absence data and for fusion of presence/absence data with presence-only data. Ecol Monogr. 89(3):e01372.

Gelman A, Rubin DB. 1992. Inference from iterative simulation using multiple sequences. Stat Sci. 7(4):457–472.

Georgian SE, Shedd W, Cordes EE. 2014. High-resolution ecological niche modelling of the cold-water coral *Lophelia pertusa* in the Gulf of Mexico. Mar Ecol Prog Ser. 506:145–161.

Georgian SE, Anderson OF, Rowden AA. 2019. Ensemble habitat suitability modeling of vulnerable marine ecosystem indicator taxa to inform deep-sea fisheries management in the South Pacific Ocean. Fish Res. 211:256–274.

Georgian SE, Kramer K, Saunders M, Shedd W, Roberts H, et al. 2020. Habitat suitability modelling to predict the spatial distribution of cold-water coral communities affected by the Deepwater Horizon oil spill. J Biogeogr. 47(7):1455–1466.

Guillera-Arroita G. 2011. Impact of sampling with replacement in occupancy studies with spatial replication. Methods Ecol Evol. 2(4):401–406.

Guinotte JM, Davies AJ. 2014. Predicted deep-sea coral habitat suitability for the US West Coast. PLoS One 9(4):e93918.

Hine AC, Brooks GR, Davis RA, Duncan DS, Locker SD, Twichell DC, Gelfenbaum G. 2003. The west-central Florida inner shelf and coastal system: a geologic conceptual overview and introduction to the special issue. Mar Geol. 200:1–17.

Hijmans RJ. 2019. raster: geographic analysis and modeling. R package version 2.8-19; [accessed 25 Oct 2020]. https://cran.r-project.org/web/packages/raster/index.html.

Hirzel A, Guisan A. 2002. Which is the optimal sampling strategy for habitat suitability modelling? Ecol Modell. 157(2):331–341.

Hourigan TF, Etnoyer PJ, McGuinn RP, Whitmire C, Dorfman DS, et al. 2015. An introduction to NOAA's national database for deep-sea corals and sponges. Silver Spring (MD): National Oceanic and Atmospheric Administration, National Ocean Service, National Centers for Coastal Ocean Science. 27 p. Report No.: NOAA Technical Memorandum NOS NCCOS 191.

Hourigan TF, Etnoyer PJ, Cairns SD. 2017. The state of deep-sea coral and sponge ecosystems of the United States. Silver Spring (MD): National Ocean and Atmospheric Administration, National Marine Fisheries Service. 467 p. Report No.: NOAA Technical Memorandum NMFS-OHC-4.

HYCOM Consortium. 2019. HYCOM + NCODA Gulf of Mexico 1/25° analysis [dataset]; [accessed 25 Oct 2020]; https://www.hycom.org/data/gomu0pt04.

Jenness J. 2013. DEM surface tools. Flagstaff (AZ): Jenness Enterprises; [accessed 25 Oct 2020]. http://www.jennessent.com/arcgis/surface_area.htm.

Jiménez-Franco MV, Kéry M, León-Ortega M, Robledano F, Esteve MA, et al. 2019. Use of classical bird census transects as spatial replicates for hierarchical modeling of an avian community. Ecol Evol. 9(2):825–835.

Kennicutt MC, Brooks JM, Bidigare RR, Fay RR, Wade TL, et al. 1985. Vent-type taxa in a hydrocarbon seep region on the Louisiana slope. Nature. 317:351–353.

Kennicutt MC, Brooks JM, Bidigare RR. 1988. Hydrocarbon seep communities: four years of study. Oceanography. 1(2):44–45.

Kéry M, Royle JA. 2008. Hierarchical Bayes estimation of species richness and occupancy in spatially replicated surveys. J Appl Ecol. 45(2):589–598.

Kéry M, Royle JA. 2016. Applied hierarchical modeling in ecology: analysis of distribution, abundance and species richness in R and BUGS, volume 1: prelude and static models. Boston (MA): Academic Press. 808 p.

Kinlan B, Poti M, Etnoyer P, Siceloff L, Jenkins C, et al. 2013. U.S. Gulf of Mexico deep sea coral habitat suitability models—digital data package [dataset]. Silver Spring (MD): National Oceanic and Atmospheric Administration, National Ocean Service, National Centers for Coastal Ocean Science; [accessed 25 Oct 2020]. https://nccospublicstor.blob.core.windows.net/projects-attachments/35/DSC_PredictiveModeling_US_Gulf_of_Mexico.zip.

Kinlan BP, Poti M, Drohan AF, Packer DB, Dorfman DS, et al. 2020. Predictive modeling of suitable habitat for deep-sea corals offshore the northeast United States. Deep Sea Res Part I. 158:103229.

Kramer KV, Shedd WW. 2017. A 1.4-billion-pixel map of the Gulf of Mexico seafloor. Eos. 98.

Lotze HK, Worm B. 2009. Historical baselines for large marine animals. Trends Ecol Evol. 24(5):254–262.

MacDonald IR, Boland GS, Baker JS, Brooks JM, Kennicutt MC, et al. 1989. Gulf of Mexico hydrocarbon seep communities. Mar Biol. 101:235–247.

MacDonald IR, Sager WW, Peccini MB. 2003. Gas hydrate and chemosynthetic biota in mounded bathymetry at mid-slope hydrocarbon seeps: Northern Gulf of Mexico. Mar Geol. 198:133–158.

MacKenzie DI, Nichols JD, Lachman GB, Droege S, Royle JA, et al. 2002. Estimating site occupancy rates when detection probabilities are less than one. Ecology. 83(8):2248–2255.

[MMS] Minerals Management Service. 2010. Notice to lessees and operators of federal oil, gas, and sulphur leases and pipeline right-of-way holders, outer continental shelf, Gulf of Mexico OCS Region. New Orleans (LA): Minerals Management Service (now BOEM); [accessed 25 Oct 2020]. https://www.boem.gov/sites/default/files/regulations/Notices-To-Lessees/2009/09-G40.pdf.

[NASA] National Aeronautics and Space Administration. 2019. OceanColor web. Greenbelt (MD): National Aeronautics and Space Administration, Goddard Space Flight Center, Ocean Biology Processing Group; [accessed 25 Oct 2020]. https://oceancolor.gsfc.nasa.gov/.

[NCEI] National Centers for Environmental Information. 2004. Multibeam bathymetry database. Stennis Space Center (MS): National Oceanic and Atmospheric Administration, National Environmental Satellite, Data, and Information Service, National Centers for Environmental Information; [updated 1 Oct 2020; accessed 25 Oct 2020]. https://www.ngdc.noaa.gov/mgg/bathymetry/multibeam.html.

Newton CR, Mullins HT, Gardulski AF. 1987. Coral mounds on the West Florida Slope: unanswered questions regarding the development of deep-water banks. Palaios. 2(4):359–367.

[NOAA] National Oceanic and Atmospheric Administration. 2019. Notice of availability of the Deepwater Horizon oil spill open ocean trustee implementation group final restoration plan 2 and environmental assessment: fish, sea turtles, marine mammals, and mesophotic and deep benthic communities and finding of no significant impact. Fed Regist. 84(12 Dec): 67929–67931.

[NOAA] National Oceanic and Atmospheric Administration. 2020a. Fisheries of the Caribbean, Gulf of Mexico, and South Atlantic; Atlantic highly migratory species; coral and coral reefs of the Gulf of Mexico; Amendment 9. Fed Regist. 85 (16 Oct): 65740–65749.

[NOAA] National Oceanic and Atmospheric Administration. 2020b. Proposed expansion of Flower Garden Banks National Marine Sanctuary. Fed Regist. 85 (May 1): 25359–25378.

[NOAA Fisheries] National Oceanic and Atmospheric Administration Fisheries. 2018 Coral habitat areas considered for habitat area of particular concern designation in the Gulf of Mexico. Final Amendment 9. Tampa (FL): Gulf of Mexico Fishery Management Council; [accessed 2020 Oct 25]. https://www.fisheries.noaa.gov/action/amendment-9-coral-habitat-areas-considered-management-gulf-mexico.

Open Ocean Trustee Implementation Group. 2019. *Deepwater Horizon* oil spill natural resource damage assessment, final restoration plan 2/environmental assessment: fish, sea turtles, marine mammals, and mesophotic and deep benthic communities; [accessed 25 Oct 2020]. https://www.gulfspillrestoration.noaa.gov/sites/default/files/2019-12%20OO%20TIG_RP2EA_PublicFinal_2019_signatures.pdf.

Paull CK, Hecker B, Commeau R, Freeman-Lynde RP, Neumann C, Corso WP, Golubic S, Hook JE, Sikes E, Curray J. 1984. Biological communities at the Florida Escarpment resemble hydrothermal vent taxa. Science. 226:965–967.

Petracca LS, Funston PJ, Henschel P, Cohen JB, Maclennan S, Frair JL. 2020. Modeling community occupancy from line transect data: a case study with large mammals in post-war Angola. Anim Conserv. 23(4):420–433.

Phillips SJ, Dudik M, Elith J, Graham CH, Lehmann A, Leathwick J, Ferrier S. 2009. Sample selection bias and presence-only distribution models: implications for background and pseudo-absence data. Ecol Appl. 19(1):181–197.

Pinheiro J, Bates D. 2004. Mixed-effects models in S and S-Plus. New York: Springer. 528 p.

Plummer M. 2018. Rjags: Bayesian graphical models using MCMC. R package version 4-8; [accessed 25 Oct 2020]. https://cran.r-project.org/web/packages/rjags/index.html.

R Core Team. 2018. R: A language and environment for statistical computing. version 3.5.2. Vienna (AT): R Foundation for Statistical Computing; [accessed 25 Oct 2020]. https://www.R-project.org/.

Roberts JM, Wheeler AJ, Freiwald A, Cairns S. 2009. Cold-water corals: the biology and geology of deep-sea coral habitats. New York (NY): Cambridge University Press. 351 p.

Rooper CN, Zimmerman M, Prescott MM. 2017. Comparison of modeling methods to predict the spatial distribution of deep-sea coral and sponge in the Gulf of Alaska. Deep Sea Res Part I. 126:148–161.

Rowe GT, Kennicutt MC, editors (Texas A&M University, College Station, TX). 2009. Northern Gulf of Mexico continental slope habitats and benthic ecology study: final report. New Orleans (LA): US Department of the Interior, Minerals Management Service. 417 p. Contract No.: 1435-01-99-CT-30991 (M99PC0001). Report No.: OCS Study MMS 2009-039; [accessed 4 Jan 2021]. https://marinecadastre.gov/espis/#/search/study/157

Ross SW, Rhode M, Brooke S. 2017. Deep-sea coral and hardbottom habitats on the west Florida slope, eastern Gulf of Mexico. Deep Sea Res I. 120:14–28.

Royle JA, Chandler RB, Yackulic C, Nichols JD. 2012. Likelihood analysis of species occurrence probability from presence-only data for modelling species distributions. Methods Ecol Evol. 3(3):545–554.

Sadoti G, Zuckerberg B, Jarzyna MA, Porter WF. 2013. Applying occupancy estimation and modelling to the analysis of atlas data. Divers Distrib. 19(7):804–814.

Scales KL, Hazen EL, Jacox MG, Edwards CA, Boustany AM, et al. 2017. Scale of inference: on the sensitivity of habitat models for wide-ranging marine predators to the resolution of environmental data. Ecography. 40(1):210–220.

Schroeder WW. 1992. Observations of *Lophelia pertusa* and the surficial geology at a deep-water site in the northeastern Gulf of Mexico. Hydrobiol. 471:29–33.

Silva M, MacDonald IR. 2017. Habitat suitability modeling for mesophotic coral in the northeastern Gulf of Mexico. Mar Ecol Prog Ser. 583:121–136.

Srivathsa A, Puri M, Kumar NS, Jathanna D, Karanth KU. 2018. Substituting space for time: empirical evaluation of spatial replication as a surrogate for temporal replication in occupancy modelling. J Appl Ecol. 55(2):754–765.

Sterne TK, Retchless D, Allee R, Highfield W. 2020. Predictive modelling of mesophotic habitats in the north-western Gulf of Mexico. Aquat Conserv Mar Freshwater Ecosyst. 30(4):846–859.

Sulak KJ, Randall MT, Luke KE, Norem AD, Miller JM, editors. 2008. Characterization of northern Gulf of Mexico deepwater hard bottom communities with emphasis on *Lophelia* coral–*Lophelia* reef megafaunal community structure, biotopes, genetics, microbial ecology, and geology (2004–2006). Reston (VA): US Department of the Interior, US Geological Survey. 42 p. Report No.: US Geological Survey Open-File Report 2008-1148 and OCS Study MMS 2008-015. [accessed 4 Jan 2021]. https://pubs.er.usgs.gov/publication/ofr20081148

Tobler W. 1970. A computer movie simulating urban growth in the Detroit region. Econ Geogr. 46:234–240.

Valavi R, Elith J, Lahoz-Monfort JJ, Guillera-Arroita G. 2019. blockCV: an R package for generating spatially or environmentally separated folds for k-fold cross-validation of species distribution models. Methods Ecol Evol. 10(2):225–232.

Vierod ADT, Guinotte JM, Davies AJ. 2014. Predicting the distribution of vulnerable marine ecosystems in the deep sea using presence-background models. Deep Sea Res Part II. 99:6–18.

Weatherall P, Marks KM, Jakobsson M, Schmitt T, Tani S, Arndt JE, Rovere M, Chayes D, Ferrini V, Wigley R. 2015. A new digital bathymetric model of the world's oceans. Earth Space Sci. 2(8):331–345.

Williams BK, Brown ED. 2019. Sampling and analysis frameworks for inference in ecology. Methods Ecol Evol. 10(11):1832–1842.

Williams SJ, Flocks J, Jenkins C, Khalil S, Moya J. 2012. Offshore sediment character and sand resource assessment of the northern Gulf of Mexico, Florida to Texas. J Coast Res. 60:30–44.

Wiltshire KH, Tanner JE, Althaus F, Sorokin SJ, Williams, A. 2018. Predicting environmental suitability for key benthic species in an ecologically and environmentally important deep-sea environment. Deep Sea Res 2 Top Stud Oceanogr. 157–158:121–133.

Winship AJ, Thorson JT, Clarke ME, Coleman HM, Costa B, et al. 2020. Good practices for species distribution modeling of deep-sea corals and sponges for resource management: data collection, analysis, validation, and communication. Front Mar Sci. 7:303.

WoRMS Editorial Board. 2020. World register of marine species. Ostend (BE): Flanders Marine Institute; [accessed 25 Oct 2020]. https://www.marinespecies.org.

Zipkin EF, DeWan A, Royle JA. 2009. Impacts of forest fragmentation on species richness: a hierarchical approach to community modelling. J Appl Ecol. 46(4):815–822.

Zipkin EF, Royle JA, Dawson DK, Bates S. 2010. Multi-species occurrence models to evaluate the effects of conservation and management actions. Biol Conserv. 143(2):479–484.

Zipkin EF, Grant EHC, Fagan WF. 2012. Evaluating the predictive abilities of community occupancy models using AUC while accounting for imperfect detection. Ecol Appl. 22(7):1962–1972.

Zuur AF, Ieno EN, Elphick CS. 2010. A protocol for data exploration to avoid common statistical problems. Methods Ecol Evol. 1(1):3–14.

A Appendix A: Survey datasets included in the synthesis of DSC and chemosynthetic community observations

A.1 Carney & Roberts Benthic Seeps (1988, 1989–1997, 1990)

Data Providers: BOEM

Principal Investigators: Robert Carney, Harry Roberts (Louisiana State University)

Year Range: 1988–1997

Vessel: R/V *Atlantis*

Vehicles (Vehicle Type): *Pisces* (HOV), *Johnson Sea Link I* (HOV), *Alvin* (HOV)

Observation Type: HOV transects (continuous)

BOEM Gulf of Mexico Planning Areas: Western, Central

Depth Zones: Mesophotic, Upper Bathyal, Lower Bathyal

Depth Range: 65–2,246 m

Dives: 141

Sites: 98

Segments: 1,875

Total Area: 50,346 m^2

Three datasets were included from this multi-year investigation. The objective of the fieldwork was to observe and sample the benthic biology and geology of seep sites. Video of the seafloor was collected by submersible cameras in various analog formats, was digitized to computer readable video files, and was archived as DVDs. Although the spatial coverage of this investigation was extensive, georeferenced information was coarse. Position was derived only from a single ship position during vehicle deployment. The areal coverage was estimated by camera frame width, and duration of surveys. Regardless of coarse coverage, these datasets were valuable due to coverage of 48 different lease block areas. A total of 3,223 clips of 5-minute duration each, representing a total of 280 hours of bottom time, comprise the digital video data archive. Chemosynthetic phenomena were previously annotated, but coral colonies were not identified. The species identification work was performed by biologists at NOAA.

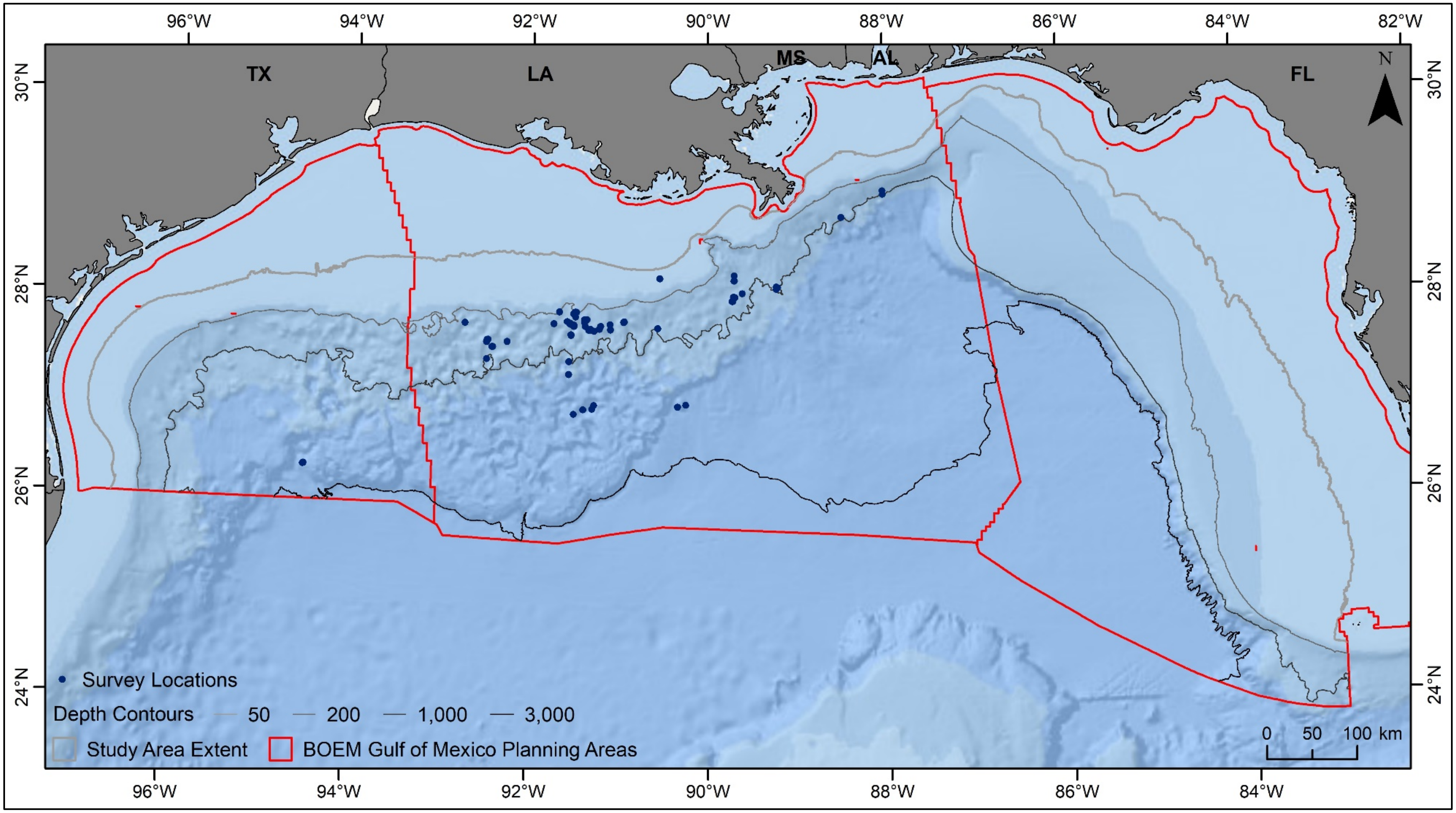

Figure A-1. Survey locations in the Carney & Roberts Benthic Seeps datasets (1988, 1989–1997, 1990).

A.2 MS-AL Pinnacle Trend Ecosystem Monitoring (MAPTEM)

Data Provider: Ian MacDonald (Florida State University)

Principal Investigators: Ian MacDonald (Florida State University), Mauricio Silva (Florida State University)

Year Range: 1997–1999

Vessel: R/V *Tommy Munro*

Vehicle (Vehicle Type): SeaROVER (ROV)

Observation Types: ROV transects, still images

BOEM Gulf of Mexico Planning Areas: Central

Depth Zones: Mesophotic

Depth Range: 57–97 m

Dives: 15

Sites: 34

Segments: 1,176

Total Area: 353 m^2

This area was chosen for monitoring based on the hard bottom community structure and dynamics. The potential sensitivity of these communities to oil and gas industry activities was of interest to the US Department of the Interior Minerals Management Service (now BOEM). The goal was benthic habitat characterization to describe and monitor biological communities and environmental conditions along the Pinnacle Trend reef carbonate mounds. All corals were identified by Mauricio Silva from still images obtained from ROV video.

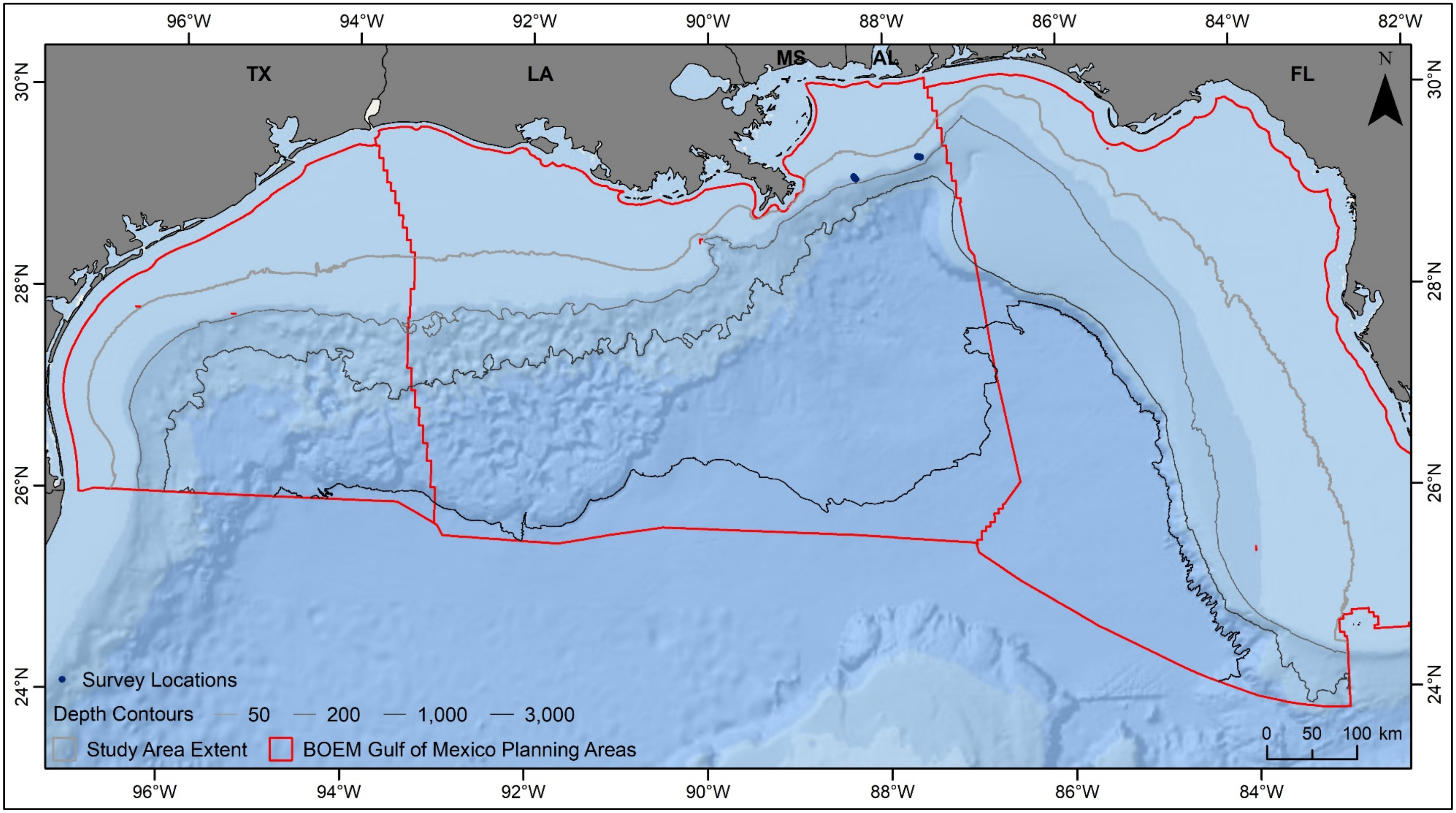

Figure A-2. Survey locations in the MS-AL Pinnacle Trend Ecosystem Monitoring dataset.

A.3 Deep Slope Chemosynthetic

Data Provider: NOAA Office of Ocean Exploration and Research (OER)

Principal Investigators: Charles Fisher (Pennsylvania State University)

Year Range: 2007

Vessel: NOAA Ship *Ronald H. Brown*

Vehicle (Vehicle Type): *Jason II* (ROV)

Observation Types: ROV photos, biological specimens

BOEM Gulf of Mexico Planning Areas: Western, Central

Depth Zones: Upper Bathyal, Lower Bathyal

Depth Range: 942–2,942 m

Dives: 16

Sites: 423

Segments: 7,821

Total Area: 58,658 m^2

The primary purpose of this research cruise was to use ROV *Jason* to conduct near bottom and photographic surveys of the prime sampling sites identified during a previous cruise. Targets for this mission were determined to have high likelihood of deep-sea chemosynthetic phenomena. The area surveyed was estimated from the image frame of the photographic record of two fixed cameras (Brow cam, Pilot cam). A third camera (Sci cam) was used for closer visualization of organisms, to aid taxonomic identification. Some organisms were identified to species level, aided by morphological identification of specimens collected, and documented in the cruise reports and Smithsonian NMNH records. Photographic observations were identified to family or genus level when appropriate or assigned the species ID of the voucher specimen.

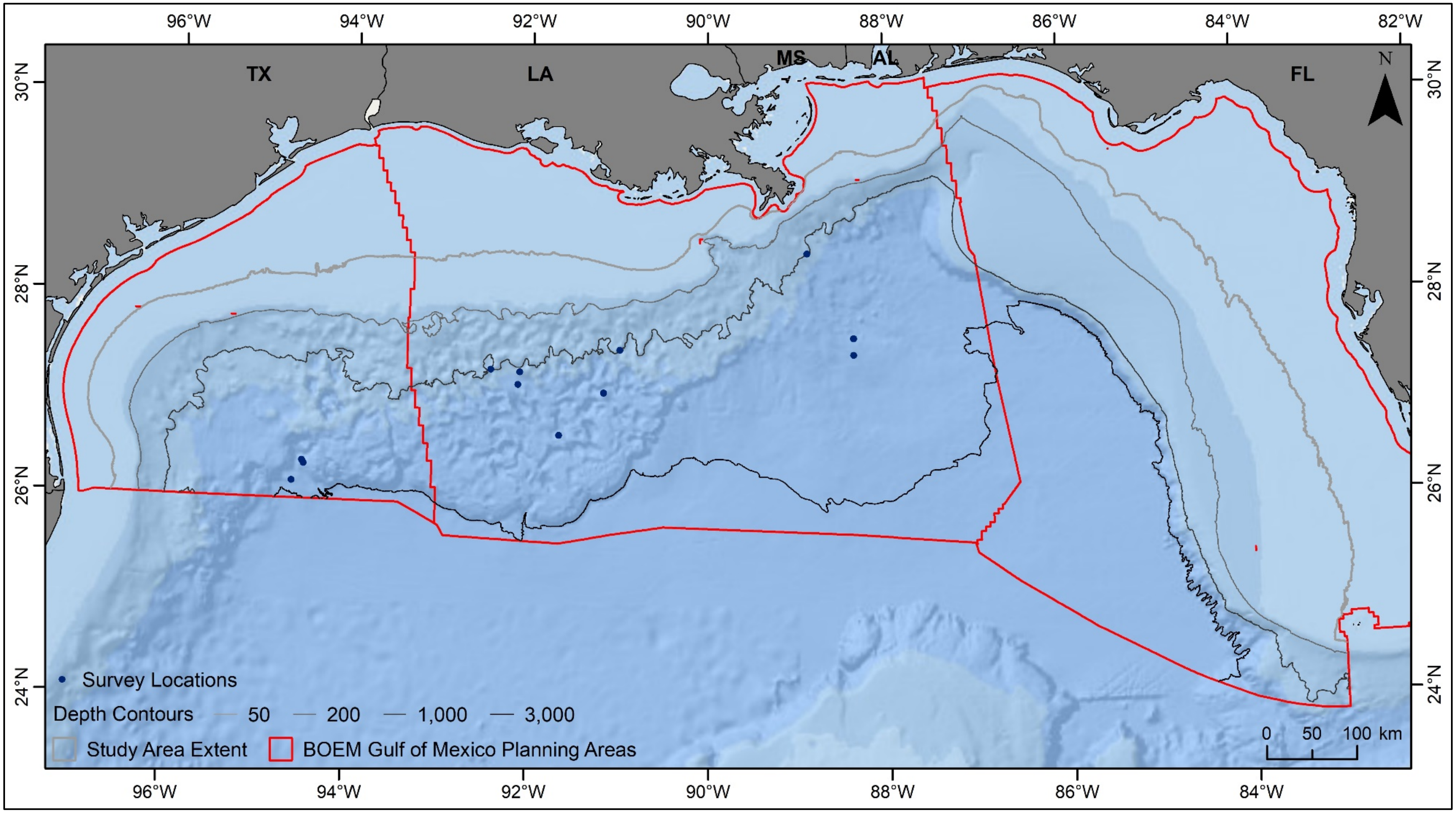

Figure A-3. Survey locations in the Deep Slope Chemosynthetic dataset.

A.4 Lophelia II 2008

Data Provider: Erik Cordes (Temple University), BOEM

Principal Investigators: Erik Cordes (Temple University), Robert Church (C & C Technologies)

Year Range: 2008

Vessel: NOAA Ship *Nancy Foster*

Vehicle (Vehicle Type): SeaEye Falcon (ROV)

Observation Types: ROV transects (exploratory)

BOEM Gulf of Mexico Planning Areas: Central

Depth Zones: Upper Bathyal

Depth Range: 250–800 m

Dives: 7

Sites: 47

Segments: 74

Total Area: 4,927 m^2

This was a multi-year investigation including five cruises from 2008–2012. This dataset is for the second leg of the first cruise, which took place in 2008. The first leg was used to characterize shipwreck sites and was not included in this dataset. The objective of the fieldwork was to obtain a robust predictive capability for the occurrence of rich cnidarian (primarily scleractinian coral) hard-ground communities in the deep Gulf of Mexico. Video of the seafloor was collected for this dataset by submersible cameras in standard definition, digitized to computer readable video files, and archived on hard drives. Although the spatial coverage of this dataset was extensive, georeferenced information was coarse due to missing navigation data. However, it was still a highly valuable dataset for this study. The areal coverage was estimated by camera frame width and duration of surveys. The species identification work was performed by biologists at NOAA.

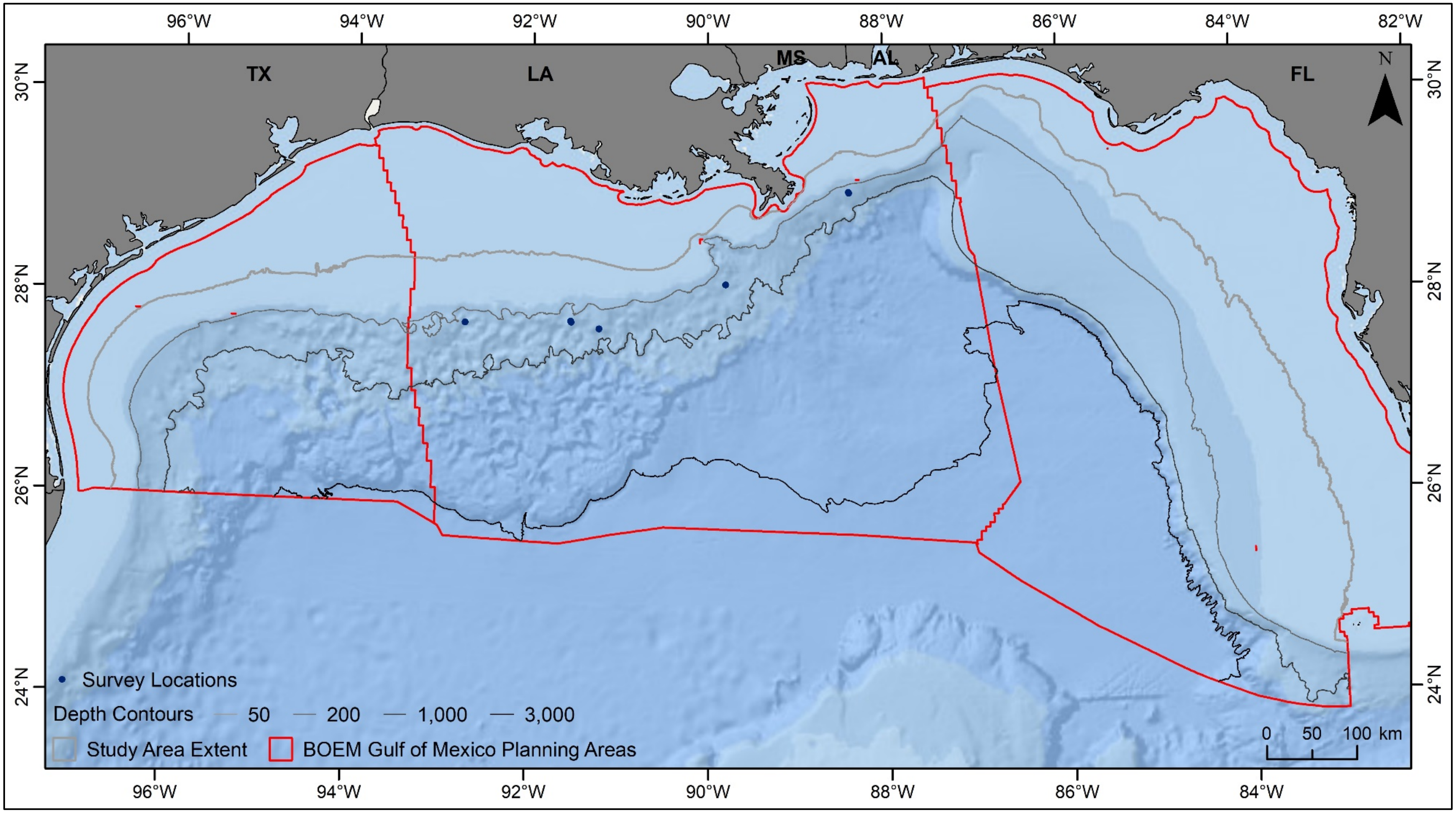

Figure A-4. Survey locations in the Lophelia II 2008 dataset.

A.5 Lophelia II 2009

Data Providers: Erik Cordes (Temple University), BOEM

Principal Investigators: Erik Cordes (Temple University), Charles Fisher (Pennsylvania State University)

Year Range: 2009

Vessel: NOAA Ship *Ronald H. Brown*

Vehicle (Vehicle Type): *Jason II* (ROV)

Observation Types: ROV transects (exploratory)

BOEM Gulf of Mexico Planning Areas: Western, Central, Eastern

Depth Zones: Upper Bathyal, Lower Bathyal

Depth Range: 400–2,455 m

Dives: 14

Sites: 69

Segments: 161

Total Area: 1,569 m^2

This was a multi-year investigation including five cruises from 2008–2012. This dataset is for the third cruise, which took place in fall 2009. Five dives took place on shipwrecks and were not included in this dataset. The objective of the fieldwork was to obtain a robust predictive capability for the occurrence of rich cnidarian (primarily scleractinian coral) hard-ground communities in the deep Gulf of Mexico. Video of the seafloor was collected for this dataset by submersible cameras in high definition, digitized to computer readable video files, and archived on hard drives. Although the spatial coverage of this dataset was extensive, georeferenced information was coarse due to missing navigation data. However, it was still a highly valuable dataset for this study. The areal coverage was estimated by camera frame width and duration of surveys. The species identification work was performed by biologists at NOAA.

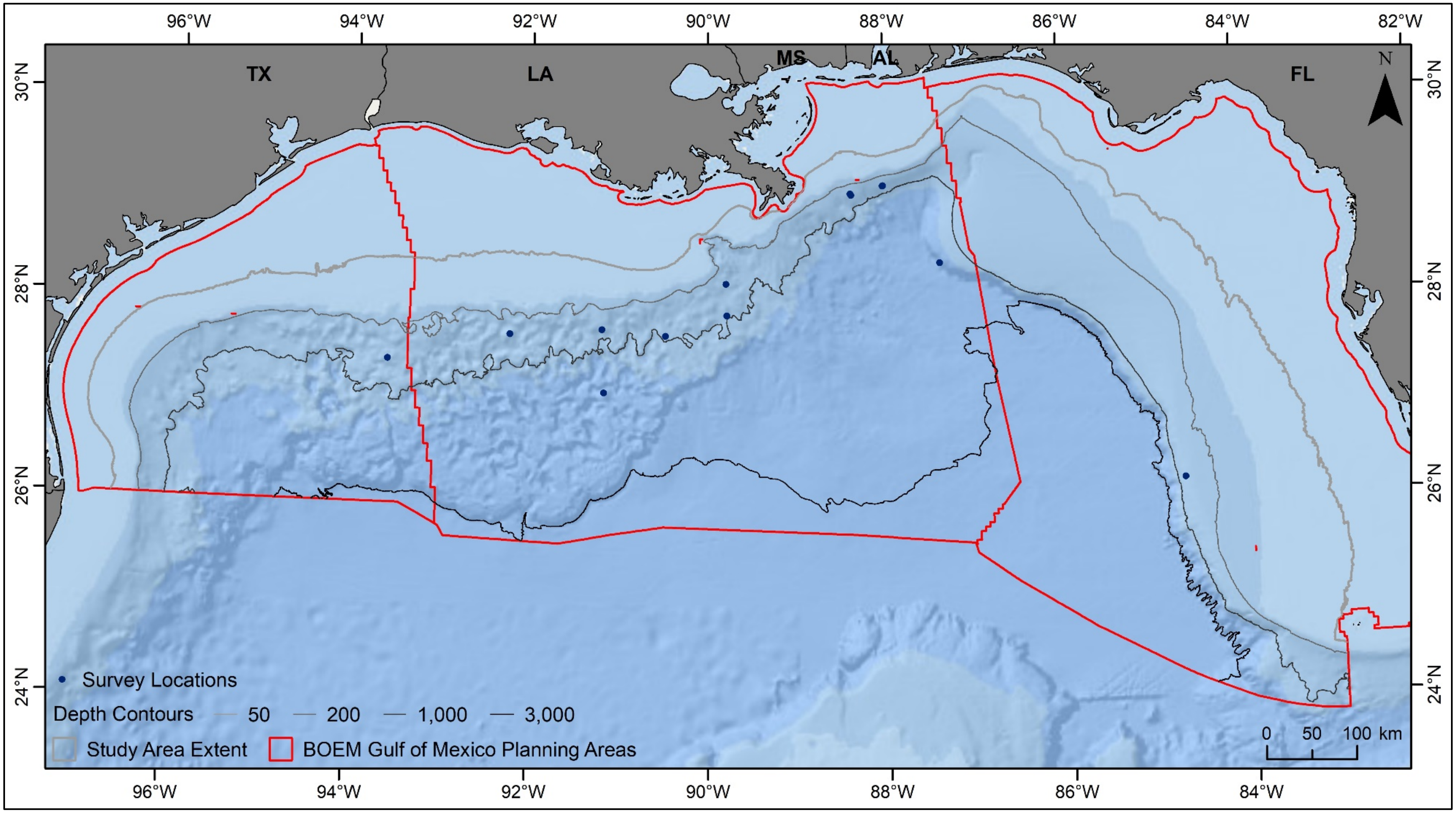

Figure A-5. Survey locations in the Lophelia II 2009 dataset.

A.6 Lophelia II 2010

Data Providers: Erik Cordes (Temple University), BOEM

Principal Investigators: Erik Cordes (Temple University), Charles Fisher (Pennsylvania State University)

Year Range: 2010

Vessel: NOAA Ship *Ronald H. Brown*

Vehicle (Vehicle Type): *Jason II* (ROV)

Observation Types: ROV transects (exploratory)

BOEM Gulf of Mexico Planning Areas: Western, Central

Depth Zones: Upper Bathyal, Lower Bathyal

Depth Range: 250–2,600 m

Dives: 15

Sites: 78

Segments: 128

Total Area: 2,131 m^2

This was a multi-year investigation including five cruises from 2008–2012. This dataset is for the fourth cruise, which took place in fall 2009. Seven previous sites from the third cruise were revisited as well as five sites never visited by ROV. The objective of the fieldwork was to obtain a robust predictive capability for the occurrence of rich cnidarian (primarily scleractinian coral) hard-ground communities in the deep Gulf of Mexico. Video of the seafloor was collected for this dataset by submersible cameras in high definition, digitized to computer readable video files, and archived on hard drives. Although the spatial coverage of this dataset was extensive, georeferenced information was coarse due to missing navigation data. However, it was still a highly valuable dataset for this study. The areal coverage was estimated by camera frame width and duration of surveys. The species identification work was performed by biologists at NOAA.

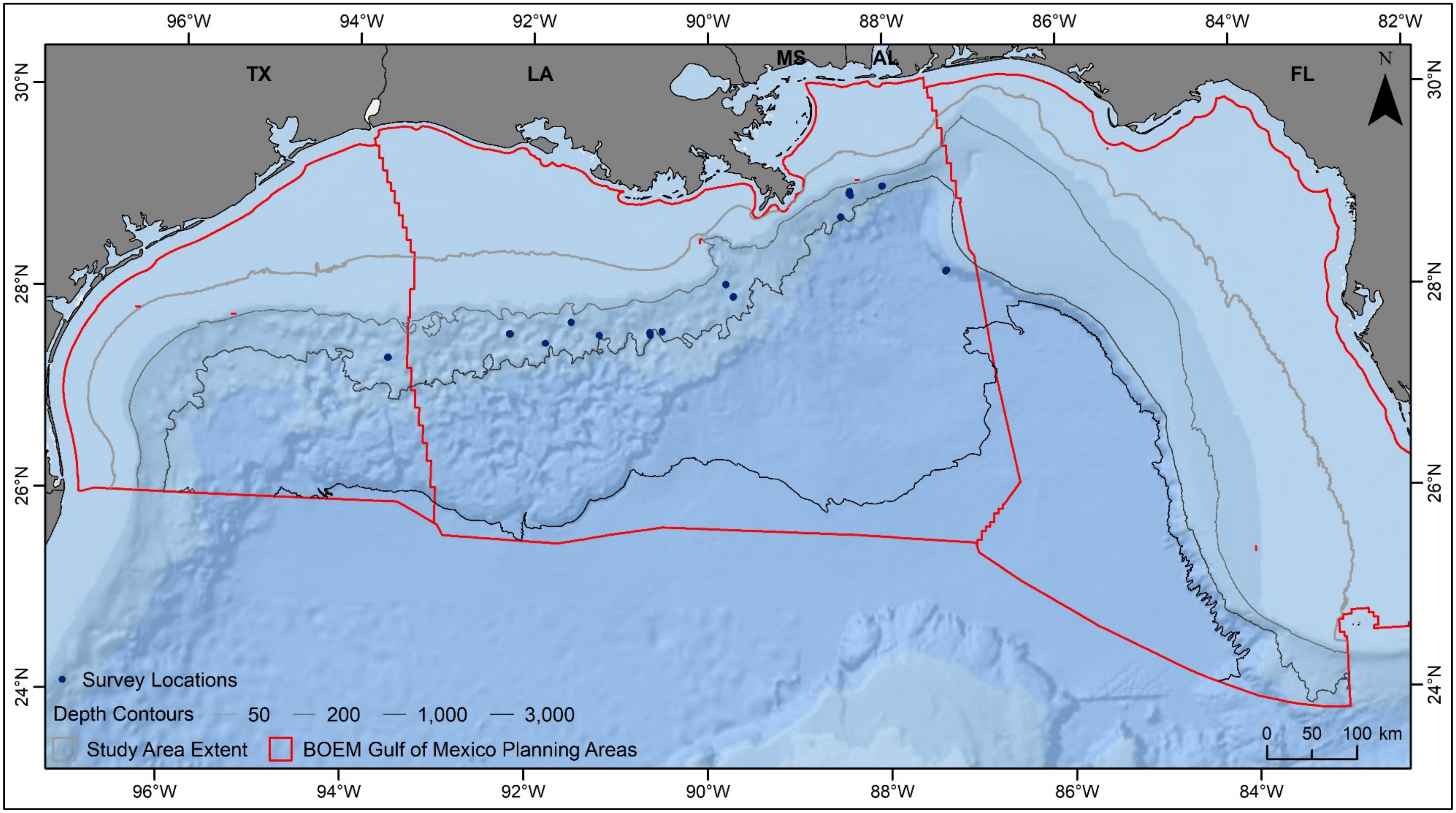

Figure A-6. Survey locations in the Lophelia II 2010 dataset.

A.7 Florida Shelf Edge Expedition (FLoSEE)

Data Providers: John Reed (Harbor Branch Oceanographic Institute)

Principal Investigators: John Reed (Harbor Branch Oceanographic Institute)

Year Range: 2010

Vessel: R/V *Seward Johnson*

Vehicle (Vehicle Type): *Johnson Sea Link II* (HOV)

Observation Types: HOV transect still photos

BOEM Gulf of Mexico Planning Areas: Eastern

Depth Zones: Mesophotic

Depth Range: 65–127 m

Dives: 13

Sites: 10

Segments: 15

Total Area: 77 m^2

Local anglers refer to an area of the West Florida Shelf as “sticky grounds” due to their experiences when attempting to bottom fish and getting their nets caught on the seafloor there. Bathymetry and side scan sonar indicated a margin of carbonate mounds in water depths of 116–135 m. The area was surveyed as part of the Florida Shelf Edge Expedition to ground truth the swath map data and to quantify and characterize benthic habitats, benthic macrofauna, fish populations, and coral/sponge cover. This study characterized for the first time this mesophotic reef ecosystem and associated fish populations. The extent and significance of associated living resources with these bottom types was particularly important in light of the 2010 *Deepwater Horizon* oil spill. The species identification work was performed by biologists at NOAA. The areal coverage was estimated by camera frame width.

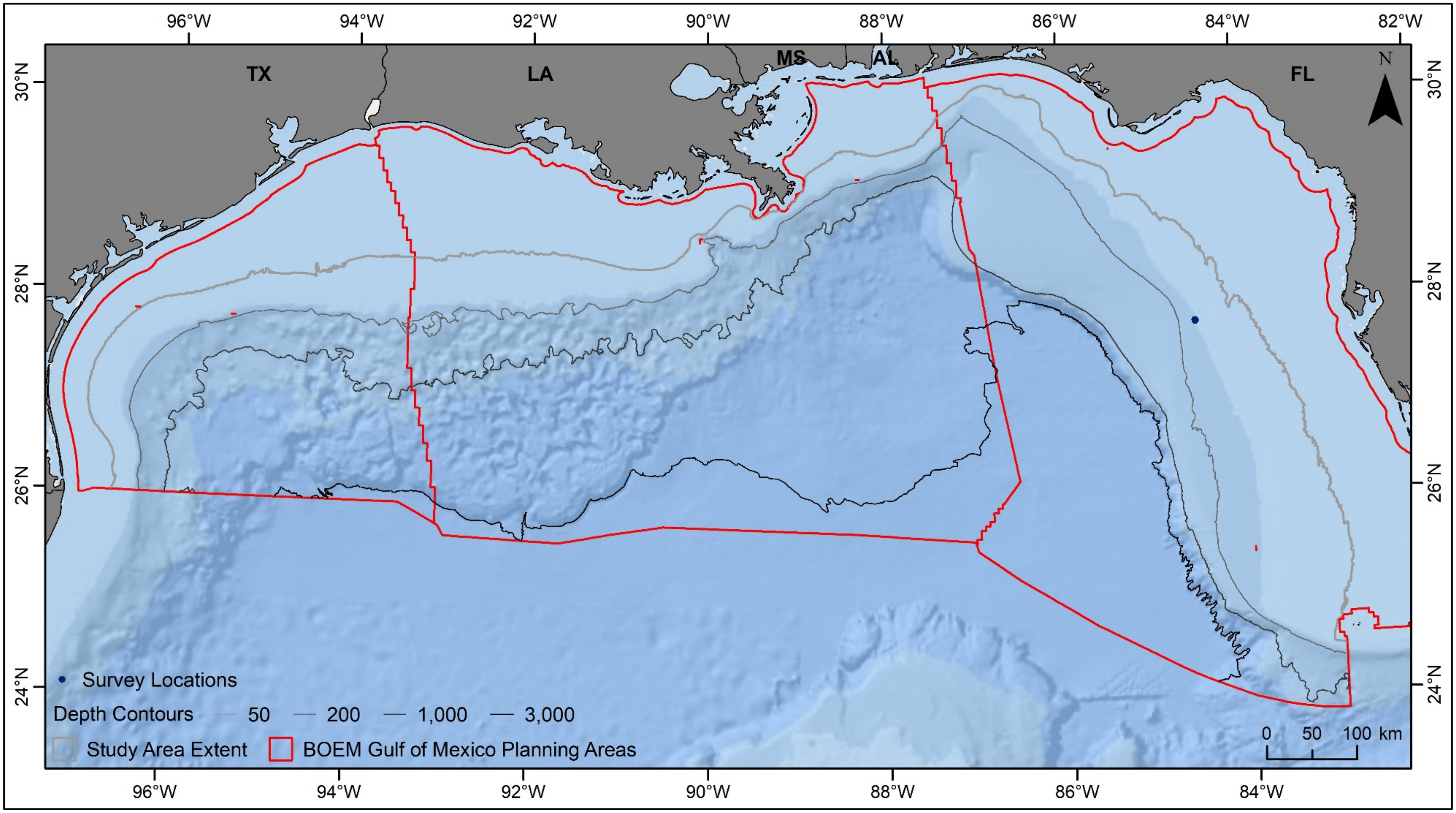

Figure A-7. Survey locations in the Florida Shelf Edge Expedition dataset.

A.8 *Deepwater Horizon* Soft Sediment Megafauna

Data Providers: Stephanie Sharuga (BOEM, formerly Louisiana State University)

Principal Investigators: Mark Benfield (Louisiana State University)

Year Range: 2011–2012

Vessel: HOS *Sweet Water*

Vehicle (Vehicle Type): Perry Triton XLS 52 (ROV)

Observation Types: ROV transects, video

BOEM Gulf of Mexico Planning Areas: Central

Depth Zones: Upper Bathyal, Lower Bathyal

Depth Range: 836–1,473 m

Dives: 6

Sites: 52

Segments: 128

Total Area: 54,630 m^2

Deepwater Horizon was a semisubmersible rig located approximately 50 miles southeast of the Mississippi River Delta in the Gulf of Mexico. An explosion and consequent loss of well control resulted in oil and gas flowing from the Macondo Prospect oil field from April 22–July 15, 2010. In the wake of the spill, there was a marked increase in demand for knowledge of Gulf of Mexico ecosystems, including the lesser known deep-sea megabenthos. The goals of this survey were to explore the effectiveness of industrial AUV and ROV technologies for studying deep-sea benthic megafaunal communities in soft sediment environments in the northern Gulf of Mexico. The survey design incorporated the use of industrial ROVs to perform a radial transect survey pattern with transects spaced at 15 degree intervals. The area surveyed by each transect was calculated as the mean field of view multiplied by the total distance traveled as obtained from the ROV navigation data. The species identification work was performed by Stephanie Sharuga, formerly at Louisiana State University and currently with BOEM.

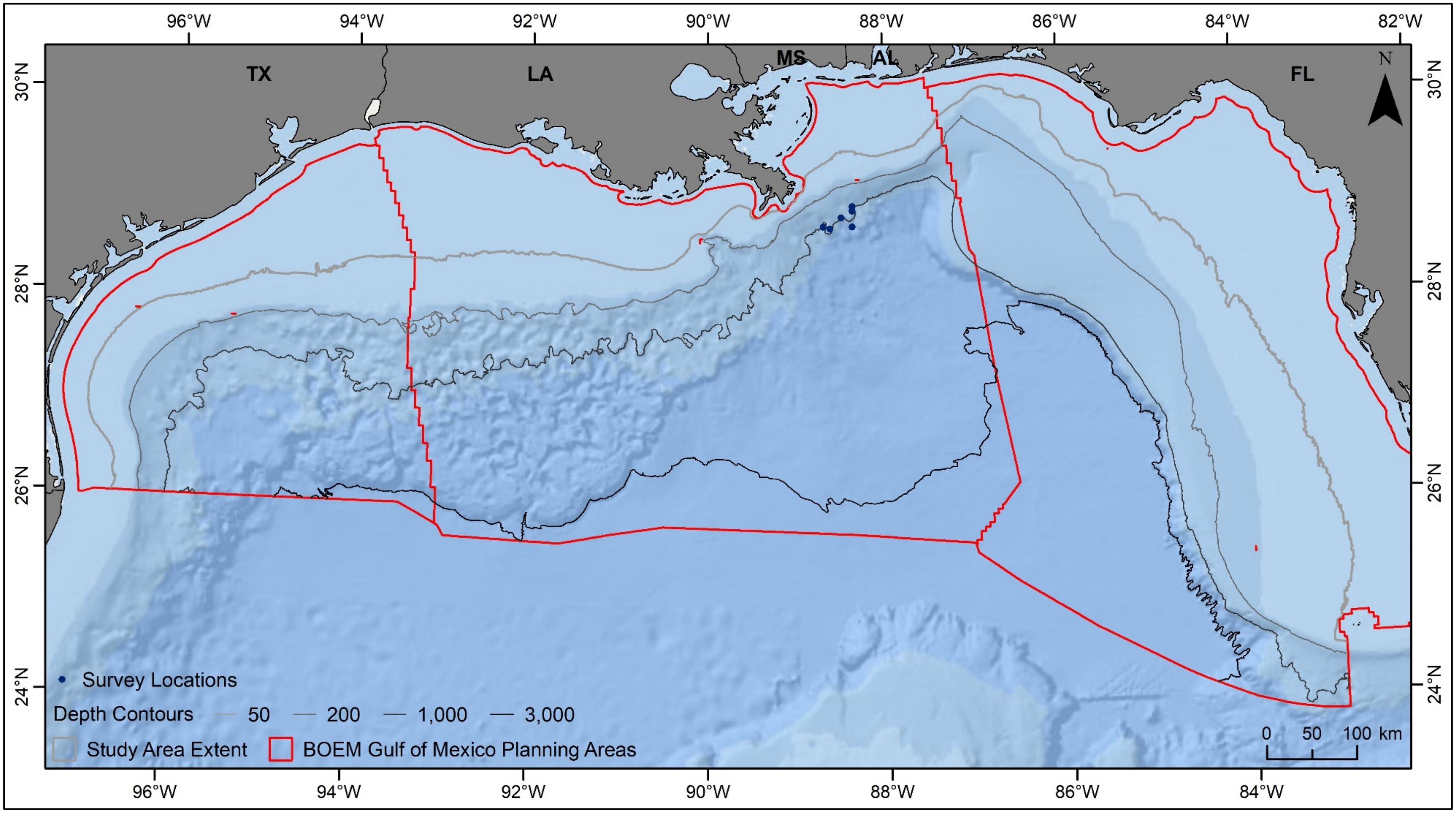

Figure A-8. Survey locations in the Deepwater Horizon Soft Sediment Megafauna dataset.

A.9 Potentially Sensitive Benthic Features

Data Providers: Flower Garden Banks National Marine Sanctuary

Principal Investigators: Marissa Nuttall, Emma Hickerson, George Schmahl (Flower Garden Banks National Marine Sanctuary)

Year Range: 2011–2013

Vessel: R/V *Manta*

Vehicle (Vehicle Type): Phantom S2 (ROV)

Observation Types: Digital still images

BOEM Gulf of Mexico Planning Areas: Western, Central

Depth Zones: Mesophotic

Depth Range: 50–200 m

Dives: 132

Sites: 682

Segments: 6,026

Total Area: 5,572 m^2

This was a multi-year investigation to explore “Potentially Sensitive Biological Features” in and around the Flower Garden Banks National Marine Sanctuary in the north-central Gulf of Mexico. The investigators visited 14 banks from 2011–2013 aboard the R/V *Manta*, to collect benthic community data. Standard definition video was collected with the ROV Phantom S2, and downward looking digital stills were taken every 30 seconds along 10-minute transects, resulting in ~1,000 photographs per bank. NOAA scientists annotated a random subset of georeferenced images, and every coral and seep present was identified. Area of the stills was calculated with PhotoQuad software, using laser points spaced 10 cm apart for scale. This dataset consisted of an abundant and diverse assortment of coral taxa.

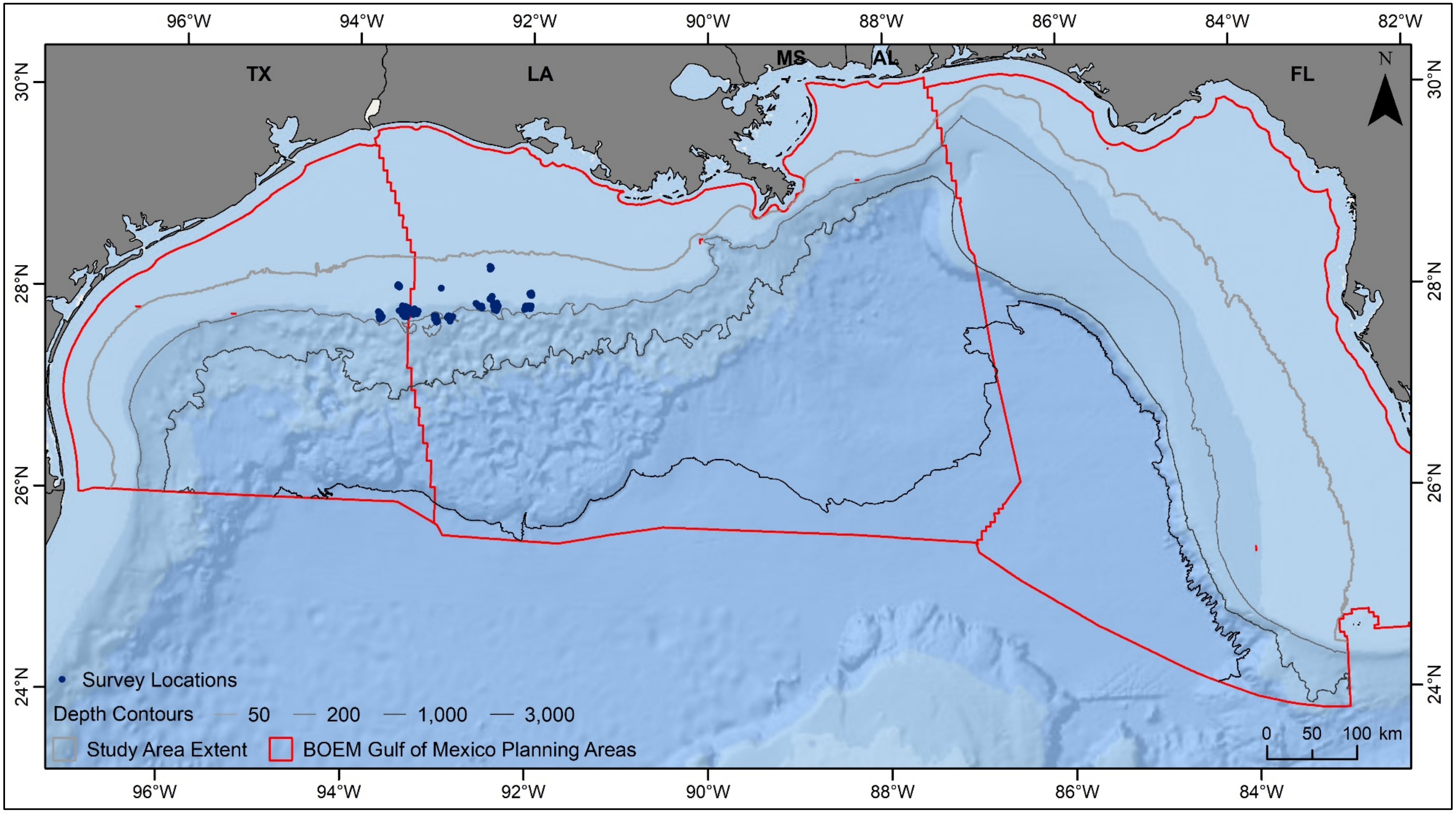

Figure A-9. Survey locations in the Potentially Sensitive Benthic Features dataset.

A.10 Ecosystem Impacts of Oil and Gas Inputs (ECOGIG)

Data Providers: Charles Fisher (Pennsylvania State University)

Principal Investigators: Charles Fisher (Pennsylvania State University), Erik Cordes (Temple University)

Year Range: 2011–2017

Vessels: E/V *Nautilus*, R/V *Falkor*, NOAA Ship *Ronald H. Brown*, NOAA Ship *Okeanos Explorer*, Offshore Supply Ship *Holiday*, Offshore Supply Ship *Ocean Inspector*, Offshore Supply Ship *Ocean Intervention II*

Vehicle (Vehicle Type): *Hercules* (ROV), *Global Explorer* (ROV), *Jason II* (ROV), *Little Hercules* (ROV), Schilling UHD (ROV)

Observation Types: ROV transects, video, samples

BOEM Gulf of Mexico Planning Areas: Central

Depth Zones: Upper Bathyal, Lower Bathyal

Depth Range: 437–1,852 m

Dives: 35

Sites: 69

Segments: 135

Total Area: 14,407 m^2

The research goal of this multi-year project was to investigate the ecosystem effects of natural oil and gas seepage to the Gulf of Mexico. The primary focus was to monitor and sample benthic communities, primarily deep-water corals, in the vicinity of the Macondo well, the location of the 2010 Gulf of Mexico oil spill. When corals were found, a marker was deployed and all the corals within 100 m^2 were individually named, with the marker number as the first part of the name. Each marker was visited several times over the course of the project and corals were imaged each time they were visited. Corals were identified morphologically by experts on the cruises as well as by genetic work done post-cruise.

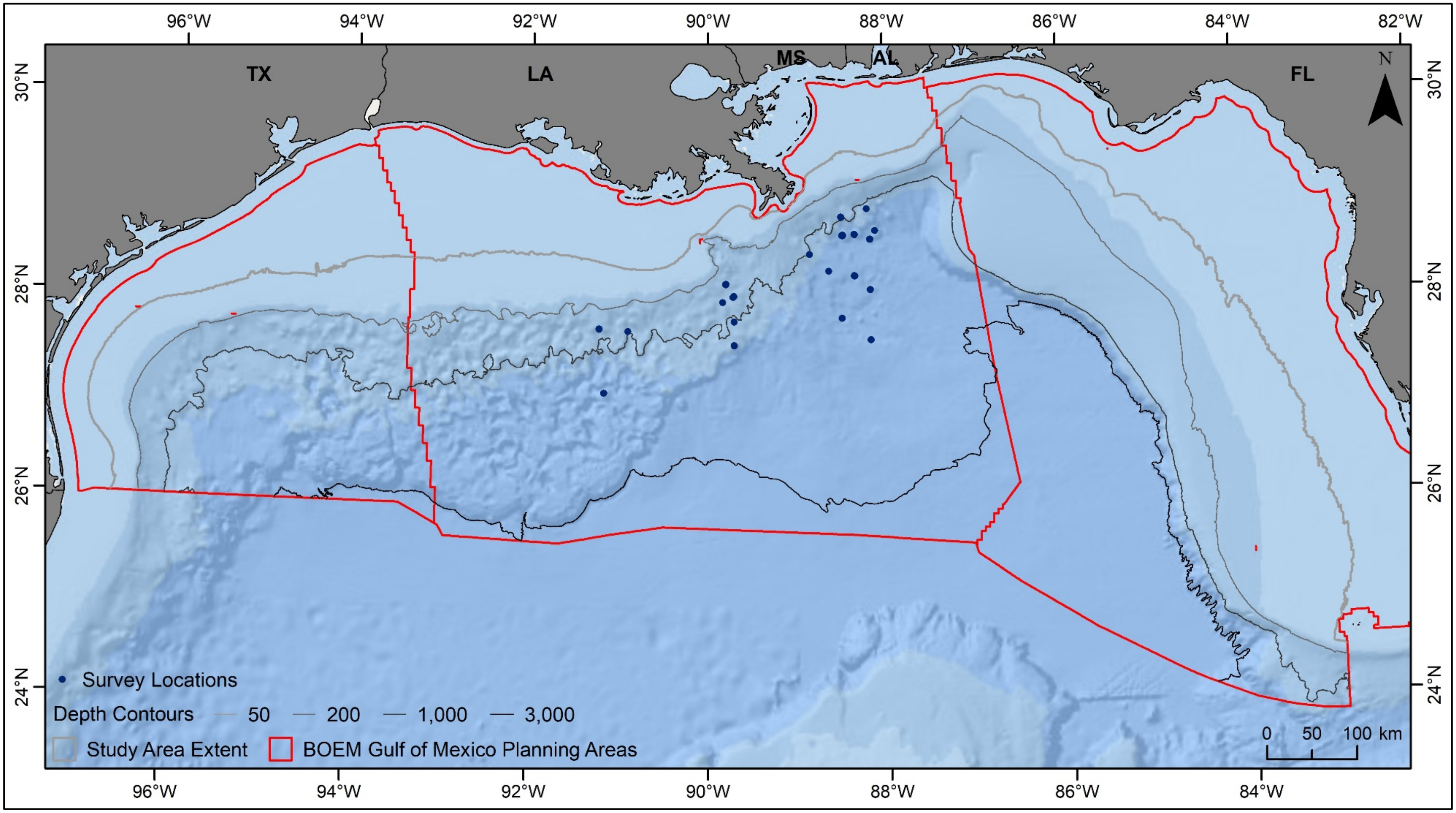

Figure A-10. Survey locations in the Ecosystem Impacts of Oil and Gas Inputs to the Gulf of Mexico (ECOGIG) dataset.

A.11 *Okeanos Explorer* 2012

Data Providers: NOAA OER

Principal Investigators: Elizabeth Lobecker (NOAA OER)

Year Range: 2012

Vessels: NOAA Ship *Okeanos Explorer*

Vehicle (Vehicle Type): *Seirios* (ROV), *Little Hercules* (ROV)

Observation Types: Digital stills

BOEM Gulf of Mexico Planning Areas: Central, Eastern

Depth Zones: Upper Bathyal, Lower Bathyal

Depth Range: 420–2,900 m

Dives: 15

Sites: 122

Segments: 2,126

Total Area: 5,614 m^2

The purpose of this expedition was to conduct exploratory investigations on the diversity and distribution of deep-sea habitats and marine life in the northern Gulf of Mexico. This dataset is for Leg 2 of the 2012 cruise. Still images were obtained from NOAA OER. Annotation was completed for the DSCs and for observed substrate using Coastal and Marine Ecological Classification Standard (CMECS) terminology. The species identification work was performed by biologists at NOAA. The areal coverage was estimated by camera frame width.

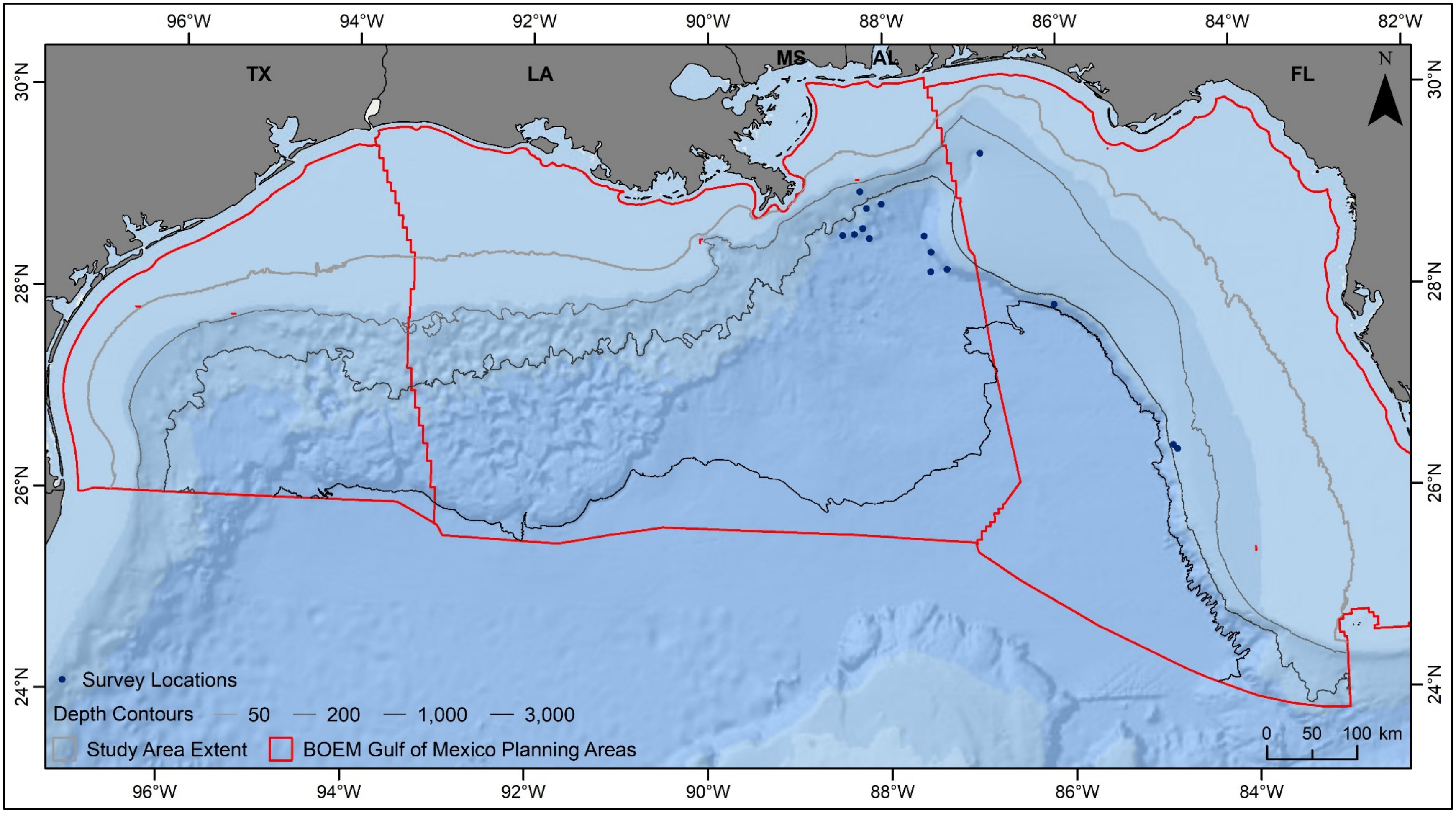

Figure A-11. Survey locations in the Okeanos Explorer 2012 dataset.

A.12 Deep Sea Coral Shakedown Cruises

Data Providers: Schmidt Ocean Institute, NOAA NCCOS

Principal Investigators: Peter Etnoyer (NOAA NCCOS), Erik Cordes (Temple University)

Year Range: 2012

Vessels: R/V *Falkor*

Vehicle (Vehicle Type): *Global Explorer* (ROV)

Observation Types: ROV video transects

BOEM Gulf of Mexico Planning Areas: Central, Eastern

Depth Zones: Upper Bathyal, Lower Bathyal

Depth Range: 517–2,120 m

Dives: 7

Sites: 41

Segments: 155

Total Area: 10,595 m^2

This series of cruises in 2012 aboard the R/V *Falkor* consisted of ROV field trials with a new *Global Explorer* ROV. They focused on developing safe practices and procedures for deployment and operation of the ROV. Video and biological samples were collected when possible, and other oceanographic instruments were tested and calibrated. 3D and HD video were collected, and split up into approximately 5 minute segments. These segments were then reviewed, and all corals were identified. Six different localities in the Gulf of Mexico were visited, and seven dives were successful. Area of segments was calculated using average frame width and start and stop navigation points for linear distance.

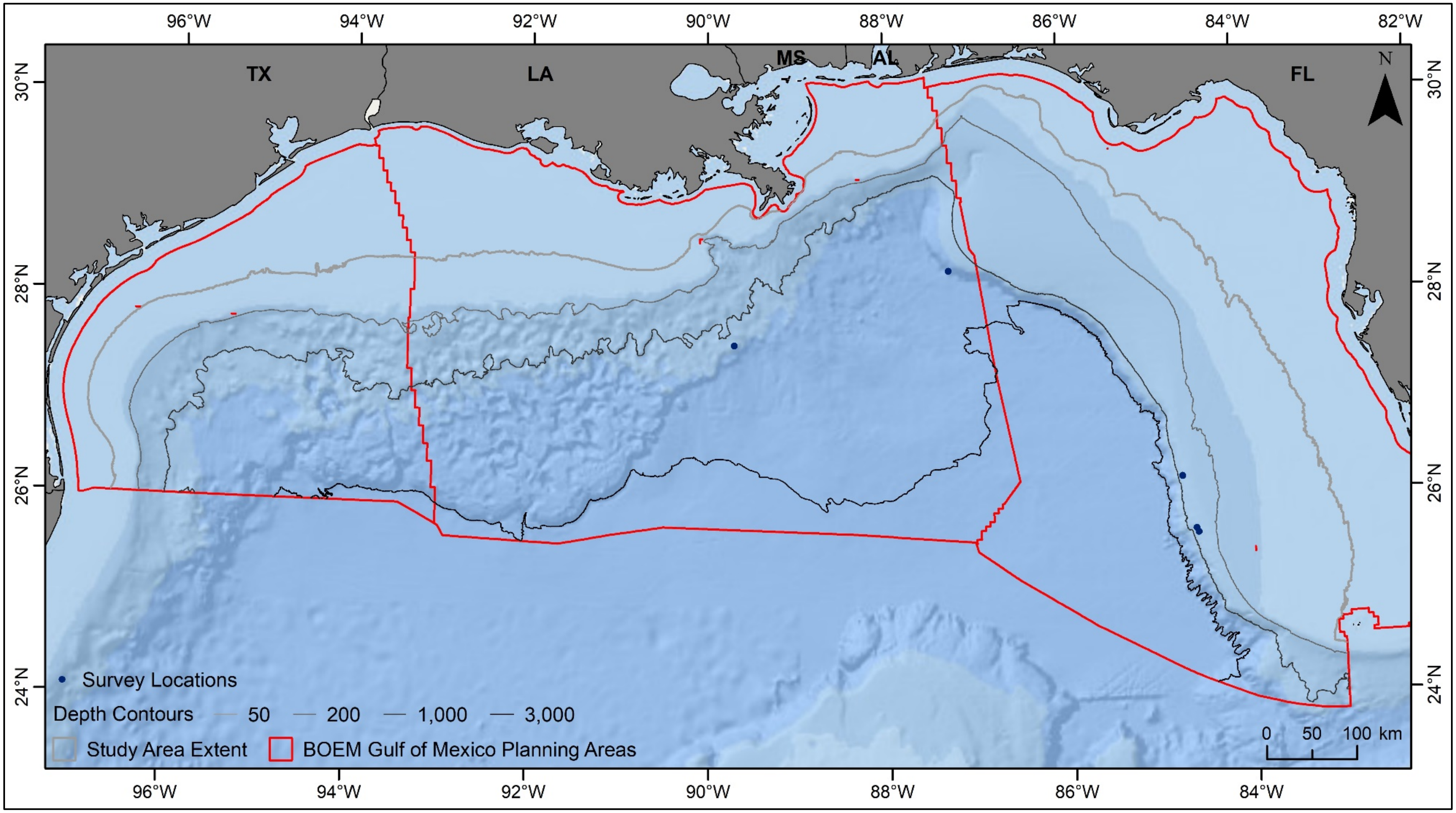

Figure A-12. Survey locations in the Deep Sea Coral Shakedown Cruises dataset.

A.13 Mapping South Texas Banks

Data Providers: Schmidt Ocean Institute, Harte Research Institute

Principal Investigators: Thomas Shirley, David Hicks (Harte Research Institute)

Year Range: 2012

Vessels: R/V *Falkor*

Vehicle (Vehicle Type): *Global Explorer* (ROV)

Observation Types: ROV transects, video, samples

BOEM Gulf of Mexico Planning Areas: Western

Depth Zones: Mesophotic

Depth Range: 55–96 m

Dives: 8

Sites: 33

Segments: 445

Total Area: 4,434 m^2

The Schmidt Ocean Institute research team used multibeam sonar systems available to map these areas in great detail, and, in many cases, these dives revealed never before seen sites. ROV dives ran video transects across the ridges, bumps and crevices of various bank areas that run along the edge of the continental shelf and collected samples. These areas had been poorly studied previously, because access to submersibles and ROVs in this region has been extremely limited, and the banks are below safe scuba diving depths. Objectives in this expedition included collecting data to determine ecological roles these banks may play, such as influencing movements of animals from the tropics to the sub-tropics. Data provided for this study is from continuous video transects approximately 30 seconds each and covering an area of approximately 10 square meters.

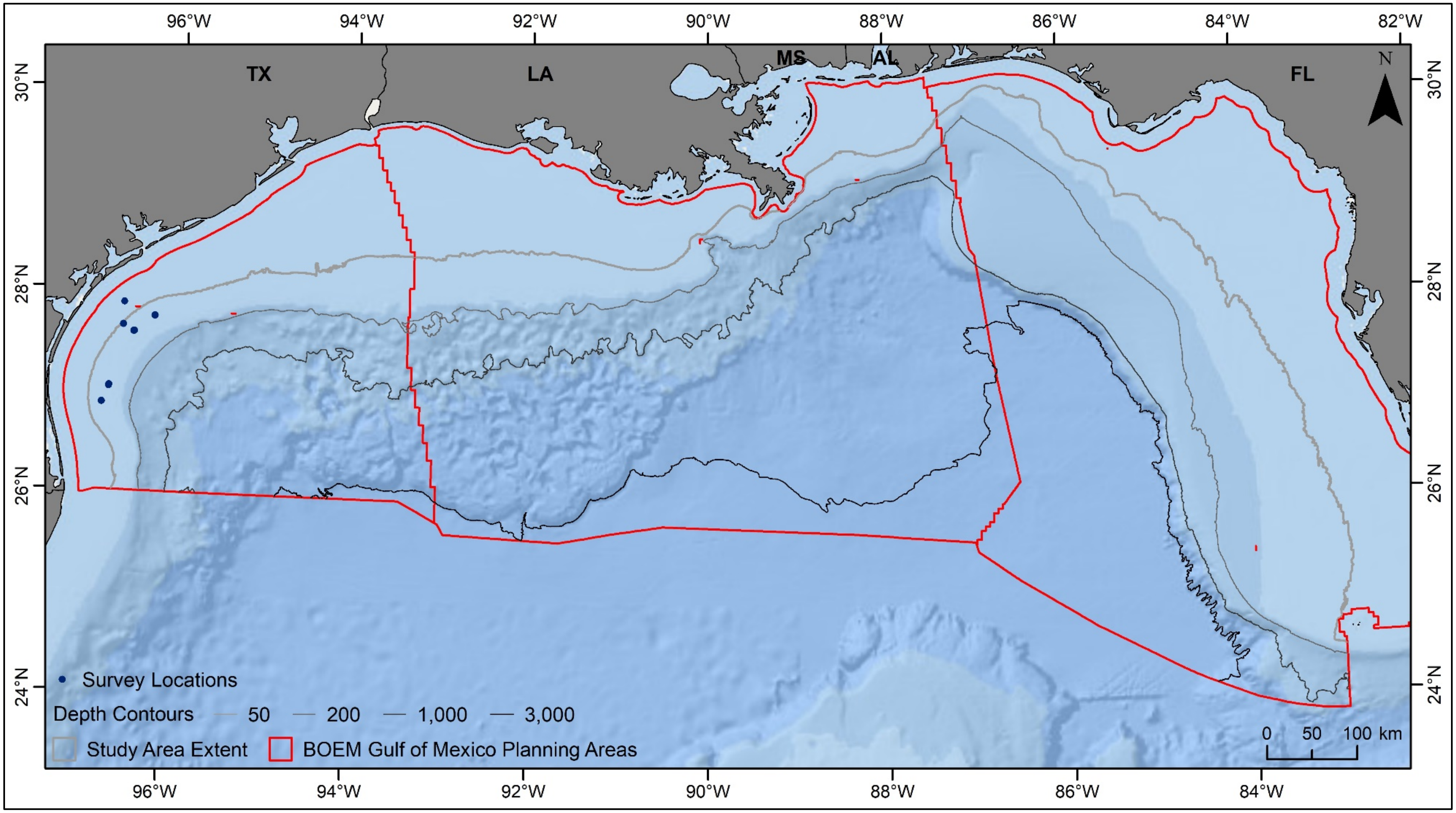

Figure A-13. Survey locations in the Mapping South Texas Banks dataset.

A.14 AT-26

Data Providers: Woods Hole Oceanographic Institution

Principal Investigators: Peter Girguis (Harvard University), Erik Cordes (Temple University), Samantha Joye (University of Georgia), Cindy Van Dover (Duke University)

Year Range: 2014

Vessels: R/V *Atlantis*

Vehicle (Vehicle Type): *Alvin* (HOV)

Observation Types: HOV transects (exploratory), still images (downlooking)

BOEM Gulf of Mexico Planning Areas: Western, Central, Eastern

Depth Zones: Mesophotic, Upper Bathyal, Lower Bathyal

Depth Range: 330–3,100 m

Dives: 58

Sites: 154

Segments: 201

Total Area: 17,392 m^2

This dataset included all legs of cruise AT-26. Due to the nature of instrument tests performed during some of the dives, not all dives will be useful for segment or transect quantification, but in totality they do provide adequate coverage, good variation of seafloor types, and state of the art georeferenced images. Still photos were collected with down-looking HD cameras every 10 seconds, and HD video was collected for several dives. The dataset for this study was obtained through collaboration with the Woods Hole Oceanographic Institution library archive and downloaded over a 3-day period. Contents of data folders were inspected for quality and completeness. Navigation was processed, and the species identification work was performed by biologists at NOAA.

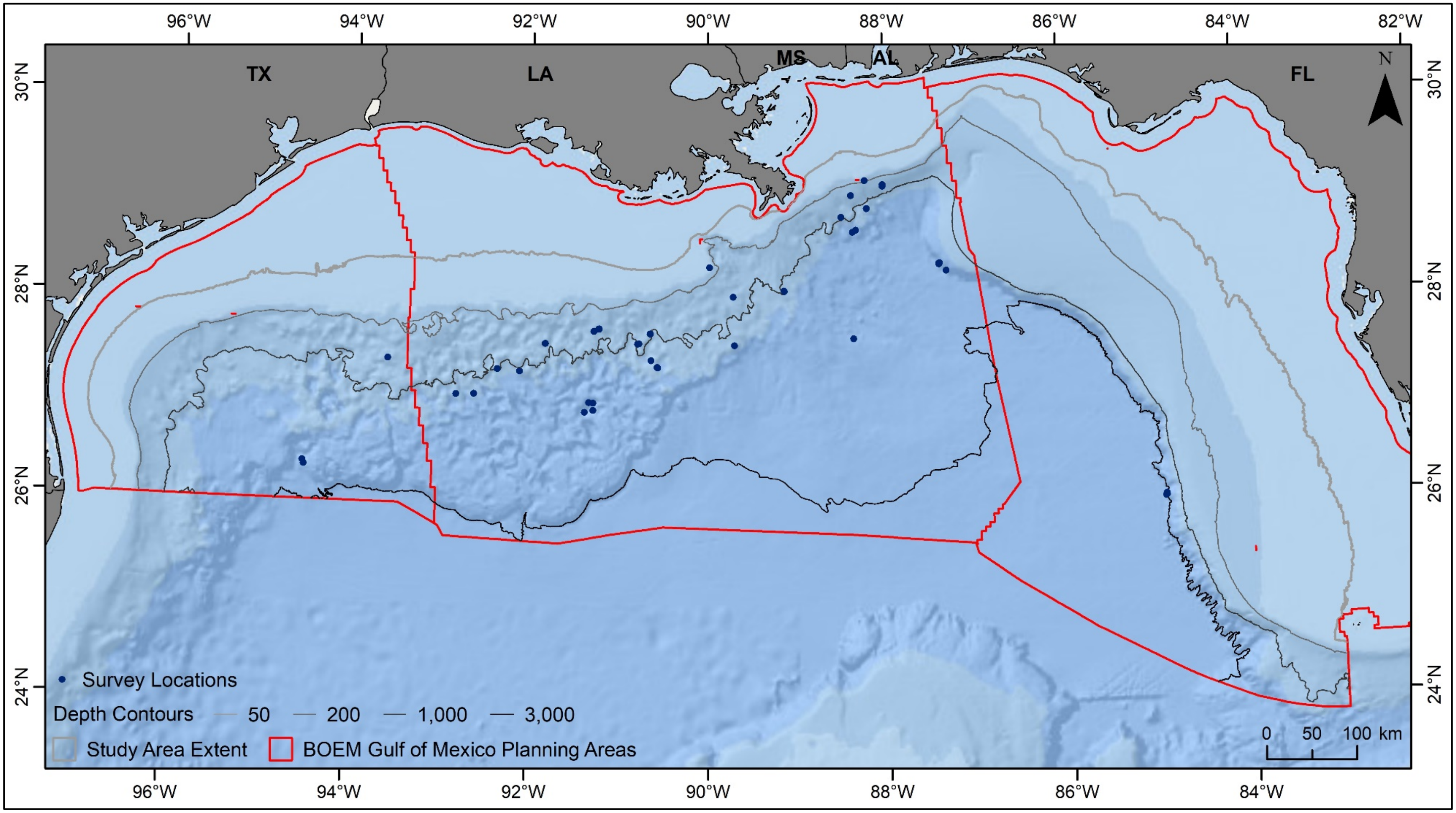

Figure A-14. Survey locations in the AT-26 dataset.

A.15 Mesophotic Pinnacles

Data Providers: NOAA NCCOS

Principal Investigators: Peter Etnoyer (NOAA NCCOS)

Year Range: 2014

Vessels: R/V *Walton Smith*

Vehicle (Vehicle Type): *Global Explorer* (ROV)

Observation Types: ROV transects (continuous)

BOEM Gulf of Mexico Planning Areas: Central, Eastern

Depth Zones: Mesophotic

Depth Range: 48–88 m

Dives: 10

Sites: 24

Segments: 30

Total Area: 9,767 m^2

This dataset consists of observations from a 2014 survey conducted to assess damage to mesophotic corals post *Deepwater Horizon* oil spill. Transects selected for this dataset were conducted for 5 minutes each, with consistent ROV altitude. Area and density measurements were obtained. Taxonomic identifications to species level were aided by samples collected, and analyzed by the NOAA NCCOS Deep Coral Ecology Laboratory. Photographic observations were identified to genus level when appropriate. These transects were selected due to inclusion of all coral taxa within the area surveyed. The segments (transects) provided were continuous, with all visible corals documented within transect lines.

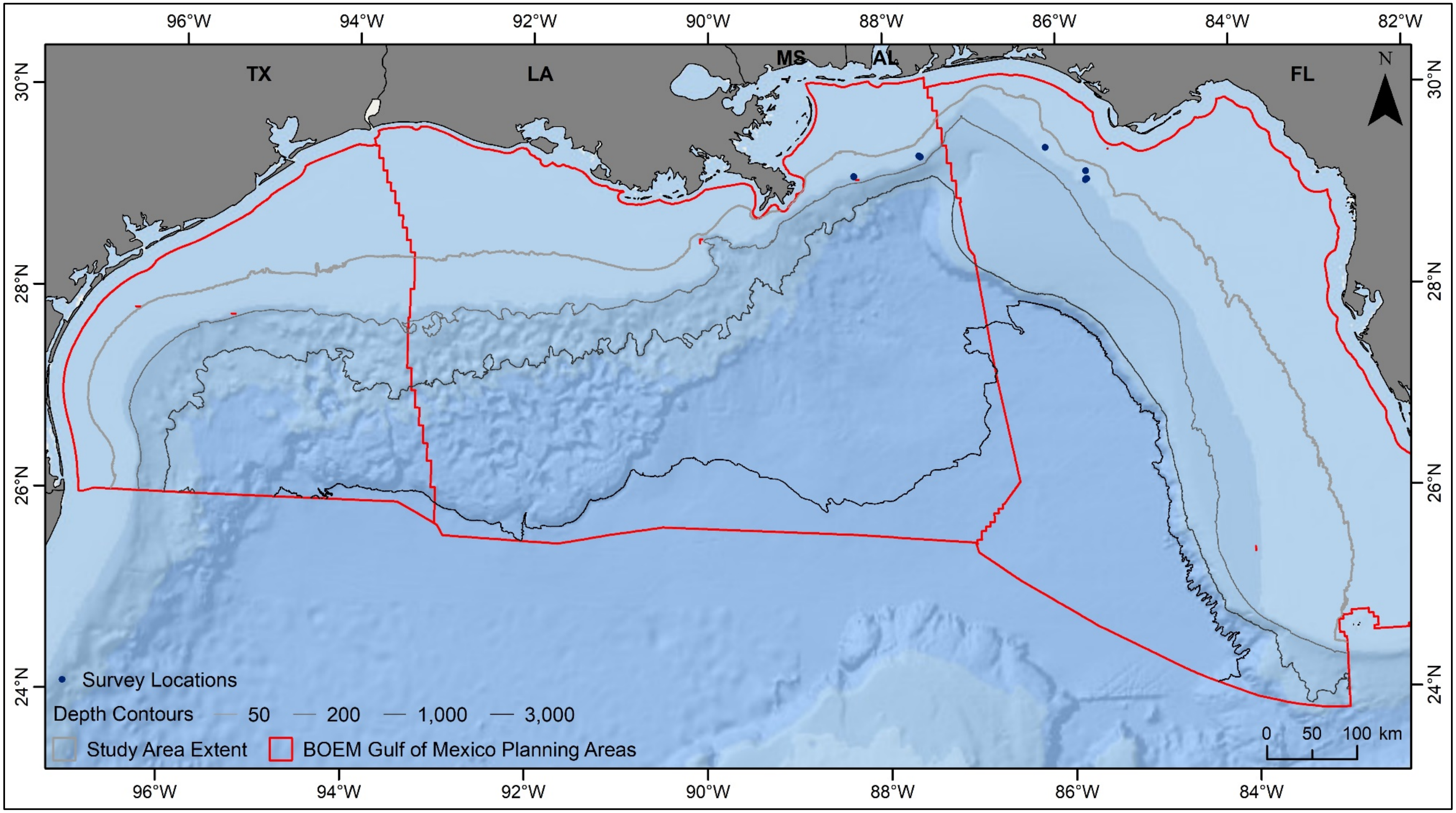

Figure A-15. Survey locations in the Mesophotic Pinnacles dataset.

A.16 Okeanos Explorer 2014

Data Providers: NOAA OER

Principal Investigators: Elizabeth Lobecker (NOAA OER)

Year Range: 2014

Vessels: NOAA Ship *Okeanos Explorer*

Vehicle (Vehicle Type): *Seirios* (ROV), *Little Hercules* (ROV)

Observation Types: Digital stills

BOEM Gulf of Mexico Planning Areas: Western, Central, Eastern

Depth Zones: Upper Bathyal, Lower Bathyal

Depth Range: 420–2,900 m

Dives: 14

Sites: 169

Segments: 2,239

Total Area: 6,619 m^2

The purpose of this expedition was to conduct exploratory investigations on the diversity and distribution of deep-sea habitats and marine life in the northern Gulf of Mexico. This dataset is for Leg 3 of the 2014 cruise. Still images were obtained from NOAA OER. Annotation was completed for the deep sea corals and for observed substrate using Coastal and Marine Ecological Classification Standard (CMECS) terminology. The species identification work was performed by biologists at NOAA. The areal coverage was estimated by camera frame width.

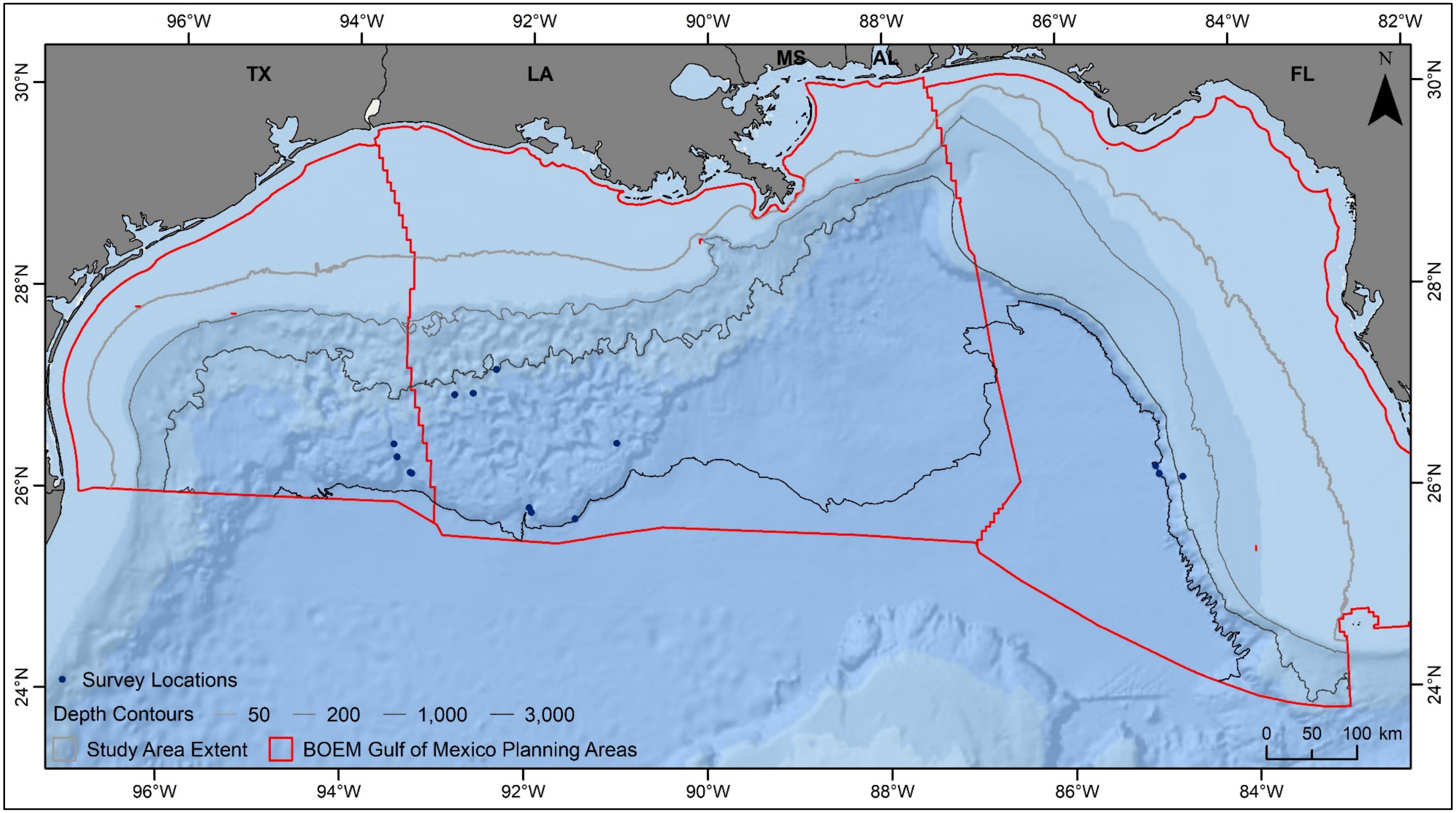

Figure A-16. Survey locations in the Okeanos Explorer 2014 dataset.

A.17 Deep Fish Habitat 28

Data Providers: Flower Garden Banks National Marine Sanctuary

Principal Investigators: Emma Hickerson (Flower Garden Banks National Marine Sanctuary)

Year Range: 2015

Vessels: R/V *Manta*

Vehicle (Vehicle Type): Mohawk (ROV)

Observation Types: ROV transects (continuous)

BOEM Gulf of Mexico Planning Areas: Western, Central

Depth Zones: Mesophotic

Depth Range: 30–200 m

Dives: 24

Sites: 67

Segments: 137

Total Area: 6,194 m^2

This cruise was conducted in collaboration with University of North Carolina Wilmington to capture video and still images of sites and biological communities of interest for sanctuary expansion purposes. Eleven dives at mesophotic depths in sites within and around the Flower Garden Banks NMS were conducted. The reporter identified video segments of usable quality for taxonomic identification with a mean duration of 2 minutes, 31 seconds, and a maximum linear distance of 155 meters. Presences of black corals, stony corals, and octocorals were recorded. Because lasers were not present, area estimates are based on distance (m) x estimated mean frame width (m).

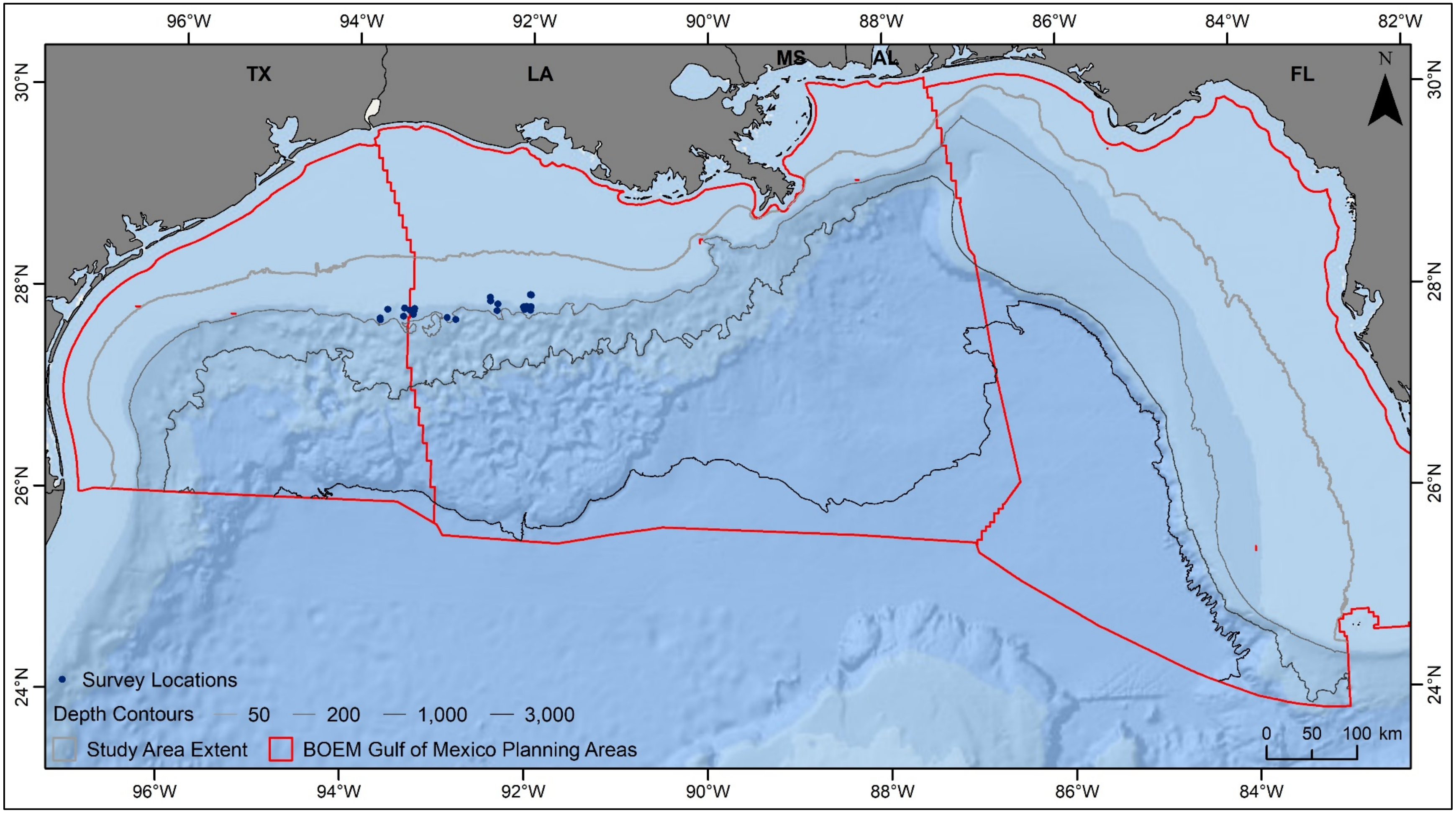

Figure A-17. Survey locations in the Deep Fish Habitat 28 dataset.

A.18 *Okeanos Explorer* 2017

Data Providers: NOAA OER

Principal Investigators: Diva Amon (Natural History Museum, London), Charles Messing (Nova Southeastern University)

Year Range: 2017

Vessels: NOAA Ship *Okeanos Explorer*

Vehicle (Vehicle Type): *Deep Discoverer* (ROV)

Observation Types: ROV transects, video, samples

BOEM Gulf of Mexico Planning Areas: Western, Central, Eastern

Depth Zones: Upper Bathyal, Lower Bathyal

Depth Range: 381–2,320 m

Dives: 17

Sites: 171

Segments: 659

Total Area: 48,862 m^2

This was a 23-day expedition to collect information and acquire data on priority areas identified by ocean management and scientific communities. Seventeen ROV dives were completed, ranging in depth from 300 to 2,321 meters (984 to 7,615 feet) to explore the diversity and distribution of deep-sea habitats and associated marine communities in the Gulf of Mexico basin. Operations focused on characterizing deep-sea coral and sponge communities; bottomfish habitats; shipwrecks; and chemosynthetic habitats such as cold seeps, mud volcanoes, asphalt seeps, and brine pools. This expedition was the first of three expeditions planned to increase our understanding of the Gulf of Mexico, with additional sites explored during spring 2018 (EX1803). Area for each segment was calculated by multiplying linear distance by field of view. Biologists at the NOAA NCCOS Deep Coral Ecology Laboratory performed the species identification work.

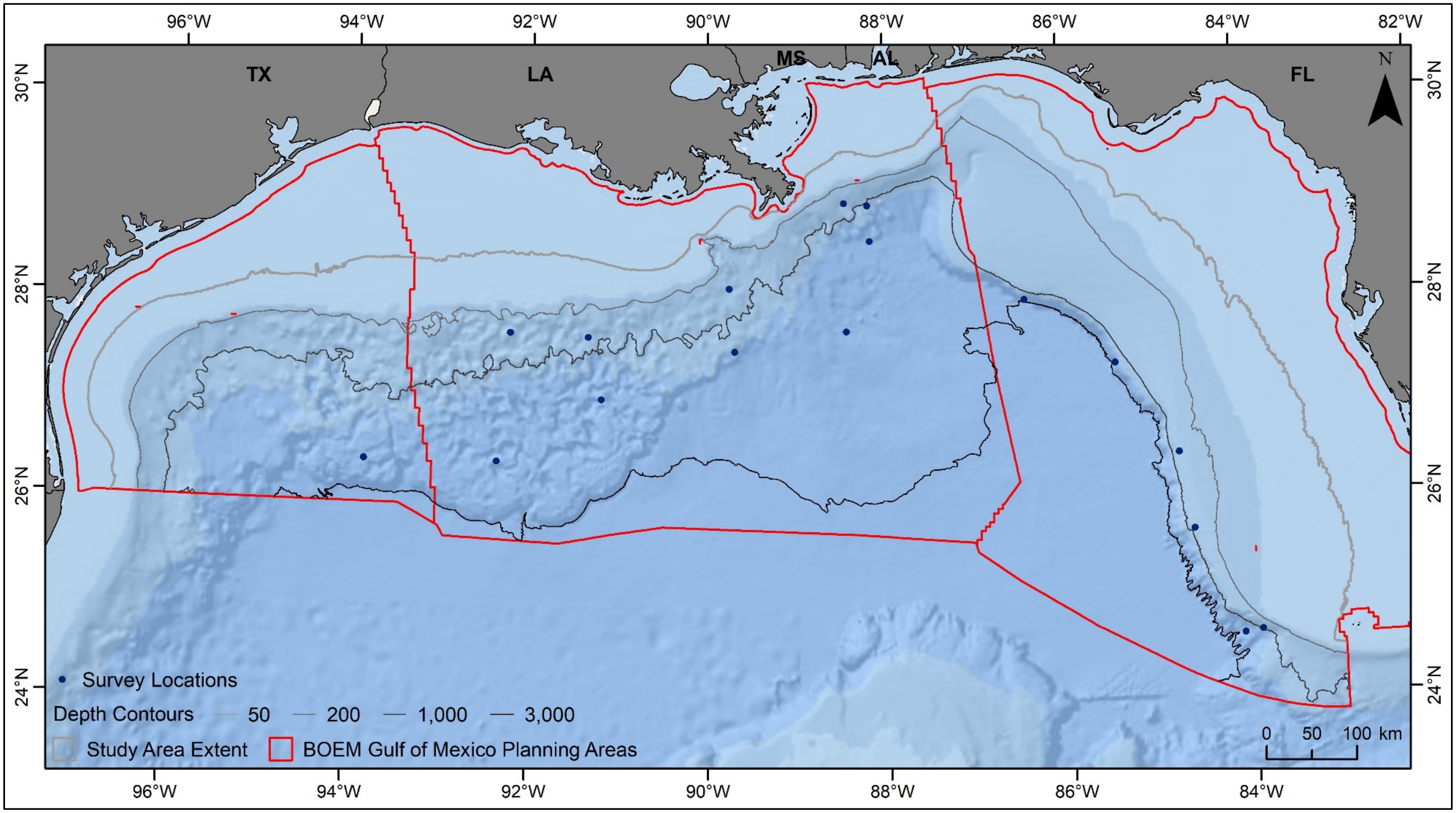

Figure A-18. Survey locations in the Okeanos Explorer 2017 dataset.

A.19 SEDCI NF1708

Data Providers: Peter Etnoyer (NOAA NCCOS)

Principal Investigators: Peter Etnoyer (NOAA NCCOS)

Year Range: 2017

Vessels: NOAA Ship *Nancy Foster*

Vehicle (Vehicle Type): *Odysseus* (ROV)

Observation Types: ROV transects, video, samples

BOEM Gulf of Mexico Planning Areas: Eastern

Depth Zones: Upper Bathyal

Depth Range: 384–698 m

Dives: 13

Sites: 95

Segments: 111

Total Area: 43,792 m^2

This expedition was part of the Southeast Deep Coral Initiative (SEDCI). The objectives of this expedition were to survey, sample, and map deep-sea coral ecosystems in the eastern Gulf of Mexico and South Atlantic Bight between ~200-1,000m depths, focusing on priority areas identified by the Gulf of Mexico Fishery Management Council and the South Atlantic Fishery Management Council. Area for each segment was calculated by multiplying linear distance by field of view. The species identification work was performed by biologists at the NOAA NCCOS Deep Coral Ecology Laboratory.

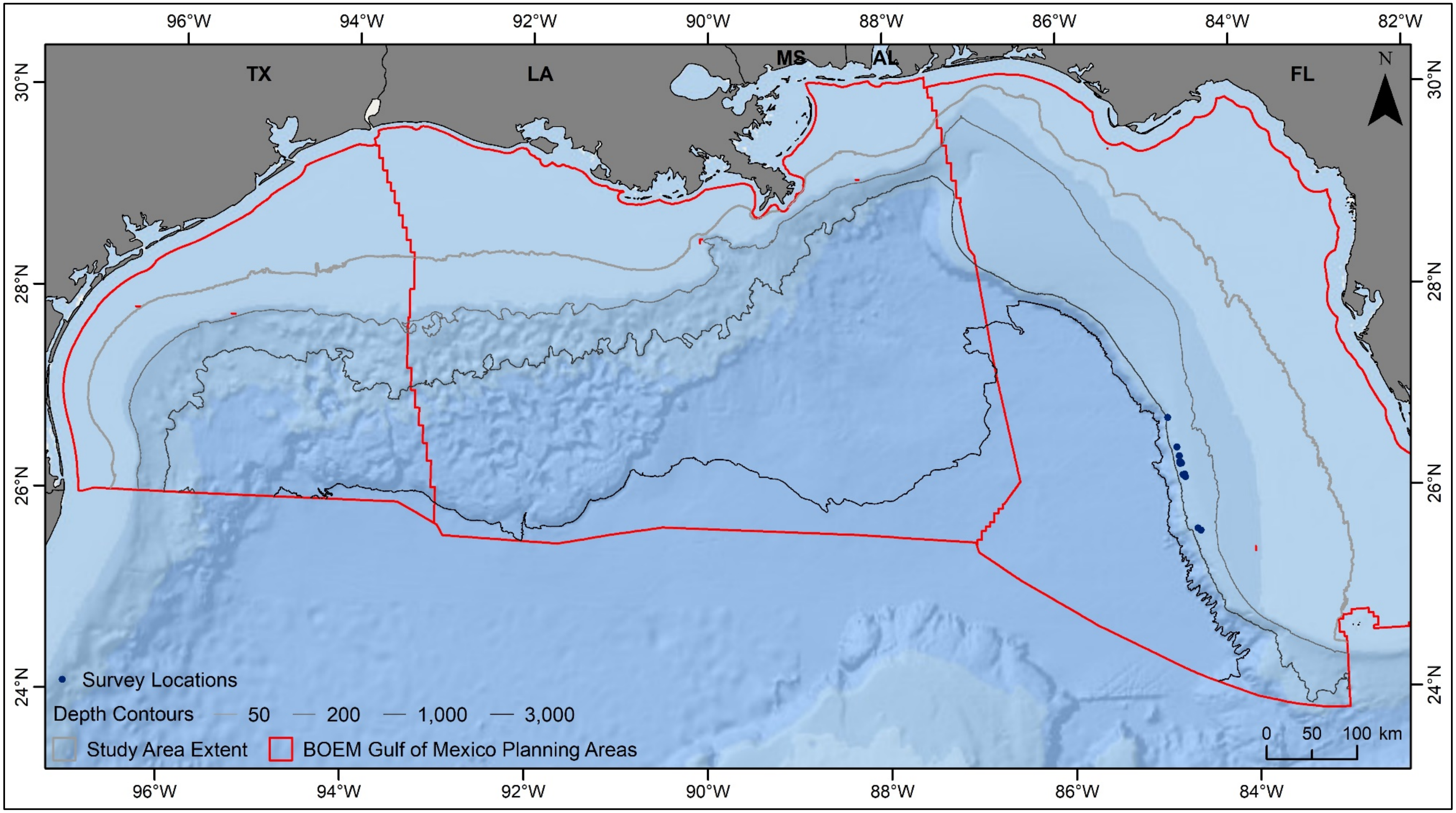

Figure A-19. Survey locations in the SEDCI NF1708 dataset.

A.20 *Okeanos Explorer* 2018 (EX1803)

Data Providers: NOAA OER

Principal Investigators: Daniel Wagner (formerly NOAA NCCOS, now with Conservation International), Adam Skarke (Mississippi State University)

Year Range: 2018

Vessels: NOAA Ship *Okeanos Explorer*

Vehicle (Vehicle Type): *Deep Discoverer* (ROV)

Observation Types: ROV transects, video, samples

BOEM Gulf of Mexico Planning Areas: Western, Central, Eastern

Depth Zones: Upper Bathyal, Lower Bathyal

Depth Range: 516–3,007 m

Dives: 13

Sites: 75

Segments: 77

Total Area: 11,453 m^2

Areas that had been scarcely, or previously unexplored were visited again from April 11 through May 3, 2018. The scientists conducted exploratory investigations into the diversity and distribution of deep-sea habitats and associated marine communities in the Gulf of Mexico basin. The 23-day expedition focused on acquiring data on priority exploration areas identified by ocean management and scientific communities. Priority areas were identified for exploration, building on the Gulf of Mexico 2017 expedition. This expedition explored deep coral and sponge communities, bottom fish habitats, undersea canyons, shipwrecks, and a variety of chemosynthetic habitats including cold seeps, mud volcanoes, and brine pools.

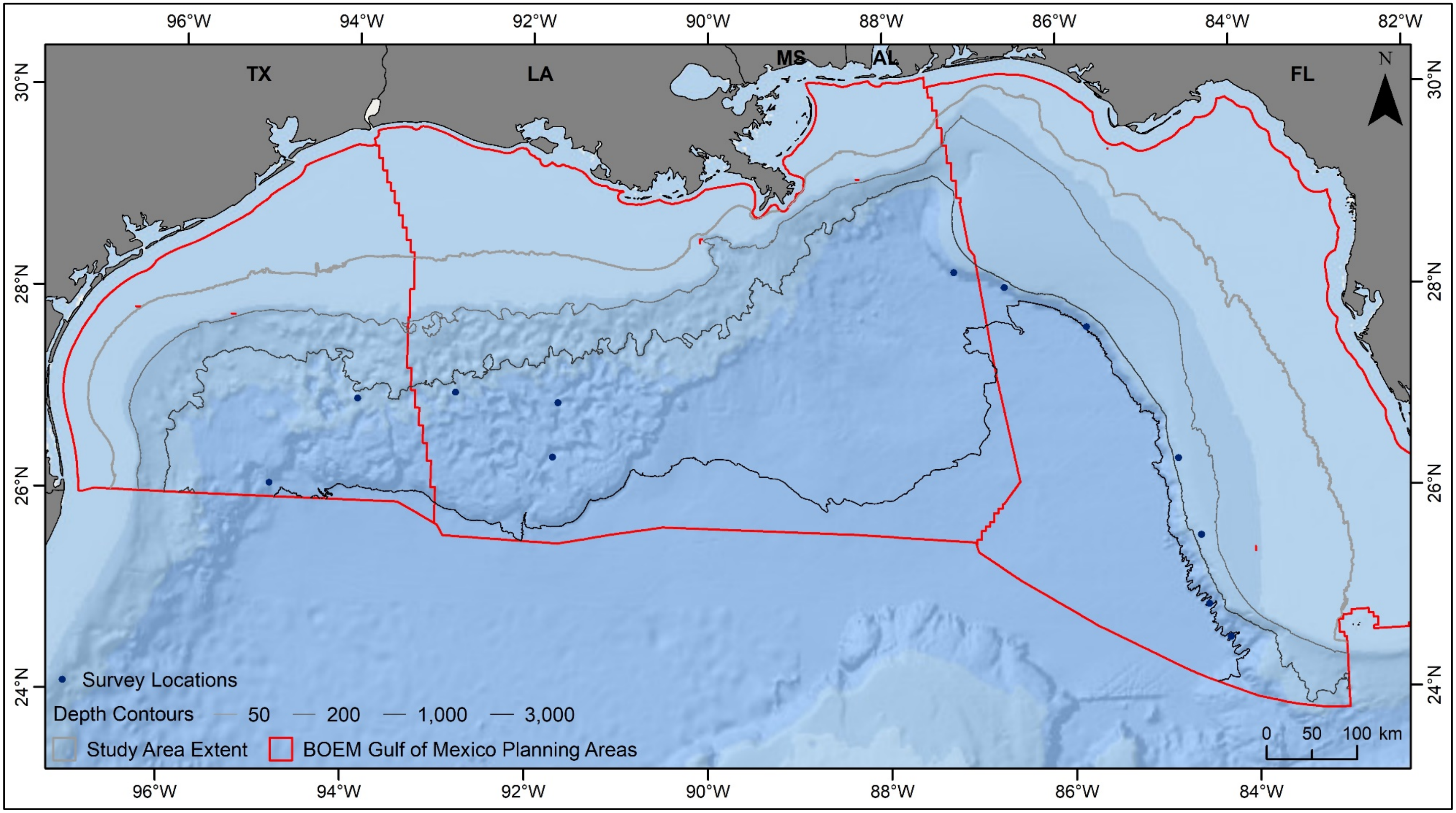

Figure A-20. Survey locations in the Okeanos Explorer 2018 dataset.

B Appendix B: Maps of the Environmental Predictor Variables

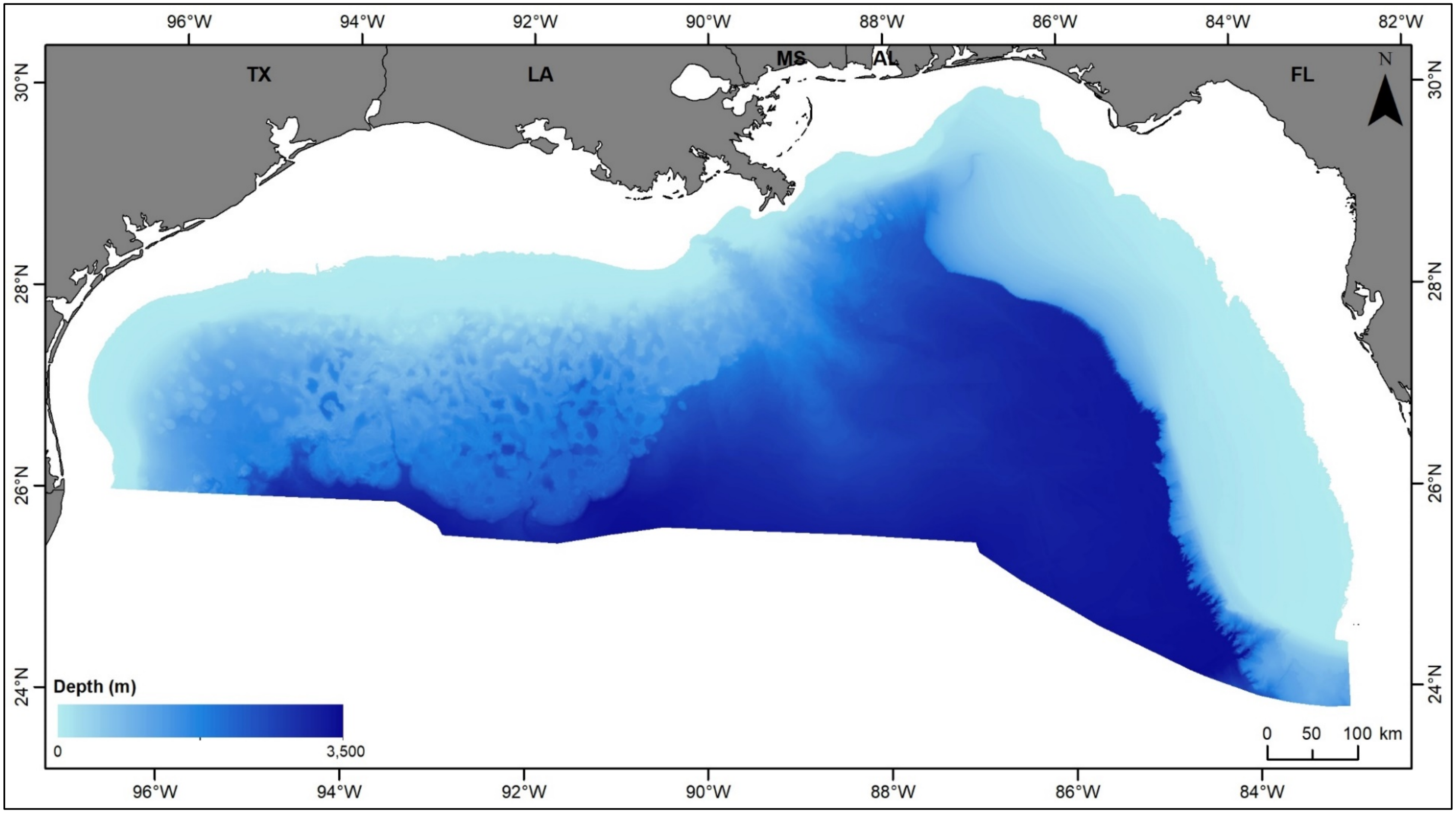

Figure B-1. Depth of the seafloor, 100 x 100 m resolution.

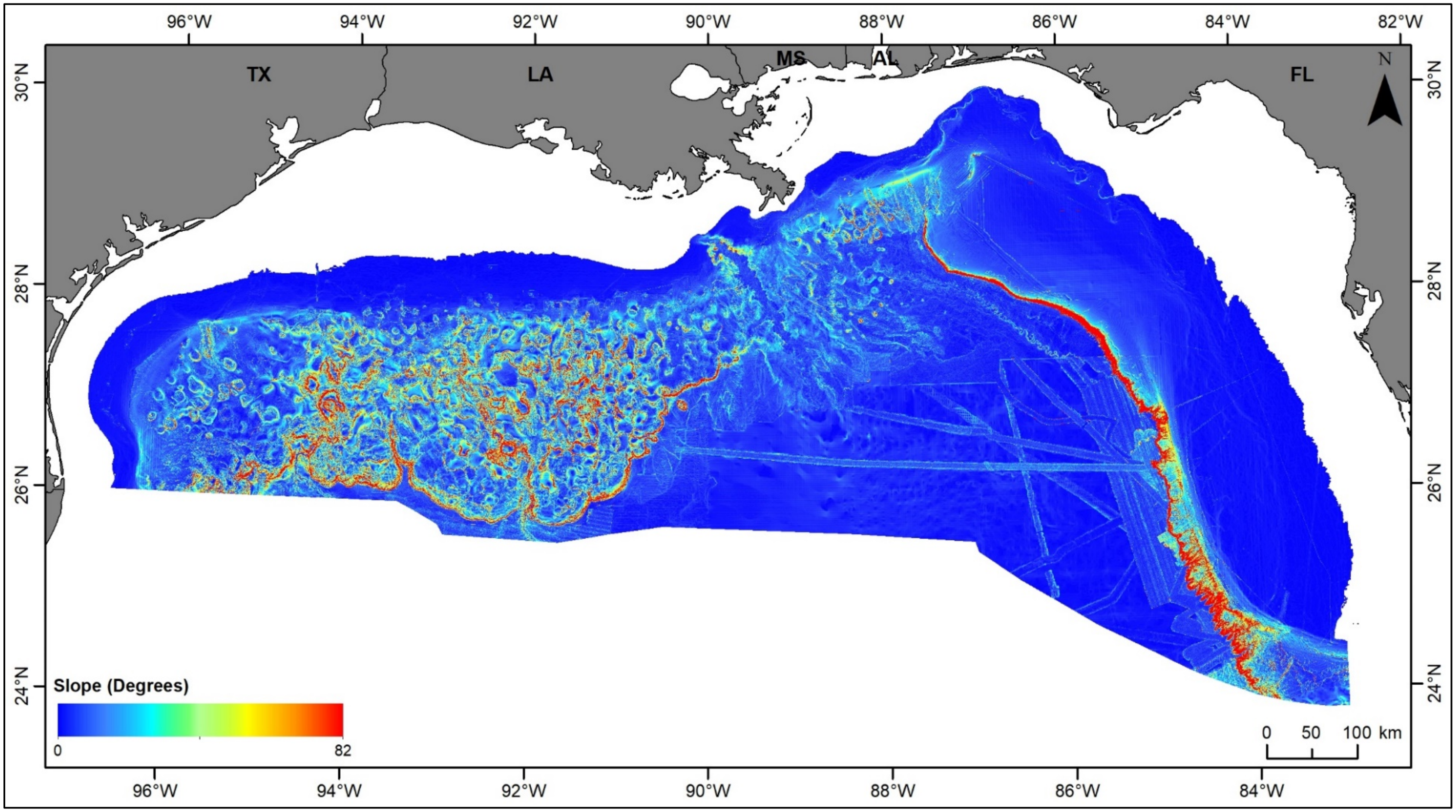

Figure B-2. Slope of the seafloor, 100 x 100 m resolution.

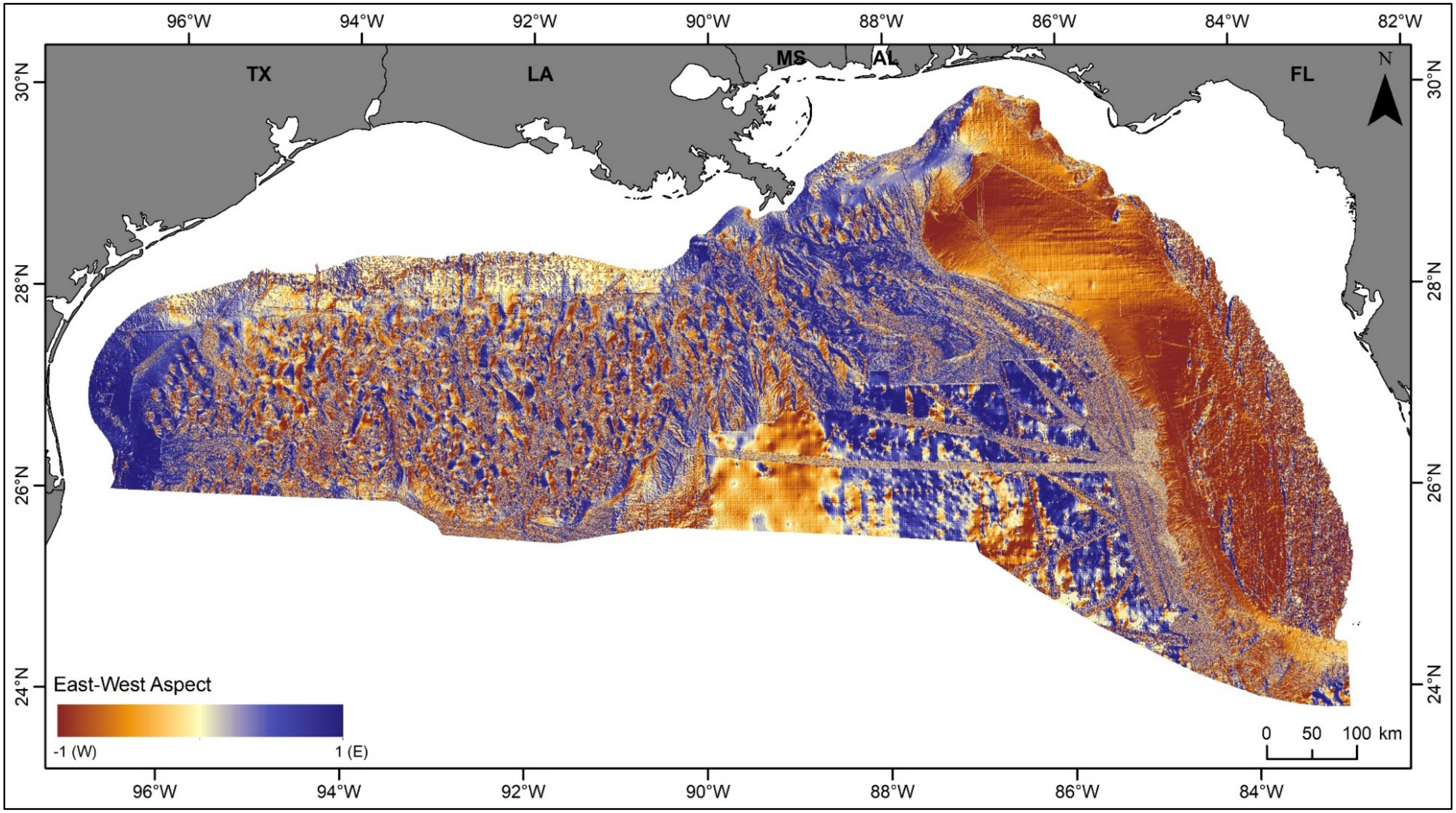

Figure B-3. East-west aspect (sine of seafloor slope direction), 100 x 100 m resolution.

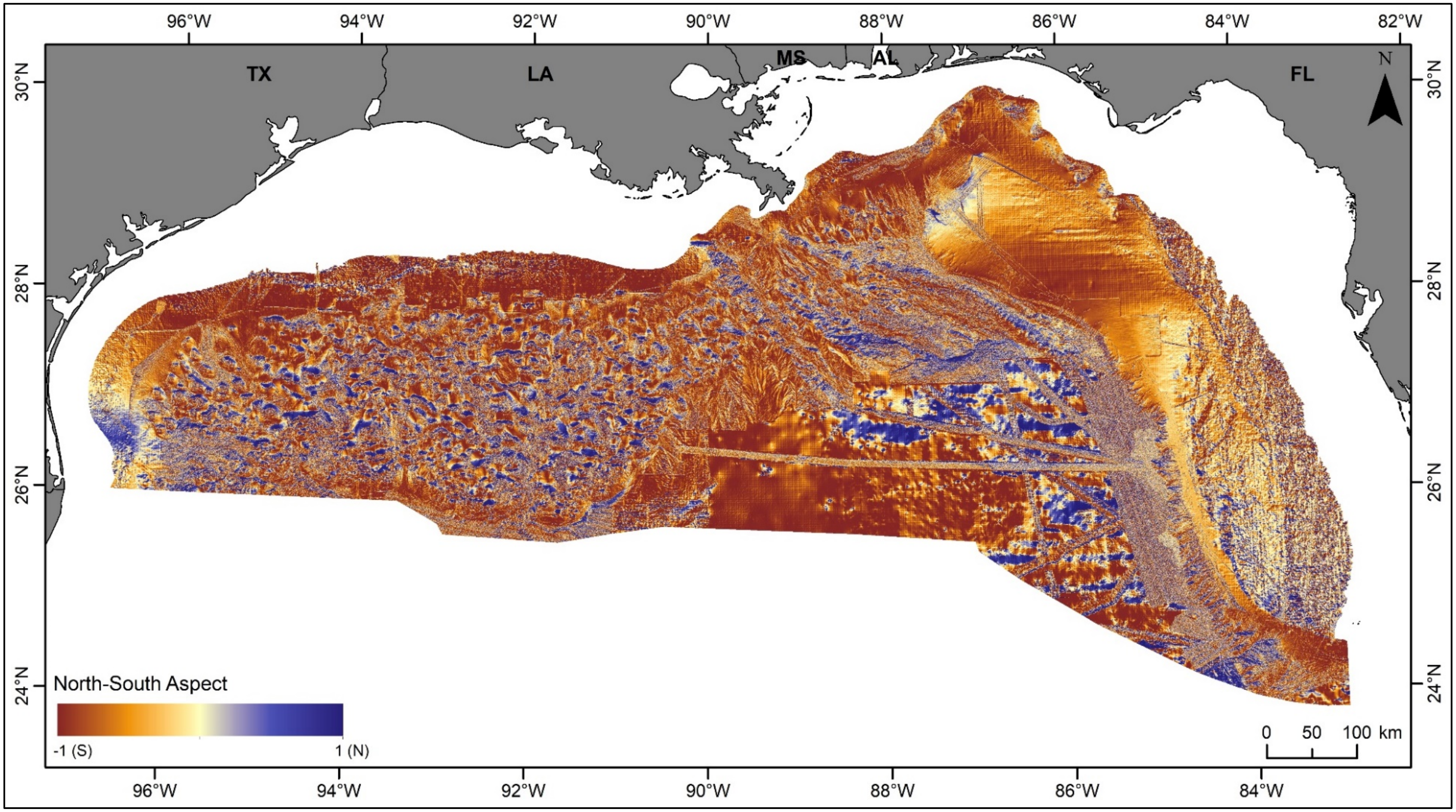

Figure B-4. North-south aspect (sine of seafloor slope direction), 100 x 100 m resolution.

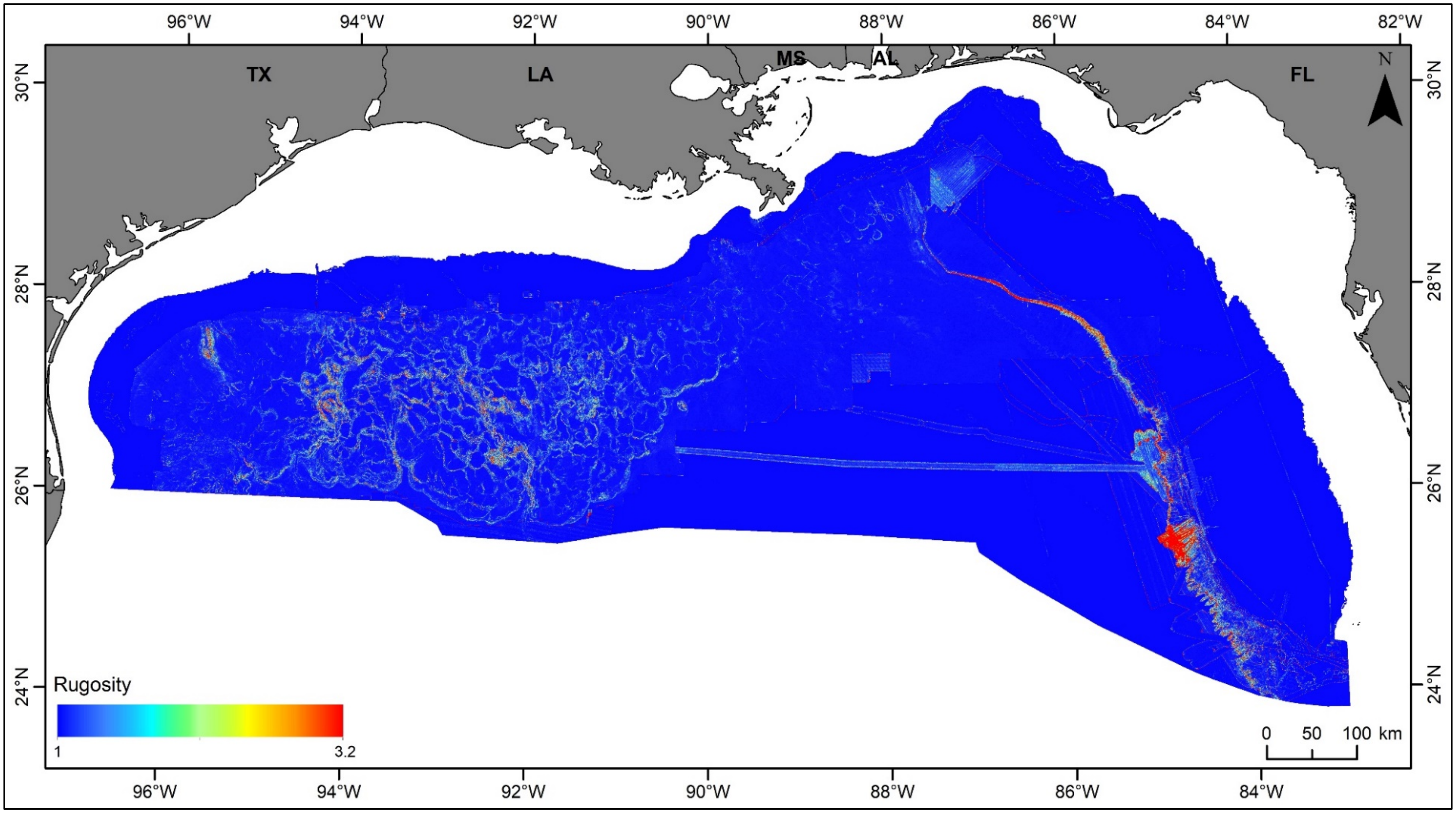

Figure B-5. Rugosity of the seafloor (arc-chord ratio method), 100 x 100 m resolution.

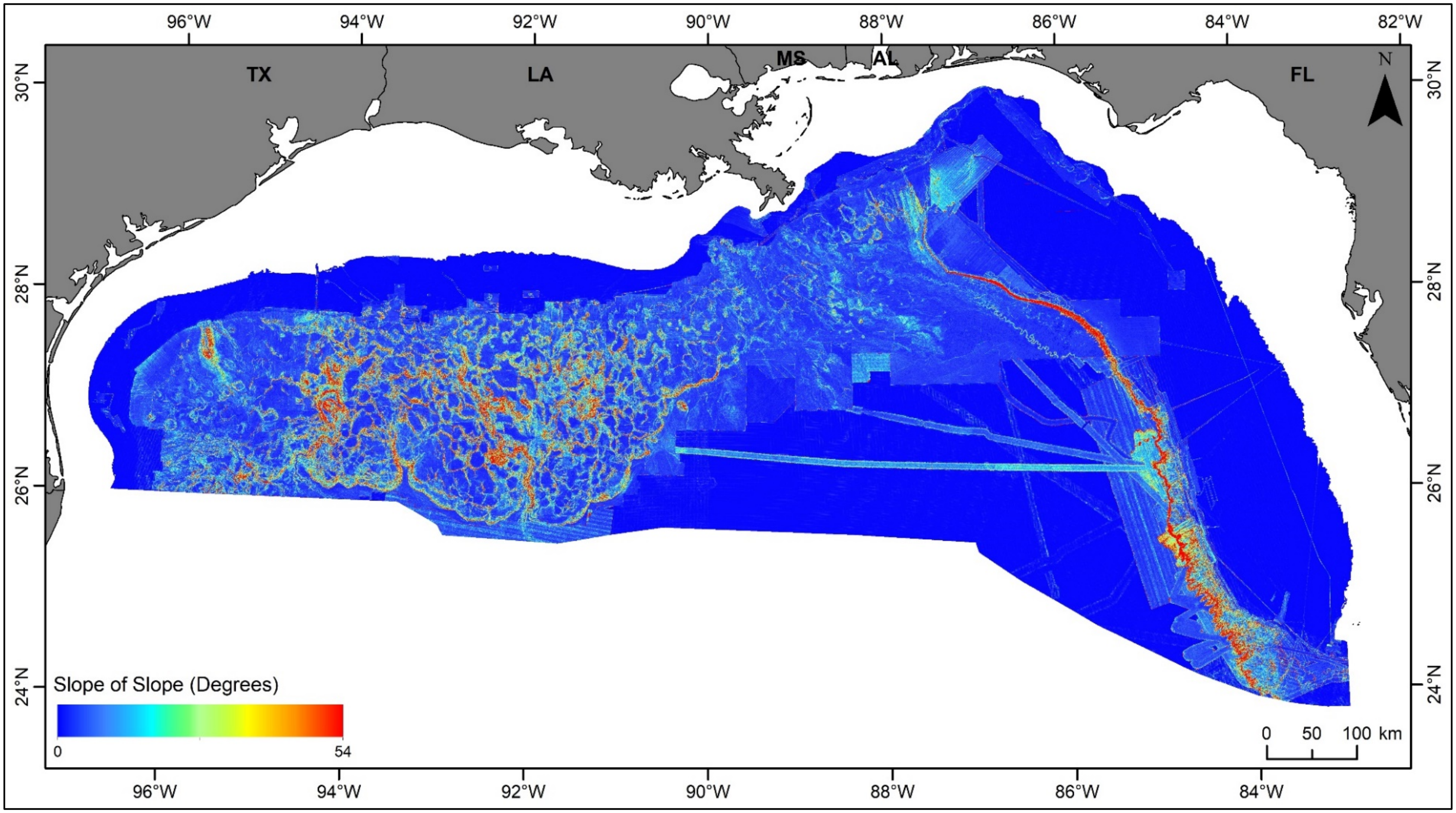

Figure B-6. Slope of slope of the seafloor, 100 x 100 m resolution.

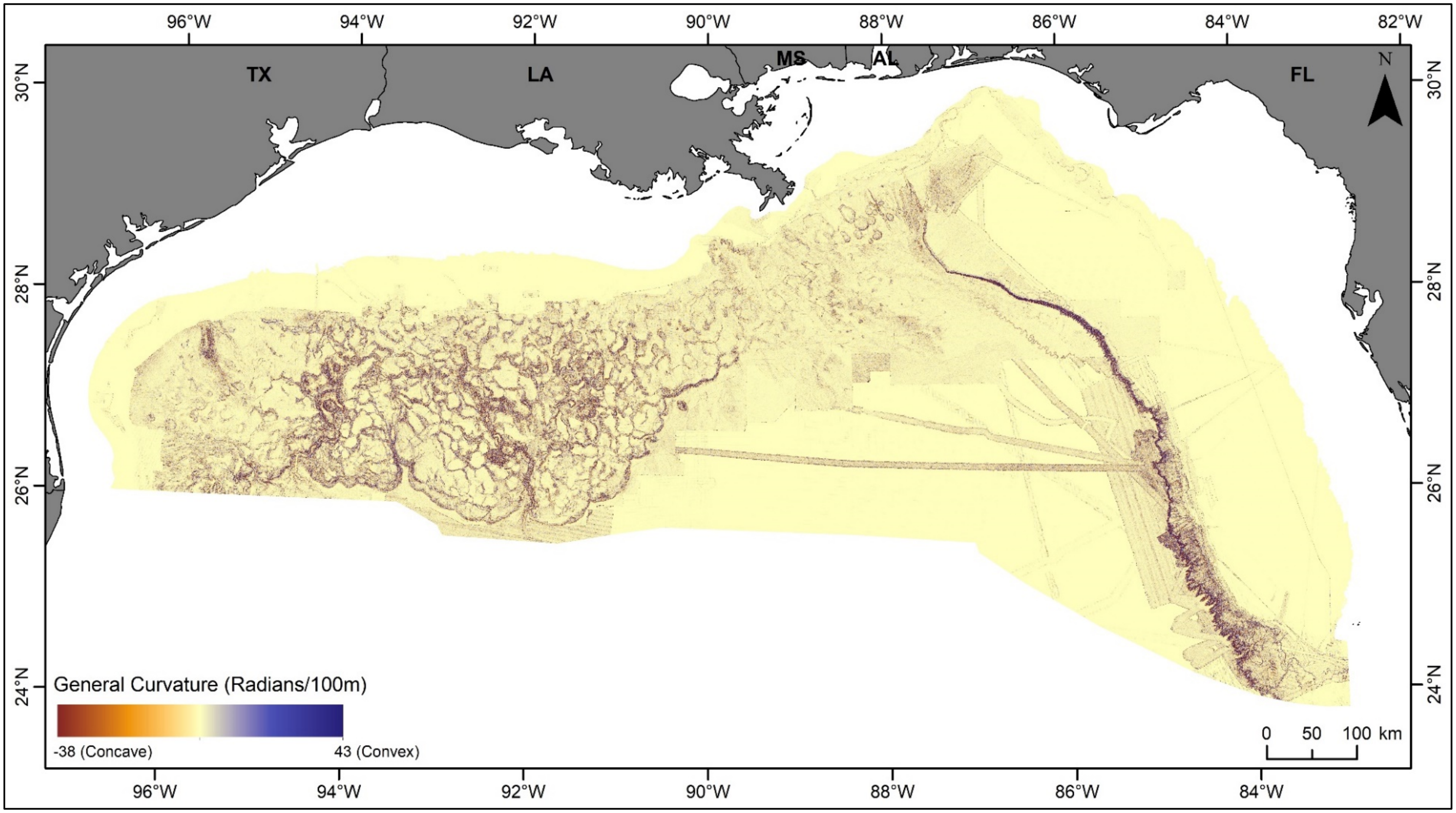

Figure B-7. General curvature of the seafloor, 100 x 100 m resolution.

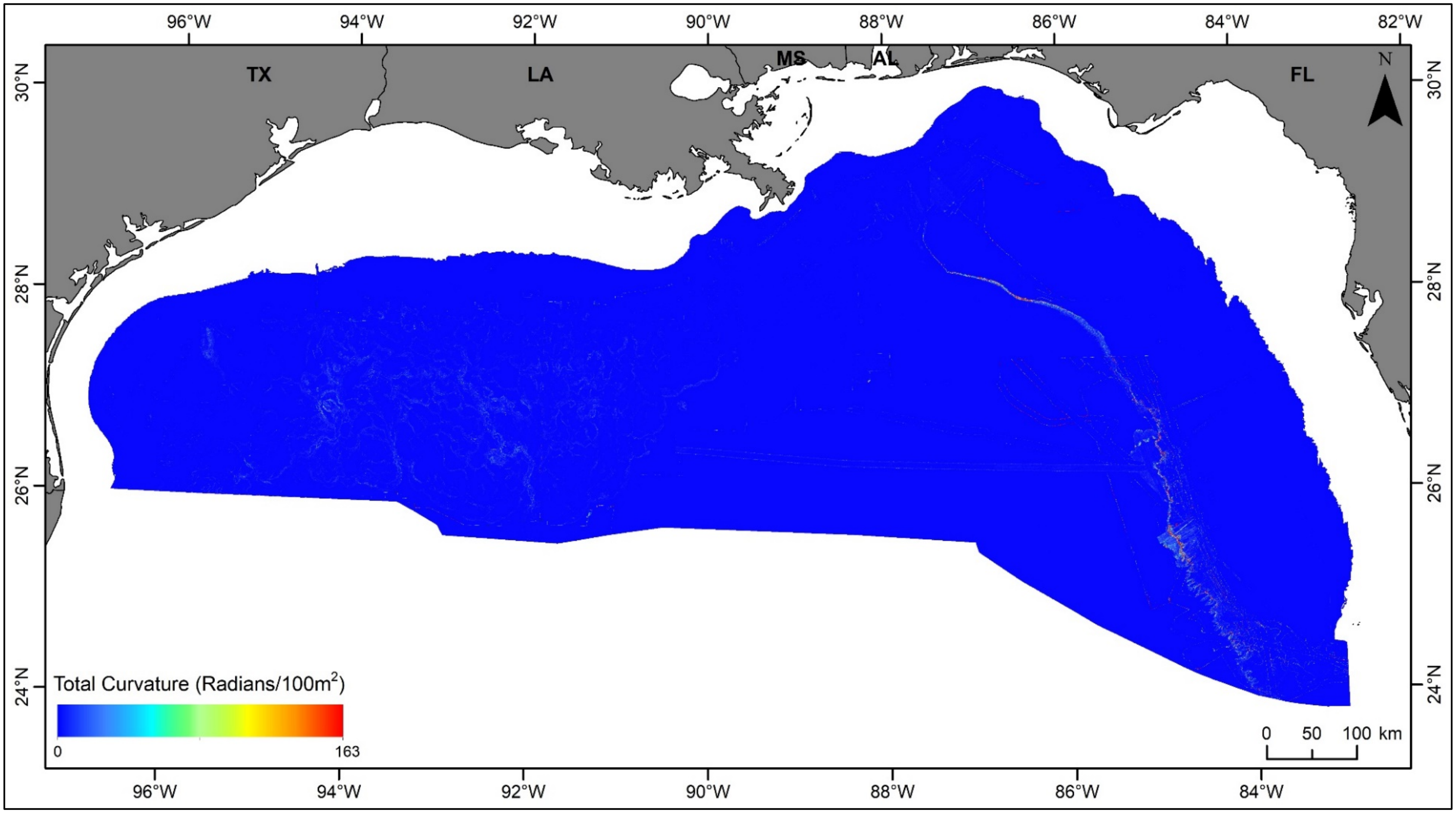

Figure B-8. Total curvature of the seafloor, 100 x 100 m resolution.

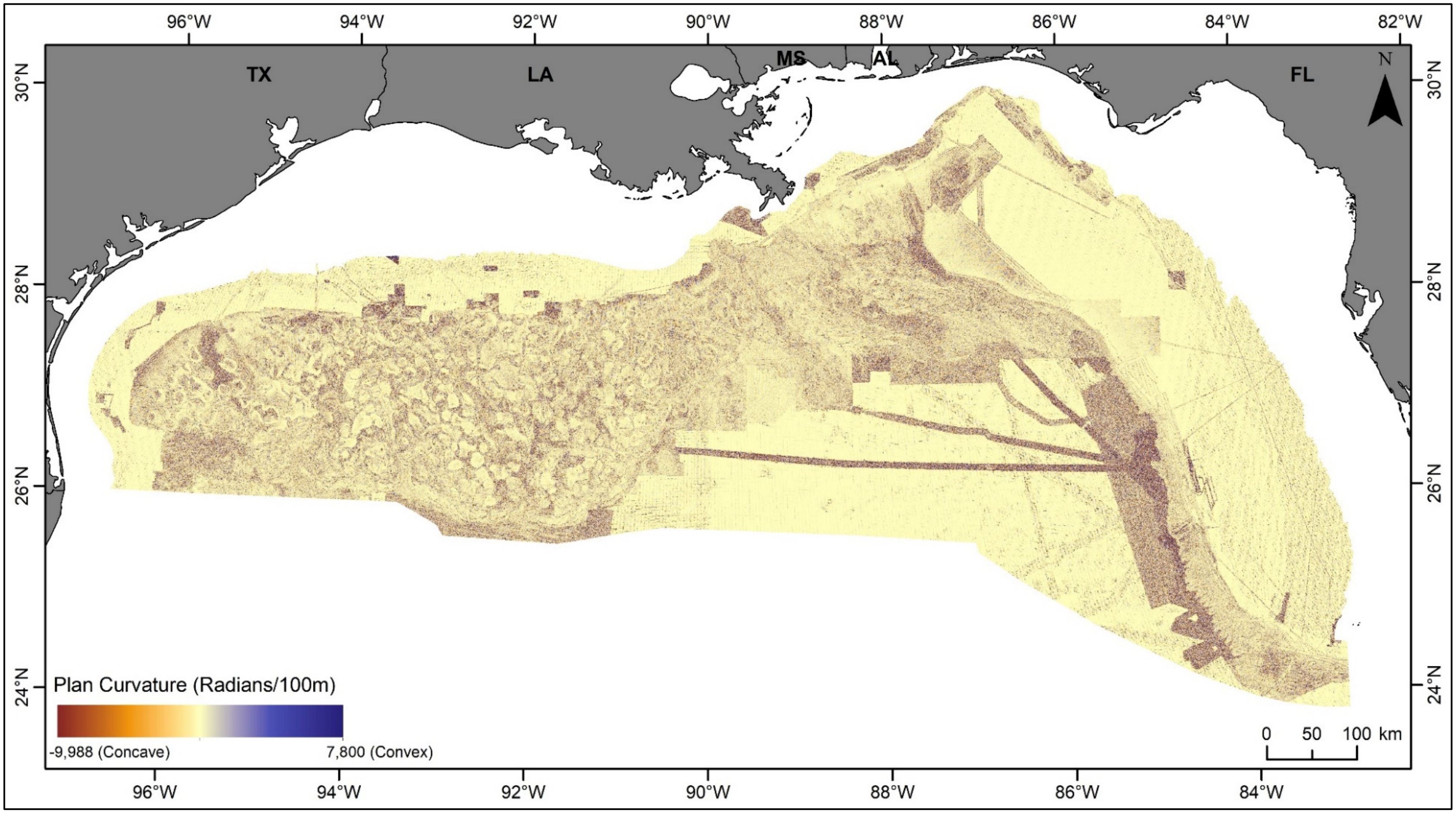

Figure B-9. Plan (i.e., planform) curvature of the seafloor, 100 x 100 m resolution.

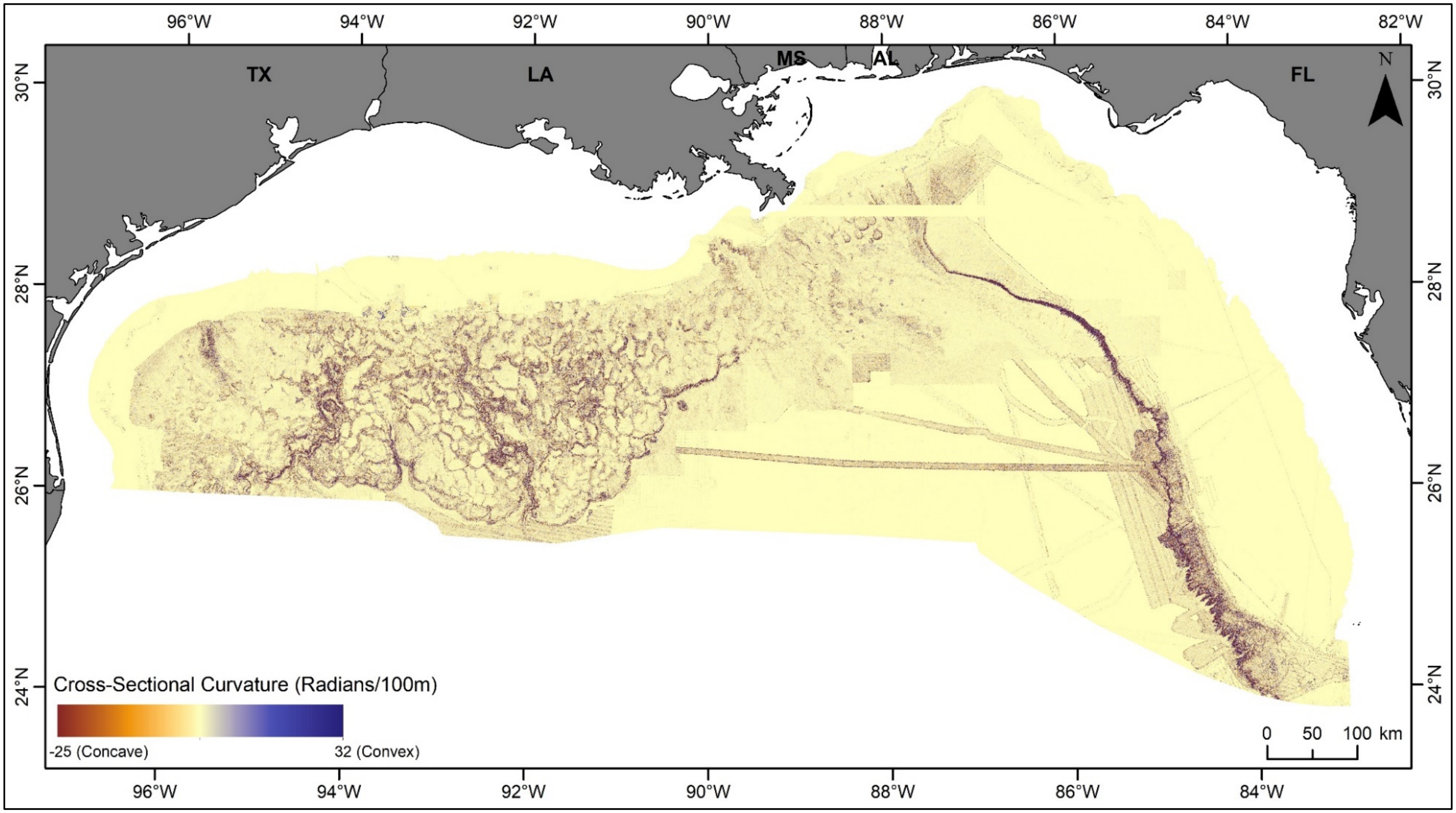

Figure B-10. Cross-sectional curvature of the seafloor, 100 x 100 m resolution.

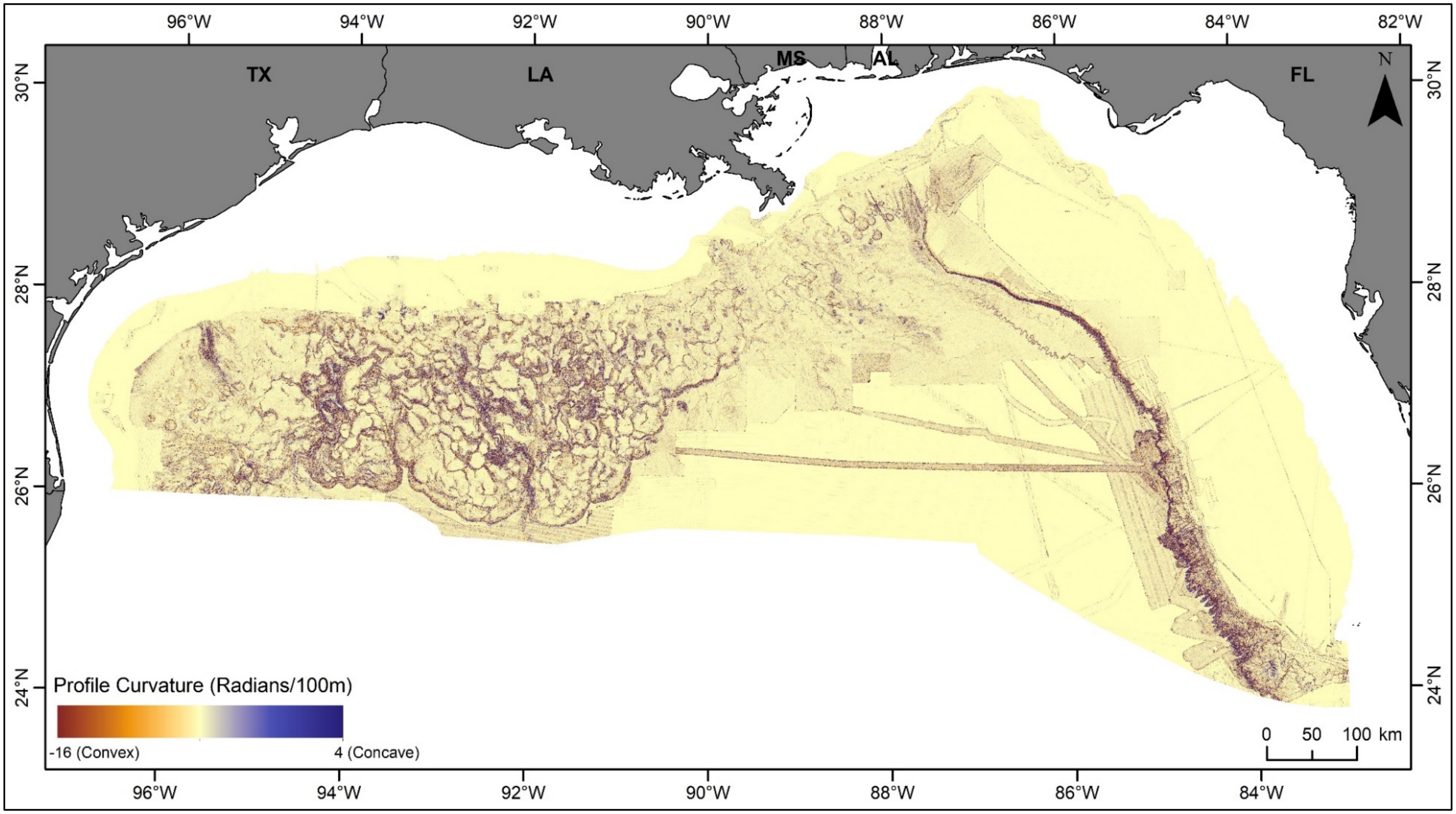

Figure B-11. Profile curvature of the seafloor, 100 x 100 m resolution.

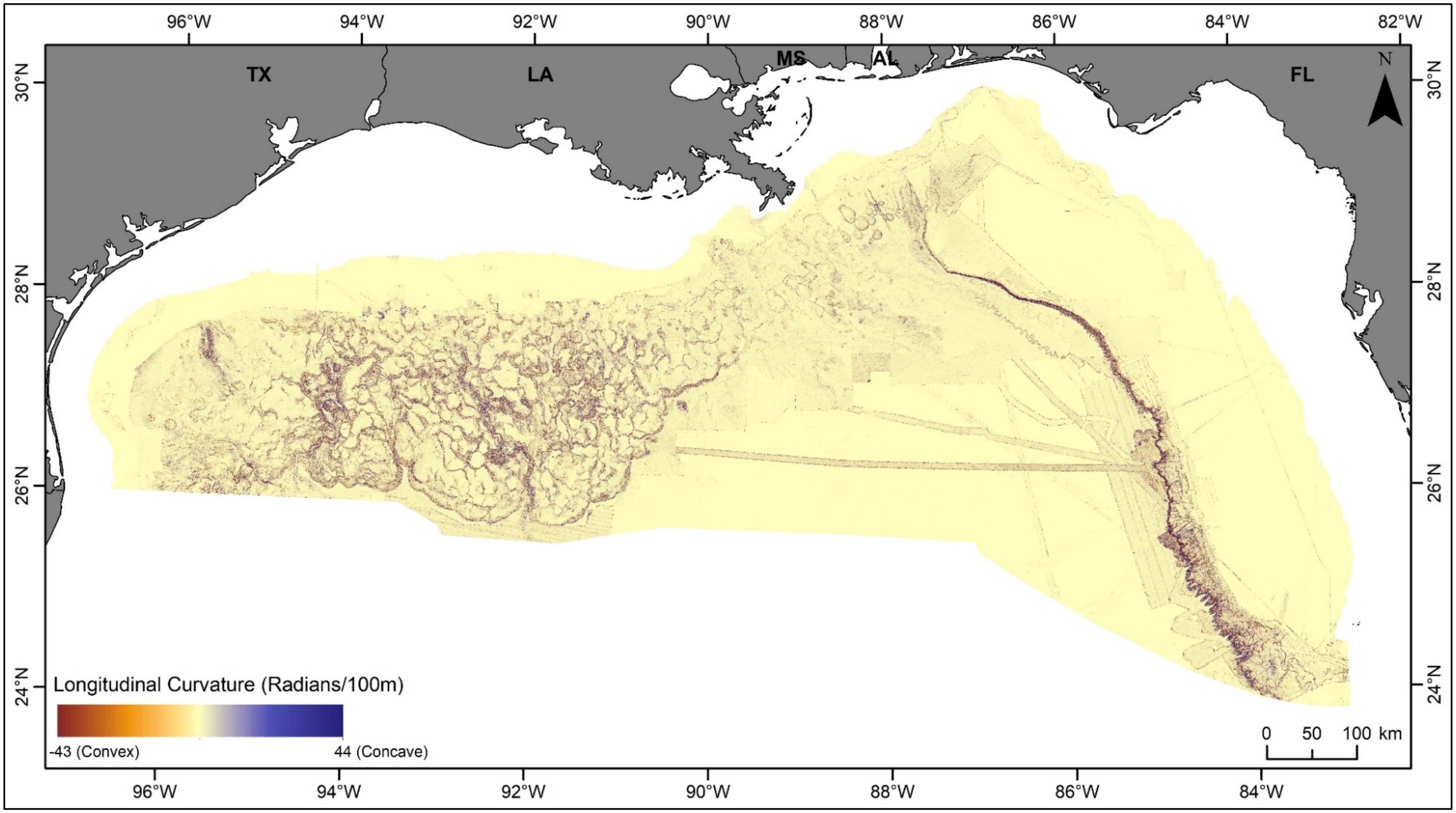

Figure B-12. Longitudinal curvature of the seafloor, 100 x 100 m resolution.

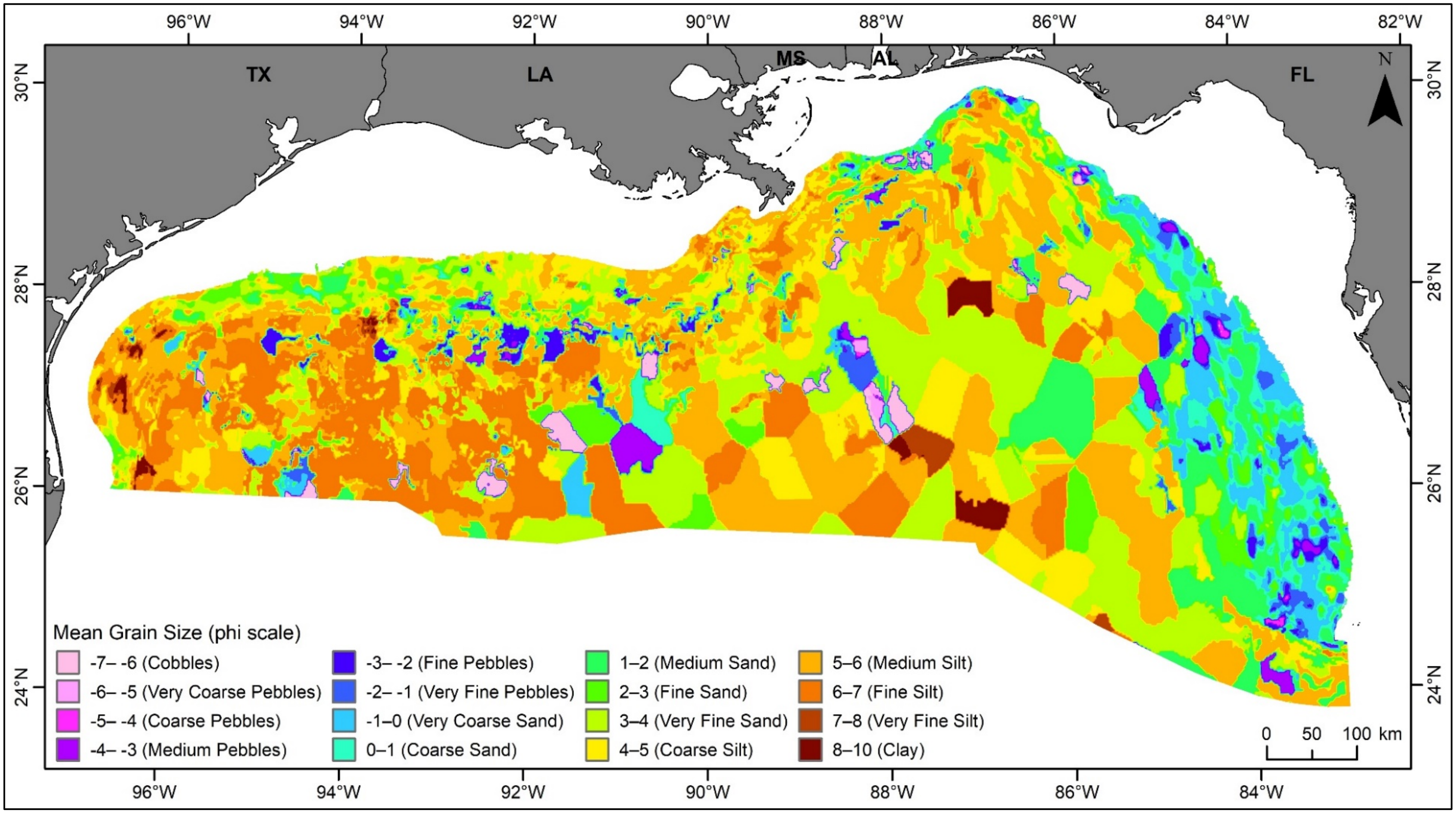

Figure B-13. Surficial sediment mean grain size, 100 x 100 m resolution.

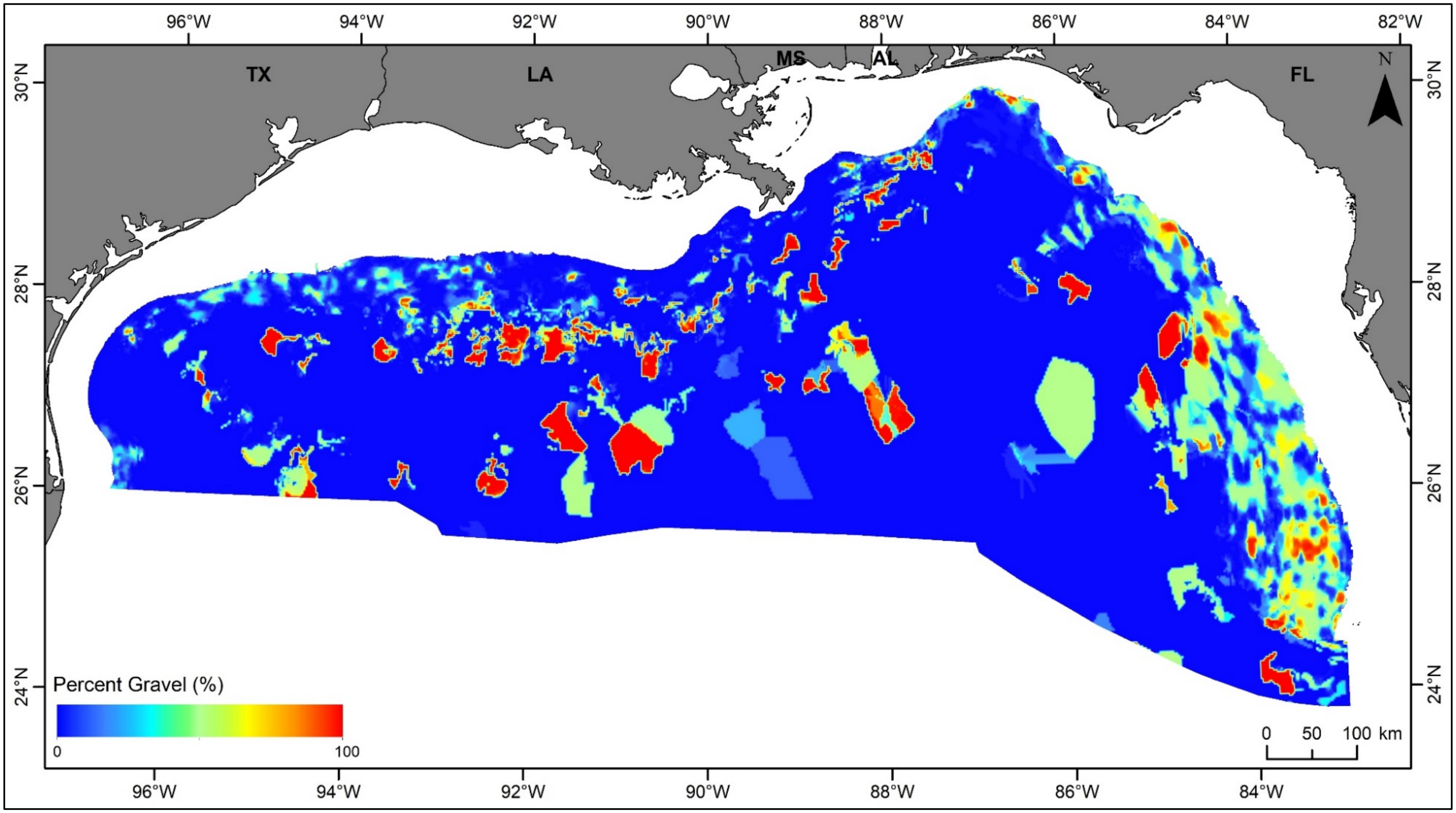

Figure B-14. Surficial sediment percent gravel, 100 x 100 m resolution.

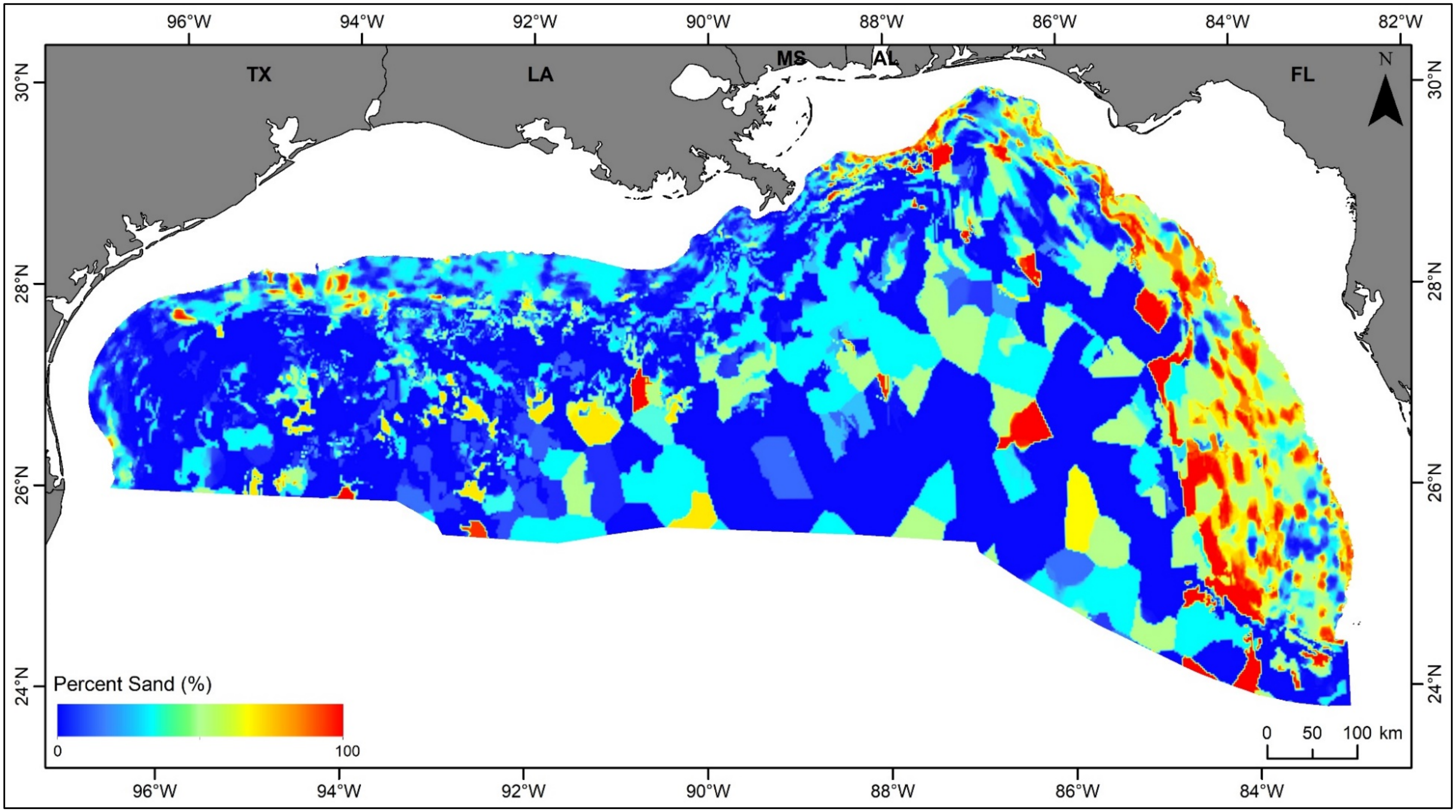

Figure B-15. Surficial sediment percent sand, 100 x 100 m resolution.

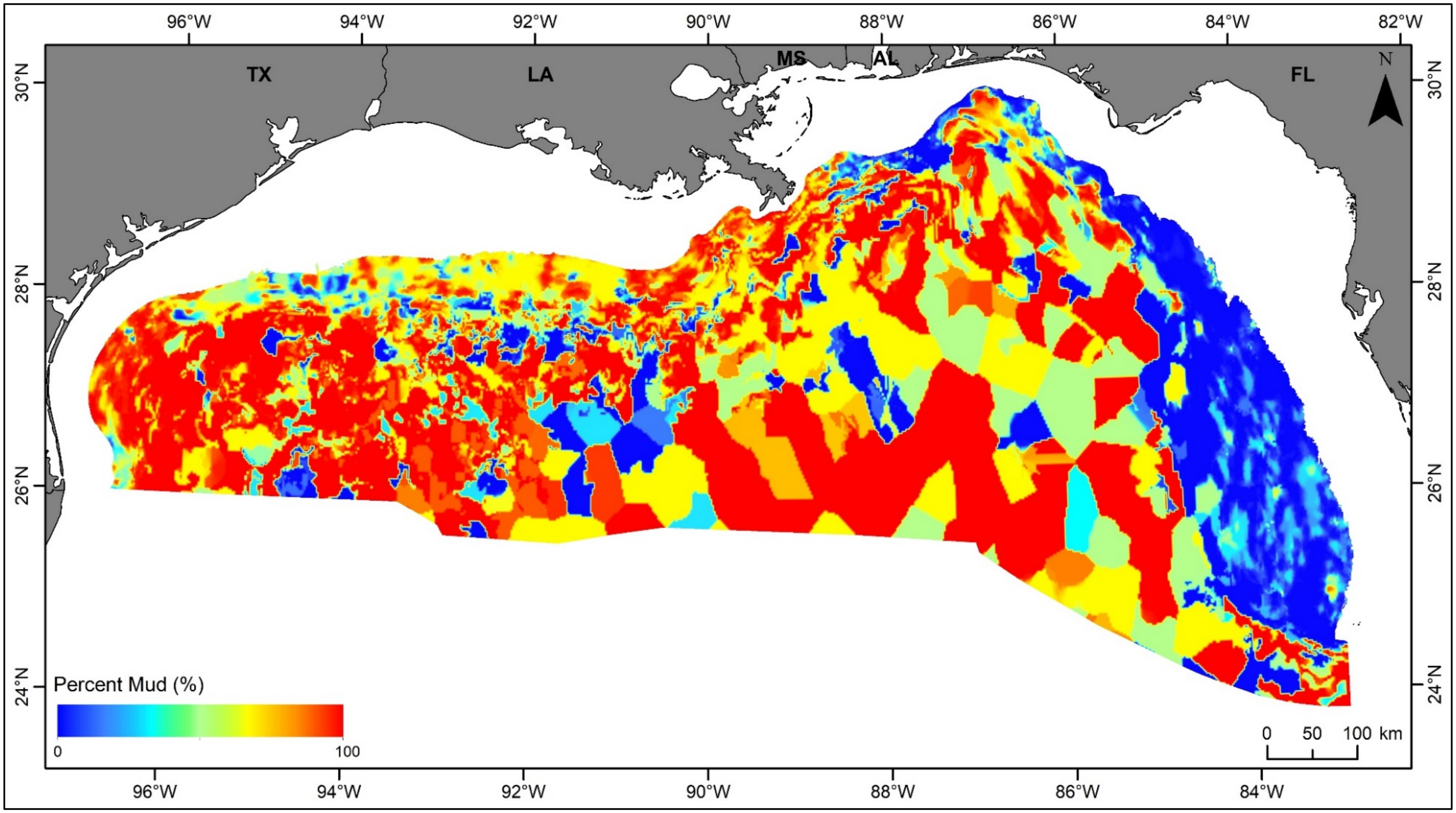

Figure B-16. Surficial sediment percent mud, 100 x 100 m resolution.

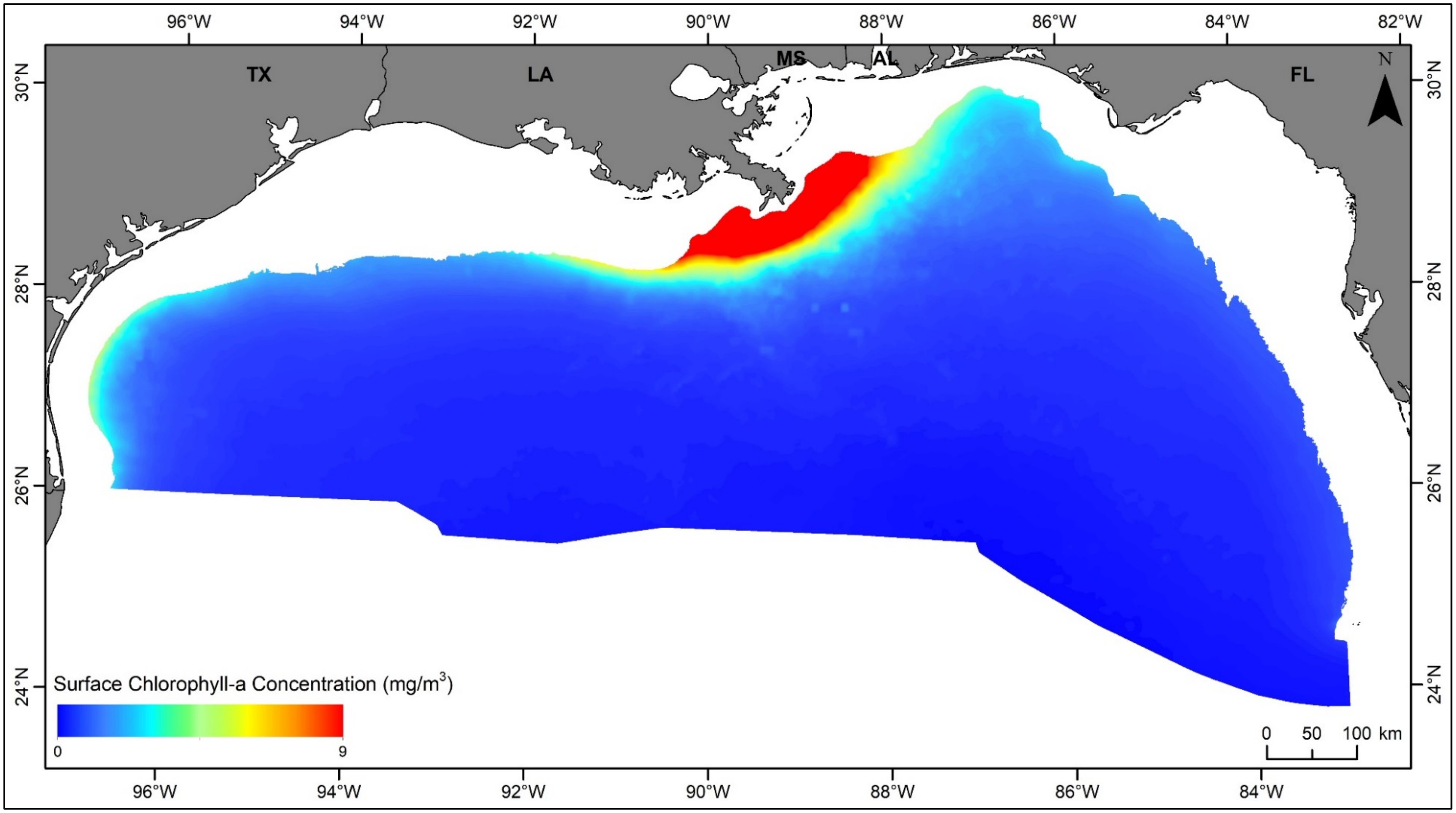

Figure B-17. Annual mean sea surface chlorophyll-a concentration, 100 x 100 m resolution.

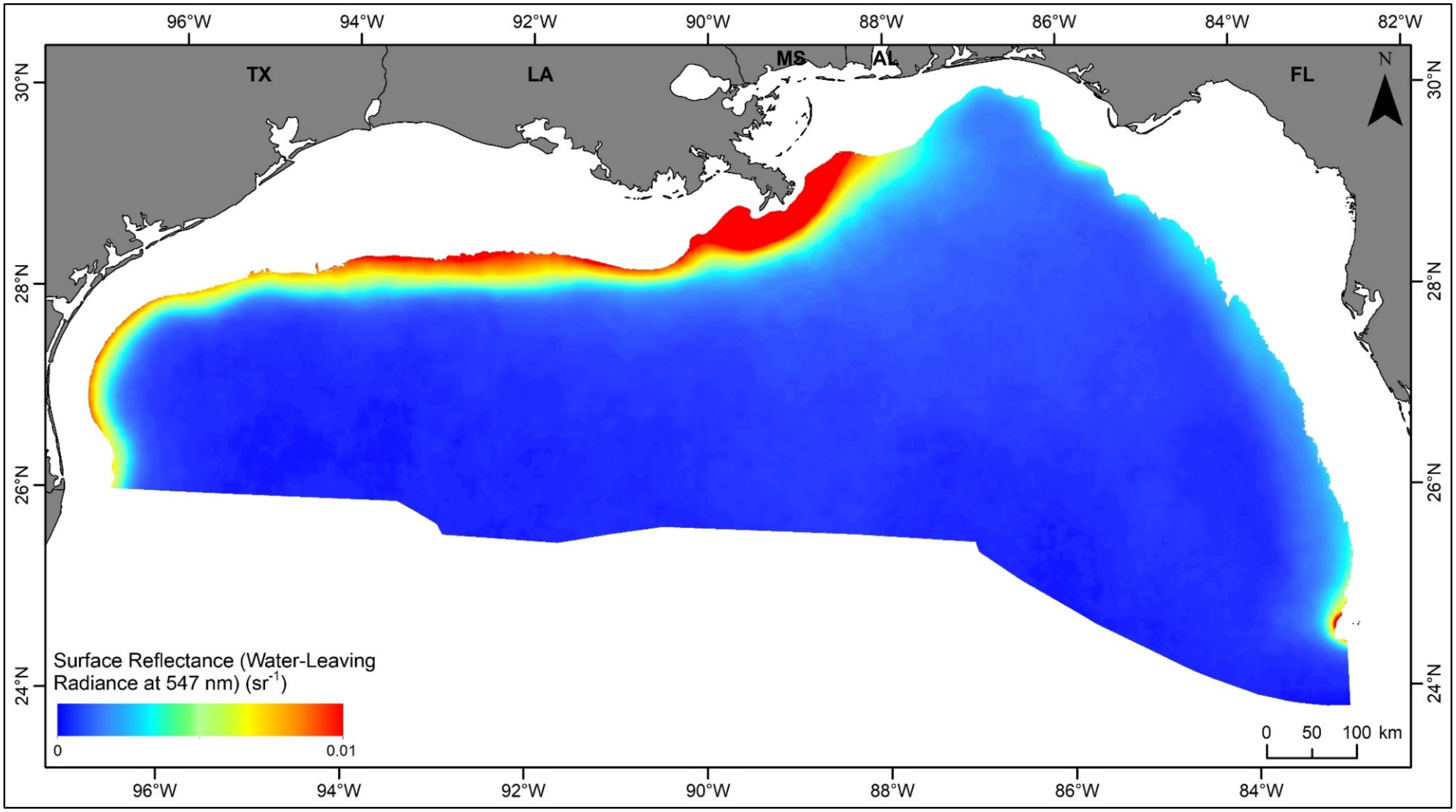

Figure B-18. Annual mean sea surface reflectance (water-leaving radiance at 547 nm), 100 x 100 m resolution.

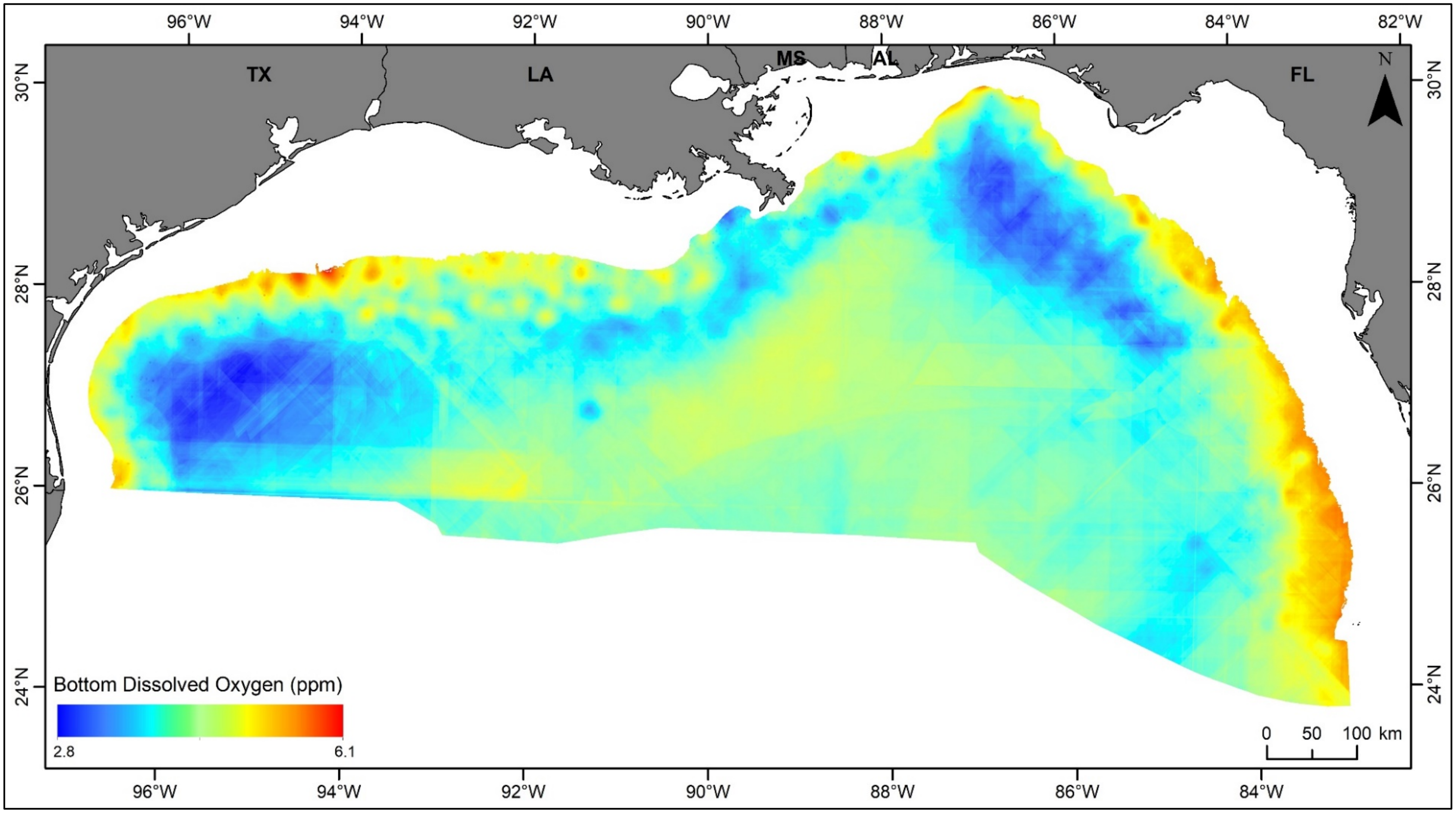

Figure B-19. Annual mean bottom dissolved oxygen, 100 x 100 m resolution.

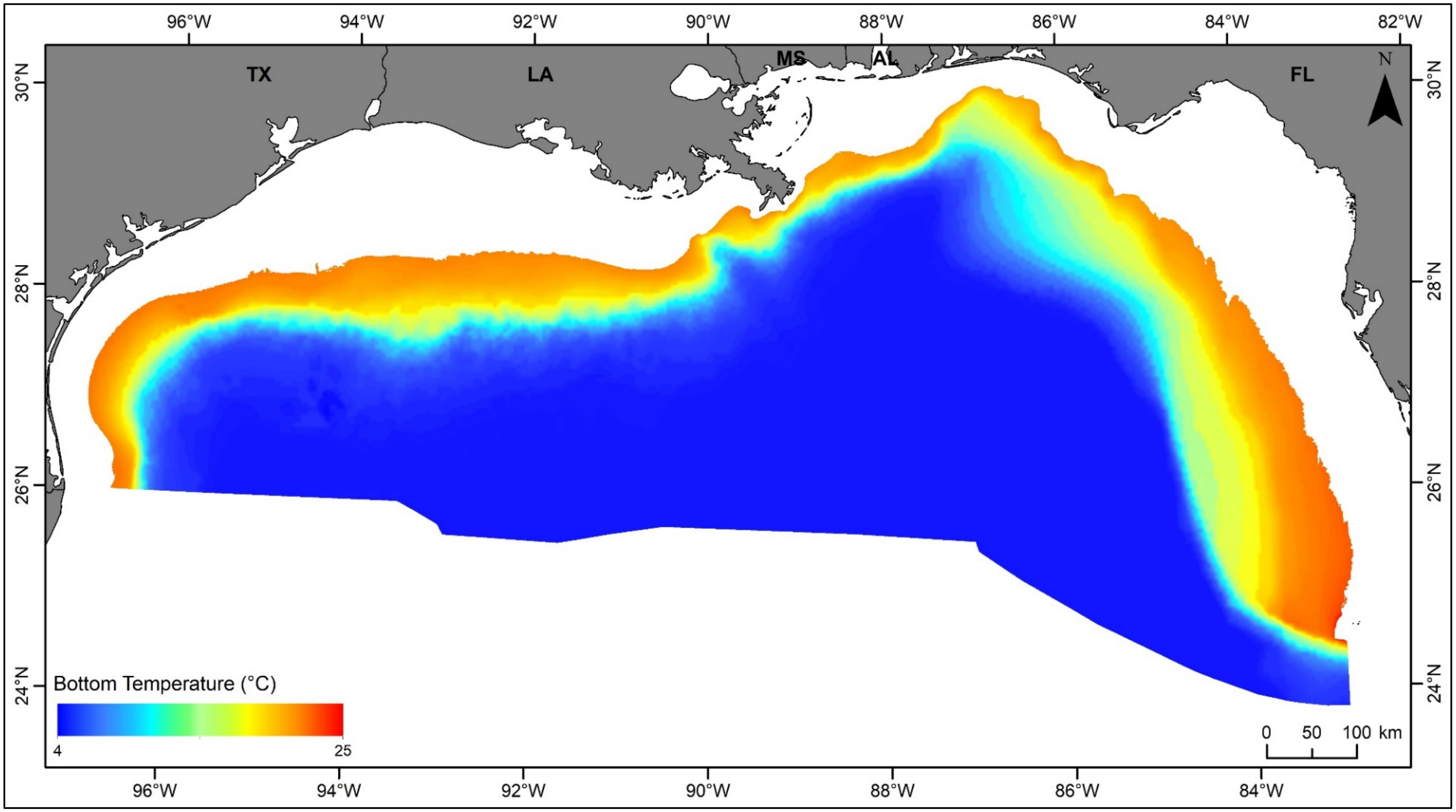

Figure B-20. Annual mean bottom temperature, 100 x 100 m resolution.

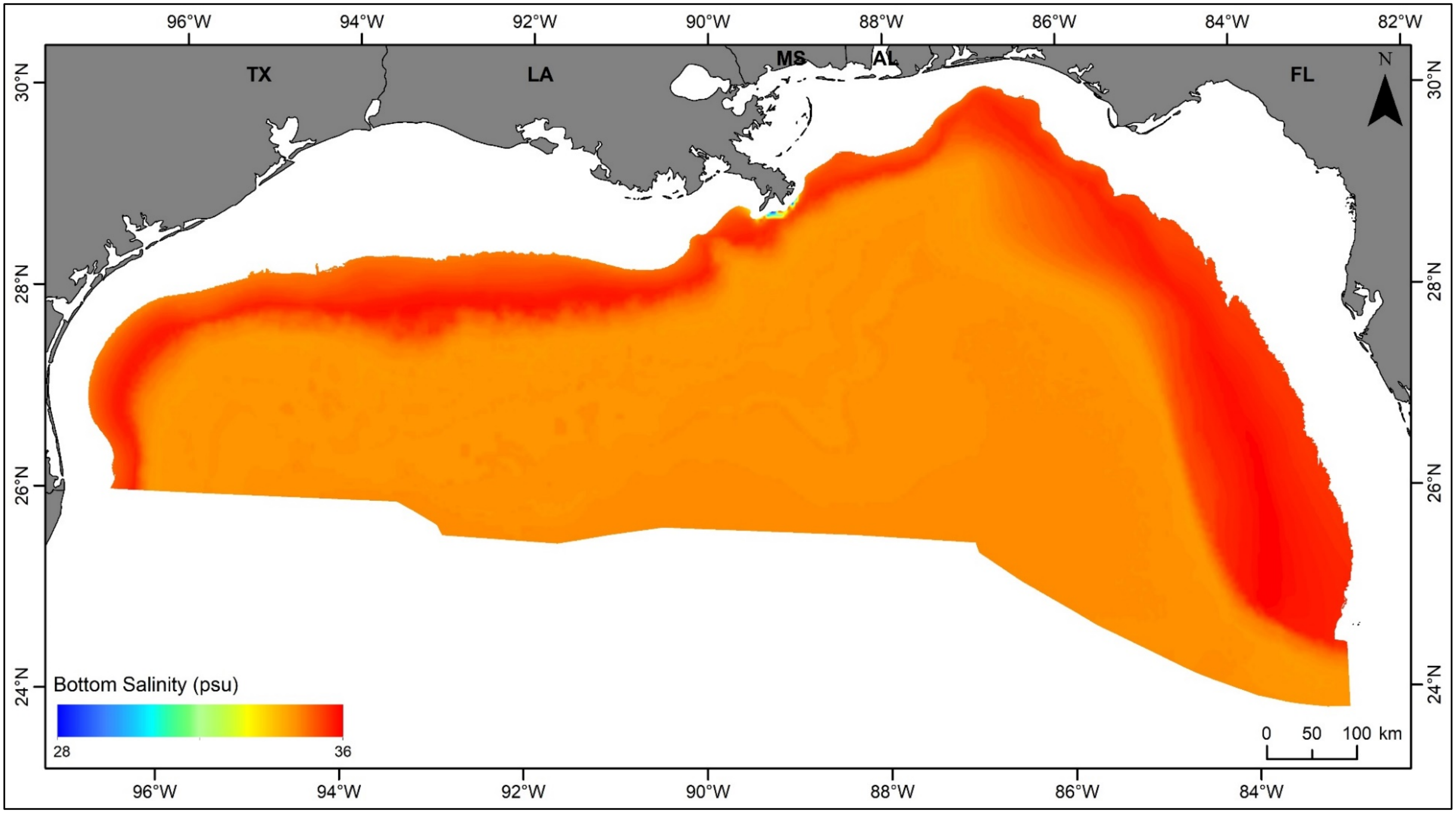

Figure B-21. Annual mean bottom salinity, 100 x 100 m resolution.

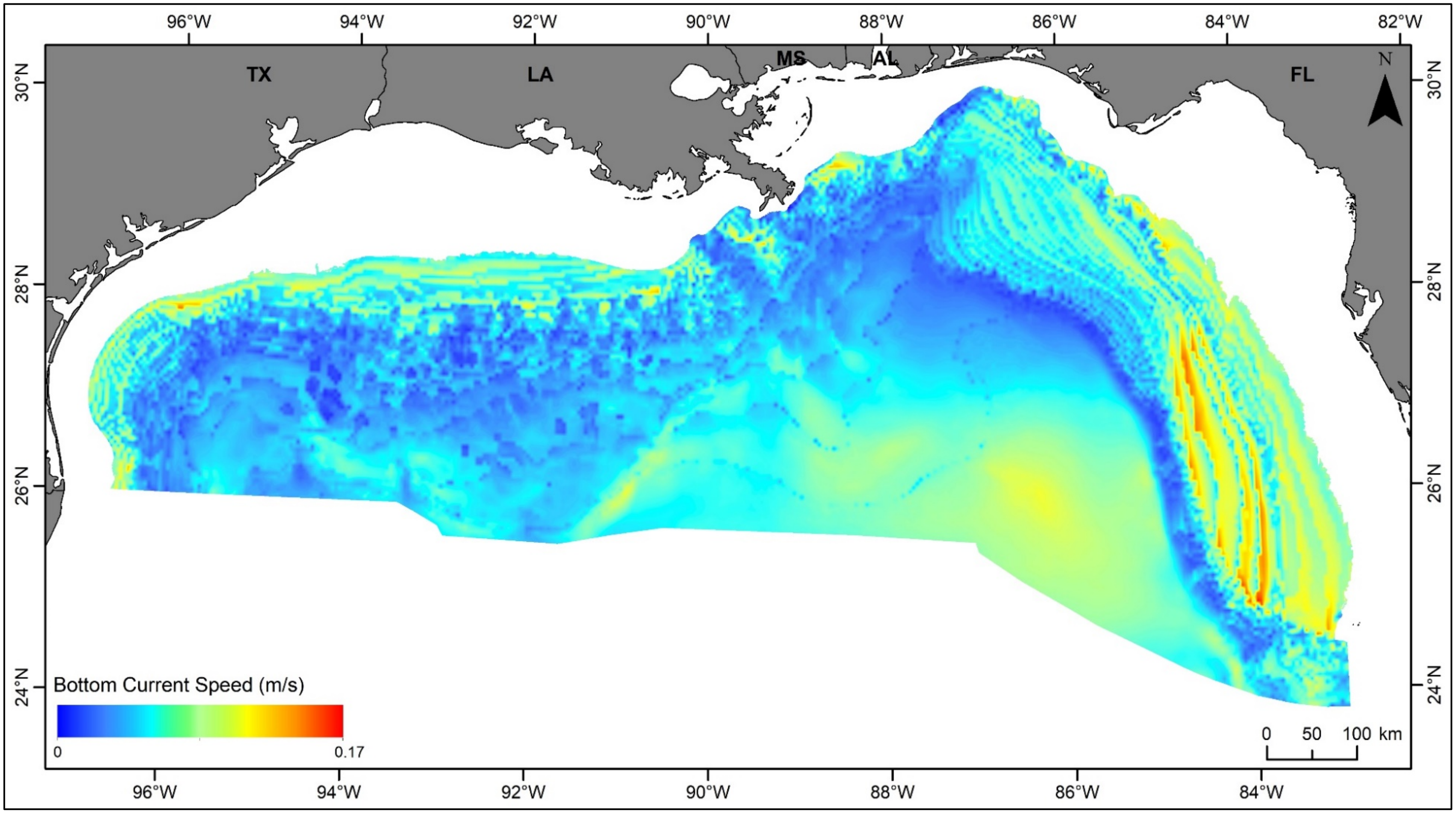

Figure B-22. Annual mean bottom current speed, 100 x 100 m resolution.

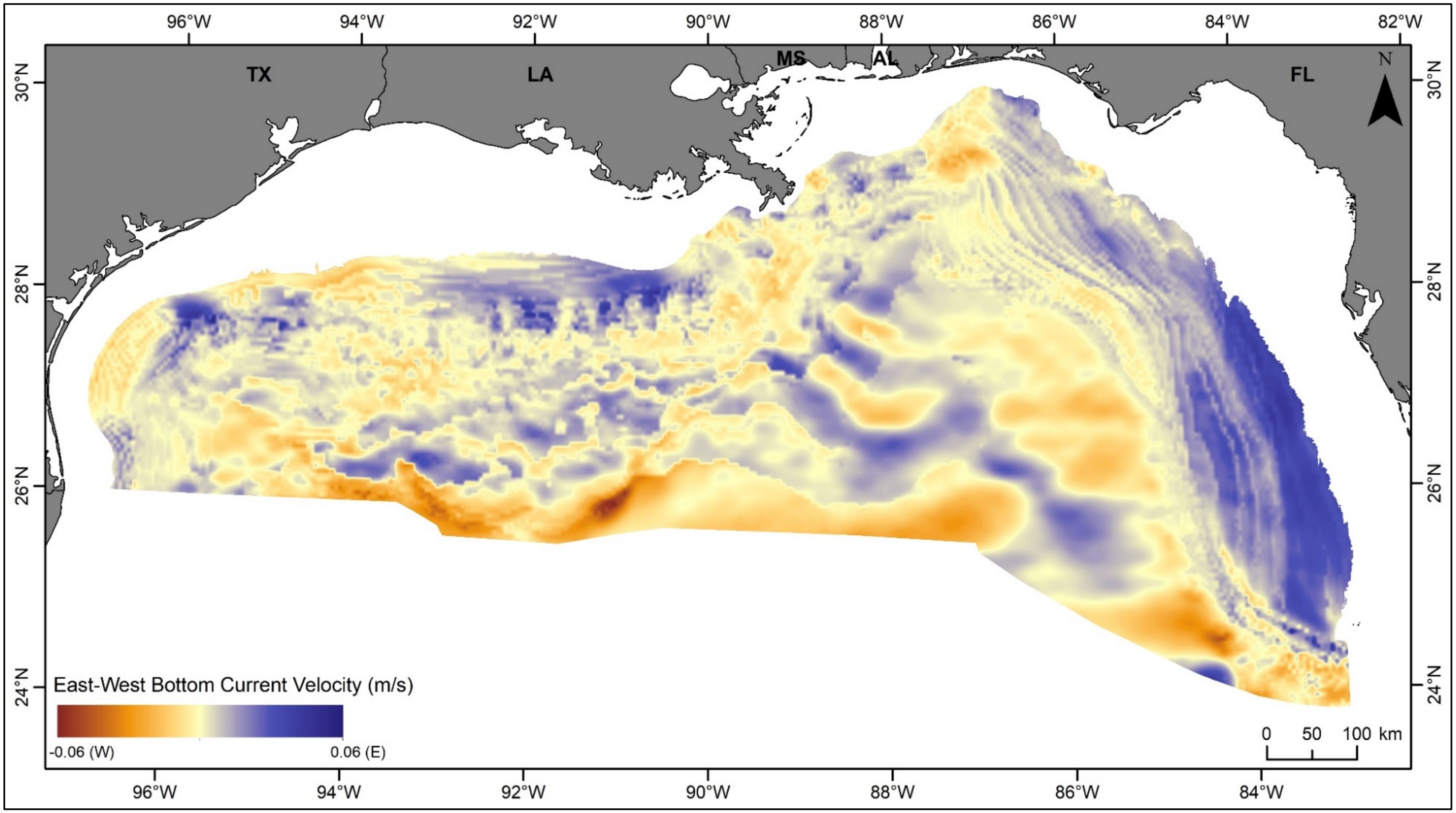

Figure B-23. Annual mean east-west bottom current velocity, 100 x 100 m resolution.

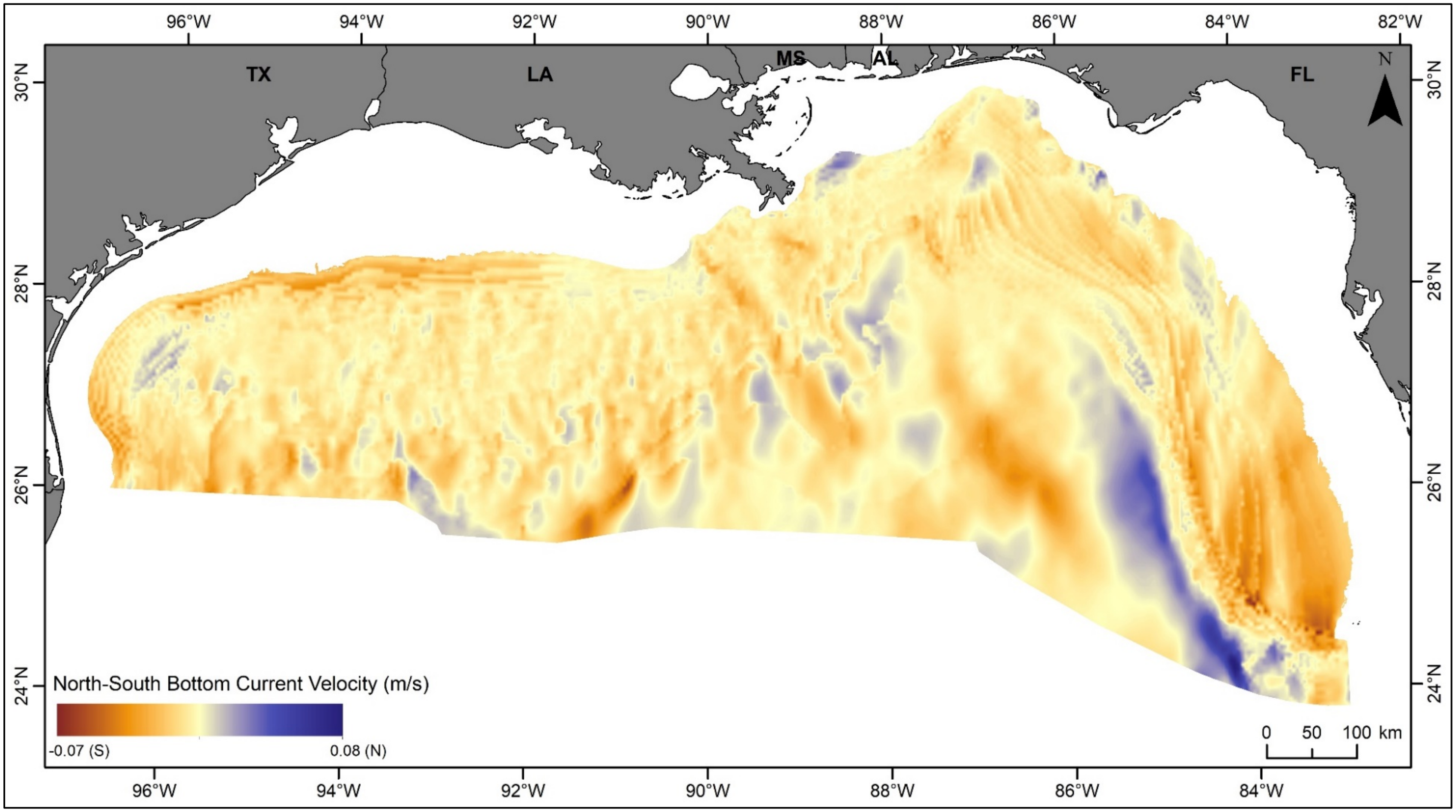

Figure B-24. Annual mean north-south bottom current velocity, 100 x 100 m resolution.

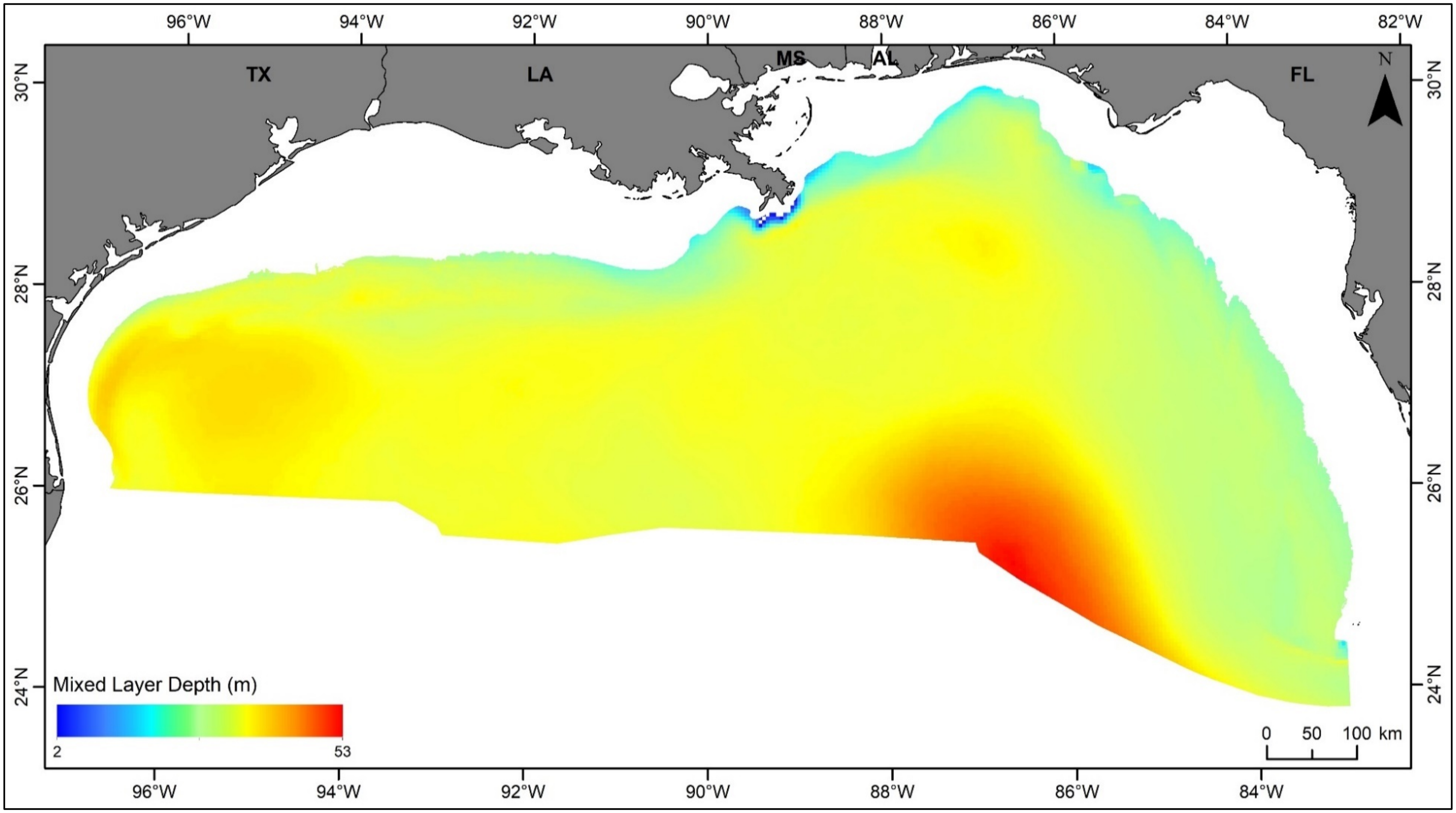

Figure B-25. Annual mean mixed layer depth, 100 x 100 m resolution.

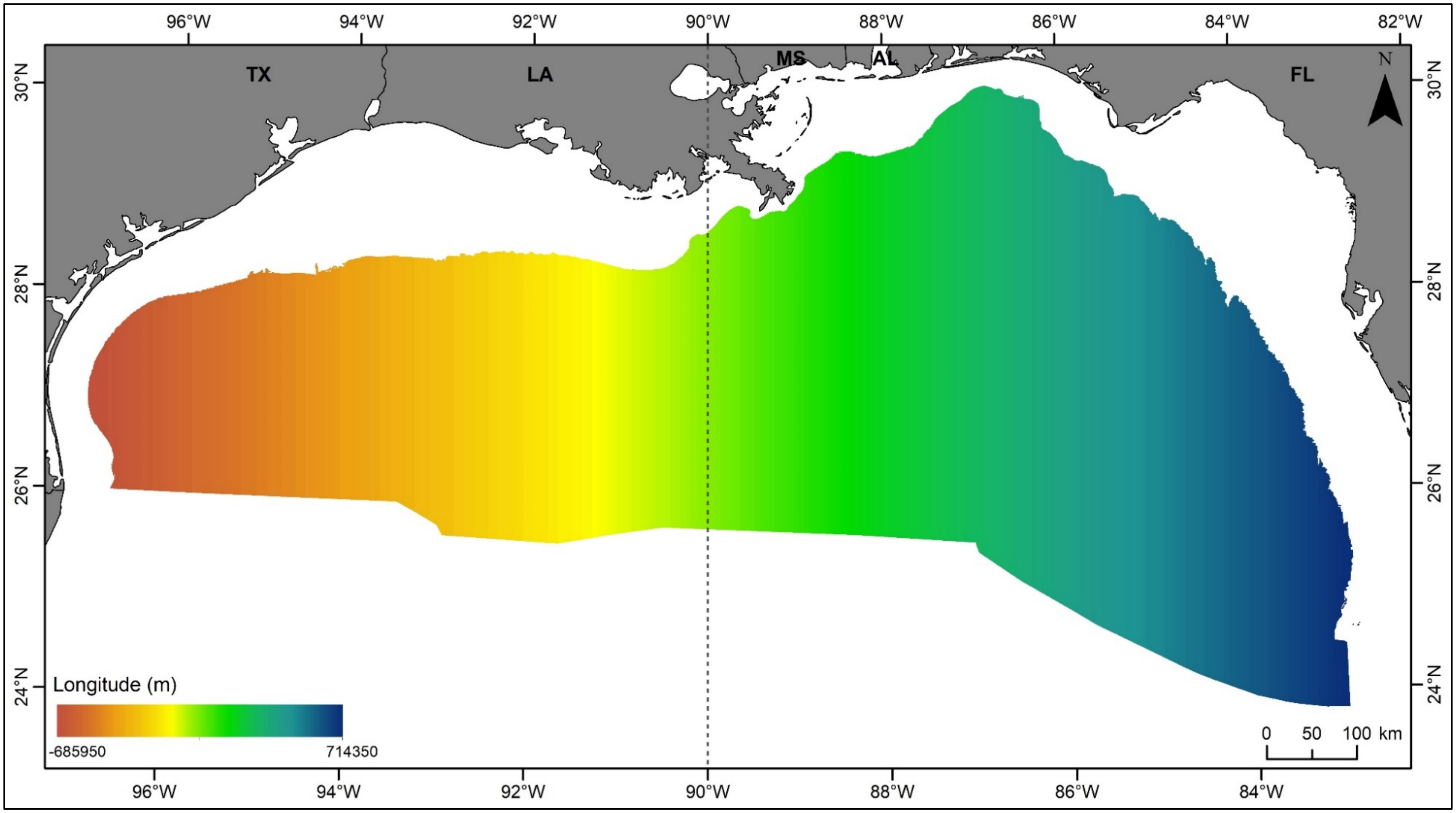

Figure B-26. Longitude (projected), 100 x 100 m resolution.

A dashed gray line depicts the longitude of origin parameter of projected coordinate system, 90 °W.

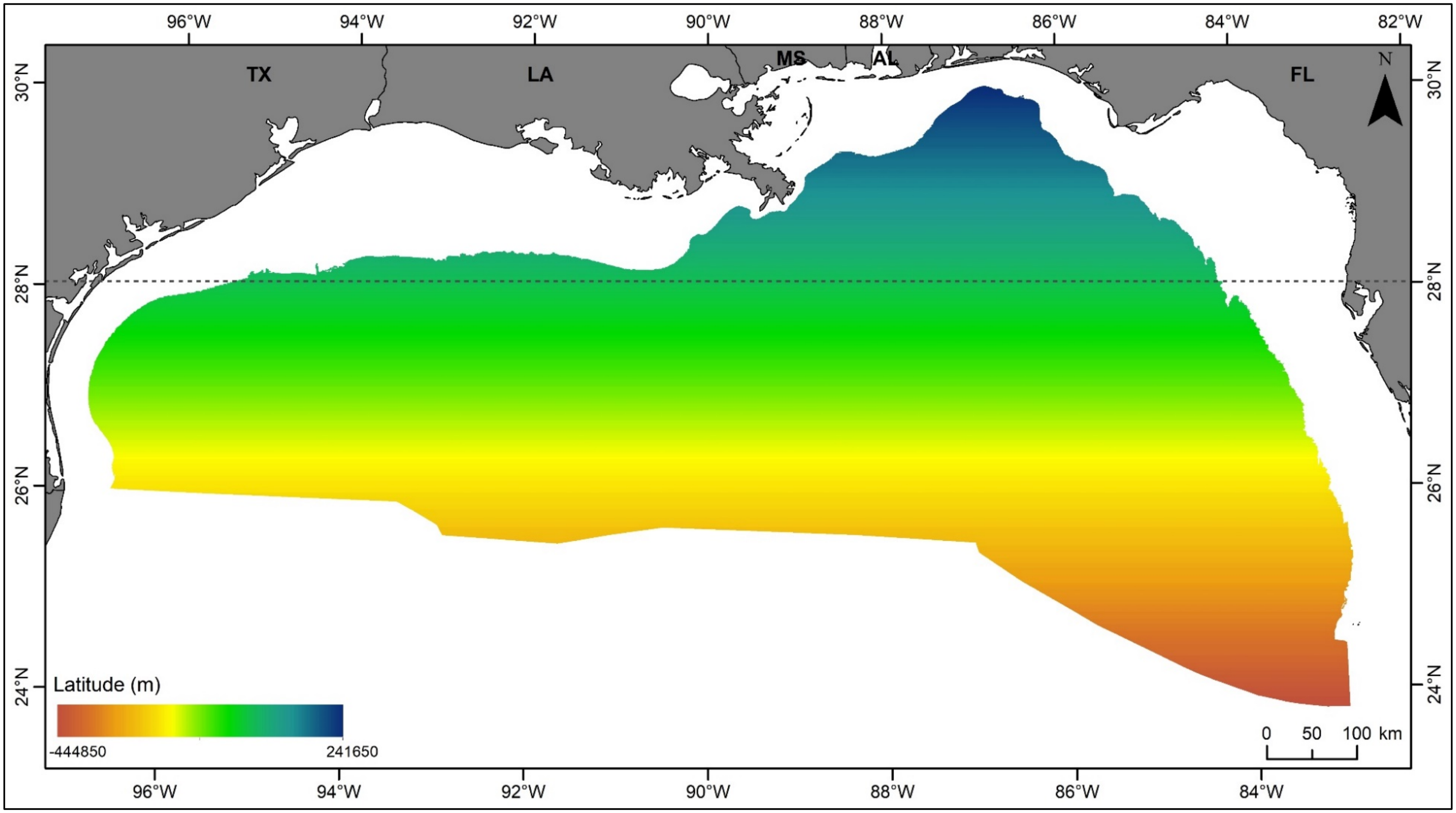

Figure B-27. Latitude (projected), 100 x 100 m resolution.

A dashed gray line depicts the latitude of origin parameter of projected coordinate system, 28 °N.

C Appendix C: High-resolution bathymetry datasets

Table C-1. Compilation of bathymetry datasets included in the bathymetry synthesis

Dataset	Data Source	Year(s)	Grid Resolution	Coordinate System
H12947_MB_8m_MLLW_Combined	eTrac	2016	8 x 8 m	WGS84 UTM Zone 16N
H12945_MB_8m_MLLW_combined	eTrac	2016	8 x 8 m	NAD83 UTM Zone 16N
H12944_MB_8m_MLLW_Combined	eTrac	2016	8 x 8 m	NAD83 UTM Zone 16N
H12943_MB_4m_MLLW_combined	eTrac	2016	4 x 4 m	NAD83 UTM Zone 16N
H12942_MB_4m_MLLW_1of1	eTrac	2016	4 x 4 m	WGS84 UTM Zone 16N
H12941_MB_4m_MLLW_Combined	eTrac	2016	4 x 4 m	WGS84 UTM Zone 16N
H12740_MB_4m_MLLW_1of1	David Evans and Associates	2015	4 x 4 m	NAD83 UTM Zone 16N
H12739_MB_8m_MLLW_combined	David Evans and Associates	2015	8 x 8 m	NAD83 UTM Zone 16N
H12738_MB_8m_MLLW_Combined	David Evans and Associates	2015	8 x 8 m	NAD83 UTM Zone 16N
H12737_MB_4m_MLLW_combined	David Evans and Associates	2015	4 x 4 m	NAD83 UTM Zone 16N
H12636_MB_2m_MLLW_combined	C & C Technologies	2014–2015	2 x 2 m	NAD83 UTM Zone 16N
H12634_MB_4m_MLLW_combined	C & C Technologies	2014-2015	4 x 4 m	NAD83 UTM Zone 16N
NF1407_FKNMS_RileysHump_2m_UTM17N	NOAA Ship *Nancy Foster*	2014	2 x 2 m	NAD83 UTM Zone 17N
NF1407_FKNMS_WestOfSanctuary_4m_UTM17N	NOAA Ship *Nancy Foster*	2014	4 x 4 m	NAD83 UTM Zone 17N
NF1708_Leg1_10m_NAD83_UTM16N	NOAA Ship *Nancy Foster*	2017	10 x 10 m	NAD83 UTM Zone 16N
H12553_MB_4m_MLLW_combined	Ocean Surveys, Inc.	2013–2014	4 x 4 m	NAD83 UTM Zone 16N
FK004E_WFL_Canyon_Survey_10m_WGS84	Schmidt Ocean Institute	2012	10 x 10 m	WGS84
NF1206_FKNMS_Rileys_Hump_South_4m_UTM17N	NOAA Ship *Nancy Foster*	2012	4 x 4 m	NAD83 UTM Zone 17N
W00422_MB_4m_MLLW_Combined	NOAA Ship *Nancy Foster*	2011	4 x 4 m	NAD83 UTM Zone 17N
W00230_MB_8m_MLLW_Combined1	NOAA Ship *Nancy Foster*	2010	8 x 8 m	NAD83 UTM Zone 16N
W00230_MB_8m_MLLW_Combined2	NOAA Ship *Nancy Foster*	2010	8 x 8 m	NAD83 UTM Zone 16N
H12059_2m_MLLW_1of6	C & C Technologies	2009	2 x 2 m	NAD83 UTM Zone 15N
H12059_2m_MLLW_5of6	C & C Technologies	2009	2 x 2 m	NAD83 UTM Zone 15N
H12059_2m_MLLW_6of6	C & C Technologies	2009	2 x 2 m	NAD83 UTM Zone 15N
NF0815_OE_CUBE_10m	NOAA Ship *Nancy Foster*	2008	10 x 10 m	WGS84 World Mercator

Dataset	Data Source	Year(s)	Grid Resolution	Coordinate System
W00397_MB_2m_MLLW_Combined	NOAA Ship *Nancy Foster*	2008	2 x 2 m	NAD83 UTM Zone 17N
W00396_MB_4m_MLLW_Combined	NOAA Ship *Nancy Foster*	2008	4 x 4 m	NAD83 UTM Zone 17N
NF0713_FGBNMS_25m_WGS84	NOAA Ship *Nancy Foster*	2007	25 x 25 m	WGS84
NF0612_FGBNMS_5m_WGS84	NOAA Ship *Nancy Foster*	2006	5 x 5 m	WGS84
H11343_4m_MLLW_1of3	NOAA Ship *Thomas Jefferson*	2004	4 x 4 m	WGS84 UTM Zone 15N
H11343_6m_MLLW_2of3	NOAA Ship *Thomas Jefferson*	2004	6 x 6 m	WGS84 UTM Zone 15N
H11343_12m_MLLW_3of3	NOAA Ship *Thomas Jefferson*	2004	12 x 12 m	WGS84 UTM Zone 15N
H11342_7m_MLLW_1of3	NOAA Ship *Thomas Jefferson*	2004	7 x 7 m	NAD83 UTM Zone 15N
H11342_9m_MLLW_2of3	NOAA Ship *Thomas Jefferson*	2004	9 x 9 m	NAD83 UTM Zone 15N
H11342_13m_MLLW_3of3	NOAA Ship *Thomas Jefferson*	2004	13 x 13 m	NAD83 UTM Zone 15N
H11340_4m_MLLW_1of3	NOAA Ship *Thomas Jefferson*	2004	4 x 4 m	NAD83 UTM Zone 17N
H11340_8m_MLLW_2of3	NOAA Ship *Thomas Jefferson*	2004	8 x 8 m	NAD83 UTM Zone 17N
H11340_12m_MLLW_3of3	NOAA Ship *Thomas Jefferson*	2004	12 x 12 m	NAD83 UTM Zone 17N
H11324_2m_MLLW_1of6	NOAA Ship *Thomas Jefferson*	2004	2 x 2 m	WGS84 UTM Zone 15N
H11324_2m_MLLW_2of6	NOAA Ship *Thomas Jefferson*	2004	2 x 2 m	WGS84 UTM Zone 15N
H11324_4m_MLLW_3of6	NOAA Ship *Thomas Jefferson*	2004	4 x 4 m	WGS84 UTM Zone 15N
H11324_4m_MLLW_4of6	NOAA Ship *Thomas Jefferson*	2004	4 x 4 m	WGS84 UTM Zone 15N
H11324_6m_MLLW_5of6	NOAA Ship *Thomas Jefferson*	2004	6 x 6 m	WGS84 UTM Zone 15N
H11324_12m_MLLW_6of6	NOAA Ship *Thomas Jefferson*	2004	12 x 12 m	WGS84 UTM Zone 15N
H10957_5m_MLLW_UTM17N	NOAA Ship *Thomas Jefferson*	2000–2004	5 x 5 m	NAD83 UTM Zone 17N
USF_2005_2008_Corridor_10m_NAD83	University of South Florida	2005–2008	10 x 10 m	NAD83 HARN
USF_2005_2006_2008_Fill_In_10m_NAD83	University of South Florida	2005–2008	10 x 10 m	NAD83
USF_2002_TwinRidges_10m_NAD83	University of South Florida	2002	10 x 10 m	NAD83
USF_2002_Madison_10m_NAD83	University of South Florida	2002	10 x 10 m	NAD83
USGS_OF_02_006_PinnaclesRegion_16m_UTM16N	USGS	2000	16 x 16 m	WGS84 UTM Zone 16N
USGS_OF_03_007_DeSotoCanyonHead_Merged_8m_UTM16N	USGS	2002	8 x 8 m	WGS84 UTM Zone 16N
USGS_OF_02_005_WestFloridaShelf_Merged_8m_UTM16N	USGS	2001	8 x 8 m	WGS84 UTM Zone 16N

Dataset	Data Source	Year(s)	Grid Resolution	Coordinate System
USGS_OF_02_005_SteamboatLumps_4m_UTM16N	USGS	2001	4 x 4 m	WGS84 UTM Zone 16N
USGS_OF_02_411_StetsonBank_5m_UTM15N	USGS	1997	5 x 5 m	WGS84 UTM Zone 15N
USGS_OF_02_411_WestFlowerGardenBank_5m_UTM15N	USGS	1997	5 x 5 m	WGS84 UTM Zone 15N
USGS_OF_02_411_EastFlowerGardenBank_5m_UTM15N	USGS	1997	5 x 5 m	WGS84 UTM Zone 15N
USGS_OF_02_411_MacNeilBank_4m_UTM15N	USGS	2002	4 x 4 m	WGS84 UTM Zone 15N
USGS_OF_02_411_BrightRankinBanks_4m_UTM15N	USGS	2002	4 x 4 m	WGS84 UTM Zone 15N
USGS_OF_02_411_GeyerBank_4m_UTM15N	USGS	2002	4 x 4 m	WGS84 UTM Zone 15N
USGS_OF_02_411_BoumaRezakSidnerMcGrailBanks_4m_UTM15N	USGS	2002	4 x 4 m	WGS84 UTM Zone 15N
USGS_OF_02_411_SonnierBank_4m_UTM15N	USGS	2002	4 x 4 m	WGS84 UTM Zone 15N
USGS_OF_02_411_AlderdiceBank_4m_UTM15N	USGS	2002	4 x 4 m	WGS84 UTM Zone 15N
USGS_OF_02_411_JakkulaBank_4m_UTM15N	USGS	2002	4 x 4 m	WGS84 UTM Zone 15N
USGS_OF_2005_1089_PulleyRidge_5m_UTM17N	USGS	1999–2003	5 x 5 m	NAD83 UTM Zone 17N
BOEM_Deepwater_Bathymetry_W	BOEM	1998–2015	12.5 x 12.5 m	NAD27 Transverse Mercator
BOEM_Deepwater_Bathymetry_E	BOEM	1998–2015	12.5 x 12.5 m	NAD27 Transverse Mercator
EX1804_MB_FNL_15m_GoMexShallow01_WGS84	NOAA Ship *Okeanos Explorer*	2018	15 x 15 m	WGS84
EX1804_MB_FNL_15m_GoMexShallow02_WGS84	NOAA Ship *Okeanos Explorer*	2018	15 x 15 m	WGS84
EX1202L1_DeSotoCanyon_20m_WGS84	NOAA Ship *Okeanos Explorer*	2012	20 x 20 m	WGS84
W00424_MB_16m_MLLW_Combined	NOAA Ship *Nancy Foster*	2011	16 x 16 m	NAD83 UTM Zone 17N
EX1804_MB_FNL_30m_SouthFlorida_WGS84	NOAA Ship *Okeanos Explorer*	2018	30 x 30 m	WGS84
EX1710_MB_FNL_30m_Florida_WGS84	NOAA Ship *Okeanos Explorer*	2017	30 x 30 m	WGS84
EX1402L3_MB_FNL_Mosaic_30m_WGS84	NOAA Ship *Okeanos Explorer*	2014	30 x 30 m	WGS84
EX1402L2_MB_FNL_02_30m_WGS84	NOAA Ship *Okeanos Explorer*	2014	30 x 30 m	WGS84
EX1203_MB_GreenCanyon_MississippiCanyon_30m_WGS84	NOAA Ship *Okeanos Explorer*	2012	30 x 30 m	WGS84
EX1202L3_MB_FNL_KeathleyCanyon_25m_WGS84	NOAA Ship *Okeanos Explorer*	2012	25 x 25 m	WGS84
FK005_MB_25m_WGS84	Schmidt Ocean Institute	2012	25 x 25 m	WGS84
FK004e_whole_30m	Schmidt Ocean Institute	2012	30 x 30 m	WGS84 World Mercator
EX1105_NorthernArea_25m_WGS84	NOAA Ship *Okeanos Explorer*	2011	25 x 25 m	WGS84

Dataset	**Data Source**	**Year(s)**	**Grid Resolution**	**Coordinate System**
EX1804_MB_FNL_40m_GoMexDeep_WGS84	NOAA Ship *Okeanos Explorer*	2018	40 x 40 m	WGS84
EX1803_MB_FNL_50m_WesternGoMex_WGS84	NOAA Ship *Okeanos Explorer*	2018	50 x 50 m	WGS84
EX1803_MB_FNL_50m_EasternGoMex_WGS84	NOAA Ship *Okeanos Explorer*	2018	50 x 50 m	WGS84
EX1802_MB_FNL_50m_WGS84	NOAA Ship *Okeanos Explorer*	2018	50 x 50 m	WGS84
EX1711_MB_FNL_50m_Mosaic_WGS84	NOAA Ship *Okeanos Explorer*	2017	50 x 50 m	WGS84
EX1403_MB_FNL01_50m_WGS84	NOAA Ship *Okeanos Explorer*	2014	50 x 50 m	WGS84
EX1402L2_MB_FNL_01_50m_WGS84	NOAA Ship *Okeanos Explorer*	2014	50 x 50 m	WGS84
EX1402L2_MB_FNL_03_50m_WGS84	NOAA Ship *Okeanos Explorer*	2014	50 x 50 m	WGS84
EX1402L1_MB_FNL_03to05_Mosaic_50m_WGS84	NOAA Ship *Okeanos Explorer*	2014	50 x 50 m	WGS84
EX1202L2_MB_FNL_50m_WGS84	NOAA Ship *Okeanos Explorer*	2012	50 x 50 m	WGS84
FK006C_whole_40m	Schmidt Ocean Institute	2012	40 x 40 m	WGS84 World Mercator
EX1106_MB_FNL_01_50m_WGS84	NOAA Ship *Okeanos Explorer*	2011	50 x 50 m	WGS84
EX1106_MB_FNL_02_50m_WGS84	NOAA Ship *Okeanos Explorer*	2011	50 x 50 m	WGS84
EX1106_MB_FNL_03_50m_WGS84	NOAA Ship *Okeanos Explorer*	2011	50 x 50 m	WGS84
EX1105_SouthernArea_50m_WGS84	NOAA Ship *Okeanos Explorer*	2011	50 x 50 m	WGS84
EX1104_MB_FNL_04_50m_WGS84	NOAA Ship *Okeanos Explorer*	2011	50 x 50 m	WGS84
EX1202L3_MB_FNL_100m_WGS84	NOAA Ship *Okeanos Explorer*	2012	100 x 100 m	WGS84
EX1202L1_Overall_100m_WGS84	NOAA Ship *Okeanos Explorer*	2012	100 x 100 m	WGS84
EX1105_Overall_100m_WGS84	NOAA Ship *Okeanos Explorer*	2011	100 x 100 m	WGS84
CCOM_GulfofMexico_FloridaEscarpment_2007_WGS84	NOAA-UNH CCOM	2007	100 x 100 m	WGS84
CCOM_GulfofMexico_SigsbeeEscarpment_2007_WGS84	NOAA-UNH CCOM	2007	100 x 100 m	WGS84
EX1203_Overview_MultibeamBathymetry_200m_WGS84	NOAA Ship *Okeanos Explorer*	2012	200 x 200 m	WGS84

UNH = University of New Hampshire, CCOM = Center for Coastal and Ocean Mapping

Department of the Interior (DOI)

The Department of the Interior protects and manages the Nation's natural resources and cultural heritage; provides scientific and other information about those resources; and honors the Nation’s trust responsibilities or special commitments to American Indians, Alaska Natives, and affiliated island communities.

Bureau of Ocean Energy Management (BOEM)

The mission of the Bureau of Ocean Energy Management is to manage development of U.S. Outer Continental Shelf energy and mineral resources in an environmentally and economically responsible way.

BOEM Environmental Studies Program

The mission of the Environmental Studies Program is to provide the information needed to predict, assess, and manage impacts from offshore energy and marine mineral exploration, development, and production activities on human, marine, and coastal environments. The proposal, selection, research, review, collaboration, production, and dissemination of each of BOEM’s Environmental Studies follows the DOI Code of Scientific and Scholarly Conduct, in support of a culture of scientific and professional integrity, as set out in the DOI Departmental Manual (305 DM 3).